

Methods in
Molecular Biology 1703

Springer Protocols

Marc Drolet *Editor*

DNA Topoisomerases

Methods and Protocols

 Humana Press

METHODS IN MOLECULAR BIOLOGY

Series Editor

John M. Walker

School of Life and Medical Sciences

University of Hertfordshire

Hatfield, Hertfordshire, AL10 9AB, UK

For further volumes:

<http://www.springer.com/series/7651>

DNA Topoisomerases

Methods and Protocols

Edited by

Marc Drolet

*Département de microbiologie, infectiologie et immunologie
Université de Montréal, Montréal, QC, Canada*

 **Humana Press**

Editor

Marc Drolet
Département de microbiologie, infectiologie et immunologie
Université de Montréal
Montréal, QC, Canada

ISSN 1064-3745 ISSN 1940-6029 (electronic)
Methods in Molecular Biology
ISBN 978-1-4939-7458-0 ISBN 978-1-4939-7459-7 (eBook)
<https://doi.org/10.1007/978-1-4939-7459-7>

Library of Congress Control Number: 2017959552

© Springer Science+Business Media, LLC 2018

This work is subject to copyright. All rights are reserved by the Publisher, whether the whole or part of the material is concerned, specifically the rights of translation, reprinting, reuse of illustrations, recitation, broadcasting, reproduction on microfilms or in any other physical way, and transmission or information storage and retrieval, electronic adaptation, computer software, or by similar or dissimilar methodology now known or hereafter developed.

The use of general descriptive names, registered names, trademarks, service marks, etc. in this publication does not imply, even in the absence of a specific statement, that such names are exempt from the relevant protective laws and regulations and therefore free for general use.

The publisher, the authors and the editors are safe to assume that the advice and information in this book are believed to be true and accurate at the date of publication. Neither the publisher nor the authors or the editors give a warranty, express or implied, with respect to the material contained herein or for any errors or omissions that may have been made. The publisher remains neutral with regard to jurisdictional claims in published maps and institutional affiliations.

Printed on acid-free paper

This Humana Press imprint is published by Springer Nature
The registered company is Springer Science+Business Media, LLC
The registered company address is: 233 Spring Street, New York, NY 10013, U.S.A.

Preface

Topological problems such as underwinding, overwinding, knotting, and tangling are inherent to the double-helical structure of the DNA. Every time the DNA is transcribed, replicated, or repaired, such problems may arise and have to be resolved to allow the normal progression and completion of DNA transactions. DNA topoisomerases (topos), which are nicking-closing enzymes with strand passage activity, are ubiquitous, unique, and essential enzymes that solve these topological problems. Over the last years, it has become more and more evident that these enzymes play major roles in the maintenance of genomic stability. However, because they cleave DNA they also have the potential to fragment the genome and trigger genomic instability and cell death. In fact, this DNA cleavage property of topoisomerases is used by some of the most potent anticancer and antimicrobial drugs.

More recently, an RNA topoisomerase activity has been described for type IA topos from bacteria, yeast, and higher eukaryotes. This suggests the occurrence of topological problems that need to be resolved during cellular processes involving RNA. What is the nature of these topological problems is currently unknown. In the field of DNA topology, a hot topic is R-loop formation during transcription. Both type IA and IB topos, by relaxing DNA, can inhibit their formation. Whether or not the RNA topo activity of type IA enzymes is also implicated in the inhibition of R-loop formation remains to be seen. Bacterial enzymes of the type IA family were the first topos to be discovered, but only recently that small molecules were shown to inhibit their activity.

The present book, I believe, very well reflects the evolution of the topo field over the last years and the fact that DNA topoisomerases are directly or indirectly involved in a myriad of cellular processes. Over the last years the topo field has largely benefited from genome-wide technologies (e.g., next-generation sequencing), single-molecule approaches as well as more sophisticated cell biology approaches. This book is intended to provide specialists and nonspecialists with an overview of selected hot topics in the field, and with state-of-the-art protocols to study DNA topology, DNA topoisomerase functions and activity as well as their inhibition by various compounds.

The first three chapters of the book are review papers on selected hot topics in the topo field, including type IA topos with an evolutionary perspective (Chap. 1), the beneficial and detrimental effects of type IB topos on genomic stability (Chap. 2), and an update about antimicrobial agents targeting topos (Chap. 3). The following six chapters present experimental protocols related to DNA topology including a basic technique to measure DNA supercoiling in bacteria (Chap. 4), the use of two-dimensional agarose gel electrophoresis to reveal the dynamic of DNA topology during replication (Chap. 5), the use of genome-wide technologies to map topo IV binding and activity sites (Chap. 6), the application of psoralen photobinding to study transcription-induced supercoiling genome-wide in eukaryotic cells (Chap. 7), the use of immunoprecipitation to map sites of R-loop formation genome-wide in yeast cells (Chap. 8), and finally the application of EdU (5-ethynyl-2'-deoxyuridine) labeling to detect replication from R-loops in bacteria by flow cytometry (Chap. 9). The next four chapters describe protocols for *in vitro* studies including the preparation of substrates for the use of magnetic tweezer for single-molecule analysis of topoisomerases (Chap. 10), the synthesis of hemicatenanes to study type IA topo activity (Chap. 11), an assay to detect RNA topo activity (Chap. 12), and two assays for Tyrosyl-DNA

phosphodiesterase I (TDP1) activity, an enzyme removing topo I-associated DNA breaks (Chap. 13). The following four chapters are related to *in vivo* studies of topoisomerase II and include a protocol for chromatin immunoprecipitation of topo II for the genome-wide mapping of their binding sites (Chap. 14), two additional protocols related to topo II with one about mitotic chromosomal defects of topo II mutants (Chap. 15) and the next one about the monitoring of topo II checkpoint in yeast (Chap. 16), and protocols describing assays to identify mutations and other forms of DNA damage, resulting from Top1-cleavage at unrepaired genomic ribonucleotides (Chap. 17). Finally, the last five chapters concern topoisomerase II inhibitors and include a protocol for a fluorescence-based assay to identify bacterial topo I inhibitors (Chap. 18), one for the detection of fluoroquinolone-gyrase cleaved complex (Chap. 19), assays for the immunodetection of topo-DNA covalent complexes in extracted genomic DNA (Chap. 20) or in agarose-embedded unfixed cells (Chap. 21), and the last one about the study of plasmid-mediated quinolone resistance in bacteria (Chap. 22).

I am grateful to the authors for their contributions and patience, as well as to John Walker for his continuous support and hope that this book will be well received in the topo field.

Montréal, QC, Canada

Marc Drolet

Contents

<i>Preface</i>	<i>v</i>
<i>Contributors</i>	<i>ix</i>
1 Type IA DNA Topoisomerases: A Universal Core and Multiple Activities	1
<i>Florence Garnier, H�el�ene Debat, and Marc Nadal</i>	
2 Topoisomerase I and Genome Stability: The Good and the Bad	21
<i>Jang-Eun Cho and Sue Jinks-Robertson</i>	
3 DNA Topoisomerases as Targets for Antibacterial Agents	47
<i>Hiroshi Hiasa</i>	
4 DNA Supercoiling Measurement in Bacteria	63
<i>Yingting Liu, Zhi-Chun Hua, and Fenfei Leng</i>	
5 DNA Catenation Reveals the Dynamics of DNA Topology During Replication	75
<i>Alicia Cast�an, Pablo Hern�andez, Dora B. Krimer, and Jorge B. Schwartzman</i>	
6 Mapping <i>E. coli</i> Topoisomerase IV Binding and Activity Sites	87
<i>Hafez El Sayyed and Olivier Esp�eli</i>	
7 The Use of Psoralen Photobinding to Study Transcription-Induced Supercoiling	95
<i>Fedor Kouzine, Laura Baranello, and David Levens</i>	
8 Immunoprecipitation of RNA:DNA Hybrids from Budding Yeast	109
<i>Aziz El Hage and David Tollervey</i>	
9 Detection of <i>oriC</i> -Independent Replication in <i>Escherichia coli</i> Cells	131
<i>Makisha Martel, Aur�elien Balleydier, Julien Brochu, and Marc Drolet</i>	
10 Single-Molecule Magnetic Tweezer Analysis of Topoisomerases	139
<i>Kathryn H. Gunn, John F. Marko, and Alfonso Mondrag�n</i>	
11 Synthesis of Hemicatenanes for the Study of Type IA Topoisomerases	153
<i>Shun-Hsiao Lee, Tao-shih Hsieh, and Grace Ee-Lu Siaw</i>	
12 An Assay for Detecting RNA Topoisomerase Activity	161
<i>Muzammil Ahmad, Dongyi Xu, and Weidong Wang</i>	
13 Studying TDPI Function in DNA Repair	173
<i>Shih-Chieh Chiang, Kirsty Liversidge, and Sherif F. El-Khamisy</i>	
14 Topoisomerase II Chromatin Immunoprecipitation	183
<i>Kayleigh A. Smith, Ian G. Cowell, and Caroline A. Austin</i>	
15 Analyzing Mitotic Chromosome Structural Defects After Topoisomerase II Inhibition or Mutation	191
<i>Juan F. Gim�enez-Abi�an, Andrew B. Lane, and Duncan J. Clarke</i>	
16 Monitoring the DNA Topoisomerase II Checkpoint in <i>Saccharomyces cerevisiae</i>	217
<i>Katherine Furniss, Amit C.J. Vas, Andrew B. Lane, and Duncan J. Clarke</i>	

17	Studying Topoisomerase I-Mediated Damage at Genomic Ribonucleotides.....	241
	<i>Jessica S. Williams and Thomas A. Kunkel</i>	
18	A Fluorescence-Based Assay for Identification of Bacterial Topoisomerase I Poisons	259
	<i>Thirunavukkarasu Annamalai, Bokun Cheng, Neelam Keswani, and Yuk-Ching Tse-Dinh</i>	
19	Fluoroquinolone-Gyrase-DNA Cleaved Complexes	269
	<i>Gan Luan and Karl Drlica</i>	
20	Detection of Topoisomerase Covalent Complexes in Eukaryotic Cells.....	283
	<i>Jay Anand, Yilun Sun, Yang Zhao, Karin C. Nitiss, and John L. Nitiss</i>	
21	Visualization and Quantification of Topoisomerase–DNA Covalent Complexes Using the Trapped in Agarose Immunostaining (TARDIS) Assay	301
	<i>Ian G. Cowell and Caroline A. Austin</i>	
22	Study of Plasmid-Mediated Quinolone Resistance in Bacteria	317
	<i>George A. Jacoby</i>	
	<i>Index</i>	327

Contributors

- MUZAMMIL AHMAD • *Genome Instability and Chromatin Remodeling Section, Lab of Genetics and Genomics, National Institute on Aging, National Institute on Health, Baltimore, MD, USA*
- JAY ANAND • *Biopharmaceutical Sciences Department, University of Illinois College of Pharmacy, Rockford, IL, USA*
- THIRUNAVUKKARASU ANNAMALAI • *Department of Chemistry and Biochemistry, Florida International University, Miami, FL, USA; Biomolecular Sciences Institute, Florida International University, Miami, FL, USA*
- CAROLINE A. AUSTIN • *Institute for Cell and Molecular Biosciences, University of Newcastle upon Tyne, Newcastle upon Tyne, UK*
- AURÉLIEN BALLEVDIER • *Département de microbiologie, infectiologie et immunologie, Université de Montréal, Montréal, QC, Canada*
- LAURA BARANELLO • *Laboratory of Pathology, NCI/NIH, Bethesda, MD, USA*
- JULIEN BROCHU • *Département de microbiologie, infectiologie et immunologie, Université de Montréal, Montréal, QC, Canada*
- ALICIA CASTÁN • *Department of Cellular and Molecular Biology, Centro de Investigaciones Biológicas (CSIC), Madrid, Spain*
- BOKUN CHENG • *Department of Pediatrics, Albert Einstein College of Medicine, Bronx, NY, USA*
- SHIH-CHIEH CHIANG • *Department of Molecular Biology and Biotechnology, Krebs Institute, University of Sheffield, Sheffield, UK*
- JANG-EUN CHO • *Department of Molecular Genetics and Microbiology, Duke University Medical Center, Durham, NC, USA*
- DUNCAN J. CLARKE • *Department of Genetics, Cell Biology & Development, University of Minnesota, Minneapolis, MN, USA*
- IAN G. COWELL • *Institute for Cell and Molecular Biosciences, University of Newcastle upon Tyne, Newcastle upon Tyne, UK*
- HÉLÈNE DEBAT • *Université Versailles St-Quentin, Institut Jacques Monod, UMR 7592 CNRS-Univ. Paris Diderot, Paris, France*
- KARL DRLICA • *Department of Microbiology, Biochemistry & Molecular Genetics, Public Health Research Institute, New Jersey Medical School, Rutgers Biomedical and Health Sciences, Rutgers University, Newark, NJ, USA*
- MARC DROLET • *Département de microbiologie, infectiologie et immunologie, Université de Montréal, Montréal, Québec, Canada*
- OLIVIER ESPÉLI • *Center for Interdisciplinary Research in Biology (CIRB), Collège de France, CNRS/UMR 7241 – INSERM U1050, PSL Research University, Paris Cedex, France*
- KATHERINE FURNISS • *Department of Genetics, Cell Biology & Development, University of Minnesota, Minneapolis, MN, USA; St. John's University, Collegeville, MN, USA*
- FLORENCE GARNIER • *Université Versailles St-Quentin, Institut Jacques Monod, UMR 7592 CNRS-Univ. Paris Diderot, Paris, France*
- JUAN F. GIMÉNEZ-ABIÁN • *Department of Cell and Molecular Biology, Synthetic Microbial Macromolecular Assemblies, CIB, CSIC, Madrid, Spain*

- KATHRYN H. GUNN • *Department of Molecular Biosciences, Northwestern University, Evanston, IL, USA*
- AZIZ EL HAGE • *Wellcome Centre for Cell Biology, University of Edinburgh, Edinburgh, UK*
- SHERIF F. EL-KHAMISY • *Department of Molecular Biology and Biotechnology, Krebs Institute, University of Sheffield, Sheffield, UK*
- PABLO HERNÁNDEZ • *Department of Cellular and Molecular Biology, Centro de Investigaciones Biológicas (CSIC), Madrid, Spain*
- HIROSHI HIASA • *Department of Pharmacology, University of Minnesota Medical School, Minneapolis, MN, USA*
- TAO-SHIH HSIEH • *Institute of Cellular and Organismic Biology, Academia Sinica, Taipei, Taiwan*
- ZHI-CHUN HUA • *School of Life Sciences, Nanjing University, Nanjing, Jiangsu, People's Republic of China; Changzhou High-Tech Research Institute of Nanjing University and Jiangsu TargetPharma Laboratories Inc., Changzhou, Jiangsu, People's Republic of China*
- GEORGE A. JACOBY • *Lahey Hospital and Medical Center, Burlington, MA, USA*
- SUE JINKS-ROBERTSON • *Department of Molecular Genetics and Microbiology, Duke University Medical Center, Durham, NC, USA*
- NEELAM KESWANI • *Department of Chemistry and Biochemistry, Florida International University, Miami, FL, USA; Biomolecular Sciences Institute, Florida International University, Miami, FL, USA*
- FEDOR KOUZINE • *Laboratory of Pathology, NCI/NIH, Bethesda, MD, USA*
- DORA B. KRIMER • *Department of Cellular and Molecular Biology, Centro de Investigaciones Biológicas (CSIC), Madrid, Spain*
- THOMAS A. KUNKEL • *Genome Integrity and Structural Biology Laboratory, National Institute of Environmental Health Sciences (NIEHS), National Institutes of Health (NIH), Research Triangle Park, NC, USA*
- ANDREW B. LANE • *Department of Genetics, Cell Biology & Development, University of Minnesota, Minneapolis, MN, USA*
- SHUN-HSIAO LEE • *Department of Structural Cell Biology, Molecular Mechanisms of DNA Repair, Max Planck Institute of Biochemistry, Martinsried, Germany*
- FENFEI LENG • *Biomolecular Sciences Institute, Florida International University, Miami, FL, USA; Department of Chemistry & Biochemistry, Florida International University, Miami, FL, USA*
- DAVID LEVENS • *Laboratory of Pathology, NCI/NIH, Bethesda, MD, USA*
- YINGTING LIU • *Biomolecular Sciences Institute, Florida International University, Miami, FL, USA; Department of Chemistry & Biochemistry, Florida International University, Miami, FL, USA; School of Life Sciences, Nanjing University, Nanjing, Jiangsu, People's Republic of China*
- KIRSTY LIVERSIDGE • *Department of Molecular Biology and Biotechnology, Krebs Institute, University of Sheffield, Sheffield, UK*
- GAN LUAN • *Department of Microbiology, Biochemistry & Molecular Genetics, Public Health Research Institute, New Jersey Medical School, Rutgers Biomedical and Health Sciences, Rutgers University, Newark, NJ, USA*
- JOHN F. MARKO • *Department of Molecular Biosciences, Northwestern University, Evanston, IL, USA; Department of Physics and Astronomy, Northwestern University, Evanston, IL, USA*
- MAKISHA MARTEL • *Département de microbiologie, infectiologie et immunologie, Université de Montréal, Montréal, QC, Canada*

- ALFONSO MONDRAGÓN • *Department of Molecular Biosciences, Northwestern University, Evanston, IL, USA*
- MARC NADAL • *Institut Jacques Monod, UMR 7592 CNRS-Université Paris Diderot, Paris, France*
- KARIN C. NITISS • *Biopharmaceutical Sciences Department, University of Illinois College of Pharmacy, Rockford, IL, USA; Biomedical Science Department, University of Illinois College of Medicine, Rockford, IL, USA*
- JOHN L. NITISS • *Biopharmaceutical Sciences Department, University of Illinois College of Pharmacy, Rockford, IL, USA*
- HAFEZ EL SAYYED • *Center for Interdisciplinary Research in Biology (CIRB), Collège de France, CNRS/UMR 7241 – INSERM U1050, PSL Research University, Paris Cedex, France*
- JORGE B. SCHVARTZMAN • *Department of Cellular and Molecular Biology, Centro de Investigaciones Biológicas (CSIC), Madrid, Spain*
- GRACE EE-LU SIAW • *Institute of Cellular and Organismic Biology, Academia Sinica, Taipei, Taiwan*
- KAYLEIGH A. SMITH • *Institute for Cell and Molecular Biosciences, University of Newcastle upon Tyne, Newcastle upon Tyne, UK*
- YILUN SUN • *Biopharmaceutical Sciences Department, University of Illinois College of Pharmacy, Rockford, IL, USA*
- DAVID TOLLERVEY • *Wellcome Centre for Cell Biology, University of Edinburgh, Edinburgh, UK*
- YUK-CHING TSE-DINH • *Department of Chemistry and Biochemistry, Florida International University, Miami, FL, USA; Biomolecular Sciences Institute, Florida International University, Miami, FL, USA*
- AMIT C. J. VAS • *Department of Genetics, Cell Biology & Development, University of Minnesota, Minneapolis, MN, USA; Biotechnology R&D, Cargill, Inc., Plymouth, MN, USA*
- WEIDONG WANG • *Genome Instability and Chromatin Remodeling Section, Lab of Genetics and Genomics, National Institute on Aging, National Institute on Health, Baltimore, MD, USA*
- JESSICA S. WILLIAMS • *Genome Integrity and Structural Biology Laboratory, National Institute of Environmental Health Sciences (NIEHS), National Institutes of Health (NIH), Research Triangle Park, NC, USA*
- DONGYI XU • *Genome Instability and Chromatin Remodeling Section, Lab of Genetics and Genomics, National Institute on Aging, National Institute on Health, Baltimore, MD, USA; State Key Laboratory of Protein and Plant Gene Research, School of Life Sciences, Peking University, Beijing, China*
- YANG ZHAO • *Biopharmaceutical Sciences Department, University of Illinois College of Pharmacy, Rockford, IL, USA; Biomedical Science Department, University of Illinois College of Medicine, Rockford, IL, USA*

Chapter 1

Type IA DNA Topoisomerases: A Universal Core and Multiple Activities

Florence Garnier, H el ene Debat, and Marc Nadal

Abstract

All the type IA topoisomerases display universal characteristics relying on a core region basically responsible for the transesterification and the strand passage reaction. First limited to the bacterial domain for a long time, these enzymes were further retrieved in Archaea and Eukarya as well. This is representative of an extremely ancient origin, probably due to an inheritance from the RNA world. As remaining evidence, some current topoisomerases IA have retained a RNA topoisomerase activity. Despite the presence of this core region in all of these TopoIAs, some differences exist and are originated from variable regions, located essentially within both extremities, conferring on them their specificities. During the last 2 decades the evidence of multiple activities and dedicated roles highlighted the importance of the topoisomerases IA. It is now obvious that topoisomerases IA are key enzymes involved in the maintenance of the genome stability. The discovery of these new activities was done thanks to the use of more accurate assays, based on new sophisticated DNA substrates.

Key words Topoisomerases, Type IA, Topoisomerase I, Topoisomerase III, Reverse gyrase, *topA*, *topB*, *toprim*

1 Introduction

1.1 *Discovery of the First Topoisomerases*

As early as their first publication about the double helix model of DNA, James D. Watson and Francis H. C. Crick pointed out that the proposed structure required enzymes able to remove DNA entanglements occurring during transactions of genetic information [1]. Indeed, two major topological issues occur when DNA is processed during DNA metabolism (replication, transcription, recombination, and repair), the production of torsional stress and catenated DNA molecules. These DNA transactions might require two types of hypothetical enzymes, a swivelase that transiently cleaves one DNA strand to relax the torsional stress, and a decatenase able to cleave both DNA strands at once to separate sister chromatids (for a recent review *see* ref. 2).

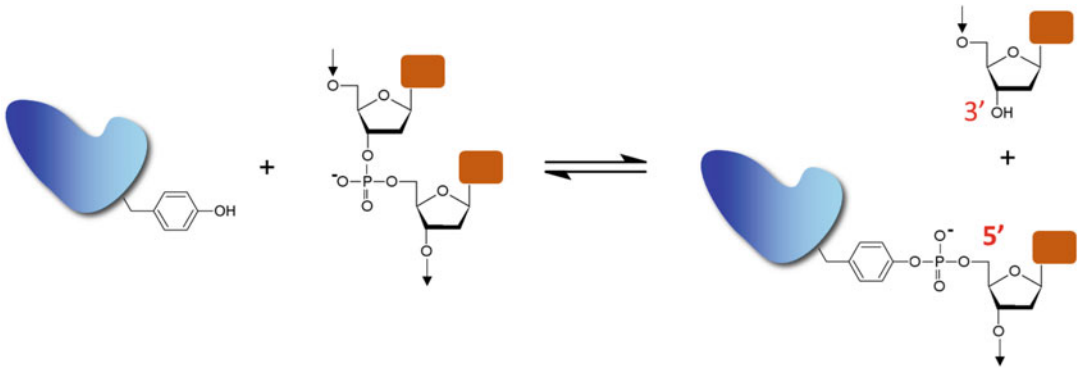


Fig. 1 Schematic representation of transesterification reaction of type IA and type II topoisomerases. The conserved tyrosine of the active site forms a transient and covalent link with the DNA by a 5' phospho-tyrosyl bond in one hand and a 3'OH end of DNA on the other hand

The first enzyme able to remove the topological constraints, the ω protein, was discovered in *Escherichia coli* by James C. Wang in 1971 and is now named topoisomerase I [3]. One year later, James J. Champoux and Renato Dulbecco discovered, in the nucleus of mouse cells, a close activity also named topoisomerase I [4]. Both enzymes are ATP-independent. Few years later, Martin Gellert and coworkers have evidenced in *E. coli*, a new topoisomerase able to negatively supercoil the DNA in the presence of ATP: the DNA gyrase [5]. Close topoisomerases, but unable to supercoil the DNA, were then found in Eukarya and referred as topoisomerase II [6].

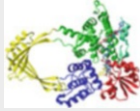
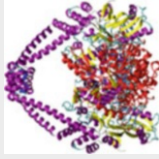
1.2 Common Catalysis of Topoisomerases

To perform their catalysis, all the DNA topoisomerases use a very efficient chemical reaction: the transesterification. The conserved tyrosine of the catalytic site cleaves a DNA strand to form a phospho-tyrosyl bond between the protein and one end of the nicked DNA strand and an OH extremity on the other end (Fig. 1). This reaction does not require energy and is fully reversible. So, to change the DNA topology, the DNA topoisomerases catalyze two transesterification reactions, the first one to break the DNA and the second one to reseal the DNA. As noticed by James C. Wang, the topoisomerases are “magicians among the magicians”, work “without leaving any trace” [7] and change the DNA linking number. The central nature of topoisomerases in the processing of the genetic information flow has made them tremendously successful therapeutic targets.

1.3 The Two Types of the DNA Topoisomerases

Based on their mechanisms, two different types of topoisomerases are considered: the enzymes able to cleave transiently only one DNA strand belong to the type I topoisomerases while the enzymes that transiently cleave simultaneously the two DNA strands belong to the type II topoisomerases (Table 1). For the type I enzymes, the

Table 1
Different types of topoisomerases and their basic properties

Type	I	II
Number of cleaved strand	1	2
Families	IA	IIB
Polarity of the DNA linkage	5'	5'
Magnesium dependence	Yes	Yes
ATP dependence	No*	Yes
Strand passage reaction	Yes	Yes
Free DNA end rotation	No	No
Domain of life	E, B, A	E, B, A
3D Structure		
Stoichiometry	α ; 3PX7	$\alpha_2\beta_2$; 5BS8
	α ; 3M4A	α ; 5HM5
	α ; 2Q2E	$\alpha_2\beta_2$; 2Q2E

A Archaea, B Bacteria, E Eukarya (when few species or only one are reported, it is indicated in *italic* or with ** respectively). For the 3D color code for topoisomerase IA see the corresponding one described in Fig. 2. For other topoisomerases alpha-helix are in purple, beta-sheet in yellow. When DNA is present it is represented in licorice. In topoisomerase IIA structure, the Toprim domain is in red. The star (*) means that all the TopoIAs is ATP-independent except the reverse gyrases. PDB references: 3PX7 [9], 3M4A [10], 5HM5 [128], 5BS8 [129] and 2Q2E [130]

second single strand can pass through the broken one while for the type II enzymes, another DNA duplex can pass through the broken double stranded DNA. Currently, topoisomerases issued from numerous organisms have been studied and all the living cells exhibit at least one copy of each type of topoisomerases.

2 Main Characteristics of the Two Types of Topoisomerases

2.1 The Type I Topoisomerases

Based on the amino acids sequences analysis and the biochemical properties, three different families have been reported for type I topoisomerases (named IA, IB, and IC) (Table 1).

As previously mentioned, all the type I topoisomerases transiently cleave one DNA strand. However, the TopoIAs are the only ones performing a strand passage reaction. By contrast, the TopoIB and IC are a real swivelase: they do not catalyze a strand passage reaction but, after the cleavage, they limit the rotation of the 5' free DNA end around the other strand before resealing the breakage (Table 1).

The TopoIB is present in all eukaryotes but it was recently shown that it is also present in some bacteria and archaea. This enzyme is the target of an important anticancer drug, camptothecin and its derivatives [2, 11]. The TopoIC is a very special enzyme present in only one species of archaea, *Methanococcus kandleri* [8, 12, 13] (Table 1). If its structure was recently solved [14–16], its origin and function are not known.

During numerous years, the study of the type IA topoisomerases (TopoIAs) was restricted to Bacteria, such as *E. coli*. Later, TopoIAs have been found in all the cells of the three domains of life (Table 1) and constitute the sole ubiquitous protein among all the topoisomerases. During the past 10 years, the importance of these topoisomerases has been highlighted partly due to their essential role in the maintenance of genome stability [2, 16, 17]. Despite the essentiality of TopoIAs, the precise mechanism(s) and function(s) of the different TopoIAs remain essentially unknown compared to type II topoisomerases. A current insight of these enzymes will be further given in detail.

2.2 The Type II Topoisomerases

The type II topoisomerases are split into two different families (named IIA and IIB) (Table 1). Type II topoisomerases are ATP-dependent enzymes that use this energy to transport a DNA duplex through one or two gates for the families IIB or IIA respectively [18–20]. Except the DNA gyrase, a TopoIIA, that negatively supercoils DNA, all the other TopoIIs relax both positively and negatively supercoiled DNA.

Three structural organizations were reported in the TopoIIA family but their overall architectures are very similar. They correspond to a heterodimer or a homodimer. The heterodimer is

composed of two copies of two different subunits, one exhibiting the ATPase site and the other the tyrosine responsible for the transesterification. The homodimer results from the fusion of the two different subunits within a single polypeptide and organized into two domains. In some viruses such as T4, a TopoIIA is present but the ATPase subunit is cleaved into two fragments leading to a heterohexameric enzyme. It is noteworthy that these enzymes are relevant targets for antibiotics such as quinolones or anticancer drugs such as etoposide [11, 16].

Similarly to some TopoIIAs, TopoIIB is a heterodimer with two copies of two different subunits. The first enzyme was discovered in Archaea [21, 22] and then in plants [9, 23]. Interestingly, the subunit responsible for the transesterification reaction was discovered in Eukarya as well as the protein responsible for the double strands breakage during the meiosis [22, 24]. Very recently, the second subunit, *i.e.*, the ATPase subunit, able to associate with the catalytic subunit was discovered both in *Arabidopsis thaliana* and in the mouse. In addition, it was proposed this heterodimer was the key enzyme to start the meiotic recombination [25–27].

The ability to cleave simultaneously both DNA strands allows the TopoIIs to change not only the DNA linking number but also the knot number and the number of links joining two different DNA molecules. Consequently, all the organisms possess, at least, one type II topoisomerase because they are essential at the end of the replication to decatenate the two newly synthesized chromosomes. These enzymes interact with numerous partners, some of them being able to directly modulate their activity (for exhaustive reviews *see* refs. 2, 9, 24, 28–34).

3 Tridimensional Structure of TopoIAs

All the TopoIAs share a common organization and are characterized by the presence of ten highly conserved amino acids motifs (Fig. 2 and [8, 9, 12, 28, 30]) which are located within three elements, the Toprim one (or Rossman fold) and the two Topofolds 1 and 2 [8, 14, 16]. The two successive Topofolds are responsible for the toroidal shape exhibited by all the TopoIAs [16, 35, 36] (Fig. 2). Despite this fold conservation, a relatively important sequence divergence occurs between the ten conserved motifs. In particular, an additional and variable domain is present in some TopoIAs into the Toprim element, between the motifs 2 and 3 (Fig. 2). The presence of an intein has been shown in some archaeal enzymes near the tyrosine of the active site [9, 18, 31, 37, 38], between the two parts of the motif 7 (Fig. 2). Moreover, outside this central core region, the carboxy-terminal part exhibits most of the DNA binding motifs; they differ both in terms of motif type and numbers of repetition. The most famous extension at the

TopoIA

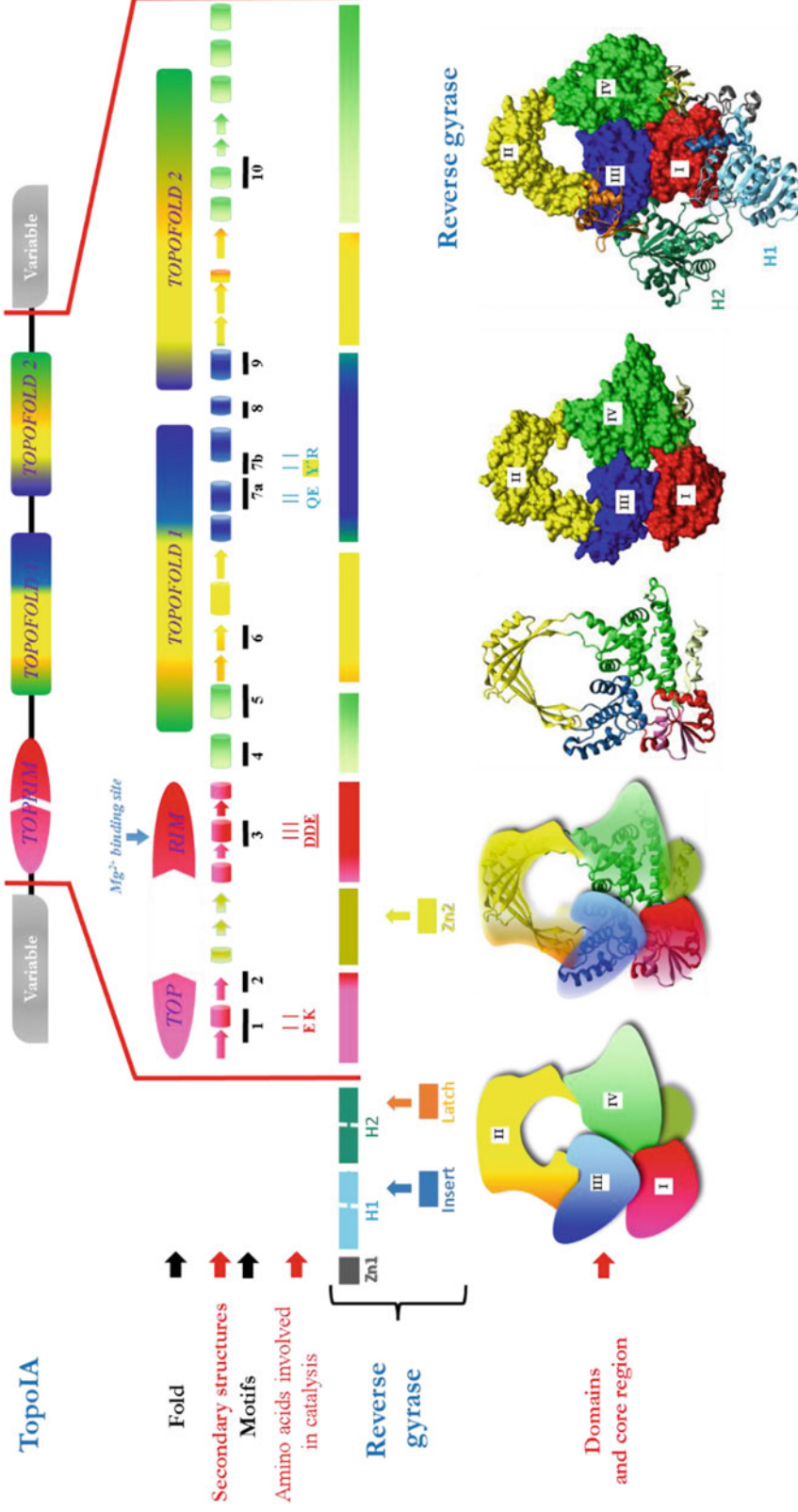


Fig. 2 TopoA overall structure representation of type IA topoisomerase. From *top* to *bottom*: **Architecture** of topoisomerase IA (**TopoIA**) with Toprim domain and two Topofolds. N-terminal and C-terminal region are variable. The **Fold** is detailed with **Secondary structures** showing insertion into Toprim domain (*green-yellow*). The presence of conserved **Motifs** [8] is shown wherein **Amino acids** are directly **involved in catalysis** (the catalytic tyrosine is underlined in *yellow* and *red*). **Reverse gyrase architecture** with an additional Zinc finger (Zn2) in Toprim domain and a large N-terminal extension with Zinc finger (Zn1) and two helicase domains (H1 and H2) each containing an insertion, in particular the Latch domain in H2. The domains I, II, III and IV define the **core region** of Topo IA and are indicated in *red, yellow, blue* and *green* respectively. At the *bottom*, the links between folds and domains are highlighted with PDB structure of *E. coli* (3PX7) [9] and compared with the reverse gyrase of *T. maritima* (*bottom right*, 4DDU)

amino terminal part corresponds to the presence of a SF2 helicase that characterizes the reverse gyrase subfamily (Fig. 2).

The structure of the core region corresponds to the 67 kDa fragment of *E. coli* TopA and has been determined more than 20 years ago [25]. It has been further retrieved in all the other type IA topoisomerase structures currently obtained [9, 24, 28–34, 39]. It can be divided in four structural domains noted I, II, III and IV (Fig. 2) forming a toroid with a central hole able to accommodate single or double stranded DNA [9, 28–30]. The ten amino acids motifs [8], conserved in all the TopoIAs, are spread within this core region (Fig. 2). There is a contact between the Toprim domain (domain I) and the domain III, but no covalent link allowing the toroid free to open. Interestingly, the Toprim domain is also present in all the type II topoisomerases and also actively participate to the catalysis [35, 36].

The 3D determination of TopoIA in interaction with an oligonucleotide for mimicking a single-stranded DNA, indicates that the DNA is bound in a deep groove formed at the interface between domains I and III partially implying the domain IV as well (Fig. 3) [9, 31, 37, 38]. The second part of the DNA binding site end by the tyrosine of the active site located at the surface of the domain II and corresponds to the 5' terminus of the oligonucleotide. Some phosphate groups of the oligonucleotide are linked to basic

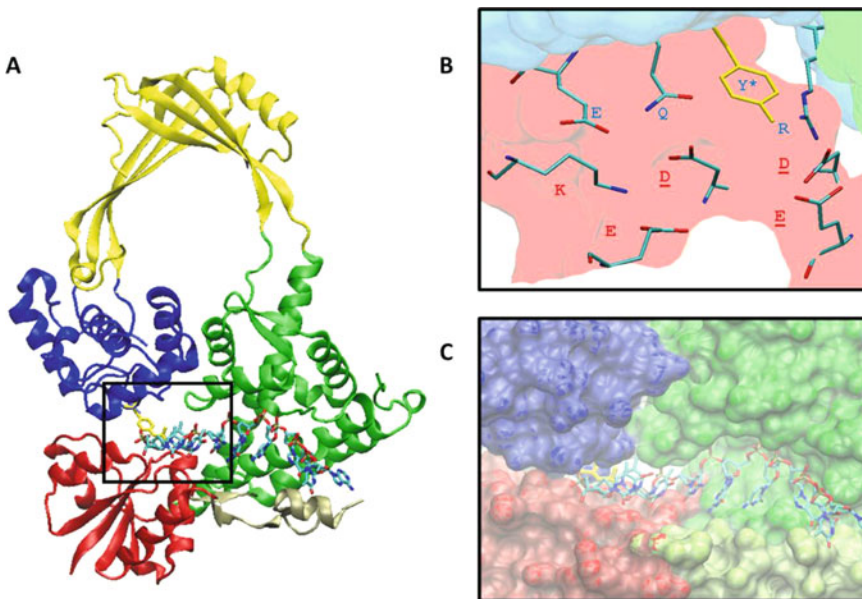


Fig. 3 Catalytic site of *E. coli* topoisomerase IA (3PX7) coupled with single strand DNA [9]. (a) The *black* frame delimits the localization of the catalytic site between domains I (*red*) and III (*blue*). The active tyrosine is represented in yellow with *. (b) Active site with the amino acids directly involved in catalysis. (c) The DNA substrate localized in the catalytic site

residues located within this cavity and allow for the cleavage reaction to occur [2–4, 9, 33]. Currently, the position of the complementary DNA strand has not been mapped yet.

4 Activity of the Core Region and Inhibitors of TopoIAs

The activity of the core region can be obtained by expressing a mutant of the *E. coli* enzyme deleted in its carboxy-terminal part [25, 40, 41] or after a mild proteolysis of *T. maritima* TopoI (*topA* gene product) [39]. In this case, the cleavage performed by the protease is close to the boundary between domains II and III, near the proposed hinge region involved in conformational changes [29]. It was shown that the core region of *E. coli* TopoI retained only the DNA cleavage reaction and not the DNA relaxation activity. By contrast, the *T. maritima* truncated TopoI is still able to relax DNA but with a lower efficiency compared with the complete protein, the DNA sequence recognition specificity being unchanged [5–7, 39, 42, 43]. This indicates that the core region is responsible for the transesterification reaction. The amino acids involved in this transesterification reaction are located at the junctions between the domains I, III, and IV.

The conserved amino acids of the motif 1 (ExxK) and motif 3 (D-D(R/T)EGE) located within the Toprim domain, are involved in the binding of the magnesium. They are also essential for the transesterification reaction and faced to the tyrosine of the active site, which is located right in front of these amino acids at the end of the Topofold 1 (Fig. 3 domain III) [40, 41]. Thus, amino acids mutations within the motifs 1 and 3 lead to a decrease or a complete suppression of the religation step [2, 9, 11, 13, 15, 17, 44, 45].

During many years, no inhibitors of TopoIA were available in spite of significant efforts [46] except an inhibition of *E. coli* TopA by phospholipids which has been reported [46, 47]. However, since a couple of years, some TopoIA inhibitors have been described [47, 48]. In particular, by using a cell-based high throughput assay, three compounds were selected for increasing the cleavage reaction. Unfortunately, the inhibitions observed were relatively low [49]. Organomercury compounds have been shown to inhibit TopoI but these inhibitions are probably not selective because they act by interacting with the cysteine residues of the Zn fingers [50, 51]. However, more specific molecules such as sec-oneolistine or norclomipramine have been discovered recently, inhibiting TopoI from *Streptococcus pneumonia* [52] or *Mycobacterium tuberculosis* [53] respectively. However, a deep characterization of these compounds on the different TopoIAs must be achieved. In particular, it would be interesting to know which reaction step is sensitive to these drugs.

5 Three Subfamilies Among TopoIAs

Despite their sequence and structure similarities and a common transesterification mechanism for all the TopoIAs, three different subfamilies of TopoIA must be considered: the TopoI, the TopoIII and the reverse gyrase subfamily.

5.1 *Their Respective Enzymatic Activities*

The TopoI subfamily is represented by *E. coli* TopA and is very efficient to relax negatively supercoiled DNA. The discovery of a second TopoIA in a TopoI deficient *E. coli* strain ($\Delta topA$) pointed out a new property, the ability to decatenate circular molecules containing a nick (DNA FII) [54]. This property is shared by topoisomerases issued from the three domains of life and is used to define functionally the second TopoIA group, the TopoIII subfamily. The TopoIII subfamily is represented by *E. coli* TopB, yeast TopoIII and the two human TopoIII α or β , all these enzymes being relatively inefficient for the relaxation but very efficient to catenate or decatenate, and knot or unknot nicked DNA. Finally, the third subfamily of TopoIA corresponds to the reverse gyrase, which is a fusion, within the same polypeptide, between a classical type IA topoisomerase and a SF2 helicase. Reverse gyrase is present only in hyperthermophilic and some thermophilic organisms and is able to introduce positive supercoils into the DNA. It was proposed that this unique activity reduces DNA melting in organisms particularly exposed to extreme life conditions, helping them to maintain genome stability [55].

Although the TopoIA core region clearly corresponds to a platform that carried out the transesterification reaction, some possible extensions, essentially located within the carboxy-terminal part make it highly variable and are likely responsible for the different activities and functions of the TopoIAs. It has been demonstrated that the cleavage specificity of TopoI and reverse gyrase is close but differs from TopoIII. Both for TopoI (but not for TopoIII) and reverse gyrase, the cleavage specificity requires a cytosine at the position -4 relatively to the cleavage site. This cytosine is in total agreement with the steric hindrance of the cavity (motif 4) for interaction [9]. We noticed that the -4 cytosine interacts with the tyrosine of this motif 4 for TopoI but with a phenylalanine residue for reverse gyrases. In addition, the bases positioned from -6 to $+1$ relatively to the cleavage site interact with domains IV and I. All the TopoIAs, including reverse gyrases, relax both negatively and positively supercoiled DNA substrates. In the second case, the substrate must possess in addition a permanent bubble [56–58]. This indicates that these enzymes require during their reaction process a single stranded DNA and the strand passage reaction is basically possible in the two directions.

5.2 Their Related Structural Specificities

5.2.1 TopoI vs. TopoIII

Amino acids comparison of the different TopoIAs indicate that major differences appear within the carboxy-terminal region, both in terms of length and composition, giving to the TopoIAs their respective specificities. It was proposed that the carboxy-terminal part of the TopoIAs contributes to discriminate between TopoI and TopoIII and it is obvious that this extension of the core region exhibits very few contact areas with the other domains [59]. It modulates the specificity of the cleavage reaction for some TopoIs. Indeed, the two zinc fingers 1 and 2 of the TopoI from *E. coli* are required for the site specificity [43] while, for *T. maritima* TopoI, the unique zinc finger is not essential. Indeed, mutation of the corresponding cysteine leads to the loss of the Zn atom but retains the activity, the cleavage specificity being unchanged [42]. If the specificity of the cleavage site can be modulated by some amino acids, it basically appears for the different TopoIA subfamilies that the amino acids extensions act mostly on the strand passage reaction. In particular, an insertion of 17 residues is located within the domain III of the *E. coli* TopoIII, in the vicinity of the tyrosine of the active site, by comparison with the *E. coli* TopoI. It was suggested that this insertion could be responsible for the catenation/decatenation of DNA catalyzed by TopoIII and was named the “decatenation loop” [30, 60]. Unfortunately, the *T. maritima* TopoI which is efficient in decatenation, does not require this loop for the decatenation [42] nor the TopoIII from *Sulfolobus solfataricus* and numerous other TopoIIIs such as yeast TopoIII or the two human TopoIIIs (unpublished results and observations). The function of this insertion in *E. coli* TopoIII remains to be elucidated and the amino acids really involved in the decatenation too. Another possibility could be the involvement of the proline residues in the hinge regions between the domain II and the domains III and IV. Indeed, important differences are observed within these regions [61]. So the strand passage mechanism seems to be different between TopoI and TopoIII and could be due to conformational changes, in particular in the domain I [9, 31, 37, 61].

5.2.2 Reverse Gyrase

Reverse gyrase is the only type I topoisomerase able to positively supercoil the DNA in an ATP-dependent manner [9, 31, 37, 62–64]. As previously mentioned, it is a chimera of the core region of the TopoIA with a SF2 helicase located at its amino-terminal part [12, 65]. The SF2 helicase is formed by two domains, H1 and H2 (Fig. 2) and have six characteristic motifs [8, 12]. This H1 helicase domain is in interaction with the domains I and III of the core region [24, 32]. Two Zn fingers, with different structural features, are present in the reverse gyrase. The first, located at the amino-terminus of the protein, interacts with the domain I, in the vicinity of the domain IV. The second is an insertion within the Toprim domain, not so far from the Zn finger 1, allowing an interaction between the two Zn fingers. The Zn finger 2 is not retrieved in

reverse gyrases issued from particular bacteria but the consequence of this lack on the activity has not been examined yet. A highly variable insertion, both in length and in amino acids composition and named the latch is present in the H2 domain (Fig. 2) and interacts with the domain III. This interaction is probably transient [66] and participates to a communication between the helicase and topoisomerase parts. This latch is not essential for the positive supercoiling activity but inhibits the relaxation activity of the topoisomerase part [67–69]. Another variable amino acids sequence is present between the motifs Ia and II (Fig. 2) [12]. An intein has been reported to be present in some reverse gyrases from Euryarchaeota. It is located between the motifs 7a and 7b, splitting the active site just before the catalytic tyrosine [70].

5.2.3 Partners of TopoIAs

The TopoIA core region can display interactions with different partners that are able to modulate their activities. Indeed, in addition to reverse gyrase, which corresponds to a permanent interaction between a SF2 helicase and a TopoIA topoisomerase, it emerges from the literature that genome stability is partly mediated by an interaction between TopoIII and SF2 helicases such as Sgs1 in yeast [71], RecQ in *E. coli* [72], BLM and WRN in human [73] and generally numerous RecQ and RecQ-like proteins [74]. These interactions exist in the three domains of life and, in hyperthermophiles, such interaction exists between the TopoIII and the helicase Hel112 in addition to the intrinsic association of corresponding domains within the two reverse gyrases [75]. In *Drosophila*, it was demonstrated that it is the carboxy-terminal domain of TopoIII α which interacts with BLM [76, 77]. The TopoIII acts in concert with two OB fold proteins, Rmi1 and Rmi2 for the maintenance of genomic stability in eukaryotes [77–79]. It was shown that Rmi1 interacts with the edge of domain II of the TopoIII (Fig. 2), a part of it being in the central hole of TopoIII α [78]. This interaction could play a major role in the decatenation of hemicatenanes [78, 80]. However, the TopoIAs are able to interact with other proteins such as RecA [80, 81]. This interaction in *E. coli* confirms the stimulation of the relaxation activity of TopoI by RecA previously described [81, 82] and could play a regulatory role in transcription. Indeed, in *E. coli*, TopoI interacts with the RNA polymerase by its carboxy-terminal extension [82–84] while in Metazoa, the TRDT3 protein, that facilitates the transcription of genes marked by methylated histones, interacts with TopoIII β [83–86]. Thus, these interactions probably allow to increase the specificity and the selectivity of the TopoIA rather than to modulate the transesterification reaction by itself. In addition, it has been shown that TopoIII β is able to knot/un knot RNA [85–88].

5.2.4 Role of the TopoIAs

During the 80's, a lot of new topoisomerases has been discovered and in a famous review entitled "DNA Topoisomerases: Why So Many?", James C. Wang tried to make sense to this multiplicity in terms of diversity of their functions. This title can be still addressed to the TopoIAs. Thus, many organisms contain more than one TopoIA involved in different processes. In Bacteria, the TopoI is clearly involved in the homeostatic regulation of the superhelical density of the chromosome [87–89]. Another essential function of TopoI is the relaxation of transcription-induced negative supercoiling [89–93]. Indeed, in *E. coli*, the absence of TopoI leads to growth defects due to R-loops accumulation and hypernegative supercoiling [82, 90–93]. This function is sustained by the interaction of TopoI with the β' subunit of the RNA polymerase [82, 94]. Both the hypernegative supercoiling and R-loops increase the genome instability by authorizing non-B DNA structure [94, 95]. Finally, TopoIII can compensate, but only partially, the default in TopoI, the cell being viable [83, 95]. In Eukarya, it has been reported that TopoIII β is also able to reduce R-loop formation induced during transcription [83, 85, 86]. Interestingly, this function could be linked to the RNA topoisomerase activity. Indeed, TopoIIIs with a RNA topoisomerase activity were reported in the three domains of life including *E. coli* TopoI and TopoIII, *S. solfataricus* and *Nanoarchaeum equitans* TopoIII, yeast TopoIII and human TopoIII β [54, 85, 86, 96].

In *E. coli*, the role of TopoIII is unclear, it poorly relaxes DNA but decatenates replication intermediates [54, 97]. So TopoIII can serve as the cellular decatenase [97, 98] and, in the presence of RecQ, is able to unlink precatenanes [98, 99]. However, in *E. coli*, decatenation is probably essentially performed by TopoIV which is much more efficient for decatenating DNA than TopoIII. Therefore TopoIII could be rather involved in other processes such as recombination [100, 101]. In this case, TopoIII prevents the formation of lethal recombination intermediates [101]. During the last decade, it is obvious that the TopoIIIs play an essential role in disentangling recombination intermediates to maintain the genome stability [74, 101]. This function is probably the most universal function of the TopoIAs. In all organisms, this role is achieved thanks to the interaction with SF2 helicase [74, 102] and, with additional partners such as Rmi1 and Rmi2 in Eukarya. In yeast, the complex TopoIII-Rmi1 is responsible for the dissolution of the D-loop formed during homologous recombination [102, 103]. In Metazoa, the complex TopoIII-SF2 helicase-Rmi1-Rmi2 is responsible for convergent branch migration of double Holliday junctions (dHj) [103, 104] and solve the double Holliday junction by dissolution instead of resolution. It is important to keep in mind that the resolution pathway induces cross-overs, a reorganization of the genome, and finally an instability of the genome [104].

In the hyperthermophiles, two or three TopoIAs are present, including at least one reverse gyrase. It is likely that reverse gyrase avoids DNA melting and increase the rate of the reannealing of the two complementary DNA strands after the passage of replication forks or transcriptional bubble [55, 105]. It seems possible to delete the unique reverse gyrase gene in Euryarcheota [106]. By contrast, in Crenarcheota, in spite of the presence of two reverse gyrase encoding genes, both are essential [18, 107]. However, this discrepancy is probably the result of major differences between the different enzymes. Some of them are inefficient, or not very efficient [18, 108, 109] while others are extraordinarily efficient [109–111] to positively supercoil the DNA, suggesting different roles for the corresponding enzymes. In *S. solfataricus*, the two reverse gyrases clearly exhibit different enzymatic properties and a specific regulation pathway, to assume different functions in the cell [75, 109–111]. Surprisingly, a third TopoIA-SF2 helicase complex exists in *Sulfolobus* cell as its TopoIII interacts with the helicase Hel112 [75]. The hyperthermophilic organisms live in environmental conditions that increase the DNA damage frequency. Some results showed that these organisms face to these difficulties by expressing constitutively most of the proteins involved directly or indirectly in DNA repair and recombination [112–114]. It is likely that TopoIA multiplicity in these organisms is the consequence of the importance of the TopoIA-SF2 helicase association in the maintenance of genome stability, which is crucial in organisms living in a particularly DNA damaging environment.

Finally, redundancy of the TopoIAs is observed in numerous organisms belonging to the three domains of life and concerns either the TopoIII or the reverse gyrase subfamily. As an example, it has been shown that three copies of TopoIA encoding gene are present in the chromosome of *Bacillus cereus* (one for TopoI and two for TopoIII), but two additional gene copies are also present in plasmids [115, 116]. A similar redundancy of the TopoIA genes is observed in *Pectobacterium atrosepticum*. It was demonstrated that the TopoIII β of this organism is involved in the maintenance of a pathogenicity island by reducing its excision from the bacterial genome both during growth or after plant infection [116].

5.2.5 Why Such a Multiplicity of TopoIAs?

Both the presence of highly conserved motifs and the same global architecture and shape strongly suggest that type IA topoisomerase is a very ancient protein that has been submitted to a very high level of selective pressure. However, gene duplications and further sub-functionalizations appeared several times over the time evolution and both lead to highly challenging phylogenetics analyses. In addition, it is most likely that more or less recent horizontal gene transfers occur [16, 115–118]. Thus, as reported, two groups of TopoIA could be distinguished easily, the TopoI family which includes the protein encoded by *E. coli topA* gene and the reverse

gyrase [16, 114]. The third group is not well defined and gathers, irrespectively with the annotation existing in the database, all the other TopoIAs, most of them being annotated as TopoIII. It seems to us that it is probably from this group that originates the most ancient enzyme which displays the universal characteristics of topoisomerases. Clearly, it is in this group that numerous duplications and subsequent subfunctionalizations may have occurred leading to the presence of several copies both in Bacteria and Eukarya. As an example, *B. cereus* exhibits two TopoIIIs as human, each of them exhibiting a specific activity and associated function(s) [86, 114]. During the last decade, the increasing amount of sequenced genomes revealed the presence, in most organisms, of several TopoIAs. Taking into account both the phylogeny and the activities, when these data exist, it is tempting to speculate that TopoIAs are very ancient enzymes that first work on RNA in the RNA world as it was suggested when their RNA topoisomerase activities were discovered [86, 119]. It is obvious that at least one gene duplication occurs in LUCA, leading to the TopoI and the TopoIII (Fig. 4). This is in accordance with the RNA topoisomerase activity of the two enzymes of *E. coli* [85, 96, 119, 121]. The

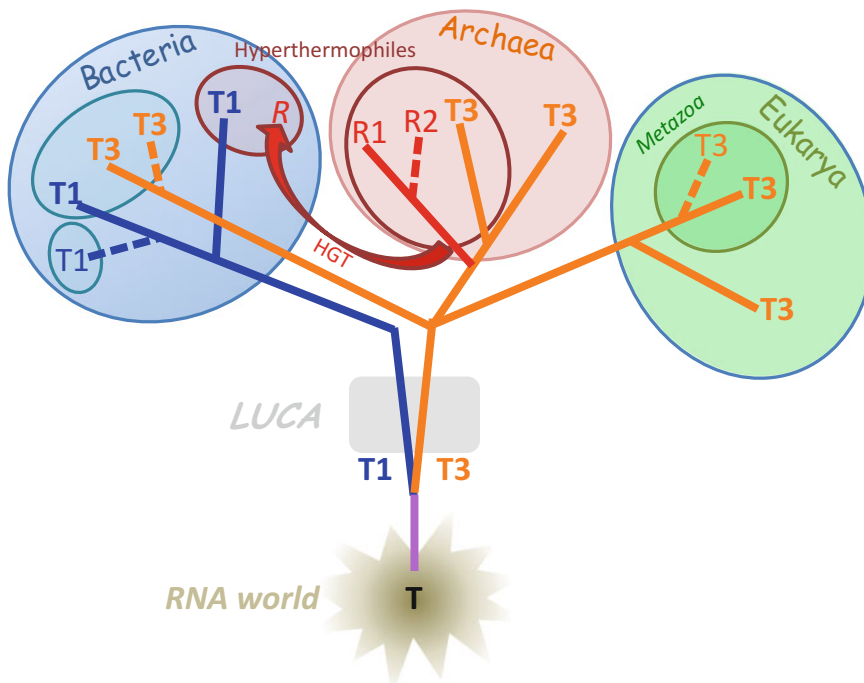


Fig. 4 Hypothetical origin and distribution of Topoisomerases IA within the tree of life. T1, T3, and R indicate the TopoI, the TopoIII, and the reverse gyrase, respectively. The enzymes with a RNA topoisomerase activity are in **bold**, the others, having lost it, are in regular. The *dashed lines* indicate that only a part of the organisms possess such enzymes. LUCA [120] and HGT mean Last Universal Cellular Ancestor and Horizontal Gene Transfer respectively. T represents the ancestor of all of the TopoIAs

TopoIII copy seems to be lost in some organisms, such as the mycobacteria while further duplications of TopoIII seem to have occurred both in Bacteria and Eukarya, probably independently, some of these copies having lost their RNA topoisomerase activity such as in Metazoa (Fig. 4). Finally, it is difficult to know exactly how the fusion of the SF2 helicase with a TopoIA occurred to form the reverse gyrase. In hyperthermophilic bacteria, it is likely that reverse gyrase has been acquired through a horizontal gene transfer (Fig. 4).

5.2.6 Concluding Remark

The multiplicity of the TopoIAs, as regards their structural and enzymatic properties, strongly suggest that TopoIA is a very ancient protein which has endured a lot of duplications followed by a subfunctionalization process giving new enzymatic properties, intrinsic or when coupled to partners. During the last decade, new enzymatic assays helped us to distinguish these new properties especially by using a panel of nucleic acid substrates which can mimic transient intermediates of recombination, replication, repair or transcription such as R-loops, hemicatenanes, Holliday junctions, or RNA-knot [85, 96, 121–123]. At the same time, single molecule experiment have been expanded, giving a more precise control of kinetics parameters [122–125] or, for the reverse gyrase, the torque produced [124–127]. Moreover, single molecule assays allow to use highly specific substrates more easily than in bulk and to discriminate between the different activities of a set of different enzymes [126, 127]. The use of these new substrates will allow us to have a better understanding of the precise mechanism of each enzyme and finally to get a better knowledge of their roles in the cells.

Acknowledgments

We are grateful to Terence Strick both for the laboratory facilities and helpful discussions.

References

1. Watson JD, Crick FH (1953) Molecular structure of nucleic acids; a structure for deoxyribose nucleic acid. *Nature* 171:737–738
2. Chen SH, Chan N-L, Hsieh T-S (2013) New mechanistic and functional insights into DNA topoisomerases. *Annu Rev Biochem* 82:139–170
3. Wang JC (1971) Interaction between DNA and an *Escherichia coli* protein omega. *J Mol Biol* 55:523–533
4. Champoux JJ, Dulbecco R (1972) An activity from mammalian cells that untwists superhelical DNA – a possible swivel for DNA replication (polyoma-ethidium bromide-mouse-embryo cells-dye binding assay). *Proc Natl Acad Sci U S A* 69:143–146
5. Gellert M, Mizuuchi K, O’Dea MH, Nash HA (1976) DNA gyrase: an enzyme that introduces superhelical turns into DNA. *Proc Natl Acad Sci U S A* 73:3872–3876
6. Liu LF, Liu CC, Alberts BM (1980) Type II DNA topoisomerases: enzymes that can unknot a topologically knotted DNA molecule via a reversible double-strand break. *Cell* 19:697–707
7. Wang JC (1991) DNA topoisomerases: why so many? *J Biol Chem* 266:6659–6662

8. Nadal M (2007) Reverse gyrase: an insight into the role of DNA-topoisomerases. *Biochimie* 89:447–455
9. Zhang Z, Cheng B, Tse-Dinh Y-C (2011) Crystal structure of a covalent intermediate in DNA cleavage and rejoining by *Escherichia coli* DNA topoisomerase I. *Proc Natl Acad Sci U S A* 108:6939–6944
10. Patel A, Yakovleva L, Shuman S, Mondragón A (2010) Crystal structure of a bacterial topoisomerase IB in complex with DNA reveals a secondary DNA binding site. *Structure* 18:725–733
11. Pommier Y, Leo E, Zhang H, Marchand C (2010) DNA topoisomerases and their poisoning by anticancer and antibacterial drugs. *Chem Biol* 17:421–433
12. Jaxel C, Bouthier de la Tour C, Duguet M, Nadal M (1996) Reverse gyrase gene from *Sulfolobus shibatae* B12: gene structure, transcription unit and comparative sequence analysis of the two domains. *Nucleic Acids Res* 24:4668–4675
13. Slesarev AI, Lake JA, Stetter KO et al (1994) Purification and characterization of DNA topoisomerase V. An enzyme from the hyperthermophilic prokaryote *Methanopyrus kandleri* that resembles eukaryotic topoisomerase I. *J Biol Chem* 269:3295–3303
14. Aravind L (1998) Toprim—a conserved catalytic domain in type IA and II topoisomerases, DnaG-type primases, OLD family nucleases and RecR proteins. *Nucleic Acids Res* 26:4205–4213
15. Rajan R, Osterman AK, Gast AT, Mondragón A (2014) Biochemical characterization of the topoisomerase domain of *M. kandleri* topoisomerase V. *J Biol Chem* 289:28898–28909
16. Duguet M, Serre M-C, Bouthier de La Tour C (2006) A universal type IA topoisomerase fold. *J Mol Biol* 359:805–812
17. Usongo V, Drolet M (2014) Roles of type IA topoisomerases in genome maintenance in *Escherichia coli*. *PLoS Genet* 10: e1004543–e1004543
18. Bouthier de la Tour C, Portemer C, Kaltoum H, Duguet M (1998) Reverse gyrase from the hyperthermophilic bacterium *Thermotoga maritima*: properties and gene structure. *J Bacteriol* 180:274–281
19. Roca J, Berger JM, Harrison SC, Wang JC (1996) DNA transport by a type II topoisomerase: direct evidence for a two-gate mechanism. *Proc Natl Acad Sci U S A* 93:4057–4062
20. Corbett KD, Berger JM (2005) Structural dissection of ATP turnover in the prototypical GHL ATPase TopoVI. *Structure* 13:873–882
21. Bergerat AA, Gabelle DD, Forterre PP (1994) Purification of a DNA topoisomerase II from the hyperthermophilic archaeon *Sulfolobus shibatae*. A thermostable enzyme with both bacterial and eucaryal features. *J Biol Chem* 269:27663–27669
22. Bergerat A, de Massy B, Gabelle D et al (1997) An atypical topoisomerase II from Archaea with implications for meiotic recombination. *Nature* 386:414–417
23. Yin Y, Cheong H, Friedrichsen D et al (2002) A crucial role for the putative Arabidopsis topoisomerase VI in plant growth and development. *Proc Natl Acad Sci U S A* 99:10191–10196
24. Rudolph MG, Del Toro Duany Y, Jungblut SP et al (2013) Crystal structures of *Thermotoga maritima* reverse gyrase: inferences for the mechanism of positive DNA supercoiling. *Nucleic Acids Res* 41:1058–1070
25. Lima CD, Wang JC, Mondragón A (1992) Crystallization of a 67 kDa fragment of *Escherichia coli* DNA topoisomerase I. *J Mol Biol* 232:1213–1216
26. Vrielynck N, Chambon A, Vezon D et al (2016) A DNA topoisomerase VI-like complex initiates meiotic recombination. *Science* 351:939–943
27. Robert T, Nore A, Brun C et al (2016) The TopoVIB-like protein family is required for meiotic DNA double-strand break formation. *Science* 351:943–949
28. Lima CD, Wang JC, Mondragón A (1994) Three-dimensional structure of the 67K N-terminal fragment of *E. coli* DNA topoisomerase I. *Nature* 367:138–146
29. Feinberg H, Lima CD, Mondragón A (1999) Conformational changes in *E. coli* DNA topoisomerase I. *Nat Struct Biol* 6:918–922
30. Mondragón A, DiGate R (1999) The structure of *Escherichia coli* DNA topoisomerase III. *Structure* 7:1373–1383
31. Changela A, DiGate RJ, Mondragón A (2001) Crystal structure of a complex of a type IA DNA topoisomerase with a single-stranded DNA molecule. *Nature* 411:1077–1081
32. Rodríguez AC, Stock D (2002) Crystal structure of reverse gyrase: insights into the positive supercoiling of DNA. *EMBO J* 21:418–426

33. Perry K, Mondragón A (2003) Structure of a complex between *E. coli* DNA topoisomerase I and single-stranded DNA. *Structure* 11:1349–1358
34. Tan K, Zhou Q, Cheng B et al (2015) Structural basis for suppression of hypernegative DNA supercoiling by *E. coli* topoisomerase I. *Nucleic Acids Res* 43:11031–11046
35. Liu Q, Wang JC (1999) Similarity in the catalysis of DNA breakage and rejoining by type IA and IIA DNA topoisomerases. *Proc Natl Acad Sci U S A* 96:881–886
36. Graille M, Cladière L, Durand D et al (2008) Crystal structure of an intact type II DNA topoisomerase: insights into DNA transfer mechanisms. *Structure* 16:360–370
37. Changela A, DiGate RJ, Mondragón A (2007) Structural studies of *E. Coli* topoisomerase III-DNA complexes reveal a novel type IA topoisomerase-DNA conformational intermediate. *J Mol Biol* 368:105–118
38. Tan K, Cao N, Cheng B et al (2015) Insights from the structure of *Mycobacterium tuberculosis* topoisomerase I with a novel protein fold. *J Mol Biol* 428:182–193
39. Cossard R, Viard T, Lamour V et al (2004) Proteolytic cleavage of the hyperthermophilic topoisomerase I from *Thermotoga maritima* does not impair its enzymatic properties. *Biochim Biophys Acta* 1700:161–170
40. Chen SJ, Wang JC (1998) Identification of active site residues in *Escherichia coli* DNA topoisomerase I. *J Biol Chem* 273:6050–6056
41. Zhu CX, Tse-Dinh YC (2000) The acidic triad conserved in type IA DNA topoisomerases is required for binding of Mg(II) and subsequent conformational change. *J Biol Chem* 275:5318–5322
42. Viard T, Lamour V, Duguet M, la Tour de CB (2001) Hyperthermophilic topoisomerase I from *Thermotoga maritima*. A very efficient enzyme that functions independently of zinc binding. *J Biol Chem* 276:46495–46503
43. Viard T, Cossard R, Duguet M, la Tour de CB (2004) *Thermotoga maritima*-*Escherichia coli* chimeric topoisomerases. Answers about involvement of the carboxyl-terminal domain in DNA topoisomerase I-mediated catalysis. *J Biol Chem* 279:30073–30080
44. Cheng B, Shukla S, Vasunilashorn S et al (2005) Bacterial cell killing mediated by topoisomerase I DNA cleavage activity. *J Biol Chem* 280:38489–38495
45. Cheng B, Annamalai T, Sorokin E et al (2009) Asp-to-Asn substitution at the first position of the DxD TOPRIM motif of recombinant bacterial topoisomerase I is extremely lethal to *E. coli*. *J Mol Biol* 385:558–567
46. Tse-Dinh YC (2007) Exploring DNA topoisomerases as targets of novel therapeutic agents in the treatment of infectious diseases. *Infect Disord Drug Targets* 7:3–9
47. Mizushima T, Natori S, Sekimizu K (1992) Inhibition of *Escherichia coli* DNA topoisomerase I activity by phospholipids. *Biochem J* 285:503–506
48. Tse-Dinh YC (2009) Bacterial topoisomerase I as a target for discovery of antibacterial compounds. *Nucleic Acids Res* 37:731–737
49. Cheng B, Liu I-F, Tse-Dinh Y-C (2007) Compounds with antibacterial activity that enhance DNA cleavage by bacterial DNA topoisomerase I. *J Antimicrob Chemother* 59:640–645
50. Cheng B, Cao S, Vasquez V et al (2012) Identification of anziaic acid, a lichen depside from *Hypotrachyna* sp., as a new topoisomerase poison inhibitor. *PLoS One* 8: e60770–e60770
51. Cheng B, Annamalai T, Sandhaus S et al (2015) Inhibition of Zn(II) binding type IA topoisomerases by organomercury compounds and Hg(II). *PLoS One* 10:e0120022
52. García MT, Blázquez MA, Ferrandiz MJ et al (2011) New alkaloid antibiotics that target the DNA topoisomerase I of *Streptococcus pneumoniae*. *J Biol Chem* 286:6402–6413
53. Godbole AA, Ahmed W, Bhat RS et al (2015) Targeting *Mycobacterium tuberculosis* topoisomerase I by small-molecule inhibitors. *Antimicrob Agents Chemother* 59:1549–1557
54. DiGate RJ, Marians KJ (1988) Identification of a potent decatenating enzyme from *Escherichia coli*. *J Biol Chem* 263:13366–13373
55. Nadal M, Mirambeau G, Forterre P et al (1986) Positively supercoiled DNA in a virus-like particle of an Archaeobacterium. *Nature* 321:256–258
56. Kirkegaard K, Wang JC (1985) Bacterial-DNA topoisomerase-I can relax positively supercoiled DNA containing a single-stranded loop. *J Mol Biol* 185:625–637
57. Slesarev AI, Kozyavkin SA (1990) DNA substrate specificity of reverse gyrase from extremely thermophilic archaeobacteria. *J Biomol Struct Dyn* 7:935–942
58. Hsieh T-S, Plank JL (2006) Reverse gyrase functions as a DNA renaturase: annealing of complementary single-stranded circles and positive supercoiling of a bubble substrate. *J Biol Chem* 281:5640–5647

59. Hansen G, Harrenga A, Wieland B et al (2006) Crystal structure of full length topoisomerase I from *Thermotoga maritima*. *J Mol Biol* 358:1328–1340
60. Li Z, Mondragón A, Hiasa H et al (2000) Identification of a unique domain essential for *Escherichia coli* DNA topoisomerase III-catalysed decatenation of replication intermediates. *Mol Microbiol* 35:888–895
61. Viard T, Bouthier de La Tour C (2007) Type IA topoisomerases: a simple puzzle? *Biochimie* 89:456–467
62. Kikuchi A, Asai K (1984) Reverse gyrase – a topoisomerase which introduces positive superhelical turns into DNA. *Nature* 309:677–681
63. Forterre P, Mirambeau G, Jaxel C et al (1985) High positive supercoiling in vitro catalyzed by an ATP and polyethylene glycol-stimulated topoisomerase from *Sulfolobus acidocaldarius*. *EMBO J* 4:2123–2128
64. Nadal M, Jaxel C, Portemer C et al (1988) Reverse gyrase of *Sulfolobus*: purification to homogeneity and characterization. *Biochemistry* 27:9102–9108
65. Confalonieri F, Elie C, Nadal M et al (1993) Reverse gyrase: a helicase-like domain and a type I topoisomerase in the same polypeptide. *Proc Natl Acad Sci U S A* 90:4753–4757
66. Lulchev P, Klostermeier D (2014) Reverse gyrase-recent advances and current mechanistic understanding of positive DNA supercoiling. *Nucleic Acids Res* 42:8200–8213
67. Rodríguez AC (2003) Investigating the role of the latch in the positive supercoiling mechanism of reverse gyrase. *Biochemistry* 42:5993–6004
68. Ganguly A, Del Toro Duany Y, Rudolph MG, Klostermeier D (2011) The latch modulates nucleotide and DNA binding to the helicase-like domain of *Thermotoga maritima* reverse gyrase and is required for positive DNA supercoiling. *Nucleic Acids Res* 39:1789–1800
69. Del Toro Duany Y, Ganguly A, Klostermeier D (2014) Differential contributions of the latch in *Thermotoga maritima* reverse gyrase to the binding of single-stranded DNA before and after ATP hydrolysis. *Biol Chem* 395:83–93
70. Chute IC, Hu Z, Liu XQ (1998) A topA intein in *Pyrococcus furiosus* and its relatedness to the r-gyr intein of *Methanococcus jannaschii*. *Gene* 210:85–92
71. Gangloff S, McDonald JP, Bendixen C et al (1994) The yeast type I topoisomerase Top3 interacts with Sgs1, a DNA helicase homolog: a potential eukaryotic reverse gyrase. *Mol Cell Biol* 14:8391–8398
72. Harmon FG, DiGate RJ, Kowalczykowski SC (1999) RecQ helicase and topoisomerase III comprise a novel DNA strand passage function: a conserved mechanism for control of DNA recombination. *Mol Cell* 3:611–620
73. Wu L, Davies SL, North PS et al (2000) The Bloom's syndrome gene product interacts with topoisomerase III. *J Biol Chem* 275:9636–9644
74. Wu L, Hickson ID (2001) RecQ helicases and topoisomerases: components of a conserved complex for the regulation of genetic recombination. *Cell Mol Life Sci* 58:894–901
75. Valenti A, De Felice M, Perugino G et al (2012) Synergic and opposing activities of Thermophilic RecQ-like helicase and topoisomerase 3 proteins in Holliday junction processing and replication fork stabilization. *J Biol Chem* 287:30282–30295
76. Chen SH, C-H W, Plank JL, Hsieh T-S (2012) Essential functions of the C-terminus of *Drosophila* topoisomerase III α in double Holliday junction dissolution. *J Biol Chem* 287:19346–19353
77. Xu D, Guo R, Sobek A et al (2008) RMI, a new OB-fold complex essential for Bloom syndrome protein to maintain genome stability. *Genes Dev* 22:2843–2855
78. Bocquet N, Bizard AH, Abdulrahman W et al (2014) Structural and mechanistic insight into Holliday-junction dissolution by topoisomerase III α and RMI1. *Nat Struct Mol Biol* 21(3):261–268
79. Mullen JR, Nallaseth FS, Lan YQ et al (2005) Yeast Rmi1/Ncc4 controls genome stability as a subunit of the Sgs1-Top3 complex. *Mol Cell Biol* 25:4476–4487
80. Banda S, Tiwari PB, Darici Y, Tse-Dinh YC (2016) Investigating direct interaction between *Escherichia coli* topoisomerase I and RecA. *Gene* 585:65–70
81. Reckinger AR, Jeong KS, Khodursky AB, Hiasa H (2007) RecA can stimulate the relaxation activity of topoisomerase I: molecular basis of topoisomerase-mediated genome-wide transcriptional responses in *Escherichia coli*. *Nucleic Acids Res* 35:79–86
82. Cheng B, Zhu C-X, Ji C et al (2003) Direct interaction between *Escherichia coli* RNA polymerase and the zinc ribbon domains of DNA topoisomerase I. *J Biol Chem* 278:30705–30710
83. Yang Y, McBride KM, Hensley S et al (2014) Arginine methylation facilitates the

- recruitment of TOP3B to chromatin to prevent R loop accumulation. *Mol Cell* 53:484–497
84. Siaw GE-L, Liu I-F, Lin P-Y et al (2016) DNA and RNA topoisomerase activities of Top3{beta} are promoted by mediator protein Tudor domain-containing protein 3. *Proc Natl Acad Sci U S A* 113:5544–5541
 85. Xu D, Shen W, Guo R et al (2013) Top3 β is an RNA topoisomerase that works with fragile X syndrome protein to promote synapse formation. *Nat Neurosci* 16:1238–1247
 86. Ahmad M, Xue Y, Lee SK et al (2016) RNA topoisomerase is prevalent in all domains of life and associates with polyribosomes in animals. *Nucleic Acids Res* 44:6335–6349
 87. Tse-Dinh YC (1985) Regulation of the Escherichia coli DNA topoisomerase I gene by DNA supercoiling. *Nucleic Acids Res* 13:4751–4763
 88. Dorman CJ (2013) Genome architecture and global gene regulation in bacteria: making progress towards a unified model? *Nat Rev Microbiol* 11:349–355
 89. Masse E, Drolet M (1999) Relaxation of transcription-induced negative supercoiling is an essential function of Escherichia coli DNA topoisomerase I. *J Biol Chem* 274:16654–16658
 90. Drolet M, Bi X, Liu LF (1994) Hypernegative supercoiling of the DNA template during transcription elongation in vitro. *J Biol Chem* 269:2068–2074
 91. Drolet M, Phoenix P, Menzel R et al (1995) Overexpression of RNase H partially complements the growth defect of an Escherichia coli delta topA mutant: R-loop formation is a major problem in the absence of DNA topoisomerase I. *Proc Natl Acad Sci U S A* 92:3526–3530
 92. Masse E, Drolet M (1999) Escherichia coli DNA topoisomerase I inhibits R-loop formation by relaxing transcription-induced negative supercoiling. *J Biol Chem* 274:16659–16664
 93. Drolet M (2006) Growth inhibition mediated by excess negative supercoiling: the interplay between transcription elongation, R-loop formation and DNA topology. *Mol Microbiol* 59:723–730
 94. Higgins NP, Vologodskii AV (2015) Topological behavior of plasmid DNA. *Microbiol Spectr* 3:1–25
 95. Stupina VA, Wang JC (2005) Viability of Escherichia coli topA mutants lacking DNA topoisomerase I. *J Biol Chem* 280:355–360
 96. Wang H, Di Gate RJ, Seeman NC (1996) An RNA topoisomerase. *Proc Natl Acad Sci U S A* 93:9477–9482
 97. Nurse P, Levine C, Hassing H, Mariani KJ (2003) Topoisomerase III can serve as the cellular decatenase in Escherichia coli. *J Biol Chem* 278:8653–8660
 98. Hiasa H, Mariani KJ (1994) Topoisomerase III, but not topoisomerase I, can support nascent chain elongation during theta-type DNA replication. *J Biol Chem* 269:32655–32659
 99. Harmon FG, Brockman JP, Kowalczykowski SC (2003) RecQ helicase stimulates both DNA catenation and changes in DNA topology by topoisomerase III. *J Biol Chem* 278:42668–42678
 100. Zechiedrich EL, Cozzarelli NR (1995) Roles of topoisomerase IV and DNA gyrase in DNA unlinking during replication in Escherichia coli. *Genes Dev* 9:2859–2869
 101. Lopez CR, Yang S, Deibler RW et al (2005) A role for topoisomerase III in a recombination pathway alternative to RuvABC. *Mol Microbiol* 58:80–101
 102. Fasching CL, Cejka P, Kowalczykowski SC, Heyer W-D (2015) Top3-Rmi1 dissolve Rad51-mediated D loops by a topoisomerase-based mechanism. *Mol Cell* 57:595–606
 103. Chen SH, Plank JL, Willcox S et al (2014) Top3 α is required during the convergent migration step of double Holliday junction dissolution. *PLoS One* 9:e83582
 104. Bizard AH, Hickson ID (2014) The dissolution of double Holliday junctions. *Cold Spring Harb Perspect Biol* 6:a016477–a016477
 105. Bell SD, Jaxel C, Nadal M et al (1998) Temperature, template topology, and factor requirements of archaeal transcription. *Proc Natl Acad Sci U S A* 95:15218–15222
 106. Atomi H, Matsumi R, Imanaka T (2004) Reverse gyrase is not a prerequisite for hyperthermophilic life. *J Bacteriol* 186:4829–4833
 107. Zhang C, Tian B, Li S et al (2013) Genetic manipulation in Sulfolobus islandicus and functional analysis of DNA repair genes. *Biochem Soc Trans* 41:405–410
 108. Hsieh T-S, Capp C (2005) Nucleotide- and stoichiometry-dependent DNA supercoiling by reverse gyrase. *J Biol Chem* 280:20467–20475
 109. Bizard A, Garnier F, Nadal M (2011) TopR2, the second reverse gyrase of Sulfolobus solfataricus, exhibits unusual properties. *J Mol Biol* 408:839–849

110. Garnier F, Nadal M (2008) Transcriptional analysis of the two reverse gyrase encoding genes of *Sulfolobus solfataricus* P2 in relation to the growth phases and temperature conditions. *Extremophiles* 12:799–809
111. Couturier M, Bizard AH, Garnier F, Nadal M (2014) Insight into the cellular involvement of the two reverse gyrases from the hyperthermophilic archaeon *Sulfolobus solfataricus*. *BMC Mol Biol* 15:18
112. Quaiser A, Constantinesco F, White MF et al (2008) The Mre11 protein interacts with both Rad50 and the HerA bipolar helicase and is recruited to DNA following gamma irradiation in the archaeon *Sulfolobus acidocaldarius*. *BMC Mol Biol* 9:25
113. Rolfsemeier ML, Laughery MF, Haseltine CA (2011) Repair of DNA double-strand breaks induced by ionizing radiation damage correlates with upregulation of homologous recombination genes in *Sulfolobus solfataricus*. *J Mol Biol* 414:485–498
114. Larmony S, Garnier F, Hoste A, Nadal M (2015) A specific proteomic response of *Sulfolobus solfataricus* P2 to gamma radiations. *Biochimie* 118:270–277
115. Li Z, Hiasa H, DiGate R (2004) *Bacillus cereus* DNA topoisomerase I and III α : purification, characterization and complementation of *Escherichia coli* TopoIII activity. *Nucleic Acids Res* 33:5415–5425
116. Vanga BR, Butler RC, Toth IK et al (2012) Inactivation of PbTopo III β causes hyperexcision of the Pathogenicity Island HAI2 resulting in reduced virulence of *Pectobacterium atrosepticum*. *Mol Microbiol* 84:648–663
117. Dai P, Wang Y, Ye R et al (2003) DNA topoisomerase III from the hyperthermophilic archaeon *Sulfolobus solfataricus* with specific DNA cleavage activity. *J Bacteriol* 185:5500–5507
118. Forterre P, Gabelle D (2009) Phylogenomics of DNA topoisomerases: their origin and putative roles in the emergence of modern organisms. *Nucleic Acids Res* 37:679–692
119. Ahmed W, Menon S, Karthik PVDNB, Nagaraja V (2015) Autoregulation of topoisomerase I expression by supercoiling sensitive transcription. *Nucleic Acids Res* 0:10881–11088
120. Forterre P (2015) The universal tree of life: an update. *Front Microbiol* 6:717
121. Chen SH, Plank JL, Willcox S et al (2013) Improved methods for creating migratable Holliday junction substrates. *Nucleic Acids Res* 41:e60
122. Dekker NH, Viard T, Bouthier de la Tour C et al (2003) Thermophilic topoisomerase I on a single DNA molecule. *J Mol Biol* 329:271–282
123. Szafran MJ, Strick T, Strzałka A et al (2014) A highly processive topoisomerase I: studies at the single-molecule level. *Nucleic Acids Res* 42:7935–7946
124. Ogawa T, Yogo K, Furuike S et al (2015) Direct observation of DNA overwinding by reverse gyrase. *Proc Natl Acad Sci U S A* 112:7495–7500
125. Ogawa T, Sutoh K, Kikuchi A, Kinoshita K (2016) Torsional stress in DNA limits collaboration among reverse gyrase molecules. *FEBS J* 283:1372–1384
126. Terekhova K, Gunn KH, Marko JF, Mondragón A (2012) Bacterial topoisomerase I and topoisomerase III relax supercoiled DNA via distinct pathways. *Nucleic Acids Res* 40:10432–10440
127. Terekhova K, Marko JF, Mondragón A (2014) Single-molecule analysis uncovers the difference between the kinetics of DNA decatenation by bacterial topoisomerases I and III. *Nucleic Acids Res* 42:11657–11667
128. Rajan R, Osterman A, Mondragón A (2016) *Methanopyrus kandleri* topoisomerase V contains three distinct AP lyase active sites in addition to the topoisomerase active site. *Nucleic Acids Res* 44:3464–3474
129. Blower TR, Williamson BH, Kerns RJ, Berger JM (2016) Crystal structure and stability of gyrase-fluoroquinolone cleaved complexes from *Mycobacterium tuberculosis*. *Proc Natl Acad Sci U S A* 113:1706–1713
130. Corbett KD, Benedetti P, Berger JM (2007) Holoenzyme assembly and ATP-mediated conformational dynamics of topoisomerase VI. *Nat Struct Mol Biol* 14:611–619

Topoisomerase I and Genome Stability: The Good and the Bad

Jang-Eun Cho and Sue Jinks-Robertson

Abstract

Topoisomerase I (Top1) resolves torsional stress that accumulates during transcription, replication and chromatin remodeling by introducing a transient single-strand break in DNA. The cleavage activity of Top1 has opposing roles, either promoting or destabilizing genome integrity depending on the context. Resolution of transcription-associated negative supercoils, for example, prevents pairing of the nascent RNA with the DNA template (R-loops) as well as DNA secondary structure formation. Reduced Top1 levels thus enhance CAG repeat contraction, somatic hypermutation, and class switch recombination. Actively transcribed ribosomal DNA is also destabilized in the absence of Top1, reflecting the importance of Top1 in ensuring efficient transcription. In terms of promoting genome instability, an aborted Top1 catalytic cycle stimulates deletions at short tandem repeats and the enzyme's transesterification activity supports illegitimate recombination. Finally, Top1 incision at ribonucleotides embedded in DNA generates deletions in tandem repeats, and induces gross chromosomal rearrangements and mitotic recombination.

Key words Top1, Ribonucleotides, R-loops, Mutation

1 Introduction

Topoisomerases resolve torsional stress that accumulates as a result of the DNA strand separation required for template access during replication and transcription, as well as intertwines between DNA molecules that arise during replication and recombination [1–3]. Strand separation overwinds DNA ahead of the corresponding machinery, resulting in the accumulation of positive supercoils that can block transcription elongation or an advancing replication fork. During transcription, DNA behind the RNA polymerase (RNAP) also becomes underwound, has increased single-stranded character, and forms negative supercoils. There are thus “twin domains” of positive and negative supercoiling during transcription [4, 5]. Topoisomerases catalyze supercoil removal through cleavage–ligation reactions that involve a covalent DNA–protein intermediate. Type I enzymes transiently nick one strand of

DNA to provide a gate for passage of the other strand, while Type II enzymes break both DNA strands to allow passage of duplex DNA. Type I topoisomerases are further divided depending on the nature of the covalent linkage to the nicked DNA molecule. Type IA enzymes form a link to a 5'-phosphate while Type IB enzymes link to a 3'-phosphate. The absence of sufficient topoisomerase activity interferes with DNA metabolic processes and is generally associated with genetic instability. Topoisomerase-mediated DNA cleavage, however, can initiate instability as well as promote genome integrity. Here, we focus on the effects of Topoisomerase I (Top1) on genome integrity, with an emphasis on studies in the budding yeast (*Saccharomyces cerevisiae*) model system.

1.1 Basics of Top1 Enzymology

Top1 is a Type IB enzyme that relaxes both positive and negative supercoils and its catalytic cycle is as follows. First, the single-subunit enzyme interacts noncovalently with duplex DNA and uses an active site tyrosine to attack one DNA strand. Although both mammalian and yeast Top1 have a weak consensus site for cleavage [5'-(G/C)(A/T)T-3'; [6, 7]] some enzymes such as vaccinia Top1 exhibit a strong cleavage site preference [5'-(T/C)CCTT-3'; [8]]. Enzyme attack results in formation of a covalent phosphotyrosyl bond with the 3'-end of nick, leaving a free 5'-hydroxyl (5'-OH) on the other side of the nick. The Top1-DNA adduct structure is called the Top1 cleavage complex (Top1cc). Controlled rotation of DNA downstream of the Top1cc relieves torsional stress, with multiple supercoils being removed during a single cleavage–ligation cycle. Nucleophilic attack of the 3'-phosphotyrosyl bond of the Top1cc by the 5'-OH then releases Top1 from DNA and restores the phosphodiester backbone. The 3'-phosphotyrosyl bond and 5'-OH must be properly aligned within the enzyme for efficient ligation to occur, and this requirement can lead to stabilization/trapping of the Top1cc. Trapping occurs *in vitro*, for example, when Top1 incises near DNA mismatches, loops, or oxidative damage, all of which distort positioning of the 5'-OH [9, 10]. In yeast, analyses of plasmid relaxation and transcription at the ribosomal DNA (rDNA) locus indicate that Top1 primarily removes negative supercoils, while the sole Type II enzyme (Top2) preferentially removes positive supercoils [11–14].

1.2 Approaches for Studying Top1 Effects on Genome Stability

To elucidate the roles of Top1 in promoting genome stability, multiple approaches have been taken to abolish or inhibit Top1 activity. In budding or fission yeast where Top1 is dispensable, the *TOP1* gene can simply be deleted. In higher eukaryotes where Top1 is essential, its levels can be depleted using RNA interference (RNAi). In addition, the chemotherapeutic drug camptothecin (CPT) and its derivatives are frequently used to inhibit Top1 activity. Top1 is the only cellular target of CPT, and CPT inhibits enzyme activity by aborting the catalytic cycle rather than

preventing interaction with DNA. CPT is a planar molecule that intercalates between the 3-phosphotyrosyl bond and the 5'-OH, reversibly blocking the religation step and trapping the enzyme in the context of a single-strand nick [15]. Interestingly, CPT extends the target site specificity of the enzyme *in vitro* to include a G preference 3' of the cleavage site [6]. In addition to the direct effects of trapped Top1cc, the resulting enzyme sequestration might limit activity elsewhere in the genome. In addition, CPT induces proteasome-dependent degradation of the Top1 protein in mammalian cells, which may ultimately decrease the amount of available Top1 [reviewed in [16]]. In budding yeast, a mutant form of Top1, Top1-T722A, has been used to mimic CPT treatment [17]. Although the Top1-T722A protein has DNA binding and cleavage activity comparable to the wild-type enzyme, its reduced religation activity is expected to elevate Top1cc levels. If genetic instability increases or decreases upon Top1 depletion/inhibition, then a role for Top1 in maintaining genome integrity or promoting instability, respectively, can be inferred. Interestingly, accumulation of Top1cc in budding yeast through CPT treatment or Top1-T722A expression has global effects on genome stability, but the absence of Top1 does not [18]. Results suggest that overexpression of Top1 also drives genetic instability in some yeast assays [19], and this may be relevant to potential consequences of Top1 overexpression in tumor cells [20–22].

1.3 CPT-Induced Damage and Repair of Top1cc

In the case of a CPT-trapped Top1, the most well-studied outcome is double-strand break (DSB) formation, which is the cause of lethality in dividing cells. DSB formation occurs primarily in the context of DNA replication and is generally assumed to reflect replication-fork runoff at the Top1cc-associated nick. There is also evidence, however, that failure to remove positive supercoils ahead of an advancing fork can cause fork reversal [23, 24]. Cleavage of the resulting chicken-foot structure may also contribute to replication-associated DSB formation.

Regardless of whether Top1 is covalently trapped in the context of a nick or a DSB, the enzyme must be removed before repair can ensue. The major player in Top1 removal is tyrosyl DNA phosphodiesterase or Tdp1 [25]. Following proteolysis of Top1, the remaining peptide is removed by Tdp1 cleavage of the phosphotyrosyl bond, leaving a 3'-phosphate end [26]. Alternatively, Top1 can be removed by the Wss1 metalloprotease [27, 28]. In yeast, the 3'-phosphate left by Tdp1 is removed by Tpp1 to generate a 3'-OH that can be extended by DNA polymerase or ligated to a 5'-phosphate [29]. The nucleases that process abasic sites (Apn1 and Apn2) as well as the Rad1-Rad10 structure-specific endonuclease provide alternative activities for creating a 3'-OH [30]. In mammals, there is a bifunctional enzyme (PNKP) that has one domain with homology to Tpp1 and a second domain with kinase

activity. PNKP functions in the repair of single-strand breaks, where its role is to convert “dirty” DNA ends to clean 3'-OH and 5'-phosphate ends [31]. Additional proteins have also been implicated in processing the Top1cc [10, 32].

1.4 Top1 Activity During Transcription

Actively transcribed genes are expected to accumulate more torsional stress than other genomic regions and thus to require more Top1 activity. Top1 association with expressed genes and its interaction with RNAP are well documented. Top1 is frequently found at promoter regions, enhancers and transcription start sites of genes actively transcribed by RNAPII [33–36]. It colocalizes with RNAPII in vivo [37], and its association with RNAPII is positively correlated with gene expression level [38]. Physical interaction between the phosphorylated C-terminal domain (CTD) of elongating RNAPII and Top1 has been reported in multiple organisms [39, 40], suggesting that Top1 removes supercoils while traveling with RNAPII. Finally, the use of biotin-trimethylpsoralen, which preferentially intercalates into underwound DNA, has provided direct evidence that negative supercoils accumulate at RNAPII-transcribed genes in the absence of Top1 [41].

A role for Top1 in ensuring the transcription of long genes is evident in neuronal tissues, where there is a positive correlation between the gene length and the expression level [42]. The particular importance of Top1 in the expression of long genes was discovered in a screen for small molecules that inhibit expression of autism-related genes. Topotecan, a CPT derivative, reduced expression of extremely long genes (generally >100 kb) in mouse and human neurons in a dose-dependent manner, as did knock-down of Top1 [43]. A *TOP1* conditional knockout mouse also was used to delete the enzyme in cultured neuron cells, and this similarly resulted in reduced expression of long genes [44]. Though only a subset of long genes affected by topotecan was also affected by Top1 knockout, the genes affected by both are exceptionally long. CPT treatment downregulates long, highly expressed genes in non-neuron cells as well, indicating that the role of Top1 in ensuring transcription of long genes is a general phenomenon [45].

2 Top1 as a Promoter of Genome Integrity

2.1 Top1 Limits R-Loop Formation

The underwinding of DNA associated with the negative supercoils that accumulate behind RNAP, especially in the absence of Top1, gives single-stranded character to both the nontranscribed strand (NTS) and the transcribed-strand (TS) DNA strands. This provides an opportunity for a nascent RNA to rehybridize with the TS as it exits RNAP, forming a stable R-loop structure composed of an RNA–DNA hybrid and the single-stranded NTS. The S9.6 antibody specifically binds to RNA–DNA hybrids and has been an

important experimental tool for detecting R-loops *in vivo*. R-loops are present in wild-type yeast strains and are enriched at highly expression regions and at long polyA tracts [46–48]. In mammalian cells, Top1 activates arginine-serine-rich (SR proteins) splicing factors via phosphorylation to promote mRNP assembly [49–52]. This limits R-loop formation by sequestering the nascent RNA and physically interfering with hybridization to the TS. Although yeast Top1 lacks a similar kinase domain, abolishment of THO/TREX complex similarly results in R-loop accumulation [53]. THO/TREX is important for mRNA export, indicating that mRNP assembly is a conserved mechanism for preventing R-loop formation [54, 55]. In prokaryotes, co-transcriptional translation [56] and the interaction of transcription termination factors such as Rho with translation-uncoupled transcripts [57] serve a similar purpose.

R-loop accumulation can impede transcription elongation [53, 58] and block replication fork progression [59–61]. Whereas reduced Top1 activity promotes R-loop formation, R-loop accumulation is counteracted by RNase H enzymes (RNase H1 and H2), which degrade the RNA component of RNA–DNA hybrids [62] or by RNA–DNA helicases that unwind R-loops [63, 64]. The standard approach to reduce R-loop levels *in vivo*, and thereby directly implicate them in genetic instability, is through overexpression of the monomeric RNase H1 protein [e.g., [53, 65]]. Elimination of all RNase H activity (loss of RNase H1 and RNase H2) elevates R-loop levels in yeast and in this genetic background, Top1 is essential [14, 58]. This lethality underscores the interplay between Top1 and RNase H activity in regulating R-loop accumulation and maintaining genetic integrity. The genome destabilizing consequences of persistent R-loops have been extensively reviewed [66–69], and we focus here on Top1-related effects.

In human cells, Top1 deficiency or loss of kinase activity causes replication defects, and chromosome breaks can be detected at highly transcribed genes during S phase [70]. Slow replication-fork progression and DSB formation are suppressed by RNase H1 overexpression, demonstrating that R-loops are responsible for the observed phenotypes. In addition to effects associated with Top1 loss, Top1 inhibition by CPT treatment also slows replication fork progression [24, 71]. Inhibition of transcription suppresses CPT-induced fork stalling and RNA-processing factors are enriched at stalled replication forks, suggesting R-loop accumulation in this system as well [71]. Consistent with this observation, a genome-wide survey of R-loop accumulation immediately after CPT exposure revealed that R-loops transiently increase in the nucleolus where rDNA is actively transcribed [34, 36]. Longer exposure to CPT, however, resulted in a disappearance of R-loops [36].

2.2 *Top1 Promotes rDNA Stability*

Loss of yeast Top1 is associated with hyperrecombination at the rDNA locus on chromosome XII, which is composed of ~120 tandem repeats, but not at the *CUPI* tandem-repeat locus [72–74]. In a *top1Δ* background, loss of a selectable marker within the rDNA array is greatly elevated and chromosome XII runs as a smear following pulsed-field gel electrophoresis. Top2 is an essential Type II topoisomerase that is required for decatenation of sister chromatids after DNA replication [3] and this enzyme is also important for rDNA stability [72]. Upon loss of both Top1 and Top2 activity, rDNA repeats are excised as circular mini-chromosomes [75]. rDNA excision is suppressed by expression of the *Escherichia coli topA* gene, which specifically resolves negative supercoils, indicating that negative supercoiling is the major cause of the rDNA hyperrecombination [75]. Finally, CPT treatment or Top1-T722A expression enhances mitotic crossing over within the rDNA locus as well as at *CUPI* tandem repeats [18].

2.3 *Top1 and Stability of G4 DNA*

R-loop formation exposes the NTS as single-strand DNA (ssDNA), providing an opportunity for it to fold into secondary structures. The guanines in G-rich DNA, for example, interact via Hoogsteen base pairing to form planar G quadruplexes, which then can stack to form a highly stable structure known as G4 DNA. G4 DNA on the NTS blocks RNAPII elongation in vitro [76]; in vivo, it interferes with replication progression and initiates genetic instability [77–79]. Yeast Top1 is important for suppressing the instability associated with sequences that can form G4 DNA [80–82]. Using a recombination assay that detects gene conversion within a highly transcribed reporter, it was demonstrated that the conversion frequency is higher when the G-rich, G4-forming sequence is on the NTS than when it is on the TS [80]. Loss of Top1 or RNase H activity (*top1Δ* or *rnh1Δ rnh201Δ* mutant, respectively) further enhanced the recombination, suggesting that unresolved negative supercoils and/or persistent R-loops contribute to the instability. Using a different system that detects genome rearrangements, highly transcribed G-rich sequences on the NTS were a hotspot for loss of heterozygosity, gross chromosomal rearrangements, internal deletions, terminal deletions and segmental duplications in the absence of Top1 [81]. Gross chromosomal rearrangements and loss of heterozygosity were specifically elevated when the reporter gene was in a head-on orientation with respect to an advancing replication fork, suggesting that Top1 also suppresses instability by preventing or resolving conflicts between replication and transcription.

Although R-loops are a consequence of either Top1 or RNase H loss, data suggest that the underlying mechanisms for G4-associated instability are different. First, RNase H1 overexpression suppresses the hyperrecombination phenotype in *rnh1Δ rnh201Δ* background, but has no effect in *top1Δ* background

[81]. Second, recombination in the *rnh1Δ rnh201Δ* background is not affected by the direction of replication, while that in a *top1Δ* background is enhanced when transcription and replication are in the head-on orientation [81]. Third, loss of Top1 specifically increases recombination when the NTS contains the G-rich sequence, while loss of RNase H activity enhances recombination even in the absence of a potential G4-forming sequence [80]. Finally, the catalytic activity of Top1 is required to suppress G4-associated recombination, but expression of the *E. coli topA* gene, which removes negative supercoils, only partially rescues Top1 loss [82]. Collectively, these results suggest that the increased recombination in an *rnh1Δ rnh201Δ* double mutant primarily reflects R-loops, while that in a *top1Δ* is also G4-specific. Top1 presumably limits the formation of G4 DNA on the NTS by removing negative supercoils, but also may actively promote G4 removal once it is formed. With regard to the latter role, Top1 binds to G4 DNA [83–85].

2.4 Top1 and Antibody Diversification

Top1 has been implicated in the two antibody diversification processes that occur in the vertebrate immune system: somatic hypermutation (SHM) and class switch recombination (CSR). During these processes, Top1 both constrains and contributes to the instability. Following the joining of V, D and J segments into a functional variable segment during B-cell development, antigen stimulation triggers SHM and CSR. SHM rapidly introduces mutations into immunoglobulin variable regions to enhance antigen-antibody affinity, while CSR alters the heavy segment that is joined to a given variable segment, thereby changing the downstream consequences of antigen-antibody interaction [reviewed in [86–88]]. Both processes require transcription of immunoglobulin genes and the expression of activation-induced deaminase (AID). AID targets ssDNA exposed during transcription [89] and converts cytosine to uracil, resulting in C>T mutations if uracil removal does not occur. Error-prone repair of uracil introduces other mutation types during SHM, and uracil removal contributes to the DNA cleavage required to initiate CSR.

AID specifically targets ssDNA, leading to the expectation that active transcription and R-loop accumulation should enhance AID-induced instability. In agreement with this, extended R-loops are detected at the AID-targeted switch (S) regions where CSR occurs [90], and expression of human AID in a yeast THO mutant background enhances transcription-associated instability of S regions [80, 91]. Top1 can limit ssDNA exposure by removing negative supercoils and discouraging R-loop formation, and Top1 depletion using siRNA increases AID-mediated CSR and SHM [41, 92, 93]. Conversely, Top1 overexpression suppresses SHM [93]. In the case of SHM, however, variable regions do not normally form R-loops [94] and AID appears to access the ssDNA

within the RNAPII-associated transcription bubble [89]. Top1 depletion increases RNAPII pausing in the variable region, thereby enhancing AID-induced instability [95]. Interestingly, AID suppresses Top1 protein translation in cells undergoing SHM [93] or CSR [92], suggesting that Top1 reduction is important for maximizing AID-mediated instability.

S regions are GC-rich and the bases are distributed asymmetrically, with the G-rich strand corresponding to the NTS. This asymmetry is important for CSR, implicating G4 DNA as well as R-loops in the corresponding rearrangements. Surprisingly, CPT treatment in Top1-depleted cells decreases DSBs in S regions and reduces both CSR and SHM [92, 93]. It has been suggested that cleavage by Top1 is important for CSR, and the degradation of CPT-trapped Top1 might reduce the enzyme below a critical level. In terms of how Top1 activity might contribute to the DSBs that initiate CSR, the enzyme binds to G4 DNA [83] and is recruited to non-B DNA by the FACT complex [41]. Subsequent cleavage by Top1 would provide transient breaks on the G-rich strand, and breaks on the complementary C-rich strand could be generated as intermediates in the repair of uracils created by AID. Frequent breaks on both strands of the S region would then produce the DSBs required for CSR. The apparent requirement of Top1 in SHM is more difficult to explain.

2.5 Top1 and CAG Repeat Stability

Human diseases such as Huntington disease and several spinocerebellar ataxias are associated with expansion of CAG trinucleotide repeats [96–98]. To identify drugs that promote repeat contraction, a selective system was established in human cells and a chemical screen was performed [99]. Briefly, a (CAG)₉₅ repeat was placed within the intron of a *HPRT* minigene under control of an inducible promoter. The presence of (CAG)₉₅ interferes with intron splicing and cells are HPRT-deficient, while repeat contraction to (CAG)₃₈ or less allows proper splicing and cells become HPRT-proficient. Restoration of HPRT activity can be selected in HAT medium, and active transcription of the reporter is required for repeat contraction. Importantly, chemicals that inhibit Top1-mediated ligation were identified in the screen, suggesting that a stabilized Top1cc triggers contraction. In support of this, reduction of TDP1, which is involved in Top1cc removal, also enhances repeat contraction, as does depletion of additional components (XRCC1 and PARP1) of the single-strand break repair complex [100]. The elevated contraction associated with reduced TDP1 was suppressed, however, by simultaneous knockdown of the transcription-coupled nucleotide-excision repair (TC-NER) pathway. Based on these observations, it was proposed that the accumulation of trapped Top1 in TDP1-depleted cells triggers TC-NER, with engagement of the TC-NER pathway leading to repeat contraction. Interestingly, TOP1 depletion alone also increased repeat

contraction, indicating that TOP1 suppresses repeat contraction under normal conditions. The enhanced contraction upon TOP1 depletion could reflect instability associated with R-loops, leading to the prediction that contraction should be repressed by over-expression of RNase H1.

3 Top1 Initiation of Genetic Instability

3.1 Deletions at Short Tandem Repeats

Two independent groups reported that Top1 is required for a specific mutation signature associated with high levels of transcription in budding yeast [101, 102]. This signature is composed of 2–5 bp deletions that occur at hotspots coincident with a low copy-number tandem repeat, with the size of the deletion matching that of the repeat unit. The catalytic activity of Top1 is essential for transcription-associated deletions, suggesting that DNA cleavage by Top1 triggers the deletion process. Given the known genome-destabilizing effects of the Top1cc, it was proposed that deletions reflect the processing of the “dirty” DNA ends formed when the enzyme is trapped within a tandem repeat (*see* Fig. 1). The removal of the Top1cc (and possibly the 5'-OH) would then generate a single-strand gap within the tandem repeat, allowing repeat-mediated realignment of the DNA strands to convert the gap to a readily ligated nick. The religated strand containing the deletion intermediate would then give rise to a permanent mutation following replication. While there is evidence that a Top1cc can indeed initiate deletion formation (*see* below), most Top1-dependent mutations reflect incision at a ribonucleotide embedded in duplex DNA. Thus far, Top1-dependent short deletions have only been documented in budding yeast.

Ribonucleotides are frequently incorporated into the yeast genome during DNA replication [103], and there are mutant forms of the replicative DNA polymerases (Pol α , Pol δ and Pol ϵ) that insert more ribonucleotides than do the wild-type enzymes [104–106]. Ribonucleotides are typically of no genetic consequence because of their efficient removal via the “ribonucleotide excision repair” pathway, which is initiated when RNase H2 incises on the 5' side of a ribonucleotide [107]. In addition to cleavage of the RNA component of long RNA–DNA hybrids, RNase H2 incises when there are only one or a few ribonucleotides embedded in DNA; this property is unique and is not shared by RNase H1 [62]. The connection between ribonucleotides and Top1-dependent deletions was made using yeast strains devoid of RNase H2 activity (typically *rnh201Δ* strains) to examine the genetic consequences of ribonucleotide persistence. In forward mutation assays, a 2–5 bp deletion signature identical to that associated with high levels of transcription was observed [108–111]. It was subsequently demonstrated that deletions in an *rnh201Δ*

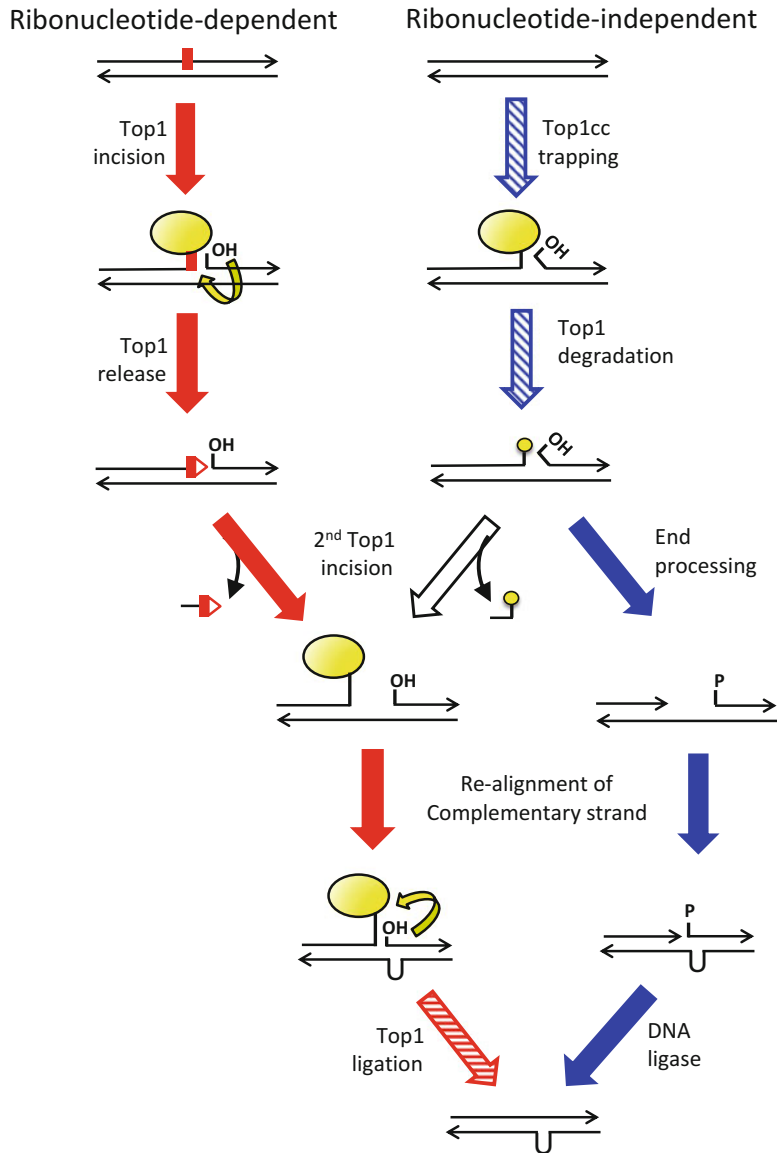


Fig. 1 Top1-dependent deletions at tandem repeats. *Black lines* indicate DNA and arrowheads designate 3'-OH ends. When a ribonucleotide (*red rectangle*) is incorporated at a Top1 incision site, deletion occurs via sequential Top1 cleavage (left side; *red or red-hatched arrows*). Top1 (*yellow ova*) cleavage at a ribonucleotide generates a 5'-OH and a covalent linkage of the enzyme to a 3'-phosphate. Nucleophilic attack of the phosphotyrosyl bond by the 2'-OH of ribose releases Top1, creating a nick flanked by a 2'3'-cyclic phosphate (*red triangle*) and a 5'-OH. A second Top1 incision 5' of the cyclic phosphate generates an oligonucleotide, the release of which traps the Top1cc. Spontaneous realignment of complementary strands brings the 5'-OH and Top1cc into close proximity to facilitate Top1-mediated ligation. The ribonucleotide-independent pathway is shown on the right and two possible mechanisms for deletion formation are illustrated. As shown, the Top1cc is stabilized by displacement of the 5'-OH, although other types of stabilization are possible. Top1 is degraded to a peptide (*yellow circle*) by the proteasome, and further end processing (*blue arrows*) generates a gap flanked by a 5'-phosphate (P) and 3'-OH. Realignment of complementary strands converts the gap to a nick that is sealed by DNA ligase. Alternatively, Top1 degradation can be followed by a second cleavage event (*white arrow*), that generates an intermediate identical to that in the ribonucleotide-dependent pathway. Realignment between complementary strands and Top1-mediated ligation generates the deletion intermediate

background are completely Top1-dependent [106, 108, 112]. Importantly, the mutation reporters in these early experiments were transcribed from their native promoters, demonstrating that very high-levels of transcription are not a prerequisite for the accumulation of Top1-dependent deletions.

3.1.1 Mechanism of Ribonucleotide-Dependent Deletions

Biochemical experiments done 20 years ago with vaccinia virus Top1 (vcTop1) demonstrated that the enzyme incises efficiently at a ribonucleotide embedded in DNA. As with a DNA-only substrate, vcTop1 cleavage on the 3' side of the ribonucleotide creates a 3'-phosphotyrosyl bond with the ribose. The 2'-OH of the ribose then attacks the 3'-phosphotyrosyl bond, releasing Top1 from DNA and leaving a nick flanked by a 2'3'-cyclic phosphate and a 5'-OH [113]. Based on these data and additional genetic evidence suggesting that the ligation activity of yeast Top1 promotes deletion formation, we proposed a sequential-cleavage model that requires two independent Top1 cleavage events [[114]; see Fig. 1]. Following the initial incision at and release from a ribonucleotide, it was proposed that a second Top1 incision occurs at a deoxyribonucleotide located a short distance upstream (5') of the 2'3'-cyclic phosphate. Whether the same or a different enzyme performs the second cleavage is not known. Sequential Top1 cleavage generates a short oligonucleotide held in place mainly by hydrogen bonding with the complementary strand. Spontaneous loss of this fragment by diffusion traps Top1, creating a short gap flanked by a Top1cc (second Top1 incision) and the 5'-OH created by the first Top1 incision. We proposed that the presence of a tandem repeat allows realignment with the complementary strand, closely juxtaposing the Top1cc and 5'-OH and facilitating efficient Top1-mediated ligation. This model has been confirmed in vitro using purified yeast or human Top1 [115–117].

3.1.2 Features of Ribonucleotide-Dependent Deletions

Studies of Top1-dependent mutagenesis in vivo have been greatly facilitated through the use of *lys2*-based deletion reporters that contain single tandem-repeat hotspots and that are positioned near a well-defined origin of replication. Fusing these reporters to a highly inducible, doxycycline-regulated promoter (*pTET*) allows the specific effects of transcription on hotspot activity to be monitored. In addition, inversion of a hotspot fragment allows the effect of Top1 cleavage-site position on the TS versus the NTS to be examined. Finally, effects associated with the direction of DNA replication can be assessed by inverting only the hotspot-containing fragment, inverting the entire reporter, or through use of mutant DNA polymerases. With these reporters, ribonucleotide-dependent versus ribonucleotide-independent hotspots are operationally defined by whether they are affected by the loss of RNase H2; only one hotspot examined thus far [the (AT)₂ hotspot] appears to be ribonucleotide-independent. Deletions at both

types of hotspots increase 10–100 fold under high-transcription conditions [102, 114], confirming enhanced association of Top1 with transcriptionally active DNA.

Factors that affect the rates of ribonucleotide-dependent deletions have been primarily characterized using hotspot-containing constructs. Under low-transcription conditions, the Srs2 helicase in conjunction with the Exo1 5' > 3' exonuclease suppresses deletion formation, presumably through removal of the 5'-OH that is required for ligation. In addition, the ribonucleotides that lead to deletion formation are incorporated primarily by the Pol ϵ leading-strand DNAP, with little contribution from the Pol δ lagging-strand DNAP [106, 118]. With one particular hotspot, this asymmetry was used to infer that the relevant Top1 cleavage occurs on the (TG)₂-containing strand rather than the complementary (CA)₂-containing strand. Under high transcription conditions, however, ribonucleotides incorporated by Pol δ appear to initiate deletion formation at the (TG)₂ hotspot as efficiently as those incorporated by Pol ϵ [118]. In addition, the location of the (TG)₂ sequence on the TS versus NTS of the reporter becomes important under high-transcription conditions, with deletions only accumulating when the Top1 cleavage sites are on NTS. The reason for the striking NTS bias is not known, but could reflect interaction of the Top1cc intermediate with RNAPII [118, 119].

In addition to the *in vivo* analyses done with the (TG)₂ hotspot, parallel *in vivo* and *in vitro* analyses have been done with a ribonucleotide-dependent (CCCTT)₂ hotspot that accumulates 5-bp deletions [117]. In this case, yeast Top1 cleaves at the terminal T of each repeat *in vitro*. The (CCCTT)₂ hotspot can be turned into a 4-bp deletion hotspot *in vivo* by deleting the first C of the second repeat, and into a 7-bp deletion hotspot by adding a 2-bp spacer between the cleavage sites. Using the same mutated sequences *in vitro*, the distance between the Top1 cleavage sites matches the deletion size observed *in vivo*. These data confirm a key feature of the sequential cleavage model: the distance between Top1 cleavage sites determines the deletion size. Although the intact (CCCTT)₂ hotspot cannot support the complete ribonucleotide-dependent deletion reaction *in vitro* when rUMP is substituted for the terminal dTMP of the second repeat, the reaction is robust when a third CCCTT repeat is added and rUMP is substituted for the terminal dTMP of the central repeat. It should be noted that Top1 clamps down on duplex DNA when cleavage occurs [120], leading to the hypothesis that is difficult for the Top1-linked end to realign/slide and base-pair with the complementary strand within the gap, as must occur if only two repeats are present. In the case of three repeats, the gap would be within the central repeat, allowing the 5'-OH end to slide toward the constrained Top1cc. In support of this interpretation, the (CCCTT)₃

hotspot produces more 5-bp deletions *in vivo* than does the (CCCTT)₂ hotspot. As with the (TG)₂ hotspot, the (CCCTT)₂ hotspot is functional only if the mapped Top1 cleavage sites are on the NTS of a highly transcribed reporter.

3.1.3 Ribonucleotide-Independent Deletions

In addition to the unligatable nick produced when Top1 cleaves at a ribonucleotide, intermediate stabilization/trapping during the Top1 catalytic cycle generates a nick flanked by a Top1cc and a 5'-OH. As noted previously, such stabilization occurs when Top1 cleaves near a mismatch or DNA damage, or when CPT intercalates at the cleavage site [10]. In addition, the encounter of RNAPII with a Top1cc on the TS displaces the 5'-OH required for ligation and traps the covalent intermediate [121]. In an early examination of transcription-dependent Top1 deletions, interaction of Top1 with the reporter gene was detected by chromatin immunoprecipitation (ChIP) without using formaldehyde as a crosslinking agent, suggesting accumulation of mutagenic, covalently linked Top1-DNA complexes [101]. More direct evidence for relevance of trapped Top1 to ribonucleotide-independent deletions was obtained by expressing the Top1-T722A protein, which has reduced religation activity. The prediction was that stabilization of the intermediate would increase those deletions due to a trapped Top1, and this was confirmed using the ribonucleotide-independent (AT)₂ hotspot [114]. As with the ribonucleotide-dependent hotspots examined to date, deletions at the (AT)₂ hotspot occur when it is inserted into the *pTET-lys2* reporter in one orientation, but not in the other (Cho JE. and Jinks-Robertson S., unpublished data). It is not currently known how Top1 is trapped or whether specific factors are required to process the Top1cc and 5'-OH so that eventual ligation occurs [102]. As noted previously, however, there are numerous activities implicated in removing peptides linked to the 3'-phosphate after proteolysis of Top1 [10].

It was previously noted that vcTop1 has a strong consensus site for cleavage: 5'-(T/C)CCTT-3'. Although the (CCCTT)₂ hotspot is ribonucleotide-dependent in the presence of yeast Top1, it is a ribonucleotide-independent hotspot when vcTop1 is expressed in a *top1Δ* background. Similar to yeast Top1 activity at the (AT)₂ hotspot, vcTop1 generates 5-bp deletions at the (CCCTT)₂ hotspot when the hotspot-containing fragment is in one orientation, but not in the other, within a highly transcribed reporter (Cho JE. and Jinks-Robertson S., unpublished data). In this case, however, the strand that is cleaved by vcTop1 is known, and cleavage of the NTS facilitates deletions. The common behavior of the ribonucleotide-dependent and -independent hotspots with regard to their function in only one orientation within the *pTET-lys2* reporter suggests that there may be an unanticipated similarity in the molecular mechanism of deletion formation. Instead of the involvement of a single

Top1 in ribonucleotide-independent deletions, it is possible that these events also occur via sequential Top1 cleavage. Without a ribonucleotide to catalyze the release of Top1 after the initial incision, however, the protein would have to be mostly or completely removed before cleavage by a second enzyme could occur (*see* Fig. 1).

If both ribonucleotide-dependent and -independent deletions occur via sequential Top1 cleavage, the key difference becomes whether the initial Top1 cleavage reaction occurs at a ribonucleotide or deoxyribonucleotide, respectively. This means a given hotspot would show ribonucleotide-dependent or -independent activity depending on the presence or absence of an appropriately positioned ribonucleotide, respectively. In vitro, the probability of inserting a ribonucleotide at a given position depends on base identity as well as sequence context [103]. In addition, replicative polymerases are not expected to incorporate a ribonucleotide at a given position during every round of DNA replication. Deletions observed in RNase H2-defective background may thus represent a mixture of ribonucleotide-dependent and -independent events. Finally, RNase H2 efficiency also could be affected by sequence context, allowing some ribonucleotide-dependent deletions to occur in a wild-type background. This possibility could be tested by examining hotspot activity in an otherwise wild-type strain that expresses a ribonucleotide-restrictive DNA polymerase, where only ribonucleotide-dependent events should be reduced. Only those additional deletions that appear upon RNase H2 loss can be definitively attributed to ribonucleotides.

3.2 Gross Chromosomal Rearrangements and Mitotic Recombination

In addition to their association with short tandem repeats in yeast, ribonucleotides embedded in genomic DNA also elevate gross chromosomal rearrangements (GCRs) and mitotic recombination in a Top1-dependent manner [110, 122–124]. In haploid yeast, the GCR rate is synergistically elevated when loss of RNase H2 (*rnh203Δ* background) is combined with the loss of a large number of genes, including *ESC2* or *SGS1* [124]. Both *Esc2* and *Sgs1* have been implicated in the processing of homologous recombination intermediates, but do so by independent mechanisms [125]. Interestingly, the elevated GCR rate in an *rnh203Δ ecs2Δ* background is suppressed by deletion of *TOP1*, but that in an *rnh203Δ sgs1Δ* background is not [124].

Loss of RNase H2 activity elevates mitotic recombination [110, 126] and the hyperrecombination phenotype is partially suppressed by Top1 loss [110, 123]. Given the similar Top1 dependence of ribonucleotide-initiated deletions and recombination, the initial assumption was that both reflect the persistence of single ribonucleotides incorporated during DNA replication. An *rnh201* separation-of-function allele (*rnh201-P45D-Y219A*) has been described that eliminates the processing of single ribonucleotides

by RNase H2 while maintaining the ability to process contiguous ribonucleotides [127]. This separation-of-function allele behaves like a null allele with respect to 2–5 bp deletions, confirming that these Top1-dependent events reflect incision at single ribonucleotides [127]. This allele does not behave as a null, however, with respect to the stimulation of recombination events [123]. This suggests that, in contrast to 2–5 bp deletions, recombination can be additionally stimulated by a more extensive RNA–DNA hybrid. Finally, overexpression or abolishment of RNase H1 does not affect the recombination rate in *rnh201Δ* background [123], suggesting that the recombinogenic RNA–DNA hybrid in a *rnh201-P45D-Y219A* mutant is not an R-loop but rather is a small number of consecutive ribonucleotides in the genome. It should be noted that *TOP1* deletion or *rnh201-P45D-Y219A* expression in *rnh201Δ* background reduced the recombination rate, but not to the wild-type level. Whether Top1-dependent recombination is associated only with single ribonucleotides or may also initiate at consecutive ribonucleotides in the genome, has not been directly tested.

Whole genome sequencing of a diploid yeast strain homozygous for *rnh201Δ* and the *pol2-M644G* allele, which elevates ribonucleotide incorporation into DNA, detected an increase in loss of heterozygosity (LOH) [122]. LOH typically reflects reciprocal crossover events, but also can result from a nonreciprocal type of recombination known as break-induced replication [128]. Elevated LOH associated with RNase H2 loss was confirmed by measuring allelic recombination on a single chromosome arm. The further exacerbation of this phenotype in an *rnh201Δ pol2-M644G* background indicates that ribonucleotides can initiate LOH. Importantly, the ribonucleotide-induced LOH in the double mutant was suppressed by loss of Top1. In a different assay, nonallelic recombination was also elevated in an *rnh201Δ pol3-L612M* (rNTP-permissive version of Pol δ) as well as in the *rnh201Δ pol2-M644G* background, and again, the hyperrecombination phenotype was suppressed by Top1 loss [122]. It should be noted, however, that use of a different LOH assay has implicated R-loops rather than genomic ribonucleotides as the primary cause of increased LOH in an *rnh201Δ* single mutant with wild-type DNAP [129]. In particular, the hyperrecombination phenotype was not suppressed by the *pol2-M644 L* allele, which encodes a mutant form of Pol ε that incorporates fewer ribonucleotides into the genome than wild-type Pol ε. It is possible, however, that ribonucleotides incorporated by a DNAP other than Pol ε are the primary source of recombination-stimulating ribonucleotides. The effect of Top1 loss on these events was not tested.

When considered altogether, the data suggest that in the absence of RNase H2, recombination can be stimulated by single ribonucleotides in DNA, a small number of consecutive ribonucleotides in DNA, or persistent R-loops. Exactly which type of

RNA–DNA hybrid is relevant to Top1-dependent recombination in individual systems is unclear. In vitro, Top1 cleaves at a single ribonucleotide embedded in duplex DNA and at consecutive ribonucleotides in an DNARNA/DNA duplex [113], suggesting that Top1 incision at either may generate recombinogenic lesions. Neither an RNA/DNA duplex nor single-stranded DNA is proper substrate for Top1, suggesting that Top1 does not cleave R-loops [130, 131]. The folding of ssDNA into a secondary structure can, however, make it a target for Top1 cleavage in vitro [131]. Top1-initiated instability at R-loops, if there is any, seems more likely to reflect an aborted Top1 reaction at a deoxyribonucleotide rather than Top1 incision at a ribonucleotide.

3.3 *Illegitimate Recombination*

Illegitimate recombination refers to recombination that is not driven by sequence homology, and Top1 has been implicated in this process. Though the outcome is similar, illegitimate recombination is distinct from nonhomologous end joining, which depends on a different suite of proteins to accomplish a ligation reaction [132]. In vitro, attack of a Top1cc by a 5'-OH on the end of a different DNA molecule ligates the DNA strands [133, 134], and this is the basis of TOPO cloning. Given the ability of Top1 to join different DNA fragments in vitro, it is not surprising that there appears to be a similar role for Top1 during illegitimate recombination in vivo. One early indication of this was the excision of chromosomally integrated SV40 DNA from mouse chromosomes to produce circular excision products [135]. Although the excision products were a mixed population, degenerate Top1 cleavage sites were noted at the crossover junctions. When tested in vitro, Top1 indeed cleaved at these positions. A general model for such excision events involves Top1 cleavage opposite a nick to form a DSB. Two such Top1-induced DSBs would give rise to a linear, double-stranded molecule that has a Top1cc on one end and a 5'-OH on the other end. Top1cc-mediated ligation using the 5'-OH on the same molecule then produces a circular excision product. In addition to catalyzing excision, Top1 activity could join two DSBs on a same chromosome to generate a deletion or inversion, or two DSBs on different chromosomes to generate a translocation. Interestingly, the human Top1 recognition site is overrepresented at breakpoint junctions of germ-line rearrangements (deletions or duplications) involving genes associated with hereditary diseases [136].

Similar observations with respect to illegitimate recombination have been made in budding yeast using a transformation-based assay [137, 138]. In this system, a linear DNA fragment carrying a selectable marker and lacking homology to the yeast genome was transformed into cells. Selection for retention of the selectable marker identified transformants with the fragment stably integrated in a yeast chromosome by illegitimate recombination. Such DNA

insertions presumably resulted from a chromosomal DSB into which the foreign DNA fragment was ligated. As seen in the SV40 excision junctions mentioned above, degenerate Top1 cleavage sites were overrepresented at the insertion junctions [137]. In addition, the frequency of illegitimate recombination was significantly reduced in a *top1Δ* background, and overexpression of either yeast or human Top1 further enhanced insertion of the introduced DNA fragment [137, 138]. Overexpression of human, but not yeast, Top1 was associated with biased insertion into the yeast rDNA locus. Most significantly, illegitimate recombination in the transformation system required prior dephosphorylation of the introduced DNA fragment, indicating that the 5'-OH is essential for ligation into the chromosome. Finally, CPT treatment decreased the frequency of fragment insertion in a dose-dependent manner. Although CPT treatment enhances Top1 trapping, it also blocks Top1cc-mediated ligation and thereby suppresses the strand transferase activity of Top1 [139].

4 Conclusions

The roles of Top1 in maintaining genome integrity mainly reflect its resolution of negative supercoils, especially those that accumulate in the wake of the transcription machinery. Negatively supercoiled DNA has single-stranded character, which promotes R-loop formation and the folding of ssDNA into secondary structures such as hairpins and G4 DNA. It should be noted that R-loops and secondary structures on the nontranscribed DNA strand are mutually reinforcing, with R-loops exposing ssDNA that can assume alternative structures and secondary structures stabilizing R-loops. With regard to G4-associated instability, studies in yeast suggest that Top1 may have an additional role after G4 DNA forms [82]. Top1 preferentially binds to G4 DNA [85], and nicking of these structures could initiate their removal. The potential targeting of G4 and other secondary structures by Top1 needs further investigation. Although the genetic instability associated with R-loops and alternative DNA structures is generally considered in a negative light, such structures are physiologically important in some contexts, with class-switch recombination in the vertebrate immune system providing an example. Finally, Top1 is important for the transcription of very long genes, and this may be particularly relevant to proper expression in neuronal tissue.

Top1 resolves supercoils by introducing a transient single-strand break in DNA, and the covalent cleavage complex (Top1cc) is stabilized by CPT and its derivatives. The encounter of a replication fork with a Top1cc leads to the formation of potentially toxic DSBs, which are the basis of CPT use as a chemotherapeutic drug. What has not been fully investigated, however,

are the collateral effects of CPT in those cells that survive. Rampant DSBs are expected to lead to many types of genome rearrangements, including deletions, inversions, duplications and translocations. These, in principle, can reflect either homologous recombination or nonhomologous end joining. In the yeast model, CPT stimulates homologous recombination that results in LOH as well as copy number variation [18]. In addition to the genome instability associated with chemical stabilization of the covalent Top1cc, other DNA metabolic processes or helical distortions also stabilize the Top1cc by displacing the 5'-OH required for religation. This provides the opportunity for a different 5'-OH to serve as a nucleophile, which can generate illegitimate recombination events and genome rearrangements. Top1-associated illegitimate events deserve further study, as they provide yet another source of genome instability and genetic plasticity.

In the yeast system, Top1 is responsible for 2–5 bp deletions that occur in low copy-number tandem repeats. These were discovered in two distinct contexts: as a mutation signature in highly transcribed DNA and a signature associated with ribonucleotides embedded in genomic DNA. Although high transcription is not a prerequisite for these events, they are strongly stimulated by transcription. The sequential-cleavage mechanism of ribonucleotide-dependent deletions has been verified *in vitro* using purified Top1, but not all deletions are ribonucleotide-dependent. Whether the latter events are generated via sequential cleavage or arise through a different mechanism is not clear, and this is an important area for future study. An anomaly of Top1-dependent mutagenesis in highly transcribed DNA is a general requirement for the cleavage site(s) to be on the NTS, but the basis of this is not known.

Mutations in the human RNase H2 complex are associated with Aicardi-Goutières syndrome (AGS), a neuro-inflammatory, autoimmune disease [140]. Although recent work suggests that R-loop accumulation is the major culprit in AGS [141], an intriguing possibility is that the ribonucleotide-dependent mutagenesis described in the yeast system may also be relevant to disease pathogenesis. Interestingly, human Top1 that is associated with actively transcribed regions is SUMOylated at K391 and K436, and these sites are lacking in yeast Top1. SUMOylation is important for human Top1 interaction with the RNAPII elongation complex and for preventing R-loop formation *in vivo*, but reduces catalytic activity of the purified protein *in vitro*. These observations have led to the proposal that human Top1 may have evolved to avoid transcription-associated mutagenesis [142, 143]. Though this is an interesting possibility, the very high conservation in basic DNA metabolic processes suggests that the Top1-dependent genome instability documented in yeast will likely have broader impact. Clearly, there remains much to be learned about the opposing effects that Top1 activity can have on the eukaryotic genome, especially with regard to actively promoting instability.

References

1. Champoux JJ (2001) DNA topoisomerases: structure, function, and mechanism. *Annu Rev Biochem* 70:369–413. <https://doi.org/10.1146/annurev.biochem.70.1.369>
2. Wang JC (2002) Cellular roles of DNA topoisomerases: a molecular perspective. *Nat Rev Mol Cell Biol* 3(6):430–440. <https://doi.org/10.1038/nrm831>
3. Pommier Y, Sun Y, Huang SN et al (2016) Roles of eukaryotic topoisomerases in transcription, replication and genomic stability. *Nat Rev Mol Cell Biol* 17(11):703–721. <https://doi.org/10.1038/nrm.2016.111>
4. Liu LF, Wang JC (1987) Supercoiling of the DNA template during transcription. *Proc Natl Acad Sci U S A* 84(20):7024–7027
5. Wu HY, Shyy SH, Wang JC et al (1988) Transcription generates positively and negatively supercoiled domains in the template. *Cell* 53(3):433–440
6. Tanizawa A, Kohn KW, Pommier Y (1993) Induction of cleavage in topoisomerase I c-DNA by topoisomerase I enzymes from calf thymus and wheat germ in the presence and absence of camptothecin. *Nucleic Acids Res* 21(22):5157–5166
7. Been MD, Burgess RR, Champoux JJ (1984) Nucleotide sequence preference at rat liver and wheat germ type I DNA topoisomerase breakage sites in duplex SV40 DNA. *Nucleic Acids Res* 12(7):3097–3114
8. Shuman S, Prescott J (1990) Specific DNA cleavage and binding by vaccinia virus DNA topoisomerase I. *J Biol Chem* 265(29):17826–17836
9. Pourquier P, Ueng LM, Kohlhagen G et al (1997) Effects of uracil incorporation, DNA mismatches, and abasic sites on cleavage and religation activities of mammalian topoisomerase I. *J Biol Chem* 272(12):7792–7796
10. Pommier Y, Barcelo JM, Rao VA et al (2006) Repair of topoisomerase I-mediated DNA damage. *Prog Nucleic Acid Res Mol Biol* 81:179–229. [https://doi.org/10.1016/S0079-6603\(06\)81005-6](https://doi.org/10.1016/S0079-6603(06)81005-6)
11. Schultz MC, Brill SJ, Ju Q et al (1992) Topoisomerases and yeast rRNA transcription: negative supercoiling stimulates initiation and topoisomerase activity is required for elongation. *Genes Dev* 6(7):1332–1341
12. Fernandez X, Diaz-Ingelmo O, Martinez-Garcia B et al (2014) Chromatin regulates DNA torsional energy via topoisomerase II-mediated relaxation of positive supercoils. *EMBO J* 33(13):1492–1501. [10.15252/embj.201488091](https://doi.org/10.15252/embj.201488091)
13. Salceda J, Fernandez X, Roca J (2006) Topoisomerase II, not topoisomerase I, is the proficient relaxase of nucleosomal DNA. *EMBO J* 25(11):2575–2583. <https://doi.org/10.1038/sj.emboj.7601142>
14. French SL, Sikes ML, Hontz RD et al (2011) Distinguishing the roles of topoisomerases I and II in relief of transcription-induced torsional stress in yeast rRNA genes. *Mol Cell Biol* 31(3):482–494. <https://doi.org/10.1128/mcb.00589-10>
15. Staker BL, Hjerrild K, Feese MD et al (2002) The mechanism of topoisomerase I poisoning by a camptothecin analog. *Proc Natl Acad Sci U S A* 99(24):15387–15392. <https://doi.org/10.1073/pnas.242259599>
16. Tomicic MT, Kaina B (2013) Topoisomerase degradation, DSB repair, p53 and IAPs in cancer cell resistance to camptothecin-like topoisomerase I inhibitors. *Biochim Biophys Acta* 1835(1):11–27. <https://doi.org/10.1016/j.bbcan.2012.09.002>
17. Colley WC, van der Merwe M, Vance JR et al (2004) Substitution of conserved residues within the active site alters the cleavage religation equilibrium of DNA topoisomerase I. *J Biol Chem* 279(52):54069–54078. <https://doi.org/10.1074/jbc.M409764200>
18. Andersen SL, Sloan RS, Petes TD et al (2015) Genome-destabilizing effects associated with Top1 loss or accumulation of Top1 cleavage complexes in yeast. *PLoS Genet* 11(4):e1005098. <https://doi.org/10.1371/journal.pgen.1005098>
19. Sloan RS (2016) Topoisomerase I (Top1)-associated genome instability in yeast: effects of persistent cleavage complexes or increased Top1 levels. Dissertation, Duke University
20. Husain I, Mohler JL, Seigler HF et al (1994) Elevation of topoisomerase I messenger RNA, protein, and catalytic activity in human tumors: demonstration of tumor-type specificity and implications for cancer chemotherapy. *Cancer Res* 54(2):539–546
21. Pfister TD, Reinhold WC, Agama K et al (2009) Topoisomerase I levels in the NCI-60 cancer cell line panel determined by validated ELISA and microarray analysis and correlation with indenoisoquinoline sensitivity. *Mol Cancer Ther* 8(7):1878–1884. <https://doi.org/10.1158/1535-7163.mct-09-0016>

22. Shamanna RA, Lu H, Croteau DL et al (2016) Camptothecin targets WRN protein: mechanism and relevance in clinical breast cancer. *Oncotarget* 7(12):13269–13284. [10.18632/oncotarget.7906](https://doi.org/10.18632/oncotarget.7906)
23. Koster DA, Palle K, Bot ES et al (2007) Antitumour drugs impede DNA uncoiling by topoisomerase I. *Nature* 448(7150):213–217. <https://doi.org/10.1038/nature05938>
24. Ray Chaudhuri A, Hashimoto Y, Herrador R et al (2012) Topoisomerase I poisoning results in PARP-mediated replication fork reversal. *Nat Struct Mol Biol* 19(4):417–423. <https://doi.org/10.1038/nsmb.2258>
25. Yang SW, Burgin AB Jr, Huiizenga BN et al (1996) A eukaryotic enzyme that can disjoin dead-end covalent complexes between DNA and type I topoisomerases. *Proc Natl Acad Sci U S A* 93(21):11534–11539
26. Debethune L, Kohlhagen G, Grandas A et al (2002) Processing of nucleopeptides mimicking the topoisomerase I-DNA covalent complex by tyrosyl-DNA phosphodiesterase. *Nucleic Acids Res* 30(5):1198–1204
27. Stingele J, Schwarz MS, Bloemeke N et al (2014) A DNA-dependent protease involved in DNA-protein crosslink repair. *Cell* 158(2):327–338. <https://doi.org/10.1016/j.cell.2014.04.053>
28. Balakirev MY, Mullally JE, Favier A et al (2015) Wss1 metalloprotease partners with Cdc48/Doa1 in processing genotoxic SUMO conjugates. *elife* 4. <https://doi.org/10.7554/eLife.06763>
29. Vance JR, Wilson TE (2001) Uncoupling of 3'-phosphatase and 5'-kinase functions in budding yeast. Characterization of *Saccharomyces cerevisiae* DNA 3'-phosphatase (TPP1). *J Biol Chem* 276(18):15073–15081. <https://doi.org/10.1074/jbc.M011075200>
30. Vance JR, Wilson TE (2001) Repair of DNA strand breaks by the overlapping functions of lesion-specific and non-lesion-specific DNA 3' phosphatases. *Mol Cell Biol* 21(21):7191–7198. <https://doi.org/10.1128/mcb.21.21.7191-7198.2001>
31. Weinfeld M, Mani RS, Abdou I et al (2011) Tidying up loose ends: the role of polynucleotide kinase/phosphatase in DNA strand break repair. *Trends Biochem Sci* 36(5):262–271. <https://doi.org/10.1016/j.tibs.2011.01.006>
32. Xu Y, Her C (2015) Inhibition of topoisomerase (DNA) I (TOP1): DNA damage repair and anticancer therapy. *Biomol Ther* 5(3):1652–1670. <https://doi.org/10.3390/biom5031652>
33. Durand-Dubief M, Persson J, Norman U et al (2010) Topoisomerase I regulates open chromatin and controls gene expression *in vivo*. *EMBO J* 29(13):2126–2134. <https://doi.org/10.1038/emboj.2010.109>
34. Marinello J, Chillemi G, Bueno S et al (2013) Antisense transcripts enhanced by camptothecin at divergent CpG-island promoters associated with bursts of topoisomerase I-DNA cleavage complex and R-loop formation. *Nucleic Acids Res* 41(22):10110–10123. <https://doi.org/10.1093/nar/gkt778>
35. Puc J, Kozbial P, Li W et al (2015) Ligand-dependent enhancer activation regulated by topoisomerase-I activity. *Cell* 160(3):367–380. <https://doi.org/10.1016/j.cell.2014.12.023>
36. Marinello J, Bertoncini S, Aloisi I et al (2016) Dynamic effects of topoisomerase I inhibition on R-loops and short transcripts at active promoters. *PLoS One* 11(1):e0147053. <https://doi.org/10.1371/journal.pone.0147053>
37. Rosenberg M, Fan AX, Lin IJ et al (2013) Cell-cycle specific association of transcription factors and RNA polymerase II with the human beta-globin gene locus. *J Cell Biochem* 114(9):1997–2006. <https://doi.org/10.1002/jcb.24542>
38. Baranello L, Wojtowicz D, Cui K et al (2016) RNA polymerase II regulates topoisomerase I activity to favor efficient transcription. *Cell* 165(2):357–371. <https://doi.org/10.1016/j.cell.2016.02.036>
39. Phatnani HP, Greenleaf AL (2004) Identifying phosphoCTD-associating proteins. *Methods Mol Biol* 257:17–28. <https://doi.org/10.1385/1-59259-750-5:017>
40. Wu J, Phatnani HP, Hsieh TS et al (2010) The phosphoCTD-interacting domain of topoisomerase I. *Biochem Biophys Res Commun* 397(1):117–119. <https://doi.org/10.1016/j.bbrc.2010.05.081>
41. Husain A, Begum NA, Taniguchi T et al (2016) Chromatin remodeller SMARCA4 recruits topoisomerase I and suppresses transcription-associated genomic instability. *Nat Commun* 7:10549. <https://doi.org/10.1038/ncomms10549>
42. Zylka MJ, Simon JM, Philpot BD (2015) Gene length matters in neurons. *Neuron* 86(2):353–355. <https://doi.org/10.1016/j.neuron.2015.03.059>
43. King IE, Yandava CN, Mabb AM et al (2013) Topoisomerases facilitate transcription of long genes linked to autism. *Nature* 501

- (7465):58–62. <https://doi.org/10.1038/nature12504>
44. Mabb AM, Simon JM, King IF et al (2016) Topoisomerase I regulates gene expression in neurons through cleavage complex-dependent and -independent mechanisms. *PLoS One* 11(5):e0156439. <https://doi.org/10.1371/journal.pone.0156439>
 45. Solier S, Ryan MC, Martin SE et al (2013) Transcription poisoning by topoisomerase I is controlled by gene length, splice sites, and miR-142-3p. *Cancer Res* 73(15):4830–4839. <https://doi.org/10.1158/0008-5472.CAN-12-3504>
 46. Chan YA, Aristizabal MJ, Lu PY et al (2014) Genome-wide profiling of yeast DNA:RNA hybrid prone sites with DRIP-Chip. *PLoS Genet* 10(4):e1004288. <https://doi.org/10.1371/journal.pgen.1004288>
 47. Wahba L, Amon JD, Koshland D et al (2011) RNase H and multiple RNA biogenesis factors cooperate to prevent RNA:DNA hybrids from generating genome instability. *Mol Cell* 44(6):978–988. <https://doi.org/10.1016/j.molcel.2011.10.017>
 48. Wahba L, Costantino L, Tan FJ et al (2016) S1-DRIP-seq identifies high expression and polyA tracts as major contributors to R-loop formation. *Genes Dev* 30(11):1327–1338. <https://doi.org/10.1101/gad.280834.116>
 49. Rossi F, Labourier E, Forne T et al (1996) Specific phosphorylation of SR proteins by mammalian DNA topoisomerase I. *Nature* 381(6577):80–82. <https://doi.org/10.1038/381080a0>
 50. Labourier E, Rossi F, Gallouzi IE et al (1998) Interaction between the N-terminal domain of human DNA topoisomerase I and the arginine-serine domain of its substrate determines phosphorylation of SF2/ASF splicing factor. *Nucleic Acids Res* 26(12):2955–2962
 51. Soret J, Gabut M, Dupon C et al (2003) Altered serine/arginine-rich protein phosphorylation and exonic enhancer-dependent splicing in mammalian cells lacking topoisomerase I. *Cancer Res* 63(23):8203–8211
 52. Malanga M, Czubyat A, Girstun A et al (2008) Poly(ADP-ribose) binds to the splicing factor ASF/SF2 and regulates its phosphorylation by DNA topoisomerase I. *J Biol Chem* 283(29):19991–19998. <https://doi.org/10.1074/jbc.M709495200>
 53. Huertas P, Aguilera A (2003) Cotranscriptionally formed DNA:RNA hybrids mediate transcription elongation impairment and transcription-associated recombination. *Mol Cell* 12(3):711–721
 54. Strasser K, Masuda S, Mason P et al (2002) TREX is a conserved complex coupling transcription with messenger RNA export. *Nature* 417(6886):304–308. <https://doi.org/10.1038/nature746>
 55. Luna R, Rondon AG, Aguilera A (2012) New clues to understand the role of THO and other functionally related factors in mRNP biogenesis. *Biochim Biophys Acta* 1819(6):514–520. <https://doi.org/10.1016/j.bbagr.2011.11.012>
 56. Gowrishankar J, Harinarayanan R (2004) Why is transcription coupled to translation in bacteria? *Mol Microbiol* 54(3):598–603. <https://doi.org/10.1111/j.1365-2958.2004.04289.x>
 57. Leela JK, Syeda AH, Anupama K et al (2013) Rho-dependent transcription termination is essential to prevent excessive genome-wide R-loops in *Escherichia coli*. *Proc Natl Acad Sci U S A* 110(1):258–263. <https://doi.org/10.1073/pnas.1213123110>
 58. El Hage A, French SL, Beyer AL et al (2010) Loss of topoisomerase I leads to R-loop-mediated transcriptional blocks during ribosomal RNA synthesis. *Genes Dev* 24(14):1546–1558. <https://doi.org/10.1101/gad.573310>
 59. Gan W, Guan Z, Liu J et al (2011) R-loop-mediated genomic instability is caused by impairment of replication fork progression. *Genes Dev* 25(19):2041–2056. <https://doi.org/10.1101/gad.17010011>
 60. Wellinger RE, Prado F, Aguilera A (2006) Replication fork progression is impaired by transcription in hyperrecombinant yeast cells lacking a functional THO complex. *Mol Cell Biol* 26(8):3327–3334. <https://doi.org/10.1128/MCB.26.8.3327-3334.2006>
 61. Zeman MK, Cimprich KA (2014) Causes and consequences of replication stress. *Nat Cell Biol* 16(1):2–9. <https://doi.org/10.1038/ncb2897>
 62. Cerritelli SM, Crouch RJ (2009) Ribonuclease H: the enzymes in eukaryotes. *FEBS J* 276(6):1494–1505. <https://doi.org/10.1111/j.1742-4658.2009.06908.x>
 63. Mischo HE, Gomez-Gonzalez B, Grzechnik P et al (2011) Yeast Sen1 helicase protects the genome from transcription-associated instability. *Mol Cell* 41(1):21–32. <https://doi.org/10.1016/j.molcel.2010.12.007>
 64. Skourti-Stathaki K, Proudfoot NJ, Gromak N (2011) Human senataxin resolves RNA/DNA hybrids formed at transcriptional pause sites to promote Xrn2-dependent termination. *Mol Cell* 42(6):794–805. <https://doi.org/10.1016/j.molcel.2011.04.026>

65. Li X, Manley JL (2005) Inactivation of the SR protein splicing factor ASF/SF2 results in genomic instability. *Cell* 122(3):365–378. <https://doi.org/10.1016/j.cell.2005.06.008>
66. Aguilera A, Garcia-Muse T (2012) R loops: from transcription byproducts to threats to genome stability. *Mol Cell* 46(2):115–124. <https://doi.org/10.1016/j.molcel.2012.04.009>
67. Skourti-Stathaki K, Proudfoot NJ (2014) A double-edged sword: R loops as threats to genome integrity and powerful regulators of gene expression. *Genes Dev* 28(13):1384–1396. <https://doi.org/10.1101/gad.242990.114>
68. Hamperl S, Cimprich KA (2014) The contribution of co-transcriptional RNA:DNA hybrid structures to DNA damage and genome instability. *DNA Repair* 19:84–94. <https://doi.org/10.1016/j.dnarep.2014.03.023>
69. Sollier J, Cimprich KA (2015) Breaking bad: R-loops and genome integrity. *Trends Cell Biol* 25(9):514–522. <https://doi.org/10.1016/j.tcb.2015.05.003>
70. Tuduri S, Crabbe L, Conti C et al (2009) Topoisomerase I suppresses genomic instability by preventing interference between replication and transcription. *Nat Cell Biol* 11(11):1315–1324. <https://doi.org/10.1038/ncb1984>
71. Ribeyre C, Zellweger R, Chauvin M et al (2016) Nascent DNA proteomics reveals a chromatin remodeler required for topoisomerase I loading at replication forks. *Cell Rep* 15(2):300–309. <https://doi.org/10.1016/j.celrep.2016.03.027>
72. Christman MF, Dietrich FS, Fink GR (1988) Mitotic recombination in the rDNA of *S. cerevisiae* is suppressed by the combined action of DNA topoisomerases I and II. *Cell* 55(3):413–425
73. Houseley J, Kotovic K, El Hage A et al (2007) Trf4 targets ncRNAs from telomeric and rDNA spacer regions and functions in rDNA copy number control. *EMBO J* 26(24):4996–5006. <https://doi.org/10.1038/sj.emboj.7601921>
74. Krawczyk C, Dion V, Schar P et al (2014) Reversible Top1 cleavage complexes are stabilized strand-specifically at the ribosomal replication fork barrier and contribute to ribosomal DNA stability. *Nucleic Acids Res* 42(8):4985–4995. <https://doi.org/10.1093/nar/gku148>
75. Trigueros S, Roca J (2002) Failure to relax negative supercoiling of DNA is a primary cause of mitotic hyper-recombination in topoisomerase-deficient yeast cells. *J Biol Chem* 277(40):37207–37211. <https://doi.org/10.1074/jbc.M206663200>
76. Tornaletti S, Park-Snyder S, Hanawalt PC (2008) G4-forming sequences in the non-transcribed DNA strand pose blocks to T7 RNA polymerase and mammalian RNA polymerase II. *J Biol Chem* 283(19):12756–12762. <https://doi.org/10.1074/jbc.M705003200>
77. Lopes J, Piazza A, Bermejo R et al (2011) G-quadruplex-induced instability during leading-strand replication. *EMBO J* 30(19):4033–4046. <https://doi.org/10.1038/emboj.2011.316>
78. London TB, Barber LJ, Mosedale G et al (2008) FANCD1 is a structure-specific DNA helicase associated with the maintenance of genomic G/C tracts. *J Biol Chem* 283(52):36132–36139. <https://doi.org/10.1074/jbc.M808152200>
79. Paeschke K, Capra JA, Zakian VA (2011) DNA replication through G-quadruplex motifs is promoted by the *Saccharomyces cerevisiae* Pif1 DNA helicase. *Cell* 145(5):678–691. <https://doi.org/10.1016/j.cell.2011.04.015>
80. Kim N, Jinks-Robertson S (2011) Guanine repeat-containing sequences confer transcription-dependent instability in an orientation-specific manner in yeast. *DNA Repair* 10(9):953–960. <https://doi.org/10.1016/j.dnarep.2011.07.002>
81. Yadav P, Harcy V, Argueso JL et al (2014) Topoisomerase I plays a critical role in suppressing genome instability at a highly transcribed G-quadruplex-forming sequence. *PLoS Genet* 10(12):e1004839. <https://doi.org/10.1371/journal.pgen.1004839>
82. Yadav P, Owiti N, Kim N (2016) The role of topoisomerase I in suppressing genome instability associated with a highly transcribed guanine-rich sequence is not restricted to preventing RNA:DNA hybrid accumulation. *Nucleic Acids Res* 44(2):718–729. <https://doi.org/10.1093/nar/gkv1152>
83. Arimondo PB, Riou JF, Mergny JL et al (2000) Interaction of human DNA topoisomerase I with G-quartet structures. *Nucleic Acids Res* 28(24):4832–4838
84. Marchand C, Pourquier P, Laco GS et al (2002) Interaction of human nuclear topoisomerase I with guanosine quartet-forming and guanosine-rich single-stranded DNA and RNA oligonucleotides. *J Biol Chem* 277(11):8906–8911. <https://doi.org/10.1074/jbc.M106372200>

85. Shuai L, Deng M, Zhang D et al (2010) Quadruplex-duplex motifs as new topoisomerase I inhibitors. *Nucleosides Nucleotides Nucleic Acids* 29(11):841–853. <https://doi.org/10.1080/15257770.2010.530635>
86. Gazumyan A, Bothmer A, Klein IA et al (2012) Activation-induced cytidine deaminase in antibody diversification and chromosome translocation. *Adv Cancer Res* 113:167–190. <https://doi.org/10.1016/b978-0-12-394280-7.00005-1>
87. Matthews AJ, Zheng S, DiMenna LJ et al (2014) Regulation of immunoglobulin class-switch recombination: choreography of non-coding transcription, targeted DNA deamination, and long-range DNA repair. *Adv Immunol* 122:1–57. <https://doi.org/10.1016/b978-0-12-800267-4.00001-8>
88. Hwang JK, Alt FW, Yeap LS (2015) Related mechanisms of antibody somatic hypermutation and class switch recombination. *Microbiol Spectr* 3(1):Mdna3-0037-2014. <https://doi.org/10.1128/microbiolspec.MDNA3-0037-2014>
89. Senavirathne G, Bertram JG, Jaszczur M et al (2015) Activation-induced deoxycytidine deaminase (AID) co-transcriptional scanning at single-molecule resolution. *Nat Commun* 6:10209. <https://doi.org/10.1038/ncomms10209>
90. Huang FT, Yu K, Balter BB et al (2007) Sequence dependence of chromosomal R-loops at the immunoglobulin heavy-chain S_μ class switch region. *Mol Cell Biol* 27(16):5921–5932. <https://doi.org/10.1128/mcb.00702-07>
91. Ruiz JF, Gomez-Gonzalez B, Aguilera A (2011) AID induces double-strand breaks at immunoglobulin switch regions and *c-MYC* causing chromosomal translocations in yeast THO mutants. *PLoS Genet* 7(2):e1002009. <https://doi.org/10.1371/journal.pgen.1002009>
92. Kobayashi M, Aida M, Nagaoka H et al (2009) AID-induced decrease in topoisomerase I induces DNA structural alteration and DNA cleavage for class switch recombination. *Proc Natl Acad Sci U S A* 106(52):22375–22380. <https://doi.org/10.1073/pnas.0911879106>
93. Kobayashi M, Sabouri Z, Sabouri S et al (2011) Decrease in topoisomerase I is responsible for activation-induced cytidine deaminase (AID)-dependent somatic hypermutation. *Proc Natl Acad Sci U S A* 108(48):19305–19310. <https://doi.org/10.1073/pnas.1114522108>
94. Ronai D, Iglesias-Ussel MD, Fan M et al (2007) Detection of chromatin-associated single-stranded DNA in regions targeted for somatic hypermutation. *J Exp Med* 204(1):181–190. <https://doi.org/10.1084/jem.20062032>
95. Maul RW, Saribasak H, Cao Z et al (2015) Topoisomerase I deficiency causes RNA polymerase II accumulation and increases AID abundance in immunoglobulin variable genes. *DNA Repair* 30:46–52. <https://doi.org/10.1016/j.dnarep.2015.03.004>
96. Gatchel JR, Zoghbi HY (2005) Diseases of unstable repeat expansion: mechanisms and common principles. *Nat Rev Genet* 6(10):743–755. <https://doi.org/10.1038/nrg1691>
97. La Spada AR, Taylor JP (2010) Repeat expansion disease: progress and puzzles in disease pathogenesis. *Nat Rev Genet* 11(4):247–258. <https://doi.org/10.1038/nrg2748>
98. Wojciechowska M, Krzyzosiak WJ (2011) CAG repeat RNA as an auxiliary toxic agent in polyglutamine disorders. *RNA Biol* 8(4):565–571. <https://doi.org/10.4161/rna.8.4.15397>
99. Hubert L Jr, Lin Y, Dion V et al (2011) Topoisomerase I and single-strand break repair modulate transcription-induced CAG repeat contraction in human cells. *Mol Cell Biol* 31(15):3105–3112. <https://doi.org/10.1128/mcb.05158-11>
100. Caldecott KW (2008) Single-strand break repair and genetic disease. *Nat Rev Genet* 9(8):619–631. <https://doi.org/10.1038/nrg2380>
101. Takahashi T, Burguiere-Slezak G, Van der Kemp PA et al (2011) Topoisomerase I provokes the formation of short deletions in repeated sequences upon high transcription in *Saccharomyces cerevisiae*. *Proc Natl Acad Sci U S A* 108(2):692–697. <https://doi.org/10.1073/pnas.1012582108>
102. Lippert MJ, Kim N, Cho JE et al (2011) Role for topoisomerase I in transcription-associated mutagenesis in yeast. *Proc Natl Acad Sci U S A* 108(2):698–703. <https://doi.org/10.1073/pnas.1012363108>
103. Nick McElhinny SA, Watts BE, Kumar D et al (2010) Abundant ribonucleotide incorporation into DNA by yeast replicative polymerases. *Proc Natl Acad Sci U S A* 107(11):4949–4954. <https://doi.org/10.1073/pnas.0914857107>
104. Nick McElhinny SA, Kumar D, Clark AB et al (2010) Genome instability due to ribonucleotide incorporation into DNA. *Nat Chem*

- Biol 6(10):774–781. <https://doi.org/10.1038/nchembio.424>
105. Lujan SA, Williams JS, Clausen AR et al (2013) Ribonucleotides are signals for mismatch repair of leading-strand replication errors. *Mol Cell* 50(3):437–443. <https://doi.org/10.1016/j.molcel.2013.03.017>
 106. Williams JS, Clausen AR, Lujan SA et al (2015) Evidence that processing of ribonucleotides in DNA by topoisomerase I is leading-strand specific. *Nat Struct Mol Biol* 22(4):291–297. <https://doi.org/10.1038/nsmb.2989>
 107. Sparks JL, Chon H, Cerritelli SM et al (2012) RNase H2-initiated ribonucleotide excision repair. *Mol Cell* 47(6):980–986. <https://doi.org/10.1016/j.molcel.2012.06.035>
 108. Kim N, Huang SN, Williams JS et al (2011) Mutagenic processing of ribonucleotides in DNA by yeast topoisomerase I. *Science* 332(6037):1561–1564. <https://doi.org/10.1126/science.1205016>
 109. Clark AB, Lujan SA, Kissling GE et al (2011) Mismatch repair-independent tandem repeat sequence instability resulting from ribonucleotide incorporation by DNA polymerase ϵ . *DNA Repair* 10(5):476–482. <https://doi.org/10.1016/j.dnarep.2011.02.001>
 110. Potenski CJ, Niu H, Sung P et al (2014) Avoidance of ribonucleotide-induced mutations by RNase H2 and Srs2-Exo1 mechanisms. *Nature* 511(7508):251–254. <https://doi.org/10.1038/nature13292>
 111. Niu H, Potenski CJ, Epshtein A et al (2016) Roles of DNA helicases and Exo1 in the avoidance of mutations induced by Top1-mediated cleavage at ribonucleotides in DNA. *Cell Cycle* 15(3):331–336. <https://doi.org/10.1080/15384101.2015.1128594>
 112. Williams JS, Smith DJ, Marjavaara L et al (2013) Topoisomerase I-mediated removal of ribonucleotides from nascent leading-strand DNA. *Mol Cell* 49(5):1010–1015. <https://doi.org/10.1016/j.molcel.2012.12.021>
 113. Sekiguchi J, Shuman S (1997) Site-specific ribonuclease activity of eukaryotic DNA topoisomerase I. *Mol Cell* 1(1):89–97
 114. Cho JE, Kim N, Li YC et al (2013) Two distinct mechanisms of topoisomerase I-dependent mutagenesis in yeast. *DNA Repair* 12(3):205–211. <https://doi.org/10.1016/j.dnarep.2012.12.004>
 115. Sparks JL, Burgers PM (2015) Error-free and mutagenic processing of topoisomerase I-provoked damage at genomic ribonucleotides. *EMBO J* 34(9):1259–1269. [10.15252/embj.201490868](https://doi.org/10.15252/embj.201490868)
 116. Huang SY, Ghosh S, Pommier Y (2015) Topoisomerase I alone is sufficient to produce short DNA deletions and can also reverse nicks at ribonucleotide sites. *J Biol Chem* 290(22):14068–14076. <https://doi.org/10.1074/jbc.M115.653345>
 117. Cho JE, Huang SN, Burgers PM et al (2016) Parallel analysis of ribonucleotide-dependent deletions produced by yeast Top1 in vitro and in vivo. *Nucleic Acids Res* 44(16):7714–7721. <https://doi.org/10.1093/nar/gkw495>
 118. Cho JE, Kim N, Jinks-Robertson S (2015) Topoisomerase I-dependent deletions initiated by incision at ribonucleotides are biased to the non-transcribed strand of a highly activated reporter. *Nucleic Acids Res* 43(19):9306–9313. <https://doi.org/10.1093/nar/gkv824>
 119. Cho JE, Jinks-Robertson S (2016) Ribonucleotides and transcription-associated mutagenesis in yeast. *J Mol Biol.* <https://doi.org/10.1016/j.jmb.2016.08.005>
 120. Stewart L, Redinbo MR, Qiu X et al (1998) A model for the mechanism of human topoisomerase I. *Science* 279(5356):1534–1541
 121. Wu J, Liu LF (1997) Processing of topoisomerase I cleavable complexes into DNA damage by transcription. *Nucleic Acids Res* 25(21):4181–4186
 122. Conover HN, Lujan SA, Chapman MJ et al (2015) Stimulation of chromosomal rearrangements by ribonucleotides. *Genetics* 201(3):951–961. <https://doi.org/10.1534/genetics.115.181149>
 123. Epshtein A, Potenski CJ, Klein HL (2016) Increased spontaneous recombination in RNase H2-deficient cells arises from multiple contiguous rNMPs and not from single rNMP residues incorporated by DNA polymerase epsilon. *Microb Cell* 3(6):248–254
 124. Allen-Soltero S, Martinez SL, Putnam CD et al (2014) A *Saccharomyces cerevisiae* RNase H2 interaction network functions to suppress genome instability. *Mol Cell Biol* 34(8):1521–1534. <https://doi.org/10.1128/mcb.00960-13>
 125. Mankouri HW, Ngo HP, Hickson ID (2009) Esc2 and Sgs1 act in functionally distinct branches of the homologous recombination repair pathway in *Saccharomyces cerevisiae*. *Mol Biol Cell* 20(6):1683–1694. <https://doi.org/10.1091/mbc.E08-08-0877>
 126. Ii M, Ii T, Mironova LI et al (2011) Epistasis analysis between homologous recombination

- genes in *Saccharomyces cerevisiae* identifies multiple repair pathways for Sgs1, Mus81-Mms4 and RNase H2. *Mutat Res* 714 (1–2):33–43. <https://doi.org/10.1016/j.mrfmmm.2011.06.007>
127. Chon H, Sparks JL, Rychlik M et al (2013) RNase H2 roles in genome integrity revealed by unlinking its activities. *Nucleic Acids Res* 41(5):3130–3143. <https://doi.org/10.1093/nar/gkt027>
128. Llorente B, Smith CE, Symington LS (2008) Break-induced replication: what is it and what is it for? *Cell Cycle* 7(7):859–864. <https://doi.org/10.4161/cc.7.7.5613>
129. O’Connell K, Jinks-Robertson S, Petes TD (2015) Elevated genome-wide instability in yeast mutants lacking RNase H activity. *Genetics* 201(3):963–975. <https://doi.org/10.1534/genetics.115.182725>
130. Shuman S, Turner J (1993) Site-specific interaction of vaccinia virus topoisomerase I with base and sugar moieties in duplex DNA. *J Biol Chem* 268(25):18943–18950
131. Been MD, Champoux JJ (1984) Breakage of single-stranded DNA by eukaryotic type I topoisomerase occurs only at regions with the potential for base-pairing. *J Mol Biol* 180(3):515–531
132. Waters CA, Strande NT, Wyatt DW et al (2014) Nonhomologous end joining: a good solution for bad ends. *DNA Repair* 17:39–51. <https://doi.org/10.1016/j.dnarep.2014.02.008>
133. Christiansen K, Svejstrup AB, Andersen AH et al (1993) Eukaryotic topoisomerase I-mediated cleavage requires bipartite DNA interaction. Cleavage of DNA substrates containing strand interruptions implicates a role for topoisomerase I in illegitimate recombination. *J Biol Chem* 268(13):9690–9701
134. Henningfeld KA, Hecht SM (1995) A model for topoisomerase I-mediated insertions and deletions with duplex DNA substrates containing branches, nicks, and gaps. *Biochemistry* 34(18):6120–6129
135. Bullock P, Champoux JJ, Botchan M (1985) Association of crossover points with topoisomerase I cleavage sites: a model for nonhomologous recombination. *Science* 230(4728):954–958
136. Kovac MB, Kovacova M, Bachraty H et al (2015) High-resolution breakpoint analysis provides evidence for the sequence-directed nature of genome rearrangements in hereditary disorders. *Hum Mutat* 36(2):250–259. <https://doi.org/10.1002/humu.22734>
137. Zhu J, Schiestl RH (1996) Topoisomerase I involvement in illegitimate recombination in *Saccharomyces cerevisiae*. *Mol Cell Biol* 16:1805–1812
138. Zhu J, Schiestl RH (2004) Human topoisomerase I mediates illegitimate recombination leading to DNA insertion into the ribosomal DNA locus in *Saccharomyces cerevisiae*. *Mol Gen Genomics* 271(3):347–358. <https://doi.org/10.1007/s00438-004-0987-7>
139. Pommier Y, Jenkins J, Kohlhagen G et al (1995) DNA recombinase activity of eukaryotic DNA topoisomerase I; effects of camptothecin and other inhibitors. *Mutat Res* 337(2):135–145
140. Behrendt R, Roers A (2014) Mouse models for Aicardi-Goutières syndrome provide clues to the molecular pathogenesis of systemic autoimmunity. *Clin Exp Immunol* 175(1):9–16. <https://doi.org/10.1111/cei.12147>
141. Lim YW, Sanz LA, Xu X et al (2015) Genome-wide DNA hypomethylation and RNA:DNA hybrid accumulation in Aicardi-Goutières syndrome. *elife* 4. <https://doi.org/10.7554/eLife.08007>
142. Li M, Pokharel S, Wang JT et al (2015) RECQ5-dependent SUMOylation of DNA topoisomerase I prevents transcription-associated genome instability. *Nat Commun* 6:6720. <https://doi.org/10.1038/ncomms7720>
143. Li M, Liu Y (2016) Topoisomerase I in human disease pathogenesis and treatments. *Genomics Proteomics Bioinformatics* 14(3):166–171. <https://doi.org/10.1016/j.gpb.2016.02.004>

DNA Topoisomerases as Targets for Antibacterial Agents

Hiroshi Hiasa

Abstract

DNA topoisomerases are proven therapeutic targets of antibacterial agents. Quinolones, especially fluoroquinolones, are the most successful topoisomerase-targeting antibacterial drugs. These drugs target type IIA topoisomerases in bacteria. Recent structural and biochemical studies on fluoroquinolones have provided the molecular basis for both their mechanism of action, as well as the molecular basis of bacterial resistance. Due to the development of drug resistance, including fluoroquinolone resistance, among bacterial pathogens, there is an urgent need to discover novel antibacterial agents. Recent advances in topoisomerase inhibitors may lead to the development of novel antibacterial drugs that are effective against fluoroquinolone-resistant pathogens. They include type IIA topoisomerase inhibitors that either interact with the GyrB/ParE subunit or form nick-containing ternary complexes. In addition, several topoisomerase I inhibitors have recently been identified. Thus, DNA topoisomerases remain important targets of antibacterial agents.

Key words Aminocoumarin, Antibacterial drugs, DNA gyrase, Fluoroquinolone, Topoisomerase I, Topoisomerase IV, Topoisomerase poison

1 Introduction

The helical structure of duplex DNA is at the root of the topological problems of DNA [1]. DNA topoisomerases are ubiquitous enzymes that alter the linking number (Lk) of double-stranded DNA [2–6]. The negative superhelicity of the chromosomes is maintained by the relaxation activity of topoisomerase I (Topo I) and the supercoiling activity of DNA gyrase in bacterial cells [7, 8]. By regulating the topology of DNA, topoisomerases facilitate critical DNA transactions vital to cell growth and survival [2–6].

There are two classes of DNA topoisomerases, type I and type II. Each class of topoisomerase is structurally and functionally conserved and forms a large protein family [2–6]. Type I topoisomerases alter the Lk in steps of one by breaking one DNA strand of duplex DNA, passing the other DNA strand through the break, and then resealing the broken strand [2–6]. There are three subtypes of

type I topoisomerases, type IA, type IB, and type IC [5, 6]. Topoisomerase III (Topo III), which is present both in bacteria and eukaryotes, and bacterial Topo I are type IA enzymes, whereas eukaryotic Topo I belongs to the type IB subtype. Type IB topoisomerases are also found in archaea and some bacteria. The discovery of a unique type I enzyme, topoisomerase V, from *Methanopyrus kandleri* prompted the creation of the type IC subtype [9]. Type II enzymes alter the Lk in steps of two by breaking both DNA strands of duplex DNA [Gate (G)-segment], passing another segment of duplex DNA [Transfer (T)-segment] through the break, and then resealing the broken strands [2–6]. Type II topoisomerases are comprised of two subtypes, Type IIA and Type IIB [2–6]. Bacterial DNA gyrase and topoisomerase IV (Topo IV), as well as eukaryotic topoisomerase II (Topo II), belong to the type IIA subtype. Since the discovery of topoisomerase VI from *Sulfolobus shibatae* [10], the prototype of the type IIB subtype, type IIB topoisomerases have been found in archaea, some plants, and a few bacteria [11].

The importance of bacterial type IIA topoisomerases is underscored by the fact that both DNA gyrase and Topo IV are the cellular targets of clinically important antibacterial drugs [12–15]. Shortly after its discovery [16], DNA gyrase was identified as the target of the coumarin and the quinolone classes of antibacterial drugs [17–19]. These DNA gyrase inhibitors also inhibit Topo IV, the second type IIA topoisomerase present in many bacteria [20, 21]. Fluoroquinolones (FQs) are one of the most successful antibacterial agents [12–15]. As is the case with many antibacterial drugs, however, drug resistance among bacterial pathogens has limited the clinical use of quinolones in recent years [22, 23]. As described below, new classes of antibacterial drugs also target DNA gyrase and Topo IV [14, 15]. Thus, bacterial type IIA topoisomerases remain as clinically important therapeutic targets.

Recently, a few small molecules have been identified as potent inhibitors of bacterial Topo I, a type IA topoisomerase and, thus, Topo I inhibitors may become effective therapeutic agents to combat infections of drug-resistant bacterial pathogens [24].

2 Bacterial DNA Topoisomerases

The four *Escherichia coli* topoisomerases have been studied most extensively [2–6, 25]. Both Topo I [26] and Topo III [27] are monomeric enzymes that require a single-stranded DNA region to bind to DNA. Topo I relaxes negative supercoils, whereas Topo III can relax negative supercoils, and catenate and decatenate nicked (or gapped) circular DNA molecules [2–6]. DNA gyrase [16, 28] and Topo IV [29] consist of GyrA and GyrB subunits and ParC and ParE subunits, respectively. GyrA and ParC subunits bind to DNA, whereas GyrB and ParE subunits hydrolyze ATP. Both subunits are required to catalyze strand-breakage and religation reactions, and

the active forms of DNA gyrase and Topo IV are an A_2B_2 tetramer. Topo IV can relax both positive and negative supercoils, and catenate and decatenate circular DNA molecules. DNA gyrase can supercoil relaxed DNA, catenate and decatenate circular DNA molecules, and, in the absence of ATP, relax negative supercoils [2–6].

As the parental duplex DNA is unwound during DNA replication, the deficit generated in positive turns must be made up elsewhere in the molecule [30]. Topoisomerase function is essential for removal of such topological constraints to maintain replication fork progression [31]. It was thought that the positive windings (+Lk) accumulated as positive supercoils ahead of the replication forks [32]. In fact, this was the conceptual basis for the original proposal that introduction of a swivel point in this region of the replicating DNA molecule would be sufficient to relieve +Lk [1]. However, it has been shown that the +Lk accumulation is not restricted to a region ahead of the advancing replication forks and can equilibrate behind the replication forks, taking the form of right-handed interwindings of the partially replicated duplexes about each other [33, 34]. Because these interwindings are identical to those of torus catenanes, they have been termed “precatenanes” [35]. In vitro studies have revealed two distinct modes of DNA unlinking during DNA replication [33]. DNA gyrase removes +Lk by relaxing the positive supercoils in front of the replication forks, whereas Topo IV decatenates precatenanes behind the forks. Interestingly, Topo III, a type IA enzyme, can also support the elongation of DNA replication by decatenating precatenanes [33, 36]. The position of a type IIA topoisomerase relative to an advancing replication fork may influence the efficacy of quinolone antibacterial drugs [12, 13, 25].

During termination of DNA replication, decatenation of two daughter chromosomes must be catalyzed by a topoisomerase to allow subsequent chromosome segregation. Although DNA gyrase was thought to be the enzyme responsible for the decatenation of daughter chromosomes [37], it has been shown that Topo IV, not DNA gyrase, catalyzes the efficient decatenation of replicating daughter DNA molecules both in vitro and in vivo [38–40]. It is noteworthy, however, that some bacteria, such as *Mycobacterium tuberculosis*, do not have Topo IV [41] and DNA gyrase alone is capable of supporting DNA replication and chromosome segregation in these bacteria [42].

3 Aminocoumarins and Simocyclinones

Novobiocin, coumermycin A1, and clorobiocin are classical aminocoumarins [43]. They are natural products that contain a 3-amino-4,7-dihydroxycoumarin ring. The ability of aminocoumarins to

inhibit DNA synthesis in bacteria was known long before the identification of DNA gyrase as their target [17]. Aminocoumarins bind to the ATP binding domain of the GyrB/ParE subunit and act as a competitive inhibitor of ATPase activity [27, 44, 45]. Unlike quinolones, aminocoumarins have found little success in the clinic due, at least in part, to their toxicity [12–15]. It is noteworthy, however, that mutations that confer resistance to aminocoumarins appear to significantly affect the activity of DNA gyrase [12]. Continued efforts to identify novel inhibitors of the ATPase activity of DNA gyrase and Topo IV, especially the discovery of potent dual inhibitors of GyrB and ParE ATPase activities, may lead to the development of clinically successful antibacterial agents [13, 15, 46].

Simocyclinones also contain the aminocoumarin moiety and target DNA gyrase [47–50]. However, simocyclinones contain an angucyclic polyketide core, which is linked to the aminocoumarin moiety through a deoxyhexose, and a tetraene side chain. Simocyclinone D8 binds to the GyrA subunit and inhibits the supercoiling activity of DNA gyrase by preventing DNA gyrase from binding to DNA [50, 51]. Simocyclinone D8 is also capable of inhibiting the decatenation activity of Topo IV, albeit less effectively [51]. Observed cross-resistance between simocyclinone D8 and FQs may limit its clinical use [50, 52].

4 Topoisomerase Poisoning

Topoisomerases form a covalent topoisomerase–DNA complex as a catalytic intermediate by forming a phosphotyrosyl bond between an active-site tyrosine and a phosphate group in the DNA backbone at the site of strand breakage [2–6]. Some topoisomerase inhibitors bind to a covalent topoisomerase–DNA complex and trap it as a topoisomerase–drug–DNA ternary complex [12–15, 24, 25]. Ternary complex formation on the chromosome triggers cytotoxic events. Thus, these drugs convert a topoisomerase (an essential enzyme) into a cytotoxic covalently attached protein adduct on the DNA (a cellular poison). Topoisomerase inhibitors that utilize this mechanism are often referred to as “topoisomerase poisons” because of their unique mode of action [12, 13, 25]. Topoisomerase poisons include both clinically successful antibacterial drugs (e.g., quinolones) and anticancer drugs (e.g., etoposide).

The formation of a topoisomerase–drug–DNA ternary complex is critical for the cytotoxicity of topoisomerase poisons, but formation of these complexes is completely reversible [12, 13, 25]. Thus, an additional event must take place at the ternary complex that leads to the disruption of the ternary complex and the generation of a DNA break. The leading candidate for this disruptive event has been the collision of a ternary complex with a replication

fork. In fact, a study of human Topo I–camptothecin–DNA ternary complexes in a cell-free SV40 replication system has shown that the collision between an advancing replication fork and a Topo I–camptothecin–DNA ternary complex results in replication fork arrest and the formation of a double-strand break (DSB) [53].

This “collision” model has frequently been used to describe the events occurring during the encounter of a type IIA topoisomerase–drug–DNA ternary complex with a replication fork [12–15]. However, a study in an *oriC* replication system reconstituted with purified *E. coli* replication proteins has revealed a different outcome in the collision between a replication fork and a ternary complex formed with an FQ and either DNA gyrase or Topo IV [54]. This collision converts the ternary complex into a nonreversible form, but does not generate a DSB. Thus, an additional step(s) is required to generate a DSB. Shortly after this study was reported, it was shown that the collision between a replication fork and a ternary complex formed with an anticancer drug and a type IIA topoisomerase also results in the inhibition of DNA replication but not the generation of a DSB [55, 56]. Thus, unlike what occurs with ternary complexes formed with type IB topoisomerases [53], encounters of advancing replication forks with topoisomerase–drug–DNA ternary complexes formed with type IIA topoisomerases only cause the inhibition of DNA replication [54–56]. The bacteriostatic activities of quinolones are mainly due to the inhibition of DNA replication by such ternary complexes [57]. The steps required for bactericidal activities of quinolones, that is the events downstream of fork arrest by the ternary complex, including the additional step(s) required for the generation of DSBs, are not completely understood [12, 13, 25, 57].

5 Quinolones

Nalidixic acid [58], the prototype of the first-generation synthetic quinolone antibacterial agents, was introduced for the treatment of urinary tract infections. The first generation quinolones are effective against gram-negative bacteria, except those from the genus *Pseudomonas* [12, 59]. The attachment of a fluorine atom to the C-6 position of the quinolone core to create the FQ norfloxacin in 1979 dramatically increased antibacterial activity and an expanded spectrum of bacterial targets [60]. Since then, a number of FQs have been developed and successfully used as broad-spectrum antibacterial drugs [12, 59]. Norfloxacin and ciprofloxacin (Fig. 1a) belong to the second-generation of quinolone compounds, which are effective against both gram-negative bacteria, including *Pseudomonas aeruginosa*, and gram-positive bacteria. Levofloxacin and moxifloxacin belong to the third- and fourth-generation quinolones, respectively.

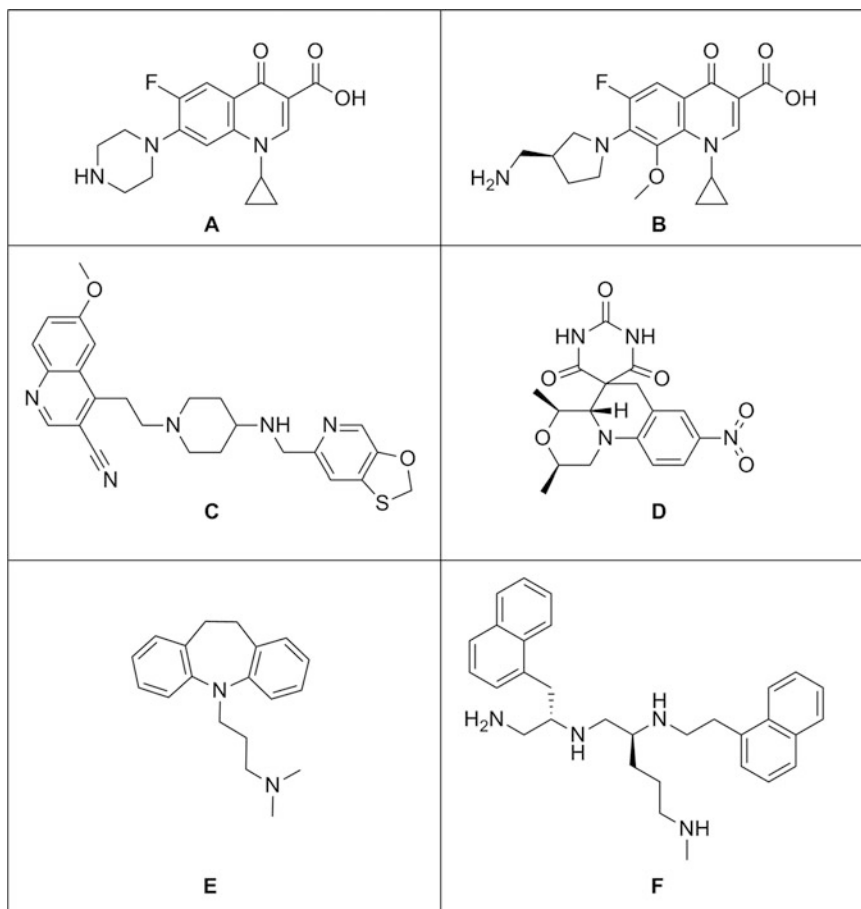


Fig. 1 Structures of bacterial topoisomerase inhibitors. Structures of ciprofloxacin (a), UING5-249 (b), GSK299423 (c), QPT-1 (d), imipramine (e), and compound 2471-80 (f) are shown

Quinolones can target and poison both DNA gyrase and Topo IV [12, 13, 25]. However, DNA gyrase is the primary target of quinolones in gram-negative bacteria, whereas Topo IV often becomes their primary target in gram-positive bacteria [61–64]. The selection of the preferred target (i.e., the topoisomerase that forms more cytotoxic ternary complexes) may be determined by several factors, including the quinolone sensitivities of the two type IIA topoisomerases, the number of active topoisomerases on the chromosome, and the position of ternary complexes relative to advancing replication forks. DNA gyrase functions in front of the replication forks, whereas Topo IV binds behind the forks during the chromosomal DNA replication in *E. coli* [33–35]. Thus, ternary complexes formed with DNA gyrase collide with the replication forks more frequently than those formed with Topo IV.

Another possibility is that differences in repairing the ternary complexes formed with DNA gyrase versus those formed with

Topo IV make the DNA gyrase–quinolone–DNA ternary complex more cytotoxic than the Topo IV–quinolone–DNA ternary complex. The loss of function of the UvrD helicase significantly increased the efficiency of the Topo IV-targeted cell killing in *E. coli*, although it has no effect on the DNA gyrase-targeted cell killing [65]. Thus, the post-replicative repair system appears to be able to repair the ternary complexes formed with Topo IV, but not those formed with DNA gyrase, in *E. coli*. It is interesting to note that the UvrD helicase alone can disrupt a Topo IV–quinolone DNA ternary complex, and generate a single-strand break in vitro [66].

Quinolone resistance-conferring mutations arise rapidly and they are clustered within a small region (between residues 67 and 106 of GyrA, often referred to as the quinolone resistance-determining region) of the *gyrA* gene in *E. coli* [64]. The structure of an *N*-terminal domain of *E. coli* GyrA has demonstrated that the quinolone resistance-determining region is located in the helix-turn-helix region (specifically in the $\alpha 3$ and $\alpha 4$ helices) of the GyrA subunit [67]. Mutational hotspots for quinolone resistance, Ser-83 and Asp-87 of *E. coli* GyrA [64], locate to the $\alpha 4$ helix, and these two amino acid residues are thought to directly interact with the quinolone drug in a gyrase–quinolone–DNA ternary complex. The structure of the *Acinetobacter baumannii* Topo IV–moxifloxacin–DNA ternary complex has revealed the presence of a Mg^{2+} -water bridge between the *C*-3, *C*-4 diketo moiety of moxifloxacin and the conserved amino acid residues Ser-84 and Glu-88 in the ParC subunit [68], which correspond to Ser-83 and Asp-87 of *E. coli* GyrA. Other structures of topoisomerase–FQ–DNA ternary complexes have also shown that two FQ molecules are intercalated between the +1 and –1 bases at the sites of strand breakage and are anchored by a Mg^{2+} -water bridge between the FQ and the GyrA/ParC subunit [69, 70]. This provides the molecular basis for the quinolone resistance conferred by amino acid substitutions at Ser-83 and Asp-87 of *E. coli* GyrA, as well as explaining why the carbonyl at the *C*-4 position is essential for antibacterial activity of FQs [57, 71].

Currently available structures of ternary complexes do not identify any differences in the topoisomerase–FQ interaction that could explain either the different levels of activities of various FQs or the distinct FQ susceptibilities among DNA gyrases and Topo IVs [68–70]. A recent study on the ternary complexes formed with *M. tuberculosis* DNA gyrase and several FQs has demonstrated that the stability of ternary complexes correlates well with the activity of FQs [70]. These results coincide with previous observations that the stability of ternary complexes correlates both with the cytotoxicity of an FQ in *E. coli* [72], and with the ability of ternary complexes to inhibit DNA replication in vitro [73].

Although the only direct interaction between an FQ and its target in a ternary complex appears to be through a Mg^{2+} -water

bridge between the FQ and the topoisomerase [68, 70], nonspecific interactions between an FQ and either DNA or a topoisomerase may contribute to the formation and the stability of a ternary complex. The walls of FQ binding sites are formed by the +1 and -1 bases and the quinolone core and these bases interact through π - π stacking and van der Waals interactions [68–70]. The C-7 moiety of an FQ also interacts with the conserved Toprim domain of the GyrB/ParE subunit via van der Waals interactions in a ternary complex [68–70]. The fact that mutations that confer resistance to either quinolones or quinazolidiones, quinolone-class drugs that cannot form a Mg^{2+} -water bridge with the GyrA/ParC subunit, have been mapped in this domain of the GyrB/ParE subunit demonstrates the importance of this interaction [74, 75].

In addition to forming the wall of quinolone binding site [68–70], DNA may play an additional role in the action of FQs. FQs can poison a topoisomerase by either stimulating the strand breakage reaction or inhibiting the religation reaction [12, 13, 71]. Biochemical and structural studies have supported the notion that type IIA topoisomerases use a variation of the classic “two-metal-ion mechanism” [76], where Mg^{2+} at metal binding site A is directly involved in the chemistry of the reaction by stabilizing the transition state and Mg^{2+} at metal binding site B plays a structural role by anchoring the -1 phosphate group [77–80]. The binding affinity of Mg^{2+} to site A is higher than that of Mg^{2+} to site B [78, 79]. A recent biochemical study has demonstrated that both FQs and quinazolidiones can promote the Topo IV-catalyzed strand breakage reaction at low Mg^{2+} concentrations where Topo IV alone cannot efficiently cleave DNA [81]. An FQ can form a ternary complex with Topo IV and DNA prior to the strand breakage reaction and induce local structural distortions in DNA [82]. It has been proposed that at low Mg^{2+} concentrations, where a topoisomerase can bind to DNA but cannot catalyze the strand breakage reaction, an FQ binds to the topoisomerase on the DNA and modulates metal binding sites to increase the affinity of Mg^{2+} to metal binding site B through the local distortion of the DNA structure [81]. This leads to the stimulation of the strand breakage reaction. At high Mg^{2+} concentrations, an FQ inhibits the religation reaction by either stabilizing Mg^{2+} binding at site B or by inhibition of the binding of Mg^{2+} to site A [81].

As effective as FQs are in the treatment of various bacterial infections, the development and spread of quinolone resistance among bacterial pathogens restricts their clinical use [22, 23]. However, recent studies on quinazolidiones may have opened the door to a new strategy to overcome quinolone resistance [83–85]. As stated above, amino acid substitutions at Ser-83 and Asp-87 of *E. coli* GyrA, mutational hot spots for quinolone resistance [64], interfere with the formation of the Mg^{2+} -water bridge between an FQ and the GyrA/ParC subunit, which is critical for the binding of the FQ to the topoisomerase in a ternary complex

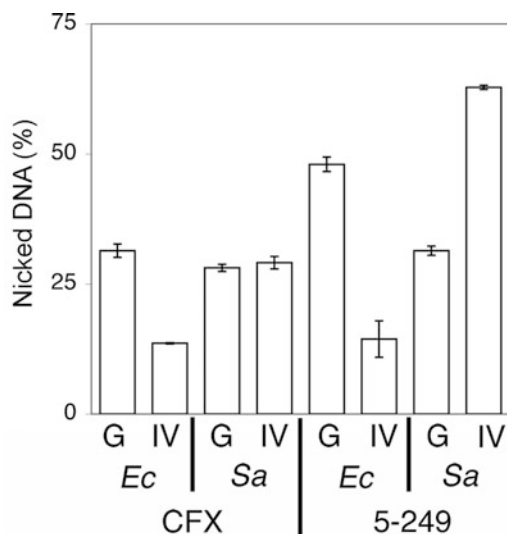


Fig. 2 Formation of nick- and DSB-containing ternary complexes. The levels of nick-containing ternary complexes (Nicked DNA) are expressed as [(nicked DNA)/(nicked DNA + linear DNA)] \times 100 (%). CFX, ciprofloxacin; 5-249, UING5-249; Ec, *E. coli*; Sa, *S. aureus*; G, DNA gyrase; and IV, Topo IV

[68, 70]. Although quinazolinones intercalate between the +1 and -1 bases at the sites of strand breakage similar to FQs, they do not form a Mg^{2+} -water bridge with the GyrA/ParC subunit [69]. Instead, the C-7 moiety of quinazolinones interacts with the Toprim domain of the GyrB/ParE subunit [69, 75]. Thus, many quinolone-resistant mutations found in the GyrA/ParC subunit have either no or reduced effects on the activity of quinazolinones [83–85]. Interestingly, a C-7 aminomethylpyrrolidine, 8-methoxy FQ, UING5-249 (Fig. 1b), also exhibits an enhanced activity against quinolone-resistant mutant DNA gyrases [83–85]. This enhanced activity appears to be due to the direct interaction between the primary amine in the C-7 aminomethylpyrrolidine side chain and the Glu-437 and Arg-418 residues in the Toprim domain of the GyrB/ParE subunit, in addition to the Mg^{2+} -water bridge between the C-3, C-4 diketo moiety of UING5-249 and the GyrA/ParC subunit [85]. Thus, introducing a side chain at the C-7 position of either an FQ or a quinazolinone that can directly interact with the GyrB/ParE subunit may lead to the development of novel antibacterial drugs with enhanced activity against quinolone-resistant strains of bacterial pathogens.

We found that UING5-249 induced more nick-containing ternary complexes than DSB-containing ternary complexes when incubated with either *E. coli* DNA gyrase or *Staphylococcus aureus* Topo IV, but not with either *E. coli* Topo IV or *S. aureus* DNA gyrase (Fig. 2; Oppgaard LM, Kerns RJ, Hiasa H, unpublished data). These results suggested that nick-containing ternary complex formation might contribute to the activity of UING5-

249. Interestingly, GSK299423, a novel bacterial topoisomerase inhibitor (NBTI), also induces nick-containing ternary complexes when it poisons *S. aureus* DNA gyrase [86]. Thus, not only DSB-containing ternary complexes but also nick-containing ternary complexes may be important for the cytotoxicity of type IIA topoisomerase poisons. The discovery of nick-containing ternary complexes formed with bacterial type IIA topoisomerases establishes nick-containing ternary complex formation as a new activity criterion to be used to identify novel type IIA topoisomerase poisons that could not be identified by other screening methods.

6 Novel Topoisomerase IIA Inhibitors

NBTIs [86] and quinoline pyrimidine trione-1 (QPT-1) [87] represent two promising, novel classes of bacterial type IIA topoisomerase inhibitors. NBTIs were discovered from an unbiased antibacterial screen by GlaxoSmithKline, and GSK299423 (Fig. 1c), the first NBTI reported, is a potent inhibitor of both *E. coli* and *S. aureus* DNA gyrases, and exhibits broad spectrum antibacterial activity, including activity against FQ-resistant strains of bacteria [86]. An *S. aureus* DNA gyrase–GSK299423–DNA complex structure has revealed that one GSK299423 molecule is bound in the middle of the two active sites [86]. The quinolone-carbonitrile group (Fig. 1c) is intercalated between the two central bases and the oxathiole-pyridine group (Fig. 1c) is bound to a hydrophobic pocket created at the GyrA dimer interface in a pre-DNA strand breakage conformation. The binding mode of GSK299423 explains why NBTIs are active against FQ-resistant strains of bacterial pathogens. Unlike ternary complexes formed with other DNA gyrase poisons that contain DSBs, *S. aureus* DNA gyrase–GSK299423–DNA complexes contain nicks [86]. A biochemical study with a derivative of GSK299423 showed that, similar to topoisomerase–FQ–DNA ternary complexes [54], topoisomerase–NBTI–DNA ternary complexes could arrest replication fork progression in vitro (Hiasa H, unpublished data).

QPT-1 (originally PNU-286607; Fig. 1d) was identified during a high-throughput screening by Pharmacia and Upjohn for compounds possessing whole cell antibacterial activity [87]. It is a synthetic compound with activity against a broad spectrum of bacterial pathogens, including FQ-resistant pathogens. QPT-1 inhibits DNA replication and the majority of QPT-1-resistant mutations were mapped in the *gyrB* gene [87]. Biochemical studies have shown that QPT-1 inhibits the catalytic activities of DNA gyrase and Topo IV, and poisons DNA gyrase. A recent structural study of the *S. aureus* DNA gyrase–QPT-1–DNA ternary complex has demonstrated that, similar to FQs, two QPT-1 molecules intercalate between the –1 and +1 bases at the sites of strand breakage

[88]. Although the QPT-1 binding site and the FQ binding site overlap, their binding modes are noticeably different. FQs interact with the GyrA subunit of DNA gyrase through a Mg^{2+} -water bridge [68, 70, 88], whereas QPT-1 interacts with the TOPRIM domain of the GyrB subunit of DNA gyrase [88]. The interaction of QPT-1 with the conserved amino acid residues in the TOPRIM domain is somewhat similar to that of either etoposide [88] or quinazolinone [69].

Since the discovery of GSK299423, a series of cyclohexylamides, amino-piperidines, and tricyclic compounds have been reported as NBTIs [89–92]. Gepotidacin (originally GSK2140944 [93], an analog of GSK299423) and AZD0914 [94–96], an analog of QPT-1, are in clinical trials. Thus, these two classes of bacterial type IIA topoisomerase inhibitors may provide us with new antibacterial drugs to fight bacterial infections, especially infections of drug-resistant pathogens.

7 Topoisomerase I Inhibitors

As is the case with DNA gyrase, bacterial Topo I, a type IA enzyme, is essential for the viability of all bacteria [7] and, thus, is a potential target of antibacterial agents. Despite the fact that Topo I was discovered in 1971 [26], and numerous attempts were made to identify selective Topo I inhibitors as antibacterial drugs, its potential as a therapeutic target has only recently been validated [24].

Several bacterial Topo I inhibitors, including phenanthrenes, bisbenzimidazoles, and anziaic acid, have been recently identified [24]. An *in silico* screening of *M. tuberculosis* Topo I inhibitors has identified imipramine (Fig. 1e), a tricyclic antidepressant, and the structurally related compound norclomipramine as potential Topo I inhibitors [97]. Biochemical characterization of these compounds shows that they inhibit the catalytic activity of mycobacterial Topo I, but not that of *E. coli* Topo I, and that they act as mycobacterial Topo I poisons. Both compounds exhibited bacteriostatic activity against *M. tuberculosis* and *Mycobacterium smegmatis* [97]. More recently, a screening of scaffold-ranking library mixtures has led to the discovery of four polyamines (one of which, compound 2471-80, is shown in Fig. 1f) that are able to inhibit the relaxation activity of either *E. coli* or mycobacterial Topo I [98]. They function as Topo I catalytic inhibitors, not as Topo I poisons, and exhibit bactericidal activity against *M. tuberculosis* and *M. smegmatis* [98].

No Topo I inhibitors are currently available for the treatment of bacterial infections [24]. However, if any of these Topo I inhibitors lead to the development of novel antibacterial drugs, they would likely to be effective against drug-resistant strains of bacterial

pathogens. Thus, these drugs may become powerful weapons in our fight against drug-resistant bacterial infections.

Acknowledgments

I would like to thank Lisa Oppegard for her contribution and critical comments on the manuscript, Fang Li for invaluable discussion, and Justine Delgado for preparation of Fig. 1 and critical comments on the manuscript. Studies from my laboratory were supported in part by National Institutes of Health grants GM59465, AI087671, and a fellowship from SmithKline Beecham Pharmaceuticals.

References

1. Watson JD, Crick FH (1953) Genetical implications of the structure of deoxyribonucleic acid. *Nature* 171:964–967
2. Champoux JJ (2001) DNA topoisomerases: structure, function, and mechanism. *Annu Rev Biochem* 70:369–413
3. Wang JC (2002) Cellular roles of DNA topoisomerases: a molecular perspective. *Nat Rev Mol Cell Biol* 3:430–440
4. Nitiss JL (2009) DNA topoisomerase II and its growing repertoire of biological functions. *Nat Rev Cancer* 9:327–337
5. Vos SM, Tretter EM, Schmidt BH, Berger JM (2011) All tangled up: how cells direct, manage and exploit topoisomerase function. *Nat Rev Mol Cell Biol* 12:827–841
6. Bush NG, Evans-Roberts K, Maxwell A (2015) DNA topoisomerases. *EcoSal Plus*. <https://doi.org/10.1128/ecosalplus.ESP-0010-2014>
7. Stupina VA, Wang JC (2005) Viability of *Escherichia coli* topA mutants lacking DNA topoisomerase I. *J Biol Chem* 280:355–360
8. Jeong KS, Xie Y, Hiasa H, Khodursky AB (2006) Analysis of pleiotropic transcriptional profiles: a case study of DNA gyrase inhibition. *PLoS Genet* 2:e152
9. Forterre P (2006) DNA topoisomerase V: a new fold of mysterious origin. *Trends Biotechnol* 24:245–247
10. Bergerat A, Gabelle D, Forterre P (1994) Purification of a DNA topoisomerase II from the hyperthermophilic archaeon *Sulfolobus shibatae*. A thermostable enzyme with both bacterial and eucaryal features. *J Biol Chem* 269:27663–27669
11. Malik SB, Ramesh MA, Hulstrand AM, Logsdon JM Jr (2007) Protist homologs of the meiotic Spo11 gene and topoisomerase VI reveal an evolutionary history of gene duplication and lineage-specific loss. *Mol Biol Evol* 24:2827–2841
12. Collin F, Karkare S, Maxwell A (2011) Exploiting bacterial DNA gyrase as a drug target: current state and perspectives. *Appl Microbiol Biotechnol* 92:479–497
13. Pommier Y (2013) Drugging topoisomerases: lessons and challenges. *ACS Chem Biol* 8:82–95
14. Mayer C, Janin YL (2014) Non-quinolone inhibitors of bacterial type IIA topoisomerases: a feat of bioisosterism. *Chem Rev* 114:2313–2342
15. Ehmann DE, Lahiri SD (2014) Novel compounds targeting bacterial DNA topoisomerase/DNA gyrase. *Curr Opin Pharmacol* 18:76–83
16. Gellert M, Mizuuchi K, O’Dea MH, Nash HA (1976) DNA gyrase: an enzyme that introduces superhelical turns into DNA. *Proc Natl Acad Sci U S A* 73:3872–3876
17. Gellert M, O’Dea MH, Itoh T, Tomizawa J (1976) Novobiocin and coumermycin inhibit DNA supercoiling catalyzed by DNA gyrase. *Proc Natl Acad Sci U S A* 73:4474–4478
18. Sugino A, Peebles CL, Kreuzer KN, Cozzarelli NR (1977) Mechanism of action of nalidixic acid: purification of *Escherichia coli* nalA gene product and its relationship to DNA gyrase and a novel nicking-closing enzyme. *Proc Natl Acad Sci U S A* 74:4767–4771
19. Gellert M, Mizuuchi K, O’Dea MH, Itoh T, Tomizawa J (1977) Nalidixic acid resistance: a second genetic character involved in DNA gyrase activity. *Proc Natl Acad Sci U S A* 74:4772–4776

20. Kato J, Suzuki H, Ikeda H (1992) Purification and characterization of DNA topoisomerase IV in *Escherichia coli*. *J Biol Chem* 267:25676–25684
21. Peng H, Marians KJ (1993) *Escherichia coli* topoisomerase IV. Purification, characterization, subunit structure, and subunit interactions. *J Biol Chem* 268:24481–24490
22. Redgrave L, Sutton S, Webber M, Piddock L (2012) Fluoroquinolone resistance: mechanisms, impact on bacteria, and role in evolutionary success. *Trends Microbiol* 22:438–445
23. Dalhoff A (2012) Resistance surveillance studies: a multifaceted problem – the fluoroquinolone example. *Infection* 40:239–262
24. Tse-Dinh YC (2015) Targeting bacterial topoisomerase I to meet the challenge of finding new antibiotics. *Future Med Chem* 7:459–471
25. Levine C, Hiasa H, Marians KJ (1998) DNA gyrase and topoisomerase IV: biochemical activities, physiological roles during chromosome replication, and drug sensitivities. *Biochim Biophys Acta* 1400:29–43
26. Wang JC, Becherer K (1983) Cloning of the gene *topA* encoding for DNA topoisomerase I and the physical mapping of the *cysB-topA-trp* region of *Escherichia coli*. *Nucleic Acids Res* 11:1773–1790
27. DiGate RJ, Marians KJ (1989) Molecular cloning and DNA sequence analysis of *Escherichia coli topB*, the gene encoding topoisomerase III. *J Biol Chem* 264:17924–17930
28. Mizuuchi K, O’Dea MH, Gellert M (1978) DNA gyrase: subunit structure and ATPase activity of the purified enzyme. *Proc Natl Acad Sci U S A* 75:5960–5963
29. Kato J, Nishimura Y, Imamura R, Niki H, Hiraga S, Suzuki H (1990) New topoisomerase essential for chromosome segregation in *E. coli*. *Cell* 63:393–404
30. Bates AD, Maxwell A (1997) DNA topology: topoisomerases keep it simple. *Curr Biol* 7: R778–R781
31. Wang JC, Liu LF (1990) DNA replication: topological aspects and the roles of DNA topoisomerases. In: Cozzarelli NR, Wang JC (eds) *DNA topology and its biological effects*. Cold Spring Harbor, Cold Spring Harbor Laboratory
32. Cairns J (1963) The bacterial chromosome and its manner of replication as seen by autoradiography. *J Mol Biol* 6:208–213
33. Hiasa H, Marians KJ (1996) Two distinct modes of strand unlinking during θ -type DNA replication. *J Biol Chem* 271:21529–21535
34. Peter BJ, Ullsperger C, Hiasa H, Marians KJ, Cozzarelli NR (1998) The structure of supercoiled intermediates in DNA replication. *Cell* 94:819–827
35. Ullsperger C, Vologodskii A, Cozzarelli NR (1995) Unlinking of DNA by topoisomerases during DNA replication. In: Lilly D, Eckstein F (eds) *Nucleic acids and molecular biology*, vol 9. Springer-Verlag, Berlin, pp 115–142
36. Hiasa H, Marians KJ (1994) Topoisomerase III, but not topoisomerase I, can support nascent chain elongation during theta-type DNA replication. *J Biol Chem* 269:32655–32659
37. Bliska JB, Cozzarelli NR (1987) Use of site-specific recombination as a probe of DNA structure and metabolism in vivo. *J Mol Biol* 194:205–218
38. Hiasa H, DiGate RJ, Marians KJ (1994) Decatenating activity of *Escherichia coli* DNA gyrase and topoisomerases I and III during *oriC* and *pBR322* DNA replication in vitro. *J Biol Chem* 269:2093–2099
39. Hiasa H, Marians KJ (1994) Topoisomerase IV can support *oriC* DNA replication in vitro. *J Biol Chem* 269:16371–16375
40. Zechiedrich EL, Khodursky AB, Cozzarelli NR (1997) Topoisomerase IV, not gyrase, decatenates products of site-specific recombination in *Escherichia coli*. *Genes Dev* 11:2580–2592
41. Cole ST, Brosch R, Parkhill J, Garnier T, Churcher C et al (1998) Deciphering the biology of *Mycobacterium tuberculosis* from the complete genome sequence. *Nature* 393:537–544
42. Aubry A, Fisher LM, Jarlier V, Cambau E (2006) First functional characterization of a singly expressed bacterial type II topoisomerase: the enzyme from *Mycobacterium tuberculosis*. *Biochem Biophys Res Commun* 348:158–165
43. Li SM, Heide L (2005) The biosynthetic gene clusters of aminocoumarin antibiotics. *Curr Med Chem* 12:419–427
44. Sugino A, Higgins NP, Brown PO, Peebles CL, Cozzarelli NR (1978) Energy coupling in DNA gyrase and the mechanism of action of novobiocin. *Proc Natl Acad Sci U S A* 75:4838–4842
45. Maxwell A, Lawson DM (2003) The ATP-binding site of type II topoisomerases as a target for antibacterial drugs. *Curr Top Med Chem* 3:283–303
46. Azam MA, Thathan J, Jubie S (2015) Dual targeting DNA gyrase B (*GyrB*) and topoisomerase IV (*ParE*) inhibitors: a review. *Bioorg Chem* 62:41–63

47. Schimana J, Fiedler HP, Groth I, Süßmuth R, Beil W et al (2000) Simocyclinones, novel cytosstatic angucyclinone antibiotics produced by *Streptomyces antibioticus* Tü 6040. I. Taxonomy, fermentation, isolation and biological activities. *J Antibiot* 53:779–787
48. Theobald U, Schimana J, Fiedler HP (2000) Microbial growth and production kinetics of *Streptomyces antibioticus* Tü 6040. *Antonie Van Leeuwenhoek* 78:307–313
49. Holzenkämpfer M, Walker M, Zeeck A, Schimana J, Fiedler HP (2002) Simocyclinones, novel cytosstatic angucyclinone antibiotics produced by *Streptomyces antibioticus* Tü 6040 II. Structure elucidation and biosynthesis. *J Antibiot* 55:301–307
50. Flatman RH, Howells AJ, Heide L, Fiedler HP, Maxwell A (2005) Simocyclinone D8, an inhibitor of DNA gyrase with a novel mode of action. *Antimicrob Agents Chemother* 49:1093–1100
51. Oppegard LM, Hamann BL, Streck KR, Ellis KC, Fiedler HP et al (2009) In vivo and in vitro patterns of the activity of simocyclinone D8, an angucyclinone antibiotic from *Streptomyces antibioticus*. *Antimicrob Agents Chemother* 53:2110–2119
52. Hearnshaw SJ, Edwards MJ, Stevenson CE, Lawson DM, Maxwell A (2014) A new crystal structure of the bifunctional antibiotic simocyclinone D8 bound to DNA gyrase gives fresh insight into the mechanism of inhibition. *J Mol Biol* 426:2023–2033
53. Tsao YP, Russo A, Nyamuswa G, Silber R, Liu LF (1993) Interaction between replication forks and topoisomerase I-DNA cleavable complexes: studies in a cell-free SV40 DNA replication system. *Cancer Res* 53:5908–5914
54. Hiasa H, Yousef DO, Marians KJ (1996) DNA strand cleavage is required for replication fork arrest by a frozen topoisomerase-quinolone-DNA ternary complex. *J Biol Chem* 271:26424–26429
55. Hong G, Kreuzer KN (2000) An antitumor drug-induced topoisomerase cleavage complex blocks a bacteriophage T4 replication fork in vivo. *Mol Cell Biol* 20:594–603
56. Lucas I, Germe T, Chevrier-Miller M, Hyrien O (2001) Topoisomerase II can unlink replicating DNA by precatenane removal. *EMBO J* 20:6509–6519
57. Drlica K, Hiasa H, Kerns R, Malik M, Mustaev A et al (2009) Quinolones: action and resistance updated. *Curr Top Med Chem* 9:981–998
58. Goss WA, Deitz WH, Cook TM (1965) Mechanism of action of nalidixic acid on *Escherichia coli* II. Inhibition of deoxyribonucleic acid synthesis. *J Bacteriol* 89:1068–1074
59. Emmerson AM, Jones AM (2003) The quinolones: decades of development and use. *J Antimicrob Chemother* 51:13–20
60. Ito A, Hirai K, Inoue M, Koga H, Suzue S et al (1980) In vitro antibacterial activity of AM-715, a new nalidixic acid analog. *Antimicrob Agents Chemother* 17:103–108
61. Kreuzer KN, Cozzarelli NR (1979) *Escherichia coli* mutants thermosensitive for deoxyribonucleic acid gyrase subunit a: effects on deoxyribonucleic acid replication, transcription, and bacteriophage growth. *J Bacteriol* 140:424–435
62. Ferrero L, Cameron B, Manse B, Lagneaux D, Crouzet J et al (1994) Cloning and primary structure of *Staphylococcus aureus* DNA topoisomerase IV: a primary target of fluoroquinolones. *Mol Microbiol* 13:641–653
63. Khodursky AB, Zechiedrich EL, Cozzarelli NR (1995) Topoisomerase IV is a target of quinolones in *Escherichia coli*. *Proc Natl Acad Sci U S A* 92:11801–11805
64. Yoshida H, Bogaki M, Nakamura M, Nakamura S (1990) Quinolone resistance-determining region in the DNA gyrase *gyrA* gene of *Escherichia coli*. *Antimicrob Agents Chemother* 34:1271–1272
65. Khodursky AB, Cozzarelli NR (1998) The mechanism of inhibition of topoisomerase IV by quinolone antibacterials. *J Biol Chem* 273:27668–27677
66. Shea ME, Hiasa H (2000) Distinct effects of the UvrD helicase on topoisomerase-quinolone-DNA ternary complexes. *J Biol Chem* 275:14649–14658
67. Morais Cabral JH, Jackson AP, Smith CV, Shikotra N, Maxwell A et al (1997) Crystal structure of the breakage-reunion domain of DNA gyrase. *Nature* 388:903–906
68. Wohlkonig A, Chan PF, Fosberry AP, Homes P, Huang J et al (2010) Structural basis of quinolone inhibition of type IIA topoisomerases and target-mediated resistance. *Nat Struct Mol Biol* 17:1152–1153
69. Laponogov I, Pan XS, Veselkov DA, McAuley DA, Fisher LM et al (2010) Structural basis of gate-DNA breakage and resealing by type II topoisomerases. *PLoS One* 5:e11338
70. Blower TR, Williamson BH, Kerns RJ, Berger JM (2016) Crystal structure and stability of gyrase-fluoroquinolone cleaved complexes from *Mycobacterium tuberculosis*. *Proc Natl Acad Sci U S A* 113:1706–1713

71. Aldred KJ, Kerns RJ, Osheroff N (2014) Mechanism of quinolone action and resistance. *Biochemistry* 53:1565–1574
72. Pfeiffer ES, Hiasa H (2004) Replacement of ParC alpha4 helix with that of GyrA increases the stability and cytotoxicity of topoisomerase IV-quinolone-DNA ternary complexes. *Antimicrob Agents Chemother* 48:608–611
73. Hiasa H, Shea ME (2000) DNA gyrase-mediated wrapping of the DNA strand is required for the replication fork arrest by the DNA gyrase-quinolone-DNA ternary complex. *J Biol Chem* 275:34780–34786
74. Yoshida H, Bogaki M, Nakamura M, Yamanaka LM, Nakamura S (1991) Quinolone resistance-determining region in the DNA gyrase *gyrB* gene of *Escherichia coli*. *Antimicrob Agents Chemother* 35:1647–1650
75. Pan XS, Gould KA, Fisher LM (2009) Probing the differential interactions of quinazolinodione PD 0305970 and quinolones with gyrase and topoisomerase IV. *Antimicrob Agents Chemother* 53:3822–3831
76. Wang J, Yu P, Lin TC, Konigsberg WH, Steitz TA (1996) Crystal structures of an NH₂-terminal fragment of T4 DNA polymerase and its complexes with single-stranded DNA and with divalent metal ions. *Biochemistry* 35:8110–8119
77. West KL, Meczes EL, Thorn R, Turnbull RM, Marshall R et al (2000) Mutagenesis of E477 or K505 in the B' domain of human topoisomerase II β increases the requirement for magnesium ions during strand passage. *Biochemistry* 39:1223–1233
78. Pitts SL, Liou GF, Mitchenall LA, Burgin AB, Maxwell A et al (2011) Use of divalent metal ions in the DNA cleavage reaction of topoisomerase IV. *Nucleic Acids Res* 39:4808–4817
79. Noble CG, Maxwell A (2002) The role of GyrB in the DNA cleavage-religation reaction of DNA gyrase: a proposed two metal-ion mechanism. *J Mol Biol* 318:361–371
80. Deweese JE, Burgin JE, Osheroff N (2008) Human topoisomerase II α uses a two-metal-ion mechanism for DNA cleavage. *Nucleic Acids Res* 36:4883–4893
81. Oppegard LM, Schwanz HA, Towle TR, Kerns RJ, Hiasa H (2016) Fluoroquinolones stimulate the DNA cleavage activity of topoisomerase IV by promoting the binding of Mg(2+) to the second metal binding site. *Biochim Biophys Acta* 1860:569–575
82. Mariani KJ, Hiasa H (1997) Mechanism of quinolone action. A drug-induced structural perturbation of the DNA precedes strand cleavage by topoisomerase IV. *J Biol Chem* 272:9401–9409
83. German N, Malik M, Rosen JD, Drlica K, Kerns RJ (2008) Use of gyrase resistance mutants to guide selection of 8-methoxyquinazoline-2,4-diones. *Antimicrob Agents Chemother* 52:3915–3921
84. Malik M, Marks KR, Mustaev A, Zhao X, Chavda K et al (2011) Fluoroquinolone and quinazolinodione activities against wild-type and gyrase mutant strains of *Mycobacterium smegmatis*. *Antimicrob Agents Chemother* 55:2335–2343
85. Drlica K, Mustaev A, Towle TR, Luan G, Kerns RJ et al (2014) Bypassing fluoroquinolone resistance with quinazolinodiones: studies of drug-gyrase-DNA complexes having implications for drug design. *ACS Chem Biol* 9:2895–2904
86. Bax BD, Chan PF, Eggleston DS, Fosberry A, Gentry DR et al (2010) Type IIA topoisomerase inhibition by a new class of antibacterial agents. *Nature* 466:935–940
87. Miller AA, Bundy GL, Mott JE, Skepner JE, Boyle TP et al (2008) Discovery and characterization of QPT-1, the progenitor of a new class of bacterial topoisomerase inhibitors. *Antimicrob Agents Chemother* 52:2806–2812
88. Chan PF, Srikannathasan V, Huang J, Cui H, Fosberry AP et al (2015) Structural basis of DNA gyrase inhibition by antibacterial QPT-1, anticancer drug etoposide and moxifloxacin. *Nat Commun* 6:10048
89. Miles TJ, Barfoot C, Brooks G, Brown P, Chen D et al (2011) Novel cyclohexyl-amides as potent antibacterials targeting bacterial type IIA topoisomerases. *Bioorg Med Chem Lett* 21:7483–7488
90. Miles TJ, Axten JM, Barfoot C, Brooks G, Brown P et al (2011) Novel amino-piperidines as potent antibacterials targeting bacterial type IIA topoisomerases. *Bioorg Med Chem Lett* 21:7489–7495
91. Miles TJ, Hennessy AJ, Bax B, Brooks G, Brown BS et al (2013) Novel hydroxyl tricyclics (e.g., GSK966587) as potent inhibitors of bacterial type IIA topoisomerases. *Bioorg Med Chem Lett* 23:5437–5441
92. Miles TJ, Hennessy AJ, Bax B, Brooks G, Brown BS et al (2016) Novel tricyclics (e.g., GSK945237) as potent inhibitors of bacterial type IIA topoisomerases. *Bioorg Med Chem Lett* 26:2464–2469
93. Ross JE, Scangarella-Oman NE, Flamm RK, Jones RN (2014) Determination of disk diffusion and MIC quality control guidelines for GSK2140944, a novel bacterial type II

- topoisomerase inhibitor antimicrobial agent. *J Clin Microbiol* 52:2629–2632
94. Jacobsson S, Golparian D, Alm RA, Huband M, Mueller J et al (2014) High in vitro activity of the novel spiropyrimidinetrione AZD0914, a DNA gyrase inhibitor, against multidrug-resistant *Neisseria gonorrhoeae* isolates suggests a new effective option for oral treatment of gonorrhoea. *Antimicrob Agents Chemother* 58:5585–5588
95. Huband MD, Bradford PA, Otterson LG, Basarab GS, Kutschke AC et al (2015) In vitro antibacterial activity of AZD0914, a new spiropyrimidinetrione DNA gyrase/topoisomerase inhibitor with potent activity against Gram-positive, fastidious Gram-negative, and atypical bacteria. *Antimicrob Agents Chemother* 59:467–474
96. Alm RA, Lahiri SD, Kutschke A, Otterson LG, McLaughlin RE et al (2015) Characterization of the novel DNA gyrase inhibitor AZD0914: low resistance potential and lack of cross-resistance in *Neisseria gonorrhoeae*. *Antimicrob Agents Chemother* 59:1478–1486
97. Godbole AA, Ahmed W, Bhat RS, Bradley EK, Ekins S et al (2015) Targeting *Mycobacterium tuberculosis* topoisomerase I by small-molecule inhibitors. *Antimicrob Agents Chemother* 59:1549–1557
98. Sandhaus S, Annamalai T, Welmaker G, Houghten RA, Paz C et al (2016) Small-molecule inhibitors targeting topoisomerase I as novel antituberculosis agents. *Antimicrob Agents Chemother* 60:4028–4036

DNA Supercoiling Measurement in Bacteria

Yingting Liu, Zhi-Chun Hua, and Fenfei Leng

Abstract

DNA supercoiling plays critical roles in several essential DNA metabolic pathways, such as replication, transcription and recombination. Typically plasmid DNA molecules are used to measure DNA supercoiling status inside bacterial cells. In this chapter, we describe how to isolate plasmid DNA molecules from *E. coli* cells and determine DNA supercoiling density by 1% agarose gel electrophoresis containing chloroquine using plasmid pACYC184 as an example.

Key words Agarose gel electrophoresis, DNA supercoiling, DNA topoisomers, Supercoiling density

1 Introduction

DNA supercoiling plays a key role in many essential DNA metabolic pathways including DNA replication, transcription, and recombination [1–6]. Many naturally occurring DNA molecules, such as plasmids, bacterial chromosomes, mitochondrial and chloroplast DNA, exist as closed circular DNA [7] and are usually negatively supercoiled, which is equivalent to unwinding of the right-handed DNA double helix, although those isolated from thermophilic archaea are positively supercoiled [8]. In *E. coli* or other bacteria, the supercoiling status of DNA is a result of counteractions of two topoisomerases, DNA topoisomerase I and gyrase [1–4].

As pointed out by James White [5, 6], DNA supercoiling can be described by one topological parameter, the linking number (Lk), and two geometric parameters, writhe (Wr) and Twist (Tw) [6–8]:

$$\text{Lk} = \text{Wr} + \text{Tw} \quad (1)$$

For definitions of Lk, Wr, and Tw, please refer to previous publications by White and colleagues for details [6]. If Lk_0 is the linking number for relaxed DNA, the linking number difference or linking difference (ΔLk) can be used to describe the negatively supercoiled DNA in solution:

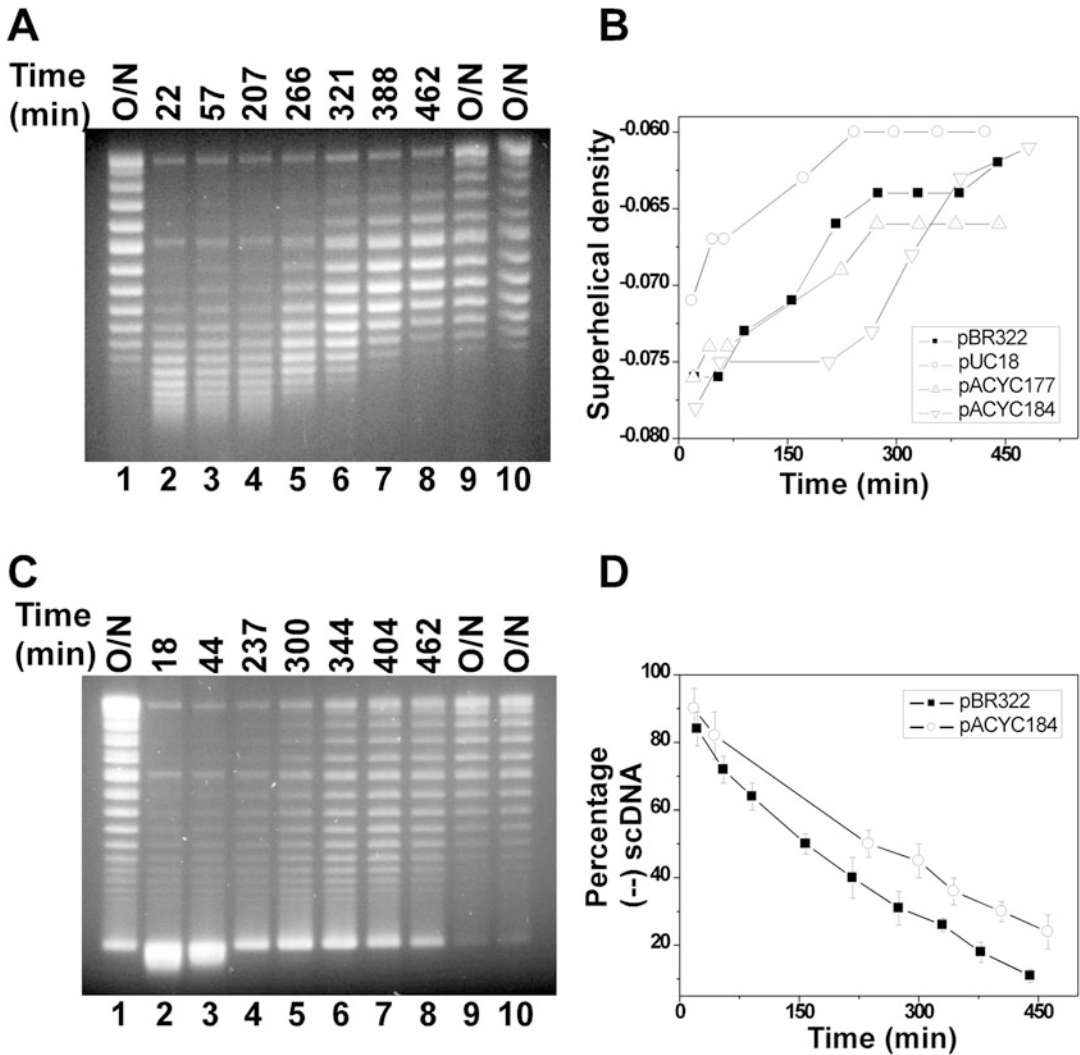


Fig. 1 Time courses of DNA supercoiling status in MG1655 (a, b) and VS111 (c, d). Overnight cultures of *E. coli* cells carrying plasmids pBR322, pUC18, pACYC177, or pACYC184 were diluted 100-fold in LB and grown to the time points indicated. The DNA molecules were isolated using the alkaline lysis assays using the QIAprep Spin Miniprep Kit. The DNA samples were subjected to 1% agarose gel electrophoresis in the presence of 5 $\mu\text{g/mL}$ of chloroquine. The DNA supercoiling densities were determined as detailed in Subheadings 3.3. The symbol of (--) represents the hypernegatively supercoiled DNA. O/N represents overnight

$$\Delta Lk = Lk - Lk_0 \tag{2}$$

Since ΔLk is dependent on the size of the DNA molecule, the specific linking difference or supercoiling (superhelical) density (σ), is used to describe DNA supercoiling:

$$\sigma = \Delta Lk / Lk_0 \tag{3}$$

To study DNA supercoiling in bacteria, we usually rely on the analysis of small circular DNA molecules. Figure 1 shows the time

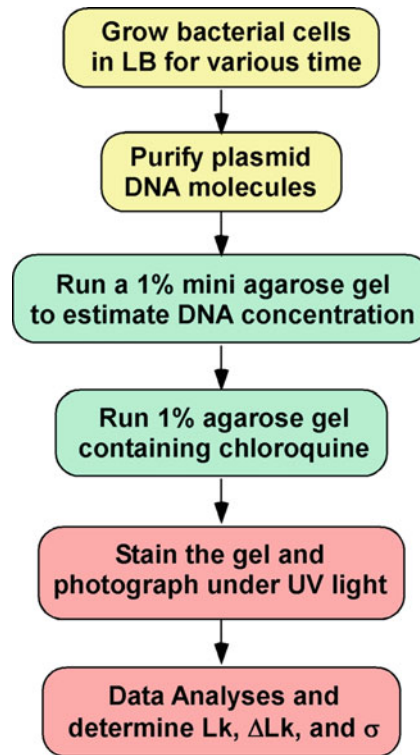


Fig. 2 An experimental procedure to determine the supercoiling density (σ) of plasmid DNA molecules isolated from bacterial cells

course of DNA supercoiling density of different plasmids in *E. coli*. In this chapter, we provide a detailed protocol to determine supercoiling density of plasmid DNA molecules in *E. coli*. Figure 2 shows an experimental procedure for this determination.

2 Materials

2.1 Extraction of Plasmid DNA Molecules from Bacterial Cells

1. *E. coli* strain FL#474: MG1655/pACYC184.
2. Luria–Bertani (LB) broth: dissolve 10 g of Bacto tryptone, 5 g of Bacto yeast extract, and 10 g of NaCl into 1 L of DI H₂O. Adjust pH to 7.0 with 5 M NaOH and autoclave. (The approximate volume of 5 M NaOH is 200 μ L).
3. Tetracycline solution (10 mg/mL): dissolve 100 mg tetracycline into 10 mL 70% ethanol.
4. Chloramphenicol solution (25 mg/mL): dissolve 250 mg Chloramphenicol into 10 mL ethanol.
5. A 37 °C air shaker.

6. A spectrophotometer (Cary 50 UV-Visible Spectrophotometer) and cuvettes.
7. QIAprep Spin Miniprep Kit or GeneJET Plasmid Miniprep Kit.
8. 50× TAE Buffer: dissolve 121 g of Tris base into 250 mL DI H₂O, and then add 28.6 mL of acetic acid and 50 mL of 0.5 M EDTA (pH 8.0) into the Tris base solution. Finally bring the total volume to 500 mL in a graduated cylinder with DI H₂O.
9. A microwave oven.
10. A UV-transparent gel tray (7 cm (W) × 10 cm (L) × 0.5 cm (H)).
11. 50 mL of 1% agarose gel: add 0.5 g of agarose into 50 mL 1× TAE in a conical flask. Heat the solution in a microwave oven for ~1 min to completely dissolve the agarose. Let the agarose solution cool down to ~55 °C and then pour the warm agarose solution into the UV-transparent gel tray mounted in a plastic mold supplied with the electrophoresis apparatus. Make sure the appropriate comb has been inserted into the tray. Allow the gel to solidify at room temperature.
12. Basic power supply for gel electrophoresis.
13. Ethidium bromide solution (10 mg/mL): dissolve 100 mg of ethidium bromide into 10 mL of DI H₂O with stirring overnight. Store at room temperature using a dark brown bottle to protect from light.
14. A UV transilluminator.
15. A gel documentation system (Kodak DEAS 290 gel imaging system) with a digital camera.
16. 6× gel loading dye: dissolve 25 mg of xylene cyanol, 25 mg of bromophenol blue, and 4 g of sucrose into 10 mL of DI H₂O. Store at 4 °C.
17. DNA marker: λ DNA HindIII Digest.

**2.2 DNA
Topoisomers
Resolution by 1%
Agarose Gel
Electrophoresis in 1×
TAE Containing
Chloroquine**

1. A CBS Scientific Co. SGU-040T-02 horizontal system for agarose gel electrophoresis.
2. A UV-transparent gel tray (18.5 cm (W) × 40 cm (L) × 0.5 cm (H)).
3. Chloroquine stock solution (10 mg/mL): dissolve 100 mg of chloroquine into 10 mL of DI H₂O, protect from light with aluminum foil. Store at 4 °C for 2 weeks.
4. 900 mL of 1% agarose gel containing 5 µg/mL Chloroquine: add 9 g of agarose into 900 mL 1× TAE in a conical flask. Heat the solution in a microwave oven for ~9 min to completely dissolve the agarose. Let the agarose solution cool down to ~55 °C and then add 450 µL of chloroquine stock solution into the agarose solution. Pour the warm agarose solution into the

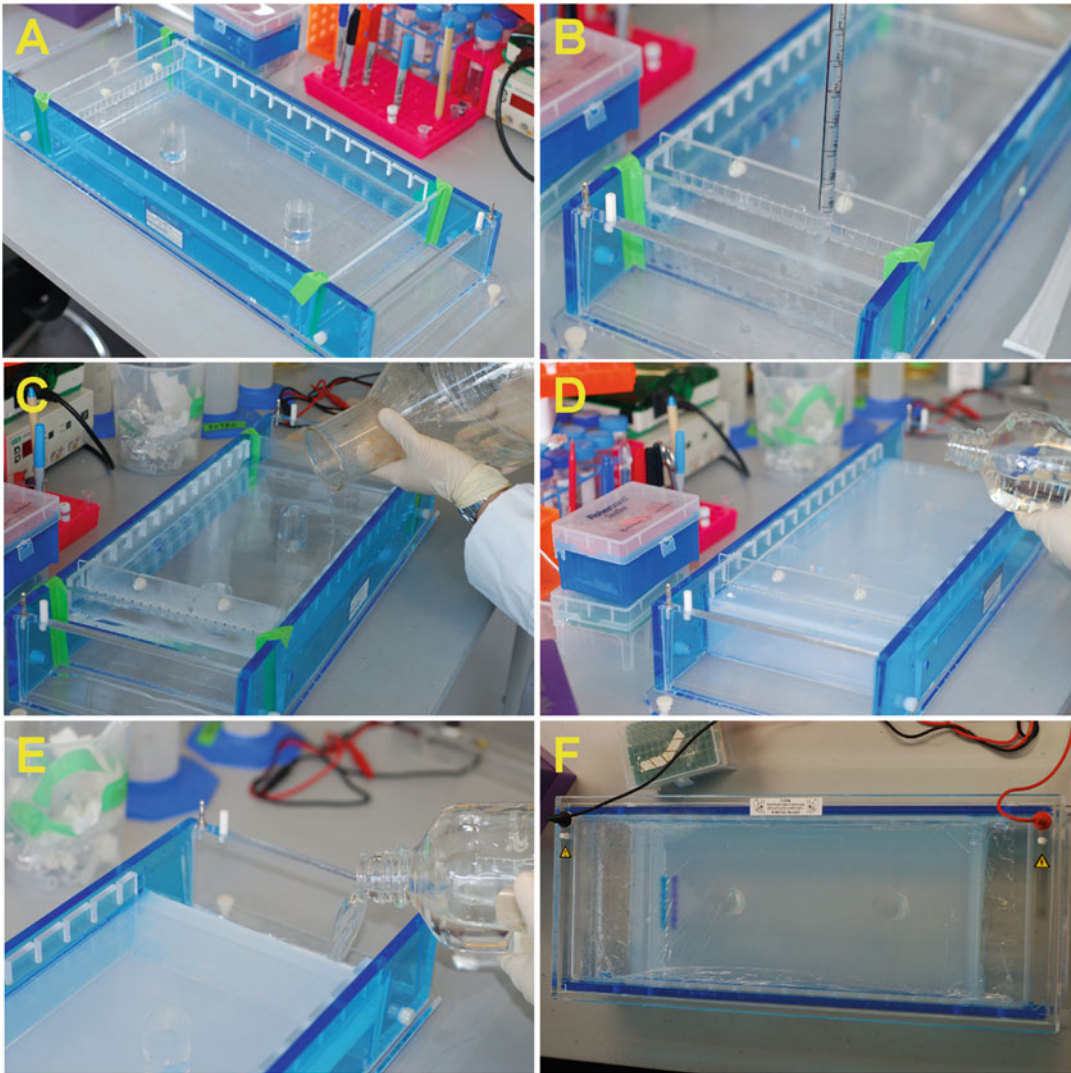


Fig. 3 Assembling of the non-submarine gel system and casting of the 1% agarose gel. (a) Assembling the modified gel system. (b) Making the agarose bridges between the gel and the TAE buffer reservoirs. (c) Pouring 1% agarose into the gel tray. (d) Adding 1× TAE on the gel surface to preventing it from drying. (e) Adding 1× TAE into reservoirs. (f) Running the gel. A layer of plastic membrane was used to cover the gel surface during gel electrophoresis

UV-transparent gel tray as described in Subheading 3.2 and Fig. 3. Allow the gel to solidify at room temperature.

5. Plastic film (Sarah wrap).

6. SYBR Gold or SYBR Green Nucleic Acid Gel Stain.

2.3 DNA Supercoiling Density Determination

1. 900 mL of 1% agarose gel containing 0, 0.5, 1, and 2.5 µg/mL chloroquine, respectively: add 9 g of agarose into 900 mL 1× TAE in a conical flask. Heat the solution in a microwave oven

for ~9 min to completely dissolve the agarose. Let the agarose solution cool down to ~55 °C and then add 0, 45, 90, and 225 µL of chloroquine stock solution into the agarose solution, respectively. Pour the warm agarose solution into the UV-transparent gel tray as described in Subheading 3.2 and Fig. 3. Allow the gel to solidify at room temperature.

2. BSA solution (100 µg/mL): dissolve 1 mg of BSA in 10 mL of DI-H₂O.
3. 10× topoisomerase I buffer: 200 mM Tris–acetate (pH 7.9), 500 mM KAc, 100 mM Mg(Ac)₂, 10 mM DTT, and 100 µg/mL BSA.
4. *E. coli* topoisomerase I (20 µM)
5. Phenol equilibrated with 10 mM Tris–HCl, pH 8.0, 1 mM EDTA.
6. Ethanol: absolute and 70%.
7. TE Buffer: 10 mM Tris–HCl, pH 8.0 and 1 mM EDTA.
8. 10 mM Tris–HCl, pH 8.5.
9. KODAK 1D Image Analysis Software.
10. Origin 7 professional software.

3 Methods

3.1 Purify Plasmid DNA Molecules from Bacterial Cells.

1. Inoculate 5 mL of LB containing appropriate antibiotics, for example 25 µg/mL of chloramphenicol and 10 µg/mL tetracycline, with a bacterial strain carrying a plasmid, such as *E. coli* strain FL#474 (MG1655/pACYC184), and grow the bacterial cells in an air shaker at 37 °C with vigorous agitation (250–300 rpm) overnight.
2. Inoculate 200 mL of LB containing 25 µg/mL of chloramphenicol and 10 µg/mL tetracycline with the overnight cell culture at 1:100 dilution. Grow the culture at 37 °C with vigorous agitation (250 rpm) to different time points, i.e., 30, 60, 120, 180, 240 min, and overnight. Determine the concentration of cells by measuring OD₆₀₀ with a spectrophotometer, such as Cary 50 UV-Visible Spectrophotometer, with the assumption of that 0.1 OD is equivalent to 1 × 10⁸ cells/mL.
3. Purify plasmid DNA molecules by alkaline lysis assay using a commercially available plasmid purification kit, such as QIAprep Spin Miniprep Kit or GeneJET Plasmid Miniprep Kit. For dilute cell samples, a floor centrifuge may be required to pellet bacterial cells. Otherwise, a desktop centrifuge is sufficient. Please follow the steps provided by manufacturers to purify

plasmid DNA molecules. We recommend using the same amount of bacterial cells for all samples for DNA purification. In the final step, use 50 μL of elution buffer (50 mM Tris-HCl, pH 8.5) to elute plasmid DNA. The eluted DNA samples can be used immediately or store at $-80\text{ }^{\circ}\text{C}$ for long-term storage (*see Note 1*).

4. To make a 1% agarose mini-gel (7 cm (W) \times 10 cm (L) \times 0.5 cm (H)), add 0.5 g of agarose into 50 mL of 1 \times TAE Buffer in a 200 mL conical flask. Heat the mixture in a microwave oven for about 1 min until the agarose is completely dissolved. Let agarose solution cool down to about $50\text{ }^{\circ}\text{C}$, usually ~ 5 min. Pour the warm gel solution into a UV-transparent gel tray (7 \times 10 cm) with an inserted comb and let it sit at room temperature until it has completely solidify (~ 30 min).
5. Run the purified DNA samples on the 1% agarose gel in 1 \times TAE buffer at 100 V for 90 min. After this step, the gel is stained by ethidium bromide for 45–60 min and photographed using a Kodak DEAS 290 gel imaging system. The DNA concentration of each sample is estimated by comparing their band density with those of a DNA standard on the same gel, such as λ DNA HindIII digest. If necessary, adjust all DNA samples to the same concentration using elution buffer (*see Note 2*).

3.2 DNA

Topoisomers

Resolution by 1%

Agarose Gel

Electrophoresis in 1 \times

TAE Containing

Chloroquine

1. A CBS Scientific Co. SGU-040T-02 horizontal system for agarose gel electrophoresis is used. Gel bed dimension is 18.5 cm (W) \times 40 cm (L) \times 0.5 cm (H). To make a 1% gel containing 5 $\mu\text{g}/\text{mL}$ of chloroquine, 9 g of agarose is added into 900 mL of 1 \times TAE in a 3800 mL conical flask. Heat the mixture in a microwave oven until the agarose is completely dissolved (~ 8 min). Cool the gel down to $55\text{ }^{\circ}\text{C}$ in a $55\text{ }^{\circ}\text{C}$ water bath (5–10 min), then add 450 μL of 10 mg/mL chloroquine solution into the gel and mix well. The gel system was slightly modified to run non-submarine gels to increase the separation resolution (Fig. 3). Two agarose bridges between the buffer reservoirs and the gel tray (Fig. 3b) are first made and the remaining gel solution is poured into the gel tray with a comb inserted (Fig. 3c), and solidified at room temperature. Remove the plates for the agarose gel bridges and the comb when the gel becomes solidified and ready to use (*see Note 3*).
2. Prepare 1500 mL of 1 \times TAE containing 5 $\mu\text{g}/\text{mL}$ of chloroquine. Add 1 \times TAE on the gel surface to prevent drying (Fig. 3d). Fill sample wells with 1 \times TAE. Add the rest of 1 \times TAE in the two reservoirs of the gel system (Fig. 3c).

3. Prepare DNA samples in 1× DNA loading dye. For instance, add 4 μL of 6× DNA loading dye to 20 μL of DNA sample and mix well. Load DNA samples in 1× DNA loading dye in each well.
4. Run the gel for 30 min at 140 V to allow the DNA samples to enter the gel. Then place a piece of plastic wrap (Saran Wrap is used in our lab) on the gel surface to prevent it from drying (Fig. 3f). After this step, run the gel for an additional 15–16 h at 110 V, usually overnight.
5. Stain the gel in 0.5 μg/mL Ethidium Bromide for ~3–4 h.
6. Visualize DNA bands under a UV light, and cut the gel to a smaller size to only keep the portion containing the DNA topoisomers.
7. Destain the gel in deionized water. Change deionized water frequently, for example once or twice per hour. If necessary, leave the gel in deionized water for overnight.
8. If necessary, stain the gel in SYBR Gold or SYBR Green for 1–3 h.
9. After the staining step, the gel is photographed using a gel documentation system, such as a Kodak DEAS 290 gel imaging system. The gel images may be analyzed by image analysis software, such as KODAK 1D Image Analysis Software.

3.3 DNA Supercoiling Density Determination

1. In order to determine the supercoiling density of a plasmid DNA molecule, it is required to generate a series of DNA samples with different supercoiling densities and resolve DNA topoisomers using 1% agarose gels containing various concentrations of chloroquine as described in Subheading 3.2. Here we use plasmid pACYC184 as an example.
2. 1.5 μg of supercoiled pACYC184 was relaxed at 37 °C for 1 h by *E. coli* topoisomerase I in 100 μL of topoisomerase I buffer in the presence of 0, 0.5, 1, 1.5, 2, 2.5, 5, and 7.5 μM of ethidium bromide (*see Note 4*).
3. Add an equal volume of phenol (100 μL) to stop the relaxation reactions. The DNA samples are centrifuged for 3 min at 13,400 rpm ($12,100 \times g$) at room temperature. The aqueous layers are transferred into new eppendorf centrifuge tubes. After adding 11 μL of 3 M NaAC, pH 5.3, the DNA samples are precipitated with 2 volumes of ethanol and centrifuged at 13,000 rpm at 4 °C for 15 min. The pellets are washed with 500 μL of 70% ethanol. After removing ethanol, the DNA samples were air dried for 10 min and dissolved into 85 μL of TE.
4. The topological status of each DNA sample was analyzed by electrophoresis in a 1% agarose gel in 1× TAE buffer in the presence of different concentrations of chloroquine (0, 0.5, 1, and 2.5 μg/mL).

5. Run the gel at 120 V for 16 h, usually overnight.
6. The gel was stained and photographed as described in Subheading 3.2. Figure 4 shows the gel images that were used to calculate σ of pACYC184.
7. The linking number (Lk_0) for relaxed pACYC184 was calculated to be 404 with an assumption of 10.5 bp per turn of DNA helix for relaxed B-form DNA [7]: $Lk_0 = 4245 \text{ bp} / 10.5 \text{ bp} = 404$ (the linking number is an integer).
8. Figures 1 and 4 were used to calculate the supercoiling density (σ) of pACYC184 isolated from *E. coli* strain FL#474. First, the topoisomers of lane 3 of Fig. 4b (that represents fully relaxed pACYC184 DNA, i.e., no Ethidium Bromide during relaxation with topoisomerase I) was used to determine Lk_0 by analyzing the intensity of the different DNA topoisomers. The intensity of DNA topoisomers were calculated by using KODAK 1D Image Analysis Software and then fit to a Gaussian distribution in Origin Data Analysis and Graphing Software (Fig. 5). The DNA linking number (Lk) was determined by band counting. σ was calculated by Eqs. 2 and 3.

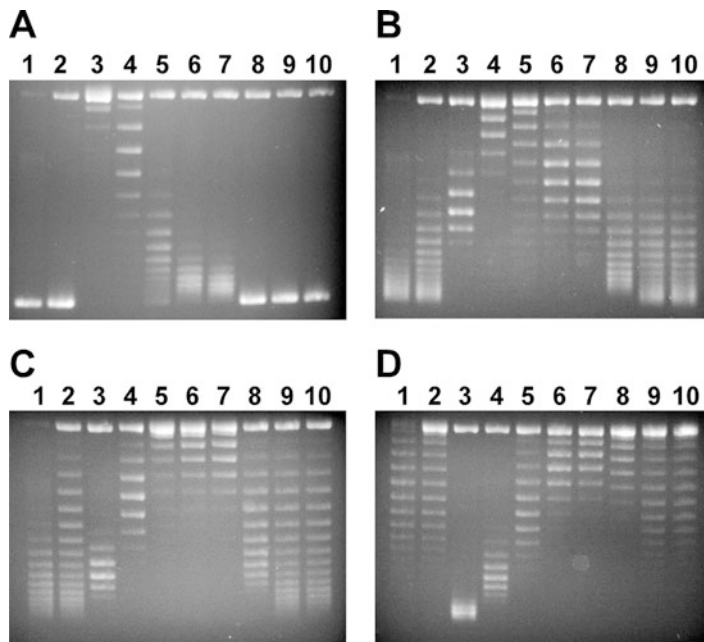


Fig. 4 Analysis of DNA topoisomers by using 1% agarose gel containing different concentrations of chloroquine. Briefly, negatively supercoiled plasmid pACYC184 DNA samples were relaxed by *E. coli* DNA topoisomerase in the presence of different concentrations of ethidium bromide (please see Subheading 3.3 for details). Panels (a), (b), (c), and (d) are 1% agarose gel in 1xTAE buffer containing 0, 0.5, 1, and 2.5 $\mu\text{g}/\text{mL}$ of chloroquine. Lanes 1 and 2 are negatively supercoiled pACYC184. Lanes 3 to 10 contain DNA samples relaxed by *E. coli* DNA topoisomerase I in the presence of 0, 0.5, 1, 1.5, 2, 2.5, 5, and 7.5 μM of ethidium bromide, respectively

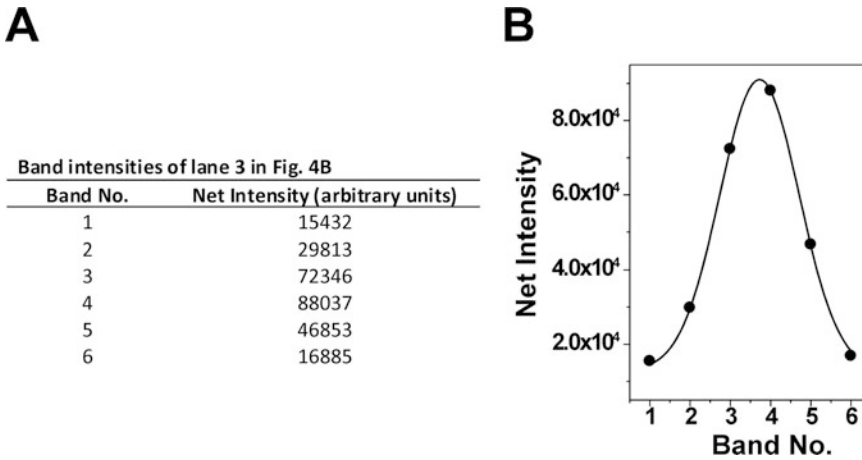


Fig. 5 Gaussian distribution of DNA topoisomers. (a) Band intensities of *lane 3* in Fig. 4b (the relaxed pACYC184) were calculated by using KODAK 1D Image Analysis Software and then (b) fit to Gaussian distribution in Origin Data Analysis and Graphing Software

4 Notes

1. It is critical to isolate plasmid DNA molecules as soon as the bacterial cell growth reaches the time point. The topological status of DNA molecules inside bacterial cells is always changing and therefore it is not recommended to store the cells at room temperature or on ice for an extended period of time. Also, since freeze and thaw will result in nicking plasmid DNA molecules, DNA samples should be stored at 4 °C for short-term storage.
2. It is always recommended to run a 1% mini gel to check the DNA concentrations for plasmid DNA molecules. Alternatively, DNA concentration can be determined by using a UV spectrophotometer.
3. In our hands, non-submarine gels always have a higher separation resolution for DNA topoisomers. Submarine gels can also be used to resolve DNA topoisomers.
4. Although *E. coli* DNA topoisomerase I was used here, eukaryotic DNA topoisomerase I, such as human topoisomerase I, may be used to relax DNA molecules. *E. coli* DNA topoisomerase I only relaxes negatively supercoiled DNA molecules.

References

1. Champoux JJ (2001) DNA topoisomerases: structure, function, and mechanism. *Annu Rev Biochem* 70:369–413
2. Snoep JL, van der Weijden CC, Andersen HW, Westerhoff HV, Jensen PR (2002) DNA supercoiling in *Escherichia coli* is under tight and

- subtle homeostatic control, involving gene-expression and metabolic regulation of both topoisomerase I and DNA gyrase. *Eur J Biochem* 269:1662–1669
3. Wang JC (1996) DNA topoisomerases. *Annu Rev Biochem* 65:635–692
 4. Zechiedrich EL, Khodursky AB, Bachellier S, Schneider R, Chen D, Lilley DM, Cozzarelli NR (2000) Roles of topoisomerases in maintaining steady-state DNA supercoiling in *Escherichia coli*. *J Biol Chem* 275:8103–8113
 5. White JH, Bauer WR (1986) Calculation of the twist and the writhe for representative models of DNA. *J Mol Biol* 189:329–341
 6. Cozzarelli NR, Boles TC, White JH (1990) A primer on the topology and geometry of DNA supercoiling. In: Cozzarelli NR, Wang JC (eds) *DNA topology and its biological effects*. Cold Spring Harbor Laboratory Press, Cold Spring Harbor, New York, pp 139–184
 7. Bates AD, Maxwell A (2005) *DNA topology*, 2nd edn. Oxford University Press, Oxford
 8. White JH, Cozzarelli NR, Bauer WR (1988) Helical repeat and linking number of surface-wrapped DNA. *Science* 241:323–327

DNA Catenation Reveals the Dynamics of DNA Topology During Replication

Alicia Castán, Pablo Hernández, Dora B. Krimer,
and Jorge B. Schwartzman

Abstract

Two-dimensional agarose gel electrophoresis is the method of choice to identify and quantify all the topological forms DNA molecules can adopt in vivo. Here we describe the materials and protocols needed to analyze catenanes, the natural outcome of DNA replication, in *Saccharomyces cerevisiae*. We describe the formation of pre-catenanes during replication and how inhibition of topoisomerase 2 leads to the accumulation of intertwined sister duplexes. This knowledge is essential to determine how replication forks blockage or pausing affects the dynamic of DNA topology during replication.

Key words *Saccharomyces cerevisiae*, Replication, Supercoiling, Catenation, 2D gels

1 Introduction

DNA catenation is the natural outcome of replication. Due to the double-stranded nature of DNA, for the genetic code to be copied the two parental strands must separate and this melting causes an increase of torsional tension ahead of the fork [1]. The accumulation of this positive (+) torsional tension is exacerbated when two forks progressing in opposite directions approach each other during termination. At some point topoisomerases simply have not enough space to bind and relax the DNA that remains to be replicated. It was suggested that one way to solve this problem is swiveling of the forks (Fig. 1) to diffuse the (+) torsional tension to the replicated region where it adopts the form of right-handed (RH) precatenanes [2]. Relaxation of the torsional tension ahead of the forks permits DNA replication to go on. Once replication is over, topoisomerase 2 would eliminate the remaining catenanes to allow sister duplexes segregation. There is still controversy, though, as to whether fork swiveling occurs all the way during replication [3] or only at the end as termination approaches [4]. In any case,

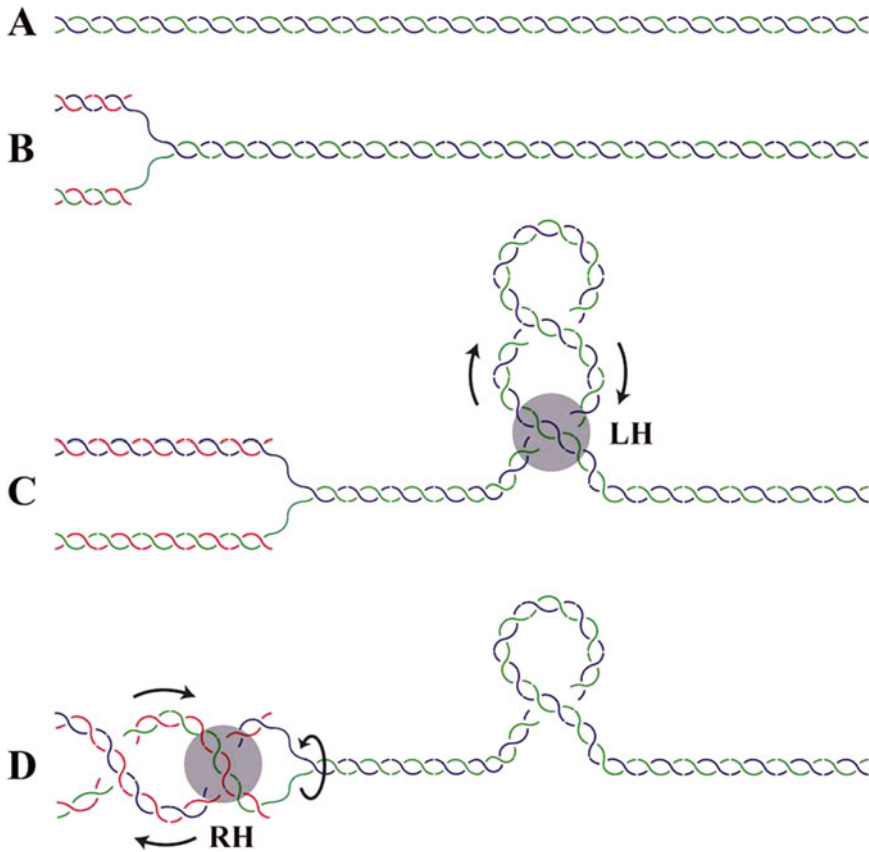


Fig. 1 Cartoons illustrating unreplicated and partially replicated molecules. (a) Unreplicated. (b) Partially replicated. (c) Progression of the replication fork generates positive (+) supercoiling showing left-handed (LH) crossings ahead. (d) Swiveling of the fork diffuses one LH crossing from the unreplicated to the replicated region, where it adopts the form of two precatenane right-handed (RH) crossings. Parental DNA is colored in blue and green and nascent DNA in red (reproduced from ref. 11 with permission from [plosone.org](https://doi.org/10.1371/journal.pone.0141111))

the final number of intertwines is directly related to the proficiency of replication progress. In other words, replication fork blockage or pausing affects precatenation and consequently the final number of catenane's intertwines. Under normal conditions replication and decatenation progress very fast and the only way to visualize catenanes is to inhibit topoisomerase 2 [5–10]. The inhibition of topoisomerase 2 can be accomplished exposing the cells to specific drugs or using conditional mutants. The latter method is preferable since drugs have secondary effects and usually cause single- and double-stranded DNA breakage [3]. The best method to identify catenated molecules so far is two-dimensional (2D) agarose gel electrophoresis (Fig. 2a). Unreplicated forms of intact circular DNA generate covalently closed monomers (CCCm) and dimers (CCCd) as well as open circles of monomers (OCm), dimers (OCd), and knotted molecules (Knm). All these forms are clearly

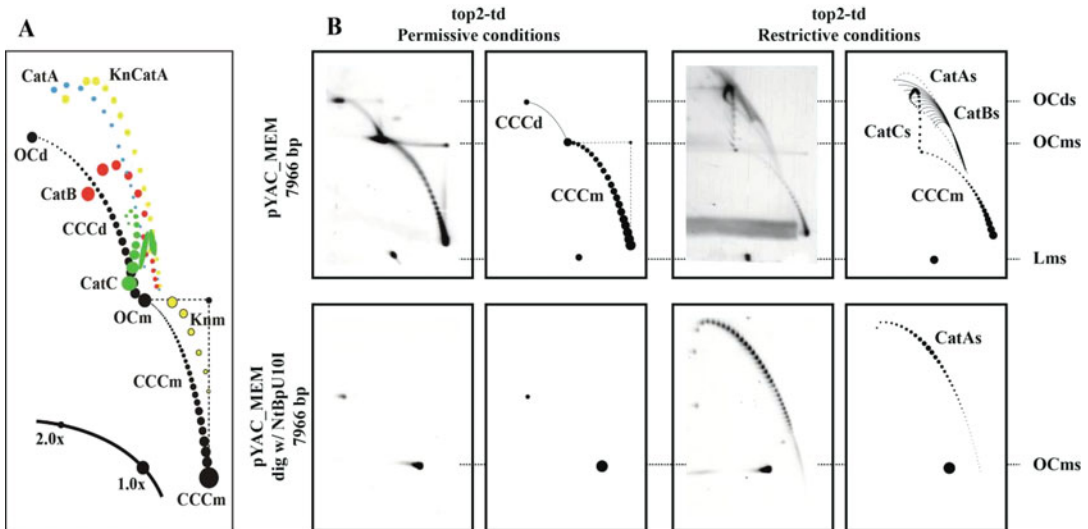


Fig. 2 Cartoons and immunograms illustrating the different patterns generated by the stereoisomers of undigested circular minichromosomes and linear DNA replication intermediates in 2D gels. **(a)** Linear forms ($1.0\times$ and $2.0\times$) and covalently closed monomers (CCCm) and dimers (CCCd) are depicted in *black*. CatA (catenanes where both rings are nicked) are depicted in *light blue*. CatB (catenanes where one ring is nicked and the other covalently closed) are depicted in *red*. CatC (catenanes where both rings are covalently closed) are depicted in *green*. KnCatA (nicked-catenanes where one or both rings are knotted) are depicted in *yellow*. And knotted monomers (Knm) are depicted in *black encircled yellow*. **(b)** Synchronized top2-td cells transformed with pYAC_MEM were fixed 80 min after their release into the S-phase under permissive (*left*) or restricted (*right*) conditions. Immunograms of 2D gels corresponding to undigested forms of pYAC_MEM are shown on top. The same DNA digested with the nicking enzyme NtBpU101 are shown on the bottom. The immunograms are shown together with corresponding diagrammatic interpretations of the most prominent signals to their right (reproduced from ref. 11 with permission from [plosone.org](https://doi.org/10.1371/journal.pone.0111111))

identified in 2D gels (Fig. 2a). The inhibition of DNA segregation leads to the accumulation of three forms of catenated molecules [5–10]: CatAs, formed by two intertwined OCs; CatBs, formed by two intertwined circles one of which is an OC and the other a CCC; and CatCs, formed by two intertwined CCCs. Exposure of all these isolated forms to a restriction endonuclease that causes single-stranded breakage (nicks) converts all catenated forms to CatAs where each dot of increased mobility in the arc corresponds to the addition of one catenation. The immunograms shown to the right in Fig. 2 correspond to intact circular forms of pYAC_MEM isolated from a top2-td strain of *Saccharomyces cerevisiae* [7, 11]. It is clearly seen that minichromosomes isolated from cells grown at the permissive temperature mainly occur as CCCm and CCCd (Fig. 2b). Nicking of these molecules converts all of them to OCm and OCd. Minichromosomes isolated from cells grown at the restrictive conditions occur as CCCm but also as catenated forms: CatAs, CatBs, and CatCs. Finally, nicking of

these molecules converts all catenated forms to CatAs allowing the precise quantification of the intertwined forms, over 50 in the corresponding immunogram.

2 Materials

2.1 *Yeast Transformation*

1. YEP medium: 1% yeast extract, 2% peptone, 60 mg/mL adenine, pH 6.5, and 40% raffinose (Raf).
2. TE: 10 mM Tris-HCl, 1 mM EDTA, pH 7.5.
3. 1 M lithium acetate (LiAc) pH 7.5 stored at 4 °C.
4. 10 mg/mL sonicated and denatured salmon sperm DNA stored at 4 °C.
5. 50% PEG (polyethylene glycol 6000) stored at 4 °C.
6. DMSO (dimethyl sulfoxide).
7. Appropriate selective medium.
8. Appropriate selective medium agar plates with 2% Raf.

2.2 *Transformation Checking*

2.2.1 *Rapid DNA Isolation*

1. Appropriate selective medium.
2. 40% Raf.
3. Breaking buffer: 2% Triton X-100, 1% SDS, 100 mM NaCl, 10 mM Tris-HCl pH 8.0, and 1 mM EDTA pH 8.0.
4. P-CIA: 25:24:1 v/v (phenol-chloroform-isoamyl alcohol) stored at 4 °C.
5. Glass beads (0.5 mm of diameter).
6. FastPrep[®]-24 Instrument.
7. TEN 100: 100 mM NaCl, 10 mM Tris-HCl pH 8.0, and 1 mM EDTA pH 8.0.
8. CIA: 24:1 v/v (chloroform-isoamyl alcohol) stored at 4 °C.
9. 100% ethanol.
10. 10 mg/mL RNase A stored at -20 °C.

2.2.2 *Unidimensional Agarose Gel Electrophoresis*

1. Agarose (Seakem LE, Lonza).
2. 5× TBE (Tris-Borate-EDTA): 0.445 M Tris base, 0.445 M boric acid, and 0.01 M EDTA pH 8.0.
3. 10× gel loading buffer: 0.1% xylene cyanol, 0.1% bromophenol blue, 30% glycerol, and 10 mM EDTA pH 8.0.

2.2.3 *Southern Blotting*

1. 37% hydrochloric acid fuming.
2. 4 M sodium hydroxide.

3. 20× SSC (saline sodium citrate): 3 M sodium chloride and 0.3 M tri-sodium citrate.
4. Whatman 3MM paper.
5. Zeta-Probe blotting membranes (Bio-Rad).

2.2.4 Nonradioactive Hybridization

1. Digoxigenin-High Prime kit (Roche).
2. 20× SSPE (saline sodium phosphate EDTA): 3.6 M sodium chloride, 0.2 M disodium phosphate, 20 mM EDTA pH 8.0.
3. 10% Blotto (nonfat powdered milk).
4. 20% SDS (sodium dodecyl sulfate).
5. 20% dextran sulfate stored at 4 °C.
6. 10 mg/mL sonicated and denatured salmon sperm DNA stored at 4 °C.
7. 20× SSC (saline sodium citrate): 3 M sodium chloride and 0.3 M tri-sodium citrate.
8. Antidigoxigenin-AP conjugate antibody stored at 4 °C.
9. CDP-Star (PerkinElmer) stored at 4 °C.

2.3 α -factor Synchronization

1. Appropriate selective medium.
2. 40% Raf.
3. YEP medium: 1% yeast extract, 2% peptone, 60 mg/mL adenine, pH 6.5.
4. 5 mg/mL α -factor.
5. 10% sodium azide.
6. 40% galactose (Gal).
7. 10 mg/mL doxycycline.

2.4 Minichromosome DNA Extraction

1. NIB (nuclear isolation buffer): 17% glycerol (v/v), 50 mM MOPS, 150 mM KAc, 2 mM MgCl₂, 500 mM spermidine, 150 mM spermine stored at 4 °C.
2. Glass beads (0.5 mm of diameter).
3. TEN 50-50-100: 50 mM Tris, 50 mM EDTA pH 8.0, 100 mM NaCl.
4. 30% sarcosyl.
5. Proteinase K (Roche).
6. P-CIA: 25:24:1 v/v stored at 4 °C.
7. CIA: 24:1 v/v stored at 4 °C.
8. 100% ethanol.
9. 10 mg/mL RNase A.

2.5 DNA Treatments

1. Appropriate endonuclease nicking enzyme.
2. Appropriate restriction buffer.

2.6 Two-Dimensional Agarose Gel Electrophoresis

1. Agarose (Seakem LE; Lonza).
2. 5× TBE (Tris–Borate–EDTA): 0.445 M Tris base, 0.445 M boric acid, and 0.01 M EDTA pH 8.0.
3. 10× gel loading buffer: 0.1% xylene cyanol, 0.1% bromophenol blue, 30% glycerol, and 10 mM EDTA, pH 8.0.

3 Methods**3.1 Yeast Transformation**

1. Transfect competent *S. cerevisiae* cells with monomeric forms of the minichromosomes to study (*see Note 1*).
2. Inoculate and grow the yeast strain in YEP medium containing 2% Raf 16–20 h at 25 °C (OD₆₀₀ has to be >1.5).
3. Dilute in 300 mL of YEP medium containing 2% Raf to get a OD₆₀₀ = 0.2–0.3.
4. Grow the culture at 25 °C up to an OD₆₀₀ = 0.5–0.6.
5. Centrifuge 50 mL in a 50 mL Falcon tube at room temperature and 1000 × *g* for 5 min.
6. Throw out the supernatant, wash the cells with 50 mL of sterile cold distilled water and centrifuge again in the same conditions.
7. Resuspend the pellet in 3 mL of 1× TE pH 7.5 and transfer 1.5 mL to a 1.5 mL Eppendorf tube.
8. Centrifuge in a microfuge at room temperature and maximum speed for 30 s.
9. Carefully resuspend the pellet in 600 µL of 1× TE/1× LiAc.
10. Mix in a Falcon tube 300–500 ng of plasmid DNA, 100 µg of denatured salmon sperm DNA, and 50 µL of competent cells.
11. Add 0.5 mL of 40% PEG/1× TE/1× LiAc and mix well.
12. Incubate the tube at 25 °C for 30 min.
13. Add 20 µL of DMSO, mix carefully and incubate at 42 °C for 15 min with moderate agitation.
14. Transfer to a sterile Eppendorf tube and centrifuge at maximum speed for 30 s.
15. Resuspend the pellet in 1 mL of appropriate selective medium containing 2% Raf and transfer to a new Falcon tube.
16. Incubate it at 25 °C for 1 h and transfer to a sterile Eppendorf tube.
17. Centrifuge in a microfuge at room temperature and maximum speed for 30 s and throw out 700 µL of supernatant.

18. Resuspend the pellet in the remaining supernatant and spread the cells on two agar plates containing the appropriate selective medium with 2% Raf (200 μ L in one plate and 100 μ L in another plate) to select for cells that incorporated the minichromosome.
19. Incubate at 25 °C for 2–3 days.
20. Streak single colonies on a new agar plate containing the appropriate selective medium with 2% Raf to generate enough cells for the next steps.

3.2 Transformation Checking

3.2.1 Rapid DNA Isolation

1. Inoculate and grow one colony in 15 mL of appropriate selective medium containing 2% Raf (as many tubes as colonies you want to check) overnight at 25 °C (OD_{600} has to be >3).
2. Harvest the cells by centrifugation at 4 °C and $1000 \times g$ for 10 min.
3. Throw out the supernatant and wash the cells with 1 mL of sterile cold distilled water and centrifuge again in the same conditions.
4. Transfer the volume to an Eppendorf tube with screw cap and centrifuge in a microfuge at maximum speed for 20 s.
5. Resuspend the pellet in 200 μ L of breaking buffer and add 0.3 g of glass beads and 200 μ L of P-CIA.
6. Lyse the cells in a FastPrep[®]-24 Instrument (2 cycles at 4 °C and 4 m/s for 20 s, waiting 20 s between cycles).
7. Add 200 μ L of TEN100 and centrifuge samples in a microfuge at room temperature and maximum speed for 5 min.
8. Transfer the supernatant to a fresh Eppendorf tube with screw cap.
9. Extract the proteins at least twice with equilibrated P-CIA pH 8.0, and once with CIA.
10. Precipitate the DNA with 2.5 volumes of cold absolute ethanol overnight at -20 °C.
11. Centrifuge and resuspend the pellet in ultra-pure water containing 1 mg/mL of RNase A.
12. Incubate at 37 °C for 1 h.

3.2.2 Unidimensional Agarose Gel Electrophoresis

1. Assemble a gel casting set with a 20-teeth (0.5×0.15 cm each) comb and pour a 0.6% agarose gel prepared in $1 \times$ TBE buffer. Let the gel solidify.
2. Place the gel into a gel tank and pour $1 \times$ TBE buffer to cover the gel. Carefully remove the comb.

3. Add 1× gel loading dye to the DNA samples and load the samples into the wells. Load your samples in both the uncut and cut form. The controls are the material which was used to transform the yeast (uncut and cut).
4. Run at 0.8 V/cm at room temperature for 15–20 h (depending on the minichromosome size).

3.2.3 Southern Blotting

1. To depurinate the DNA prior to transfer, submerge the gels for 15 min in 500 mL of 0.25 M hydrochloric acid with moderate shaking at room temperature.
2. Next, set up the blot transfer as follows avoiding the formation of air bubbles: Place three sheets of Whatman 3 MM paper that has been soaked with 0.4 M sodium hydroxide on top of a “bridge” that rests in a shallow reservoir of 0.4 M sodium hydroxide. Place the gel on top of the three soaked sheets of Whatman 3 MM paper. Roll a sterile pipette over the sandwich to remove all air bubbles that often form between the gel and the paper. Cut a piece of positively charged Zeta-probe blotting membrane to the size of the gel. Presoak the membrane in distilled water and place it on top of the gel. Use a pipette to eliminate air bubbles as above. Complete the blot assembly by adding three sheets of Whatman 3 MM paper soaked in 0.4 M sodium hydroxide, a stack of paper towels, a glass plate, and a 200–500 g weight (*see Note 2*).
3. Allow the blot to transfer overnight in transfer buffer (0.4 M sodium hydroxide).
4. After the transfer, peel the membrane from the gel; rinse it twice in 2× SSC for 5 min.

3.2.4 Nonradioactive Hybridization

1. Label the DNA probes with digoxigenin using the DIG-High Prime kit (Roche) according to manufacturer's recommendations.
2. Meantime, prehybridize the membranes in a 20 mL prehybridization solution (2× SSPE, 0.5% Blotto, 1% SDS, 10% dextran sulfate, and 0.5 mg/mL sonicated and denatured salmon sperm DNA) in hybridization bottles on a rotisserie inside a hybridization oven set at 65 °C for 4–6 h.
3. Denature the labeled DNA probe by heating it at 95–100 °C for 5 min and chill it quickly in an ice bath.
4. Add the probe to the hybridization bottles, place the bottles back into the oven and hybridize for 12–16 h.

5. Wash the hybridized membranes sequentially with $2 \times$ SSC and 0.1% SDS at room temperature for 5 min twice, and then twice with $0.1 \times$ SSC and 0.1% SDS at 68 °C for 15 min.
6. Perform the detection with an antidigoxigenin-AP conjugate antibody (Roche) and CDP-Star (PerkinElmer) according to the instructions provided by the manufacturer.

3.3 α -factor Synchronization

3.3.1 In the Presence of Topo 2

1. Inoculate and grow the yeast strain in 20 mL of appropriate selective medium containing 2% of Raf at 25 °C until saturation.
2. In 150 mL of selective medium containing 2% of Raf and grow the cells at 25 °C to an OD_{600} of 0.7 (14–16 h).
3. Dilute to an OD_{600} of 0.03 in 300 mL of YEP medium with 2% of Raf and grow at 25 °C until midlog ($OD_{600} = 0.7$).
4. Add 5 $\mu\text{g}/\text{mL}$ of α -factor to arrest cells at G1 and incubate them at 25 °C until 90% or more have *shmoo* morphology (approximately 3 h).
5. Harvest the cells by centrifugation at room temperature and $1700 \times g$ for 2 min.
6. Wash the cells 4 times with the same volume of YEP medium with 2% Raf to remove the α -factor and start the release.
7. Incubate them at 25 °C for 80 min. Time 0 was defined as the time of the first wash.
8. Add 0.1% of sodium azide to stop the growth and harvest the cells by centrifugation at 4 °C and $1300 \times g$ for 10 min.
9. Wash the cells twice with cold sterile distilled water (after this step the cells can be frozen at -80 °C).

3.3.2 In the Absence of Topo 2

1. To accomplish inhibition of topo 2 start growing top2-td cells as described before until α -factor addition. In this case 100–120 min after α -factor addition (~50% of cells have *shmoo* morphology) add 2% galactose to express the degron ligase ubiquitin and incubate at 25 °C for 30–45 min (until ~90% of cells have *shmoo* morphology).
2. Add 50 $\mu\text{g}/\text{mL}$ doxycycline to repress the top2 gen promoter and incubate at 25 °C for 30 min.
3. Transfer the culture to the restrictive temperature (37 °C) and incubate for 90 min to induce the degron ligase ubiquitin.
4. Harvest cells by centrifugation at room temperature and $1700 \times g$ for 2 min.
5. To start the release wash the cells 4 times with YEP medium with 2% of Gal and 50 $\mu\text{g}/\text{mL}$ doxycycline at 37 °C.
6. Incubate at 37 °C for 80 min.

7. Add 0.1% of sodium azide to stop the growth and harvest the cells by centrifugation at 4 °C and $1300 \times g$ for 10 min.
8. Wash the cells twice with cold sterile distilled water (after this step the cells can be frozen at -80 °C).

3.4 Minichromosome DNA Extraction

1. Resuspend the cells in cold NIB to get a 2.0×10^9 cells/mL final concentration and add the same volume of glass beads.
2. Shake the tubes in a vortex shaker at 4 °C and maximum speed for 30 s. Put the tubes on ice for 30 s. Repeat this step until you get 90% broken yeasts (check under the microscope).
3. Transfer the supernatant to a clean tube and wash the glass beads twice using the same NIB volume. Save the washes.
4. Pool the two washes with the original supernatant.
5. Centrifuge at 4 °C and $4500 \times g$ for 20 min.
6. Resuspend the pellet in 5 mL of preheated (37 °C) TEN50-50-100 containing 1.5% of sarcosyl.
7. Add 300 µg/mL proteinase K and mix carefully.
8. Incubate at 37 °C for 1 h and centrifuge at 4 °C and $1700 \times g$ for 5 min.
9. Transfer the supernatant to a clean tube and centrifuge again in the same conditions.
10. Extract the proteins at least three times with equilibrated P-CIA at pH 8.0, and once with CIA.
11. Precipitate the DNA with 2.5 volumes of cold absolute ethanol overnight at -20 °C.
12. Centrifuge and resuspend the pellet in ultra-pure water containing 1 mg/mL of RNase A.
13. Incubate at 37 °C for 1 h.
14. Precipitate the DNA with 2.5 volumes of cold absolute ethanol overnight at -20 °C and resuspend it in ultrapure water containing 1 mg/mL of RNase A.
15. Incubate at 37 °C for 1 h.

3.5 DNA Treatments

Add the endonuclease nicking enzyme and perform the reaction according to the instructions provided by the manufacturer.

3.6 Two- Dimensional Agarose gel Electrophoresis

1. The first dimension is as described in Subheading [3.2.2](#) but using 0.4% agarose concentration gel and running it at 0.4 V/cm for 22–28 h (*see* **Note 3**).
2. Stop the first dimension run.
3. Take the gel-casting tray with the gel out of the tank and place it on a clean surface. Cut out each migration lane from the first dimension and place each of them on top of one gel casting tray

oriented 90° with respect to the first dimension, so that the well of the first dimension slice is on the left side of the second dimension.

4. Melt 0.5–1.2% agarose gel in $1\times$ TBE, cool it down to $50\text{--}55^\circ\text{C}$ and pour over the slices from the first dimension. Let the gel solidify.
5. Place the gel into a gel tank and pour cold $1\times$ TBE to cover the gel.
6. Run the second dimension at $0.9\text{--}5\text{ V/cm}$ at 4°C for $8\text{--}14\text{ h}$ (depending on the minichromosome size).
7. After electrophoresis, perform Southern blotting (Subheading 3.2.3) and nonradioactive hybridization (Subheading 3.2.4).

4 Notes

1. As described by Murray and Szostak in 1983 [12], a circular artificial minichromosome needs specific elements to replicate extrachromosomally in an autonomous manner:
 - (a) ARS (autonomously replicating sequence): This element acts as a replication origin and confers the ability to replicate extra-chromosomally.
 - (b) CEN (centromere): increases mitotic stability. Without this element minichromosomes are mitotically unstable and are rapidly lost when there is no selective pressure. The presence of CEN also controls copy number which is $20\text{--}50$ copies per cell in its absence but only $1\text{--}2$ copy per cell in its presence.
 - (c) In addition the minichromosome must bear a gene allowing to select the cells that have incorporated the minichromosome after transformation.
 - (d) The minichromosome should also carry a replication origin active in *E. coli* cells and a selectable marker.
2. Make sure there is no shortcut between the transfer buffer and the paper towels, i.e., they should not touch each other. The capillary force created by the dry paper towels has to go through the gel only, for the DNA to migrate from the gel to the membrane. A cling film or other wrap is often placed around the gel to prevent short-cuts.
3. Intact circular DNA molecules are analyzed in N/N 2D gels as described before [13]. Electrophoresis conditions, though, vary significantly depending on the mass of the molecules to be analyzed. Finding the correct electrophoresis conditions for small or large molecules may require some experimentation using molecules of known masses. In our hands, for molecules

~2.5 Kbp the first dimension is usually run in a 0.5% agarose gel at 1 V/cm for approximately 20–24 h. The second dimension is run in a 1.2% agarose gel at 5–6 V/cm for 8–12 h at 4 °C. Molecules larger than 6–8 Kbp must be run under conditions of lower agarose concentration and lower voltage in both dimensions in order to separate the different topoisomers successfully. For example, for plasmids of ~10 Kbp the first dimension is usually run in a 0.28% agarose gel at 0.45 V/cm for approximately ~70 h. The second dimension is run in a 0.58% agarose gel at 0.9 V/cm for ~90 h at room temperature.

Acknowledgments

This work was supported by grant BFU2014-56835 from the Spanish Ministerio de Economía y Competitividad to JBS. We thank Jonathan Baxter and Luis Aragón for plasmids and DNA sequence data. The authors also acknowledge Alicia Rodríguez-Bernabé for technical help.

References

- Schwartzman JB, Stasiak A (2004) A topological view of the replicon. *EMBO Rep* 5:256–261
- Champoux JJ, Been MD (1980) Topoisomerases and the swivel problem. In: Alberts B (ed) *Mechanistic studies of DNA replication and genetic recombination*, ICN-UCLA symposium on molecular and cellular biology. Academic Press, New York, pp 809–815
- Cebrián J, Castán A, Martínez V, Kadomatsu-Hermosa MJ, Parra C, Fernández-Nestosa MJ, Schaerer C, Hernández P, Krimer DB, Schwartzman JB (2015) Direct evidence for the formation of precatenanes during DNA replication. *J Biol Chem* 290:13725–13735
- Schalbetter SA, Mansoubi S, Chambers AL, Downs JA, Baxter J (2015) Fork rotation and DNA precatenation are restricted during DNA replication to prevent chromosomal instability. *Proc Natl Acad Sci U S A* 112:4565–4570
- Adams DE, Shekhtman EM, Zechiedrich EL, Schmid MB, Cozzarelli NR (1992) The role of topoisomerase-IV in partitioning bacterial replicons and the structure of catenated intermediates in DNA replication. *Cell* 71:277–288
- Baxter J, Diffley JF (2008) Topoisomerase II inactivation prevents the completion of DNA replication in budding yeast. *Mol Cell* 30:790–802
- Baxter J, Sen N, Martínez VL, De Carandini ME, Schwartzman JB, Diffley JF, Aragón L (2011) Positive supercoiling of mitotic DNA drives decatenation by topoisomerase II in eukaryotes. *Science* 331:1328–1332
- Martínez-Robles ML, Witz G, Hernández P, Schwartzman JB, Stasiak A, Krimer DB (2009) Interplay of DNA supercoiling and catenation during the segregation of sister duplexes. *Nucleic Acids Res* 37:5126–5137
- Sundin O, Varshavsky A (1980) Terminal stages of SV40 DNA replication proceed via multiply intertwined catenated dimers. *Cell* 21:103–114
- Sundin O, Varshavsky A (1981) Arrest of segregation leads to accumulation of highly intertwined catenated dimers dissection of the final stages of SV40 DNA replication. *Cell* 25:659–669
- Cebrián J, Monturus E, Martínez-Robles ML, Hernández P, Krimer DB, Schwartzman JB (2014) Topoisomerase 2 is dispensable for the replication and segregation of small yeast artificial chromosomes (YACs). *PLoS One* 9:e104995
- Murray AW, Szostak JW (1983) Construction of artificial chromosomes in yeast. *Nature* 305:189–193
- Martín-Parras L, Lucas I, Martínez-Robles ML, Hernández P, Krimer DB, Hyrien O, Schwartzman JB (1998) Topological complexity of different populations of pBR322 as visualized by two-dimensional agarose gel electrophoresis. *Nucleic Acids Res* 26:3424–3432

Chapter 6

Mapping *E. coli* Topoisomerase IV Binding and Activity Sites

Hafez El Sayyed and Olivier Espéli

Abstract

This methods article described a protocol aiming at mapping *E. coli* Topoisomerase IV (Topo IV) binding and cleavage activity sites on the genome. The approach is readily applicable to any Type II topoisomerase on a broad variety of gram-positive and gram-negative bacterial species. Conventional ChIP-seq of flag tagged Topo IV subunits and a novel method aimed at trapping only DNA bound to active Topo IV (called NorfliP) are described. NorfliP relies on the ability of norfloxacin, a quinolone drug, to cross-link the 5' ends of the DNA breaks with the catalytic tyrosine of bacterial Type II topoisomerases. These methods give complementary results and their combination brought important insights on both the function and regulation of Topo IV.

Key words Topoisomerase IV, ChIP-seq, NorfliP, Norfloxacin

1 Introduction

Topoisomerase IV is the main chromosome decatenase of *E. coli* and most bacteria [1]. Topo IV is a heterotetramer formed by dimers of ParC and ParE subunits [2] which present a high degree of structural homology with the GyrA and GyrB subunits of DNA gyrase, respectively. Alteration of Topo IV leads to severe chromosome segregation defects [2] but do not halt chromosome replication [3]. Recently a role for Topo IV in the segregation of replicating sister chromatids has been demonstrated [3, 4]. It is therefore proposed that Topo IV works behind replication forks to remove precatenation links [5, 6] that are formed by the rotation of the replication fork when DNA gyrase cannot eliminate the positive superhelical tension generated by replication. Sister chromatids segregation is not a homogeneous process in *E. coli*, some regions of the chromosome appear to segregate a long time after their replication while some others segregate within minutes following their replication. Among the late segregation regions is the SNAPs regions that are enriched for GATC sequences that might recruit high amounts of SeqA protein that would inhibits Topo IV

[7]. The terminus region of the chromosome also exhibits late segregation due to a combination of events: (i) the MatP-septal ring interaction [8]; (ii) the MatP-MukB interaction and (iii) the MukB-Topo IV interaction [9]. These observations suggested that the decatenation activity of Topo IV is highly regulated in time and space. This is in good agreement with observations that Topo IV works preferentially late in the cell cycle [10] and in the chromosome terminus region at the *dif* site [12]. To get more insight into Topo IV regulation, we performed whole genome analysis of Topo IV binding and cleavage activity [11]. Topo IV has access to most of the genomic regions of *E. coli* but only selectively cleaves distinct genomic regions. Among the cleaved sites is the *dif* site which is by far the strongest, confirming that for almost every cell cycle, decatenation events take place at *dif* on fully replicated chromosomes. To verify these observations we performed ChIP seq experiments and developed a new Topo IV-DNA co-immunoprecipitation method aimed at trapping only active Topo IV (which we called NorfliP). These two methods are described in the present protocol.

2 Materials

All solutions must be prepared using ultrapure water (by purifying deionized water, to attain a sensitivity of 18 M Ω -cm at 25 °C).

Prepare the following buffers and stock solutions. Unless otherwise specified, filter solutions using a 0.2 μ m low protein binding nonpyrogenic membranes.

2.1 Strains

1. MG1655 *parE::flag* [11].
2. MG1655 *parC::flag*.
3. MG1655 *nalR parE::flag* (see Note 1).
4. MG1655 *nalR parC::flag*.
5. MG1655 *parC::3xflag* (see Note 2).

2.2 Culture Preparation and Fixation

1. LB broth.
2. 20% glucose in H₂O.
3. 20% casaminoacids in H₂O.
4. 10 \times Minimum Medium A: for 1 L, 35 g KH₂PO₄, 10 g K₂HPO₄, 3 g tri-sodium citrate, 0.5 g MgSO₄, 5 g (NH₄)₂SO₄.
5. Norfloxacin 10 mM.
6. Formaldehyde 37% (Sigma) fresh bottle.
7. Glycine 2.5 M sterilized.

2.3 DNA Shearing

1. Ice- cold PBS buffer 1×.
2. Ready-Lyse™ Lysozyme Solution (Epicentre® Biotechnologies).
3. ChIP lysis buffer: 50 mM Tris-HCl pH 7.4, 150 mM NaCl, 1 mM EDTA, 1% Triton X-100, 1 pill/50 mL buffer cComplete protease inhibitor cocktail (Roche).
4. 1.5 mL Bioruptor® Plus TPX microtubes (Diagenode).
5. Bioruptor® sonicator (Diagenode).
6. Eppendorf® LoBind microcentrifuge tubes Protein, volume 1.5 mL (Sigma).

2.4 Immuno-precipitation and Elution

1. Agarose Anti-FLAG M2 (Sigma-Aldrich).
2. TBS buffer; 50 mM Tris-HCl PH 7.5, 150 mM NaCl.
3. TBS Tween: 50 mM Tris-HCl PH 7.5, 150 mM NaCl, 0.06% Tween 20.
4. 3× Flag peptide (Sigma): 5 mg/mL.
5. Proteinase K (Thermo Fisher Scientific): 20 mg/mL.
6. RNase A (Thermo Fisher Scientific): 10 mg/mL.
7. Qubit dsDNA HS Assay Kit (Thermo Fisher Scientific).

3 Methods

3.1 Culture Preparation and Cross-Linking

1. Grow strains carrying flag-tagged Topo IV subunits until OD₆₀₀ 0.3, in 100 mL of LB or Minimal medium A supplemented with 0.2% glucose and 0.2% casaminoacids.
2. *For ChIP-seq*: Cross-link protein-DNA complexes by adding Formaldehyde (1% final concentration) for 30 min at room temperature with shaking at 100 rpm. Cross-linking is then quenched by adding Glycine to a final concentration of 250 mM for a 5-min incubation.
3. *For Norflip*: Cross-linked Topo IV-DNA cleavage complexes is obtained by adding Norfloxacin to the culture to a final concentration of 2 μM for 10 min.
4. Centrifuge cross-linked cultures at 3500 × *g* for 10 min at 4 °C and discard supernatant.
5. Wash the pellet with 10 mL ice-cold 1× PBS followed by centrifugation at 3500 × *g* for 10 min at 4 °C.
6. Repeat this step three times to remove excess cross-linking agents from cell pellets.
7. Flash freeze pellets immediately and store at -80 °C for further processing.

8. From here on, ChIP-seq and NorflIP sample processing follows the same protocol for either cross-linking methods until sequencing data analysis. One exception being the de-cross-linking step which slightly different between ChIP-seq and NorflIP methods.

3.2 DNA Shearing

1. Resuspend cross-linked cell pellets in 1 mL ChIP Lysis buffer and incubate with 3.5 units of Ready-Lyse™ Lysozyme solution at RT for 10 min shaking at 20 rpm.
2. Divide each sample into $4 \times 250 \mu\text{L}$ and transfer to 1.5 mL Bioruptor® Plus TPX microtubes and incubate on ice for 10 min prior to sonication.
3. Vortex samples briefly followed by a fast spin to bring down all sample volume.
4. Sonicate samples using a Bioruptor® sonicator (Diagenode) at 4°C for 15 cycles full power (30 s ON, 30 s OFF)
5. Centrifuge tubes for 10 min at $10,000 \times g$ at 4°C to eliminate cell debris and transfer the supernatant to a clean tube.
6. Run five microliters of sonication product on 1.5% agarose gel to check for shearing quality. Fragment sizes should range between 100 and 500 bp.
7. After ensuring that sonication gave the required size range, pool the sonication samples in one tube.
8. Keep 100 μL aside as the input sample and use the remaining 900 μL for immunoprecipitation.

3.3 Immuno-precipitation and Elution

The following steps should be carried out at 4°C unless otherwise indicated.

1. For every 900 μL sample prepare 40 μL of Agarose Anti-FLAG M2 gel pack and equilibrate it by three successive washes with 1 mL TBS buffer, discard the supernatant after centrifugation at $8000 \times g$ for 30 s.
2. Equilibrate the Agarose Anti-FLAG M2 by washing once with 1 mL ChIP Lysis Buffer.
3. Mix the 900 μL sample with the Agarose Anti-FLAG M2 gel and complete to 1 mL with ChIP Lysis Buffer.
4. Incubate overnight on a rotating wheel.
5. The next day perform two-times 500 μL washes in TBS Tween and four-times washes in TBS buffer, discard the supernatant every time.
6. Add 200 μL of 150 ng/mL $3 \times$ FLAG peptide diluted in TBS.
7. Incubate for 1 h on a rotating wheel.

8. Centrifuge beads for 30 s at $8000 \times g$ and recover the Topo IV-DNA complex found in the supernatant (IP sample).
9. The ChIP-seq IP and input samples are de-cross-linked and proteins are degraded overnight at 65 °C with 1 mg/mL proteinase K. The NorflIP IP and input samples are treated overnight at 65 °C with 1 mg/mL proteinase K and 1% SDS to degrade Topo IV covalently linked to the 5' end of DNA at the cleavage site.
10. Add 0.2 mg/mL RNase A and incubate for 30 min at 37 °C.
11. Purify IP and input samples with a DNA cleanup kit and elute in 30 μ L of Milli-Q water. Alternatively, the Mini - elute kit from Qiagen can be used to limit DNA loss during the cleaning process.
12. Measure DNA quality and quantity using Qubit dsDNA HS kit (*see Note 3*).
13. IP/input enrichment can then be preliminarily tested by qPCR using *dif* and *gapA* probes.

3.4 Library Preparation and Sequencing

Libraries were prepared according to Illumina's instructions accompanying the DNA Sample Kit (FC-104-5001). Briefly, DNA was end-repaired using a combination of T4 DNA polymerase, E. coli DNA Pol I large fragment (Klenow polymerase) and T4 polynucleotide kinase. The blunt, phosphorylated ends were treated with Klenow fragment (3' to 5' exo minus) and dATP to yield a protruding 3-'A' base for ligation of Illumina's adapters which have a single 'T' base overhang at the 3' end. After adapter ligation DNA was PCR amplified with Illumina primers for 15 cycles and library fragments of ~250 bp (insert plus adaptor and PCR primer sequences) were band isolated from an agarose gel. The purified DNA was captured on an Illumina flow cell for cluster generation. Libraries were sequenced on the Genome Analyzer following the manufacturer's protocols with single read for 50 cycles.

3.5 Sequencing Data Processing and Analysis

Sequencing results were processed by the IMAGIF facility. Base calls were performed using CASAVA version 1.8.2. ChIP-seq and NorflIP reads were aligned to the E. coli NC_000913 genome using BWA 0.6.2. A custom made pipeline for the analysis of sequencing data was developed with Matlab (available upon request). Briefly, the number of reads for the input and IP data was smoothed over a 200 bp window. Forward and reverse signals were added, reads were normalized to the total number of reads in each experiment, strong nonspecific signals observed in unrelated experiments were removed, data were exported to the UCSC genome browser (<http://archaea.ucsc.edu>) for visualization and comparisons.

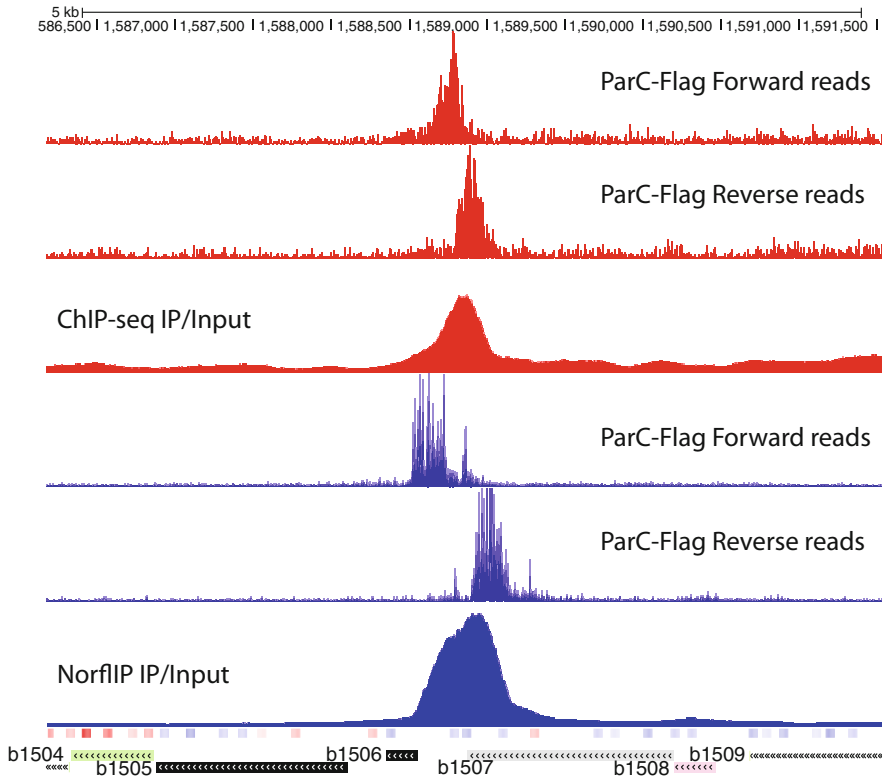


Fig. 1 Illustration of the sequencing results obtained from the Topo IV ChIP-seq (*red*) and NorfIIP (*blue*) experiments. Single read sequencing produces reads that can be aligned either on the forward (*top*) or the reverse (*middle*) genome strand. From these data a custom matlab data processing and analysis pipeline identify TopoIV binding (*red*) and cleavage (*blue*) activity sites (*bottom*). The *dif* region is represented on this genomic map

3.5.1 Peak Calling for ChiP-Seq Experiments

Several highly-enriched sites were observed in the IP samples. Interestingly one of these sites corresponds to the *dif* site (position 1.58 Mb), which has previously been identified as a strong Topo IV cleavage site in the presence of norfloxacin [12]. We also observed strong enrichment over rRNA operons, tRNA and IS sequences. To address the significance of the enrichment at rRNA, tRNA, and IS, we monitored these sites in ChIP-seq experiments performed in the same conditions with a MatP-flag strain and mock IP performed with strain that did not contain any flag tagged protein. Both MatP and Mock IP presented significant signals on rRNA, tRNA, and IS loci. This observation suggested that Topo IV enrichment at rRNA, tRNAs and IS was an artifact of the ChIP-Seq technique. By contrast no enrichment was observed at the *dif* site in the MatP and mock-IP experiments, we therefore considered *dif* to be a genuine Topo IV binding site and compared every enriched region (>2 fold) with the *dif*IP. We filtered the raw data for regions presenting the highest Pearson correlation with the *dif* signal

($P > 0.7$). This procedure discarded many highly enriched regions. An example of a site presenting a selected Topo IV IP/input signal suggesting a specific binding is presented on Fig. 1 (red graphs).

3.5.2 Peak Calling for NorflIP Experiments

The strongest IP/input ratio was observed at *dif* and a locus close to the *yebV* gene (1.9 Mb). They present a characteristic shape (Fig. 1 blue graphs, see Note 4) that allows the automatic detection of lower amplitude peaks but preserving the characteristic shape. We measured Pearson correlation coefficient with the *dif* and the *yebV* site for 600 bp sliding windows over the entire genome. Peaks with a Pearson correlation above 0.7 were considered as putative Topo IV cleavage sites. Interestingly in the NorflIP experiments nonspecific signal was observed over rRNA and IS regions but not on tRNA. This suggested that immunoprecipitation signals over tRNA are artefacts linked to formaldehyde but not to the Flag immunoprecipitation.

4 Notes

1. Both Gyrase and Topo IV are sensitive to Norfloxacin. To avoid altering Gyrase function during Topo IV trapping, we used a strain with a Gyrase *nalR* allele conferring Norfloxacin resistance. It is noteworthy that since the NorflIP method involves a specific flag tag immunoprecipitation of Topo IV the experiment is doable in a wild type context.
2. While immunoprecipitation of ParE and ParC tagged with a single flag epitope gave robust ChIP-seq and NorflIP signals we noticed for conventional ChIP qPCR experiments that immunoprecipitation of ParC tagged with a triple flag gave better signal–noise ratio and more reproducible results.
3. The amount of DNA recovered in the IP samples varies according to the experiments. We obtained successful sequencing results with DNA yields varying from 0.5 to 3 ng/ μ L in 30 μ L samples. Ten to twenty nanograms of DNA was used to build the Illumina library.
4. The NorflIP peaks correspond to a ~170 bp forward and reverse enrichment signals separated by a 130 bp segment, which is not enriched (Fig. 1, Blue). This pattern is the consequence of the covalent binding of Topo IV to the 5' bases at the cleavage site. After Proteinase K treatment the cleaving tyrosine residue bound to the 5' extremity resulted in poor ligation efficiency and infrequent sequencing of the cleaved extremities. This observation confirmed that we were observing genuine Topoisomerase cleavage sites.

Acknowledgments

This research was supported by funding to O.E. from Agence Nationale pour la Recherche (HiResBaCS ANR-15-CE11-0023).

References

1. Zechiedrich EL, Khodursky AB, Cozzarelli NR (1997) Topoisomerase IV, not gyrase, decatenates products of site-specific recombination in *Escherichia coli*. *Genes Dev* 11:2580–2592
2. Kato J, Nishimura Y, Imamura R, Niki H, Hiraga S, Suzuki H (1990) New topoisomerase essential for chromosome segregation in *E. coli*. *Cell* 63:393–404
3. Wang X, Reyes-Lamothe R, Sherratt DJ (2008) Modulation of *Escherichia coli* sister chromosome cohesion by topoisomerase IV. *Genes Dev* 22:2426–2433
4. Lesterlin C, Gigant E, Boccard F, Espéli O (2012) Sister chromatid interactions in bacteria revealed by a site-specific recombination assay. *EMBO J* 31:3468–3479
5. Cebrián J, Castán A, Martínez V, Kadomatsu-Hermosa MJ, Parra C, Fernández-Nestosa MJ, Schaerer C, Hernández P, Krimer DB, Schwartzman JB (2015) Direct evidence for the formation of precatenanes during DNA replication. *J Biol Chem* 290:13725–13735
6. Peter BJ, Ullsperger C, Hiasa H, Marians KJ, Cozzarelli NR (1998) The structure of supercoiled intermediates in DNA replication. *Cell* 94:819–827
7. Joshi MC, Magnan D, Montminy TP, Lies M, Stepankiw N, Bates D (2013) Regulation of sister chromosome cohesion by the replication fork tracking protein SeqA. *PLoS Genet* 9: e1003673
8. Espéli O, Borne R, Dupaigne P, Thiel A, Gigant E, Mercier R, Boccard F (2012) A MatP-divisome interaction coordinates chromosome segregation with cell division in *E. coli*. *EMBO J* 31:3198–3211
9. Nolivos S, Upton AL, Badrinarayanan A, Müller J, Zawadzka K, Wiktor J, Gill A, Arciszewska L, Nicolas E, Sherratt D (2016) MatP regulates the coordinated action of topoisomerase IV and MukBEF in chromosome segregation. *Nat Commun* 7:10466
10. Espeli O, Levine C, Hassing H, Marians KJ (2003) Temporal regulation of topoisomerase IV activity in *E. coli*. *Mol Cell* 11:189–201
11. El Sayyed H, Le Chat L, Lebailly E, Vickridge E, Pages C, Cornet F, Cosentino Lagomarsino M, Espéli O (2016) Mapping topoisomerase IV binding and activity sites on the *E. coli* genome. *PLoS Genet* 12: e1006025
12. Hojgaard A, Szerlong H, Tabor C, Kuempel P (1999) Norfloxacin-induced DNA cleavage occurs at the dif resolvase locus in *Escherichia coli* and is the result of interaction with topoisomerase IV. *Mol Microbiol* 33:1027–1036

The Use of Psoralen Photobinding to Study Transcription-Induced Supercoiling

Fedor Kouzine, Laura Baranello, and David Levens

Abstract

Proteins manipulating intracellular DNA necessarily impart torsional stress, which redistributes across the DNA. Overtwisting and undertwisting of the double helix result in the manifestation of positive and negative DNA supercoiling. A growing body of evidence indicates that DNA topology is an important player in the key regulatory steps of genome function, highlighting the need for biochemical techniques to detect dynamic changes in the DNA structure. Psoralen binding to DNA *in vivo* is proportional to the level of supercoiling, providing an excellent probe for the topological state of nuclear DNA. Here we describe a psoralen-based methodology to detect transcription-induced DNA supercoiling genome-wide. The DNA samples generated with this approach can be hybridized to microarray platforms or high-throughput sequenced to provide a topological snapshot of the whole genome.

Key words DNA topology, DNA supercoiling, Psoralen, Transcription, Topoisomerases, Chromatin, High-throughput genomics

1 Introduction

Rather than being a static helix, DNA possesses structural variability. DNA supercoiling plays a major role in the dynamic variation of the double helix. In supercoiled DNA, the torsional stress results in an excess or a deficiency in helical turns of the double helix. Notably, this torsional energy can be used during many critical steps of genes transcription [1, 2]. In eukaryotes, DNA supercoiling is believed to be generated dynamically and primarily by protein complexes, such as the RNA polymerase (RNAP) translocating along the double helix [3–5]. During transcription the active site of the RNAP tracks the helical path of DNA, which requires polymerase rotation relative to the DNA. The rotation of the polymerase may be hindered due to viscous drag or to tethering to nuclear structures (Fig. 1a), inducing overtwisting and undertwisting of the double helix in front of and behind the RNAP (positive and negative supercoiling, respectively). Increasing evidence suggests

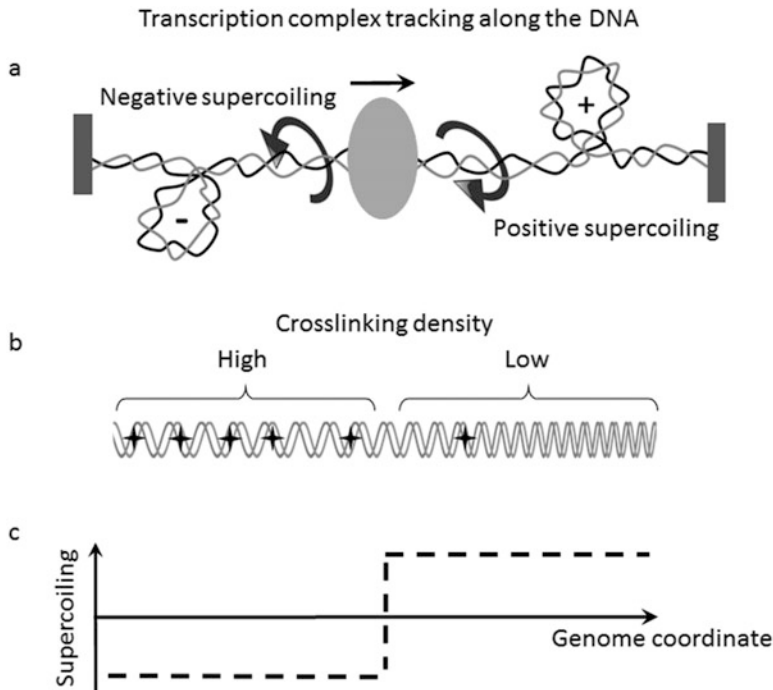


Fig. 1 Transcription-generated supercoiling and psoralen crosslinking as a probe for DNA supercoiling in vivo. (a) Transcription complex (shown as an *ova*) tracking along the DNA introduces negative and positive supercoiling. (b) Psoralen crosslinking density in vivo is high for negatively supercoiled DNA and low for positively supercoiled DNA. (c) Crosslinking density is a measure of DNA supercoiling in vivo

that biophysical mechanisms couple supercoiling to different DNA-dependent processes. Yet, we are still far from fully understanding the interplay between DNA topology and genome biology. The study of DNA topology has been hindered by experimental difficulties associated with detecting supercoiling and assessing its regulation in vivo, especially in eukaryotic cells [6].

A powerful approach to detect DNA supercoiling relies on the properties of the molecule psoralen [7, 8]. Psoralen's planar aromatic structure allows it to penetrate cellular membranes and to intercalate preferentially between the base pairs of negatively supercoiled DNA. Positively supercoiled DNA shows reduced psoralen binding (Fig. 1b). Upon exposure to UV light, the intercalated psoralen molecules crosslink complementary strands of the double helix via the formation of covalent bonds at each end of the molecules. The variation in the density of crosslinking can be used to detect and quantify DNA supercoiling in living cells (Fig. 1c). Though for several decades psoralen-based assays have been used to probe supercoiling averaged over entire genomes or in selective regions [9–11], only recently has this method been combined with genome-wide approaches, providing a global view of the functional dynamics of DNA supercoiling in vivo [12–16].

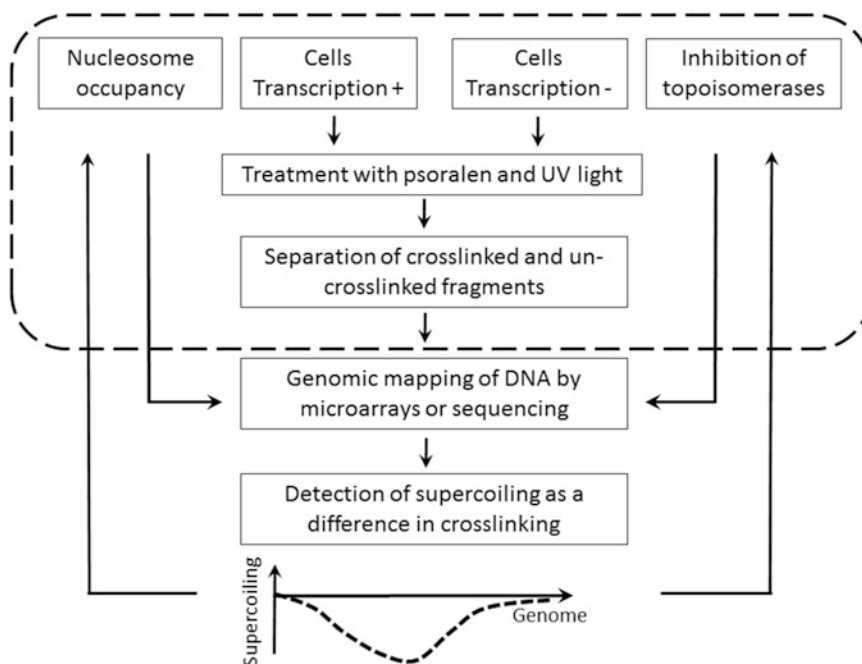


Fig. 2 Flow chart of psoralen-based approach. (*Middle*) Grow two batches of cells in culture. Cells in the first batch are grown under normal condition. Cells in the second batch are treated with transcription inhibitor. Add psoralen and introduce DNA interstrands crosslinks by exposing the cells to UV light. Using gel electrophoresis, separate and purify crosslinked and non-crosslinked fragments of genomic DNA after glyoxal denaturation. The crosslinked fraction is enriched for DNA negatively supercoiled at the moment of UV-irradiation. Genomic mapping of crosslinked DNA is achieved by hybridization to oligonucleotide microarrays or by direct high-throughput sequencing. Construction of the genome-wide pattern of transcription-generated supercoiling as a difference in crosslinking density between normal cells and cells treated with transcription inhibitor. (*Left*) To confirm that the crosslinking difference is due to transcription-generated supercoiling, verify that chromatin structure does not change at genomic regions of interest. (*Right*) To reveal the dynamic character of supercoiling and to examine its regulation, treat cells with topoisomerases inhibitors. *Dotted line* marks experimental methods presented in this chapter

We have developed a methodology that is particularly suitable to detect and study transcription-induced dynamic supercoiling. Our method is based on the different electrophoretic mobility in agarose gel of crosslinked versus uncrosslinked DNA fragments after denaturation of sonicated genomic DNA from cells treated with psoralen and UV light. The crosslinked and uncrosslinked DNA fragments are separated, purified and can be tested for enrichment throughout the genome by microarray or direct sequencing (Fig. 2). Because psoralen intercalation is also affected by DNA sequence composition and DNA-protein interactions [8], corrections for sequence and chromatin structure must be made to detect and estimate supercoiling inside the cells. A crosslinking difference between intact cells and cells treated with a transcriptional inhibitor is intrinsically normalized for the effect of sequence composition

and chromatin, providing a measure of transcription-generated supercoiling [13]. Genome-wide mapping of nucleosome occupancy is an important control experiment in our psoralen-based approach to insure that inhibition of transcription does not alter nucleosome deposition on the studied DNA regions, that otherwise might influence the level of crosslinking and confound the detection of DNA supercoiling [17]. Treatment of the cells with topoisomerases inhibitors (topoisomerases are enzymes which can relax DNA supercoiling) magnifies the results and helps to illuminate the mechanism of DNA topological homeostasis inside cells (Fig. 2). Details of the microarray hybridizations, high-throughput sequencing and transcriptome study as well as subsequent analysis have been reported elsewhere [13, 18, 19] and are not the focus of the protocol described here.

Our approach has already been adopted by other groups [20, 21]. It will allow researchers to study in detail the physical organization of chromosome and investigate the role of dynamic supercoiling in genome functioning.

2 Materials

2.1 Reagents

1. Proteinase K (Solution, 20 mg/mL).
2. Phenol–chloroform–isoamyl alcohol 25:24:1 v/v/v, Tris pH 8.0 saturated.
3. Ethanol 100%.
4. Sodium acetate 3.0 M, pH 5.2.
5. 1 M CaCl₂ solution.
6. RNase, DNase-free, 500 µg/mL.
7. 10% SDS.
8. 0.5 M EDTA.
9. 37% formaldehyde.
10. Glycogen: 20 mg/mL stock solution.
11. UltraPure Agarose (Invitrogen).
12. NuSieve 3:1 Agarose (Cambrex).
13. Dimethyl sulfoxide (DMSO), for molecular biology, >99.9%.
14. Glyoxal aldehyde solution, for molecular biology, 40% in H₂O.
15. Amberlite Mixed Bed Exchanger Amberlite MB-150, Sigma.
16. 5,6-dichloro-1-β-D-ribofuranosylbenzimidazole (DRB), 50 mM solution in DMSO.
17. Camptothecin (CPT), 10 mM solution in DMSO.
18. β-Lapachone (LAP), 40 mM solution in DMSO.

19. 4,5',8-trimethylpsoralen (psoralen), 0.9 mg/mL solution in ethanol.
20. MNase.
21. SYBR Green Nucleic Acid Gel Stain.
22. Dialysis tube, cellulose tubular membrane, MWCO ~8000.

2.2 Buffers

1. TE buffer: 10 mM Tris-HCl, 1 mM EDTA, pH 8.0.
2. Denaturing solution: 0.5 M NaOH, 1.5 M NaCl.
3. Neutralizing solution: 1.5 M NaCl, 500 mM Tris-HCl pH 8.0, 1 mM EDTA.
4. TAE buffer: 40 mM Tris pH 7.6, 20 mM acetic acid, 1 mM EDTA.
5. 0.1 M sodium phosphate buffer, pH 7.0.
6. PBS: 137 mM NaCl, 2.7 mM KCl, 10 mM Na₂HPO₄, 2 mM KH₂PO₄, without calcium and magnesium, pH 7.4.
7. Lysis buffer: 10 mM Tris-HCl pH 7.5, 10 mM NaCl, 3 mM MgCl₂, 0.5% NP-40, 0.15 mM spermine, 0.5 mM spermidine.
8. MNase digestion buffer: 10 mM Tris-HCl pH 7.4, 15 mM NaCl, 60 mM KCl, 0.15 mM spermine, 0.5 mM spermidine.

2.3 Equipments

1. Gel electrophoresis apparatus with a gel tray up to 20 cm.
2. Ultraviolet lamp; model B-100 A, Ultra-Violet Products, Inc.
3. Perkin Elmer MBA 2000 UV/VIS Spectrometer.
4. Thermoblock.
5. Sonicator, Ultrasonic processor XL, MISONIX Inc.
6. Rocker, tube wheel rotator, vacuum dryer, water bath, aspirator, and thermomixer.

2.4 Kits

1. QIAquick Gel Extraction Kit (Qiagen).

3 Methods

3.1 Preparing Genomic DNA from the Cells Treated with Psoralen and UV-Light

1. Grow Raji cells in RPMI 1640 medium with 10% FBS and 2 mM of L-glutamine (*see Note 1*). Split cells into fresh medium at a density of 0.2×10^6 cell/mL in 50 mL (175 cm² flask) and add DMSO (1.5% final concentration). Allow cells to grow for 4 days (*see Note 2*).
2. Count cells and transfer the suspension to a centrifuge tube. Recover the cell pellet by centrifugation at $500 \times g$ for 10 min at room temperature (RT). Remove the supernatant by aspiration and gently resuspend the cells in fresh medium without DMSO at a concentration of 1×10^6 cells/mL. Allow cells to

grow for 6 h (*see Note 3*). For a typical experiment, we use 1×10^7 cells per condition.

3. A typical experiment requires condition #I, cells not exposed to UV-light; #II, cells exposed to UV-light; #III, cells treated with an inhibitor of transcription (we chose DRB) and exposed to UV-light (*see Note 4*). Write these numbers on the bottom part of the 6 cm tissue culture dishes. If topoisomerase inhibitors will be used, prepare also sample #IV, cells treated with camptothecin and sample #V, cells treated with β -Lapachone. Other topoisomerase inhibitors can be used, according to the purpose of the experiment. For simplicity, in the protocol described below we will consider only treatments #I, #II, and #III.
4. Transfer the cells to a centrifuge tube and recover them by centrifugation at $500 \times g$ for 10 min at RT. Resuspend the cells to have 2×10^6 cell/mL and transfer 1×10^7 cells (5 mL) into 6 cm tissue culture dishes (*see Note 5*).
5. Add 40 μ M of DRB (final concentration) to dish #III. After 26 min of incubation at 37 °C, add 70 μ L of psoralen solution to each dish (*see Note 6*), mix by rocking, and incubate for 4 min at 37 °C in shadow light environment (*see Note 7*).
6. Place dishes #II and #III on an ice bed and expose them to $\sim 3.6 \text{ kJ m}^{-2}$ of 365-nm light (ultraviolet lamp; model B-100 A, Ultra-Violet Products, Inc. at a distance of 12 cm from the top of the light filter to the surface of the cell-containing media during 40 s) (*see Note 8*).
7. Immediately lyse the cells in each dish by adding SDS, EDTA and Proteinase K, giving final concentrations of 0.5%, 100 mM, and 100 μ g/mL, respectively.
8. Transfer cellular lysates to the 50 mL Falcon tube, mix by shaking, and incubate the lysates for 5 h (or overnight) at 55 °C.
9. Cool the solution to room temperature (RT) and add an equal volume of phenol–chloroform. Mix the two phases by shaking the tube for a few minutes, and separate the two phases by centrifugation at $3500 \times g$ for 10 min at RT. Transfer the aqueous phase to a new 50 mL Falcon tube.
10. Repeat **step 3.1.9**. Add to the aqueous phases 0.1 volume of 3 M sodium acetate and 2 volumes of ethanol stored at RT. Swirl the tubes to thoroughly mix solutions and precipitate the DNA by centrifugation at $3500 \times g$ for 10 min. Remove as much of the ethanol solution as possible, using an aspirator.
11. Add 5 mL of TE (pH 8.0) to each tube and 5 μ g of RNase, DNase-free. Place the tubes on a tube wheel rotator and incubate the solution overnight at RT with gentle agitation until

the DNA is completely dissolved. Repeat **step 3.1.9** and the ethanol precipitation. Wash the DNA precipitates with 70% ethanol. Remove as much ethanol as possible and air-dry the pellet for 15 min.

12. Dissolve the DNA pellet by vortexing it in 100 μL of TE (pH 8.0) for 1 hour and by heating it in a water bath to 55 $^{\circ}\text{C}$. Save 5 μL of DNA to use in **step 3.1.13** and fragment the remaining DNA by sonication. Sonication is performed on ice with an ultrasonic sonicator (Sonicator, Ultrasonic processor XL, MISONIX Inc. at 15% of power) by pulsing 20 times for 30 s, cooling in an ice-bath for 30 s between pulses.
13. Quantify the DNA of both unsonicated and sonicated samples spectrophotometrically and run 0.3 μg of DNA on a 0.6% agarose gel. The average DNA length of sonicated DNA should be around 200–300 bp with the distribution of fragment size ranging from 100 bp up to 500 bp. Unsonicated DNA should not show any sign of degradation, evidenced by smearing of DNA below the high-molecular band.

3.2 Separation of Psoralen Crosslinked and Uncrosslinked DNA Fragments

1. Run a preparatory 0.6% agarose gel electrophoresis in TAE buffer. Load DNA from each sample (#I, #II, #III) into the 1 cm wide gel wells, 5 μg of DNA per well. Run 20 cm gel for 2 h at 5 V/cm.
2. Divide DNA distribution into two parts: part I is from 300 bp to 100 bp and part 2 is from 500 bp to 300 bp. Cut the gel into slices with the DNA falling into these ranges. Purify the DNA by QIAquick Gel Extraction Kit (*see Note 9*). Label purified DNA as #I-1, #I-2, #II-1, #II-2, #III-1, and #III-2. Add to the purified DNA 20 μg of glycogen, 2 volumes of ice-cold ethanol 100%, and 0.1 volume of 3.0 M sodium acetate. Incubate at -20°C for 30 min and precipitate by centrifugation at $13,000 \times g$ for 10 min at $+4^{\circ}\text{C}$. Wash DNA pellets with 70% ethanol. Air-dry the pellet and dissolve DNA in 18 μL of water.
3. Incubate glyoxal aldehyde with “Amberlite Mixed Bed Exchanger Amberlite MB-150” (Sigma) at 2 to 1 volume ratio for 30 min at constant rotation (*see Note 10*). Prepare a master stock by mixing of 150 μL of 40% glyoxal aldehyde and 630 μL of DMSO right before use in next step.
4. Add 9 μL of 100 mM sodium phosphate buffer (pH 7.0) to each tube with DNA. Mix samples by vortex. Boil the samples for 1 min. Immediately add 78 μL of master stock from **step 3.2.3** to the denatured DNA (*see Note 11*). Incubate the samples for 1 h at 55 $^{\circ}\text{C}$. Reduce the volume of the samples to approximately $\frac{1}{4}$ by vacuum dryer.

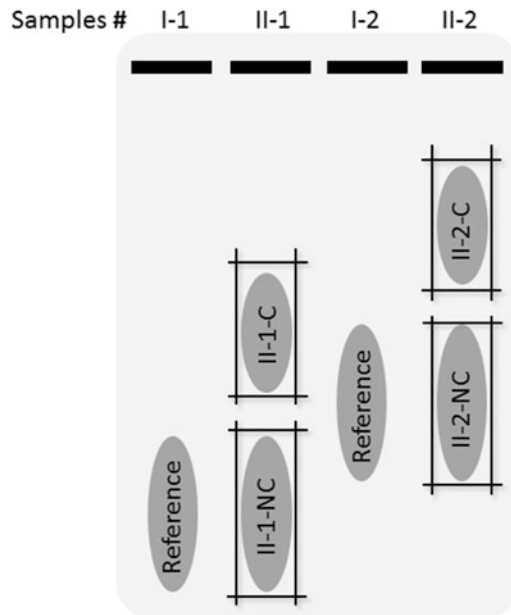


Fig. 3 Guide for preparative selection of crosslinked (-C) and uncrosslinked (-NC) DNA fragments on a hypothetical agarose gel. Uncrosslinked DNA from the cells not treated with UV light (samples # I-1 and I-2) serves as a reference marker to better resolve different DNA species in the experimental samples # II-1 and II-2. Use scalpel to excise the bands as shown by the *black lines*

5. Add the appropriate amount of loading buffer to the samples. Separate crosslinked and non-crosslinked DNA fragments by electrophoresis on a 3% agarose gel in 10 mM sodium phosphate buffer (pH 7.0) at 2 V/cm while recirculating the buffer for approximately 10 h (*see Note 12*). The length of the gel is 20 cm. To cast gel, use 1.2:1.8 mixture of UltraPure Agarose from Invitrogen and NuSieve 3:1 Agarose from Cambrex (*see Note 13*).
6. Incubate the gel with denaturing solution at 65 °C for 3 h to reverse psoralen crosslinks. Then incubate the gel with neutralizing solution for 1 h with constant agitation. Equilibrate the gel in the TAE buffer overnight. Stain the DNA in the gel with SYBR Green in TAE buffer for 16–18 h while changing the buffer three times.
7. Examine the stained gel by UV illumination. Locate the DNA “clouds” that belongs to the uncrosslinked (migrates faster) and crosslinked (migrates slower) DNA fragments. As a reference, chose the DNA “cloud” from the cells not treated with UV light (samples #I-1, #I-2). Use a sharp scalpel to cut out a slice of agarose containing the DNA of interest (Fig. 3). The ratio of non-crosslinked to crosslinked fragments should be ~3:1 to insure unsaturated conditions for crosslinking.

8. Close one end of a dialysis tube with a clip. Fill the dialysis tube with TAE buffer and transfer the gel slice into the buffer-filled tube. Squeeze out most of the buffer and seal the tube with a second dialysis tube clip. Label the clip with the name of DNA sample. For example, #II-1-NC means uncrosslinked DNA from sample #II-1, #II-1-C means crosslinked DNA from sample #II-1. Immerse the tube in a horizontal electrophoresis tank and apply an electric current through the tube (5 V/cm) for 2 h. After finishing the elution, massage the tube to redistribute DNA into the buffer.
9. Transfer the eluted DNA solution into a 15 mL Falcon tube and extract DNA twice with an equal volume of phenol–chloroform. Aliquot the extracted DNA into the Eppendorf tubes (0.5 mL in each) and precipitate the DNA with 2 volumes of ice-cold ethanol 100% in the presence of 0.3 M sodium acetate and 20 µg of glycogen after incubation at –20 °C for 30 min. Dissolve DNA pellets from each Eppendorf tube in 30 µL of TE buffer and combine DNA corresponding to each sample. Repeat ethanol precipitation in the presence of 0.3 M sodium acetate.
10. Wash DNA pellets with 70% ethanol, air-dry and dissolve DNA in 50 µL of TE buffer (pH 8.0). Combine purified DNA in the following order. C+ is crosslinked DNA from the untreated cells: #II-1-C and #II-2-C. NC+ is uncrosslinked DNA from the untreated cells: #II-1-NC and #II-2-NC. C- is crosslinked DNA from the cells treated with DRB: #III-1-C and #III-2-C. NC- is uncrosslinked DNA from the cells treated with DRB: #III-1-NC and #III-2-NC. Measure DNA concentrations by spectrometer (*see Note 14*).
11. Repeat the experiment generating required number of biological replicates (*see Note 15*).
12. The resulting DNA samples are ready for downstream steps, which can involve either hybridization on a microarray platform or high throughput sequencing of single-stranded DNA, accordingly the scheme presented in Fig. 4. In our laboratory, we performed DNA labeling, hybridization, detection, data extraction, and quality assessment using the commercial microarray service. Algorithm of computational data analysis can be found at *Supplementary Information* of Kouzine et al. [13].

3.3 Inhibition of Topoisomerases

1. Starting from **step 3.1.5** of the current protocol, having ready dishes #III, VI and V. Add 40 µM of DRB (final concentration) to dish # III. After 21 min of incubation at 37 °C, add 10 µM (final concentration) CPT to dish # IV. Add 10 µM (final concentration) LAP to dish #V (*see Note 16*). Mix by rocking for 30 s. After additional 5 min of incubation at 37 °C, add

DNA samples	Description	Equivalence
C+ or C+ versus NC+	Enrichment (or relative enrichment) of crosslinked DNA in untreated cells	Crosslinking density due to cumulative effects of DNA sequence, chromatin structure and transcription-induced supercoiling
C- or C- versus NC-	Enrichment (or relative enrichment) of crosslinked DNA in DRB-treated cells	Crosslinking density due to cumulative effects of DNA sequence and chromatin structure
	Difference in crosslinking density between DRB-treated and untreated cells	Transcription-induced DNA supercoiling
C-CPT or C-CPT versus NC-CPT	Enrichment (or relative enrichment) of crosslinked DNA in CPT-treated cells	
	Difference in crosslinking density between DRB-treated and cells treated with CPT	Transcription-induced DNA supercoiling in cells treated with CPT
C-LAP or C-LAP versus NC-LAP	Enrichment (or relative enrichment) of crosslinked DNA in LAP-treated cells	
	Difference in crosslinking density between DRB-treated and cells treated with LAP	Transcription-induced DNA supercoiling in cells treated with LAP

Fig. 4 Definition of DNA samples and equivalence of genomic data

70 μ L of psoralen solution to each dish, mix by rocking, and incubate for 4 min at 37 °C in the shadow light environment.

2. Follow **steps 3.1.6–3.2.10** of the current protocol to obtain the following DNA samples: C-CPT is crosslinked DNA from the CPT treated cells; NC-CPT is uncrosslinked DNA from the CPT treated cells; C-L is crosslinked DNA from the LAP treated cells; NC-L is uncrosslinked DNA from the LAP treated cells.
3. Continue to **steps 3.2.11** and **3.2.12** of the current protocol (*see* Fig. 4).

3.4 Preparation of Nucleosomal DNA

1. Use cells treated or not with DRB for 30 min. Cross-link 15–20 million cells in each condition by adding formaldehyde (1% final concentration) directly to the medium and incubate for 5 min at RT (*see* **Note 17**). Wash the cells twice with ice-cold PBS and lyse the cells in 1 mL of ice-cold lysis buffer in Eppendorf tubes. After 5 min of incubation on ice, spin the

tubes at $1000 \times g$ for 5 min at 4 °C. Wash the pellets of nuclei twice with ice-cold MNase digestion buffer. Resuspend the nuclei in 1 mL of MNase digestion buffer and add CaCl_2 , giving 1 mM final concentration. Keep the nuclei on ice.

2. Add 0, 0.01, 0.02, 0.04, 0.08, 0.15, 0.3, 0.6, 1.0, and 2.0 U of MNase to 10 Eppendorf tubes and aliquot 100 μL of nuclei solution into each tube. Incubate the reaction mixture at 37 °C for 10 min. Stop the reaction by adding SDS, EDTA, and Proteinase K, giving final concentrations of 0.5%, 100 mM, and 100 $\mu\text{g}/\text{mL}$, respectively. Incubate the mixture at 65 °C for overnight.
3. Extract DNA twice with phenol–chloroform, add 20 μg of glycogen as a carrier and precipitate the DNA with 2 volumes of ethanol 100% in the presence of 0.3 M sodium acetate after incubation at -20 °C for 30 min. Wash DNA pellets with 70% ethanol, air-dry and dissolve DNA in 20 μL of TE buffer (pH 8.0).
4. Add an appropriate amount of loading buffer to 10 μL of each sample and run 0.6% agarose gel electrophoresis in TAE buffer (20 cm gel for 2 h at 5 V/cm) to resolve the nucleosome ladder. Examine the gel stained with SYBR Green by UV illumination. Use a sharp scalpel to cut out a slice of agarose covering mononucleosome DNA only from lines containing 3–8 bands in the nucleosome ladder.
5. Purify the DNA by QIAquick Gel Extraction Kit. Resulting DNA samples are ready for downstream analysis by using microarray platform or high throughput sequencing.

3.5 Transcription Activity Assays

To generate cellular transcriptome required to correlate the map of DNA supercoiling with transcriptional activity, in our experiments we used microarray-based method to quantify gene expression level from cDNA (complementary DNAs generated from the RNA) signal at the annotated genes [13]. However, a recently developed technique called RNA Sequencing (RNA-Seq) uses high-throughput sequencing to build transcriptome of genomes at a far higher resolution than in microarray-based methods [18]. Thus, we recommend using RNA-Seq assay to create a reference map for transcription-generated DNA supercoiling. An independent measure of transcriptional activity and pausing state of RNA polymerase II might be obtained by RNA polymerase ChIP-sequencing assay [19].

4 Notes

1. The DMSO treatment for 96 h will synchronize Raji cells at early G1 cell cycle phase. While this step is not necessary, it might reduce variation in the crosslinking density due to other reasons than transcription (DNA replication, mitosis etc.).
2. This protocol is designed for suspension cells. If adherent cells are used, grow them in 6 cm tissue culture dishes. The number of dishes should fulfill the requirement to have 10 million cells per condition: #I, #II and #III. Start the protocol for adherent cells from **step 3.1.5**, preferably working with no more than three dishes simultaneously.
3. At this step, synchronized cells are in the middle of G1 phase of the cell cycle.
4. DRB rapidly enters cells, specifically inhibits CDK9 phosphorylation of the C-terminal domain of RNA polymerase II, and blocks transcription within a minute after administration.
5. The small size of the dish is chosen to ensure uniform irradiation of the cells. However, other commercially available light sources might accommodate larger dishes.
6. Psoralen is light sensitive and its exposure to light should be minimized. It should be stored in the dark. When added to cells, we typically reduce lighting, avoid sunlight, etc. Psoralen is a powerful mutagen and carcinogen and should be handled with care.
7. Following the UV irradiation, all subsequent manipulations of the cells, of the cellular lysates and of the DNA are performed under shadow light conditions, with the cells and DNA being subjected only to indirect lighting.
8. If using other types of the fluorescent lamps or other type of cells, in a pilot experiment, expose dishes to various doses of 365-nm light, starting from 3.0 kJ m^{-2} with an incident light intensity of about 0.3 kJ m^{-2} up to 3.9 kJ m^{-2} . Then go through all steps until **step 3.2.7** and choose the conditions which satisfy 3:1 ratio between uncrosslinked and crosslinked DNA fragments to perform the main experiment.
9. Be careful to not exceed the DNA binding capacity of the QIAquick membranes (10 μg).
10. Glyoxal is readily air-oxidized. By mixing the glyoxal solution with the mixed bed, we remove oxidation products the same day as the DNA samples are prepared.
11. Glyoxal reacts with DNA by introducing an additional ring onto guanosine residues, thus sterically hindering the formation of G-C base pairs and consequently the renaturation of DNA double helix.

12. To better estimate the time of running, mix all leftover DNA samples in one tube and load the mixture in one well on the side of the gel. After few hours of electrophoresis, cut a slice of the gel containing the mixture of DNA loaded in this well, stain it with SYBR Green in TAE buffer, and calculate the exact time required to run the gel.
13. It is important to use agarose with high melting temperature (NuSieve 3:1) to successfully perform **step 3.2.19** with an addition of typical agarose (UltraPure Agarose) to insure durability of the gels in the subsequent steps.
14. At this step DNA exist in the partially denatured state. Single-stranded DNA fragments might anneal with each other to form mesh-like structure complex. To measure accurately the DNA concentration, we boil DNA for 1 min and then transfer 1 μ L of DNA solution to the 100 μ L of ice-cold TE buffer. The concentration of resulting DNA solution is measured by Perkin Elmer MBA 2000 UV/VIS Spectrometer.
15. Microarrays and high-throughput sequencing have been routinely used for the ChIP-Chip and ChIP-Seq experiments, where the enrichment of sequences is 10–100-fold higher than the background. The relative enrichment of psoralen crosslinking at negatively supercoiled DNA is only two folds in comparison to relaxed DNA. In addition, psoralen binding sites are not focal, rather continuously distributing across the genome. However, from our experience, even for high noise experiments such as microarrays, 3 replicates are sufficient to achieve a required level of accuracy. With high-throughput sequencing this number will come down further to two replicates, insuring the reproducibility of experiment.
16. Different inhibitors act on different topoisomerases and affect different steps in the topoisomerase reaction cycle. Changes in crosslinking density will reflect their mode of action; confirming the results of the main experiment and revealing the mechanisms of topological homeostasis inside the cells (*see* also Fig. 4).
17. The crosslinking with formaldehyde is required to avoid possible redistribution of nucleosomes upon nuclei preparation and MNase digestion.

References

1. Kouzine F, Levens D, Baranello L (2014) DNA topology and transcription. *Nucleus* 5 (3):195–202
2. Ma J, Wang M (2014) Interplay between DNA supercoiling and transcription elongation. *Transcription* 5(3):e28636
3. Nelson P (1999) Transport of torsional stress in DNA. *Proc Natl Acad Sci U S A* 96 (25):14342–14347
4. Liu LF, Wang JC (1987) Supercoiling of the DNA template during transcription. *Proc Natl Acad Sci U S A* 84(20):7024–7027

5. Droge P (1994) Protein tracking-induced supercoiling of DNA: a tool to regulate DNA transactions in vivo? *BioEssays* 16(2):91–99
6. Freeman LA, Garrard WT (1992) DNA supercoiling in chromatin structure and gene expression. *Crit Rev Eukaryot Gene Expr* 2(2):165–209
7. Sinden RR, Bat O, Kramer PR (1999) Psoralen cross-linking as probe of torsional tension and topological domain size in vivo. *Methods* 17(2):112–124
8. Bermudez I et al (2010) A method for genome-wide analysis of DNA helical tension by means of psoralen-DNA photobinding. *Nucleic Acids Res* 38(19):e182
9. Ljungman M, Hanawalt PC (1992) Localized torsional tension in the DNA of human cells. *Proc Natl Acad Sci U S A* 89(13):6055–6059
10. Jupe ER, Sinden RR, Cartwright IL (1993) Stably maintained microdomain of localized unrestrained supercoiling at a drosophila heat-shock gene locus. *EMBO J* 12(3):1067–1075
11. Sinden RR, Carlson JO, Pettijohn DE (1980) Torsional tension in the DNA double helix measured with trimethylpsoralen in living *E. coli* cells: analogous measurements in insect and human cells. *Cell* 21(3):773–783
12. Naughton C et al (2013) Transcription forms and remodels supercoiling domains unfolding large-scale chromatin structures. *Nat Struct Mol Biol* 20(3):387–395
13. Kouzine F et al (2013) Transcription-dependent dynamic supercoiling is a short-range genomic force. *Nat Struct Mol Biol* 20(3):396–403
14. Teves SS, Henikoff S (2014) Transcription-generated torsional stress destabilizes nucleosomes. *Nat Struct Mol Biol* 21(1):88–94
15. Matsumoto K, Hirose S (2004) Visualization of unconstrained negative supercoils of DNA on polytene chromosomes of *Drosophila*. *J Cell Sci* 117(Pt 17):3797–3805
16. Joshi RS, Pina B, Roca J (2010) Positional dependence of transcriptional inhibition by DNA torsional stress in yeast chromosomes. *EMBO J* 29(4):740–748
17. Sinden RR (2013) The helix turns at 60: writhing free in chromosomes. *Nat Struct Mol Biol* 20(3):251–253
18. Podnar J et al (2014) Next-generation sequencing RNA-Seq library construction. *Curr Protoc Mol Biol* 106:4.21.1–4.2119
19. Baranello L et al (2016) RNA polymerase II regulates Topoisomerase I activity to favor efficient transcription. *Cell* 165(2):357–371
20. Benarroch-Popivker D et al (2016) TRF2-mediated control of telomere DNA topology as a mechanism for chromosome-end protection. *Mol Cell* 61(2):274–286
21. Lal A et al (2016) Genome scale patterns of supercoiling in a bacterial chromosome. *Nat Commun* 7:11055

Immunoprecipitation of RNA:DNA Hybrids from Budding Yeast

Aziz El Hage and David Tollervey

Abstract

During transcription, the nascent transcript behind an elongating *RNA polymerase* (RNAP) can invade the DNA duplex and hybridize with the complementary DNA template strand, generating a three-stranded “R-loop” structure, composed of an RNA:DNA duplex and an unpaired non-template DNA strand. R-loops can be strongly associated with actively transcribed loci by all RNAPs including the *mitochondrial RNA polymerase* (mtRNAP). In this chapter, we describe two protocols for the detection of RNA:DNA hybrids in living budding yeast cells, one that uses conventional *chromatin immunoprecipitation* (ChIP-qPCR) and one that uses *DNA:RNA immunoprecipitation* (DRIP-qPCR). Both protocols make use of the S9.6 antibody, which is believed to recognize the intermediate A/B helical RNA:DNA duplex conformation, with no sequence specificity.

Key words *Saccharomyces cerevisiae*, RNA:DNA hybrids, R-loop, Chromatin immunoprecipitation (ChIP), DNA:RNA immunoprecipitation (DRIP), S9.6 antibody

1 Introduction

In the budding yeast *Saccharomyces cerevisiae* (*S. cerevisiae*), RNA:DNA hybrids can be generated by reverse transcription of the messenger RNAs of TY retrotransposons, within the viral-like particles in the cytoplasm (for a review *see ref. 1*). Short RNA:DNA hybrids can serve for the initiation of DNA synthesis in both the leading and lagging strands (for a review *see ref. 2*). Short RNA:DNA hybrids (~7–9 bp) are also located within transcription bubbles (for a review *see Nudler 2009 [3]*). RNA:DNA hybrids are also represented by R-loop structures which are most frequently generated by invasion of the DNA duplex by the nascent transcript *in cis* behind the RNAP, but can also form *in trans* (reviewed in [4–9]). R-loops play integral roles in the replication of T4 bacteriophage, *E. coli* ColE1 plasmid and mammalian mtDNA (reviewed in [4]), and also in immunoglobulin class switch recombination (CSR) in B-cells ([10]; for a recent review *see ref. 11*). Besides, R-loops have been recently reported to

play beneficial roles in diverse other mechanisms including gene expression (e.g., transcription initiation and termination), telomere maintenance, and chromatin structure (for a recent review *see* ref. 8). Conversely, however, R-loops can be detrimental for transcription and replication of the genomic DNA (gDNA) and can present a major threat for genome stability (reviewed in [4, 7–9]). Moreover, they can be associated with neurological diseases and cancer (reviewed in [6, 8, 9]).

A myriad of factors playing roles in RNA and/or DNA metabolism, including topoisomerases, ribonucleases, RNA/DNA helicases, RNA processing and packaging factors, RNA splicing, proteins implicated in DNA repair, etc. have been implicated in the resolution and/or prevention of R-loops (for a recent review *see* ref. 8). The first evidence showing that R-loops can accumulate *in vivo* came from studies performed by Drolet and colleagues [12]. This study showed that overexpression of *E. coli* RNase HI, an enzyme that cleaves the RNA strand in R-loops, partially compensates for the lack of *E. coli* TopoI, a type IA topoisomerase that can relieve negative (–) DNA torsional stress (TS) behind the RNAP. In budding yeast, Top1 and Top2 can relax both (+) and (–)TS, ahead, and behind, of the transcription machinery, respectively (for a review *see* ref. 13). Importantly, while Top1 can relax both (+) and (–)TS with similar efficiency, Top2 can be more proficient in quickly relaxing (+)TS than (–)TS [14]. Consistent with this notion, loss of Top1 in budding yeast enhances (–)TS and R-loop formation behind RNAP I (which is responsible for the transcription of the 35S ribosomal RNA (35S rRNA) into the 18S, 25S, and 5.8S rRNAs), while the loss of Top2 enhances (+)TS ahead of RNAP I [15, 16]. Remarkably, accumulation of stable R-loops at the 35S rRNA locus in triple mutants lacking both RNase HI and RNase H2 activities and depleted of Top1p (for a review on eukaryotic RNases H *see* ref. 17) can: (i) impose persistent transcription blocks by RNAP I [15], (ii) prime origin-independent replication [18], and (iii) lead to irreparable and lethal DNA replication blocks [19]. Moreover, the expression of non-coding RNAs by RNAP II from the rDNA intergenic spacers is highly increased in these triple mutants [15], strongly suggesting that accumulation of RNA:DNA hybrids at those sequences relieves silencing of transcription by RNAP II and leads to the instability of the highly repetitive rDNA loci [20]. In line with these observations, it was reported that the budding yeast Ataxin-2 protein Pbp1 plays important roles at the rDNA intergenic spacers by binding noncoding RNAs, suppressing RNA:DNA hybrids and preventing aberrant recombination [21]. Finally, failure to suppress (–)TS and/or (+)TS at genes transcribed by RNAP II in budding yeast mutants lacking Top1 or Top2 can lead to chromosome breakage and genome instability [22, 23].

R-loops can be predicted *in silico* in nucleic acid sequences of mammals and other organisms including yeast (*see* <http://rloop.bii.a-star.edu.sg> and [24]). R-loops can be detected in living cells by different procedures including nondenaturing or native bisulfite sequencing, immunostaining of chromosome spreads, dot blots, electron microscopy, and immunoprecipitation (outlined in [3, 25]). To date, the mouse monoclonal S9.6 antibody [26] has been widely used for the detection of RNA:DNA hybrids, including: (i) R-loop structures (references outlined in [25]), (ii) cytosolic RNA:DNA hybrids that are generated by reverse transcription in TY retrotransposons of budding yeast or in virus-infected mammalian cells [27, 28], (iii) cytosolic RNA:DNA hybrids in virus-free human cell lines [29], and (iv) RNA:DNA hybrids in microarray studies [30].

We initially used the S9.6 antibody in a conventional ChIP-qPCR approach (i.e., immunoprecipitation of formaldehyde-crosslinked and sonicated chromatin combined with quantitative PCR) in order to detect R-loops at the actively transcribed rRNA genes in *S. cerevisiae* [15]. In a subsequent study, we recovered the DNA fragments from the S9.6 ChIP and processed them for high-throughput sequencing (referred to herein as ChIP-seq) [27]. Our genome-wide study revealed that R-loops are mainly associated with the highly expressed genes by RNAPs I, II, and III. These findings were corroborated by another genome-wide study in which conventional ChIP was combined with hybridization on tiling microarrays (referred to herein as DRIP-chip) [31]. For instance, the abundance of R-loops at RNAP III genes, in particular the tRNA genes, was found to be increased in double mutants *rnh1Δ rnh201Δ* which lack all RNase H activities [27, 31] and also in mutants impaired for Sen1, an RNA/DNA helicase [31]. In concordance with these observations, R-loops were reported to be enriched at tRNA genes in mutants lacking RNases H in *S. pombe* [32]. Interestingly, accumulation of R-loops at tRNA genes in the budding yeast *rnh1Δ rnh201Δ* mutants has been linked to increased rates of mobility of Ty1 retrotransposons to the 5'-flanking regions of tRNA genes [27], and also to increased rates of APOBEC3B-induced-cytidine-deamination and hypermutability of tRNA genes [33]. In the same line of evidence, accumulation of RNA:DNA hybrids in budding yeast mutants impaired for Sen1 was reported to be detrimental for genome stability [34], DNA replication [35], and transcription termination [36]. Regarding the differences in findings between the R-loop genome-wide studies mentioned above [27, 31], the DRIP-chip study revealed that R-loop prone-sites are enriched at telomeric repeats, at genes which are associated with anti-sense transcripts, at snoRNA genes (in mutants impaired for Sen1), and at Ty1 and Ty2 retrotransposons. In concordance with these observations, it was reported in budding yeast that RNA:DNA hybrids affect telomere maintenance

[37, 38], and that the GAL *long non-coding RNAs* (lncRNAs) promote transcriptional induction in trans by formation of lncRNA:DNA hybrids [39]. The ChIP-seq study [27] reported, however, that a noticeable fraction of RNA:DNA hybrids that accumulate at the Ty1 retrotransposons in mutants lacking RNases H is associated with Ty1 complementary DNAs (cDNAs). Indeed, cDNA molecules generated by reverse transcription of cellular messenger RNAs (mRNAs) in budding yeast mutants *rnh1Δ rnh201Δ* can serve as templates for the repair of chromosomal double strand breaks (DSBs) (for a review see ref. 40). In addition, stable RNA:DNA hybrids created by hybridization of nascent transcripts to their cognate gDNAs *in cis* in double mutants *rnh1Δ rnh201Δ* can play important roles in DNA repair at the sites of DSBs, in *S. cerevisiae* [40] and *S. pombe* [41]. Finally, ChIP-seq [27] further revealed that R-loop accumulation is more prominent over exonic than intronic sequences of highly expressed, intron-containing mRNA genes. R-loops are also highly enriched at the mtDNA in single mutants *rnh1Δ* [27]. The role of RNase H1 in mitochondria is indeed conserved through evolution as degradation of RNA:DNA hybrids is essential for mtDNA maintenance in the developing mouse [42].

More recently, R-loops were mapped genome-wide in budding yeast by a technology named S1-DRIP-seq [43]. This consisted mainly in using naked, S1 nuclease-treated and sonicated DNA, instead of formaldehyde-crosslinked and sonicated chromatin. Overall, only a subset of the hybrid-prone sites found in the S1-DRIP-seq study matched previously identified sites; specifically, mtDNA, rDNA loci, telomeres, Ty retrotransposons, tRNA genes and highly expressed mRNA genes. The S1-DRIP-seq study found, however, that RNA:DNA hybrids can significantly accumulate at specific sites on moderately and weakly expressed mRNA genes, in particular over promoter and/or terminator regions. Moreover, the S1-DRIP-seq study found that polyA tracts, as well as highly expressed genes, account for a large fraction of hybrids in the yeast genome. Importantly, the budding yeast R-loop genome-wide studies came to the same conclusion, that high transcription levels are likely to be a major determinant of R-loop formation. This positive correlation between gene expression and R-loop formation may be universal, as a recent genome-wide study in human and mice cells using an RNA-based strand-specific genome-wide approach revealed that R-loops are indeed strongly associated with highly expressed mRNA genes ([44]; reviewed in [45]). It is thus possible that the robust appearance of R-loops at highly expressed genes is simply the consequence of high rates of transcription. In line with this idea, accumulation of stable R-loops at highly expressed genes in yeast were reported to hinder

transcription by RNAP I [15], block DNA replication [46], and lead to deleterious mutations and rearrangements in gDNA (reviewed in [47]).

Our ChIP-qPCR and ChIP-seq studies showed that the R-loop signal at the highly transcribed mRNA genes was only a few fold higher than background levels [27]. Importantly, however, the R-loop signal over the highly transcribed 35S rRNA genes and mt genes was several fold higher than background levels (compare Figs. 1 and 4 with S9 in [27]). Furthermore, the R-loop signal at moderately/weakly expressed mRNA genes was near background levels (*see* Figs. 5A, 5C and S9 in [27]). It is possible that formaldehyde crosslinking of chromatin at mRNA genes, in particular the moderately/weakly expressed ones, could shield RNA:DNA hybrids, which could thus be partly accessible/inaccessible for binding to the antibody. Conversely, an open chromatin structure, for example at highly transcribed mRNA genes, or the lack of nucleosomes, for example at actively transcribed rRNA and mt genes, could favor binding of the antibody to cross-linked RNA:DNA hybrids (for a thorough investigation regarding the immunoprecipitation efficiencies of RNA:DNA hybrids using antibody S9.6, *see* ref. 25). In conclusion, different variants of immunoprecipitation and analysis of RNA:DNA hybrids on a genome-wide scale in *S. cerevisiae* lead to similar but not identical findings regarding the location and/or the abundance of R-loops [27, 31, 43, 48]. This is also true for studies applied to the mammalian genome (*see* refs. 25, 45). It is also important to emphasize that the S9.6 antibody has high affinity to RNA:DNA hybrids, but may also have low affinity toward double stranded RNAs (dsRNAs) [49]. Thus, it is very important to perform a control with RNase H to confirm that nucleic acids that are recovered by this antibody are genuine RNA:DNA hybrids (*see* also **Notes 13** and **24** in this chapter).

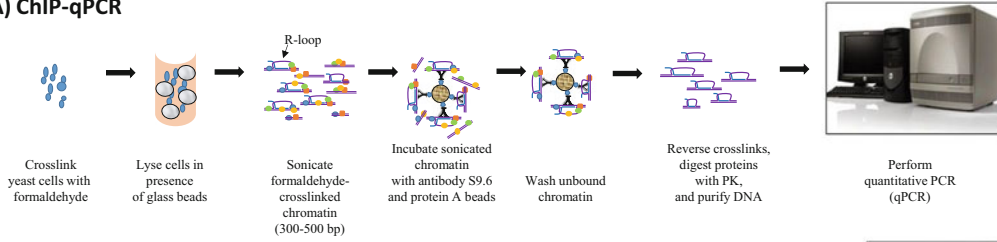
In this chapter, we describe two methodologies for the detection of R-loops using antibody S9.6: (i) “ChIP-qPCR” approach that uses formaldehyde-crosslinked and sonicated chromatin (*see* Fig. 1A), and (ii) “DRIP-qPCR” approach that uses naked and restriction endonuclease (RE)-fragmented DNA (*see* Fig. 1B).

2 Materials

2.1 Equipment Common for Both ChIP-qPCR and DRIP- qPCR

1. Tubes: 1.5 ml safe-lock (e.g., Eppendorf, catalog number 0030 120.086), 1.5 ml standard, 5 ml safe-lock (e.g., Eppendorf, catalog number 0030119401), 15 ml standard, and 50 ml standard.
2. Autoclave.
3. Rotating wheel and shaking platform.

A) ChIP-qPCR



B) DRIP-qPCR

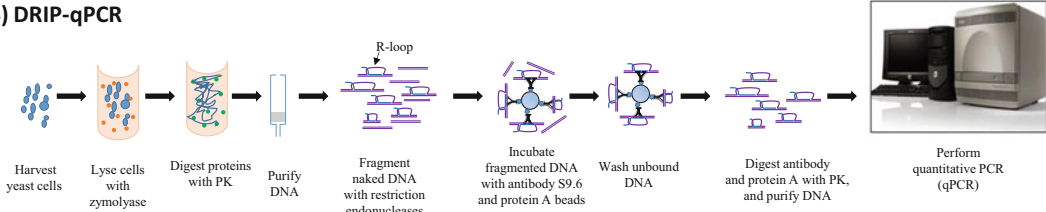


Fig. 1 Cartoon illustrating the main steps in the workflows for ChIP-qPCR (panel **a**) and DRIP-qPCR (panel **b**) methodologies. Abbreviations: PK (*proteinase K*) and gDNA (*genomic DNA*)

4. Heating block (e.g., Thermomixer C with thermoblock, Eppendorf).
5. Apparatus for running a small agarose gel.
6. PhosphorImager for scanning SYBR-stained nucleic acids (e.g., Fuji FLA-5100).
7. 96 well plates (96-well plates semi-skirted and optical cap 8 × strip, e.g., Agilent Technologies, catalog numbers 401334 and 401425, respectively).
8. Real-time PCR machine (e.g., MX3005P, Agilent Technologies).

2.2 Equipment

Unique to ChIP-qPCR

1. Multi-vortexer (e.g., Genie 2T, Scientific Industries).
2. Sonicator Bioruptor PICO (or similar) and 1.5 ml Bioruptor Microtubes (Diagenode, catalog number C30010016).
3. Syringe 5 ml and needle 25G.

2.3 Equipment

Unique to DRIP-qPCR

1. 200 µl and 1000 µl wide-orifice tips with filter (e.g., Starlab, catalog numbers E1011-8618 and E1011-9618, respectively).
2. Magnetic racks for 1.5 ml and 15 ml tubes.
3. Qubit Fluorometer (Thermofisher Scientific).

2.4 Reagents

Common for Both ChIP-qPCR and DRIP-qPCR

1. FA-1 buffer: 50 mM HEPES-KOH pH 7.5, 140 mM NaCl, 1 mM EDTA pH 8, 1% Triton X-100, 0.1% w/v sodium deoxycholate. Filter-sterilize. Store at 4 °C.
2. Complete Protease inhibitor cocktail containing EDTA (e.g., Sigma/Roche, catalog number 11697498001). For 25 × stock

solution, dissolve one pellet in 2 ml of water. The solution can be stored at 4 °C up to 1 month.

3. Anti-DNA:RNA Hybrid antibody (1 µg/µl), clone S9.6, mouse IgG2a (e.g., Millipore, catalog number MABE1095 or Kerafast, catalog number ENH001).
4. FA-2 buffer: as FA-1 buffer but with 500 mM NaCl. Filter-sterilize. Store at 4 °C.
5. FA-3 buffer: 20 mM Tris-HCl pH 8, 0.25 M LiCl, 0.5% Nonidet P-40, 0.5% w/v sodium deoxycholate, 1 mM EDTA pH 8. Filter-sterilize. Store at 4 °C. (Nonidet P-40 substitute, e.g., Sigma/Roche, catalog number 11 754 599 001).
6. TE 1×: 10 mM Tris-HCl pH 8, 1 mM EDTA pH 8. Filter-sterilize. Store at 4 °C.
7. RNase A, DNase-free: for stock of 10 mg/ml, dissolve powder in water, aliquot in small volumes and store for long term at -20 °C. For elution of DNA from Qiagen Minelute columns prepare 0.1 mg/ml ChIP-RNase A in buffer containing 10 mM Tris-HCl pH 7.5 and 15 mM NaCl (aliquot and store as above).
8. Proteinase K (PK), recombinant, PCR Grade (e.g., Sigma/Roche, catalog number 3115836001): for stock of 20 mg/ml, dissolve powder in water, aliquot and store for long term at -20 °C.
9. Sodium Dodecyl Sulfate (SDS) 20%.
10. DNA purification kit, e.g., Minelute PCR purification kit (Qiagen, catalog number 28004).
11. Q-PCR mix: e.g., SYBR premix and Ex Taq II Tli RNase H Plus (Clontech/Takara, catalog number RR820L).
12. Standard agarose gel loading dyes: e.g., Orange (6×) and Purple (6×) (New England Biolabs, catalog numbers B7022S and B7024S, respectively).
13. SYBR Safe DNA gel stain (e.g., Thermofisher Scientific, catalog number S33102)
14. 1 Kb plus DNA ladder (Invitrogen, 10787-018)
15. Double distilled-autoclaved water.

2.5 Reagents Unique to ChIP-qPCR

1. Formaldehyde, stock 36.5–38% (e.g., Sigma, catalog number F8775).
2. Glycine 2.5M (sterilized by autoclaving).
3. Phosphate buffered saline (PBS) 1× pH 7.4: 137 mM NaCl, 2.7 mM KCl, 4.3 mM Na₂HPO₄, 1.47 mM KH₂PO₄ (sterilized by autoclaving).
4. Glycerol stock 100% (sterilized by autoclaving).

5. 425–600 μm glass beads (e.g., Sigma, catalog number G8772).
6. Sepharose CL-4B beads (e.g., Sigma, catalog number CL4B200).
7. Protein A sepharose CL-4B beads (e.g., VWR International/GE Healthcare, catalog number 17-0780-01).

2.6 Reagents Unique to DRIP-qPCR

1. Zymolyase (R) 20T (e.g., Amsbio, catalog number 120491–1): for a stock of 1000 units/ml, dissolve 40–45 mg powder in 1 ml water. Aliquot 100 units per tube and store at $-20\text{ }^{\circ}\text{C}$.
2. Spheroplasting buffer: 1 M sorbitol, 2 mM Tris–HCl pH 8, 100 mM EDTA. Filter-sterilize. Store at room temperature (RT).
3. DNA extraction kit for yeast cells, e.g., Blood & Cell Culture DNA Mini Kit (Qiagen, catalog number 13323).
4. Five restriction endonuclease (RE) enzymes: BsrGI (10.000 units/ml), EcoRI–HF (20.000 units/ml), HindIII–HF (20.000 units/ml), SspI (5000 units/ml), and XbaI (20.000 units/ml) (New England Biolabs, catalog numbers R0575, R3101, R3104, R0132, and R0145, respectively).
5. Spermidine (e.g., Sigma, catalog number S2626).
6. NEB buffer 2.1 containing 100 $\mu\text{g}/\text{ml}$ BSA (New England Biolabs, catalog number B7202S).
7. Phase lock gel light, 2 ml tubes (5 Prime, catalog number 2302820).
8. Phenol–chloroform–isoamyl alcohol (PCI) at 25:24:1 v/v/v: we make the mixture ourselves by using a phenol solution pH 6.7 ± 0.2 , equilibrated with 10 mM Tris–HCl pH 8 and 1 mM EDTA, (Sigma, catalog number P4557).
9. Sodium acetate 3M pH 5.2.
10. GlycoBlue coprecipitant 15 mg/ml (e.g., Thermofisher Scientific, catalog number AM9515).
11. Ethanol 100% and 70%.
12. Isopropanol 100%.
13. Dynabeads Protein A for immunoprecipitation (e.g., Thermofisher Scientific, catalog number 10002D).
14. Tween 20 (e.g., Scientific Laboratory Supplies, catalog number CHE3852).
15. Qubit dsDNA HS Assay Kit and assay tubes (Thermofisher Scientific, catalog numbers Q32851 and Q32856, respectively).

3 Methods

3.1 ChIP-qPCR

Here we describe a protocol for immunoprecipitation of RNA:DNA hybrids from formaldehyde-crosslinked and sonicated chromatin (ChIP), which is modified from [50] (*see* Fig. 1a). We process three samples in parallel, the “input DNA,” the “No-antibody control,” and the “S9.6-immunoprecipitate.”

3.1.1 Formaldehyde Crosslinking of Yeast Cells

1. Use 10^9 yeast cells (~ 50 OD₆₀₀ of mid-log phase growth at ~ 0.6 ; for this protocol we used a derivative of yeast strain BY4741).
2. Add 1% formaldehyde and swirl gently and occasionally at RT (18–25 °C) for 25 min (*see* Note 1).
3. Add 137.5 mM glycine in order to quench formaldehyde. Swirl gently and occasionally at RT, for at least 5 min (*see* Note 1).
4. Collect cells in 50 ml tubes. Spin at $3000 \times g$ for 5 min at 4 °C. Discard supernatants. Wash cell pellets with 35 ml ice-cold 1× PBS. Spin as before. Discard supernatant and repeat washes twice. Remove all traces of supernatant by pipetting. Cell pellets can be stored in the 50 ml tube (or in 1.5 ml safe-lock tube) at -20 °C for several months (or at -80 °C for long term).

3.1.2 Cell Lysis

1. Add 400 μ l FA-1* buffer (*see* Note 2) on top of the cell pellets, on ice. Wait for few minutes until pellet is completely thawed. Resuspend cells by pipetting up and down several times using 1 ml tips. Pour ~ 500 μ l glass beads into a 1.5 ml safe-lock tube. Add the 400 μ l of resuspended cells on top of the glass beads. Close the tube tightly. Place on a multi-vortexer, setting maximum, in the cold room at 4 °C. Vortex for 45 min.
2. Pull the plunger from a 5 ml syringe and discard it. Place the 1.5 ml tube (containing glass beads and cell lysate) in the emptied syringe. Place the whole set in an uncapped 15 ml tube, on ice. Proceed by puncturing the 1.5 ml tube with a hot needle, firstly in the cap and secondly in the bottom. Collect the whole cell lysate in the 15 ml tube by centrifuging at low speed $335 \times g$ for 1 min at 4 °C. Add 100 μ l FA-1* buffer to wash the glass beads from residual cell lysates. Spin as previously. Transfer the cell lysate in a new 1.5 ml tube.
3. Spin at $16,000 \times g$ for 10 min at 4 °C. Remove the supernatant by pipetting (*see* Note 3) and make sure to recover only the cell pellet. Resuspend the lysed cell pellet in 600 μ l FA-1* buffer, on ice.

3.1.3 Sonication of the Crosslinked Chromatin

1. Switch on the sonicator and wait until the water cools down to 4 °C. Split the whole cell extract into two 1.5 ml bioruptor microtubes (300 μ l each tube, i.e., ~ 25 OD₆₀₀ cells per tube).

Close the tubes tightly and place them in the water bath of the sonicator (*see Note 4*). Sonicate for 30 s ON, 30 s OFF, 15–20 cycles.

2. Pool sonicated chromatin in one 1.5 ml tube, on ice. Spin for 15 min at $16,000 \times g$, 4 °C. Transfer ~570 μ l supernatant into a 5 ml tube (*see Notes 5 and 6*). Top-up with FA-1* buffer for a total volume of ~1600 μ l. Add 80 μ l of glycerol 100% (final ~5%) (*see Note 7*). Mix on a rotating wheel for 5–10 min at 4 °C.

3.1.4

Immunoprecipitation of Cross-Linked RNA:DNA Hybrids

1. Add ~1680 μ l sonicated chromatin to ~150 μ l bed of pre-washed sepharose CL-4B beads (*see Note 8*) in a new 5 ml tube, on ice. Pre-clear the sonicated chromatin by mixing on a rotating wheel for 1 h at 4 °C. At the end of the process, spin at $335 \times g$ for 1 min at 4 °C and transfer the supernatant to a fresh 5 ml tube.
2. Prepare sample “Input chromatin”: Transfer 20 μ l of “pre-cleared-sonicated-chromatin” to a safe-lock 1.5 ml tube. Keep overnight at 4 °C.
3. Prepare samples “S9.6-immunoprecipitate” and “No-antibody control”: For “S9.6-immunoprecipitate” add ~800 μ l of pre-cleared-sonicated-chromatin and 10–20 μ g of the S9.6 antibody (*see Note 9*) to ~50–60 μ l bed of Protein A sepharose CL-4B beads (*see Note 10*), in a safe-lock 1.5 ml tube, on ice. Repeat the same for the “No-antibody control” sample but without adding antibody. Mix samples overnight (12–16 h) on a rotating wheel at 4 °C.

3.1.5 *Washing of Protein A Sepharose Beads*

1. Recover protein A beads by centrifugation for 1–2 min, at low speed ($100\text{--}400 \times g$), 4 °C. Discard supernatant by pipetting gently (*see Note 11*).
2. Wash protein A sepharose beads, using a rotating wheel at 4 °C (*see Notes 12 and 13*), subsequently as follow: 3×10 min with FA-1* buffer, 1 ml each wash; 20 min with 1 ml FA-2* buffer; 15 min with 1 ml FA-3* buffer; 3×10 min with $1 \times$ TE, 1 ml each wash. At the end of the washings, remove all traces of supernatant by pipetting.

3.1.6 *Crosslink Reversal and Purification of DNA*

1. Perform reversal of crosslinked-sonicated-chromatin for three samples, i.e., “input chromatin,” “no-antibody control,” and “S9.6-immunoprecipitate.” Add 150 μ l of $1 \times$ TE buffer containing 1% SDS and 1 mg/ml PK. Vortex mildly. Incubate overnight (12–16 h) at 65 °C (*see Note 14*) in a thermomixer, preferably with shaking at 500 rpm.
2. Purify DNA using Qiagen MinElute kit (follow manufacturer’s conditions; *see also Note 15*). Elute DNA with 26 μ l buffer EB

Table 1

Sequence of primer pairs used routinely as a control for the efficiency of immunoprecipitation with the S9.6 antibody, in ChIP-qPCR and DRIP-qPCR. Primer pairs *CEN16* and *ARS504* can be used for normalization in ChIP-qPCR and DRIP-qPCR, respectively

Name of primer	Sequence of primer	Specifications of amplified region
1-18S2-forward	TCCAATTGTTTCCTCGTTAAG	18S rDNA (gDNA)
1-18S2-reverse	ATTCAGGGAGGTAGTGACAA	18S rDNA (gDNA)
21S-1-forward	CGAAAGCAAACGATCTAACT	21S rDNA (mtDNA)
21S-1-reverse	AGCTATCTGCAAACCAGATT	21S rDNA (mtDNA)
CEN16-1-forward	TGAGCAAACAATTTGAACAG	<i>CEN16</i> (Centromere of chr XVI)
CEN16-1-reverse	CCGATTTGCTTTAGAAC	<i>CEN16</i> (Centromere of chr XVI)
ARS504-forward	TCCTTTAAGAGGTGATGGTG	<i>ARS504</i> (chr V)
ARS504-reverse	GTGCGCAGTACTTGTGAAA	<i>ARS504</i> (chr V)

containing 0.5 µg/ml ChIP-RNase A. Wait for 5 min. Spin column for 1 min at $20,000 \times g$, RT. Repeat elution once, in order to obtain a total of ~50 µl DNA. Dilute 1:1 by adding 50 µl EB (containing 0.5 µg/ml ChIP-RNase A), for a total of ~100 µl.

3.1.7 Amplification of DNA by qPCR

1. Perform reactions in triplicate using a real-time PCR machine. 10 µl reactions contain: 5 µl of $2 \times$ SYBR premix, 2 µl of “S9.6-immunoprecipitate” (or 2 µl of “no-antibody” control, or 2 µl of 1:10 dilution of input chromatin), 0.4 µl of 10 µM primers (mix of forward and reverse at 1:1), 0.04 µl of Rox II; 2.56 µl of water. In order to look for S9.6 immunoprecipitation efficiencies, we usually test loci that are known to be highly enriched in R-loops (e.g., rDNA and mtDNA, *see* Table 1 and [27]).
2. Set program “Sybr green with dissociation curve.” Set parameters of qPCR as follow: 1 cycle of (95 °C 30 s) and 38 cycles of (95 °C 5 s, 55 °C 15 s, 72 °C 15 s). Set parameters of dissociation curve as follow: 1 cycle of (95 °C 1 min, 55 °C 30 s, 95 °C 30 s).
3. For calculation of qPCR values *see* Note 16.

3.2 DRIP-qPCR

Here we describe a protocol adapted for immunoprecipitation of RNA:DNA hybrids using naked DNA (*see* Note 17), which is fragmented by a cocktail of five RE as described in [51] (*see* Fig. 1b). We process two samples in parallel, the “input DNA” and the “S9.6-immunoprecipitate.”

3.2.1 Preparation of Naked DNA

We used a Blood & Cell Culture DNA Mini Kit (Qiagen) for extraction of yeast DNA. We followed the instructions in the manual with some modifications.

1. Harvest $7\text{--}8 \times 10^8$ yeast cells ($35\text{--}40$ OD₆₀₀ of mid-log phase growth at ~ 0.6 ; in this protocol we tested a derivative of yeast strain YPH54) in 50 ml tubes, by centrifuging at $3000 \times g$ for 5 min at 4 °C. Discard supernatant. Wash cell pellet once with 35 ml ice-cold $1 \times$ TE. Spin as above, discard the supernatant and store the pellet in a safe-lock 1.5 ml tube at -80 °C.
2. Add 1 ml of spheroplasting buffer (supplemented freshly with 0.1% β -mercaptoethanol) on top of the frozen cell pellet, at RT. Wait until pellet is completely thawed. Add 100 μ l zymolyase (stock 1000 units/ml). Mix by inverting the tube several times. Incubate at 30 °C for 1 h in a thermomixer with shaking at 500 rpm. In addition, mix by inverting the tube occasionally.
3. Spin for 10 min at $5000 \times g$ and 4 °C. Discard the supernatant by pipetting gently without disturbing the lysed cell pellet. Add 1 ml water on top of the lysed cell pellet. Remove the water by gentle pipetting. This step helps to get rid of any residues of zymolyase.
4. Add 1 ml of buffer G2 (provided in the kit, *see Note 18*) on top of the spheroplast pellet and transfer by pipetting to a 5 ml tube containing already 1 ml buffer G2. Resuspend the spheroplast by pipetting gently, 30–50 times with a 1000 μ l wide-orifice filter tip (*see Note 19*).
5. Add 50 μ l PK (stock 20 mg/ml). Mix by inverting the tube several times. Incubate at 37 °C for 1 h or more (*see Note 20*), with shaking at 500 rpm. In addition, mix by inverting the tube occasionally.
6. Spin at $5000 \times g$ for 10 min at 4 °C. Transfer ~ 2 ml supernatant to a fresh 5 ml tube, using a 1000 μ l, wide-orifice filter tip, without touching the white precipitate in the bottom of the tube.
7. Add 2 ml buffer QBT (provided in the kit). Mix the 4 ml sample quickly and thoroughly, by inverting the tube several times. Avoid vortexing.
8. Pre-equilibrate a genomic tip 20/G with 1 ml buffer QBT (as recommended by the manufacturer). Apply 2×2 ml sample to the column, using a 1000 μ l, wide-orifice filter tip.
9. Wash the column with 3×1 ml buffer QC (provided in the kit).
10. Preheat 2 ml buffer QF (provided in the kit) at 50 °C. Elute the DNA with 2 ml preheated buffer QF in a new 15 ml tube.
11. Add 1.4 ml of 100% isopropanol (final concentration $\sim 41\%$) to the eluted DNA in the 15 ml tube. Close the tube and mix by

inverting several times. Spin briefly. Transfer $3 \times \sim 1.13$ ml to three 1.5 ml tubes.

12. Spin at $20,000 \times g$, 5 min, RT. Remove supernatant carefully by pipetting. Add 400 μ l of 70% ethanol in each tube. Dislodge DNA pellets in to ethanol 70% by pipetting, using a wide-orifice 1000 μ l tip. Pool three supernatants in 1 tube (total ~ 1200 μ l). Spin at $20,000 \times g$, 2 min, RT. Remove supernatant carefully by pipetting. Spin briefly at full speed. Remove all traces of ethanol by pipetting. Avoid air-drying the DNA pellet. Add immediately 50 μ l $1 \times$ TE.
13. Leave the DNA pellet to dissolve at RT for 1–2 h or overnight at 4 °C.
14. Flick the tube several times in order to ensure that the DNA is homogeneously resuspended in TE buffer. Store DNA at 4 °C.
15. Measure DNA concentration using 1 μ l of 1:5 dilution and Qubit dsDNA HS Assay Kit (as recommended by the manufacturer). The DNA yield can vary between preparations and strains (e.g., for 35–40 OD₆₀₀ cells the expected DNA yield can vary between ~ 10 and 20 μ g; *see also Note 21*).

3.2.2 Fragmentation of Naked DNA by RE Digestion

1. Set up a 250 μ l reaction in 1.5 ml safe-lock tube as follow: 152 μ l H₂O, 50 μ l DNA (10–15 μ g in $1 \times$ TE), 25 μ l $10 \times$ NEB buffer 2.1, 0.5 μ l 1 M spermidine, 2.5 μ l HindIII-HF, 2.5 μ l EcoRI-HF, 2.5 μ l XbaI, 10 μ l SspI, and 5 μ l BsrGI. Mix gently using a wide-orifice 1000 μ l tip. Incubate at 37 °C (17–24 h) in a thermomixer, with shaking 500 rpm. Spin tube briefly at the end of the incubation (*see Note 22*).
2. Pre-spin a 2 ml light phase lock tube, for 30 s, $12,000 \times g$, RT (as recommended by the manufacturer). Add 255 μ l $1 \times$ TE to the 245 μ l RE digestion reaction. Transfer ~ 500 μ l to the pre-spun light phase lock tube. Add 500 μ l PCI. Mix gently on a rotating wheel (or shaking platform) at least for 10 min, RT (*see Note 23*). Spin for 5 min at $12,000 \times g$, RT. Recover about ~ 500 μ l of the aqueous phase. Transfer 2×250 μ l to two 1.5 ml safe-lock tubes.
3. Precipitate DNA by adding 0.75 μ l GlycoBlue, 1:10 volume 3M sodium acetate, and 3 volumes 100% ethanol. Mix by inverting the tube several times (*see Note 23*). Place in freezer -80 °C for 30 min (or overnight at -20 °C). Spin at $16,000 \times g$ for 10 min, 4 °C. Discard supernatant. Add 750 μ l 70% ethanol and mix on a rotating wheel for 5 min at 4 °C (*see Note 23*). Spin at $16,000 \times g$ for 5 min. Discard all traces of ethanol and leave the “blue” DNA pellet to air-dry. Add 16 μ l $1 \times$ TE in each tube (*see Note 24*). After 10 min, resuspend DNA by pipetting using a cutoff filter tip, on ice. Pool DNA (~ 30 μ l in total) and store at 4 °C.

4. Measure DNA concentration by using 1 μ l of 1:5 dilution and Qubit dsDNA HS Assay Kit (follow instructions given by the manufacturer). We usually obtain from a starting material of ~13 μ g of undigested DNA, ~10–11 μ g of RE digested DNA.

3.2.3 Immunoprecipitation of Naked RNA:DNA Hybrids

1. Add 4–5 μ g fragmented DNA to a 1.5 ml tube containing FA-1* buffer, for a total volume of 400 μ l. Mix by inverting the tube several times (*see Note 23*). For sample “input DNA,” keep 8 μ l (input fraction ~2%, *see Note 29*) in a 1.5 ml tube overnight at 4 °C.
2. For sample “S9.6-immunoprecipitate,” place the remaining ~392 μ l fragmented DNA in to a 1.5 ml tube containing ~40 μ l prewashed protein A dynabeads (*see Note 25*), on ice. Add 10 μ l antibody S9.6 (~10 μ g) (*see Note 9*). Mix on a rotating wheel overnight (~16–18 h) at 4 °C (*see Note 26*).

3.2.4 Washing of Protein A Dynabeads and Purification of DNA

1. Recover the beads using a magnetic rack (*see Note 25*). Wash beads with FA-1* buffer as follow: Add 1 ml buffer to the beads, on ice. Close the tube and flick it several times, in order to bring the beads in resuspension. Mix by inverting several times. Recover the beads using a magnetic rack (*see Note 25*). Repeat the washing procedure twice. Similarly, wash sequentially with buffers FA-2*, FA-3*, and 1 \times TE (supplemented with Tween 0.05%), three times each, 3 \times 1 ml. Following the wash with 1 \times TE, remove all traces of buffer by pipetting.
2. Add in tubes “input DNA” and “S9.6-immunoprecipitate” 150 μ l of 1 \times TE buffer containing 1% SDS and 1 mg/ml PK. Vortex gently. Incubate at 55 °C for 2 h in a thermomixer, preferably with shaking 500 rpm. Vortex the tubes occasionally and gently (*see Note 27*).
3. Purify and elute DNA as in Subheading 3.1.6, step 2.

3.2.5 Amplification of DNA by qPCR

1. Perform qPCRs as in Subheading 3.1.7, steps 1 and 2 (*see Note 28*).
2. DRIP-qPCR data can be calculated by using the Percent Input Method (*see Note 29*).

4 Notes

1. Swirl the cells occasionally during the cross-linking procedure to avoid settling in the bottom of the flask/bottle. Crosslinking time is empirical but should be kept constant between experiments and samples. It is important to note that immunoprecipitation efficiencies of RNA:DNA hybrids may vary according

to the length of crosslinking times. In case the signal-to-noise ratio is very low (e.g., at mRNA genes and/or non-coding loci that are weakly transcribed by RNAP II) crosslinking times could be decreased or the crosslinking step can be totally omitted (*see ref. 41*). Alternatively, the crosslinking step could be maintained but reversal of crosslinking could be performed after the sonication procedure and before immunoprecipitation with the S9.6 antibody (*see refs. 25, 39, 52*).

2. Star (*) indicates complete protease inhibitor cocktail containing EDTA at a working concentration of 1×. FA-1*, FA-2* and FA-3* buffers should be kept always on ice.
3. This step is optional and is usually performed to get rid of proteins that are not associated with the chromatin fraction and of any impurities that may interfere with the immunoprecipitation process.
4. The sample should be maintained at 4 °C throughout the sonication process.
5. Make sure not to touch the pellet of cell debris when pipetting the supernatant. Keep the supernatant and discard the pellet.
6. The size of sonicated chromatin (in the range of 300–500 bp) can be checked on a standard agarose gel. Add 10 µl of sonicated DNA to 150 µl mixture of 1x TE containing 1% SDS and 1 mg/ml PK, in a 1.5 ml safe-lock tube. Mix by vortexing. Incubate at 65 °C overnight (for reversal of cross-links and digestion of proteins). Purify DNA using MinElute PCR purification kit and elute DNA with 10 µl EB buffer. Treat with RNase A, e.g., 0.25 µg/µl, for 30 min at 37 °C (note that RNase A at high concentrations, e.g., 0.25 µg/µl, may stick to the DNA, which can make it difficult to assess the size of sonicated DNA on a gel. If so, decrease the amount of RNase A.). Mix with gel loading dye Orange (1× final) and run on a standard agarose gel (stained with 1x SYBR Safe) alongside with a DNA ladder. Visualize by scanning the gel in a phosphorImager. In case the DNA fragments are not in the range of 300–500 bp, the sonication parameters can be adjusted accordingly. If the formaldehyde-crosslinking of chromatin is to be omitted, the sonication time as well as the number of cycles should be reduced (for example *see ref. 41*).
7. We noticed that the addition of glycerol to a final concentration 5% could preserve the chromatin from precipitation after cycles of freezing–thawing. At this stage, the sonicated chromatin can be stored at –20 °C for long term and for further use.
8. Pre-wash sepharose Cl-4B beads with FA-1* buffer. For instance, add 1 ml FA-1* buffer to ~150 µl bed of sepharose Cl-4B beads, in a 1.5 ml tube, on ice. Rotate for 5 min at 4 °C. Spin at 400 × *g* for 1 min at 4 °C. Discard the supernatant

completely by pipetting. Repeat washing once. All pipetting of beads should be done with cutoff tips and centrifugations at low speed $100\text{--}400 \times g$, at 4°C .

9. The amount of antibody required is empirical and may vary between batches. The efficiency of the antibody could be assessed after immunoprecipitation by testing by qPCR some loci that are known to be highly enriched in R-loops, e.g., the gDNA and mtDNA (*see* Table 1 and [27]).
10. The powder of sepharose Protein A Cl-4B beads should be pre-swollen in water, on ice. The swollen beads should be washed subsequently, twice with water, and twice with FA-1* buffer (*see* also **Note 8**).
11. It is important to take extra care when pipetting to avoid losses of beads, i.e., the bed of beads should be neither perturbed nor aspirated in the tip.
12. Number and time of washes are empirical. After each wash, spin beads at low speed ($100\text{--}400 \times g$), 4°C , for 1–2 min. Discard all traces of buffer by pipetting (*see* also **Note 11**). Samples should be kept on ice as much as possible.
13. As a control for the specificity of the S9.6 antibody, protein A beads from sample “S9.6-immunoprecipitate” can be treated with recombinant RNase HI (e.g., New England Biolabs, catalog number M0297), as described in [27]. Alternatively, the DNA recovered from sample “S9.6-immunoprecipitate” (Sub-heading 3.1.6, **step 2**) can be treated with recombinant RNase HI and reimmunoprecipitated with the antibody S9.6 (*see* supplementary material and Fig. S5 in [15]). We noticed that a small fraction of immunoprecipitated RNA:DNA hybrids associated with the rDNA and mtDNA can be refractory to recombinant RNase HI treatment. This could be due to several reasons, including: (i) The complexity/length of such hybrids (*see* ref. 53), and/or (ii) the association of cross-linked hybrids with endogenous proteins, which could make them refractory to digestion by recombinant RNase HI (*see* Sub-heading 1), and/or (iii) the presence in such hybrids of dsRNA structures that are refractory to digestion by recombinant RNase HI but are amenable to immunoprecipitation by antibody S9.6 [49].
14. As PK from *Pichia pastoris* retains its full activity at 65°C (according to the manufacturer), both steps, i.e., reversal of crosslinking and protein digestion can be combined and performed overnight at 65°C . Alternatively, crosslinking can be reversed by incubation in $1 \times$ TE buffer containing 1% SDS at 65°C overnight, and digestion of proteins with PK can be performed the following day at 55°C for 2–3 h.

15. Before proceeding with elution of DNA make sure that no residual traces of ethanol are left in the MinElute spin column, as traces of ethanol can inhibit subsequent qPCR reactions. We usually place the column in a fresh 1.5 ml tube, spin for 1 or 2 min at $20,000 \times g$, and repeat the procedure (by replacing the 1.5 ml tube with a new one) up to several times, until no residual traces of ethanol are observed in the bottom of the tube. Finally, make sure to elute the DNA in a fresh 1.5 ml tube.
16. The ChIP protocol presented herein gives a very low qPCR signal of RNA:DNA hybrids at the locus *CEN16*. We thus normalize the ChIP-qPCR values to *CEN16* (*see* Table 1 and [27]), in order to compensate for differences in immunoprecipitation efficiencies within and between samples. Calculate the average of triplicates of Ct values and apply the following formulas:

$$\frac{\Delta\Delta Ct \text{ "no-antibody control" target gene}}{\Delta\Delta Ct \text{ "no-antibody control" } CEN16} = \frac{2^{-(Ct \text{ "no-antibody control" target gene} - Ct \text{ "input chromatin" target gene})}}{2^{-(Ct \text{ "no-antibody control" } CEN16 - Ct \text{ "input chromatin" } CEN16)}}$$

$$\frac{\Delta\Delta Ct \text{ "S9.6-immunoprecipitate" target gene}}{\Delta\Delta Ct \text{ "S9.6-immunoprecipitate" } CEN16} = \frac{2^{-(Ct \text{ "S9.6-immunoprecipitate" target gene} - Ct \text{ "input chromatin" target gene})}}{2^{-(Ct \text{ "S9.6-immunoprecipitate" } CEN16 - Ct \text{ "input chromatin" } CEN16)}}$$
17. RNA:DNA hybrids embedded in naked DNA could be sensitive to degradation by RNase A at low salt concentrations (*see* [25]). To avoid RNase contamination, use filter tips, RNase-free tubes, and filter-sterilized solutions.
18. Do not add RNase A in buffer G2 (for the same reason as in **Note 17**).
19. Place the wide-orifice tip in the bottom of the tube. Pipette gently until all white filaments are homogeneously dissolved in the G2 buffer. Avoid vortexing, in order to preserve the integrity of RNA:DNA hybrids.
20. We avoided heating the DNA sample at 50 °C in presence of PK for the same reason as in **Note 19**.
21. Due to omission of RNase A in buffer G2 we observed that the DNA can be contaminated with total RNA (degree of contamination varies between preparations and strains; in some mutants the RNA/DNA ratio can be much lower than in the wild-type). RNA concentration can be measured using 1 µl of a dilution 1:25 of the naked DNA and Qubit RNA HS Assay kit (ThermoFisher Scientific, catalog number Q32852) as recommended by the manufacturer.
22. The RE digestion could be checked on a standard agarose gel as follow: Mix in a 1.5 ml tube 4 µl DNA, 3.5 µl of $1 \times$ TE, and 2.5 µl of 1 mg/ml RNase A. Vortex and incubate for ~30 min at 37 °C. Add 2 µl gel loading dye purple 6× and mix by

vortexing. Run sample on a standard 0.8% agarose gel (stained with 1× SYBR Safe) alongside with a DNA ladder. Visualize by scanning the gel in a phosphorImager. DNA fragments form a smear that run below ~3000–2000 bp. In theory, 26,909 fragments should be generated by the Cocktail of five enzymes (XbaI, SspI, HindIII, EcoRI, and BsrGI) and 60% of the genome should be represented by fragments ≥ 100 bp and ≤ 1 kbp.

23. Avoid mixing by vortexing for the same reason as in **Note 19**.
24. The specificity of the antibody S9.6 could be checked by performing a control with RNase H, e.g., recombinant RNase HI (*see* **Note 13**). Split the RE-fragmented DNA in to two halves: One as a mock (i.e., without adding RNase HI) and one for treatment with RNase HI (as recommended by the manufacturer, *see* also **Note 13**). Incubate both samples overnight at 37 °C. Stop RNase HI reaction by adding 10 mM EDTA. Precipitate the DNA and resuspend it in 15 μ l 1× TE (as described in Subheading 3.2.2, **step 3**). Incubate both DNA samples, i.e., mock and RNase H-treated, with protein A dynabeads and the S9.6 antibody (proceed as described in Subheading 3.2.3 and the following sections).
25. To prewash protein A dynabeads, transfer ~40 μ l beads, using a cutoff tip, to a 1.5 ml tube containing already 250 μ l FA-1* buffer, on ice. Invert the tube several times. To recover the beads, place the tube on a magnetic rack at RT, wait for 1 min and discard the supernatant by pipetting. Repeat washing once. For several DNA samples, e.g., for ten samples, wash ~400 μ l beads with 2.5 ml FA-1* buffer, in a 5 ml tube. Use an appropriate magnetic rack for large tubes to recover the beads. Add 2.5 ml FA-1* buffer, invert several times and aliquot beads equally in 10 small tubes of 1.5 ml. Recover the beads as mentioned above.
26. We did not include a “no-antibody control” sample as incubation of naked DNA with protein A dynabeads without adding the S9.6 antibody gave a very low signal to noise, for most of the loci tested with qPCR.
27. This step helps unlinking the DNA from the beads, by digestion with PK of both protein A and the S9.6 antibody.
28. Avoid designing/ordering qPCR primer pairs that amplify DNA sequences endowed with cutting sites for either of the 5 RE [i.e., BsrGI (T[^]GTACA), EcoRI-HF (G[^]AATTC), HindIII-HF (A[^]AGCTT), SspI (AAT[^]ATT), and XbaI (T[^]CTAGA)], as these sequences should be broken during the RE-fragmentation of naked DNA.

29. For “Percent Input Method” refer for example to (<https://www.thermofisher.com/uk/en/home/life-science/epigenetics-noncoding-rna-research/chromatin-remodeling/chromatin-immunoprecipitation-chip/chip-analysis.html>). For instance, herein, the starting input fraction is ~2%. As 2 μ l of a dilution 1:10 were used in the qPCR reaction, this brings the starting input fraction to ~0.4%. A dilution factor of 250 or 7.96 cycles (i.e., \log_2 of 250) is subtracted from the Ct value of diluted input (i.e., Adjusted input target gene = Ct Input target gene – 7.96). To express the Ct values of “S9.6-immunoprecipitate” of target gene as percent of input, calculate the average of Ct values of triplicates, and then apply the formula: Percent input of target gene = $100 \times 2^{(\text{Adjusted input target gene} - \text{Ct “S9.6-immunoprecipitate” target gene})}$. The values could be further normalized to a non-transcribed region, e.g., *ARS504* (see Table 1).

Acknowledgments

We thank Kim Kotovic for initial help with the ChIP technique, members of Jean Beggs lab for giving us access to the bioruptor PICO, and Shaun Webb for help with bioinformatics analysis. We thank Andres Aguilera, Frederic Chedin, Martin Reijns, and Leonel Sanz for sharing protocols and/or reagents. We thank Frederic Chedin, Benoit Palancade, and Ralf Wellinger for critically reading the manuscript. We apologise to the colleagues whose work is not cited in this chapter due to space constraints. This work was supported by a Wellcome Trust Fellowship to DT (077248) and by core funding to the Wellcome Trust Centre for Cell Biology (092076).

References

1. Lesage P, Todeschini AL (2005) Happy together: the life and times of Ty retrotransposons and their hosts. *Cytogenet Genome Res* 110(1–4):70–90
2. Lujan SA, Williams JS, Kunkel TA (2016) DNA polymerases divide the labor of genome replication. *Trends Cell Biol* 26(9):640–654
3. Nudler E (2009) RNA polymerase active center: the molecular engine of transcription. *Annu Rev Biochem* 78:335–61. doi: <https://doi.org/10.1146/annurev.biochem.76.052705.164655>. Review. PMID:19489723
4. Aguilera A, Garcia-Muse T (2012) R loops: from transcription byproducts to threats to genome stability. *Mol Cell* 46(2):115–124
5. Drolet M (2006) Growth inhibition mediated by excess negative supercoiling: the interplay between transcription elongation, R-loop formation and DNA topology. *Mol Microbiol* 59(3):723–730
6. Groh M, Gromak N (2014) Out of balance: R-loops in human disease. *PLoS Genet* 10(9): e1004630
7. Hamperl S, Cimprich KA (2014) The contribution of co-transcriptional RNA:DNA hybrid structures to DNA damage and genome instability. *DNA Repair (Amst)* 19:84–94
8. Santos-Pereira JM, Aguilera A (2015) R loops: new modulators of genome dynamics and function. *Nat Rev Genet* 16(10):583–597
9. Skourti-Stathaki K, Proudfoot NJ (2014) A double-edged sword: R loops as threats to genome integrity and powerful regulators of gene expression. *Genes Dev* 28(13):1384–1396

10. Yu K et al (2003) R-loops at immunoglobulin class switch regions in the chromosomes of stimulated B cells. *Nat Immunol* 4 (5):442–451
11. Pefanis E, Basu U (2015) RNA exosome regulates AID DNA Mutator activity in the B cell genome. *Adv Immunol* 127:257–308
12. Drolet M et al (1995) Overexpression of RNase H partially complements the growth defect of an Escherichia coli delta topA mutant: R-loop formation is a major problem in the absence of DNA topoisomerase I. *Proc Natl Acad Sci U S A* 92(8):3526–3530
13. Pommier Y et al (2016) Roles of eukaryotic topoisomerases in transcription, replication and genomic stability. *Nat Rev Mol Cell Biol* 17(11):703–721
14. Fernandez X et al (2014) Chromatin regulates DNA torsional energy via topoisomerase II-mediated relaxation of positive supercoils. *EMBO J* 33(13):1492–1501
15. El Hage A et al (2010) Loss of topoisomerase I leads to R-loop-mediated transcriptional blocks during ribosomal RNA synthesis. *Genes Dev* 24(14):1546–1558
16. French SL et al (2011) Distinguishing the roles of topoisomerases I and II in relief of transcription-induced torsional stress in yeast rRNA genes. *Mol Cell Biol* 31(3):482–494
17. Cerritelli SM, Crouch RJ (2009) Ribonuclease H: the enzymes in eukaryotes. *FEBS J* 276 (6):1494–1505
18. Stuckey R et al (2015) Role for RNA:DNA hybrids in origin-independent replication priming in a eukaryotic system. *Proc Natl Acad Sci U S A* 112(18):5779–5784
19. Amon JD, Koshland D (2016) RNase H enables efficient repair of R-loop induced DNA damage. *elife* 5. <https://doi.org/10.7554/eLife.20533>.
20. Christman MF, Dietrich FS, Fink GR (1988) Mitotic recombination in the rDNA of *S. cerevisiae* is suppressed by the combined action of DNA topoisomerases I and II. *Cell* 55(3):413–425
21. Salvi JS et al (2014) Roles for Pbp1 and caloric restriction in genome and lifespan maintenance via suppression of RNA-DNA hybrids. *Dev Cell* 30(2):177–191
22. Pannunzio NR, Lieber MR (2016) Dissecting the roles of divergent and convergent transcription in chromosome instability. *Cell Rep* 14 (5):1025–1031
23. Yadav P, Owiti N, Kim N (2016) The role of topoisomerase I in suppressing genome instability associated with a highly transcribed guanine-rich sequence is not restricted to preventing RNA:DNA hybrid accumulation. *Nucleic Acids Res* 44(2):718–729
24. Jenjaroenpun P et al (2017) R-loopDB: a database for R-loop forming sequences (RLFS) and R-loops. *Nucleic Acids Res* 45(D1):D119–D127
25. Halasz L et al (2017) RNA-DNA hybrid (R-loop) immunoprecipitation mapping: an analytical workflow to evaluate inherent biases. *Genome Res* 27(6):1063–1073
26. Boguslawski SJ et al (1986) Characterization of monoclonal antibody to DNA:RNA and its application to immunodetection of hybrids. *J Immunol Methods* 89(1):123–130
27. El Hage A et al (2014) Genome-wide distribution of RNA-DNA hybrids identifies RNase H targets in tRNA genes, retrotransposons and mitochondria. *PLoS Genet* 10(10):e1004716
28. Rigby RE et al (2014) RNA:DNA hybrids are a novel molecular pattern sensed by TLR9. *EMBO J* 33(6):542–558
29. Koo CX et al (2015) RNA polymerase III regulates cytosolic RNA:DNA hybrids and intracellular microRNA expression. *J Biol Chem* 290(12):7463–7473
30. Hu Z et al (2006) An antibody-based microarray assay for small RNA detection. *Nucleic Acids Res* 34(7):e52
31. Chan YA et al (2014) Genome-wide profiling of yeast DNA:RNA hybrid prone sites with DRIP-chip. *PLoS Genet* 10(4):e1004288
32. Legros P et al (2014) RNA processing factors Swd2.2 and Sen1 antagonize RNA Pol III-dependent transcription and the localization of condensin at Pol III genes. *PLoS Genet* 10(11):e1004794
33. Saini N et al (2017) APOBEC3B cytidine deaminase targets the non-transcribed strand of tRNA genes in yeast. *DNA Repair (Amst)* 53:4–14
34. Mischo HE et al (2011) Yeast Sen1 helicase protects the genome from transcription-associated instability. *Mol Cell* 41(1):21–32
35. Alzu A et al (2012) Senataxin associates with replication forks to protect fork integrity across RNA-polymerase-II-transcribed genes. *Cell* 151(4):835–846
36. Grzechnik P, Gdula MR, Proudfoot NJ (2015) Pcf11 orchestrates transcription termination pathways in yeast. *Genes Dev* 29(8):849–861
37. Balk B et al (2013) Telomeric RNA-DNA hybrids affect telomere-length dynamics and senescence. *Nat Struct Mol Biol* 20 (10):1199–1205
38. Pfeiffer V et al (2013) The THO complex component Thp2 counteracts telomeric R-loops

- and telomere shortening. *EMBO J* 32 (21):2861–2871
39. Cloutier SC et al (2016) Regulated formation of lncRNA-DNA hybrids enables faster transcriptional induction and environmental adaptation. *Mol Cell* 61(3):393–404
 40. Keskin H, Meers C, Storici F (2016) Transcript RNA supports precise repair of its own DNA gene. *RNA Biol* 13(2):157–165
 41. Ohle C et al (2016) Transient RNA-DNA hybrids are required for efficient double-strand break repair. *Cell* 167(4):1001–1013.e7. <https://doi.org/10.1016/j.cell.2016.10.001>
 42. Holmes JB et al (2015) Primer retention owing to the absence of RNase H1 is catastrophic for mitochondrial DNA replication. *Proc Natl Acad Sci U S A* 112(30):9334–9339
 43. Wahba L et al (2016) S1-DRIP-seq identifies high expression and polyA tracts as major contributors to R-loop formation. *Genes Dev* 30 (11):1327–1338
 44. Sanz LA et al (2016) Prevalent, dynamic, and conserved R-loop structures associate with specific Epigenomic signatures in mammals. *Mol Cell* 63(1):167–178
 45. Chedin F (2016) Nascent connections: R-loops and chromatin patterning. *Trends Genet* 32(12):828–838
 46. Santos-Pereira JM et al (2013) The Npl3 hnRNP prevents R-loop-mediated transcription-replication conflicts and genome instability. *Genes Dev* 27(22):2445–2458
 47. Kim N, Jinks-Robertson S (2012) Transcription as a source of genome instability. *Nat Rev Genet* 13(3):204–214
 48. Wang IX et al (2016) RNA-DNA sequence differences in *Saccharomyces cerevisiae*. *Genome Res* 26(11):1544–1554
 49. Phillips DD et al (2013) The sub-nanomolar binding of DNA-RNA hybrids by the single-chain Fv fragment of antibody S9.6. *J Mol Recognit* 26(8):376–381
 50. Aparicio O et al (2005) Chromatin immunoprecipitation for determining the association of proteins with specific genomic sequences in vivo. *Curr Protoc Mol Biol* Chapter 21: p. Unit 21 3
 51. Ginno PA et al (2012) R-loop formation is a distinctive characteristic of unmethylated human CpG island promoters. *Mol Cell* 45 (6):814–825
 52. Zhao DY et al (2016) SMN and symmetric arginine dimethylation of RNA polymerase II C-terminal domain control termination. *Nature* 529(7584):48–53
 53. Brown TA, Tkachuk AN, Clayton DA (2008) Native R-loops persist throughout the mouse mitochondrial DNA genome. *J Biol Chem* 283 (52):36743–36751

Detection of *oriC*-Independent Replication in *Escherichia coli* Cells

Makisha Martel, Aurélien Balleydier, Julien Brochu, and Marc Drolet

Abstract

In bacteria, replication of the chromosome is normally initiated following the binding of DnaA proteins to the *oriC* region. However, under certain circumstances, replication can also be initiated independent of the *oriC*/DnaA system. This is the case, for example, in *Escherichia coli* cells lacking RNase HI (*rnhA* mutants) or type IA topoisomerase activity (*topA topB* mutants). Here, we present a protocol in which replication from the *oriC*/DnaA system is first inhibited by the addition of the protein synthesis inhibitor, spectinomycin, to exponentially growing bacterial cell cultures. The thymidine analog, 5-ethynyl-2'-deoxyuridine (EdU) is then added to the cells, and after 1 h the cells are fixed and the Alexa Fluor® 488 dye is conjugated to EdU by the click-iT® reaction. The *oriC*-independent replication is detected in fixed cells by flow cytometry and can be visualized by fluorescence microscopy.

Key words DNA replication, EdU, Bacteria, R-loop, *oriC*, Topoisomerases

1 Introduction

The accurate copying of the genetic material, DNA replication, is an essential step of the cell cycle in all living organisms. Replication is initiated by the binding of specific proteins to replication origins which induces DNA opening [1]. Replicative helicases can then be loaded to more extensively unwind DNA, a prerequisite for the addition of the replisome and the ensuing bidirectional replication [2]. For bacteria, replication of the circular chromosome is initiated following the binding of a specific protein, DnaA, to a specific nucleotide sequence named *oriC* [1].

Interestingly, replication from outside normal origins has been detected in various organisms from the three domains of life [3–8]. In non growing stationary phase *E. coli* cells, evidence for stress-induced mutagenesis being initiated by R-loop-dependent replication has been presented [9]. R-loop formation generally occurs during transcription, when the nascent RNA rehybridize with the template strand behind the moving RNA polymerase

(RNAP), thus leaving the nontemplate strand single-stranded [10–12]. The first evidence for R-loop formation in vivo came from work done in *E. coli topA* (topoisomerase I, a type IA topo) mutants [13, 14]. It was shown that a major function of topo I is to relax transcription-induced negative supercoiling, to inhibit R-loop formation [10, 15]. Such negative supercoiling promotes DNA opening, a prerequisite for R-loop formation.

Because an R-loop opens the DNA, it can potentially be used to initiate replication, providing that an alternative system, i.e., other than DnaA/*oriC*, is available to load the replicative helicase. In fact, such a system exists, the PriA-dependent primosome [16], and replication from R-loops was first described in *E. coli* cells lacking RNase HI (*rnhA*) [3], an enzyme degrading the RNA in the R-loop, and more recently in *topA topB* null mutants [17]. This replication was named “constitutive stable DNA replication” (cSDR) because, as opposed to the normal one from the chromosomal origin *oriC* (requiring de novo DnaA synthesis), it could continue for several hours following protein synthesis inhibition. Moreover, cells lacking RNase HI were found to be viable in the absence of the DnaA/*oriC* system [3].

In the classical procedure to detect cSDR, cells are treated with protein synthesis inhibitors to prevent replication initiation from *oriC*. [³H]-thymine is added to the cell culture and its incorporation during *oriC*-independent replication is measured following cells lysis, precipitation of nucleic acids on membrane filters with trichloroacetic acid and radioactivity measurement of the dried filters [18, 19]. However, this protocol is time-consuming, more or less accurate, requires the use of bacterial strains with specific genotypes and, most of all, because it involves cell lysis and total DNA extraction it only gives the average DNA replication level in a population of cells.

To study cSDR in *E. coli* cells lacking type IA topoisomerase activity [17], we have recently adapted the protocol of Ferullo et al. [20] in which the click-iT[®] reaction is used to conjugate the Alexa Fluor[®] 488 dye to the thymidine analog EdU incorporated during DNA synthesis, in order to visualize DNA replication in fixed cells by fluorescence microscopy. Here, we describe a protocol using EdU and the click-it[®] reaction with the Alexa Fluor[®] 488 dye, in which exponentially growing *E. coli* cells are initially exposed to spectinomycin for 2 h to allow the complete inhibition of *oriC*-dependent replication. *oriC*-independent replication is then measured and visualized respectively by flow cytometry and fluorescent microscopy.

2 Materials

2.1 EdU Labeling

1. LB medium (*see Note 1*) supplemented with required antibiotics and supplements.
2. 250 mL Erlenmeyer flasks.
3. Water bath shaker.
4. Spectrophotometer.
5. 50 mL glass tubes with ventilation caps.
6. 50 mL disposable centrifuge tubes.
7. Filtered spectinomycin (Sigma-Aldrich) solution at 50 mg/mL in deionized water.
8. EdU. We use the Click-iT[®] EdU Imaging Kits from Invitrogen. EdU can also be obtained from Sigma-Aldrich. EdU is prepared as a 10 mM stock solution in DMSO and stored at -20 °C. The stock solution is stable for 1 year.

2.2 Cell Fixation and Permeabilization

1. Methanol solution 90%.
2. Filtered PBS, pH 7.4.
3. 0.5% Triton X-100 in filtered PBS.

2.3 EdU Detection

1. Click-iT[®] EdU Imaging Kits from Invitrogen. See the Methods section for the preparation of the reaction cocktail.
2. Deionized water.
3. Filtered PBS, pH 7.4.

2.4 Measurement of EdU Incorporation by Flow Cytometry

1. Flow cytometer. We use a BD FACSCanto[™] II apparatus.
2. Software for data analysis. We use the BD FACSDiva[™] software (BD sciences).

2.5 Visualization of EdU Incorporation by Fluorescence Microscopy

1. Microscope slides.
2. Poly-L-Lysine (Sigma-Aldrich) solution 10%.
3. Prolong Diamond Antifade Mountant (Molecular Probes).
4. Cover glasses.
5. Fluorescent microscope. We use a Nikon TE2000U microscope equipped with a CoolSnap fx 12 bits CCD camera (Photometrics) and a GFP filter.
6. Software for images processing. We use the freely available ImageJ software (<https://fiji.sc/>).

3 Methods

3.1 EdU Labeling and Cell Fixation

1. Prepare overnight (ON) cultures of the *Escherichia coli* strains in LB medium at the appropriate temperature (37 °C or 30 °C for thermosensitive mutants). Add appropriate antibiotics and supplements.
2. Dilute the ON cultures to an OD₆₀₀ of 0.01 in 30 mL LB medium (supplemented with required antibiotics and supplements) in a 250 mL Erlenmeyer flask. Incubate in a water bath at the appropriate temperature with vigorous shaking (*see Note 2*) up to an OD₆₀₀ of 0.3.
3. At this stage three 2 mL aliquots of the cell cultures are withdrawn. The first one is directly transferred to a 50 mL disposable centrifuge tube containing 13 mL of methanol 90% (*see Note 3*). This is the negative control (*see Note 4*). The tube is kept on ice or in a refrigerator at 4 °C (fixed cells in methanol can be kept at 4 °C for a week).
4. The second 2 mL aliquot is transferred to a 50 mL glass tube (with a ventilation cap) that contains 24 µL of the 10 mM EdU solution (0.12 mM final; *see Note 5*). This tube is incubated in a water bath with shaking for 1 h and the cell culture is transferred to a 50 mL disposable centrifuge tube containing 13 mL of methanol 90%, as indicated in **step 4**. This is the positive control (*see Note 6*).
5. The third 2 mL aliquot is transferred to a 50 mL glass tube (with a ventilation cap) that contains 16 µL of the 50 mg/mL spectinomycin solution (400 µg/mL final; *see Note 7*). This tube is incubated in a water bath with shaking for 2 h (*see Note 8*) before the addition of 24 µL of the 10 mM EdU solution. After 1 h of incubation, the cell culture is transferred to a 50 mL disposable centrifuge tube containing 13 mL of methanol 90%, as indicated in **step 4**.

3.2 Cell Permeabilization

1. Centrifuge the cells fixed in methanol at 5000 × *g* for 15 min at 4 °C.
2. Resuspend them in 1.5 mL of filtered PBS, pH 7.4.
3. Centrifuge at 13,000 × *g* for 4 min at 4 °C.
4. Carefully resuspend the cells (no vortexing; *see Note 9*) in 100 µL of 0.5% Triton X-100 in filtered PBS.
5. Incubate the cells in the Triton X-100 solution for 30 min at room temperature (permeabilization).
6. Pellet the cells by centrifugation at 13,000 × *g* for 3 min at 4 °C.
7. Carefully resuspend them in 1.5 mL of filtered PBS, pH 7.4.

3.3 EdU Detection

1. Centrifuge the cells at $13,000 \times g$ for 4 min at 4 °C.
2. Resuspend in 200 μ L of the Click-iT[®] reaction cocktail. This reaction cocktail must be used within 15 min of preparation. 1 mL of the Click-iT[®] reaction cocktail is prepared by mixing in the order 860 μ L of 1 \times Click-iT[®] reaction buffer prepared by adding 4 mL of the 10 \times Click-iT[®] reaction buffer to 36 mL of deionized buffer (stable for up to 6 month at 4 °C), 20 μ L of CuSO₄, 2.5 μ L of Alexa Fluor[®]-azide solution in DMSO (*see Note 10*), and 100 μ L of reaction buffer additive.
3. Protect from light (use aluminum foil) and incubate at room temperature for 30 min. From this step it is important to minimize light exposure.
4. Centrifuge at $13,000 \times g$ for 3 min at 4 °C.
5. Resuspend the cells in 1.5 mL of filtered PBS, pH 7.4.
6. Wash again in PBS and centrifuge.
7. Resuspend in 1 mL of filtered PBS, pH 7.4.
8. Store at 4 °C protected from light. The Alexa Fluor[®] 488 labeling signal is stable for 2–3 weeks when the samples are kept in the refrigerator.

3.4 Measurement of EdU Incorporation by Flow Cytometry

1. The labeled cells are analyzed by flow cytometry with at least 10,000 events per sample. The side scatter (SSC) threshold is set at 200 to eliminate as much background noise as possible. Since we use Alexa Fluor[®] 488, the BD FACSCanto™ II apparatus is set for 488 nm (laser) with the 530/30 filter. For a different apparatus and dye, use the parameters recommended by the manufacturer. We recommend performing the experiments with gates to minimize variations from one sample to another within the same experiment. For every experiment it is also recommended to perform a wild-type strain control.
2. Use the appropriate software to analyze and present the data. We use the BD FACSDiva™ software (BD sciences). An example is presented in Fig. 1.

3.5 Visualization of EdU Incorporation by Fluorescence Microscopy

1. Prepare the microscope slides by covering them with a 10% Poly-L-Lysine solution for 5 min. Rinse with deionized water and dry the slides at room temperature ON.
2. Spot 3 μ L of the concentrated labeled cells (concentrated 3–5 times in PBS) on the microscopic slides.
3. Air-dry at room temperature.
4. Add one drop of Prolong Diamond Antifade Mountant (Molecular Probes) to the slides and seal with cover glasses.
5. Take pictures (fluorescence (Alexa Fluor[®] 488) and DIC) at random with a fluorescent microscope. We use a Nikon

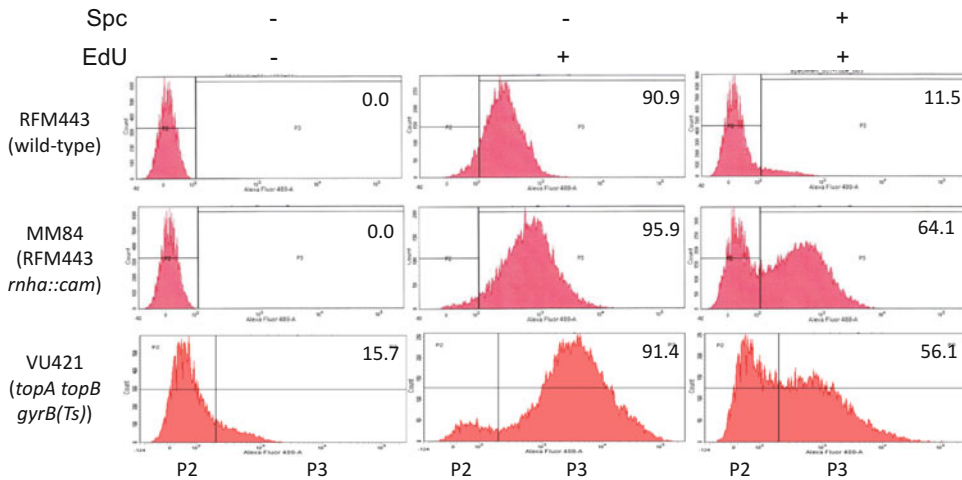


Fig. 1 Flow cytometry to measure EdU incorporation during replication in different strains of *Escherichia coli* as indicated. MM84 (*rnhA*⁻) and VU421 (*topA*⁻, *topB*⁻, *gyrB(Ts)*) are derivatives of the RFM443 wild-type strain. RFM443 and MM84 were grown at 37 °C, whereas VU421 was grown at 30 °C to reactivate gyrase. P2 and P3 zones respectively represent the nonspecific binding of Alexa Fluor[®] 488 (mostly observed in the negative control no EdU) and actively replicating cells (mostly observed in the positive control, with EdU but no *spc*). Cells with cSDR activity are found in the P3 zone in the samples treated with *spc* before the addition of EdU. The number in the upper right corner of the panels indicates the percentage of cells actively incorporating EdU (cells in the P3 zone). EdU is 5-ethynyl-2'-deoxyuridine and *Spc* is spectinomycin at 400 µg/mL

TE2000U microscope equipped with a CoolSnap fx 12 bits CCD camera. We use the GFP filter and an exposure time of 1 s.

6. Process the images with an appropriate software. We use ImageJ that is freely available (<https://fiji.sc/>).

4 Notes

1. Although minimal medium may also work well, we obtained better results when we used rich media such as LB. As cSDR depends on R-loops, rich media supporting high transcriptional activity may be more appropriate for cSDR than poor media.
2. A small volume of medium in a 250 mL Erlenmeyer flask and vigorous shaking promote high growth rates, which in turn should favor replication, including cSDR (*see Note 1*).
3. We use methanol to fix cells. Although we have not tested it, 3.7% formaldehyde in PBS can also be used in principle.
4. The negative control is used to show the background (nonspecific) binding of the Alexa Fluor[®] dye to the cells.
5. Avoid using a limited amount of EdU for labeling. We have found that reducing by half the amount of EdU (0.06 mM final

instead of 0.12 mM for 1 h incubation) did not affect the results.

6. The positive control shows the replication capacity of the cell culture before the inhibition of *oriC*-dependent replication by the addition of spectinomycin.
7. In principle, various antibiotics inhibiting protein synthesis can be used. Apart from spectinomycin, we have found that chloramphenicol and amikacin can also give good results. For any antibiotics to be used, it is important to determine the minimal concentration for which no replication (EdU labeling) is detected, after a 2-h treatment. For spectinomycin, we have found this concentration to be 400 µg/mL [17]. Instead of antibiotics, a *dnaA*(Ts) strain can also be used. In this case, the cells are incubated for 2 h at the nonpermissive temperature (42 °C) to fully terminate *oriC*-dependent replication.
8. Bidirectional replication from *oriC* is fully completed within 2 h. After 2 h of exposure to spectinomycin, no EdU labeling is detected in wild-type cells [17].
9. From this step and up to the end, the cells must be manipulated with great care to avoid lysis.
10. We used Alex Fluor® 488, but kits are also available with Alex Fluor® 555, 594 or 647. The click-iT® detection reaction can also be used with fluorescein and allophycocyanin.

Acknowledgments

This work was supported by a Discovery Grant from the Natural Sciences and Engineering Research Council of Canada (NSERC) to MD. AB and MM were supported by an Undergraduate Student Research Award from the NSERC.

References

1. Leonard AC, Méchali M (2013) DNA replication origins. *Cold Spring Harb Perspect Biol* 5 (10):a010116
2. Bell SP, Kaguni JM (2013) Helicase loading at chromosomal origins of replication. *Cold Spring Harb Perspect Biol* 5(6):a010124
3. Kogoma T (1997) Stable DNA replication: interplay between DNA replication, homologous recombination, and transcription. *Microbiol Mol Biol Rev* 61:212–238
4. Stuckey R, Garcia-Rodriguez N, Aguilera A, Erik Wellinger R (2015) Role for RNA:DNA hybrids in origin-independent replication priming in a eukaryotic system. *Proc Natl Acad Sci U S A* 112:5779–5784
5. Hawkins M, Malla S, Blythe MJ, Nieduszynski CA, Allers T (2013) Accelerated growth in the absence of DNA replication origins. *Nature* 503:544–547
6. Ohbayashi R, Watanabe S, Ehira S, Kanesaki Y, Chibazakura T, Yoshikawa H (2016) Diversification of DnaA dependency for DNA replication in cyanobacterial evolution. *ISME J* 10:1113–1121
7. Lombrana R, Almeida R, Alvarez A, Gomez M (2015) R-loops and initiation of DNA

- replication in human cells: a missing link? *Front Genet* 6:158
8. Sandoval PY, Lee PH, Meng X, Kapler GM (2015) Checkpoint activation of an unconventional DNA replication program in tetrahymena. *PLoS Genet* 11(7):e1005405
 9. Wimberly H, Shee C, Thornton PC, Sivaramakrishnan P, Rosenberg SM, Hastings PJ (2013) R-loops and nicks initiate DNA breakage and genome instability in non-growing *Escherichia coli*. *Nat Commun* 4:2115
 10. Masse E, Drolet M (1999) *Escherichia coli* DNA topoisomerase I inhibits R-loop formation by relaxing transcription-induced negative supercoiling. *J Biol Chem* 274:16659–16664
 11. Drolet M, Broccoli S, Rallu F, Hraiky C, Fortin C, Masse E, Baakli I (2003) The problem of hypernegative supercoiling and R-loop formation in transcription. *Front Biosci* 8:d210–d221
 12. Roy D, Yu K, Lieber MR (2008) Mechanism of R-loop formation at immunoglobulin class switch sequences. *Mol Cell Biol* 28:50–60
 13. Drolet M, Bi X, Liu LF (1994) Hypernegative supercoiling of the DNA template during transcription elongation *in vitro*. *J Biol Chem* 269:2068–2074
 14. Drolet M, Phoenix P, Menzel R, Masse E, Liu LF, Crouch RJ (1995) Overexpression of RNase H partially complements the growth defect of an *Escherichia coli delta topA* mutant: R-loop formation is a major problem in the absence of DNA topoisomerase I. *Proc Natl Acad Sci U S A* 92:3526–3530
 15. Drolet M (2006) Growth inhibition mediated by excess negative supercoiling: the interplay between transcription elongation, R-loop formation and DNA topology. *Mol Microbiol* 59:723–730
 16. Gabbai CB, Mariani KJ (2010) Recruitment to stalled replication forks of the PriA DNA helicase and replisome-loading activities is essential for survival. *DNA Repair* 9:202–209
 17. Martel M, Balleydier A, Sauriol A, Drolet M (2015) Constitutive stable DNA replication in *Escherichia coli* cells lacking type 1A topoisomerase activity. *DNA Repair* 35:37–47
 18. Kogoma T (1978) A novel *Escherichia coli* mutant capable of DNA replication in the absence of protein synthesis. *J Mol Biol* 121:55–69
 19. Ogawa T, Pickett GG, Kogoma T, Kornberg A (1984) RNase H confers specificity in the dnaA-dependent initiation of replication at the unique origin of the *Escherichia coli* chromosome *in vivo* and *in vitro*. *Proc Natl Acad Sci U S A* 81:1040–1044
 20. Ferullo DJ, Cooper DL, Moore HR, Lovett ST (2009) Cell cycle synchronization of *Escherichia coli* using the stringent response, with fluorescence labeling assays for DNA content and replication. *Methods* 48:8–13

Single-Molecule Magnetic Tweezer Analysis of Topoisomerases

Kathryn H. Gunn, John F. Marko, and Alfonso Mondragón

Abstract

Magnetic tweezers (MT) provide a powerful single-molecule approach to study the mechanism of topoisomerases, giving the experimenter the ability to change and read out DNA topology in real time. By using diverse DNA substrates, one can study different aspects of topoisomerase function and arrive at a better mechanistic understanding of these fascinating enzymes. Here we describe methods for the creation of three different DNA substrates used in MT experiments with topoisomerases: double-stranded DNA (dsDNA) tethers, “braided” (intertwined or catenated) DNA tether pairs, and dsDNA tethers with single-stranded DNA (ssDNA) regions. Additionally, we discuss how to build flow cells for bright-field MT microscopy, as well as how to noncovalently attach anti-digoxigenin to the coverslip surface for tethering digoxigenin-labeled DNAs. Finally, we describe procedures for the identification of a suitable DNA substrate for MT study and data collection.

Key words Single-molecule, Magnetic tweezers, Functionalized DNA, Flow cell, Noncovalent antibody attachment, Bright-field microscopy, Topoisomerases

1 Introduction

Single-molecule force experiments conducted with magnetic tweezers (MT) have provided insights into how topoisomerases alter DNA topology [1]. In MT experiments, DNA molecules are tethered at one end to a surface and at the other end to a paramagnetic bead, which can be manipulated using a magnetic field. MTs are ideally suited for studying topoisomerases since it is relatively easy to rotate the magnetic bead attached to the DNA and introduce supercoiling of individual DNA molecules or catenations (“braids”) of pairs of DNAs, mimicking supercoiled and catenated DNA configurations found in the cell. Single molecule MT experiments have provided a better understanding of the enzyme-bridged strand passage mechanism for type IA and IIA topoisomerases and the constrained swivel mechanism for type IB and IC [2–8]. They have also allowed comparisons between topoisomerases in the same

sub-type and different homologs. Furthermore, single molecule MT experiments have uncovered aspects of topoisomerase mechanism, such as rates along multistep pathways that could not be discerned from bulk experiments [9, 10].

Some of the most time-consuming aspects of magnetic tweezer experiments are the steps leading up to data collection: making DNA substrates, generating DNA tethers, and identifying a suitable tether for data collection. Part of what makes these tasks challenging is the variety of methods available to achieve them. For MT experiments a DNA substrate is needed that has been functionalized on both ends. In most experiments, at one end the DNA has a digoxigenin (dig) functionalization (dig handle) for attachment to an anti-dig coated coverslip. At the other end, a biotin (bio) functionalization (bio handle) is used for attachment to streptavidin coated paramagnetic beads.

Once the DNA is attached on one end to a glass slide and on the other to a paramagnetic bead, thus creating a DNA tethered bead, a magnetic force is applied. The magnetic field causes the DNA substrate to stretch, whereas rotation of the magnets rotates the bead and concomitantly the DNA. Monitoring the height of the bead allows determination of the length of the DNA tether. By rotating the magnetic bead, excess supercoils or braids can be introduced into the DNA, which in turn affects the height of the DNA substrate. The activity of topoisomerases on the DNA can then be monitored by tracking in real time the height of the bead, which is directly related to the number of turns introduced.

Here we discuss general methods used in our laboratory for magnetic tweezer experiments, including the creation of three types of DNA substrates, flow cells for bright-field MT microscopy, noncovalent attachment of anti-digoxigenin (anti-dig) to the cover glass (which can be used for both bright and dark-field microscopy), and generation and characterization of DNA tethers for data collection. We do not discuss the design, construction, and operation of MT instruments, which have been described elsewhere, for example in [11, 12].

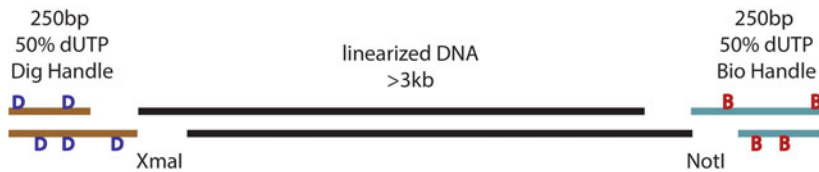
2 Materials

2.1 *Creation of the DNA Substrate*

1. Plasmid DNA of the desired tether length with appropriate restriction enzyme sites (a large range of sizes can be used, with shorter DNA (~6 kilobases (kb) or shorter) providing less noisy data than longer DNA molecules (~10 kb), but fewer supercoils can be introduced into shorter DNA tethers). We have based a number of studies on the plasmid pFOS1 (~10 kb) and on derivatives of the pMAL-pIII plasmid (~6.7 kb), mutated to contain the desired cut sites [9, 10].

2. Restriction enzymes appropriate for creating the desired tether length (in our experiments, NotI, XmaI, SacI, ApaI), T4 DNA ligase, T4 Polynucleotide Kinase (PNK) (New England Biolabs (NEB)).
3. Digoxigenin-11-dUTP alkali stable (Dig-dUTP) (11093088910, Roche) and Biotin-16-dUTP (Bio-dUTP) (11093070910, Roche).
4. For single attachment DNA—DNA oligonucleotides with a single 5' biotin or digoxigenin functionalization designed to amplify the desired size of DNA via PCR (Integrated DNA Technologies (IDT)). Singly attached DNA is used when only one strand of the duplex needs to be attached, leaving the second strand free to rotate [10, 13]. This type of attachment is used in braiding experiments where it is desirable to let the duplex rotate without supercoiling. The drawback of singly attached DNAs is that they are fragile and the DNA can detach easily under force. For example to create a 6 kb tether from pFOS1 use these two primers:
 Dig handle: 5'-(Dig) GCTCGTCGTTTGGTATGGCTT-CATTC-3'
 Bio handle: 5'-(Bio) GATGAAGGTAAACTGCCACCGATC-3'
5. For multiple attachment DNA—DNA oligonucleotides for amplification of ~250 base pairs (bp) functionalized handles with cleavage sites (Bio handle—NotI cleavage site; Dig handle—XmaI or ApaI cleavage site) and amplification of a spacer (ApaI and SacI cleavage sites) (IDT) (*see Fig. 1*). DNA with

a Multiple attachment dsDNA scheme



b Multiple attachment dsDNA with ssDNA bulge scheme

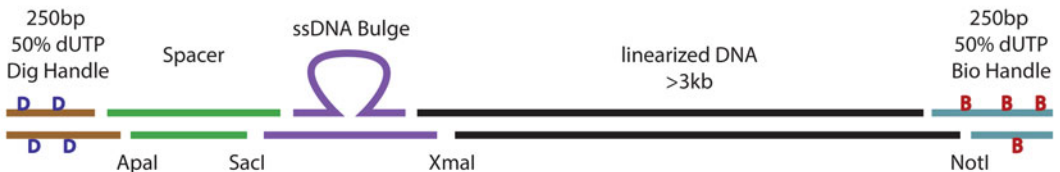


Fig. 1 DNA molecule construction. **(a)** A multiple attachment dsDNA tether can be used to study a variety of topoisomerases using either *negative* or *positive* supercoils. After PCR amplification and digestion of the Bio and Dig functionalized handles, they are ligated to a linearized DNA. **(b)** For studying type IA topoisomerases, introducing a ssDNA bulge provides a binding site even when the DNA is positively supercoiled. After PCR amplification and digestion with SacI, the spacer can be ligated to the annealed ssDNA bulge and gel purified. Next the spacer/ssDNA bulge construct is digested with ApaI and ligated to the Dig handle. The Dig handle/spacer/ssDNA bulge is then phosphorylated at the XmaI site and ligated to the linearized DNA and the Bio handle

multiple attachment sites in both strands is more resistant to high forces and ideal for supercoiling experiments.

6. Standard reagents and equipment for PCR, dNTPs, Taq polymerase, PfuTurbo polymerase.
7. PCR purification and gel extraction kits (Qiagen).
8. Annealing buffer: 10 mM Tris pH 8.0, 50 mM NaCl, and 1 mM EDTA.

2.2 Fabrication of Flow Cells for Bright-Field Magnetic Tweezers

1. Streptavidin-coated paramagnetic beads (many different sizes and brands are available, we use Dynabeads MyOne Streptavidin T1, 65601, Invitrogen or Streptavidin Magnetic Beads, S1420S, NEB).
2. Vortexer.
3. Bovine serum albumin (BSA) (many different purities available, we use A7030_10G, Sigma-Aldrich).
4. Phosphate buffered saline (PBS) (17-516Q, Lonza) and ethanol for dilutions.
5. Micro Mill (MF70, Proxxon).
6. Cylinder Diamond Drill Bit— $\frac{3}{4}$ mm.
7. 25×75 mm microscope glass slides.
8. 24×50 mm microscope glass coverslips (12-544E, Thermo Fisher Scientific).
9. Double sided tape and epoxy for sealing the flow cells.
10. Sheep anti-Digoxigenin (anti-dig) Fab fragments (11214667001, Roche).

2.3 Identifying DNA Substrate

1. Tube rotator.
2. Magnetic tweezers instrument.
3. Single molecule buffer. The buffer should be selected based on the topoisomerase to be studied. For example, our buffer for bacterial topoisomerase I is: 50 mM Tris-HCl pH 8.0, 120 mM NaCl, 1 mM MgCl₂, 0.2 mg/mL BSA. The BSA concentration can be increased if more passivation is needed.

3 Methods

3.1 Creation of the DNA Substrate

3.1.1 dsDNA Tether with Single Attachment (for Creation of Braided Double Tethers)

When creating braided DNA molecules, two DNA molecules are attached to the same magnetic bead, so that when the magnet is turned, the DNA molecules twist around each other, braiding the molecules together and thus mimicking two catenated DNA molecules. To create braids it is necessary to either nick the DNA or to create DNA substrates that have only one attachment to the coverslip and bead, respectively. In this way the tethers cannot be

supercoiled, but can still form braids. Here we describe how to make single attachment tethers. Another alternative is to follow the protocol for multiple attachment tethers and introduce a nick into the DNA using a nickase [10].

1. After deciding the length of DNA tether desired, design two oligonucleotides to amplify by PCR a portion of a plasmid to create the desired length DNA (3 kb to >10 kb; we typically use 6 kb, which results in a ~2 μm DNA tether). Purchase one of the oligonucleotides with a 5' digoxigenin group incorporated, for example from IDT, which will be used for attaching to the anti-dig coated coverslip surface. To the second oligonucleotide add a 5' biotin group, which will attach to the streptavidin coated magnetic bead. For a 6-kb tether made from plasmid pFOS1 use the primers listed in Subheading 2.1, **item 4**.
2. The oligonucleotides serve as primers for use in a standard PCR procedure for PfuTurbo polymerase to create a linear DNA fragment. For the 6 kb DNA from pFOS1 use an annealing temperature of 55 °C and an extension time of 6 min.
3. Purify the resulting DNA using standard commercially available PCR purification kits. Store concentrated stock at -20 °C. Dilute a working stock to ~0.5 ng/ μL just before using (*see Note 1*).

3.1.2 dsDNA Tether with Multiple Attachments (for Single Unnicked DNA Tethers)

In order to supercoil a single tether, multiple attachments are required between the dig and bio functionalized DNA and the coverslip and bead, respectively. If there is only a single attachment on either end, the tether can rotate around the attachment, which prevents supercoiling. The presence of nicks in the DNA backbone also results in an inability to supercoil. To achieve multiple attachments approximately 25 bio or dig functionalized dUTPs are randomly incorporated into the DNA on either end of the substrate to increase the likelihood of two or more attachments, including one on each strand of the DNA.

1. Decide on the DNA length desired and chose (or create) a plasmid close to the desired size, so that when digested with two restriction enzymes the resulting product can be purified (the piece cut should be <50 bp, so it can be readily removed using standard PCR purification kits). The choice of enzymes for digestion is also important, since ideally the cut sites would not have any T's in them, as in later steps this DNA will be ligated to handles where the T's are replaced by U's for functionalization (the presence of U's might inhibit later digestion). Typically we use NotI and XmaI with a derivative of pMAL-pIII plasmid that has been mutated to have the appropriate cut sites (*see Fig. 1a*). After digestion purify the product using a PCR purification kit, leaving only a long linearized DNA.

2. Using an oligonucleotide which introduces a single restriction site (either a NotI or XmaI site) amplify a shorter DNA region, we typically use 250 bases long, which will serve as a functionalized handle. We use NotI for the Bio handle and XmaI for the Dig handle. Taq polymerase is used for creating the handles by PCR, since Taq polymerase can incorporate functionalized dUTPs. The ratio of Bio-dUTP or Dig-dUTP to dTTP determines the amount of random incorporation of the functional groups in the handle. For shorter handles (~250 bp) we use a high percentage (50%), whereas for longer handles (1000 bp) we use a lower one of 10%. For the 250 bp handle PCR reactions, we use 50% functionalized dUTP or a 1:1 ratio of dUTP to dTTP. Specifically, we use 1 μ L of functionalized dUTP (1 mM) per 50 μ L reaction, and 1 μ L of a 50 \times stock of dNTPs containing 2 mM dATP, 2 mM dGTP, 2 mM dCTP, and 1 mM dTTP (*see Note 2*).
3. After making the handles by PCR, purify the products using a PCR purification kit. Follow this by digestion with either NotI (for Bio handle) or XmaI (for Dig handle) and PCR purify again.
4. In one tube, mix 75 ng each of the Bio and Dig functionalized handles with 250 ng of the long, linearized double stranded DNA and ligate overnight at 16 $^{\circ}$ C (*see Fig. 1a*). Stop the reaction by denaturing the ligase at 65 $^{\circ}$ C for 15 min and store the reaction at 4 $^{\circ}$ C. The ligated DNA can be used for up to 3 days, although the ability to form tethers diminishes with time. On the first day of use, we typically find that ~1 in 4 single tethers are intact, i.e., the DNA made multiple attachments and was not nicked (*see Note 3*).

**3.1.3 dsDNA Tether
with a ssDNA Bulge
with Multiple Attachments
(for Type IA
Topoisomerases
Experiments)**

Type IA topoisomerases require a single stranded binding region for activity. Negatively supercoiled DNA has melted regions that provide a substrate for the type IA topoisomerases in vivo. When using a MT, there is less noise in the data at higher forces, however, at forces >0.4 pN the DNA melts when negative supercoils are introduced resulting in no change in the height of the DNA [14]. To overcome this issue, it is typical to introduce a ssDNA region to the dsDNA tether, so that when the DNA is positively supercoiled there is still an available substrate for the type IA topoisomerase to bind to [2]. This allows data to be collected at higher forces (>0.4 pN).

1. Follow Subheading 3.1.2, steps 1–3 for creating multiple attachment dsDNA tethers, but replacing XmaI in the Dig Handle with ApaI, as in this case the ligation will be to a spacer instead of the long linearized DNA (*see Fig. 1b*). This allows the use of the same linearized DNA used in Subheading 3.1.2.

2. Use a standard procedure to amplify by PCR a spacer DNA region to position the ssDNA bulge at the desired distance from the Dig handle. The spacer would have ApaI and SacI restriction sites on either end. After digestion with only SacI, purify the spacer using a PCR purification kit. Typically, we start with 100 μg of spacer, since multiple purification steps cause significant loss of product.
3. Purchase oligonucleotides with at least 20 bp of overlapping complementary regions on either side of the desired bulge, which is located in the middle of one of the oligos. For a 27 nucleotide (nt) bulge we use the sequence 5'-AATCGGCATTGCGCAAACCAAGACAG-3' and for a 12 nt bulge 5'-AACGTGCCAAGA-3' [9]. The oligonucleotides should have overhanging sticky ends that allow for ligation to the digested spacer (SacI) and the long linearized DNA (XmaI) respectively. The SacI overhang for the annealed oligonucleotides needs to be 5' phosphorylated; we purchase the oligonucleotides prephosphorylated. Anneal the oligonucleotides by heating in a heat block to 95 °C for 3 min and allow cooling to room temperature (RT) in the heat block in annealing buffer (*see Note 4*).
4. Conduct a test to find the best ligation conditions. It is necessary to find appropriate conditions to minimize self-ligation of the annealed oligonucleotides or the SacI digested spacer. Typically we supply excess of the annealed oligonucleotides compared to the spacer. It is important to identify the desired ligation product in a gel before scaling up to a larger reaction. Once the best conditions have been identified, ligate the spacer DNA to the annealed oligonucleotide containing the bulge and gel-purify (*see Note 5*).
5. Digest the other side of the spacer (corresponding to the Dig handle) with ApaI and ligate the Spacer/Bulge to the digested Dig handle. Gel-purify the product as in Subheading 3.1.3, step 4.
6. In a 40 μL reaction, phosphorylate 75 ng of the Dig handle/Spacer/Bulge with T4 PNK following the manufacturer's protocol (using T4 DNA ligase buffer to facilitate the next step). This will phosphorylate the overhang on the bulge oligonucleotides corresponding to XmaI.
7. After denaturing the T4 PNK, take the 40 μL reaction and add 75 ng of digested Bio Handle and 250 ng of linearized DNA, ligating overnight at 16 °C (*see Fig. 1b*). Denature the ligase at 65 °C for 15 min and store the DNA at 4 °C. DNA can be used for up to 3 days, although the ability to form tethers diminishes with time. On the first day of use, we typically find ~1 in 30 single tethers can be supercoiled (not nicked).

3.2 Creation of Flow Cells for Bright-Field Magnetic Tweezers

Magnetic tweezer instruments can either illuminate the flow cell through the objective or by passing light through the flow cell to the objective, for dark-field or bright-field imaging respectively. In both cases the anti-dig coated coverslip must be the one closer to the objective. We use an inverted bright-field microscope, which requires the coverslip to be on the bottom side of the flow cell and closer to the objective [15]; a different flow cell construction is used when the objective is above the flow cell. The flow cell described here was adapted from ones used for fluorescence microscopy [16].

1. Clean the commercial streptavidin coated paramagnetic beads by taking 20 μL from the bottle (vortexed prior to evenly suspend the beads) and dilute with 200 μL of PBS. Vortex for at least 1 min. Pellet the beads with a magnet and remove the PBS. Repeat three times. Resuspend the beads in 120 μL of 0.4 mg/mL BSA for a final concentration of ~ 0.6 mg/mL and store at 4 $^{\circ}\text{C}$ (*see Note 6*).
2. Deposit reference beads on the coverslip by mixing 5 μL of cleaned beads with 45 μL of 100% ethanol. Spread the mixture on the coverslip and place the coverslip on a heat plate set at 80 $^{\circ}\text{C}$ until the liquid has evaporated (~ 15 s) [17].
3. Drill two holes diagonally from each other (*see Fig. 2*) in a glass slide using a micro mill equipped with a $\frac{3}{4}$ mm diamond drill

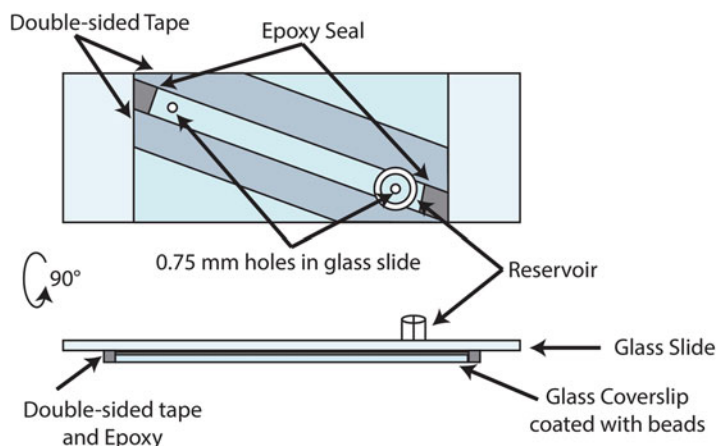


Fig. 2 Flow cell construction. For bright field microscopy, this flow cell uses capillary flow to gently change the buffer, without affecting the tethered DNA. The flow channel is created between two holes drilled in a glass slide using double sided tape to delineate the width of the channel. A glass coverslip coated with beads is gently applied to the double sided tape and pressed firmly down. Epoxy glue is then used to seal the edges of the flow cell. A reservoir is constructed using the end of a pipet tip and sealed to the glass slide with epoxy glue to prevent leakage [16]

bit. Using double-sided tape create a channel between the inlet and outlet as shown in Fig. 2. Place the coverslip on top (with the bead-coated side facing the glass slide) and gently, but firmly press until the coverslip and tape are completely affixed. Carefully cut-off the excess tape. Mix a small amount of 5-min epoxy glue and apply it to the gaps in the tape at the ends of the coverslip. Allow it to sit for 30 s and wipe clean, so no excess epoxy remains. The epoxy will have seeped under the coverslip and sealed both ends of the flow cell (*see* Fig. 2). If the epoxy glue does not form a good seal, more epoxy glue can be added for an additional 15 s and then wiped away. To create a liquid reservoir, cut the end off of a pipet tip and place it around the inlet. Apply epoxy glue to create a watertight seal for the reservoir. Allow to dry [16].

4. Resuspend anti-dig at 1 mg/mL with PBS, aliquot, and freeze at -20°C for long term storage. Take a working stock out and store at 4°C . For noncovalent attachment, add 10 μL of 1 mg/mL anti-dig to 40 μL of PBS, mix well by pipetting, and use the pipet to introduce liquid into the flow cell through the inlet until it emerges from the outlet. Pipet slowly to allow the liquid to spread out in the flow cell. After the flow cell is filled, liquid can enter the flow cell by capillarity, but flow can be aided by wicking with a tissue on the output end of the flow cell. 50 μL should completely fill the channel and leave a small amount in the reservoir to prevent drying [18]. Place the slide into a sealed plastic box on a raised platform, with PBS in the bottom of the box to maintain humidity, and incubate overnight at 4°C (*see* Note 7).
5. For dark field microscopy, noncovalent attachment can also be used (in these flow cells the coverslip is on the top side of the cell). On the day of the experiment mix 5 μL of cleaned beads with 43 μL of 100% ethanol and 2 μL of 1 mg/mL anti-dig. Spread the mixture on a coverslip and lay on a heat plate set at 80°C until evaporated (~ 15 s) (*see* Note 8).
6. Before using a flow cell, flow in at least four flow cell volumes (FCV) of 0.4 mg/mL BSA (~ 200 μL) and incubate for at least 5 min to passivate the flow cell. Add the BSA to the reservoir and pull through the flow cell using a tissue. Longer incubation with BSA can reduce the ability to form tethers and for this reason it is important to adjust the time of incubation.

3.3 Creating the Tether and Identifying the DNA Substrate

In order to successfully conduct an experiment the generation of tethered DNA molecules attached to both the coverslip and the bead is essential. Since many tethers may not be torsionally constrained (having either nicks or too few attachments), it is important to create many tethered molecules and to examine them for their suitability for the experiments.

1. Mix the DNA with cleaned beads by creating two identical tubes, each containing 2 μL of ~ 0.5 ng/ μL of the DNA substrate and 2 μL of the cleaned beads (~ 0.6 mg/mL). Do not mix by pipetting the DNA and beads as pipetting can introduce nicks into the DNA. Place the tubes on a tube rotator for 5 min. Dilute the beads/DNA with PBS to a volume of ~ 55 μL . Pipet the mix into the flow cell reservoir and pull through by placing a tissue at the outlet. Add an additional 55 μL of PBS to the reservoir to prevent drying, but do not flow. Incubate the beads/DNA mix in the flow cell for 10 min (*see Note 9*).
2. Place the flow cell in the magnetic tweezer set up and apply magnetic force to the flow cell by lowering the magnets. Beads that are not well attached will float up to the top of the flow cell; turning the magnet can help to detach poorly tethered beads (*see Note 10*). If after looking at the slide more tethers are desired, repeat BSA passivation and redo Subheading 3.3, **step 1**. As many as three repetitions are sometimes necessary to generate a good covering of tethers, particularly if the DNA is not fresh.
3. To find a suitable DNA tether for the experiments, a reference bead and tethered DNA bead must be in close proximity, so that both can be tracked simultaneously. The reference bead and the tethered bead can be distinguished as they will be at different heights. For longer tethers, the two beads will be in very different focal planes and are easy to distinguish. Very short tethers are more difficult to distinguish and sometimes it is necessary to observe the movement of the beads to assess whether they are attached or tethered. In addition, turning the magnet a few turns at low force will result in a change of height of the tethered bead due to supercoiling. Intact tethered beads will not only be of the correct length, they will also change height when the magnet is turned [19]. A good reference bead will not move at all when the magnet is turned (these are the beads deposited with the EtOH). The proximity of the tether and reference bead will be determined by the size of the imaging field [12].
4. After locating a DNA tether suitable for the experiment, a look-up table is created by changing the height of the microscope objective by known amounts and taking a radial profile of the reference and tethered bead separately [12]. In this way, it is possible to measure the length of the tethered DNA with respect to the reference bead. Once the look-up table is available, it is possible to calibrate the force by measuring the variance of the bead movements and relating it to the position of the magnets. Measuring the force at several magnet positions allows a calibration so a desired force can be set (*see Note*

11). After these two calibrations are done, a plot of the height of the DNA against the number of turns introduced can be generated for different forces. For a single DNA tether start with a curve at ~ 0.4 pN, since at this force the height will change for both positively and negatively supercoiled tethers, allowing for manual recentering of the tether if necessary (*see Note 12*). After the force has been calibrated and the tethered DNA has been centered, it is necessary to collect an extension vs. turns curve for the force(s) planned for the experiment. These plots have a characteristic shape (“hat curves”) and significant deviation from the expected shape indicates that the DNA substrate is unsuitable for the experiments [14] (*see Fig. 3*).

5. The linear portion of the hat curve can be used to translate extension into excess linking number or number of braids introduced for data analysis [12]. For experiments, single molecule buffer is introduced by capillary flow, since it is very gentle and reduces the likelihood of breaking the tether. Liquid pooled at the outlet can be absorbed by a tissue. The protein of interest is also diluted in single molecule buffer and introduced to the flow cell (2 nM is a good starting protein concentration in our experience).

4 Notes

1. In some cases, the DNA does not readily create tethers between the coverslip and bead (few tethers are seen when examined with the microscope), in these cases diluting a new aliquot of DNA can be helpful. Increasing working stock to 1 ng/ μ L can also increase the number of double tethers.
2. The ratio of functionalized dUTPs is important, since handles without sufficient functional groups can form fewer attachments. If this happens, when the magnet is rotated the DNA appears to be nicked (nonsupercoilable), as it can rotate around the single attachment.
3. Instead of ligation the day before the experiment, the DNA can also be ligated in bulk, gel purified, and stored at -20 °C, like the single attachment tether. However, significant amounts of the DNA can be lost in the gel purification step and the likelihood of DNA nicking is increased, as opposed to using the DNA directly from the ligation reaction.
4. The full oligonucleotides [9] used for the creating the 27 nt ssDNA bulge are:
Oligo containing overhangs for both SacI and XmaI ligation (opposite the bulged oligo): 5'- CCGGCCGCATTA

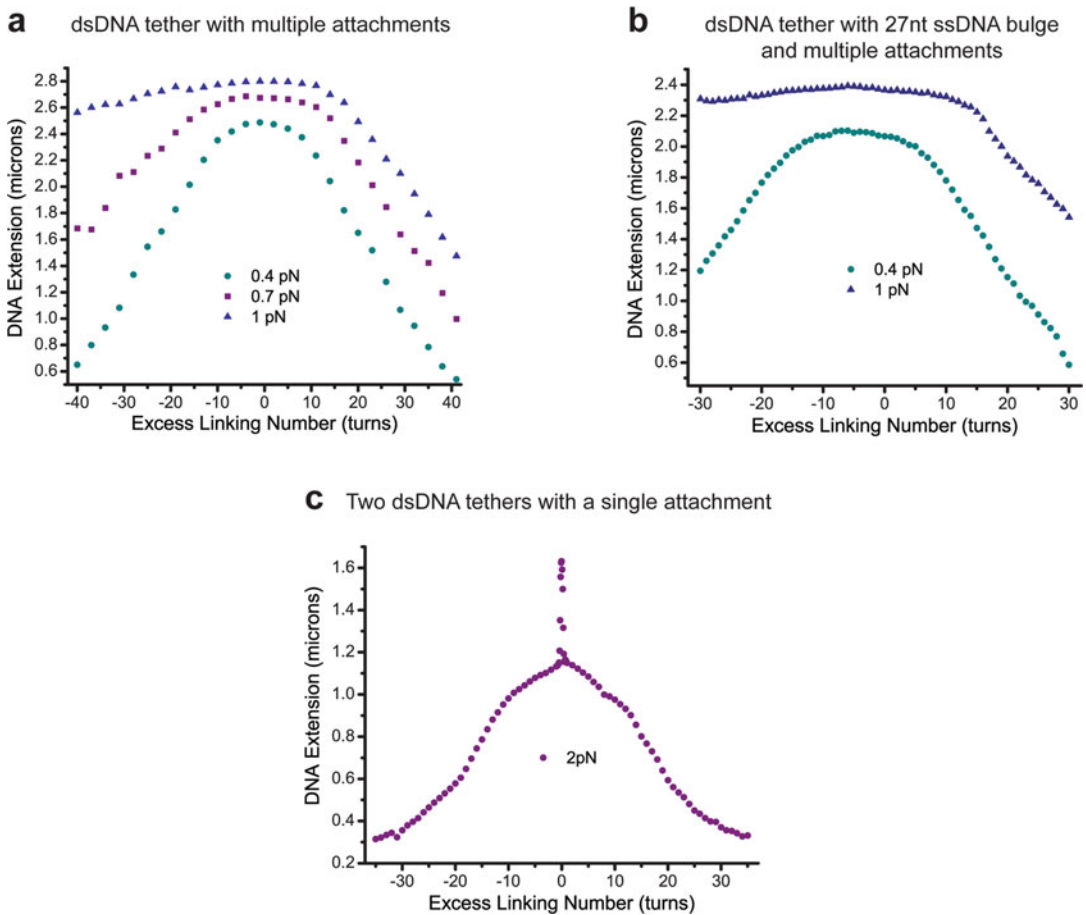


Fig. 3 Characterization curves. **(a)** Typical hat curves showing the change in DNA extension when turns are introduced into a dsDNA tether. At a force of 0.4 pN, it is possible to introduce both negative and positive supercoils. As the force increases, the DNA melts when negative supercoils are introduced, no longer changing its length. The curve was measured using a 9.5 kb dsDNA tether which has multiple bio and dig attachments. The linear region of the hat curve, after plectonemes have begun to appear, can be used to translate DNA extension data into excess linking number. **(b)** When a ssDNA region is introduced into a DNA tether, the hat curve becomes slightly asymmetric [9]. However, it still has the same overall characteristics as a dsDNA tether; at low forces introduction of negative supercoils changes the DNA extension, whereas at high forces the DNA melts. The hat curve was measured using a 9.5 kb DNA tether with a 27 nt ssDNA bulge. **(c)** When two single-strand attached dsDNA tethers are anchored to the same bead, it is possible to “braid” (intertwine) the two DNA molecules, which mimics catenated DNA molecules [10]. The introduction of the first turn causes a drastic change in length due to the introduction of the first braid. The hat curve was measured using a 6 kb single attachment dsDNA tether at 2 pN

GCAGCGTACGCTCAGCTTGGCGATCACGTAGTGGGCG
AAATCTGTACGCT-3'

Oligo containing the 27 nt bulge (5' phosphorylated for ligation): 5'- /5Phos/CCCTGACAG ATTCGCCCCACTACGT
GATCGAATCGGCATTGCGCAAACCAAGACAGCCCAAG
CTGAGCGTACGCTGCTTTAATGCGG-3'

5. For smaller spacers, a 2% agarose gel can help separate the ligation products, making it easier to excise the correct fragment.
6. Volumes can be adjusted based on the concentration of the original beads. Over time the beads become more concentrated and should be resuspended in larger volumes.
7. The amount of anti-dig used can be adjusted depending on the application. To create more double tethers, use more anti-dig. If too many double tethers are seen, use less anti-dig.
8. This procedure can also be used with the bright-field flow cell, but is slowed by the drying time for the epoxy. Increasing the amount of anti-dig used leads to more aggregation of the beads on the coverslip.
9. The incubation time outside and inside the flow cell can be adjusted depending on the substrate. Longer incubation of the DNA and beads before adding to the flow cell can increase the amount of multiply tethered beads, while longer incubation in the flow cell can increase the number of tethered beads observed. When trying to form double tethers, double both incubation times (as well as increasing the anti-dig).
10. These beads can later cause problems in bright-field imaging, since the free beads stay at the upper surface between the slide and the light source. This problem can be alleviated by flowing in PBS or buffer with the magnet lifted, to push the free beads out of the flow cell.
11. For double tethers it is important to do the force calibration after ensuring that the DNA molecules are not braided, which is apparent by looking at a height vs. turns plot. Any braids in the DNA will affect the force calibrations.
12. We have found that tethers can gain twists during the preparation process and are not always centered at zero. For tethers with bulges, there will be a slight asymmetry in the curve, which makes it more difficult to assess the centering of the molecule. For double tethers there will be a high point at the center of the curve [20], which results from a large drop in height after the introduction of the first braid.

Acknowledgments

We thank members of the Mondragón and Marko laboratories for discussions and assistance. Research was supported by the NIH (R01 GM051350 to A.M., and R01 GM105847 and U54 CA193419 (CR-PS-OC) to J.F.M.) and the NSF (MCB-1022117 and DMR-1206868 to J.F.M.). K.H.G. was supported by a Dr. John N. Nicholson Fellowship and an NRSA predoctoral training grant (T32 GM008382).

References

- Charvin G, Strick TR, Bensimon D, Croquette V (2005) Tracking topoisomerase activity at the single-molecule level. *Annu Rev Biophys Biomol Struct* 34:201–219. <https://doi.org/10.1146/annurev.biophys.34.040204.144433>
- Dekker NH, Rybenkov VV, Duguet M, Crisona NJ, Cozzarelli NR, Bensimon D, Croquette V (2002) The mechanism of type IA topoisomerases. *Proc Natl Acad Sci U S A* 99 (19):12126–12131. <https://doi.org/10.1073/pnas.132378799>
- Baker NM, Rajan R, Mondragon A (2009) Structural studies of type I topoisomerases. *Nucleic Acids Res* 37(3):693–701. <https://doi.org/10.1093/nar/gkn1009>
- Taneja B, Schnurr B, Slesarev A, Marko JF, Mondragon A (2007) Topoisomerase V relaxes supercoiled DNA by a constrained swiveling mechanism. *Proc Natl Acad Sci U S A* 104 (37):14670–14675. <https://doi.org/10.1073/pnas.0701989104>
- Basu A, Parente AC, Bryant Z (2016) Structural dynamics and mechanochemical coupling in DNA gyrase. *J Mol Biol* 428(9 Pt B):1833–1845. <https://doi.org/10.1016/j.jmb.2016.03.016>
- Koster DA, Croquette V, Dekker C, Shuman S, Dekker NH (2005) Friction and torque govern the relaxation of DNA supercoils by eukaryotic topoisomerase IB. *Nature* 434(7033):671–674. <https://doi.org/10.1038/nature03395>
- Strick TR, Croquette V, Bensimon D (2000) Single-molecule analysis of DNA uncoiling by a type II topoisomerase. *Nature* 404 (6780):901–904. <https://doi.org/10.1038/35009144>
- Ogawa T, Yogo K, Furuike S, Sutoh K, Kikuchi A, Kinosita K Jr (2015) Direct observation of DNA overwinding by reverse gyrase. *Proc Natl Acad Sci U S A* 112(24):7495–7500. <https://doi.org/10.1073/pnas.1422203112>
- Terekhova K, Gunn KH, Marko JF, Mondragon A (2012) Bacterial topoisomerase I and topoisomerase III relax supercoiled DNA via distinct pathways. *Nucleic Acids Res* 40 (20):10432–10440. <https://doi.org/10.1093/nar/gks780>
- Terekhova K, Marko JF, Mondragon A (2014) Single-molecule analysis uncovers the difference between the kinetics of DNA decatenation by bacterial topoisomerases I and III. *Nucleic Acids Res* 42(18):11657–11667. <https://doi.org/10.1093/nar/gku785>
- Lionnet T, Allemand JF, Revyakin A, Strick TR, Saleh OA, Bensimon D, Croquette V (2012) Magnetic trap construction. *Cold Spring Harb Protoc* 2012(1):133–138. <https://doi.org/10.1101/pdb.prot067496>
- Gosse C, Croquette V (2002) Magnetic tweezers: micromanipulation and force measurement at the molecular level. *Biophys J* 82 (6):3314–3329. [https://doi.org/10.1016/S0006-3495\(02\)75672-5](https://doi.org/10.1016/S0006-3495(02)75672-5)
- Bai H, Sun M, Ghosh P, Hatfull GF, Grindley ND, Marko JF (2011) Single-molecule analysis reveals the molecular bearing mechanism of DNA strand exchange by a serine recombinase. *Proc Natl Acad Sci U S A* 108(18):7419–7424. <https://doi.org/10.1073/pnas.1018436108>
- Strick TR, Allemand JF, Bensimon D, Bensimon A, Croquette V (1996) The elasticity of a single supercoiled DNA molecule. *Science* 271(5257):1835–1837. <https://doi.org/10.1126/science.271.5257.1835>
- Gunn KH, Marko JF, Mondragon A (2017) An orthogonal single-molecule experiment reveals multiple-attempt dynamics of type IA topoisomerases. *Nat Struct Mol Biol* 24 (5):484–490. <https://doi.org/10.1038/nsmb.3401>
- Joo C, Ha T (2012) Preparing sample chambers for single-molecule FRET. *Cold Spring Harb Protoc* 2012(10):1104–1108. <https://doi.org/10.1101/pdb.prot071530>
- Burnham DR, De Vlaminck I, Henighan T, Dekker C (2014) Skewed brownian fluctuations in single-molecule magnetic tweezers. *PLoS One* 9(9):e108271. <https://doi.org/10.1371/journal.pone.0108271>
- Graham JS, Johnson RC, Marko JF (2011) Counting proteins bound to a single DNA molecule. *Biochem Biophys Res Commun* 415(1):131–134. <https://doi.org/10.1016/j.bbrc.2011.10.029>
- Seol Y, Neuman KC (2011) Single-molecule measurements of topoisomerase activity with magnetic tweezers. *Methods Mol Biol* 778:229–241. https://doi.org/10.1007/978-1-61779-261-8_15
- Charvin G, Bensimon D, Croquette V (2003) Single-molecule study of DNA unlinking by eukaryotic and prokaryotic type-II topoisomerases. *Proc Natl Acad Sci U S A* 100 (17):9820–9825. <https://doi.org/10.1073/pnas.1631550100>

Chapter 11

Synthesis of Hemicatenanes for the Study of Type IA Topoisomerases

Shun-Hsiao Lee, Tao-shih Hsieh, and Grace Ee-Lu Siaw

Abstract

Hemicatenane is a structure that forms when two DNA duplexes are physically linked through a single-stranded crossover. It is proposed to be an intermediate resulting from double Holliday junction (dHJ) dissolution, repair of replication stalled forks and late stage replication. Our previous study has shown that hemicatenane can be synthesized and dissolved *in vitro* by hyperthermophilic type IA topoisomerases. Here we present the protocol of hemicatenane synthesis and its structure detection by 2D agarose gel electrophoresis. The generated product can be used as a substrate to study the biochemical mechanism of hemicatenane processing reactions.

Key words Type IA topoisomerases, Hemicatenane, Double Holliday junction, 2D agarose gel electrophoresis

1 Introduction

Type IA DNA topoisomerases are highly conserved and ubiquitous enzymes with essential biological functions. They release DNA topological stress that arises during the processes of replication, transcription, recombination, repair, and chromatin remodeling [1–3]. These enzymes use a catalytic tyrosine as a nucleophile to attack the DNA backbone, generating a transient covalent linkage with a 5' hydroxyl group. The “enzyme bridging” mechanism allows another DNA strand to pass through the tethered DNA gate and the single-stranded break is then resealed through the reverse reaction [4]. Previous studies have shown that type IA topoisomerases not only have the function of maintaining DNA topology in the cell but also participate in the dissolution of double Holliday junction (dHJ), a cytotoxic DNA intermediate generated during homologous recombination [5]. In human cells, the BTR complex which comprises Bloom helicase (BLM), topoisomerase III α , RMI1 and RMI2 has a critical role in eliminating recombination intermediates to maintain genomic integrity [6,7]. Biochemical

studies have demonstrated that human, yeast and *Drosophila* homologs of the BTR complex can dissolve dHJ presumably through convergent branch migration to yield non-crossover products [8–10].

Hemicatenane is a form of physical linkage between two DNA duplexes in which a strand from each duplex creates a single topological linkage to connect a pair of DNA duplexes. This structure is proposed as the final intermediate that forms when two Holliday junctions converge to each other during the dissolution process [10], and it can also be generated from late stage replication and the repair of stalled replication forks [11–14]. The single-stranded interlocks of hemicatenanes are proposed to be disentangled by type IA topoisomerases through its single-stranded DNA passage activity. Our previous study has demonstrated that hyperthermophilic type IA topoisomerases are able to synthesize and dissolve hemicatenane structure in vitro [15], supporting the hypothesis that type IA topoisomerases might be a key factor in removing hemicatenane in the cells.

A suitable substrate is essential to study the biochemical properties of hemicatenanes. There are a few publications on hemicatenane synthesis and preparation, which involve strand-annealing procedures [16, 17]. Here we describe a simple system as an approach to investigate the mechanistic insights into the generation and dissolution of hemicatenanes. A step-by-step protocol is presented for the generation of plasmid-based hemicatenane synthesized by topoisomerase III from a hyperthermophilic archaeum, *Nanoarchaeum equitans*, followed by its detection by 2D agarose gel electrophoresis and Southern blot. The reaction is carried out using a low concentration of active enzyme at high temperature. Under these conditions, single-stranded DNA bubbles are presumably created and the hemicatenation is promoted by DNA condensation effect due to the high concentration of catalytic dead enzyme. The expected hemicatenation products are purified for further identification and downstream applications. For the detection of hemicatenane structures by 2D agarose gel electrophoresis, the DNA sample is first run under native conditions to resolve the DNA species according to their molecular weight. Separation in the second dimension is subsequently performed under alkaline conditions to disentangle DNA molecules without covalent linkages.

2 Materials

2.1 Enzyme Reaction

1. *Nanoarchaeum equitans* Topoisomerase III (wild-type and active site mutant Y293F) (*see Note 1*).
2. pUC19 plasmid DNA (450 ng/ μ l in TE buffer) (*see Note 2*).
3. 1 \times TE buffer: 10 mM Tris-HCl pH 8.0, 0.1 mM EDTA.

4. 10× TKEM buffer: 100 mM Tris-HCl pH 8.0, 500 mM KCl, 1 mM EDTA, 100 mM MgCl₂.
5. Gelatin (1 mg/ml autoclaved).
6. Mineral oil.
7. Proteinase K (20 mg/ml).
8. Stop solution: 5% SDS, 250 mM EDTA, pH 8.0.
9. Water bath.

2.2 DNA Extraction

1. Phenol (saturated, pH 7.9).
2. Phenol-chloroform-isoamyl alcohol mixture 25:24:1 (v/v/v).
3. 3.0 M sodium acetate pH 5.2.
4. Ethanol, absolute and 70%.
5. Refrigerated benchtop centrifuge.

2.3 2D Agarose Gel Electrophoresis and Southern Blot

1. Agarose (Lonza).
2. 1× DNA loading buffer: 2.5% Ficoll-400, 11 mM EDTA, 3.3 mM Tris-HCl pH 8.0, 0.017% SDS, 0.015% bromophenol blue.
3. 10× TPE buffer: 890 mM Tris-phosphate, 20 mM EDTA, final pH 7.5.
4. Alkaline buffer: 30 mM NaOH, 1 mM EDTA.
5. Random primer labeling kit: Rediprime II DNA Labeling System, GE Healthcare.
6. Deoxycytidine 5'-triphosphate, [α -³²P] (3000 Ci/mmol, 10 μ Ci/ μ l, PerkinElmer).
7. Denaturation buffer: 0.5 N NaOH, 1.5 M NaCl.
8. Neutralization buffer: 0.5 M Tris-HCl pH 7.0, 1.5 M NaCl.
9. 20× SSC buffer: 3.0 M NaCl, 0.3 M sodium citrate, pH 7.0.
10. 10% SDS solution.
11. Vacuum transfer system (VacuGene XL Vacuum Blotting system, GE Healthcare).
12. Nylon blotting membrane (Amersham HybondTM-N⁺, GE Healthcare).
13. Ultraviolet crosslinker (UVP).
14. Prehybridization buffer: 6× SSC, 5× Denhardt's reagent, 0.5% SDS, 1 μ g/ml Poly (A), 100 μ g/ml Salmon sperm DNA.
15. Medium-sized horizontal electrophoresis system (Owl EasyCast B3, Thermo Scientific).
16. Large-sized horizontal electrophoresis system (Owl EasyCast A5, Thermo Scientific).
17. Hybridization oven and bottles.
18. Phosphorimager (Typhoon FLA 7000, GE Healthcare).

3 Methods

3.1 Synthesis of Hemicatenane

1. Set up a 200 μ l NeqTop3 reaction on ice containing 1 \times TKEM buffer, 4.5 μ g pUC19 DNA, 50 ng/ μ l gelatin, 16 nM wild-type NeqTop3, and 128 nM NeqTop3 Y293F active site mutant in a microcentrifuge tube (*see Note 3*).
2. Add three drops of mineral oil on top of the reaction to avoid evaporation at high temperature.
3. Initiate the reaction by putting the tubes in 80 °C water bath for 90 s (*see Note 4*).
4. Stop reaction by adding 1.2 μ l stop solution and deproteinize with 0.75 mg/ml proteinase K at 45 °C for 30 min.
5. Transfer the solution to a new tube and avoid the mineral oil.
6. Add equal volume of phenol and mix thoroughly by pipetting several times.
7. Centrifuge at 15,000 $\times g$ for 3 min and transfer the aqueous phase to a new tube, avoid the precipitated protein on the interface.
8. Repeat the extraction using equal volume of phenol–chloroform–isoamyl alcohol 25:24:1 and transfer the aqueous phase to a new tube.
9. Add 1/10 volume of 3.0 M sodium acetate pH 5.2 and 2.5 \times volume of absolute ethanol, incubate at –80 °C for 15 min.
10. Centrifuge at 20,000 $\times g$ for 20 min at 4 °C, small white pellet should be seen at the bottom, carefully remove all the solution.
11. Wash pellet with 1 ml 70% ethanol and repeat the centrifugation step.
12. Repeat the wash step to obtain better quality of DNA.
13. Remove the remaining wash solution and dry the pellet for 10 min at room temperature (*see Note 5*).
14. Resuspend DNA pellet in 50 μ l 1 \times TE buffer and store at 4 °C.

3.2 Detection of Hemicatenane by 2D Agarose Gel Electrophoresis and Southern Blot

1. Mix 1.5 g agarose powder and 135 ml H₂O in a flask and dissolve by heating in a microwave.
2. Add 15 ml 10 \times TPE buffer and cool down to around 50 °C.
3. Pour the warm agarose solution into a 14 \times 12 cm gel casting chamber.
4. Make one loading well on the upper left side (we usually use a plastic stick with a 2 mm diameter and fix it on the original comb).
5. Fill 1 l of 1 \times TPE buffer in electrophoresis chamber and load 500 ng DNA sample on the well.

6. Run electrophoresis at 1 V/cm for 12 h at room temperature (*see Note 6*).
7. Soak the agarose gel into 1 l alkaline solution (30 mM NaOH, 1 mM EDTA) for 30 min twice.
8. Put the gel on another large electrophoresis apparatus and turn 90° clockwise. Fill the apparatus with 2 l of alkaline solution (precool at 4 °C).
9. Run electrophoresis in the second dimension at 4 V/cm for 3 h at cold room (*see Note 7*).
10. Soak the gel with 500 ml denaturation buffer (0.5 N NaOH, 1.5 M NaCl) for 30 min on shaker.
11. Soak the gel twice with 500 ml neutralization buffer (0.5 M Tris-HCl pH 7.0, 1.5 M NaCl) for 30 min on shaker.
12. Put the gel on a vacuum transfer equipment, filled with 1 l 20× SSC buffer, transfer DNA to nitrocellulose membrane at 90 mbar for 3 h.
13. Crosslink the DNA with UV light (254 nm, 0.15 J/cm²).
14. Put the membrane into a hybridization bottle and add 10 ml prehybridization buffer, rotate in hybridization oven at 65 °C overnight.
15. Hybridize the DNA at 65 °C for 4 h by adding 25 µl of radioactive random primer in prehybridization buffer (*see Note 8*).
16. Wash membrane with high stringency buffer (0.5× SSC, 0.1% SDS) at 65 °C for 30 min, repeat four times.
17. Vacuum dry the membrane and detect the signal with a phosphorimager.

4 Notes

1. Enzymes are expressed and purified from *E. coli* host cells through column chromatography; details are described in previous publication [15]. The activity of wild-type NeqTop3 might vary between each protein preps. This variation can be compared using the specific activity, with one unit defined as the amount of enzyme required to relax 500 ng of negatively supercoiled pUC19 DNA in a reaction volume of 30 µl at 80 °C for 30 min.
2. High quality plasmid DNA should be purified by twice cesium chloride–ethidium bromide equilibrium density ultracentrifugation, even though commercial Maxi-prep kits also work well.

3. For large amount of sample preparation, we scale up the reaction to 6 ml and split into multiple tubes to minimize the variation from heat conduction between different reactions.
4. Since the reaction is fast and sensitive to temperature, a time course assay can be done to optimize the level of hemicatenation. We incubate 90 s to obtain simple hemicatenane and 7 min for complex hemicatenane networks.
5. Centrifugal vacuum concentrator is an alternative, but do not overdry the DNA.
6. Electrophoresis with TPE buffer has to be done under constant circulation to avoid the ion gradient. Our electrophoresis apparatus comes with built-in circulation system, connecting the setup to an external pump is an alternative. Using other general electrophoresis buffers, such as TAE and TBE is optional.
7. Running the alkaline gel at high voltage generates more heat than native gel electrophoresis, therefore it is recommended to perform this step at low temperature.
8. For random primer labeling, we followed the instructions of the Amersham Rediprime II DNA Labeling System.

Acknowledgments

This work is dedicated to our late mentor, Dr. Tao-shih Hsieh, who passed away during the preparation of this chapter. We would like to thank Dr. Christian Biertümpfel for critical reading of the manuscript. This work was supported by National Institutes of Health Grant GM29006 and Academia Sinica intramural funding (to Tao-shih Hsieh).

References

1. Wang JC (2002) Cellular roles of DNA topoisomerases: a molecular perspective. *Nat Rev Mol Cell Biol* 3(6):430–440
2. Wang JC (2009) Untangling the double helix. DNA entanglement and the action of the DNA topoisomerases. Cold Spring Harbor Laboratory Press, Cold Spring Harbor, New York
3. Chen SH, Chan NL, Hsieh TS (2013) New mechanistic and functional insights into DNA topoisomerases. *Annu Rev Biochem* 82:139–170
4. Schoeffler AJ, Berger JM (2008) DNA topoisomerases: harnessing and constraining energy to govern chromosome topology. *Q Rev Biophys* 41(1):41–101
5. Wu L, Hickson ID (2003) The Bloom's syndrome helicase suppresses crossing over during homologous recombination. *Nature* 426 (6968):870–874
6. Singh TR, Ali AM, Busygina V, Raynard S, Fan Q, Du CH, Andreassen PR, Sung P, Meetei AR (2008) BLAP18/RMI2, a novel OB-fold-containing protein, is an essential component of the bloom helicase-double Holliday junction dissolvosome. *Genes Dev* 22 (20):2856–2868
7. Xu D, Guo R, Sobeck A, Bachrati CZ, Yang J, Enomoto T, Brown GW, Hoatlin ME, Hickson ID, Wang W (2008) RMI, a new OB-fold complex essential for bloom syndrome protein to maintain genome stability. *Genes Dev* 22 (20):2843–2855
8. Plank JL, Wu J, Hsieh TS (2006) Topoisomerase IIIalpha and Bloom's helicase can resolve a

- mobile double Holliday junction substrate through convergent branch migration. *Proc Natl Acad Sci U S A* 103(30):11118–11123
9. Raynard S, Zhao W, Bussen W, Lu L, Ding YY, Busygina V, Meetei AR, Sung P (2008) Functional role of BLAP75 in BLM-topoisomerase III α -dependent holliday junction processing. *J Biol Chem* 283(23):15701–15708
 10. Cejka P, Plank JL, Bachrati CZ, Hickson ID, Kowalczykowski SC (2010) Rmi1 stimulates decatenation of double Holliday junctions during dissolution by Sgs1-Top3. *Nat Struct Mol Biol* 17(11):1377–1382
 11. Liberi G, Maffioletti G, Lucca C, Chiolo I, Baryshnikova A, Cotta-Ramusino C, Lopes M, Pellicoli M, Haber JE, Foiani M (2005) Rad51-dependent DNA structures accumulate at damaged replication forks in sgs1 mutants defective in the yeast ortholog of BLM RecQ helicase. *Genes Dev* 19(3):339–350
 12. Nurse P, Levine C, Hassing H, Marians KJ (2003) Topoisomerase III can serve as the cellular decatenase in *Escherichia Coli*. *J Biol Chem* 278(10):8653–8660
 13. Lucas I, Hyrien O (2000) Hemicatenanes form upon inhibition of DNA replication. *Nucleic Acids Res* 28(10):2187–2193
 14. Robinson NP, Blood KA, McCallum SA, Edwards PA, Bell SD (2007) Sister chromatid junctions in the hyperthermophilic archaeon *Sulfolobus solfataricus*. *EMBO J* 26(3):816–824
 15. Lee SH, Siaw GE, Willcox S, Griffith JD, Hsieh TS (2013) Synthesis and dissolution of hemicatenanes by type IA DNA topoisomerases. *Proc Natl Acad Sci U S A* 110(38):E3587–E3594
 16. Gaillard C, Strauss F (2000) DNA loops and semicatenated DNA junctions. *BMC Biochem* 1:1
 17. Gaillard C, Strauss F (2015) Construction of DNA hemicatenanes from two small circular DNA molecules. *PLoS One* 10(3):e0119368

Chapter 12

An Assay for Detecting RNA Topoisomerase Activity

Muzammil Ahmad, Dongyi Xu, and Weidong Wang

Abstract

RNA topoisomerase activity has recently been detected in multiple Type IA DNA topoisomerases from all three domains of life: bacteria, archaea, and eukarya. Many, but not all, Type IA topoisomerases are found to possess activities for not only DNA, but also RNA, suggesting that they may solve topological problems for both types of nucleic acids. Here we describe a detailed assay used by our group to detect RNA topoisomerase activity for many Type IA topoisomerases. We discuss the strategy, experimental procedures, troubleshooting, and limitations for this assay.

Key words Topoisomerase, Top3 β , Circular RNA, Knot

1 Introduction

Topoisomerases solve essential problems produced during metabolic reactions on DNA, such as replication, transcription, recombination, repair, and segregation [1, 2]. These enzymes have a unique strand passage activity that can alter the topological states of DNA. Type I topoisomerases can create a transient break on one strand of DNA duplex, whereas type II topoisomerases can produce breaks on both strands. The topoisomerase then allows the other strand to pass through the break, and rejoin the broken ends. As a result, supercoils created during DNA metabolism can be removed, interlocked DNA rings can be separated (decatenation), and knots can be introduced into or removed from DNA circles. The importance of topoisomerases can be reflected by the fact that they are broadly present in all species [3], and that their inactivation can often lead to slow growth, lethality, and diseases [1, 4–6].

While DNA topoisomerases have been extensively characterized during the past four and half decades, RNA topoisomerases have been largely ignored. *E.coli* Topoisomerase III (EcoTop3), a Type IA topoisomerase, was the first enzyme that was shown to be capable to catalyze strand passage reactions using circular RNA as substrates in 1996 [7]. However, no follow-up studies have been

reported, so that the biological relevance of the observed RNA topoisomerase activity is unclear. The RNA topoisomerase has finally attracted some attention after the discovery that human Top3 β is an RNA topoisomerase that works with an RNA-binding protein, FMRP, to bind mRNAs, associate with translation machinery, and to promote neurodevelopment; and its deletion is linked to schizophrenia and intellectual disability [4, 8]. To date, RNA topoisomerase activity has been detected in many Type IA topoisomerases from all domains of life, bacteria, archaea, and eukarya. In particular, some of the most-commonly studied topoisomerases, including Top1 (EcoTop1) and Top3 (EcoTop3) of *E.coli*, Top3 of yeast, Top3 β of human (humTop3 β) and *Drosophila*, have all been shown to possess RNA topoisomerase activity [7–10]. Moreover, Top3 β from several animal species (human, chicken, and *Drosophila*), have been shown to associate with mRNA translation machinery [4, 8, 9], suggesting that these enzymes may solve RNA topological problems during mRNA translation. Furthermore, a bona fide RNA-binding domain, RGG-box, has been identified in Top3 β , but not its paralog, Top3 α , in Type IA enzymes from animals [8]. Deletion of this domain diminishes the RNA topoisomerase activity of Top3 β . These data provide structural basis for why the former, but not the latter, possesses RNA topoisomerase activity.

Here we describe a detailed assay used by our group to detect the RNA topoisomerase activity for Type IA topoisomerases from all three domains of life. We believe that this assay can be broadly applied to examine RNA topoisomerase activity for this family of topoisomerases.

1.1 Strategy

The original assays used to detect RNA topoisomerase activity for EcoTop3 were designed elegantly by Seeman and his colleagues [7]. They engineered a circular single-stranded RNA substrate consisting two pairs of complementary regions of 10 bp each, which are separated by four intervening spacers, which are also 10 bp each (Fig. 1a) [7]. The two complementary regions are thermodynamically favored to form two short duplexes. However, only through a strand-passage reaction catalyzed by a topoisomerase, can both regions form normal duplexes. After the strand-passage reaction, the circular RNA substrate will be converted to a trefoil with a single knot (Fig. 1a). The trefoil knot product can be distinguished from its circular substrate by denaturing polyacrylamide electrophoresis (PAGE) analysis (Fig. 1b). Using this assay, RNA topoisomerase activity was detected for EcoTop3, but not EcoTop1 [7].

We used the same strategy designed by Seeman and colleagues, but modified their circular RNA substrate by increasing the complementary regions from 10 to 12 bps [8]. We reasoned that the increased length should further stabilize the duplex regions, and make the reaction thermodynamically more favorable. Indeed,

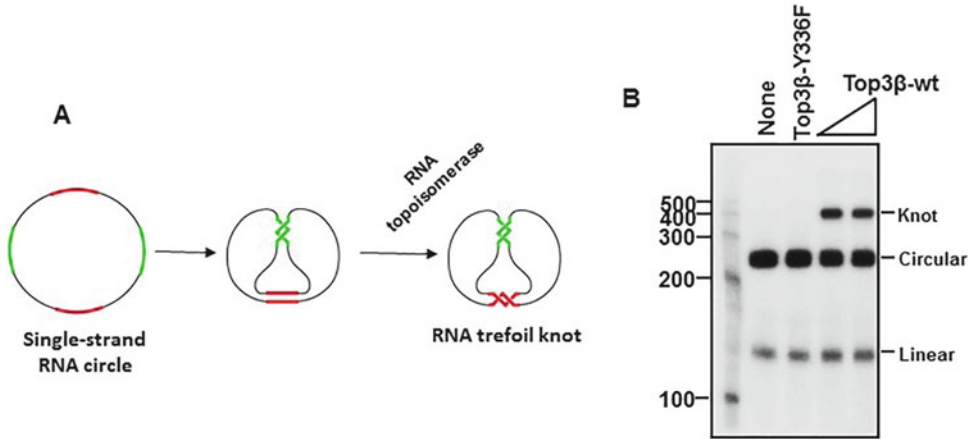


Fig. 1 A trefoil knot formation assay to show that human Top3β protein has RNA topoisomerase activity. (a) Schematic representation of an RNA topoisomerase assay that is based on conversion of an RNA circle to a trefoil knot. Two complementary regions are marked by red and green colors, whereas the spacer regions are marked by black. The circle substrate and the knot are indicated. (b) An autoradiograph shows that wild type human Top3β, but not the catalytic mutant Y336F, has RNA topoisomerase activity that can convert the RNA circle substrate to a trefoil knot product. 5 nM of protein was used in the assay

using our substrate, we found that EcoTop1 does have robust RNA topoisomerase activity, and this activity is comparable to that of hum Top3β [9]. Because the new substrate allowed us to detect the RNA topoisomerase activity in EcoTop1, whereas that used by Seeman and colleagues did not, we conclude that the new substrate makes the assay more sensitive. We have since used the new substrate to detect RNA topoisomerase activity for many type IA topoisomerases.

2 Materials

2.1 Preparation of Radiolabeled Linear RNA Substrate

1. MEGAshortscript™ T7 Kit (Ambion) for in vitro transcription reactions.
2. The synthetic DNA oligo sequences needed to make the circular RNA substrate are listed in Table 1. A single-strand RNA (GGGAGAUUUUUUUUUUUUUUUUUUUUUUUUGUCAGACGGAUCUUUUUUUUUUUUUUUUUUUUUUUUUUUUUCUCCCGACUGGUUUUUUUUUUUUUUUUUUUUUUUUUUUUGAUCCGUCUGACUUUUUUUUUUUUUUUUUUUUUUUUUUUUUCCAGUC) was transcribed by MEGAshortscript™ T7 Kit (Ambion) from an annealed DNA template consisting of synthetic oligos K128f and K128r (Table 1).
3. All purification steps for RNA topoisomerases should be performed in ice cold buffers. All solutions for RNA topoisomerase reactions should be prepared in RNase-free, DNase-free, and DEPC-treated molecular biology grade water. Work place

Table 1
A list of DNA oligo sequences used for making the circular RNA substrate

Oligos used in the RNA topoisomerase assay	
DNA oligos	Sequence
K128f	ACTTCGAAATTAATACGACTCACTATAGGGAGATTTTTTTTTTT TTTTTTTTTTTGTCCAGACGGATCTTTTTTTTTTTTTTTTTTTT TCTCCCGACTGGTTTTTTTTTTTTTTTTTTTTTTTGATC CGTCTGACTTTT TTTTTTTTTTTTTTTTTTCCAGTC
K128r	GACTGGAAAAAAAAAAAAAAAAAAAAAAAAAGTCAGACGGATCAA AAAAAAAAAAAAAAAAAAAAACCAGTCGGGA GAAAAAAAAAAAAAAAAAAAAAGATCCGTCTGACAAAAAAAAA AAAAAA AAAAATCTCCCTATAGTGAGTCGTATTAATTTCAAGT
K128link	GATCCGTCTGACAAAAAAAAAAAAAAAAAAAAAATCTCCCGACTGGAAAAA

This table has been taken from Supplemental Fig. 5 of a previous publication for the convenience of readers [8]

and pipettes should be wiped with RNaseZap (Ambion) solution to avoid RNase contamination. It is advised to use autoclaved RNase free microcentrifuge tubes. RNA substrates should be kept on Ice (unless the temperature is specified for particular reaction) while working, and stored at -80° freezers for long-term storage.

4. RNase free-DNase: Turbo DNase (Ambion).
5. 6% TBE-Urea polyacrylamide gel (Invitrogen).
6. Molecular weight marker mixture of 100–500 bases (Ambion).
7. 6% TBE-Urea polyacrylamide gel containing a single well.
8. Surgical blade.
9. D-Tube dialyser (EMD Millipore) filled with TE.
10. TBE.
11. Phenol–chloroform–isopropanol mixture (Invitrogen).
12. Cold absolute ethanol.
13. NanoDrop to determine the concentration of the RNA preps.
14. 50–60 μ Ci of γ -p32-ATP, 6000 Ci/mmol, 10 mCi/ml (PerkinElmer).
15. Kinase Max™ kit (Ambion).
16. NucAway spin column (Ambion).
17. Geiger counter.

2.2 Circularization of the Radiolabeled Linear RNA

1. 10 \times annealing buffer: 100 mM Tris pH 7.5, 1 mM NaCl.
2. Heat block.
3. T4 RNA ligase with buffer (Ambion).

4. RNaseout (Invitrogen).
5. Gel Loading Buffer II (Provided with the MEGAshortscript T7™ kit).
6. 15% TBE-Urea polyacrylamide gel (Invitrogen).
7. RNase-free water.

2.3 The RNA Strand Passage Reaction

1. 5× reaction buffer: 100 mM Tris–HCl pH 7.5, 500 mM NaCl, 50 mM MgCl₂, 0.5 mg/ml BSA, 25% glycerol. DTT (2 mM final concentration) and PEG400 (10% final concentration or 1 μl in 10 μl reaction) are added just before setting up the reaction.
2. Purified type 1A topoisomerase.
3. 5× stop buffer: 1 mg/ml proteinase K, 2.5% SDS, 100 mM EDTA.
4. Gel Loading Buffer II (Provided with the MEGAshortscript T7™ kit).
5. 15% TBE-Urea polyacrylamide gel (Invitrogen).

3 Methods

3.1 Preparation of Radiolabeled Linear RNA Substrate

1. Oligos K128f and K128r (Table 1) were annealed to produce the DNA template for in vitro transcription to produce a linear RNA. For the annealing reaction, 500 ng of each oligo was mixed with 1 μl of 10× transcription buffer from the MEGAshortscript™ T7 Kit and appropriate amount of H₂O, so that the final volume is 10 μl.
2. The tube containing the reaction mixture was first incubated at 95 °C for 5 min, and then placed into boiling water in a beaker to let it slowly cool down to room temperature. This will take about 2 h. The tube was centrifuged for 10 s when temperature reaches to about 60 °C, to re-collect the liquid that was evaporated and condensed on the cap of the microcentrifuge tube. The annealed template will be used for in vitro transcription to produce linear RNA using the MEGAshortscript™ kit from Ambion as described below.
3. Take 9 μl of the annealed mixture and add 2 μl of each ribonucleotide (75 μM rATP, rUTP, rCTP and rGTP), 1.0 μl 10× transcription buffer (0.9 μl is already present in the annealing mix), 2 μl of T7 polymerase, and water to make the final reaction volume at 20 μl. Incubate the reaction mixture at 37 °C for 2 h. Afterward, add 2 μl of turbo DNase (Ambion) and incubate the mixture at 37 °C for 15 min to degrade the DNA template.

4. The mixture was added with equal volume of Gel Loading Buffer II (Provided with the MEGAscript T7™ kit). The RNA product was purified by electrophoresis on a 6% TBE-Urea polyacrylamide gel (Invitrogen) at 180 V for 40–50 min. A molecular weight marker mixture of 100–500 bases (Ambion) was included during electrophoresis. The gel needs a prerun for 30 min at 180 V before being used for purification of RNA.
5. We noticed that the linear RNA product can sometimes form irreversible dimers or multimers when it was boiled in the loading buffer. It is possible that the linear RNA molecules become tangled between each other to form knots and other structures that can no longer be separated on denaturing gels. To avoid this to happen, the RNA mixture (40 µl) can be added with 500 µl of Loading buffer to reduce the RNA concentration. After heat denaturation, the mixture can be purified using a preparative 6% TBE-Urea gel containing a single wide well (a special gel comb is needed to make such a gel).
6. After electrophoresis, the RNA product (128 base) was visualized by UV shadowing, excised from the gel using a surgical blade, and transferred to a D-Tube dialyzer (EMD Millipore) filled with TE.
7. The RNA product was then eluted by electroelution against 1X TBE at 120 V for 1–1.5 h. It was purified by extraction with equal volume of phenol–chloroform–isopropanol mixture (In Vitrogen) once. The aqueous layer containing the RNA product was collected. The RNA was then precipitated by adding 2.5 volumes of 100% ethanol and incubated at –20 °C for overnight. On the next day, the RNA was collected by centrifugation using a tabletop centrifuge at 13,500 rpm (14000 × *g*) for 10 min at 4 °C. The pellet was then washed once with cold 80% ethanol, centrifuged again, air-dried for 5 min, and dissolved in RNase-free water. The RNA should not be over-dried, which will make it difficult to dissolve. The concentration of RNA was measured using NanoDrop. Its concentration was adjusted to 2 µg/µl using water.
8. The linear RNA of 20–40 µg (2 µg/µl) was labeled with γ -p32-ATP at its 5' end using the Kinase Max™ kit as per the manufacturer protocol (Ambion). Briefly, 20 µl of RNA was added to 3 µl 10× phosphatase buffer, 3 µl calf intestine alkaline phosphatase, and water to final volume to 30 µl. The mixture was incubated for 1 h at 37 °C to remove the 5'-phosphate on the linear RNA. Equal volume of phosphatase removal buffer was added to the mix and incubated at room temperature for 3 min with intermittent shaking. The mixture was then centrifuged at 13,000 rpm (13000 × *g*) for 30 s.

Carefully remove the supernatant that was now approximately 40–45 μl . The mixture was then added with 6 μl 10 \times kinase buffer, 50–60 μCi of γ -p32-ATP (6000 Ci/mmol 10 mCi/ml, PerkinElmer), and 6 μl of T4 polynucleotide kinase enzyme, and appropriate amount of water to adjust the reaction volume to 60 μl . The mixture was then incubated at 37 $^{\circ}\text{C}$ for 1 h. The kinase reaction was terminated by heating at 95 $^{\circ}\text{C}$ for 2 min. The free radioactive nucleotides were removed using NucAway spin column (Ambion). The success of the radiolabeling reaction can be verified by measuring the radioactivity in the linear RNA using a Geiger counter or a scintillation counter (*see Note 1*).

3.2 Circularization of the Radiolabeled Linear RNA

1. The p32-labeled linear RNA was annealed with the DNA linker oligo K128link (Table 1). This linker oligo has sequence complementary to both ends of the linear RNA. When both ends of RNA are annealed to the same DNA linker, the linear RNA becomes circularized, although its 5' and 3' ends are not covalently linked. An RNA ligase will then be added to ligate the two free ends.
2. For the annealing reaction, a mixture of 15 μl was made by mixing 12 μl of p32-labelled linear RNA, 1.5 μl of K128 linker oligo (100 μM), and 1.5 μl of 10 \times annealing buffer (100 mM Tris pH 7.5, and 1 M NaCl). We found that the 10 \times RNA ligase buffer (Ambion) can also be used. The annealing mixture was heated at 95 $^{\circ}\text{C}$ in heat block for 5 min, and transferred to a water bath at 70 $^{\circ}\text{C}$. The water bath was then turned off, so that the mixture will be cooled down gradually until the water temperature reaches to the room temperature. The liquid condensed on the cap of the tube can be collected by centrifugation.
3. For ligation: the 15 μl mixture was added with 2 μl of 10 \times T4-RNA ligation buffer, 2 μl T4 RNA ligase (Ambion), 0.5 μl of RNascout (Invitrogen), and water to make the final volume to 20 μl . The mixture was incubated for 3 h at 37 $^{\circ}\text{C}$. If the yield of circular RNA is unsatisfactory, the mixture can be incubated at 16 $^{\circ}\text{C}$ overnight.
4. To remove the DNA linker oligo after RNA circularization, 2 μl of DNase (5 U/ μl) was added, and the mixture was incubated for 15 min at 37 $^{\circ}\text{C}$. The reaction was terminated by adding equal volume of Gel Loading Buffer II. The RNA-containing mixture was then denatured at 95 $^{\circ}\text{C}$ for 5 min, loaded on 15% TBE-Urea gel (Invitrogen)(which should be no more than 20 days old), and resolved by electrophoresis at 150 V for 10–11 h. The radiolabeled RNA products were detected by X-ray autoradiography. To avoid contamination of radioactivity, the gel should be wrapped carefully with a saran wrap before being exposed to the X-ray film for 0.5–1 h.

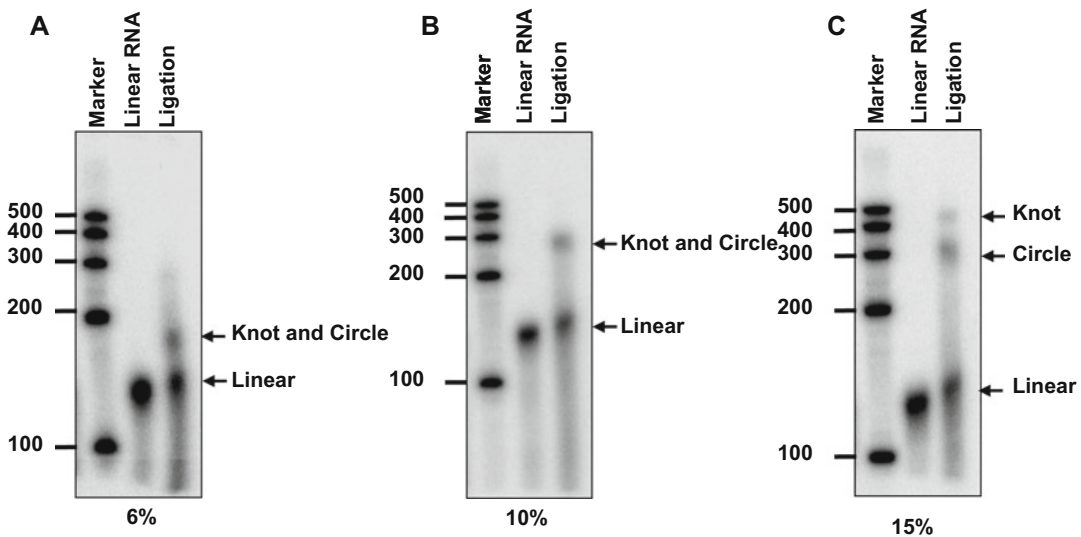


Fig. 2 Distinguishing the circular, linear, and knot forms of RNA by electrophoresis on polyacrylamide gels of different concentrations. (a) An autoradiograph shows that the RNA circle and knot have mobility similar to that of the 200 base marker on a 6% denaturing gel, whereas the corresponding linear substrate has mobility comparable to that of its expected size of 128 bases. Ligation refers to the RNA mixture in which the linear RNA substrate has been ligated using T4 ligase. (b) An autoradiograph shows that the RNA circle and knot display mobility similar to that of the 300 base marker on a 10% polyacrylamide–urea gel, while the linear substrate runs at its expected size of 128 bases. (c) An autoradiograph shows that the RNA knot has mobility similar to that of the 500 base marker, and the RNA circle runs at mobility similar to that of the 300 base marker, whereas the linear substrate runs at its expected size of 128 bases. Overall, the circular and knot forms of RNA have reduced mobility in contrast to their linear counterpart

5. The circular product can be distinguished from its linear and other forms (such as trefoil knots) based on its mobility variation on different percentages of polyacrylamide gels (Fig. 2a–c). Comparing to known molecular weight markers (Ambion), the circular RNA exhibits variation in its mobility on different percentage of gels, whereas the linear RNA does not. The relative position of the knot versus the circle also varies: the knot has slower mobility than the circle on high percentage gels, but has equal or faster mobility on low percentage gels. The conversion from a circle to a knot can be inhibited when the self-annealing of the two complementary regions of the circle is blocked by adding a competing oligo that is complementary to one of the regions.
6. The gel slice containing the circular RNA was excised, extracted by electroelution described above, precipitated by adding 1/10th volume of 3 M sodium acetate pH 5.0, and 2.5 volume of 100% ethanol, and incubated overnight at -20°C . The RNA was collected by centrifugation, and dissolved in RNase-free water (40 μl). The radioactivity of RNA was measured by scintillation counter. We typically obtain radioactivity of about 8000–12,000 CPM/ μl .

**3.3 The RNA Strand
Passage Reaction that
Converts the RNA
Circle to Trefoil Knot**

1. Make 5× reaction buffer as follows: 100 mM Tris–HCl, pH 7.5; 500 mM NaCl, 50 mM MgCl₂, 0.5 mg/ml BSA, 25% glycerol. DTT (2 mM final concentration) and PEG400 (10% final concentration or 1 μl in 10 μl reaction) should be added freshly just before setting up the reaction. We often add 4 units RNaseOut (Invitrogen) to the 1× reaction mixture to minimize RNA degradation.
2. The strand passage reaction was set up by mixing the following components: the purified Type IA topoisomerase (such as hum Top3β or EcoTop1), the p32-labeled circular RNA substrate (2500–3000 CPM), 5× reaction buffer, DTT, PEG400, and water. The final volume is 10 μl.
3. The concentration of the topoisomerase used in the reaction needs to be determined empirically (*see Note 2*). This is because too much topoisomerase in the reaction can inhibit the strand passage reaction. This may be because that if the complementary regions of the substrate are fully coated by the enzymes, they will no longer be able to form duplexes, which are the driving force for the strand-passage reaction that converts the circle to knot. For humTop3β, its optimal concentration is about 1–4 nM concentration.
4. The optimum reaction temperature for some topoisomerases, particularly those from thermo-resistant bacteria and archaea, may be higher than 37 °C. We often use 50 °C for enzymes from these species.
5. The mixture was incubated at 37 °C for 90 min. The reaction was terminated adding 2 μl 5× stop buffer (1 mg/ml Proteinase K, 2.5% SDS, 100 mM EDTA). The mixture was incubated at 50 °C for 30 min to allow degradation of proteins by the Proteinase K. The mixture was then extracted by phenol–chloroform and precipitated with ethanol.
6. We found that for many topoisomerases, such as hum Top3β and EcoTop1, the step of phenol–chloroform extraction can be omitted, as proteinase K digestion is sufficient to degrade these enzymes. However, for other topoisomerases (such as yeast Top3), this step is necessary. These topoisomerases can form strong RNA–protein complexes that are resistant to Proteinase K digestion and heat-denaturation. The complexes can produce gel shift on denaturing gels that has similar mobility as the trefoil knot (Fig. 3). Phenol–chloroform extraction can efficiently disrupt these RNA–protein complexes, remove the protein, and avoid the confusion of mistaking these gel shifts as trefoil knots.
7. After ethanol precipitation, the RNA mixture was redissolved with 5 μl water and 5 μl Gel loading dye II, denatured by heat at 95 °C for 3–5 min, and fractionated on a 15% TBE–urea gel

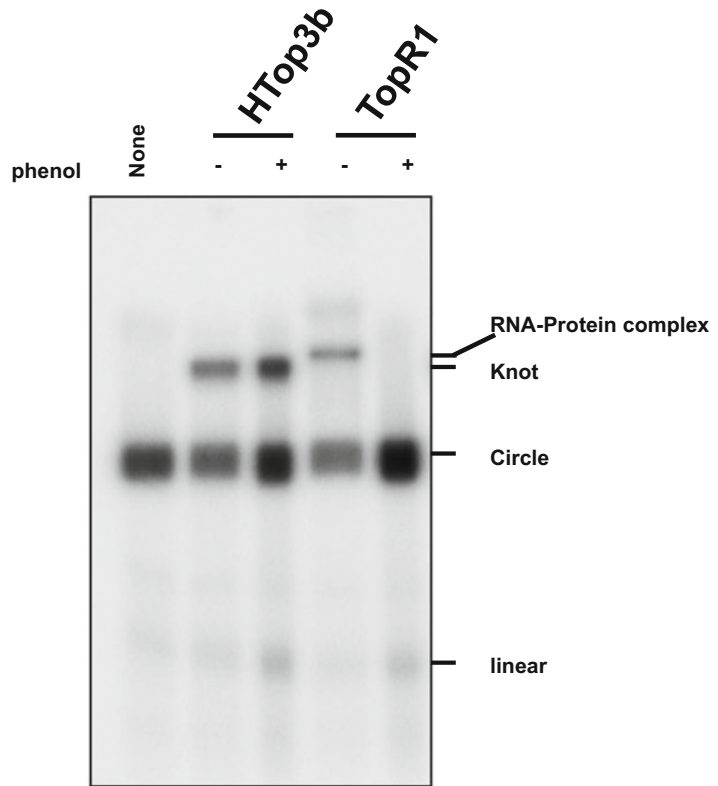


Fig. 3 Phenol–chloroform extraction distinguishes the RNA knot from a gel shift caused by stable RNA–protein complexes. An autoradiograph shows that the RNA knot produced by humTop3 β RNA topoisomerase (4 nM) does not disappear after phenol chloroform extraction (Lane 2 and 3). In contrast, the product produced by a reverse gyrase from an archaea species, TopR1 (4 nM) of *Sulfolobus solfataricus*, was disrupted by phenol chloroform extraction, indicating that the latter reaction did not produce the RNA knot. Instead, the latter reaction generated a highly stably RNA–protein complex containing the circular RNA substrate and the enzyme, which results in the gel shift. Yeast topoisomerase 3 can also form a gel shift when incubated with the circular RNA substrate at high protein concentrations (*data not shown*)

(Invitrogen). Gels that are more than 3 weeks old should not be used because they often have poor resolution (*see Note 3*). After electrophoresis at 150 V for about 5–6 h, the gel was analyzed by Storm 860 Molecular Imager (Molecular Dynamics).

8. To improve the image quality, the radiolabeled RNA in the gel can be first transferred to a Nylon membrane by electrophoresis (similar to Western blotting), and then analyzed by Storm 860 Molecular Imager. Because the membrane is much thinner

than the gel, the radiolabeled RNA becomes more concentrated after the transfer, and thus produces a much sharper signal on the Imager.

3.4 RNA Substrate for Type IA Topoisomerase Assays

The trefoil knot formation assay described here has been used to detect RNA topoisomerase activity for many Type I enzymes from all three domains of life, which include humTop3 β , yeast Top3, *E. coli* Top1, *Nanoarchaeum equitans* Top3, and *Sulfolobus solfataricus* Top3 [9]. However, it failed to detect RNA topoisomerase activity for Type IA enzymes (Top1) from *Mycobacterium tuberculosis* and *Mycobacterium smegmatis*. It is possible that the latter two enzymes lack RNA topoisomerase activity. However, it is equally possible that our assay may not be sensitive enough for detecting the RNA topoisomerase activity in all Type IA topoisomerases. One way to improve the sensitivity of the assay is to further increase the length of the complementary regions of the substrate to make the reaction thermodynamically more favorable. The length of the spacer region can also be optimized to favor the knot formation. New assays may be developed that are more sensitive and test different features of these topoisomerases. Indeed, Hsieh and colleagues have recently described a new RNA topoisomerase assay based on annealing of two complementary single-stranded RNA circles to produce a double-strand RNA circle [10]. Using the new assay, they also observed RNA topoisomerase activity in Type IA enzymes from *E. coli*, archaea, and *Drosophila*. All these data support the notion that RNA topoisomerase activity is broadly present in Type IA topoisomerases in all domains of life, which can solve topological problems for both DNA and RNA.

4 Notes

1. We found that it is important to have the p32-labeled circular substrate with high specific radioactivity. If specific radioactivity of the substrate is too low, the conversion from the circle to knot will be less efficient.
2. It is essential to make good preparations of topoisomerases. We found the RNA topoisomerase activity of humTop3 β varies between different preparations. Moreover, careful titration of the topoisomerase is also needed to find the optimal concentration of the enzyme for the reaction. Too little or too much enzymes may give poor conversion of the RNA circle to knot.
3. One should avoid using old gels, because their resolution is poor that they may not efficiently separate the RNA circle from the knot.

Acknowledgment

The experimental protocols described here have been previously reported in less detail in two previous publications of our group [8, 9]. This work is supported in part by the Intramural Research Program of the National Institute on Aging (Z01 AG000657-08), National Institutes of Health; the National Basic Research Program of China (2013CB911002); and National Natural Science Foundation of China (31271435).

References

1. Wang JC (2002) Cellular roles of DNA topoisomerases: a molecular perspective. *Nat Rev Mol Cell Biol* 3:430–440
2. Pommier Y, Sun Y, Huang SN, Nitiss JL (2016) Roles of eukaryotic topoisomerases in transcription, replication and genomic stability. *Nat Rev Mol Cell Biol* 17(11):703–721
3. Forterre P, Gribaldo S, Gadelle D, Serre MC (2007) Origin and evolution of DNA topoisomerases. *Biochimie* 89:427–446
4. Stoll G, Pietilainen OP, Linder B, Suvisaari J, Brosi C, Hennah W, Leppä V, Torniaainen M, Ripatti S, Ala-Mello S et al (2013) Deletion of TOP3beta, a component of FMRP-containing mRNPs, contributes to neurodevelopmental disorders. *Nat Neurosci* 16:1228–1237
5. Kwan KY, Greenwald RJ, Mohanty S, Sharpe AH, Shaw AC, Wang JC (2007) Development of autoimmunity in mice lacking DNA topoisomerase 3beta. *Proc Natl Acad Sci U S A* 104:9242–9247
6. Kwan KY, Wang JC (2001) Mice lacking DNA topoisomerase IIIbeta develop to maturity but show a reduced mean lifespan. *Proc Natl Acad Sci U S A* 98:5717–5721
7. Wang H, Di Gate RJ, Seeman NC (1996) An RNA topoisomerase. *Proc Natl Acad Sci U S A* 93:9477–9482
8. Xu D, Shen W, Guo R, Xue Y, Peng W, Sima J, Yang J, Sharov A, Srikantan S, Fox D 3rd et al (2013) Top3beta is an RNA topoisomerase that works with fragile X syndrome protein to promote synapse formation. *Nat Neurosci* 16:1238–1247
9. Ahmad M, Xue Y, Lee SK, Martindale JL, Shen W, Li W, Zou S, Ciaramella M, Debat H, Nadal M et al (2016) RNA topoisomerase is prevalent in all domains of life and associates with polyribosomes in animals. *Nucleic Acids Res* 44:6335–6349
10. Siaw GE, Liu IF, Lin PY, Been MD, Hsieh TS (2016) DNA and RNA topoisomerase activities of Top3beta are promoted by mediator protein Tudor domain-containing protein 3. *Proc Natl Acad Sci U S A* 113(38):E5544–E5551

Studying TDP1 Function in DNA Repair

Shih-Chieh Chiang, Kirsty Liversidge, and Sherif F. El-Khamisy

Abstract

Topoisomerase poisons act by inducing abortive topoisomerase reactions, which generate stable protein–DNA breaks (PDBs) that interfere with transcription elongation and progression of replication forks. In vertebrates, Tyrosyl-DNA phosphodiesterase 1 (TDP1) plays a major role in removal of topoisomerase I-associated PDBs in the nucleus and mitochondria by hydrolyzing the 3'-phosphotyrosine bond. Depletion of TDP1 sensitizes tumor cells with defective DNA repair capacity to the genotoxic effect of TOP1 poisons, while homozygous mutation of the catalytic residue of TDP1 is associated with cerebellar degeneration and ataxia. We describe here two fluorescence based biochemical assays for measuring TDP1 phosphodiesterase activity in cellular lysates. The Gyraseol assay is sensitive, high-throughput, and useful for screening potential TDP1 inhibitors or cell lines that are likely to develop resistance to TOP1 poisons. The gel-shift assay is low cost and simple to set up, and is also suitable for screening cell lines that are likely to develop resistance to TOP1 poisons, as well as for diagnostic screening for individuals with hereditary ataxias.

Key words TDP1, Topoisomerase, Assay, High-throughput screen, Cell-based, Drug discovery

1 Introduction

Topoisomerases fulfil their roles in unwinding and untangling DNA strands through potentially dangerous mode of catalysis—generating DNA strand breaks while remaining covalently attached to the ends while the torsional stress is released. These bulky protein adducts can interfere with progression of the DNA replication and transcription machineries. Fortunately, these are normally reaction intermediates that are extremely short-lived, as the hydroxyl group of the DNA backbone promptly attacks the phosphotyrosine bond between the protein and phosphate backbone, releasing the protein adduct and restoring the backbone continuity [1].

However, occasionally, nicking by a topoisomerase in the proximity of a preexisting DNA strand break or an abasic site prevents religation of the nick, as the required hydroxyl group is lost or absent. This forms a persistent protein–DNA break (PDB) that

signals DNA damage repair. TDP1 and TDP2 are the only currently known factors that specifically cleave the phosphotyrosine bond between the topoisomerase and DNA phosphate backbone following proteolytic degradation of the topoisomerase [2, 3]. In the case of TDP1, activity against 3'-phosphotyrosine generated by Topoisomerase 1 (TOP1) is much greater than 5' phosphotyrosine generated by Topoisomerase 2 (TOP2), and vice versa for TDP2. The resulting 3' phosphate ends are then processed by 3' phosphatase PNKP to yield a "clean" 3' hydroxyl end amenable to repair by DNA ligase III.

The 3' phosphodiesterase activity of TDP1 is highly relevant in cancer biology, as it can counteract the genotoxic effect of commonly used antineoplastic agents. In preclinical studies, cells depleted of TDP1 accumulate more DNA breaks and lose replicative potential following camptothecin (CPT), ionizing radiation, and alkylating agents [4–9], while overexpression of TDP1 increases resistance to CPT.

Currently, published high throughput assays for TDP1 activity have been based on chromogenic substrate [10], electrochemiluminescent (ECL) substrate [11], AlphaScreen technology-based assay [12], fluorescence-based AP site-cleavage activity based assay, and a hairpin-biosensor type of fluorescence assay [13]. Here, we describe another high throughput assay based on the Gyrasol assay technology, that has the advantages of being highly sensitive, specific, cost-effective, and versatile application.

The Gyrasol assay technology for TDP1 activity relies on a trivalent metal ion sensor that binds to the phosphate backbones of the dsDNA oligonucleotide substrate. Upon binding it quenches electrons from the nearby 3' fluorophore on the substrate and fluorescence signal is diminished. Upon addition of TDP1, the fluorophore is cleaved off the substrate. When the distance between the fluorophore and oligonucleotide is more than 1 nm, quenching stops and fluorescence signal is detected (Fig. 1). The steps to set up the Gyrasol TDP1 activity assay involves preparation of cellular lysates; quantification of total proteins; dilution of cell lysates and substrate in 1× reaction buffer; incubate lysate with substrate in 1× reaction buffer for a fixed time; mix the reaction with the sensor and enhancer solution, which also stops TDP1 activity; detect fluorescence with a microplate reader immediately.

The gel-shift assay relies on gel electrophoresis to detect the shift in size of the metabolite relative to the substrate after cleavage of the 3' phosphotyrosine by TDP1. It requires a dsDNA oligonucleotide substrate with 3' phosphotyrosine group, and a fluorophore at the 5' end for detection by a gel imaging system. The gel-shift assay has additional advantage over the Gyrasol assay in that it can be used in cell lines expressing fluorophore-tagged proteins.

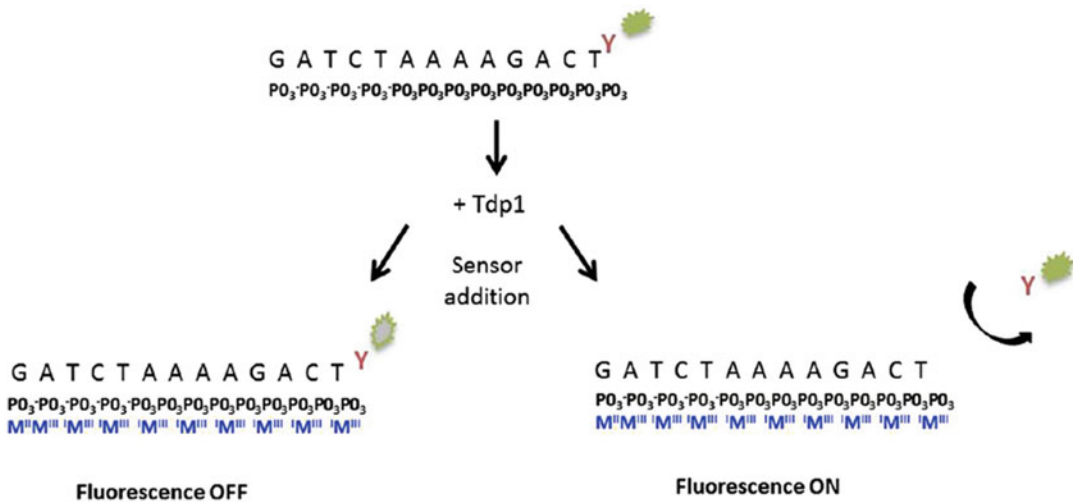


Fig. 1 Gyrasol assay technology. A 13mer oligo with a 30-tyrosine-conjugated FITC molecule was produced. The phosphodiester bond between the tyrosine and the DNA can be hydrolyzed by tyrosyl-DNA-phosphodiesterase 1 (TDP1). Addition of a small molecular, nonfluorescent trivalent metal ion sensor (MIII) (Gyrasol Technologies, USA) binds to the phosphate bone of the ss-DNA oligo. The fluorescence of any fluorophore in close proximity to the sensor is quenched by electron transfer, while any fluorophore separated from the DNA (1 nm; 10 Å) is too distant for electron transfer quench

2 Materials

2.1 Gyrasol Assay

2.1.1 Preparation of Whole Cell Extract

1. General lab equipment: vortex mixer, cooling microcentrifuge.
2. 1.5 ml microcentrifuge tubes.
3. Phosphate-buffered saline (PBS).
4. Cell Lysis Buffer: 20 mM Tris-HCl pH 7.5, 10 mM EDTA pH 8.0, 100 mM NaCl, 1% Triton X-100. Add 1× protease inhibitors cocktail and 25 U.ml⁻¹ benzonase just before use. Base lysis buffer can be stored at 4 °C long term.
5. Cell lines: test, positive control (e.g., wild-type), and negative control (e.g., TDP1 depleted/knockout).

2.2 Protein Quantification

1. General lab equipment: spectrophotometer or microplate reader.
2. Cuvettes specific to spectrophotometer, or clear flat-bottom 96-well plates.
3. Bradford Reagent (e.g., Bio-Rad Protein Assay Kit). Store at 4 °C.
4. Bovine serum albumin (BSA). Store at 4 °C.

2.2.1 TDP1 Fluorescence Assay

1. General lab equipment: fluorescence microplate reader.
2. Black flat-bottomed microplate. The assay setup described is optimized for the 384-well format.

3. Gyrase Assay Buffer: 50 mM Tris, pH 8.0, 5 mM MgCl₂, 80 mM KCl, 0.05% Triton X-100. Store at 4 °C.
4. 200 mM dithiothreitol (DTT) dissolved in water. Aliquot into single-use volumes. Store at -20 °C.
5. FITC-labeled substrate (*see Note 1*) diluted to 100 μM. Store at -20 °C.
6. (Optional) Purified TDP1 protein (*see Note 2*) at 200 μM. Store at -80 °C.
7. Enhancer & Sensor Buffers (Gyrase Technologies, KS, USA).

2.3 Gel-Shift Assay

Same materials required as Subheadings 2.1 and 2.2. In addition:

2.3.1 TDP1 Biochemical Assay

1. General lab equipment: PCR machine or water bath.
2. 0.2 ml PCR tubes or 1.5 ml Eppendorf tubes.
3. 10× Assay buffer: 250 mM HEPES, pH 8.0, 1.3 M KCl, 10 mM DTT. Aliquot and store at -20 °C.
4. 5' fluorophore-labeled substrate. We used a Cy5.5-labeled 13mer dsDNA substrate (*see Note 3*). Dilute to 100 μM in DMSO. Store at -20 °C.
5. 10 mM DTT. Store at -20 °C.

2.3.2 Gel Electrophoresis

1. General lab equipment: vertical gel electrophoresis system (e.g., Bio-Rad Mini PROTEAN), gel imaging system with fluorescence filter specific to substrate.
2. 2× Loading buffer: 44% deionized formamide, 2.25 mM Tris-borate, 0.05 mM EDTA, 0.01% xylene cyanol, 1% bromophenol blue. Store at -20 °C.
3. Urea gel constituents (e.g., SequaGel, National Diagnostics).
4. 10% w/v ammonium persulfate (APS) dissolved in distilled water.
5. 1,2-Bis(dimethylamino)ethane (TEMED).
6. 10× TBE buffer: 108 g Tris, 55 g boric acid, 40 ml of 0.5 M EDTA (pH 8.0), make up to 1 l with distilled water.

3 Methods

3.1 Gyrase Assay

3.1.1 Preparation of Whole Cell Lysates

1. Centrifuge cell suspension at $200 \times g$ for 5 min, remove supernatant.
2. Wash once with cold PBS, centrifuge as before, remove supernatant.
3. Resuspend cell pellet in lysis buffer at ~1:4 pellet volume to lysis buffer. Leave on ice for ~30 min, vortexing intermittently.

4. Centrifuge at $>16000 \times g$ at 4°C for 15 min.
5. Carefully transfer the supernatant to a clean Eppendorf tube.
6. Keep lysates on ice or alternatively if not needed immediately, store at -80°C .

3.1.2 Protein Quantification

1. Leave Bradford reagent at room temperature for 30 min prior to use.
2. Dilute Bradford reagent in distilled water to $1\times$ as required.
3. Reconstitute BSA as required. Store aliquots at -20°C .
4. Prepare five dilutions of BSA ranging from 0.2 to 0.9 mg/ml in distilled water.
5. Mix together the Bradford reagent with BSA standard or sample at ratio specified by manufacturer. Samples are measured in triplicates.
6. Incubate reaction at room temperature for at least 5 min.
7. Measure absorbance at 595 nm.
8. Calculate concentration of samples using the BSA standard curve. If concentrations lie outside the linear range, dilute the samples accordingly and repeat absorbance measurement (*see Note 4*).

3.1.3 TDP1 Fluorescence Assay

1. Set up the fluorescence microplate reader: specify plate type, sample layout, end-point reading, filter spectrum for excitation λ of 490 nm and emission λ of 520 nm, temperature at 30°C .
2. Calculate the number of reactions required: test samples, positive controls (e.g., lysate from wild-type cell line and/or purified TDP1), biological negative control (e.g., TDP1 knockout cells), three technical negative controls (no lysate, no substrate, and Assay buffer alone). All in triplicates.
3. Add 5 μl 200 mM DTT per 1 ml of Gyrasol Assay Buffer (final concentration of 1 mM) just before use, make enough for all samples and controls (in triplicates), and for diluting the substrate and purified TDP1 (if using).
4. Dilute substrate to 30 nM in Gyrasol Assay Buffer with 1 mM DTT.
5. Dilute purified TDP1 (if using) to 6.25 pM in Gyrasol Assay Buffer with 1 mM DTT.
6. Dilute cell lysates to $\sim 2 \mu\text{g}/\mu\text{l}$ in Assay Buffer with DTT (amount used to be optimized for each cell line).
7. Add 8 μl of Assay Buffer with DTT to each well of the plate, followed by 2 μl of lysate, and 5 μl of the substrate (final substrate concentration of 10 nM).
8. Mix by gently tapping the side of the plate.

9. Incubate reaction at room temperature for 10 min.
10. Mix together 30 μl of Enhancer and 2 μl Sensor buffers per well of reaction just before end of the 10 min incubation. Make enough for pipetting errors.
11. Stop the reaction by adding 32 μl of Enhancer and Sensor mixture to each well.
12. Place plate in the plate reader immediately. Adjust the gain intensity to 70–90% of maximum. Record measurement.

3.2 Gel-Shift Assay

Whole cell lysates are prepared as described in Subheadings 3.1 and 3.2. Serially dilute cell lysates to 20–100 ng/ μl in cell lysis buffer (amount used to be optimized for each cell line).

3.2.1 TDP1 Biochemical Assay

1. Dilute substrate to 3 μM in 1 \times Assay Buffer. Make enough for 0.25 μl per reaction. Excess dilute substrate can be freeze-thawed 3–5 times.
2. In a 10 μl reaction, add 1 μl of 10 \times Assay Buffer, 1 μl of 10 mM DTT, 0.25 μl of substrate, and 5.75 μl of distilled H_2O . A mastermix can be made for all reactions required plus enough for pipetting errors.
3. Transfer 8 μl of the mastermix to each 0.2 ml PCR tube, add 2 μl of cell lysate or lysis buffer (for negative control) and mix by pipetting, without introducing bubbles.
4. Incubate reaction at 37 $^\circ\text{C}$ for 1 h in a PCR machine.
5. Add 10 μl of the 2 \times Loading Buffer to stop the reaction. Mix by pipetting, then incubate at 90 $^\circ\text{C}$ for 10 min in a PCR machine (with heated lid) to remove secondary structures in the substrate.
6. The samples can be stored at -20 $^\circ\text{C}$ long-term.

3.2.2 Gel Electrophoresis

1. Make 20% urea gel: for a 10 ml gel, mix 8 ml SequaGel Concentrate with 1 ml SequaGel Diluent and 1 ml SequaGel Buffer. Add 40 μl of 10% APS and 4 μl TEMED. Mix by pipetting.
2. Pour the gel into a gel cast right up to the top edge, insert a clean gel comb (12-well or 15-well).
3. Leave to set at room temperature.
4. Dilute 10 \times TBE buffer with distilled water to 1 \times .
5. Once urea gel is set, transfer to the gel tank and secure. Fill tank with 1 \times TBE buffer.
6. Heat the gel (with the comb in place) by running 190 V of current through the electrophoresis system for 30 min to remove excess urea.

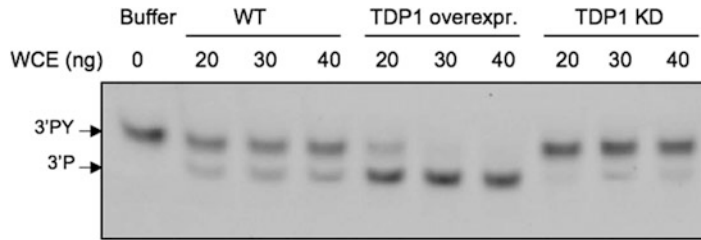


Fig. 2 Example of TDP1 gel-shift assay showing the increase in cleaved product (3'-P) from the substrate (3'-PY) in cell lysates from wild type ("WT"), TDP1 overexpressing ("TDP1 overexpr."), or TDP1 knockdown cells

7. Slowly remove the gel comb without disturbing the wells. Wash out gel debris in the wells by pipetting up and down over the wells using a P1000 pipette.
8. Load 10 μ l (for a 15-well gel) or 15 μ l (for a 12-well gel) per well including the negative control, which serves as marker for the unprocessed substrate with 3'-PY end.
9. Run the electrophoresis at constant voltage (up to 150 V for a Bio-Rad Mini PROTEAN system) for 1 h.
10. Remove gel from glass plates (*see Note 5*). Visualize gel using the gel imager with fluorescence filter specific to the fluorescent label of the substrate. There should be a lower band just below the 3'-PY marker level, indicating the processed substrate, 3'-P (Fig. 2).
11. Measure the fluorescence intensity with the gel imager or a third party software, e.g., ImageJ.
12. To quantify TDP1 processing activity, divide the fluorescence intensity of the lower band by the total intensity of both bands.

4 Notes

1. Oligonucleotides of 13mer with a 3'-phosphotyrosyl bond conjugated with an FITC molecule, 5'-(FITC) GATCTAAAAGACT(pY)-3, were purchased from Midland Certified Reagent (Texas, USA).
2. A codon-optimized synthetic gene, encoding the catalytic domain of human TDP1, was purchased from GenScript USA Inc. Details of the expression construct are consistent with that described in Interthal et al. [14]. Recombinant protein was expressed in, then purified from *Escherichia coli* strain Rosetta2 (DE3) (Merck, Darmstadt, Germany) using standard chromatography techniques, following the protocol described by Interthal et al. [14].
3. Cy5.5 labeled 13mer oligonucleotides containing a 3'-phosphotyrosyl group, 5'-(Cy5.5) GATCTAAAAGACT

(pY)-3' were purchased from Midland Certified Reagent (Texas, USA).

4. Incubation period in Bradford assay should not exceed 1 h. Accurate reading of cell lysate concentration is crucial, as no loading control is included.
5. Urea gels dry out quickly. It may be necessary to wet the gel with distilled water before or during the imaging process. Alternatively, with some gel cast cassettes that are optically clear for UV, it is not necessary to remove the gel from the cassette. This has the advantage of performing further electrophoresis on the gel if further separation of the bands is required.
6. The gel-shift assay can be used on whole blood samples. Crude fractionation of the leukocytes by centrifugation is sufficient, and cell lysis can be performed as described. However, staining by hemoglobin precludes protein quantification by Bradford assay. In our hands, 3–5 serial dilutions by tenfold is usually sufficient to identify the optimal lysate concentration for detecting the processed product. The gel-shift assay can also be used on mitochondrial lysate. To minimize contamination by nuclear TDP1, the mitochondrial pellet can be treated by 20 ng RNase-free proteinase K per 5 µg of mitochondria for 30 minutes on ice. Around 100 ng of mitochondrial lysate (cell line dependent) is required per 10 µl reaction [15].

References

1. Wang JC (2002) Cellular roles of DNA topoisomerases: a molecular perspective. *Nat Rev Mol Cell Biol* 3:430–440
2. Lin CP, Ban Y, Lyu YL, Desai SD, Liu LF (2008) A ubiquitin-proteasome pathway for the repair of topoisomerase I-DNA covalent complexes. *J Biol Chem* 283:21074–21083
3. Lin CP, Ban Y, Lyu YL, Liu LF (2009) Proteasome-dependent processing of topoisomerase I-DNA adducts into DNA double strand breaks at arrested replication forks. *J Biol Chem* 284:28084–28092
4. Katyal S, el-Khamisy SF, Russell HR, Li Y, Ju L, Caldecott KW, McKinnon PJ (2007) TDP1 facilitates chromosomal single-strand break repair in neurons and is neuroprotective in vivo. *EMBO J* 26:4720–4731
5. Murai J, Huang SY, Das BB, Dexheimer TS, Takeda S, Pommier Y (2012) Tyrosyl-DNA phosphodiesterase 1 (TDP1) repairs DNA damage induced by topoisomerases I and II and base alkylation in vertebrate cells. *J Biol Chem* 287:12848–12857
6. Alagoz M, Wells OS, El-Khamisy SF (2014) TDP1 deficiency sensitizes human cells to base damage via distinct topoisomerase I and PARP mechanisms with potential applications for cancer therapy. *Nucl Acids Res* 42:3089–3103
7. Barthelmes HU, Habermeyer M, Christensen MO, Mielke C, Interthal H, Pouliot JJ, Boege F, Marko D (2004) TDP1 overexpression in human cells counteracts DNA damage mediated by topoisomerases I and II. *J Biol Chem* 279:55618–55625
8. Nivens MC, Felder T, Galloway AH, Pena MM, Pouliot JJ, Spencer HT (2004) Engineered resistance to camptothecin and antifolates by retroviral coexpression of tyrosyl DNA phosphodiesterase-I and thymidylate synthase. *Cancer Chemother Pharmacol* 53:107–115
9. Jakobsen AK, Lauridsen KL, Samuel EB, Proszek J, Knudsen BR, Hager H, Stougaard M (2015) Correlation between topoisomerase I and tyrosyl-DNA phosphodiesterase 1 activities in non-small cell lung cancer tissue. *Exp Mol Pathol* 99:56–64

10. Cheng TJ, Rey PG, Poon T, Kan CC (2002) Kinetic studies of human tyrosyl-DNA phosphodiesterase, an enzyme in the topoisomerase I DNA repair pathway. *Eur J Biochem* 269:3697–3704
11. Antony S, Marchand C, Stephen AG, Thibaut L, Agama KK, Fisher RJ, Pommier Y (2007) Novel high-throughput electrochemiluminescent assay for identification of human tyrosyl-DNA phosphodiesterase (Tdp1) inhibitors and characterization of furamidine (NSC 305831) as an inhibitor of Tdp1. *Nucleic Acids Res* 35:4474–4484
12. Marchand C, Lea WA, Jadhav A, Dexheimer TS, Austin CP, Inglese J, Pommier Y, Simeonov A (2009) Identification of phosphotyrosine mimetic inhibitors of human tyrosyl-DNA phosphodiesterase I by a novel AlphaScreen high-throughput assay. *Mol Cancer Ther* 8:240–248
13. Jensen PW, Falconi M, Kristoffersen EL, Simonsen AT, Cifuentes JB, Marcussen LB, Fröhlich R, Vagner J, Harmsen C, Juul S, Ho YP, Withers MA, Lupski JR, Koch J, Desideri A, Knudsen BR, Stougaard M (2013) Real-time detection of TDP1 activity using a fluorophore-quencher coupled DNA-biosensor. *Biosens Bioelectron* 48:230–237
14. Interthal H, Pouliot JJ, Champoux JJ (2001) The tyrosyl-DNA phosphodiesterase Tdp1 is a member of the phospholipase D superfamily. *Proc Natl Acad Sci U S A* 98:12009–12014
15. doi: [10.1126/sciadv.1602506](https://doi.org/10.1126/sciadv.1602506)

Chapter 14

Topoisomerase II Chromatin Immunoprecipitation

Kayleigh A. Smith, Ian G. Cowell, and Caroline A. Austin

Abstract

Chromatin immunoprecipitation is a method to isolate a protein of interest coupled to DNA following cross-linking with formaldehyde and to quantify the relative abundance or occupancy of the protein at specific genomic loci. After immunoprecipitation of protein–DNA complexes protein–DNA cross-links are reversed and the DNA is extracted. Various methods exist to identify binding sites and determine relative occupancy of the protein of interest; these include quantitative PCR, probing microarrays or sequencing the isolated DNA (ChIP-seq). This chapter details the method of chromatin immunoprecipitation of TOP2 to the point of DNA extraction from the precipitated protein–DNA complexes.

Key words Topoisomerase II, TOP2, Chromatin immunoprecipitation

1 Introduction

DNA topoisomerase enzymes catalyze transient DNA strand breaks in the DNA backbone enabling changes in DNA topology to relieve torsional stress. Type II topoisomerases such as mammalian TOP2 introduce a staggered double-strand break to enable strand passage. The topoisomerase protein becomes covalently linked to the cleaved DNA via active-site tyrosine residues in a 5'-DNA phosphotyrosyl linkage. At the end of the reaction cycle strand breaks are resealed and the enzyme released. Drugs can interfere at different points in the TOP2 reaction cycle, and one class of drugs, the topoisomerase poisons are widely used in anticancer therapy. This group of drugs includes etoposide, mitoxantrone, and anthracyclines such as doxorubicin.

Chromatin immunoprecipitation can be used to isolate proteins associated with DNA, it relies on specific antibodies that enable isolation of proteins associated with chromatin. Mammals have two isoforms of type II topoisomerase, TOP2A and TOP2B, both have been isolated by chromatin immunoprecipitation from murine or human cells [1–16].

2 Materials

2.1 Equipment

1. Real time PCR machine (Bio-Rad My iQ).
2. Sonicator (Bandelin Sonopuls HD2070 sonicator).
3. Rotator (Stuart Scientific rotator drive STR4).
4. Magnetic separator (Millipore).
5. Microfuge (Eppendorf Centrifuge 5424).
6. Vacuum pump (KnF laboport Neuberger).
7. Temperature controlled incubator (HYBAID MINI10).
8. Tube heater (Stuart Scientific test tube heater SHT 2D).
9. DNA and Protein LoBind tubes (Eppendorf, Cambridge, UK).
10. Electrophoresis equipment for agarose gels.

2.2 Reagents

1. Chromatin Immunoprecipitation Kit such as Millipore (Magna ChIP A, 17-610/EZ-Magna ChIP A, 17-408).
2. PBS buffer.
3. Tween 20.
4. Protease inhibitor cocktail.
5. RNase A.
6. Proteinase K.
7. Formaldehyde.
8. Agarose.
9. Antibodies: antibodies to TOP2 and negative control antibody (*see Note 1*).

2.3 Chromatin Immunoprecipitation

The method described below is based on a reagent kit supplied by Millipore (Magna ChIP A, 17-610/EZ-Magna ChIP A, 17-408). However, other suppliers also produce chromatin immunoprecipitation kits.

3 Methods

3.1 Cell Treatment, Collection, and Lysis

The following protocol is based on TOP2 ChIP performed in MCF7 cells treated with estradiol. The protocols for treating cells will depend on the nature of the compound/s of interest and the cells used.

1. Treat cells at approximately 9×10^5 cells/mL with estradiol (10 nM) for 30 min (*see Note 2*).
2. Add formaldehyde to a final concentration of 1% and incubate for 10 min at room temperature to cross-link proteins and DNA (*see Note 3*).

3. Neutralize unreacted formaldehyde by adding $1 \times$ glycine from the kit and incubating the cells on ice for 5 min.
4. Wash adherent cells in $1 \times$ PBS and trypsinize, then pellet in medium at $1000 \times g$ for 3 min.
5. Wash cells in $1 \times$ PBS and pellet at $1000 \times g$ for 3 min.
6. Repeat the above wash.
7. Resuspend the cells in $1 \times$ PBS with protease inhibitor cocktail (PI) from the kit.
8. Pellet the cells by spinning at $800 \times g$ for 5 min at 4°C .
9. Either store pellets at -80°C or lyse pellets sequentially with cell and nuclear lysis buffers with protease inhibitor cocktail (PI) from the kit.

3.2 Sonication

1. Sonicate chromatin for 20 cycles using a Bandelin Sonopuls HD2070 sonicator at 15 s per cycle and 20% power (*see Note 4*).
2. Remove the equivalent of 1×10^5 cells (5 μL) from the sonicated chromatin samples to verify size distribution of sonicated chromatin (*see Note 4*).
3. Centrifuge the chromatin at 4°C at $12,000 \times g$ for 10 min, to remove insoluble material.
4. Remove the supernatant, store at -80°C .

3.3 Immuno-precipitation, Elution, and DNA Purification

Chromatin immunoprecipitation using protein A magnetic beads, incubated with selected antibodies.

1. Take protein A magnetic beads from the kit and wash in PBS (adjusted to pH 8.0) followed by PBS (pH 8.0) + 0.1% Tween 20.
2. For each IP add 25 μL of beads per IP to Protein LoBind tubes and incubate for 30 min on ice with the appropriate concentration of antibody (*see Note 1*).
3. For each IP, take 50 μL of chromatin (from approx. 1×10^6 cells) and dilute 1:10 in ChIP dilution buffer + PI and incubate with the 25 μL beads + antibody (from **step 2**) of interest (1–7 μg) at 4°C for 4.5 h on a rotator.
4. Collect the magnetic beads using a magnetic separator.
5. Wash chromatin immunoprecipitates sequentially in low salt, high salt, LiCl and TE wash buffers respectively, use a vacuum pump (such as KnF laboport Neuberger) to remove the supernatant.
6. Add 100 μL of ChIP elution buffer (containing SDS) + 1 μL proteinase K (10 mg/mL) to each IP and to 2.5 μL (5%) of sonicated/non-IP chromatin per treatment (input DNA).

7. Rotate IPs and input samples for 2 h at 65 °C to reverse the formaldehyde cross-links.
8. Incubate all samples at 95 °C for 10 min and leave at room temperature overnight to cool.
9. Remove magnetic beads with a magnetic separator and transfer the supernatants to DNA LoBind tubes.
10. Add 500 µL of binding reagent to each tube and transfer to spin columns from the kit and centrifuge at 12,000 × *g* for 30 s.
11. Discard the flow through, add 500 µL of wash buffer B to each column, and spin the columns at 12,000 × *g* for 30 s.
12. Discard the flow through and centrifuge the columns at 12,000 × *g* for 1 min.
13. Transfer the spin filters to collection tubes and add 80 µL of elution reagent directly to each spin filter. Incubate at room temperature for 5 min then centrifuge at 12,000 × *g* for 1 min.
14. Discard the spin filters and store the samples at 4 °C for up to 1 week before analyzing by real-time PCR (*see Note 5*) or store at –80 °C prior to processing further e.g., ChIP-Seq (*see Note 6*).

4 Notes

1. *Antibodies*: In addition to an antibody to your protein of interest, e.g., TOP2B, A negative control is essential. An antibody to GFP is a good negative control; an alternative is total rabbit IgG. We found in ChIP assays an anti-GFP antibody gave a lower background when compared to total rabbit IgG.
Antibodies used for chromatin immunoprecipitation need to meet certain criteria. Antibodies must be specific for the protein of interest; this can be tested first by western blotting or immunofluorescence. Not all antibodies work on formaldehyde fixed proteins, testing on paraformaldehyde fixed cells is one way to check this. Some commercial suppliers sell validated ChIP grade antibodies. In addition, secondary characterization of antibodies is recommended in the ENCODE ChIP-seq guidelines [17]. Antibodies that enrich for proteins at least fivefold above the negative control are reported to work well in ChIP-sequencing assays [18].
2. *Treatment conditions*: Subheading 3 describes MCF7 cells treated with an estradiol concentration of 10 nM for 30 min, based on the concentrations used in [2, 4].
3. *Formaldehyde conditions*: Formaldehyde should be prepared fresh and used within 2 weeks.

4. *Optimization of chromatin fragment size*: Sonication conditions yielding desired DNA fragment size (200–1000 base pairs) need to be determined for each cell line and cross-linking combination, using agarose gel electrophoresis. Sonicate chromatin for 5, 10, 15, and 20 cycles using a Bandelin Sonopuls HD2070 sonicator at 15 s per cycle and 20% power. Remove the equivalent of 1×10^5 cells (5 μ L) from the sonicated chromatin samples. Add 1 μ L of RNase A (10 mg/mL) and incubate at 37 °C for 30 min. Add 1 μ L of proteinase K (10 mg/mL) to samples and incubate at 65 °C for 2 h to reverse cross-links. Run samples on a 2% agarose gel in 1xTBE buffer containing ethidium bromide (0.5ug/mL), also run DNA markers (e.g., 100 bp ladder) to determine size distribution. Once conditions are determined, they don't need to be checked in each experiment.
5. *Real-time PCR*: Real-time PCR analysis of DNA isolated from chromatin immunoprecipitations is routinely used.

We used the Bio-Rad My iQ Single color dual time PCR detection system. Quantitation of DNA was carried out using the SYBR green assay, using 5 μ L of ChIP DNA (approx. 50 ng) per reaction. PCR reactions should be performed in triplicate in 96 well plates. Positive control ChIP DNA (AcH3) was amplified using primers to the GAPDH gene, supplied with the chromatin immunoprecipitation kit, and immunoprecipitations using either GFP or IgG antibodies was used as a negative control. A “no DNA” control was included on each plate as well as a standard curve using a PCR product amplified by the relevant primer set as a template.

Real-time PCR analysis: Data was analyzed using the Δ CT method and Microsoft Excel. The following equation was used to generate % input values for each antibody/treatment:

$$\% \text{ input} = 100/2[\text{Sample Ct} - (\text{INPUT Ct} - \text{Log}_2\text{INPUT dilution fold})]$$

Experiments were repeated 3–4 times per antibody/primer and the variance expressed as mean \pm standard error of the mean (S.E.M). Graphpad Prism 4 software (Oxford, UK) was used to generate graphical representations of the data.

It is essential to ensure that the efficiency of the positive control AcH3 antibody was >100 fold higher than the GFP negative control values, as recommended by Millipore.

6. *ChIP-seq*: The encode ChIP-seq guidelines [17] give a good description of the factors to bear in mind when sequencing DNA fragments isolated by chromatin immunoprecipitation. Most laboratories outsource the library preparation and sequencing and the bioinformatics analysis. Key points to ensure are that you have robust negatives controls, for example

ChIP seq from a cell line knocked out for your protein of interest and to have sufficient biological replicates.

References

1. Lyu YL, Lin CP, Azarova AM, Cai L, Wang JC, Liu LF (2006) Role of topoisomerase IIbeta in the expression of developmentally regulated genes. *Mol Cell Biol* 26:7929–7941
2. BG J, Lunyak VV, Perissi V, Garcia-Bassets I, Rose DW, Glass CK, Rosenfeld MG (2006) A topoisomerase IIbeta-mediated dsDNA break required for regulated transcription. *Science* 312:1798–1802
3. Sano K, Miyaji-Yamaguchi M, Tsutsui KM, Tsutsui K (2008) Topoisomerase IIbeta activates a subset of neuronal genes that are repressed in AT-rich genomic environment. *PLoS One* 3(12):e4103. <https://doi.org/10.1371/journal.pone.0004103>
4. Perillo B, Ombra MN, Bertoni A, Cuzzo C, Sacchetti S, Sasso A, Chiariotti L, Malorni A, Abbondanza C, Avvedimento EV (2008) DNA oxidation as triggered by H3K9me2 demethylation drives estrogen-induced gene expression. *Science* 319:202–206
5. McNamara S, Wang H, Hanna N, Miller WH Jr (2008) Topoisomerase IIbeta negatively modulates retinoic acid receptor alpha function: a novel mechanism of retinoic acid resistance. *Mol Cell Biol* 28(6):2066–2077
6. McNamara S, Nichol JN, Wang H, Miller WH Jr (2010) Targeting PKC delta-mediated topoisomerase II beta overexpression subverts the differentiation block in a retinoic acid-resistant APL cell line. *Leukemia* 24(4):729–739
7. Haffner MC, Aryee MJ, Toubaji A, Esopi DM, Albadine R, Gurel B, Isaacs WB, Bova GS, Liu W, Xu J, Meeker AK, Netto G, De Marzo AM, Nelson WG, Yegnasubramanian S (2010) Androgen-induced TOP2B-mediated double-strand breaks and prostate cancer gene rearrangements. *Nat Genet* 42(8):668–675
8. Tiwari VK, Burger L, Nikolettou V, Deogracias R, Thakurela S, Wirbelauer C, Kaut J, Terranova R, Hoerner L, Mielke C, Boege F, Murr R, Peters AH, Barde YA, Schübeler D (2012) Target genes of topoisomerase II β regulate neuronal survival and are defined by their chromatin state. *Proc Natl Acad Sci U S A* 109(16):E934–E943
9. Thakurela S, Garding A, Jung J, Schübeler D, Burger L, Tiwari VK (2013) Gene regulation and priming by topoisomerase II α in embryonic stem cells. *Nat Commun* 4:2478
10. Cowell IG, Sondka Z, Smith K, Lee KC, Manville CM, Sidorczuk-Lesthuruge M, Rance HA, Padget K, Jackson GH, Adachi N, Austin CA (2012) Model for MLL translocations in therapy-related leukemia involving topoisomerase II β -mediated DNA strand breaks and gene proximity. *Proc Natl Acad Sci U S A* 109(23):8989–8994
11. Naughton C, Avlonitis N, Corless S, Prendergast JG, Mati IK, Eijk PP, Cockroft SL, Bradley M, Ylstra B, Gilbert N (2013) Transcription forms and remodels supercoiling domains unfolding large-scale chromatin structures. *Nat Struct Mol Biol* 20(3):387–395. <https://doi.org/10.1038/nsmb.2509>
12. Smith KA, Cowell IG, Zhang Y, Sondka Z, Austin CA (2014) The role of topoisomerase II beta on breakage and proximity of RUNX1 to partner alleles RUNX1T1 and EVI1. *Genes Chromosomes Cancer* 53(2):117–128
13. Zuchegna C, Aceto F, Bertoni A, Romano A, Perillo B, Laccetti P, Gottesman ME, Avvedimento EV, Porcellini A (2014) Mechanism of retinoic acid-induced transcription: histone code, DNA oxidation and formation of chromatin loops. *Nucleic Acids Res* 42(17):11040–11055
14. Madabhushi R, Gao F, Pfenning AR, Pan L, Yamakawa S, Seo J, Rueda R, Phan TX, Yamakawa H, Pao PC, Stott RT, Gjonneska E, Nott A, Cho S, Kellis M, Tsai LH (2015) Activity-induced DNA breaks govern the expression of neuronal early-response genes. *Cell* 161(7):1592–1605
15. Manville CM, Smith K, Sondka Z, Rance H, Cockell S, Cowell IG, Lee KC, Morris NJ, Padget K, Jackson GH, Austin CA (2015) Genome-wide ChIP-seq analysis of human TOP2B occupancy in MCF7 breast cancer epithelial cells. *Biol Open* 4(11):1436–1447
16. Uusküla-Reimand L, Hou H, Samavarchi-Tehrani P, Rudan MV, Liang M, Medina-Rivera A, Mohammed H, Schmidt D, Schwalie P, Young EJ, Reimand J, Hadjur S, Gingras AC, Wilson MD (2016) Topoisomerase II beta interacts with cohesin and CTCF at topological domain borders. *Genome Biol* 17(1):182
17. Landt SG, Marinov GK, Kundaje A, Kheradpour P, Pauli F, Batzoglou S, Bernstein BE, Bickel P, Brown JB, Cayting P, Chen Y, DeSalvo G, Epstein C, Fisher-Aylor KI,

Euskirchen G, Gerstein M, Gertz J, Hartemink AJ, Hoffman MM, Iyer VR, Jung YL, Karmakar S, Kellis M, Kharchenko PV, Li Q, Liu T, Liu XS, Ma L, Milosavljevic A, Myers RM, Park PJ, Pazin MJ, Perry MD, Raha D, Reddy TE, Rozowsky J, Shoresh N, Sidow A, Slattery M, Stamatoyannopoulos JA, Tolstorukov MY, White KP, Xi S, Farnham PJ, Lieb JD,

Wold BJ, Snyder M (2012) ChIP-seq guidelines and practices of the ENCODE and mod-ENCODE consortia. *Genome Res* 22 (9):1813–1831

18. Kidder BL, Hu G, Zhao K (2011) ChIP-Seq: technical considerations for obtaining high-quality data. *Nat Immunol* 12(10):918–922

Analyzing Mitotic Chromosome Structural Defects After Topoisomerase II Inhibition or Mutation

Juan F. Giménez-Abián, Andrew B. Lane, and Duncan J. Clarke

Abstract

For analyzing chromosome structural defects that result from topoisomerase II (topo II) dysfunction we have adapted classical cell cycle experiments, classical cytological techniques and the use of a potent topo II inhibitor (ICRF-193). In this chapter, we describe in detail the protocols used and we discuss the rationale for our choice and for the adaptations applied. We clarify in which cell cycle stages each of the different chromosomal aberrations induced by inhibiting topo II takes place: lack of chromosome segregation, undercondensation, lack of sister chromatid resolution, and lack of chromosome individualization. We also put these observations into the context of the two topo II-dependent cell cycle checkpoints. In addition, we have devised a system to analyze phenotypes that result when topo II is mutated in human cells. This serves as an alternative strategy to the use of topo II inhibitors to perturb topo II function.

Key words Topoisomerase II, Chromatid resolution, Condensation, Chromosome individualization, ICRF-193, Topo II checkpoint

1 Introduction

Topoisomerase II (topo II) is required for several mitotic processes that prepare chromosomes for accurate segregation in anaphase. Topo II is the major eukaryotic enzyme that can decatenate/concatenate DNA; that is, it can transiently break a double strand of DNA, pass another double strand through the gap and then reseal the gap. Given that interchromatid catenations arise as a consequence of DNA replication, the first expected consequence of the lack of topo II activity is a block to the segregation process. In fact, this was the first phenotype to be described, when yeast topo II (*top2*) mutants were analyzed. The, so described, *cut* phenotype (*Chromosomes Untimely Torn*) corresponded to attempts at cytokinesis in the absence of genome segregation [1]. However, detailed analysis of topo II inhibition in mammalian cells, which carry considerably larger chromosomes, has revealed a wide variety of different phenotypes (Fig. 1) depending on the precise moment in

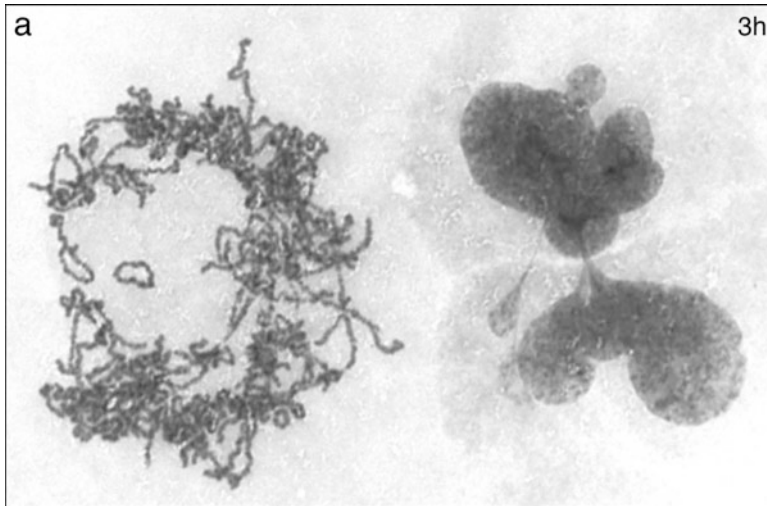


Fig. 1 Long treatments with topo II inhibitors (ICRF-193, 2 $\mu\text{g}/\text{mL}$) generate a wide variety of phenotypes coexisting in the same preparation. The cell on the left is a metaphase cells in polar view (i.e., as if the observer is at the spindle pole) and displays: (1) Lack of chromosome segregation (this cell would end up attempting cytokinesis in the absence of segregation as has occurred in the case of the cut phenotype displayed by the cell on the right); (2) chromosome undercondensation (chromosomes are long and thin); (3) lack of sister chromatid resolution (sister chromatids are indistinguishable and chromosomes appear as a single rod); and (4) deficient chromosome individualization: the chromosomes have intrachromosomal tangles (these are described as Ω - figures, based on their shape, and can be seen in the left cell at the top) and are also tangled with each other. Identification of the cell cycle stage at which each phenotype is produced requires the use of cell cycle synchrony protocols and cytological techniques which are described in detail in this chapter

which topo II activity is perturbed [2, 3]. These phenotypes include (Fig. 2):

- Block of sister chromatid segregation (i.e., when the cell reaches metaphase, the chromosomes are unable to separate their sister chromatids and eventually proceed to cytokinesis in the absence of chromosome segregation) (Fig. 3).
- Deficient chromosome condensation (i.e., chromosomes that condensed in the presence of topo II inhibitors are longer than control chromosomes when topo II is inhibited prior to late metaphase) (Figs. 4–7).
- Lack of sister chromatid resolution (i.e., chromosomes of cells that enter mitosis in the presence of topo II inhibitors do not display distinguishable sister chromatids in metaphase) (Figs. 5–7).
- Lack of chromosome individualization (i.e., chromosomes of cells that enter G_2 in the presence of topo II inhibitors reach metaphase with intrachromosomal and interchromosomal tangles) (Figs. 6 and 7).

Double thymidine block/release

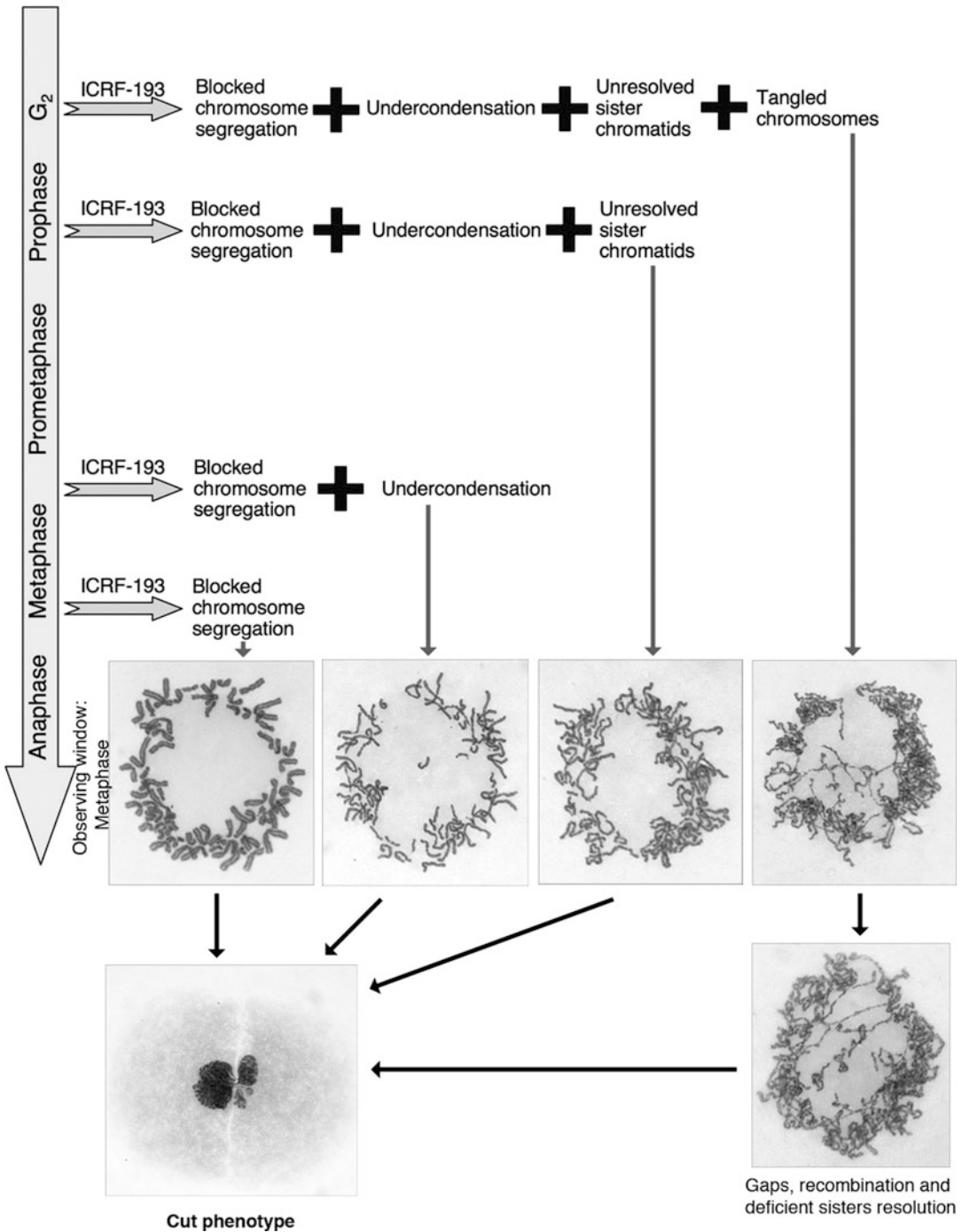


Fig. 2 Schemes representing the rationale for the protocols described in this chapter. Cells are presynchronized by a double thymidine block schedule then released into S-phase. We add the topo II inhibitor (ICRF-193) at different times as the cells progress through the cell cycle and we keep the drug present until the peak of the metaphase wave (10–10.5 h after the release from the second thymidine block). Then we fix the material

Taking a fixed window of observation (e.g., metaphase), the longer the elapsed time since addition of the topo II inhibitor to the cells, the greater the variety there is in the different phenotypes that accumulate within the same cell (Fig. 2). Thus, it is important to be able to study chromosome morphology and mitotic stages in great cytological detail in order to understand the consequences of topo II perturbation at different times during the cell cycle.

Recent advances allowing manipulation of protein levels in cells (e.g., RNA interference, CRISPR/Cas9 technologies) have made it increasingly feasible to study effects of introducing mutant versions of proteins into human cells. We describe one such strategy that allows analysis of chromosomes in topo II α mutant cell lines, in the absence of topo II inhibitors.

1.1 Strategies for Performing Mitotic Cytological Analyses When Topo II Is Perturbed

There are two general strategies that can be used to perturb Topo II, and thus allow cytological analyses of mitosis in the context of Topo II loss-of-function or when Topo II mutant proteins are expressed. The mechanism through which Topo II is experimentally perturbed dictates the factors that must be considered when examining the cytological outcomes. Here we consider the use of Topo II inhibitors, versus cell lines expressing mutant forms of Topo II.

1.1.1 Topo II Inhibitor Treatment

Using Topo II inhibitors to perturb the enzyme cycle allows the investigator to employ a constant observation window, e.g., metaphase, after the cells progress into mitosis in the presence of the drug (Fig. 2). The fixed window of observation, for chromosome cytology, is preferably metaphase (Figs. 4, 5, and 7) or prometaphase (Fig. 6) because most chromosome characteristics related to topo II function are observed at these cell cycle stages: lack of segregation, lack of condensation, lack of sister chromatid resolution (the ability to distinguish both sister chromatids), and lack of individualization (the physical separation of the chromosomes from the intertwined interphase chromosomes). This approach is only practically relevant when using topo II inhibitors. The topo II inhibitor can be added at different times prior to fixation of the cells, typically with Carnoy's solution. For example, if the observation window is metaphase and the cells are fixed 10 min after adding the inhibitor, defects will be revealed that are related to topo II inhibition in early metaphase and late prometaphase. If the inhibitor is added 3 h before fixation, a cell in metaphase at the time of fixation will display the cumulative effects of topo II inhibition

Fig. 2 (continued) and compare the effects of different length treatments at a single observation window: metaphase in the case of the scheme shown and as illustrated in Figs 3–5 or prometaphase as illustrated in Fig. 6. Comparing phenotypes seen after the different length treatments allows one to determine at which cell cycle stage topo II activity is required for a specific function. All of the different categories eventually end up, after some delay, undergoing the cut phenotype

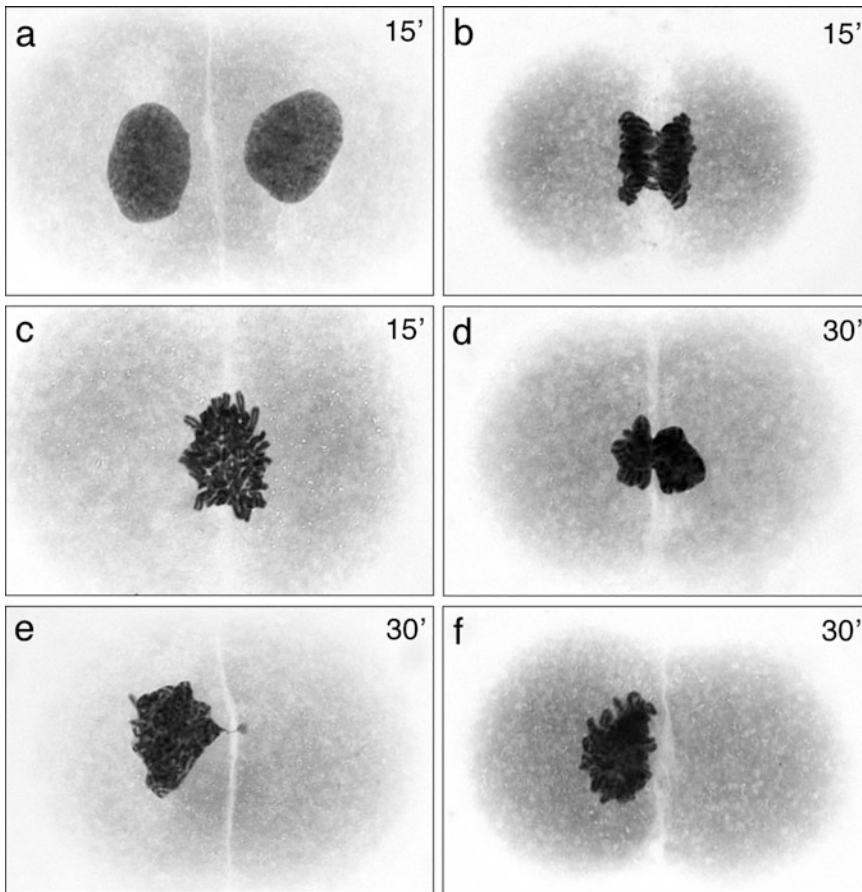


Fig. 3 The *Cut* (*Chromosomes Untimely Torn*) phenotype. As described in the protocols section we use presynchronized HeLa cells and we add ICRF-193 at different times before the peak of the metaphase wave; the longer the treatment the more complex the mixture of phenotypes observed; the shorter the treatment the lesser the extent of different phenotypes. 10 min is the minimum treatment time required to obtain a detectable phenotype. The *Cut* (*Chromosomes Untimely Torn*) phenotype is the first phenotype to be observed after short topo II inhibitor treatment. At first, this phenotype coexists with control-like telophase or early G1 cells (**a**). Though it is commonly remarked that failed segregation attempts result in the ingression of the cytokinesis ring into the chromatin mass (**b**), this phenotype is extremely infrequent. Most commonly there is no observable chromosome segregation attempt and no separation of the centromeres (or the chromosome arms) is observed, but cytokinesis takes place to one side of the chromatin mass (**c**). These cells also display a delay in the process of chromosome decondensation as chromosomes can be clearly observed while cells are entering G1 (**c**, **f**, judging by the advanced stage of cytokinesis). During the deficient attempt at cell division, the trapped unsegregated chromosomes usually take up a position away from the center of the cell (**c**, **d**) and are progressively displaced towards one of the daughter cells (**e**, notice a small chromatin fragment on the right side cell) or are completely included within one of the daughters (**f**). We interpret these cut phenotypes as the result of cells being inhibited at late/very late metaphase stages (i.e., after the metaphase topo II checkpoint). Slightly longer treatments result in an increase in cells delayed in metaphase, which can remain in metaphase for up to 1–1.5 h (example shown in Fig. 3), that show no signs of undercondensation, indicating that the cell was already in metaphase when the inhibitor was added

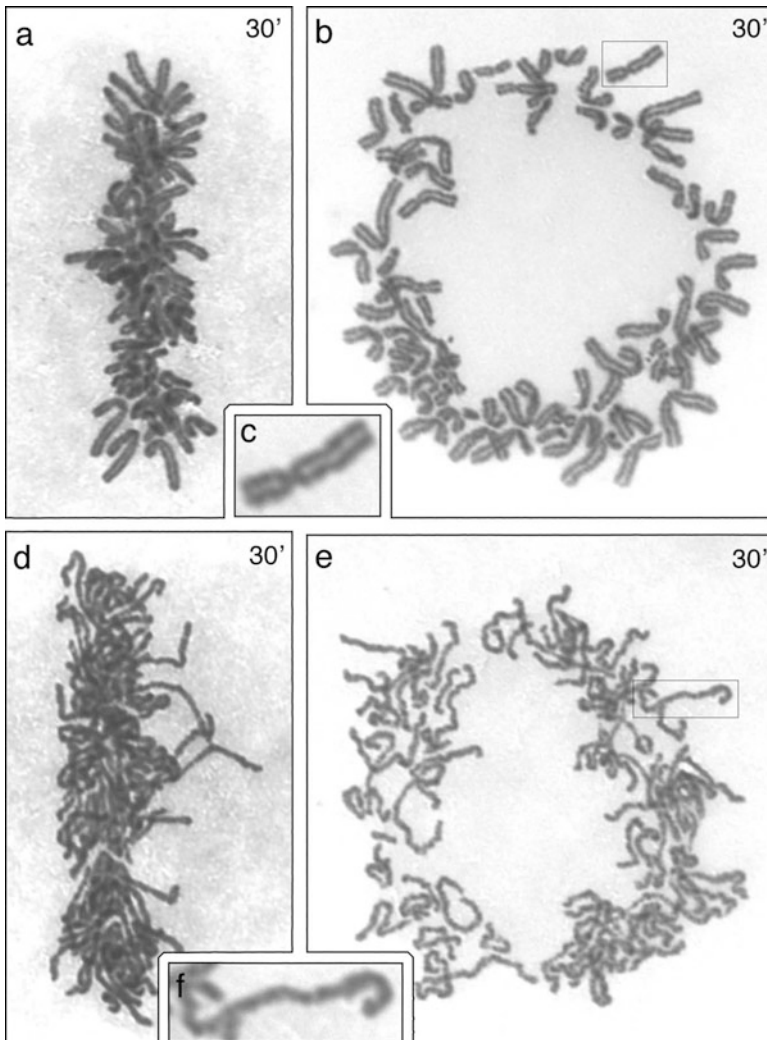


Fig. 4 Transient arrest in metaphase. Longer ICRF treatments (30'-1.5 h) result in the appearance of cells that are blocked/delayed in metaphase (**a**, *side view*; **b**, *polar view*). These cells were already in metaphase at the time the inhibitor was added (otherwise they would show chromosome undercondensation, not shown). The chromosomes in these cells show control-like sister chromatid resolution (sisters are distinguishable, insert **c**). They are easily differentiated from cells hit with the inhibitor in late prophase in which case the cells also reach metaphase during the length of the treatment (**d**, *side view*; **e**, *polar view*) but, in addition to the lack of chromosome segregation they show undercondensed chromosomes and a lack of sister chromatid resolution (chromosome in insert **f**) as sister chromatids are cytologically undifferentiated. Sister chromatid resolution takes place in late prophase in HeLa cells and in early prometaphase in *M. muntjac* cells. These latter cells also delay in metaphase and so they can appear in treatments as long as 3 h

through G2, prophase, prometaphase, and metaphase. The phenotypes that are observed after treatments differing in length can be compared and subtracted: the longer the treatments, the more complex will be the phenotypes that are observed.

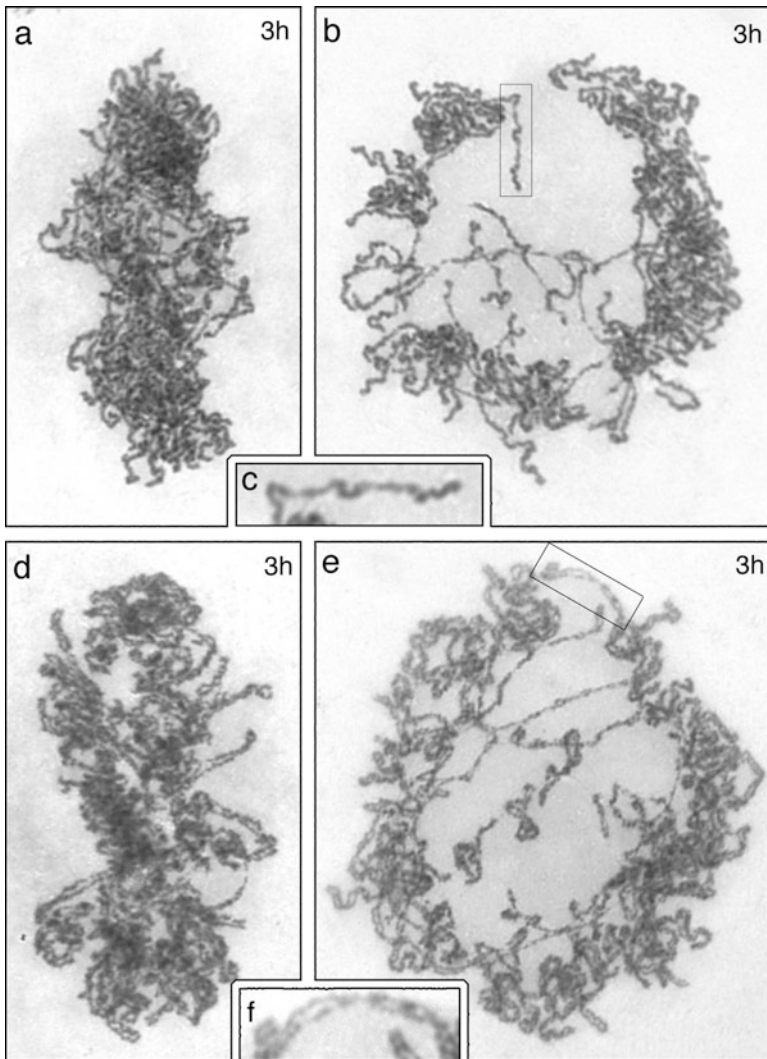


Fig. 5 Interchromosomal and intrachromosomal tangles. Treatments with topo II inhibitors (ICRF-193) initiated 1.5–3 h before the peak of the metaphase wave (i.e., when the cells were in late interphase) render new phenotypes mixed with the phenotypes described in Figs. 1–4. As before, cells show a lack of chromosome segregation, chromosome undercondensation and lack of sister chromatid resolution; but now a new phenotype appears: intrachromosomal and interchromosomal tangles, which reveal a deficiency in chromosome individualization. Part (a) represents a metaphase cell in side view while (b) shows a polar view of a metaphase cell. In both cases the tangling between chromosomes is obvious. The selected chromosome in (c) displays three (different in size) Ω -figures visualized as chromosome bents that we interpret as intrachromosomal tangles. These cells also delay in metaphase but the morphology of their chromosomes changes with time and despite being unable to segregate they end up resolving their sister chromatids which now become visible (d, metaphase in side view; e, polar view metaphase). Sister chromatids become visible but they show a discontinuous appearance (f) and chromosome recombination events can sometimes be observed (d, e). This latter category of cell appears after 3 h of inhibitor treatment and becomes more frequent after longer (up to 4–5 h) treatments

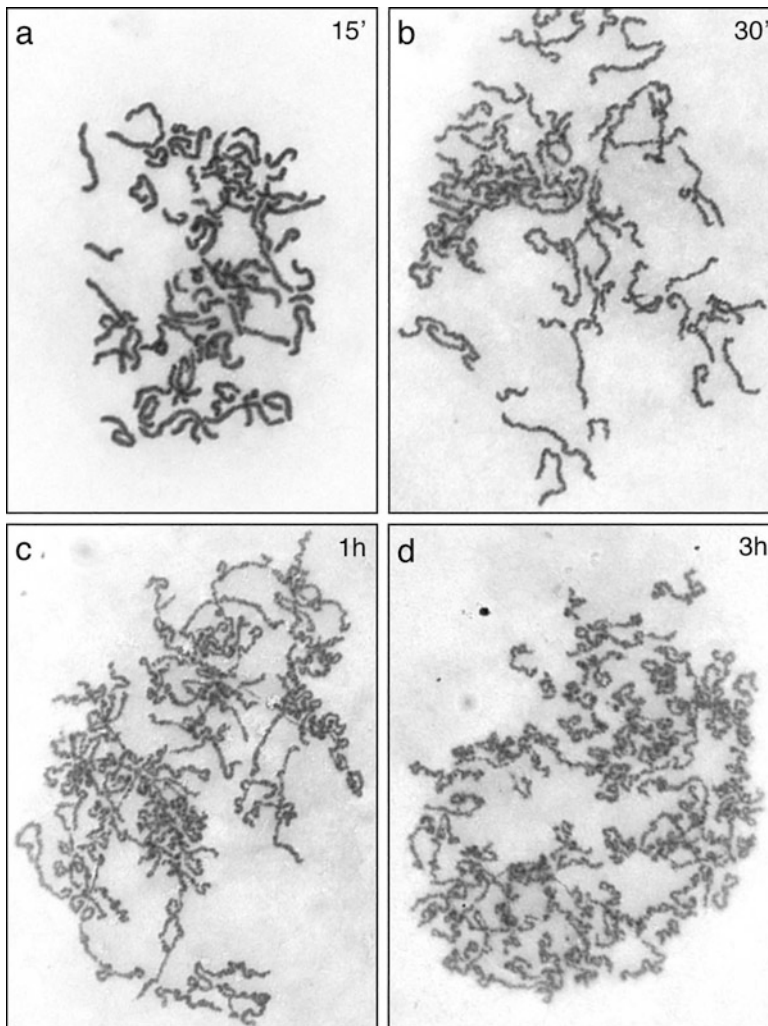


Fig. 6 Prometaphase as the observation window. In the previous figures (Figs. 2, 4 and Fig. 5) we have shown typical results obtained when following the protocols described above, when a fixed observation window (metaphase) is used. The same kind of analysis can be performed using a different observation window. In this figure we show prometaphases obtained after different length treatments with the same topo II inhibitor (ICRF-193). **(a)** Shows a prometaphase cell after a short time (15') with ICRF-193; the chromosomes display undercondensation and a lack of sister chromatid resolution indicating that the cell was hit with drug before sister chromatid resolution, which takes place in control cells in late prophase. **(b)** Is a very similar cell which displays more severe undercondensation, indicating that it was hit with drug earlier in prophase than the previous cell. **(c)** The presence of massive numbers of Ω -figures (chromosome bents and kinks) and interchromosomal tangles adds a new phenotype, said to be a deficiency in chromosome individualization (in addition to undercondensation and a lack of sister chromatid resolution), suggesting that the cell was hit with drug in interphase. **(d)** Is a more severe display of each of these phenotypes, indicating that this cell was hit with drug earlier in interphase than the cell in **(c)**

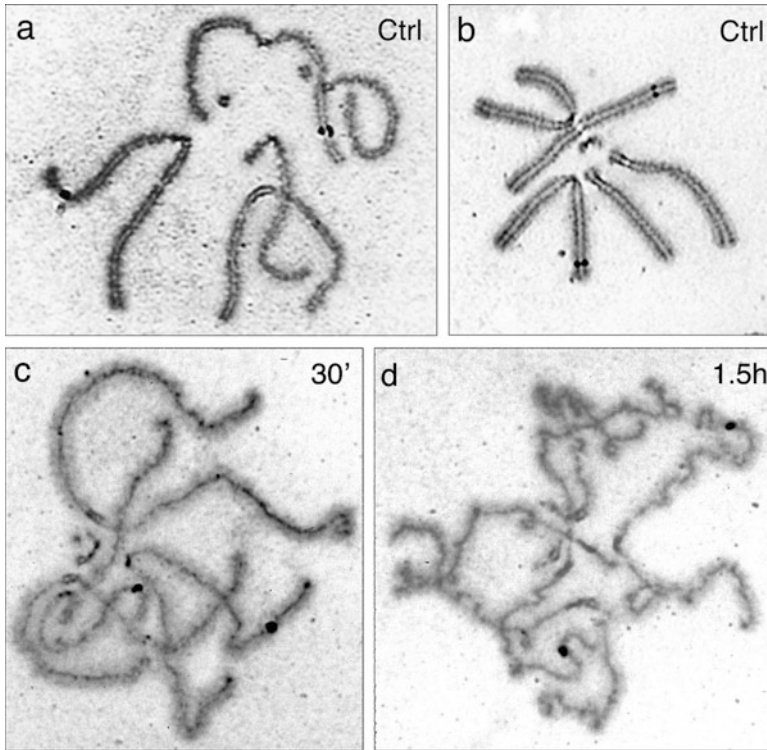


Fig. 7 Silver staining of chromosome cores. Silver staining of chromosome cores is a simple procedure but which suffers from poor reproducibility. It allows the visualization of several chromosome and cellular features, such as the chromatin halo (*yellow-orange*), the chromosome core (*brown-black*), the NOR (Nucleolar Organizing Regions) in *black* and kinetochores (*black*). The cells shown here are of *M. muntjac*, a small deer with a very low chromosome number and very large chromosomes. The cell in (a) is a control prometaphase cell in the process of resolving its sister chromatids, thus, together with regions of the chromosomes showing two sister chromatid cores we can observe stretches of apparently single core regions (unresolved regions). (b) Is a metaphase cell; two cores are observed per chromosome (sisters are already resolved) and the long muntjac kinetochores (in *black*) are grouped in the center of the cell (the metaphase plate). Two chromosomes bear near distal *black dots* which correspond to the NORs. (c) Shows a metaphase cell after a 30' treatment with ICRF-193; kinetochores are grouped and are under spindle tension (they are seen as double unlike the chromosome arms), the chromosomes are largely undercondensed and lack sister chromatid resolution (both sister chromatid cores are apposed, running through the middle of each chromosome). (d) This cell has in addition to the phenotypes in (c), the presence of multiple interchromosomal and intrachromosomal (numerous Ω -figures involving the chromosome cores are observed) tangles, impeding chromosome individualization

1.1.2 Cell Lines Expressing Mutant Forms of Topo II α

Using this approach, typically, the endogenous Type 2 Topoisomerases must be depleted and at the same time a mutant form of Topo II α is expressed exogenously. Since these manipulations cannot be accomplished instantaneously (as is the case with inhibitor addition), most cells will reach the observation window, mitosis, after relying solely on the mutant Topo II α for most of the cell cycle (S-phase, G2 and early mitosis). Phenotypes will therefore be more homogenous than when using inhibitors, and will therefore present

as the most severe phenotype that result from the particular Topo II α mutant being expressed. An additional possibility using this approach is to use a mutant Topo II α that is tagged with a fluorescent protein such as GFP, to allow direct observation of the enzyme [4].

1.1.3 Cell Cycle Synchrony

To achieve the pseudosynchronous passage of mammalian cells into and through mitosis, the cells can be presynchronized by a double-thymidine block/release protocol. For HeLa cells, for instance, a good working protocol is 15 h with 2 mM thymidine, 10 h release in normal medium, 15 h with thymidine, final release (*see* Subheading 2.1). Different cells, even different HeLa isolates, require adjustments to the timing of the protocol (*see* **Note 1**). Essentially, during the first thymidine block, the cells in G2, mitosis and in G1 cycle through and accumulate at the beginning of S-phase, while cells that were in S-phase at the time of thymidine addition remain dispersed through the S-phase period. During the first 10 h release all cells progress and leave S-phase. The second thymidine block then allows all of the cells to accumulate at the beginning of S-phase. The second release thus renders a synchronous cell cycle wave involving the whole cell population, though synchrony is lost to some extent as the cells reach mitosis. The topo II inhibitor can be added at different times after the release of the second thymidine block. The first cells will reach mitosis after about 8–10 h following the thymidine removal. Cells are then collected and processed at a fixed time after adding the inhibitor. This protocol, however, presents two main problems: (1) during the synchronization protocol, because some cells will have spent more time arrested in S-phase than others, cell mass differs as well as chromosome damage that might arise as a consequence of S-phase arrest. For these reasons, the cells progress at different rates towards mitosis, and there is some cell cycle desynchronization. The further through the cell cycle from the release point the wider becomes the synchrony wave; (2) the assays described here rely on studying chromosome structure cytologically. Most cell cycle stages are recalcitrant to the study of chromosome structure as the chromosomes need to be reasonably well condensed, as they are in prometaphase and metaphase. For example, studying chromosome structure in G2-phase following a 1 h treatment at the end of S-phase would be complicated due to the lack of condensation. This limitation can be overcome by combining the methods described here with the induction of premature chromosome condensation (PCC), which itself requires some expertise and a good PCC-inducer (for example, Calyculin A-treatment or cell-fusion experiments). Furthermore, not all cell lines are amenable to PCC protocols. Thus, we do not include these methods here, but refer the reader to published work [2].

In our hands a robust protocol for analyzing the cytological effects of topo II inhibition is a combination of two previously described methods: we use presynchronized cells and we add the topo II inhibitor at different times during the cell cycle wave keeping the inhibitor present until we fix the cells at the peak of the mitotic wave (Fig. 2). Sometimes caffeine can be added to avoid the G2-phase topo II checkpoint as this allows interphase cells with inhibited topo II to reach mitosis without delay. Caffeine addition renders higher frequencies of cells with aberrations generated in interphase (so it can be important in studies of cell cycle timing or when frequencies of aberrations are being determined) but its addition can be omitted given the leaky nature of the G2-phase topo II checkpoint, especially when only chromosome structural defects are of interest.

When it is desirable to study cytology in the absence of a topo II inhibitor, in a cell line expressing a mutant topo II, then the cell cycle synchrony method can be applied coincident with depletion of endogenous topoisomerases (*see* Subheading 3.6). In this case, all cells should reach mitosis with similar degrees of cytological aberrations, dependent on the efficiency of topoisomerase depletion and the consequences of expressing the mutant form of topo II.

1.2 Mitotic Chromosome Preparations

To analyze the cytology of mitotic cells and chromosomes, we routinely perform chromosome preparations similar to previous descriptions but with modifications that are described in this chapter [2, 3, 5]. Most chromosome preparation methods, typically used in cytogenetics, aim to spread the chromosomes well, so that chromosome aberrations can be scored. However, in this chapter we describe modifications to this procedure that allow analysis of chromosomes “in situ” on the mitotic spindle. The method allows visualization of individual chromosomes and chromatids and differentiation of telomeres, arms and centromeres within each chromosome. Remarkably, under these conditions mitotic cells appear in one plane but possess the major features of well-preserved 3D mitotic morphologies. The idea is to be able to study chromosome behavior during mitosis and to be able to accurately distinguish the different mitotic stages. This allows, in particular, the transition from metaphase to anaphase to be studied with clarity. This method is applicable to the study of the effects of any treatment on the mitotic process, but we have found it particularly effective in analyzing chromosome structural defects and aberrant chromosome behavior after topoisomerase II perturbation.

1.3 Impregnation of Silver into Chromosomes

Of particular relevance to the study of the mitotic functions of topo II is the analysis of the chromosome core, or scaffold. This is thought to be a proteinaceous structure that forms the skeleton of the mitotic chromosome, to which loops of chromatin are

attached and on which they become organized during chromosome condensation. Topo II is a component of the chromosome core [2, 6]. Silver impregnation produces a range of color tints including the black of nucleoli, the dark brown of chromosomal cores and the golden color of interphase nuclei and the chromatin halo that surrounds chromosome cores. Reproducible silver staining requires attention to detail and, unavoidably, some good luck!

2 Materials

2.1 Cell Culture and Synchrony

1. Mammalian cells growing as monolayers (*see Note 1*).
2. Tissue culture medium: DMEM (Dulbecco's Minimal Essential Medium) supplemented with final concentrations of 10% FCS (fetal calf serum), 2 mM L-glutamine, and antibiotics.
3. Trypsin solution: 0.1–0.5% Trypsin–EDTA.
4. ICRF-193 (MP Biomedicals): 4 mg/mL stock of 4-[2-(3,5-Dioxo-1-piperazinyl)-1-methylpropyl]piperazine-2,6-dione dissolved in dimethylsulfoxide. Freeze aliquots at -20°C . Use at a final concentration of 2 $\mu\text{g}/\text{mL}$.
5. Thymidine: 50 mM stock of thymidine in tissue culture medium. Filter to sterilize (when prepared) and store at 4°C .
6. Caffeine: 50 mM caffeine stock solution in tissue culture medium (*see Note 2*). Filter to sterilize (when prepared) and store at 4°C .

2.2 RNA Interference to Deplete Endogenous Type 2 Topoisomerases

1. pGIPZ lentiviral shRNA vectors (GE Dharmacon) targeting human TOP2A and TOP2B (*see Note 3*).
2. HEK 293T cells growing as monolayers.
3. Lentivirus packaging plasmids (e.g., ΔNRF and pMDG).
4. PEI: 1 mg/mL stock of polyethylenimine dissolved in sterile water.
5. Polybrene: 8 mg/mL stock of hexadimethrine dissolved in sterile water.

2.3 Construction of FLP-in Topo II α Mutant Cell Lines

1. HeLa EM2-11ht cells growing as monolayers (*see Note 4*).
2. S2F-IMCg vector containing TOP2A cDNA (*see Note 5*).
3. FLP-o vector.
4. pTRE-2 vector, with puromycin resistance marker.
5. GenJet + (SignaGen Laboratories).
6. Puromycin: 3.3 mg/mL stock dissolved in sterile water.
7. Ganciclovir: 100 mM stock dissolved in DMSO.
8. Doxycycline: 250 $\mu\text{g}/\text{mL}$ stock dissolved in sterile water.

2.4 Chromosome Preparations

1. Carnoy's Fixative: 75% methanol, 25% glacial acetic acid. Make fresh every hour (*see* **Notes 6** and **7**).
2. Clean microscope slides (*see* **Note 8**).
3. Giemsa solution: 7% Giemsa (EMD) made in phosphate buffer, pH 6.8 (Harleco) (*see* **Note 9**). It can be reused 2–3 times.
4. Entellan mounting agent (Merck) (*see* **Note 10**).

2.5 Silver Impregnation

1. 2×SSC: 300 mM sodium chloride, 30 mM sodium citrate. Adjust to pH 7.0 with 1 N HCl.
2. Silver staining solution: freshly prepare 0.05% formic acid (*see* **Note 11**) in water and then add 150 μ L of this to 0.1 g of silver nitrate (obtained from Probus or Panreac; *see* **Notes 12** and **13**). The solution should be prepared immediately before use as the silver will precipitate rapidly. Shake the mixture for 30 s (tapping) to dissolve the silver nitrate.

3 Methods

3.1 Growing and Synchronizing the Cells in Preparation for Topo II Inhibitor Treatment

The double thymidine block/release protocol is an inexpensive and reliable method to efficiently synchronize cells at the G1/S boundary. The timing of the steps in this protocol should be adjusted for each cell line depending on the doubling time and on the relative duration of each cell cycle phase (*see* **Note 1**). We should say, however, that this protocol does not work for rodent cells or for *M. muntjac* cell lines. Here we describe the protocol used for our stock of the HeLa cell line that has a doubling time of approximately 24 h.

1. Culture monolayers of HeLa cells in a tissue culture incubator under standard conditions of growth at 37 °C with 5% CO₂ (*see* **Note 14**).
2. 3 days before the experiment, seed the exponentially growing HeLa cells at 10–30% confluence in tissue culture dishes with tissue culture medium. Incubate the cells for at least 24 h (*see* **Note 15**).
3. Add prewarmed (37 °C) thymidine to a final concentration of 2 mM. Incubate the cells for 15 h (During this time cells in mitosis, G2 and G1 at the time of the thymidine addition will progress through the cell cycle and accumulate at the G1/S boundary while cells in S-phase delay/block their progression and remain at different stages of the S-phase.).
4. Release the thymidine block by removing the tissue culture medium from the cells and replacing it with prewarmed tissue culture medium without thymidine (*see* **Note 16**).

5. 10 h after the thymidine was removed, again add thymidine to a final concentration of 2 mM. Incubate the cells for 15 h. (During the thymidine release both the group of cells blocked at the G1/S boundary and those dispersed through the S period, progress beyond the S-phase. Thus, this second thymidine block gathers together all of the cells at the next G1/S boundary.)
6. Release the cells from the second thymidine block as described in **step 3**.
7. At the desired time following release from the second thymidine block (*see* Subheading **1.1**), add the prewarmed topo II inhibitor (ICRF-193) to achieve a final concentration of 2 $\mu\text{g}/\text{mL}$ (*see* **Notes 17** and **18**). (Optional: add prewarmed caffeine to achieve a final concentration of 2 mM; *see* **Note 19**.)

3.2 Preparation of Mitotic Chromosome Morphologies that Maintain the 3D-Organization of Chromosomes on the Mitotic Spindle

1. Carefully aspirate off the majority of the tissue culture medium from the dish (*see* **Note 20**).
2. Transfer the mitotic cells in about 2–3 mL of tissue culture medium into a 15 mL tube (shake-off or scrape the cells from the dish; *see* **Notes 20–22**).
3. Hypotonic treatment: Add tap water (rapidly) so that the ratio is 40% medium/60% water (i.e., hypotonic) to swell the cells. For 2 mL of medium plus cells add 3 mL of tap water (*see* **Note 23**).
4. Leave the cells for 5.5 min at room temperature (*see* **Note 24**).
5. Stop the hypotonic treatment by rapidly adding at least an equal volume of freshly prepared Carnoy's solution (i.e., fill the rest of the 15 mL tube with Carnoy's) (*see* **Notes 25** and **26**). This procedure results in rapid fixation ("freezing") of the cells.
6. Pellet the cells by centrifugation at $800\text{--}1000 \times g$, ~4–5 min.
7. Quickly aspirate off the liquid using a vacuum pump assembly taking care not to disturb the cell pellet (*see* **Notes 27** and **28**).
8. Resuspend the cells by tapping the side of the tube (*see* **Note 29**).
9. Gently fill the tube with Carnoy's solution (along the side of the tube), and mix the cells and fixative gently by inverting the capped tube twice.
10. Let the tube stand for ~5 min at room temperature.
11. Pellet the cells by centrifugation at $800\text{--}1000 \times g$, ~4–5 min, resuspend the cell pellet and add fresh Carnoy's fixative, as described in **steps 6–9**. Repeat this process so that the fixative is changed at least four times (the cells should go through at

least 3× changes in pure fixative with no water or tissue culture medium) (*see Note 30*).

12. After the final wash, resuspend the cell pellet in 2–5 mL of Carnoy's solution so that the cells are at an appropriate dilution for making the chromosome spreads (half a mL of cells in 4 mL of fixative) and store at 4 °C overnight (*see Note 31*).
13. For spreading the cells on microscope slides, first let the fixations warm to room temperature then drop (a small drop) from a 5 cm height onto precleaned glass slides and allow the cells to dry at room temperature (*see Note 32*).
14. Stain the air-dried slides in a Coplin jar in freshly made 5% Giemsa solution for 7 min (*see Notes 33 and 34*).
15. After staining, wash the slides briefly in tap water, let them air-dry.
16. Mount the slides with Entellan (Merck).
17. Analyze on the microscope (*see Note 35*).

3.3 Impregnation of Silver into Fixed Mitotic Chromosomes

1. Collect the cells and perform the hypotonic swelling, fixation and chromosome spreads as described in Subheading 3.2, steps 1–13 (*see Notes 36 and 37*).
2. Incubate the dried slides with 2 × SSC in a Coplin jar placed in a water bath at 60 °C for 23 min (*see Note 38*).
3. Rinse the slides with running tap water for 5 min in the Coplin jar and then briefly rinse in distilled water.
4. Allow the slides to air-dry.
5. Prepare the silver staining solution as described in Subheading 2.5 (*see Note 39*).
6. Put three drops (about 20 µL each) of silver staining solution onto each slide and then immediately cover with a coverslip (50–60 mm) and place the slides immediately into a wet, hot chamber at 70–80 °C.
7. After 3–4 min remove the slides from the chamber and monitor for staining intensity under the microscope. (The slides become yellow-brownish; *see Note 40*).
8. Once the staining is sufficiently intense, remove the coverslips under tap water and rinse the slides for 20 s to completely remove the silver staining solution (*see Note 41*).
9. Allow the slides to air-dry.
10. Mount with Entellan.

Transient transfection can result in overexpression of exogenous alleles; in the case of TOP2A (encoding Topo II α), leading to rapid toxicity. To circumvent this, cell lines can be used in which mutant

Table 1
EM2-11ht Cell line characteristics

Feature	Description	Resistance
Advanced rtTA	Reverse Tet-transactivator (Tet-on) protein. Required for response to doxycycline	G418 (400 µg/mL)
FRT/F3 FLP directional FLP recombinase sites	A pair of asymmetric recombination sites at the 5q31.3 locus, which can be induced to recombine with matching sites on the S2F-IMCg plasmid when the FLP recombinase is co-transfected on an expression plasmid	N/A
Hyg/TK cassette	This cassette containing two genes is situated between the FRT/F3 sites in the genome. It contains a positive and a negative selection marker, and is removed on successful insertion of the gene of interest	Hyg: Resistance to hygromycin (300 µg/mL). TK: Confers sensitivity to ganciclovir (100 µM). When removed, the cells are no longer sensitive to ganciclovir. The parental EM2-11ht cells are thus resistant to hygromycin and sensitive to ganciclovir
Key S2F-IMCg plasmid characteristics		
Feature	Description	
IMCg bidirectional promoter	Promoter that allows insertion of genes upstream and downstream under doxycycline inducible control	
F/F3 recombination sites	Flank the insertion cassette; allow directional recombination of gene between them into HeLa-EM2-11ht genome at the 5q31.3 locus	

3.4 Integration of Doxycycline-Inducible Mutant TOP2A Alleles at the 5q31.3 Locus

TOP2A is inducibly expressed, using doxycycline, close to normal levels and the endogenous Type 2 topoisomerase proteins can be efficiently depleted [7]. This allows study of null and hypomorphic Topo II mutants in stable, homogenous cell lines. The approach combines a doxycycline-inducible transgenic Topo II α with viral shRNA knockdown of the endogenous protein. A TOP2A allele of interest is integrated at the “silent-but-activatable” genomic 5q31.3 locus using the HeLa EM2-11ht cell line and the S2F-IMCg vector [8]. Using the locus avoids detectable expression in the absence of doxycycline. The key characteristics of the cell line and plasmid are described in Table 1.

1. Culture monolayers of HeLa EM2-11ht cells in a tissue culture incubator under standard conditions of growth at 37 °C with 5% CO₂.

2. Split the cells into wells of a 6-well plate, 2.5×10^5 cells/well, one well for each cell line to be constructed, plus two additional negative control wells. Culture the cells overnight.
3. Replace the medium on the cells with fresh tissue culture medium.
4. Per 6-well, prepare two 1.5 mL tubes as follows (Tube A is the same for each well and so it can be made in one large batch) (*see Note 42*):
Tube A:
 - (i) 2 μ L GenJet+.
 - (ii) 200 μ L tissue culture medium without serum.
Tube B:
 - (i) 0.5 μ g S2F-IMCg vector.
 - (ii) 1 μ g Flp-o.
 - (iii) 0.5 μ g pTRE-2.
 - (iv) 200 μ L tissue culture medium without serum.
5. Add Tube A to Tube B rapidly and mix immediately. Incubate at room temperature, 20 min. Add dropwise to cells, swirl, and incubate cells overnight.
6. For each well of the 6-well dish, trypsinize and plate 50% of the cells into one 10 cm dish, and 5% into a second 10 cm dish.
7. Add 1 μ L puromycin per mL of medium to each dish (final concentration of 3.3 μ g/mL). Incubate the cells overnight (*see Note 43*).
8. Change to tissue culture medium without puromycin and add 1 μ L ganciclovir per mL of medium (100 μ M final concentration).
9. Every 2–3 days replace with fresh medium as in **step 8**.
10. After 12–14 days, transfer colonies to individual wells of a 12-well plate and culture in tissue culture medium without ganciclovir (*see Note 44*).
11. When confluent, split each clone into two wells of a 6-well plate.
12. Add 1 μ L doxycycline per mL of medium (250 nM final concentration) to one set of wells. Culture for 48 h.
13. Examine induction of the mCherry-TOP2A gene as follows. Trypsinize the cells from the wells with doxycycline, transfer to a microscope slide and view by fluorescence microscopy.
14. Make permanent stocks of the selected clones after expanding the wells to which doxycycline was not added.

3.5 Production of Lentivirus Particles (VSV-g Pseudotyped Lentiviral Particles) Containing shRNA Targeting TOP2A and TOP2B

To allow phenotypes to be observed that result from the exogenous expression of mutant Topo II α , the endogenous Topo II α and Topo II β enzymes must be depleted. Knockdown of Topo II α alone significantly slows the growth of cells but knockdown of both Topo II α and Topo II β strongly decreases the proliferation rate. Topo II β knockdown alone at equivalent virus concentrations has no apparent effect on proliferation. To employ this strategy, the exogenous Topo II α mutant of interest, integrated at the 5q31.3 genomic locus (*see* Subheading 3.4) must be rendered insensitive to the shRNA construct by introducing silent mutations in the target site prior to integration (*see* **Note 45**). An efficient method of introducing the shRNA into cells is via lentivirus delivery, as follows.

1. Culture monolayers in 10 cm dishes of HEK 293T cells in a tissue culture incubator under standard conditions of growth at 37 °C with 5% CO₂ to an approximate confluent of 70% (*see* **Note 46**).
2. For each shRNA to be produced (per 10 cm dish of HEK 293T), prepare solutions in sterile 1 mL tubes as follows, where Tube B is the same for each shRNA and so can be made in one large batch (*see* **Note 47**):

Tube A:

- (i). 8 μ g pGIPZ vector DNA.
- (ii). 5.4 μ g Δ NRF vector DNA.
- (iii). 2.7 μ g pMDG vector DNA.
- (iv). 600 μ L serum-free tissue culture medium (DMEM).

Tube B:

- (i). 50 μ L PEI.
 - (ii). 600 μ L Serum-free tissue culture medium (DMEM).
3. Add tube B to tube A; vortex well. Incubate in tissue culture hood at RT for 20 min. Mix tube by pipetting up and down a few times, then add the mixture to the 10 cm dish of cells, drop-by-drop over the plate surface. Culture cells for 24 h.
 4. **Important Safety Information:** From here on, cells and media should be considered to contain active virus (*see* **Note 48**).
 5. Aspirate the medium from the 10 cm dish into a flask containing bleach. Replace with fresh DMEM containing 10% FCS and antibiotics. To keep the virus particles as concentrated as possible, use the minimum amount of DMEM necessary to cover the cells (e.g., 6 mL for a 10 cm plate). Culture the cells for 24 h (*see* **Note 49**).
 6. Transfer the cell medium containing the virus particles to a 15 mL centrifuge tube. Spin at 800–1000 $\times g$, 2 min in a

bucket centrifuge to remove cells and debris. Transfer the supernatant to a new 50 mL tube and store at 4 °C overnight. (*see Note 50*).

7. Add fresh tissue culture medium to the culture dishes as per **step 5**. Culture the cells for 24 h.
8. Repeat **step 6**, combining the supernatant with the previous day's supernatant stored at 4 °C (*see Note 51*).
9. Aliquot the combined supernatants into sterile 1.5 mL tubes (1 mL each) and store at –80 °C.

3.6 Synchrony of HeLa FLP-in Cells, Depletion of Endogenous Topoisomerase $II\alpha$ and Topoisomerase $II\beta$, and Induction of Mutant Topoisomerase $II\alpha$

1. Culture monolayers of HeLa cells in a tissue culture incubator under standard conditions of growth at 37 °C with 5% CO₂ (*see Notes 11 and 12*).
2. 1 day before the virus transduction, seed the exponentially growing HeLa cells at 30–50% confluence in 10 cm tissue culture dishes with tissue culture medium. Incubate the cells for 24 h (*see Note 52*).
3. Add 1 µL Polybrene per mL of medium to each 10 cm dish (8 µg/mL final concentration).
4. Add 500 µL each of virus (harvested in Subheading 3.5) to deliver shRNA targeting TOP2A and TOP2B (*see Note 53*).
5. Add 1 µL doxycycline per mL of medium to each 10 cm dish (250 ng/mL final concentration) to induce expression of the exogenous TOP2A.
6. Incubate the cells for 52 h, then proceed with the synchrony protocol (*see Subheading 3.1, steps 3–6*).
7. At the peak of the mitotic wave (10–12 h after releasing from the second thymidine block), proceed with the cytological preparation of chromosomes (*see Subheading 3.2*).

4 Notes

1. The protocols described in this chapter, especially the synchrony protocols, are optimized for HeLa cells but are applicable to a variety of immortalized mammalian cell lines. Some further optimization may be needed in some cases, for example the timing of the thymidine addition and release can be optimized for each cell line. In our experience, even different isolates of HeLa cells require some optimization of the protocol timing ranging from 14 h/8.5 h/14 h to 16 h/11 h/16 h. There are some notable exceptions that we have encountered. Primary cultures of human cells, rodent cell lines and *M. muntjac* cell lines are difficult to synchronize using the double thymidine approach.

2. Dissolving the caffeine requires warming up the solution. Caffeine does not lose activity as a result of heating (think about hot coffee).
3. The pGIPZ lentiviral shRNA vectors (GE Dharmacon) targeting human TOP2A and TOP2B are provided in *E. coli* as follows: TOP2A V3LHS_327878, TOP2B V2LHS_94084.
4. The HeLa EM2-11ht cell line was generated and characterized by Weidenfeld et al. [8] and possesses Flp recombinase sites that allow integration of alleles at the “silent but inducible” 5q31.3 locus (*see* Table 1).
5. Transgenic Topo II α and mutants of interest were rendered insensitive to the shRNA construct (that would be used to deplete endogenous Topo II α) by introducing silent mutations in the target site prior to integration.
6. It is important that the fixative is made fresh, at least every hour. Both methanol and acetic acid (glacial) should be of high quality. If old bottles of methanol and acetic acid are used, the quality of fixation can be diminished substantially.
7. The acetic acid is noxious. Take care not to breathe it in. It also burns the skin and appropriate care must be taken. Never keep acetic acid anywhere near a fluorescence microscope; in the event of an accidental spill, the acid will strip the coating from expensive microscope filters.
8. Sometimes the cytoplasm stains strongly. In that case the slides should be cleaned with methanol before being used.
9. The source of the Giemsa solution is important and Giemsa solution that works well for chromosome banding is not necessarily ideal for the analysis described here. In this protocol, the chromosomes ought to be solid-stained with the Giemsa solution and the extent of staining is important in terms of yielding maximal optical resolution.
10. Entellan. DPX mounting medium (BDH Laboratory Supplies, Poole, England) can also be used. Be careful not to touch the microscope objectives with the mounting agent before it is completely dried.
11. There are different sources of formic acid at different concentrations. Keep this in mind while preparing the silver nitrate solution (we usually obtain formic acid at 18%).
12. We have used different silver nitrate sources and, surprisingly, high quality sources such as from Merck give worse results (except when silver staining for electron microscopy).
13. Larger amounts of silver nitrate are not recommended as they tend to precipitate.

14. During the routine culturing of the cells, make sure that the cells do not reach confluence or become starved. Subculture the cells every 3 days at a dilution that allows the cells to grow exponentially at all times. It is also important that the cells do not spend too much time in the presence of the trypsin solution as this will increase the time needed for recovery of growth. Monitor the trypsinization of the cells under the inverted microscope and inactivate the trypsin by the addition of tissue culture medium as soon as the cells detach from the dish.
15. It is important to be sure that cells are plated at the proper density and growing exponentially. Leave the cells at least 24 h to settle down before starting a synchrony.
16. Most protocols suggest washing the dishes twice with PBS or medium. In our hands the washing step should be skipped as it takes too much time and results in the cooling down of the cells which causes a cell cycle delay [9]. For obtaining a proper synchrony great care must be taken to avoid the cooling down of the cells at any step. When doing experiments with large numbers of dishes, we take only four dishes out of the incubator each time.
17. For very long treatments, replacement of the medium plus ICRF-193 should be considered (i.e., every 12–24 h).
18. ICRF-193 is taken up rapidly by the cells and its inhibition of topo II is almost instant; the first effects can be observed after only 10 min.
19. The effects of caffeine and uptake by the cells are very fast and, when cells are blocked in G₂, its addition can result in the massive entrance of the cells into mitosis within 30 min–1 h.
20. By removing most of the medium from the dish before doing the mitotic shake-off or scraping the cells from the dish, the final volume of medium that the cells are transferred to the 15 mL tube can be kept to around 2–3 mL. This saves a centrifugation step diminishing the disturbance of cells before fixation. It is important to take care during this step, so as to not detach too many mitotic cells from the dish. These would be lost during the aspiration.
21. Cells can be harvested either by mitotic shake off, cell scraping or by trypsin treatment, depending on the experimental requirements. For best chromosome morphology and good quality pictures mitotic shake off is preferred, though for statistical analysis scraping must be performed (in order to include the whole cell population). For the shake off, do it strongly and rapidly but once it is done do not disturb the cells.

22. We usually take the content of a shake off from three 150 mm, almost confluent, dishes into a 15 mL tube, or the content of one 150 mm dish when the cells are being scraped (higher concentrations of cells do not fix well, so use more tubes when necessary).
23. If the volume of cells plus medium plus water is too large (i.e., more than 8 mL), quickly pellet the cells by centrifugation at $800 \times g$ to reduce the volume to 2 mL. Tap the tube to resuspend the cells.
24. We have monitored hypotonic treatments by video microscopy of H2B-GFP HeLa cell lines and no disturbance of the positioning of the chromosomes on the spindle is observed during the 5.5 min incubation. However, longer incubation times will not only disturb the position of chromosomes on the spindle but will also perturb mitotic progression.
25. Mix the cells and fixative gently by inverting the tube twice (NB. The fixative is added rapidly and strongly to the tube and then the mixing of the cells should be done gently).
26. The mixture has far too much water to be a good fixative and so the water should be removed rapidly by the successive centrifugation steps.
27. Aspirating the acetic acid may cause damage to typically used vacuum pump assemblies. Acid resistant pumps are available but they are expensive. An alternative is to pipette off the liquid, but care must be taken not to disturb the pellet, which is quite fluffy. Moreover, the initial steps of fixation need to be done rapidly to achieve optimum fixation.
28. Leave just 1–2 mm of liquid above the pellet so that it does not dry out when resuspending. Leaving more liquid will result in an excess of water in the fixative. This is a very important step because it is when the cells are going to receive the true fixation mixture after being “stopped and prefixed” in the previous step.
29. It should be efficient as cells not resuspended at this step will not resuspend in the later steps.
30. The quality of the fixation improves with each wash in fresh Carnoy’s. At least three washes are required. Fixed material can be stored for many years at -20°C .
31. The fixed material can be dropped onto microscope slides immediately following the last wash (we commonly do it), though the quality of the preparations is typically improved by the overnight storage at 4°C . The fixed material can be stored for years, but changes of fixative (every year) improve preservation.

32. A 200 μ micropipette is commonly used for convenient drop size. We usually add three drops evenly distributed on the same slide. Slides with frosted edges and labeled in pencil will be resistant to the fixative. If wider spreading of the chromosomes is required, put the slides in methanol, let them half-dry and then when the interference edges appear, drop the cells onto the slide. Help the material to dry out by gently blowing wet air across the slide surface (wet your lips continuously).
33. Quite commonly, a silvery-greenish surface is observed at the top of the Giemsa solution during the staining procedure. That surface results in dirtiness in some regions of the slide. To get rid of it, remove as much as possible from the Giemsa solution surface with a tissue paper (while staining). In addition, place a slide with useless cells on one side of the Coplin jar, next to the slides from the experiment. After staining, remove the Giemsa solution by tilting the Coplin jar in the direction of the useless slide. This will ensure that the useless slide receives the tainted surface from the solution.
34. The color of the chromosomes will depend largely on the time of staining. Short times (5–6 min) give reddish chromatin while long times (8 min) give blue chromatin. Ideally, stop the staining when the chromosomes are just changing color from pink to violet. This will ensure the best contrast under the microscope.
35. Notes on microscopy. We find that an accurate representation of the stained chromatin (in terms of color, contrast, and resolution) can be achieved using a Zeiss Axioplan II microscope with an alpha Plan Fluar 100 \times /1.45 n.a. objective, captured by an AxioCam MRC5 camera using Axiovision software.
36. We have observed that the reproducibility of the technique is greatly reduced when a standard hypotonic treatment in 25% HBSS is used.
37. When cells that are blocked in mitosis are required, mitotic arrest induced by high pressure nitrous oxide treatment is preferable to nocodazole- or colcemid-induced arrest. These latter treatments more rapidly produce hypercondensed chromosomes that are not easily impregnated with silver.
38. We have optimized the length of the SSC treatment specifically for Indian muntjac chromosomes. Other mammalian cell types may require treatments of 15–30 min and this must be determined empirically.
39. Silver staining should be performed on the same day as the 2 \times SSC pretreatment.

40. The staining largely stops as the slides cool (monitor the cells really fast in case the slides need to go back to the hot chamber), but there is still some increase in the background precipitation.
41. Rinse the slides over a surface lacking cells otherwise loss of material is prone to occur.
42. The control wells include: (a) a nontransfected well that serves to test the efficiency of the initial Puromycin treatment; (b) where the Flp-O plasmid is omitted from Tube B, to provide a background number of colonies that arise in the absence of recombinase.
43. After the overnight incubation the puromycin treatment should have killed 100% of the control untransfected cells. Of the remaining dishes, most cells should be dead, but a large number of living cells should remain adhered.
44. In general, around 50% of colonies are found to be expressing. Some of these clones appear not to grow robustly. It is suggested that around 24 colonies are picked to ensure at least 4–5 expressing clones that grow robustly are isolated.
45. The silent mutations made in the Topo II α cDNA to render it resistant to the shRNA were as follows: base pairs 1968–1996 of the wild type cDNA (ACAGATAGATGATCGAAAGGAATGGTTAA) were mutated to ACAAATCGACGACAGGAAAGAATGGCTAA.
46. Grow cells in DMEM tissue culture medium with 10% FCS, 1% penicillin/streptomycin solution. Large amounts of viral particles can be produced easily. As a guideline, consider that each plate will produce twice the culture medium volume of viral supernatant. For example, a 10 cm plate with 6 mL media will produce 12 mL total viral supernatant.
47. Two packaging plasmids are necessary for production of viral VSV-g pseudotyped lentiviral particles: pMDG and Δ NRF, both are ampicillin resistant).
48. When working with active virus take appropriate precautions as per the requirements of your institution, including but not limited to: wear gloves, safety glasses, and respiration mask; aspirate liquid waste into a flask containing bleach; autoclave solid waste).
49. The cells will be expressing GFP by now; this can be checked by viewing the cells on an inverted fluorescence microscope under low power.
50. The tubes should be in secondary containment to avoid contaminating the refrigerator.
51. Virus particles can be concentrated in an ultracentrifuge at 120,000 $\times g$ for 1 h at 4 °C.

52. Cells can be trypsinized and reseeded at desired density at the same time as adding virus. It is not necessary to wait for cells to attach to the dish.
53. Titering the virus can be carried out using an MTS assay and constructing a kill curve when cells are treated with puromycin at various concentrations of virus. From this kill curve, an approximate virus titer can be calculated.

Acknowledgments

The chromosome preparation technique was originally devised in Prof. Robert T Johnson's laboratory (Mammalian Cell DNA Repair Group, University of Cambridge, UK) and has been modified over the years by Drs. Giménez-Abián and Clarke. Silver impregnation was developed for mammalian mitotic chromosomes by Dr. Giménez-Abián, but is based on methods used to stain meiotic grasshopper chromosomes by Rufas et al. [10, 11]. HeLa EM2-11ht cells were provided by Weidenfeld et al. [8]. Development of the protocols described in this chapter was partly dependent on funding from grants BFU2008-03579/BMC and 2008201165 from the VICT (MCI, Spain) and NIH grant CA099033 to DJC.

References

1. Hirano T, Funahashi SI, Uemura T, Yanagida M (1986) Isolation and characterization of *Schizosaccharomyces pombe* cut mutants that block nuclear division but not cytokinesis. *EMBO J* 5:2973–2979
2. Giménez-Abián JF, Clarke DJ, Mullinger AM, Downes CS, Johnson RT (1995) A postprophase topoisomerase II-dependent chromatid core separation step in the formation of metaphase chromosomes. *J Cell Biol* 131:7–17
3. Giménez-Abián JF, Clarke DJ, Devlin J, Giménez-Abián ML, De la Torre C, Johnson RT, Mullinger AM, Downes CS (2000) Premitotic chromosome individualization in mammalian cells depends on topoisomerase II activity. *Chromosoma* 109:235–244
4. Tavormina PA, Côme MG, Hudson JR, Mo YY, Beck WT, Gorbsky GJ (2002) Rapid exchange of mammalian topoisomerase II alpha at kinetochores and chromosome arms in mitosis. *J Cell Biol* 158:23–29
5. Hauf S, Cole RW, LaTerra S, Zimmer C, Schnapp G, Walter R, Heckel A, van Meel J, Rieder CL, Peters JM (2003) The small molecule Hesperadin reveals a role for aurora B in correcting kinetochore-microtubule attachment and in maintaining the spindle assembly checkpoint. *J Cell Biol* 161:281–294
6. Earnshaw WC, Halligan B, Cooke CA, Heck MM, Liu LF (1985) Topoisomerase II is a structural component of mitotic chromosome scaffolds. *J Cell Biol* 100:1706–1715
7. Lane A, Giménez-Abián JF, Clarke DJ (2013) A novel chromatin tether domain controls topoisomerase II α dynamics and mitotic chromosome formation. *J Cell Biol* 203:471–486
8. Weidenfeld I, Gossen M, Löw R, Kentner D, Berger S, Görlich D, Bartsch D, Bujard H, Schönig K (2009) Inducible expression of coding and inhibitory RNAs from retargetable genomic loci. *Nucleic Acids Res* 37(7):e50
9. Mikhailov A, Shinohara M, Rieder CL (2005) The p38-mediated stress-activated checkpoint. A rapid response system for delaying progression through antepause and entry into mitosis. *Cell Cycle* 4:57–62
10. Rufas JS, Suja JA, Garcia de la Vega C (1987) Chromosome organization in meiosis revealed by light microscopy of silver stained cores. *Genome* 29:706–712
11. Sentis C, Rodriguez-Campos I, Stockert L, Fernandez-Piqueras J (1984) Morphology of the axial structures in the neo-XY sex bivalent of *Pycnogaster cucullata* (Orthoptera) by silver impregnation. *Chromosoma* 90:317–321

Monitoring the DNA Topoisomerase II Checkpoint in *Saccharomyces cerevisiae*

Katherine Furniss, Amit C.J. Vas, Andrew B. Lane, and Duncan J. Clarke

Abstract

Topoisomerase II activity is crucial to maintain genome stability through the removal of catenanes in the DNA formed during DNA replication and scaffolding the mitotic chromosome. Perturbed Topo II activity causes defects in chromosome segregation due to persistent catenations and aberrant DNA condensation during mitosis. Recently, novel *top2* alleles in the yeast *Saccharomyces cerevisiae* revealed a checkpoint control which responds to perturbed Topo II activity. Described in this chapter are protocols for assaying the phenotypes seen in *top2* mutants on a cell biological basis in live cells: activation of the Topo II checkpoint using spindle morphology, chromosome condensation using fluorescently labeled chromosomal loci and cell cycle progression by flow cytometry. Further characterization of this novel checkpoint is warranted so that we can further our understanding of the cell cycle, genomic stability, and the possibility of identifying novel drug targets.

Key words Topoisomerase II checkpoint, Anaphase, Spindle elongation, Chromosome condensation, Budding yeast

1 Introduction

In order to perform mitosis successfully, DNA topoisomerase II (Topo II) must resolve catenanes between the sister chromatid DNA molecules [1, 2]. This is essential for the separation of the sister chromatids in anaphase [3, 4]. Topo II also contributes to the process of chromosome condensation, which facilitates accurate chromosome segregation in anaphase [4–9]. When Topo II activity is perturbed, cell cycle checkpoints are triggered which delay mitotic progression [10–17]. The budding yeast, *Saccharomyces cerevisiae*, has a single Topo II protein, Top2 [18]. Top2 functions in both chromosome condensation and segregation and a pre-anaphase (G2/M) cell cycle checkpoint is activated in strains possessing mutant *top2* alleles [11]. In the following sections we will explain how to perform cell cycle synchronization of cultures of *S. cerevisiae* cells so that the checkpoint induced in response to

perturbed Top2 can be analyzed. This employs a “population analysis” approach and combines FACScan determination of DNA content and characterization of cell cycle stage using spindle morphology as a criterion. In addition we describe an alternative method to measure checkpoint activation that employs live single-cell imaging. We also describe a method that allows measurement of chromosome condensation defects in *top2* mutants [9]. Use of these assays will allow further characterization of the Topo II checkpoint and to study the process of chromosome condensation in a genetically tractable eukaryote.

1.1 Cell Cycle Synchronization of Yeast Cells

All of the yeast strains used in these assays are mating type a (*MATa*) and are *bar1Δ*. This genotype is important for the cell cycle synchronization in G1 phase. Yeast that are mating type a respond to a peptide mating pheromone called α -factor, which in the wild is secreted by mating type α cells. The pheromone induces the *MATa* cells to prepare for mating by arresting in G1 phase of the cell cycle. Upon arrest the cells form a mating projection called a shmoo which is employed in the conjugation process. We can exploit this behavior to achieve cell cycle synchrony in G1 and the shmoo is a useful marker for efficient G1 arrest. *MATa* cells that have the *BARI* locus deleted (i.e., *bar1Δ* strains) are unable to degrade α -factor and therefore can be arrested in G1 in the presence of low concentrations of the mating pheromone. This is an advantage because the peptide mating pheromone is expensive.

1.2 “Population Analysis” of Spindle Morphologies in Yeast Cells

The “population analysis” described below (Subheading 3.1) allows monitoring of cell cycle progression by taking samples at intervals following release from G1 synchronization. Each time point sample is used to score spindle morphologies visualized in cells expressing a GFP-Tub1 fusion protein (GFP fused to the alpha tubulin protein) [19]. There are two advantages to using this approach. Firstly, it avoids the need to immuno-stain the microtubules in order to visualize the mitotic spindle. Secondly, the cells can be visualized live (i.e., there is no need to fix the cells before performing the microscopy). Analysis of spindle morphologies gives an accurate view of cell cycle progression (see Figs. 1–9). When a yeast cell is in G1 the GFP-Tub1 reveals a single, bright dot with small projections; these are the spindle pole body and the astral microtubules (Fig. 1). As the cell enters S phase (which corresponds to the emergence of a bud) it duplicates its spindle pole body; however, because the spindle pole bodies do not immediately separate, a single bright dot, or two very closely aligned dots, are seen. Again, the duplicated spindle pole bodies are associated with astral microtubule projections (Fig. 2). Approximately coincident with the completion of DNA replication, and defined as the beginning of G2/M phase, the spindle pole bodies separate and the mitotic spindle assembles (Fig. 3). At this stage, the spindle is first viewed as a short (1–2 μm) long bar of microtubules with a

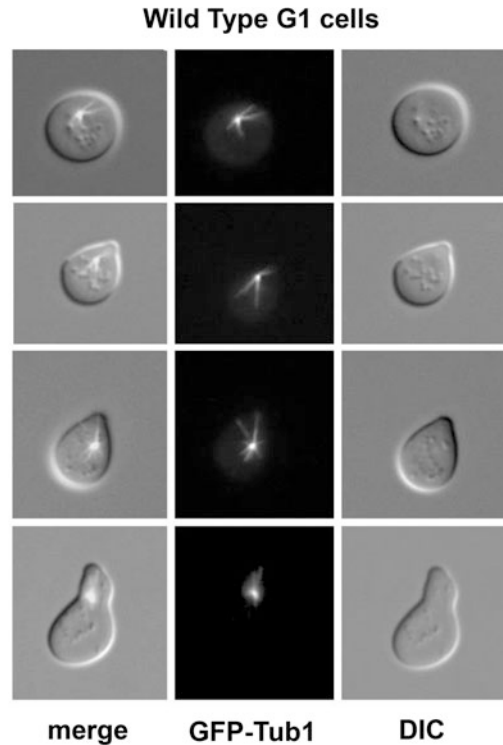


Fig. 1 Microtubule morphologies in wild type G1 cells. Wild type G1 cells visualized using the DIC setting on the microscope as well as the green fluorescence channel to observe the GFP-Tub1 fusion protein. G1 cells appear round and unbudded. However, when *bar1* Δ cells are exposed to α factor, projections called shmoos form (these are the mating projections that cells of opposite mating type form in order to initiate conjugation). The mating projections can be confused with buds. Notice that buds have a pinched (constricted) neck while the projections do not (compare the images in Figs. 1 and 2). The GFP-Tub1 fusion protein in G1 phase cells localizes to a single, bright spot which is the spindle pole body as well as to the astral microtubules that can be seen to project from the spindle pole body. When scoring the % of G1 cells in a population, combine the % of cells that are round and unbudded with the % of cells that are unbudded with a shmoos

bright dot at each end (the spindle pole bodies). The spindle pole bodies have astral microtubule projections pointing toward the edges of the mother cell (commonly in the vicinity of the bud neck) and the edges of the daughter bud. The spindle continues to elongate and can reach about 3–4 μm but remains thick and bright. At this stage, a lower density of microtubules in the middle region of the spindle can often be observed. This is because kinetochore microtubules (those that connect the spindle pole bodies to each kinetochore) do not reach all the way to the middle of the spindle [20, 21]. There are 16 kinetochore microtubules in each half of the spindle. A smaller number of overlap microtubules

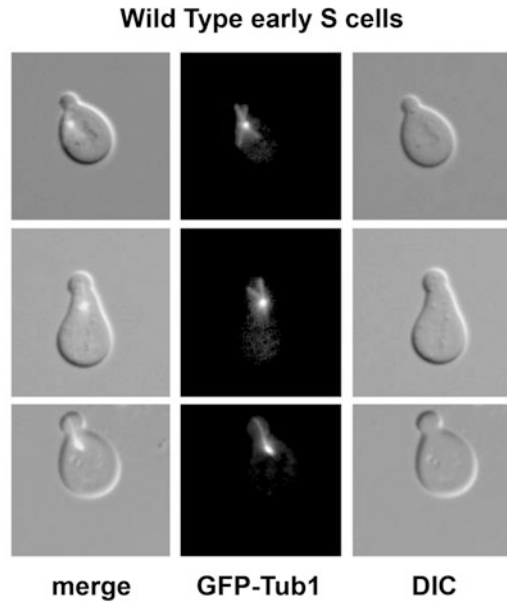


Fig. 2 Microtubule morphologies in wild type early S-phase cells. Wild type early S-phase cells visualized using the DIC setting on the microscope as well as the green fluorescence channel to observe the GFP-Tub1 fusion protein. The onset of DNA replication (when S-phase begins) coincides with the initiation of bud formation. S-phase cells have relatively small buds, up to a maximum of about 2/3 of the mother cell volume. The bud can form at the tip of the shmoo (as seen in the second image) or in a new location on the cell surface. In S-phase, cells duplicate their spindle pole body and this is initiated along with budding and DNA replication. However, the spindle pole bodies do not separate until late S-phase and a single fluorescent spot is visualized. Astral microtubules emanate from the spindle pole bodies

emanate from both spindle pole bodies and are crosslinked in the middle region of the spindle. Once anaphase begins the G2/M bar spindle morphology is dramatically changed. The anaphase spindle is much longer (typically 7–10 μm when fully elongation) and is markedly thinner so that it is no longer as bright as the G2/M spindle (Fig. 4). This is because the kinetochore microtubules shorten during chromosome segregation toward the spindle pole bodies and it is the smaller number of overlap microtubules that are seen in the anaphase spindle. Finally, in telophase, the elongated spindle begins to break down. At this stage the spindle pole bodies are seen close to the extremities of the mother and daughter cell, with short astral microtubules connecting them to the cells edges. The cell then completed the cell cycle and following cytokinesis, the mother and daughter cells return to G1 and possess a single spindle pole body with astral microtubule projections. Because the yeast topoisomerase II checkpoint extends the G2/M phase of the cell cycle, checkpoint duration can be assayed by measuring the interval

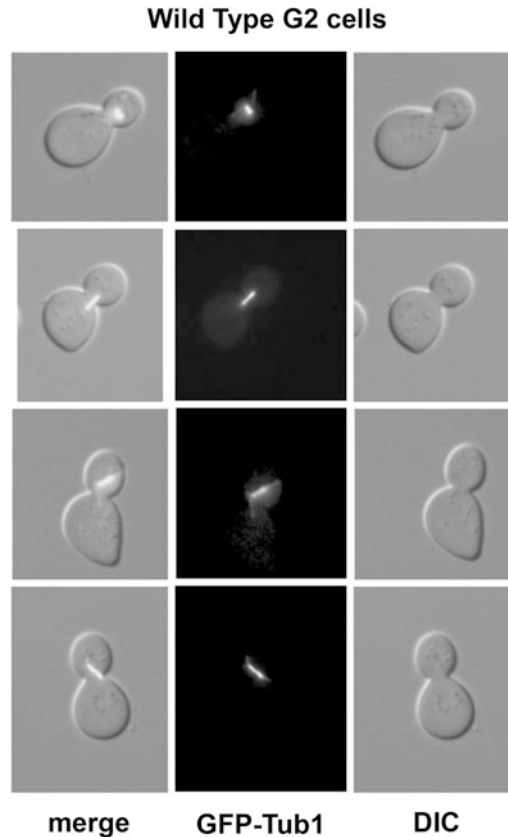


Fig. 3 Microtubule morphologies in wild type G2/M cells. Wild type G2/M cells visualized using the DIC setting on the microscope as well as the green fluorescence channel to observe the GFP-Tub1 fusion protein. In G2/M phase, the buds have grown to about 2/3 of the mother cell volume. The spindle pole bodies have separated and a thick, bright metaphase spindle can be seen. Upon assembly the metaphase spindle is initially 1–2 μm in length but typically increases in length up to about 3–4 μm during G2/M-phase. The cell at the top of this figure is an early G2/M-phase cell, its spindle pole bodies have begun to separate—the GFP-Tub1 image shows that there are two fluorescent dots. Astral microtubules can sometimes be seen to emanate from both spindle pole bodies. The spindle pole body that will ultimately remain in the mother cell has astral microtubules which contact the mother cell cortex, usually close to the neck of the bud. The spindle pole body that will ultimately segregate to the daughter cell has astral microtubules which contact the bud cortex

between spindle assembly (i.e., at the beginning of G2/M phase) and spindle elongation (i.e., at the onset of anaphase). In wild type cells that have normal levels of topoisomerase II activity (i.e., when the checkpoint has not been triggered) and also in mutant cells that lack the checkpoint response, the G2/M period is typically around 15 min [11] (see Fig. 9). In *top2* mutants that activate the

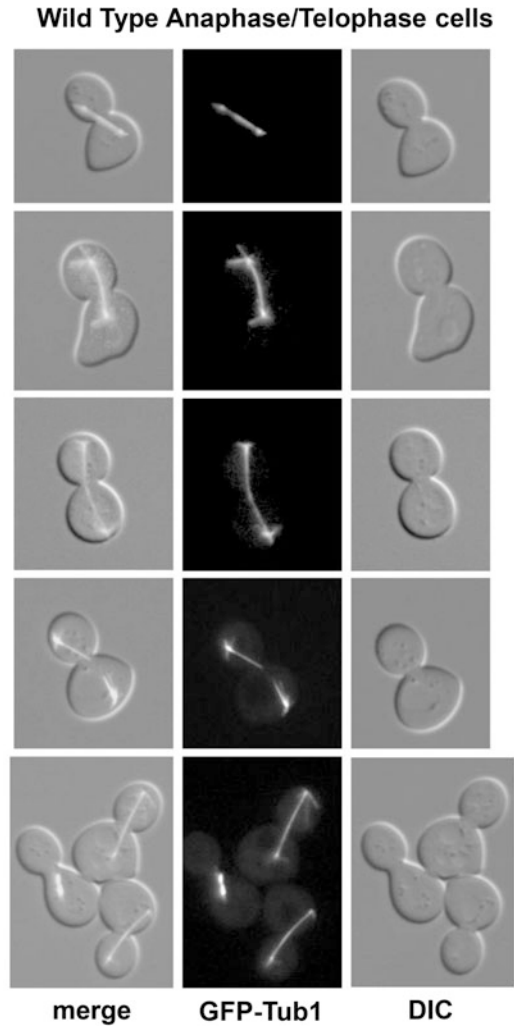


Fig. 4 Microtubule morphologies in wild type anaphase/telophase cells. Wild type anaphase/telophase cells visualized using the DIC setting on the microscope as well as the green fluorescence channel to observe the GFP-Tub1 fusion protein. Cells in anaphase and telophase also have buds that are approximately 2/3 the size of the mother cell. The spindle elongates as the spindle pole bodies migrate away from each other. The elongated spindle is composed of fewer microtubules and so it appears fainter than G2/M spindles. In the fourth image (from the top; telophase) the spindle has broken in preparation for cytokinesis. Astral microtubules can be seen to emanate from the SPBs to contact the cell cortexes. The image at the bottom has one G2/M cell (on the left) and two anaphase/telophase cells. This image contrasts the size and brightness of G2/M versus anaphase/telophase spindles

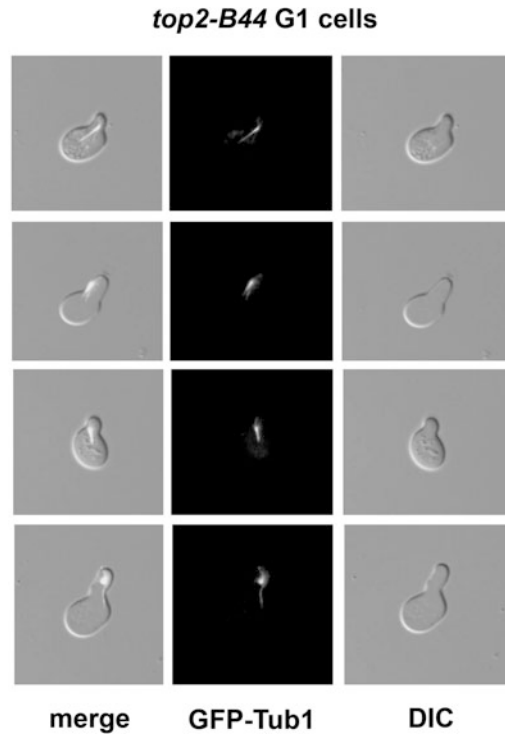


Fig. 5 Microtubule morphologies in *top2-B44* G1 cells. *top2-B44* G1 cells visualized using the DIC setting on the microscope as well as the green fluorescence channel to observe the GFP-Tub1 fusion protein. Mutant cells can look similar to wild type cells, but some different morphologies that are seen are depicted here. As shown in Fig. 1 there is a single spindle pole body with astral microtubule projections

checkpoint response, the G2/M period can be extended by at least at additional 30 min [11].

1.3 Live Single-Cell Analysis of Spindle Dynamics

In the above section (Subheading 1.2) spindle morphologies allow scoring of cell cycle position by categorization of cells by eye. This “population assay,” where samples are collected and cells categorized every 10–15 min allows plots of % cells with a G2/M (metaphase) spindle and % cells with an anaphase, versus time. This yields a plot which reveals the approximate interval between spindle assembly and anaphase spindle elongation, which can be used to define the approximate duration of G2/M (metaphase). Alternatively, time-lapse microscopy of spindles yields the precise timing of spindle assembly and anaphase spindle elongation in single cells, (typically with an error within ± 2 min). Such analysis reveals the exact metaphase duration in each cell, rather than an average metaphase length value that is derived from analyzing a population of cells (as in Subheading 1.2). Logistically, analyzing such data is straightforward, once time lapse movies have been produced that capture Tub1-GFP fluorescence of cells progressing through the

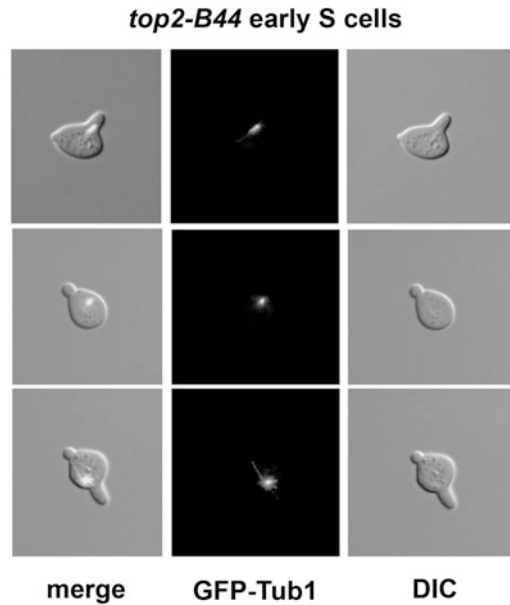


Fig. 6 Microtubule morphologies in *top2-B44* early S-phase cells. *top2-B44* early S-phase cells visualized using the DIC setting on the microscope as well as the green fluorescence channel to observe the GFP-Tub1 fusion protein. Much like the wild type cells shown in Fig. 2 these cells have formed a small bud, identified by the constriction at the bud neck. Two of the cells have both a bud and a shmoo, the buds are at the *top left* of the cells. The spindle pole body has duplicated but has not yet separated so a single dot with astral microtubules is present

cell cycle. For each individual cell, spindle length is measured at each time point until the completion of anaphase. At time points before spindle assembly occurs, the diameter of the spindle pole body is measured. When spindle length is plotted versus time, this reveals the moment of spindle pole body separation and anaphase onset to accuracy within a few minutes (*see* Fig. 10a). When individual cells are aligned on the x-axis at the moment of pole separation, and average spindle length is calculated for each time point, plots reveal small error bars during G2/M (metaphase) and large error bars during anaphase (*see* Fig. 10b). G2/M (metaphase) length can be defined as the interval between pole separation and anaphase onset, to yield the average metaphase duration after analyzing 25–50 cells (*see* Fig. 10).

The live single-cell analysis method also allows the study of nonsynchronized cultures of cells. It does, however, require an elaborate microscopy system to record Tub1-GFP fluorescence, including the capacity to maintain the cells at a fixed temperature during imaging, as well as a microfluidic chamber or other housing that keeps the cells fixed in position. It should also be noted that the duration of metaphase calculated from “population analysis,”

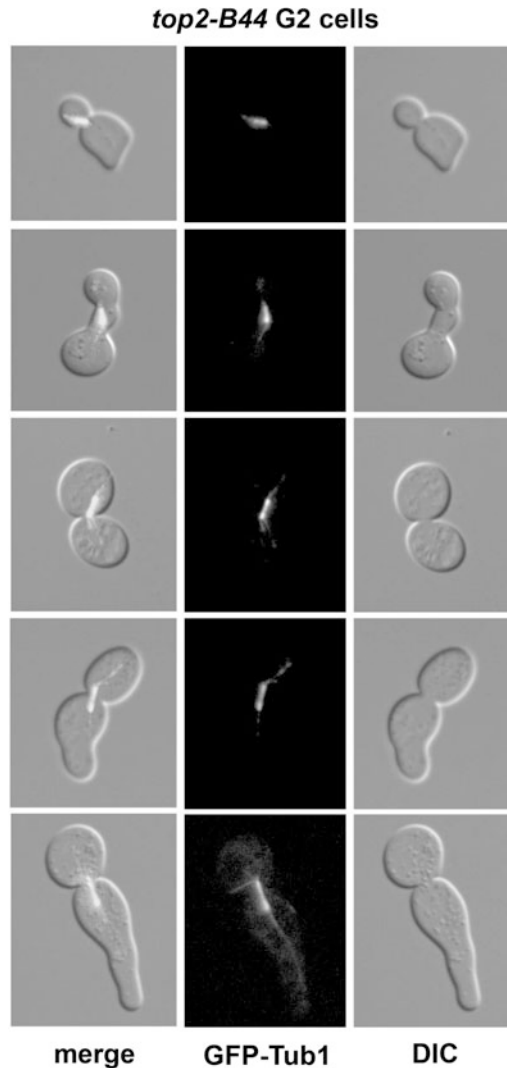


Fig. 7 Microtubule morphologies in *top2-B44* G2/M cells. *top2-B44* G2/M phase cells visualized using the DIC setting on the microscope as well as the green fluorescence channel to observe the GFP-Tub1 fusion protein. Because the Topo II checkpoint is activated in these cells they spend about three times the normal time in G2/M-phase. During this delay the bud, and to some extent the mother cell, continue growth. As a result the bud can reach the size of the mother cell. Mutant cells can have a variety of shapes. In the second image the bud has formed at the end of an elongated shmoo so that there is a long neck between the shmoo and bud. In the bottom two figures the shmoo has enlarged greatly and the bud has formed at the opposite end. As seen in Fig. 3 the spindle pole bodies have separated and the spindle is thick and bright with astral microtubules projecting from the spindle pole bodies. Because the overall cell size can be larger than wild type G2/M cells, the metaphase spindle can also become slightly longer than is typical

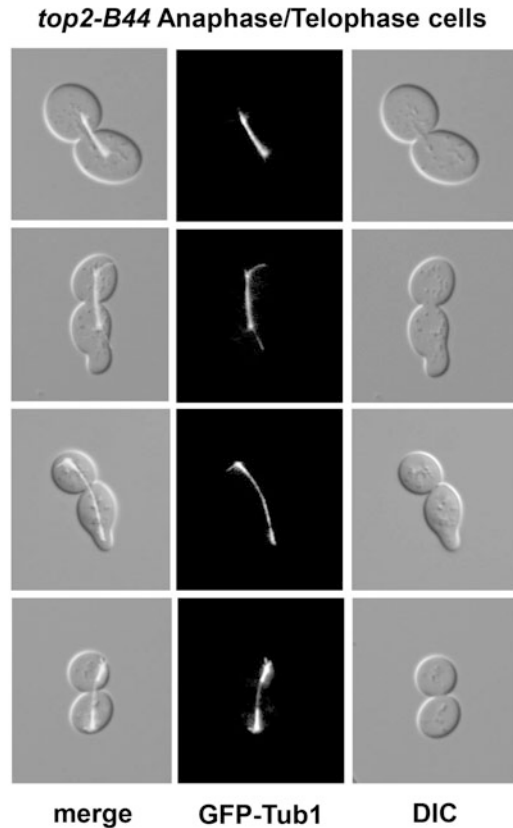


Fig. 8 Microtubule morphologies in *top2-B44* Anaphase/Telophase cells. *top2-B44* anaphase/telophase cells visualized using the DIC setting on the microscope as well as the green fluorescence channel to observe the GFP-Tub1 fusion protein. In mutant cells with G2/M delays the daughter cell can continue to grow and therefore become approximately equal in size to the mother cell. As in Fig. 4 the spindle has elongated and thinned so that it is less bright. The bottom image is of a cell in which the spindle is about to break just prior to cytokinesis

versus the single-cell method, will differ. In single-cell analysis, the kinetics of cell cycle progression is elongated because cells are grown in a static chamber instead of the conditions used for the population analysis where cells are subjected to vigorous shaking in a water bath.

1.4 Analysis of Chromosome Arm Condensation in Yeast Cells

Chromosome condensation is a necessary prerequisite for segregation of the genome in mitosis. As such, this process is regulated through the cell cycle. Through the end of S-phase, the genome is in a decondensed state. However, approximately at the onset of G2/M phase of the cell cycle, the chromosome becomes compacted and condensed, a topoisomerase II-dependent process [9]. This cell cycle stage in yeast is thought to correspond with prophase of mitosis in higher eukaryotes, where the condensation

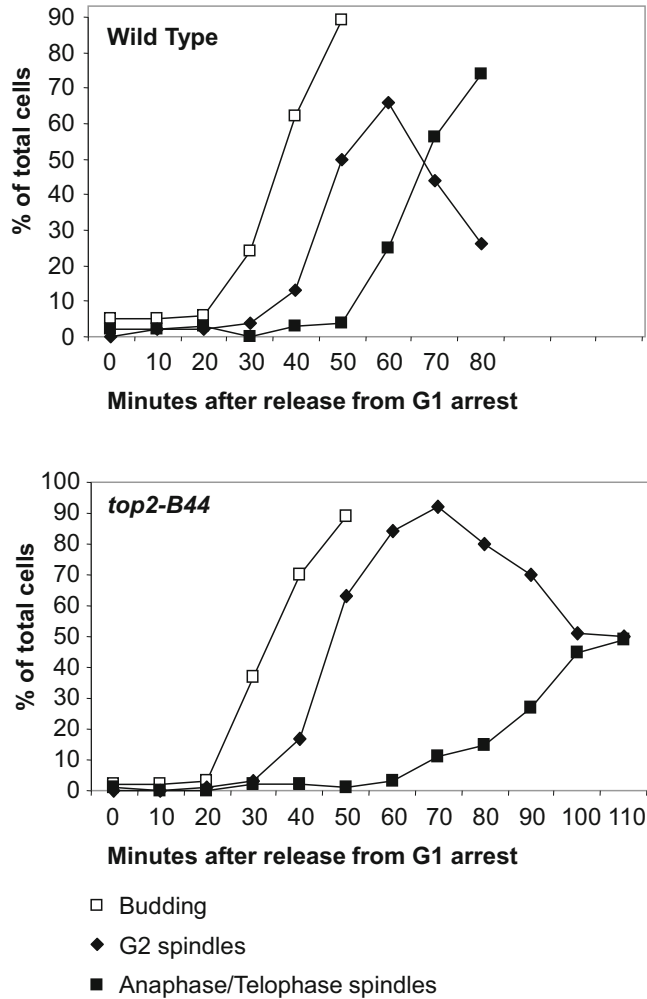


Fig. 9 A typical time course experiment in which spindle morphologies were monitored. Wild type and *top2-B44* cells were counted according to the previously defined categories of spindle morphologies (Figs. 1–8). In a typical time course of wild type cells budding begins to increase around 30 min and peaks around 80–90% between 50 and 60 min after release from G1. The formation of G2 spindles increases at an approximately equal rate but with about a 10 min delay. Anaphase spindle formation should also increase in an approximately equal rate, about 14–18 min after G2 spindle formation. In a typical time course of *top2-B44* cells, budding and G2 spindle formation occur with kinetics similar to wild type cells. However, in this mutant, due to Topo II Checkpoint activation, there is a delay between G2 spindle formation and anaphase spindle elongation of about 300%, such that anaphase spindles are seen 46 min after G2 spindles. Additionally, because of the delay the yeast cells do not undergo anaphase as synchronously as wild type cells

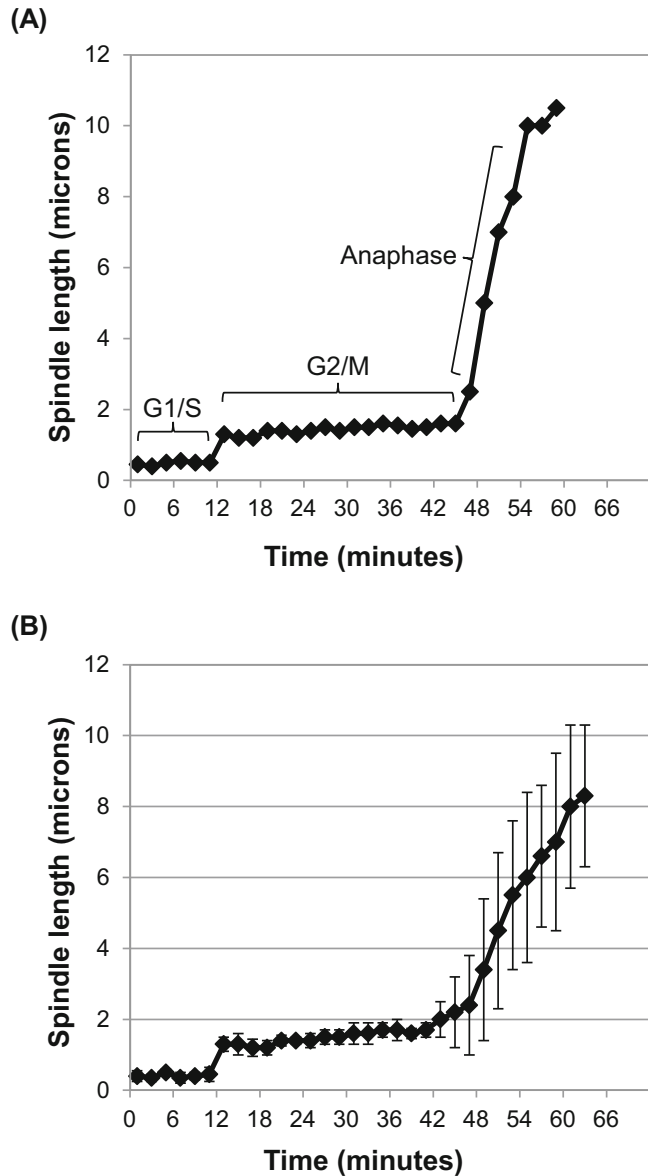


Fig. 10 Single-cell assay to monitor the kinetics of spindle assembly and elongation in yeast. Following time-lapse microscopy to capture Tub1-GFP fluorescence, spindle length is determined at each time point for each cell. The data can be plotted as follows. (a) Spindle length (or Spindle Pole Body diameter; before separation of the duplicated Spindle Pole Bodies) versus time for a single cell. Cell cycle stages are indicated that correspond to when cells are in G1/early S-phase (before Spindle Pole Body separation), G2/M (metaphase) and anaphase. (b) Average spindle length (or Spindle Pole Body diameter; before separation of the duplicated Spindle Pole Bodies) versus time. Data for each single cell are aligned on the x-axis at the moment of Spindle Pole Body separation. Standard deviation of spindle length shows that Spindle Pole Body diameters and G2/M (metaphase) spindle lengths do not vary greatly. However, the standard deviation of spindle lengths increases at time points where some cells are in anaphase

of the chromosomes is a cytologically dramatic event. In yeast, because chromosomes are very small, molecular tools needed to be developed to allow the analysis of the condensation process [9, 22]. These methods allow the monitoring of chromosome condensation in live cells and can provide insight into aspects of Topoisomerase II function under experimental conditions.

A GFP-LacR fusion protein in combination with *LacO* sequences integrated into the yeast genome was utilized to produce a suitable strain (a “condensation strain”) that can be used to monitor linear condensation of a chromosome arm during G2/M phase [9]. This system exploits features of the Lac operon in which the GFP-LacR fusion protein binds with sequence specificity to *LacO* DNA sequences. In the condensation strain, long stretches of tandemly repeated *LacO* sequences were inserted at two loci: one at the *trp1* locus (512 copies of *LacO*) and one at the *lys4* locus (256 copies of *LacO*). As GFP-LacR localizes to these repeats, it renders the *trp1* and *lys4* loci visible by fluorescent microscopy. When the chromosome is decondensed, the loci are separated by the intervening chromatin and appear as two discrete GFP foci under the microscope; the centers of the dots are separated on average by 1.6 μm [9]. As the chromosome condenses, however, the foci coalesce and appear as two tightly associated GFP foci, or in some cases one single GFP focus, with an average distance of 0.6 μm between their centers [9]. Examples are given in Figs. 11 and 12 shows a typical cell cycle analysis of condensation.

2 Materials

2.1 Yeast Strains and Plasmids

The following yeast strains and plasmids are available from the authors of the papers in which they were originally described. All of the yeast strains described below are derived from BF264-15 15DU: *MATa ura3 Δ ns ade1 his2 leu2-3112 trp1-1a* [23].

1. pAFS91: a plasmid used to integrate *GFP-TUB1* (GFP-tagged α -tubulin) into the yeast genome at the *URA3* locus. The *GFP-TUB1* gene fusion is located in the KpnI to XhoI sites of plasmid pRS306. Integration at the *URA3* locus requires digestion of the plasmid with StuI followed by transformation into a *ura3* strain and selection for transformants on solid medium lacking uracil [19].
2. DCY1671: *MATa bar1 Δ ura3::HIS3:GFP-TUB1(URA3) ARG4*. This is a yeast strain, mating type **a**, that has the *bar1* locus deleted. The *ura3* gene is replaced with the GFP-tagged α -tubulin fusion gene which is under the control of the *HIS3* promoter. The integrated construct is linked to *URA3* so that this yeast strain is *URA3* [24].

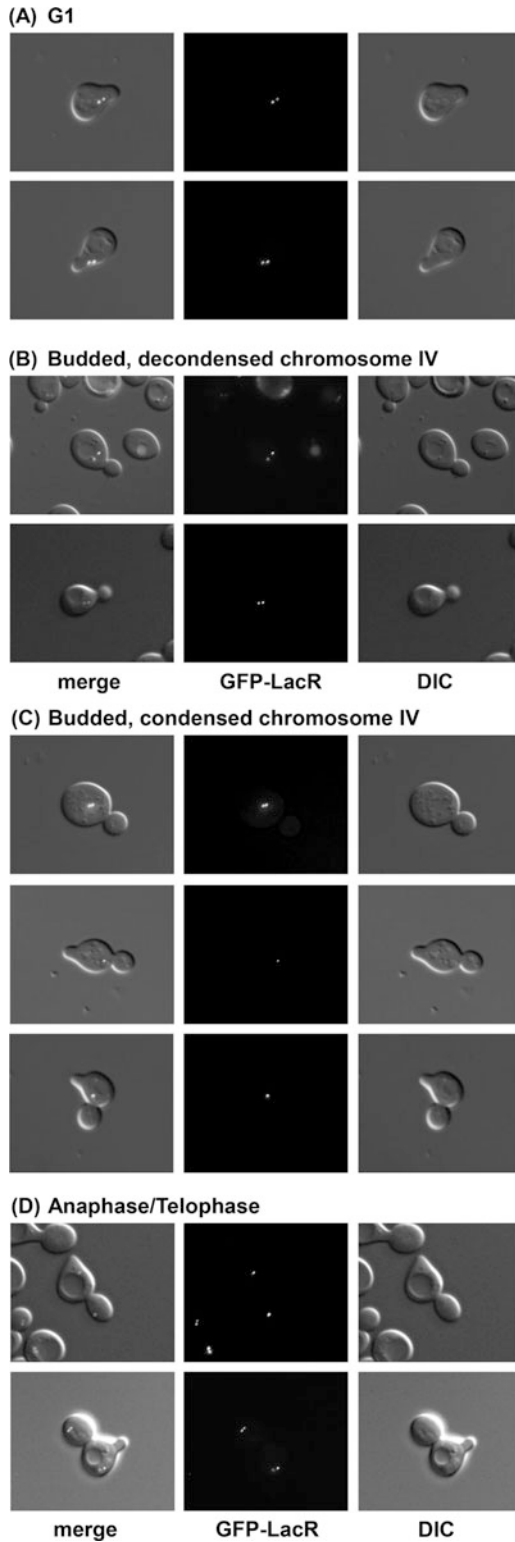


Fig. 11 Visualization of the linear compaction of the chromosome IV right arm. Yeast cells visualized using the DIC setting on the microscope as well as the green fluorescence channel to observe the GFP-LacR fusion protein in the “condensation strain” described in Subheading 1.4. (a) In G1 cells, the chromosome IV arm is

3. DCY2769: *MATa bar1Δ top2::top2-B44(KAN) ura3::HIS3:GFP-TUB1(URA3)*. This is a yeast strain, mating type **a**, that has the *bar1* locus deleted. The endogenous *TOP2* locus has been replaced with a recessive hypomorphic mutant allele of *TOP2* that causes activation of the Topo II Checkpoint at temperatures that are semipermissive for growth. This strain is temperature sensitive at 37 °C. This replacement is linked to resistance to Kanamycin [11].
4. DCY2299: *MATa bar1Δ top2-4 ura3::HIS3:GFP-TUB1(URA3)*. This is a yeast strain, mating type **a**, that has the *bar1* locus deleted. The endogenous *TOP2* locus has been replaced with an allele of *TOP2* that causes a chromosome condensation defect but does not cause activation of the Topo II Checkpoint. This allele is temperature sensitive at 30 °C [11].
5. ACY461: *MATa bar1Δ trp1::LacO(TRP1, LEU2) LYS4::LacO(LEU2) his3::GFP-LacI(HIS3)* [9]. This is the condensation strain described in Subheading 1.4.
6. ACY91: *MATa bar1Δ top2-4 trp1::LacO(TRP1, LEU2) LYS4::LacO(LEU2) his3::GFP-LacI(HIS3)* [9]. This is the condensation strain described in Subheading 1.4 and carries a temperature sensitive allele of *TOP2*.

2.2 Yeast Cell Growth and Synchronization

1. YPD: 2% glucose, 1% yeast extract, and 2% Bacto peptone in distilled H₂O. Autoclave and store the solution at room temperature.

←

Fig. 11 (continued) decondensed and thus two GFP foci are seen. If cells have not been arrested in α -factor, there is often only a single GFP focus visible in G1 cells. This is because round cells can lie in any orientation on the microscope slide and the two GFP foci can be vertically stacked, thus appearing as one dot or closely opposed dots. In α -factor arrested cells, the shmoo mating projection constrains the orientation in which the cells can lie on the slide and seems to cause the foci to more often appear next to each other rather than vertically stacked. The centers of the dots, which correspond to the *TRP1* and *LYS4* loci on the chromosome IV right arm, are separated by about 1.6 μ m. This corresponds to a distance of \sim 450 kb between *TRP1* and *LYS4*. **(b)** Budded cells with decondensed chromosomes: As the cells enter S-phase, a small bud appears. During this phase, the chromosome remains decondensed, indicated by two visible GFP foci. For the purposes of this assay, the chromosome arm is considered to be decondensed if the distance between the dots is greater than approximately 2–3 times the width of the GFP focus as seen under the fluorescent microscope. Care should be taken to focus up and down to search the entire cell for GFP foci as they may not appear in the same focal plane. **(c)** Budded cells with condensed chromosomes: As the cells enter G2/M, the bud continues to grow and the chromosomes condense. Cells are judged to have condensed chromosomes when the two GFP foci appear closely associated (less than about one GFP focus-width apart) or as a single focus. **(d)** Anaphase/Telophase cells: When cells enter anaphase/telophase, one pair of closely associated GFP foci (i.e., corresponding to one copy of the condensed chromosome IV) will move through the bud neck and appear in the daughter bud. The other pair of closely associated GFP foci segregates the extremity of the mother cell. The chromosomes often decondense rapidly once chromosome segregation has occurred

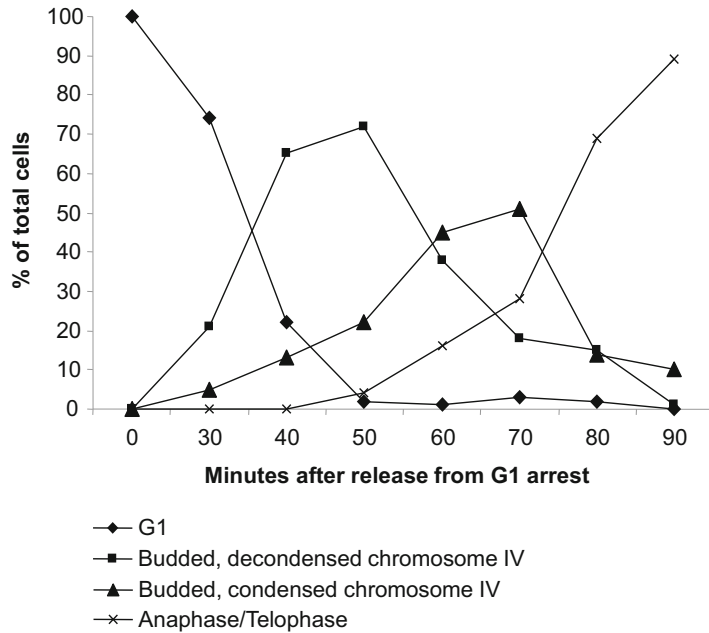


Fig. 12 A typical time course experiment in which chromosome condensation was monitored. To meaningfully relate chromosome condensation to cell cycle progression, the GFP-LacR condensation assay is coupled with analysis of budding, an indicator of entry into S-phase and therefore a useful cell cycle “landmark”. This is useful, as cells will not synchronously release from G1 if too much α -factor is used or if they are left in α -factor for longer than approximately 2½ h. In the graph shown, cells are considered to pass through the four states shown in Fig. 11. In a normal cell cycle following release from α -factor arrest, approximately 90% of cells are budded within 50–60 min (Fig. 11b). Chromosome condensation, indicated by the appearance of closely apposed GFP foci, or a single GFP focus (Fig. 11c), peaks at approximately 70 min. By 90 min, 90% of cells have completed anaphase (Fig. 11d). Because the period between chromosome condensation and the onset of anaphase is relatively short, the peak for the category in Fig. 11c is relatively low

- SD-Ura: 2% glucose, 0.67% yeast nitrogen base, 0.5% casamino acids, 0.005% adenine, and 0.005% tryptophan in distilled H₂O. Autoclave and store the solution at room temperature.
- SDC: 2% glucose, 0.67% yeast nitrogen base, 0.5% casamino acids, 0.005% adenine, 0.005% tryptophan, and 0.005% uracil in distilled H₂O. Autoclave and store the solution at room temperature.
- α -factor (mating pheromone peptide used for inducing G1 arrest in yeast): dissolve 1 mg/mL of α -factor peptide in distilled H₂O. Store aliquots at $-20\text{ }^{\circ}\text{C}$ (see Note 1).
- 100 \times adenine solution: 0.3 g of adenine in 100 mL of distilled H₂O. Autoclave and store the solution at room temperature.

2.3 FACSscan Analysis.

1. 50 mM Tris-HCl pH 8.0. Store at room temperature.
2. Sytox green (Molecular Probes): 1:1000 dilution of SYTOX Green stock solution (5 mM in DMSO; store at -20 °C) in 50 mM Tris-HCl pH 8.0. Make up the solution immediately before use.
3. Pepsin solution: 5 mg/mL of pepsin dissolved in acidified water. Make up the solution immediately before use add 45 μ L of concentrated HCl to 10 mL of distilled H₂O and then add 50 mg of pepsin.
4. 1 mg/mL of RNaseA in 50 mM Tris-HCl pH 8.0. Make up the solution immediately before use, boil it for 10 min to ensure the complete inactivation of contaminating DNase and then let it cool to room temperature.
5. 70% ethanol: store at -20 °C and transfer to ice before use.

2.4 Live Single-Cell Microscopy of Yeast

1. Fluorescence Microscope with a cooled CCD camera and fitted with an imaging chamber suitable for live cell microscopy of yeast cells (*see Note 2*).
2. Imaging analysis software: ImageJ (<https://fiji.sc/>).

3 Methods

3.1 Cell Culture and Synchronization for "Population Analysis" of Cell Cycle Progression

1. Grow cultures of *S. cerevisiae* overnight in 25 mL of SD-Ura containing 500 μ L of 100 \times adenine solution (*see Note 3*) at 30 °C in a conical flask in a shaking water bath (*see Note 4*). Aim for a late log phase culture that is near to reaching stationary phase, typically with an OD₆₀₀ of 2–5 (*see Note 5*).
2. To synchronize the cells, dilute the cultures to an OD₆₀₀ of 0.2 in 25 mL of YPD supplemented with α -factor solution (diluted in the range of 1:1000–1:5000 from the stock solution) and containing 500 μ L of 100 \times adenine solution (*see Note 6*). Grow the cells for 1.5–2.5 h at 30 °C in a shaking water bath (*see Note 7*).
3. Verify the completion of the G1 arrest as follows: take a 500 μ L aliquot of the culture, pellet the cells by centrifugation briefly at 14,000 $\times g$ in a microcentrifuge, resuspend the cells in 10 μ L of distilled H₂O and place on a microscope slide with a coverslip on top. Score G1 arrest according to the criteria described in Fig. 1.
4. When the G1 arrest is complete (ideally greater than 90%), pellet the entire culture by centrifugation at 3000 $\times g$ for 5 min.

5. Wash the α factor from the cells by resuspending two times in 1 mL of distilled H₂O and sedimenting by centrifugation briefly at $14,000 \times g$ in a microcentrifuge (*see Note 8*).
6. Release the cells from the synchrony by resuspending the pellet in 1 mL of YPD and inoculating this into 25 mL of prewarmed YPD in a conical flask in a shaking water bath (*see Note 8*).
7. Take samples at time-points every 10 min beginning at the time of the release from the synchrony by removing 1 mL of the culture into a 1.5 mL tube. Sediment the cells by brief centrifugation at $14,000 \times g$ in a microcentrifuge. Decant the supernatant.
8. Process the samples as described below for analysis by: fluorescence microscopy to assay spindle morphologies (Subheadings 3.2 and 3.2.1); fluorescence activated cell scanning to determine DNA content (Subheading 3.3); fluorescence microscopy to assay chromosome condensation (Subheadings 3.2 and 3.2.2).

3.2 Processing the Samples for Analysis by Fluorescence Microscopy

1. Wash each sample with 1 mL of water and sediment the cells by brief centrifugation at $14,000 \times g$ in a microcentrifuge. Decant the supernatant (*see Note 9*) and store the sample on ice if unable to visualize immediately (*see Notes 10 and 11*).
2. To prepare the samples on microscope slides for analysis, completely resuspend the sample in the remaining supernatant by pipetting up and down. Put 3 μ L of the resuspended sample on a microscope slide and place a coverslip over the sample on the slide (*see Note 12*).

3.2.1 Analysis of Spindle Morphologies

1. Score the cells into the following categories based on the analysis of spindle morphology and budding: G1, G2/M, Anaphase/Telophase. Images and descriptions of the morphological criteria are found in Figs. 1–8.
2. For each sample, count a total of 100–300 cells in triplicate. A graph of a typical time course is found in Fig. 9.

3.2.2 Analysis of Chromosome Condensation

1. Score the cells into the following categories based on the analysis of the fluorescent signals marking the *TRP1* and *LYS4* loci, as well as bud morphology: G1, S-phase and G2/M decondensed chromosome IV, S-phase and G2/M condensed chromosome IV, Anaphase/Telophase. Images and descriptions of the morphological criteria are found in Fig. 11.
2. For each sample, count a total of 100–300 cells in triplicate. A graph of a typical time course is found in Fig. 12.

**3.3 Fluorescence
Activated Cell
Scanning (FACScan)
Analysis of DNA
Content**

1. To process the samples for FACScan analysis, pellet the cells by centrifugation in a microcentrifuge at $14,000 \times g$ for 30 s.
2. Discard the liquid supernatant and add 1 mL of distilled H₂O to the 1.5 mL tube to resuspend the pellet and wash the cells by vortexing the sample for 3–5 s.
3. Centrifuge the sample for 30 s at $14,000 \times g$ to pellet the cells. Discard the supernatant.
4. Fix the cells by adding 1 mL of ice cold 70% ethanol to the pellet and vortexing the sample until any cell clumps are completely resuspended (*see Note 13*). Store the cells at 4 °C for a minimum of 12 h to ensure complete fixation prior to processing the cells further.
5. The day prior to the FACScan analysis of the samples, wash the fixed cells in Tris–HCl solution: First, pellet the cells by centrifugation in a microcentrifuge at $3000 \times g$ for 5 min. After discarding the ethanol add 1 mL of Tris–HCl solution to the cell pellet and vortex briefly to resuspend.
6. Treat the cells with RNase A to degrade RNA in the cells (preferably this is done at the end of the working day): Centrifuge the washed cells at $3000 \times g$ for 5 min and resuspend the pelleted cells in 200 µL of RNase A solution. Incubate the cells at 37 °C for 12 h.
7. Wash the cells with Tris–HCl solution: pellet the cells by centrifugation in a microcentrifuge at $3000 \times g$ for 5 min. After discarding the supernatant, resuspend the cells in 1 mL of Tris–HCl solution by vortexing.
8. Add 200 µL of pepsin solution to the cells from the previous step. Incubate the samples at 37 °C for 25–30 min (*see Note 14*).
9. Add 1 mL of Tris–HCl solution to the samples and centrifuge the samples in a microcentrifuge at $3000 \times g$ for 5 min. Discard the supernatant and resuspend the pelleted cells in 500 µL of Tris–HCl solution.
10. Stain the cellular DNA with SYTOX Green dye: First, label suitable FACScan analysis tubes and then aliquot 500 µL of the SYTOX Green solution into the tubes. Add 100 µL of processed cells to the FACScan analysis tubes and store the samples in the dark at 4 °C for 2 h (*see Note 15*).
11. Just prior to FACScan analysis of the samples, gently sonicate the cells for 2–5 s in order to disrupt any cell clumps in the sample (*see Note 16*).

**3.4 Live Single-Cell
Analysis of Cell Cycle
Progression.**

1. To prepare the *S. cerevisiae* strains for live cell microscopy [25], follow **steps 1–5** in Subheading 3.1 (*see Note 17*).

2. Release the cells from the synchrony by resuspending the pellet in 25 mL of SDC medium containing 500 μ L of 100 \times adenine solution.
3. Inoculate the cell suspension into the imaging chamber housed on the microscope stage (*see Note 18*).
4. Capture images at 2 min intervals (*see Note 19*) using the minimal exposure time needed to observe Tub1-GFP fluorescence (*see Note 20*) for 2–3 h (*see Note 21*).
5. To derive spindle length versus time information from the time lapse movies, measure the spindles at each movie time point using image analysis software such as ImageJ. Only analyze cells that traverse an entire cell cycle.
6. To yield a histogram plot of approximate average G2/M (metaphase) length, calculate the time interval from spindle pole separation to the onset of anaphase spindle elongation for each cell, and then average these values.
7. To yield a plot of average spindle length versus time, align the spindle length data for each single cell at the first time point where the spindle poles are separated. Then calculate the average spindle length between all the cells for each time point and plot this value against time (*see Fig. 10b*).

4 Notes

1. The volume of the aliquots should correspond to the typical amount used in each experiment so that the peptide is not thawed and refrozen, which would reduce activity.
2. Required capabilities of the microscope system include: a constant temperature chamber, such as a microfluidics system, capable of holding the yeast cells in a fixed position, heated microscope stage and objective or a microscope housed in a fully enclosed environmental chamber, highly sensitive cooled CCD camera, piezo stage capable of rapid and highly reproducible XYZ movements. In general, the system must be able to capture images with sufficient signal-to-noise to measure spindle lengths at exposure times that do not bleach the sample or cause phototoxicity. Exposure times should typically be in the range of not more than 5–10 ms.
3. Addition of the adenine reduces the background fluorescence.
4. 30 °C is the optimum growth temperature, but this should be adjusted if the strains being used are temperature sensitive.
5. In late log phase the proportion of cells in G1 will be increased and this will aid in synchronizing the cells upon the addition of mating pheromone. If the cells are over grown and have

become stationary, then the release from the synchrony will not be efficient and this will reduce the synchrony of cell cycle progression.

6. α -factor differs in its effectiveness between batches and vendors. It is useful to empirically determine an appropriate working concentration for each batch because it is an expensive reagent. Each batch should be titrated to obtain 90% G1 arrest within 2 h of yeast growth at 30 °C. If there is an insufficient α -factor concentration, the cells will not arrest during this time frame. If the concentration is too high, the cells will not release synchronously upon removal of the peptide. A minimum concentration of α factor present for a minimum amount of time will provide an optimally synchronous release. The concentration of α -factor and the time required for 90% arrest will vary according to each strain used. Typically, mutant strains require more time and higher concentrations of α -factor to achieve arrest. If more than 3.5 h is required to achieve the G1 arrest, then the cells rarely release synchronously.
7. α -factor treatment should arrest 85–100% of cells in G1. Do not leave cells in the α -factor for longer than 3.5 h as the cells will not release synchronously.
8. Water for washing the cells and the medium the cells will be released into should be prewarmed to the release temperature so that the cells release as quickly and as synchronously as possible. If the synchrony is performed at a low temperature and then release at high temperature is desired (for example when working with temperature sensitive mutants), care must be taken to avoid heat-shocking the cells which would result in G1 arrest at the START transition point. Two methods can be used to avoid heat-shocking: (1) after inoculating the cells into medium at the low temperature, allow the water bath to transition to the high temperature over a period of about 10 min; (2) inoculate the cells into medium at the low temperature, incubate with shaking for 10–15 min to allow the cells to pass the START transition then transfer the flask of cells to another water bath set at the high temperature.
9. When decanting, pour the supernatant off but leave a small amount of liquid, usually about 50–100 μ L.
10. Washing the cells decreases the background fluorescence.
11. Storing the samples on ice will prevent the cells from continuing through the cell cycle. However, long term storage on ice can lead to microtubule breakdown so it is preferable to visualize the spindle morphologies as quickly as possible. Alternatively, the cells can be fixed which will provide more time to perform the analysis. However, fixation reduces the fluorescence intensity of the GFP and can make the spindle

morphologies more difficult to characterize. If fixation is required, add a final concentration of 3.7% formaldehyde solution directly to the cells in medium, incubate at room temperature for 10 min then wash the cells with 1 mL of phosphate buffered saline.

12. The goal is to immobilize the cells between the glass surfaces. Performing the microscopy when the cells are moving across the slide surface is almost impossible. Several factors will lead to the cells moving: (1) if too large a sample volume is applied; (2) if the cells are too concentrated; (3) if the cells are not fully resuspended.
13. Store the 70% ethanol at -20°C and transfer to ice before use to achieve optimal fixation. Less variance within the sample (in the widths of the G1 and G2 peaks for DNA content) can be obtained by dripping the ethanol into the 1.5 mL tube while vortexing the sample to be fixed. The use of SYTOX Green rather than other DNA dyes such as propidium iodide also significantly reduces sample variance [26].
14. Do not treat the cells with pepsin for more than 30 min as this can result in increased sample variance.
15. Cells stained with SYTOX Green must be kept in the dark until analysis as the dye is sensitive to light.
16. Settings for the sonicator must be determined empirically to achieve an appropriate level of cell disruption. Too much disruption can cause cell breakage and too little disruption can leave clumps of cells. The amount of cell disruption required can also vary between yeast strains.
17. For live single-cell imaging, the synchrony step can be omitted. In this case, complete **step 1** of Subheading 3.1, then culture the cells to mid-log phase in SDC medium containing 500 μL of $100\times$ adenine solution, and then proceed to **step 3** of Subheading 3.4).
18. If the imaging temperature is different from the temperature used to culture and/or synchronize the cells, then heat-shock must be avoided so that the cells do not arrest in G1. In this case, place the 25 mL culture into a conical flask and shake in a water bath where the temperature gradually increases to the desired imaging temperature—about 15 min—then inoculate the cell suspension into the imaging chamber housed on the microscope stage.
19. This generally provides enough temporal resolution to detect the timing of spindle pole body separation and the moment of anaphase onset. If the imaging set up permits further temporal resolution without bleaching the GFP or causing the cells to

arrest due to UV phototoxicity, then it will be advantageous to decrease the time interval.

20. The exposure time must be minimized to prevent UV phototoxicity which will cause the cells to arrest and to prevent photobleaching of the GFP. However, it is also important to capture Z-stacks of images to ensure both ends of the spindle can be observed. Use of the CCD camera's binning function will be useful in this respect.
21. It is usually necessary to capture Z-stacks of fields of cells at several X-Y stage coordinates. This is to ensure enough single cells are imaged.

References

1. Porter AC, Farr CJ (2004) Topoisomerase II: untangling its contribution at the centromere. *Chromosome Res* 12:569–583
2. Warburton PE, Earnshaw WC (1997) Untangling the role of DNA topoisomerase II in mitotic chromosome structure and function. *Bioessays* 19:97–99
3. Holm C, Stearns T, Botstein D (1989) DNA topoisomerase II must act at mitosis to prevent nondisjunction and chromosome breakage. *Mol Cell Biol* 9:159–168
4. Uemura T, Ohkura H, Adachi Y, Morino K, Shiozaki K, Yanagida M (1987) DNA topoisomerase II is required for condensation and separation of mitotic chromosomes in *S. Pombe*. *Cell* 50:917–925
5. Adachi Y, Luke M, Laemmli UK (1991) Chromosome assembly in vitro: topoisomerase II is required for condensation. *Cell* 64:137–148
6. Wood ER, Earnshaw WC (1990) Mitotic chromatin condensation in vitro using somatic cell extracts and nuclei with variable levels of endogenous topoisomerase II. *J Cell Biol* 111:2839–2850
7. Roberge M, Th'ng J, Hamaguchi J, Bradbury EM (1990) The topoisomerase II inhibitor VM-26 induces marked changes in histone H1 kinase activity, histones H1 and H3 phosphorylation, and chromosome condensation in G2 phase and mitotic BHK cells. *J Cell Biol* 111:1753–1762
8. Newport J, Spann T (1987) Disassembly of the nucleus in mitotic extracts: membrane vesicularization, lamin disassembly, and chromosome condensation are independent processes. *Cell* 48:219–230
9. Vas AC, Andrews CA, Kirkland Matesky K, Clarke DJ (2007) In vivo analysis of chromosome condensation in *Saccharomyces Cerevisiae*. *Mol Biol Cell* 18:557–568
10. Clarke DJ, Vas AC, Andrews CA, Diaz-Martinez LA, Gimenez-Abian JF (2006) Topoisomerase II checkpoints: universal mechanisms that regulate mitosis. *Cell Cycle* 5:1925–1928
11. Andrews CA, Vas AC, Meier B, Gimenez-Abian JF, Diaz-Martinez LA, Green J, Erickson SL, Vanderwaal KE, Hsu WS, Clarke DJ (2006) A mitotic topoisomerase II checkpoint in budding yeast is required for genome stability but acts independently of Pds1/securin. *Genes Dev* 20:1162–1174
12. Skoufias DA, Lacroix FB, Andreassen PR, Wilson L, Margolis RL (2004) Inhibition of DNA decatenation, but not DNA damage, arrests cells at metaphase. *Mol Cell* 15:977–990
13. Mikhailov A, Shinohara M, Rieder CL (2004) Topoisomerase II and histone deacetylase inhibitors delay the G2/M transition by triggering the p38 MAPK checkpoint pathway. *J Cell Biol* 166:517–526
14. Gimenez-Abian JF, Weingartner M, Binarova P, Clarke DJ, Anthony RG, Calderini O, Heberle-Bors E, de la Moreno Diaz ES, Bogre L, De la Torre C (2002) A topoisomerase II-dependent checkpoint in G2-phase plant cells can be bypassed by ectopic expression of mitotic cyclin B2. *Cell Cycle* 1:187–192
15. Deming PB, Flores KG, Downes CS, Paules RS, Kaufmann WK (2002) ATR enforces the topoisomerase II-dependent G2 checkpoint through inhibition of Plk1 kinase. *J Biol Chem* 277:36832–36838
16. Deming PB, Cistulli CA, Zhao H, Graves PR, Piwnicka-Worms H, Paules RS, Downes CS, Kaufmann WK (2001) The human

- decatenation checkpoint. *Proc Natl Acad Sci U S A* 98:12044–12049
17. Downes CS, Clarke DJ, Mullinger AM, Giménez-Abián JF, Creighton AM, Johnson RT (1994) A topoisomerase II-dependent G2 cycle checkpoint in mammalian cells. *Nature* 372:467–470
 18. Goto T, Wang JC (1984) Yeast DNA topoisomerase II is encoded by a single-copy, essential gene. *Cell* 36:1073–1080
 19. Straight AF, Marshall WF, Sedat JW, Murray AW (1997) Mitosis in living budding yeast: anaphase a but no metaphase plate. *Science* 277:574–578
 20. Winey M, Mamay CL, O’Toole ET, Mastro-
narde DN, Giddings TH Jr, McDonald KL,
McIntosh JR (1995) Three-dimensional ultra-
structural analysis of the *Saccharomyces Cere-
visiae* mitotic spindle. *J Cell Biol* 129:1601–1615
 21. Pearson CG, Maddox PS, Salmon ED, Bloom
K (2001) Budding yeast chromosome struc-
ture and dynamics during mitosis. *J Cell Biol*
152:1255–1266
 22. Straight AF, Belmont AS, Robinett CC, Mur-
ray AW (1996) GFP tagging of budding yeast
chromosomes reveals that protein-protein
interactions can mediate sister chromatid cohe-
sion. *Curr Biol* 6:1599–1608
 23. Richardson HE, Wittenberg C, Cross FR,
Reed SI (1989) An essential G1 function for
cyclin-like proteins in yeast. *Cell*
59:1127–1133
 24. Clarke DJ, Segal M, Mondesert G, Reed SI
(1999) The Pds1 anaphase inhibitor and
Mec1 kinase define distinct checkpoints cou-
pling S phase with mitosis in budding yeast.
Curr Biol 9:365–368
 25. Furniss K, Tsai H-J, Byl JAW, Lane AB, Vas
AC, Hsu WS, Osheroff N, Clarke DJ (2013)
Direct monitoring of the strand passage reac-
tion of DNA topoisomerase II triggers check-
point activation. *PLoS Genetics* 9(10):
e1003832
 26. Haase SB, Reed SI (2002) Improved flow cyto-
metric analysis of the budding yeast cell cycle.
Cell Cycle 1:132–136

Chapter 17

Studying Topoisomerase 1-Mediated Damage at Genomic Ribonucleotides

Jessica S. Williams and Thomas A. Kunkel

Abstract

Ribonucleotides incorporated into DNA by the DNA polymerases can be incised by Topoisomerase 1 (Top1) to initiate removal of ribonucleotides from the genome. This Top1-dependent ribonucleotide removal has been demonstrated to result in multiple forms of genome instability in yeast. Here, we describe both quantitative and qualitative assays to identify mutations and other forms of DNA damage resulting from Top1-cleavage at unrepaired genomic ribonucleotides.

Key words DNA replication, Ribonucleotide excision repair, RNase H2, Topoisomerase 1, Replication stress, Mutagenesis, Genome instability

1 Introduction

Although DNA polymerases are proficient at excluding ribonucleotides from incorporation during DNA synthesis, this exclusion is imperfect. Consequently, ribonucleotides are stably incorporated into DNA during replication and, if not properly removed, can cause genome instability that includes mutations and DNA breaks (reviewed in [1]). Ribonucleotide Excision Repair (RER), initiated by cleavage at a ribonucleotide by RNase H2, is the major pathway by which ribonucleotides are removed from the genome [2, 3]. However, failure of RER through deletion or mutation of the genes encoding the subunits of yeast RNase H2 (RNH201, 202, 203) causes RNA-DNA damage phenotypes that are initiated when Topoisomerase 1 (Top1) incises the DNA containing a ribonucleotide [4–6]. When this nick occurs within a tandem repeat sequence, it can be converted into a short deletion [7–10]. Other forms of genome instability including cell cycle distribution defects,

Electronic supplementary material: The online version of this chapter (https://doi.org/10.1007/978-1-4939-7459-7_17) contains supplementary material, which is available to authorized users.

Marc Drolet (ed.), *DNA Topoisomerases: Methods and Protocols*, Methods in Molecular Biology, vol. 1703, https://doi.org/10.1007/978-1-4939-7459-7_17, © Springer Science+Business Media, LLC 2018

replication stress and genome integrity checkpoint activation are also observed following Top1-cleavage at genomic ribonucleotides [4, 5].

Studies of Top1-dependent mutagenesis and genome instability in yeast have been enabled by the use of wild type and variant forms of the DNA replicases (including M644G Pol ϵ , L612 M Pol δ and L868M Pol α) that have increased capacity for stable incorporation of ribonucleotides during synthesis [7, 11–13]. A combination of in vitro and in vivo analyses has provided evidence for ribonucleotide incorporation and removal by measuring alkali sensitivity of DNA, which is hydrolyzed at the site of a ribonucleotide in the presence of alkali. Methods to detect the strand-specific positions of ribonucleotides in RNase H2-deficient yeast strains at defined genomic locations [14] as well as across the genome [13, 15] have been published elsewhere. Cleavage at these unrepaired ribonucleotides by Top1 results in their removal, but removal is problematic due to the generation of unligatable DNA ends possessing a 5'-hydroxyl and 2'/3'-cyclic phosphate that cannot be directly ligated and require further processing for repair. This can result in a deletion mutation when the ribonucleotide is present in a repetitive DNA sequence. In an RNase H2-deficient yeast strain expressing the M644G Pol ϵ allele (*pol2-M644G*) with increased ribonucleotide incorporation during leading strand synthesis, ribonucleotide removal by Top1 is also accompanied by a defect in cell cycle progression, replication stress and checkpoint activation. Each of these phenotypes is reduced or alleviated by deletion of *TOP1*. In this chapter, we outline approaches that allow characterization of the negative biological phenotypes associated with cleavage at unrepaired genomic ribonucleotides by Top1.

2 Materials

2.1 Spontaneous Mutagenesis and Specificity Measurements

2.1.1 Yeast Media

1. YPDA broth. Add 20 g dextrose, 20 g Bacto peptone, 10 g Bacto yeast extract, and deionized water up to 1 L. Dissolve ingredients and autoclave for 30 min at 121 °C to sterilize. Once cooled, add 2 mL of 0.5% adenine sulfate solution that has been made up in deionized water and filter-sterilized (*see Note 1*).
2. YPDA agar. As for YPDA broth, but also add 20 g Bacto agar prior to autoclaving. Cool media to 60 °C before dispensing 30–35 mL into sterile petri plates.
3. Synthetic Complete (COM) agar plates. Add 1.3 g SC dropout powder [16], 1.7 g yeast nitrogen base without amino acids or $(\text{NH}_4)_2\text{SO}_4$, 5 g $(\text{NH}_4)_2\text{SO}_4$, 20 g dextrose, 20 g Bacto agar

and deionized water up to 1 L. Dissolve ingredients and autoclave for 30 min at 121 °C to sterilize.

4. 5-fluoroorotic acid monohydrate (5-FOA; US Biological F5050).
5. 5-FOA selection plates. Add 1.3 g SC-Ura dropout powder [16], 1.7 g yeast nitrogen base without amino acids or $(\text{NH}_4)_2\text{SO}_4$, 5 g $(\text{NH}_4)_2\text{SO}_4$, 20 g dextrose, 20 g Bacto agar, 25 mg uracil and dissolve components in 800 mL deionized H_2O (*see Note 2*). Autoclave for 15 min at 121 °C and cool to 56 °C. Using sterile technique, add 200 mL of a 0.5% 5-FOA solution that has been filter-sterilized. Mix well and dispense into sterile petri plates.

2.1.2 Overall Mutation Rate Determination

1. Yeast strains that have a chromosomal copy of the *URA3* mutation reporter gene.
2. Sterile 20 mL glass culture tubes (20 × 150 mm).
3. Roller drum for culture tube growth.
4. 30 °C incubator.
5. Centrifuge.
6. Sterile water.
7. Sterile 96-well plates.
8. 3 mm beads (Fisher 11-312A) sterilized by autoclaving.
9. Analysis spreadsheet (Worksheet 1).

2.1.3 Mutational Specificity

1. Sterile toothpicks.
2. Primers for amplification of *URA3*. Design a 5'-forward oligonucleotide and a 3'-reverse oligonucleotide (that is the reverse complement of your sequence) that anneal approximately 50–100 bp upstream or downstream of the *URA3* reporter gene in its genomic location (*see Note 3*).
3. SeqMan Pro analysis software (DNASTAR) or equivalent.

2.2 Analysis of Cell Cycle Distribution by Flow Cytometry

2.2.1 DNA Isolation and Staining

1. Spectrophotometer.
2. Sterile H_2O .
3. Microfuge.
4. 70% ethanol.
5. 1 M Tris-HCl, pH 8.0.
6. 50 mM Tris-HCl, pH 8.0.
7. 3 M Sodium acetate, pH 5.2.
8. 10 mM sodium acetate, pH 5.2: Add 33 μL of 3 M solution to 9.97 mL sterile water.
9. Boiling water bath.

10. RNase A, Type IIA from Bovine pancreas (Sigma R-5000).
11. RNase A digestion solution: First make a 10 mg/mL RNase A solution by adding 20 mg of RNase A to 2 mL of 10 mM sodium acetate, pH 5.2. This will be enough for 20 samples and can be scaled accordingly. Boil for 15 min, cool slowly to room temperature on the bench and add 200 μ L 1 M Tris-HCl, pH 8.0. Dilute RNase A to 1 mg/mL final concentration by adding 18 mL 50 mM Tris-HCl, pH 8.0.
12. Propidium iodide (Sigma P4170).
13. Propidium iodide staining buffer: 180 mM Tris base, 190 mM NaCl, pH adjusted to 7.5 with HCl.
14. Pepsin A (Sigma P-7012).
15. 37 °C heat block.
16. Pepsin digestion solution: 5 mL H₂O, 25 μ L concentrated HCl, 25 mg Pepsin A.
17. Propidium iodide staining solution. To 100 mL of the Tris/NaCl pH 7.5 solution add 1.42 g MgCl₂·6H₂O and 5 mg propidium iodide. Store protected from light at -20 °C and thaw immediately before use.

2.2.2 Sample Processing and Analysis

1. Sample tubes (Falcon 352058, 12 × 75 mm, 5 mL polystyrene round-bottom).
2. Branson Sonifier 450 sonicator (or equivalent).
3. LSR II Flow Cytometer equipped with FACSDiva software (BD Biosciences).
4. ModFit software (Verity Software House, Topsham, ME).
5. GraphPad Prism.

2.3 Spot Dilution Assay of Genotoxin Sensitivity

1. Hydroxyurea (HU; Sigma H8627).
2. 2 M HU stock solution: dissolve 3.8 g HU powder in 25 mL H₂O, filter-sterilize and store at -20 °C.
3. YPDA agar plates.
4. YPDA agar plates containing HU at different concentrations: after autoclaving medium, cool to 60 °C. Aliquot media and supplement with concentrations of HU between 10 and 200 mM before pouring.
5. Spectrophotometer.
6. Multichannel pipettes (P-20, P-200).
7. 96-well round bottom plates (Sarstedt 82.1582.001).
8. Replica pronger (Sigma, R2383) (*see Note 4*).

2.4 Immunoblotting to Detect Spontaneous Checkpoint Activation

2.4.1 Preparation of Whole Cell Extracts

1. Spectrophotometer.
2. Centrifuge.
3. Sterile H₂O.
4. Microfuge.
5. β -mercaptoethanol (β -ME).
6. 2 M sodium hydroxide (NaOH).
7. β -mercaptoethanol/NaOH solution: 1 mL 2 M NaOH +70 μ L β -ME.
8. Trichloroacetic acid (TCA; Sigma T0699).
9. Acetone.
10. Liquid nitrogen.
11. Screw-cap Eppendorf tubes.
12. 70 °C heat block.

2.4.2 Western Blotting for Rnr3

1. 4 \times NuPage LDS sample buffer (Life Technologies NP0007).
2. 1 \times NuPage LDS sample buffer: add 250 μ L of 4 \times sample buffer to 700 μ L H₂O, add 50 μ L β -ME.
3. Bechmark™ Prestained protein ladder (Life Technologies 10748-010).
4. 20 \times NuPage Transfer buffer (Life Technologies NP0006).
5. 1 \times NuPage Transfer buffer: dilute 20 \times in water.
6. 20 \times MES SDS Running buffer (Life Technologies NP0002).
7. 1 \times MES SDS Running buffer: dilute 20 \times in water.
8. Extra thick blot paper filter paper (Biorad 1703966).
9. Novex Nitrocellulose membrane filter paper sandwich, 0.45 μ M pore size (Life Technologies LC2001).
10. XCell Sure Lock Novex minicell gel and transfer apparatus (Life Technologies E10001).
11. 10 \times Tris-buffered saline, pH 7.5 (TBS): 100 mM Tris base, 150 mM NaCl.
12. Tween 20.
13. 1 \times TBST: dilute 10 \times TBS in water, add Tween 20 to a final concentration of 0.1%.
14. Bovine serum albumin (BSA, Sigma A3059).
15. WesternBright™ Sirius™ Chemiluminescent HRP substrate (Advansta; K-12043-D10).
16. Anti-Rnr3 antibody (rabbit; Agrisera AS09 574).
17. Mouse anti-rabbit secondary antibody HRP conjugate (Thermo Fisher 31464).

3 Methods

3.1 Measuring Spontaneous Mutagenesis and Specificity

3.1.1 Overall Mutation Rate Determination

The most striking biological phenotype caused by Top1 cleavage at ribonucleotides is the generation of short deletion mutations in repetitive DNA sequences. This has been determined, in yeast, by determination of spontaneous mutation rates and specificity in RNase H2-deficient strains and comparison with values determined for a *top1*Δ mutant. Mutation rate and specificity measurements can therefore be informative when testing mutant yeast strains hypothesized to have effects on ribonucleotide-dependent mutagenesis involving Top1. Here we describe a *URA3* forward mutation assay that allows determination of mutation rate by fluctuation analysis, as mutation of *URA3* confers resistance to the toxic uracil analog, 5-FOA. The fluctuation test of Luria and Delbruck (1943) is used to determine mutation rate by growing many replicate cultures over enough time for many of them to have experienced a mutation. Following plating on selective (5-FOA) and nonselective (COM) media and growth at 30 °C, colonies are counted to determine average population size and number of mutants. Mutation rate (μ) is the probability of a mutation per cell per division.

In setting up this type of experiment, there are a number of variables to consider, including the number of isolates, cultures, strains, and also growth conditions and how many plates will need to be counted. It is advisable that two or more independently generated isolates per genotype are tested for each strain (using a total of 12–24 cultures per strain). Test as many strains as possible on the same day using the same batch of liquid and solid medium.

1. Inoculate a single yeast colony from a YPDA agar plate into 5 mL YPDA broth (*see Note 5*). Grow at 30 °C for 36–48 h.
2. Centrifuge at 1750 × *g* for 5 min at 4 °C.
3. Pour off the supernatant and wash the cell pellet with 5 mL sterile H₂O.
4. Centrifuge at 2500 rpm for 5 min at 4 °C.
5. Pour off the supernatant and add 0.5 mL sterile H₂O. Vortex extensively to resuspend the pellet.
6. Prepare dilutions in 96-well plates for selection on COM and 5-FOA plates. Aim for 30–300 colonies per plate. For COM plates, plating 50–100 μL of a 1/1,600,000-fold dilution (1/160,000-fold final dilution because the cells were concentrated 10-fold when going from a 5 mL culture to 0.5 mL following the final H₂O wash) yields the desired number of colonies in our experiments. For 5-FOA plates, plating 100 μL straight from the culture tube is usually appropriate for a wild type strain or mutant that is anticipated to have a low spontaneous mutation rate. For mutants anticipated to have a higher

mutation rate, plating 100 μL of a 1/10 or 1/50 dilution may be required (*see* **Note 6**).

7. For each culture tube, plate directly or using the appropriate dilution onto both COM and 5-FOA plates. After mixing, add liquid and beads and shake until the plate surface is dry (*see* **Note 7**). Beads can then be poured off and discarded.
8. Incubate plates at 30 °C for 3–5 days before counting.
9. Count the visible colonies on each plate.
10. For mutation rate calculation, complete Worksheet 1 (attached). Data can be entered into any of the yellow cells. Any cell that is colored green should not be adjusted as these are the calculated output values.

Column A: Strain name.

Column B: Culture number.

Column C: V_{tot} is the volume of culture grown (mL).

Column D: C_{com} is the number of colonies counted on the COM plate.

Column E: V_{com} is the volume of culture plated (mL) on the COM plate.

Column F: D_{com} is the dilution factor used for COM plates. This number is 160,000 assuming a 5 mL culture was grown, resuspended in 0.5 mL H_2O after washing, and then a 1/1,600,000 dilution was plated.

Column G: C_{sel} is the number of colonies counted on the 5-FOA plate.

Column H: V_{sel} is the volume of culture plated (mL) on the 5-FOA plate.

Column I: D_{sel} is the dilution factor used for 5-FOA plates. This number is 0.1 if plating straight from the culture tube (with cell pellet resuspended in 0.5 mL H_2O). This number is 0.5 if plating a 1/5 dilution.

Column J: f is the mutant frequency.

Column K: μ_2 is the mutation rate.

11. Calculate the mutation rate (displayed as the median ($\times 10^{-7}$) and 95% confidence interval (CI) for each strain. The 95% confidence intervals (CI) are calculated as described [17].

3.1.2 Mutational Specificity

A forward mutation reporter system allows detection of any type of mutation that inactivates gene function. However, this requires sequencing of the entire 804 bp *URA3* gene in order to determine the spectrum of mutations. Specific mutation rates are calculated as the proportion of each type of event among the total mutants sequenced, multiplied by the overall mutation rate for each strain as calculated in Subheading 3.1.1.

Table 1
Mutation rates and sequencing data for the RNase H2-deficient yeast strains expressing the *URA3* reporter in orientation 2

<i>TOP1</i>	+	-	+	-
	<i>rnh201Δ</i>		<i>pol2-M644G rnh201Δ</i>	
Strain mutation rate ($\times 10^{-8}$)	4.2	2.1	72	11
95% CI	(2.1–6.5)	(1.1–2.9)	(50–98)	(6.5–17)
<i>ura3</i> mutants sequenced	273	141	138	182
Single base substitutions	89	71	8	70
Single base indels	14	16	7	34
Total 2–5 base deletions	96	0	123	2
Other ^a	13	6	0	7

^aOther includes mutations involving multiple bases (deletions of >5 bases, insertions of >1 base, duplications and complex mutations). All mutation rate data is from [4], as is the sequencing data for the *pol2-M644G rnh201Δ top1Δ* strain. Sequencing data for the *rnh201Δ* strain is from [18]. Sequencing data for the *pol2-M644G rnh201Δ* strain is from [7]

1. For a single 5-FOA-resistant colony from each plate, submit either the colony or purified genomic DNA for DNA sequencing.
2. Primers to use for PCR-amplification of *ura3* are: URA3-F and -R. These primers should flank the *URA3* reporter to allow for amplification of the entire gene. Ideally, the same primers can be used for sequencing.
3. Align sequences with the 804 bp reference *URA3* gene to identify mutations. (*see Note 8*).
4. Data can be displayed in table format (Table 1) and also presented as a mutation spectrum.
5. Calculate the specific mutation rates of mutation classes, including the rate of 2–5 bp deletions (Fig. 1). For example, if there were 96 2–5 bp deletion events out of 273 mutants sequenced and the overall mutation rate for this strain was 4.2×10^{-8} , then the specific mutation rate for 2–5 bp deletions is 1.5×10^{-8} .

3.2 Analysis of Cell Cycle Distribution by Flow Cytometry

Yeast strains containing a high density of leading strand ribonucleotides (for example, the *pol2-M644G rnh201Δ* mutant) grow slowly and have an altered cell cycle distribution profile. Cells accumulate in S and G₂/M phases as measured by flow cytometry analysis of DNA content in an asynchronous culture, and deletion of *TOP1* reduces the percentage of cells in G₂/M.

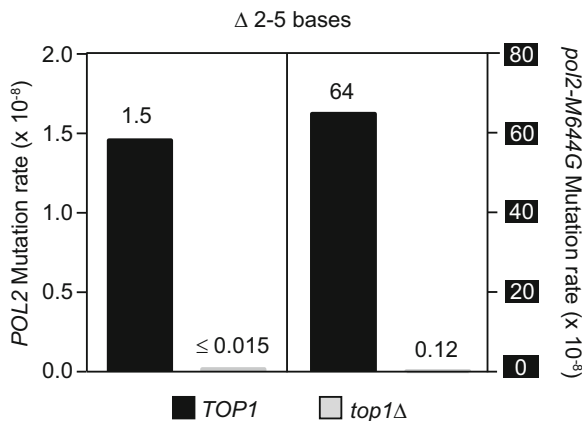


Fig. 1 The specific mutation rates for deletions of between 2 and 5 bases in size ($\Delta 2-5$ bases) are presented for strains expressing wild-type Pol ϵ (*POL2*) on the *left*, or the M644G Pol ϵ variant (*pol2-M644G*) with increased ribonucleotide incorporation propensity on the *right*. Values were calculated using *URA3* spontaneous mutation rate and sequencing data presented in Table 1 as the fraction of 2–5 base deletion events among the total mutants sequenced, multiplied by the overall mutation rate for each strain. All strains are deficient in RNase H2 (*rnh201Δ*)

3.2.1 DNA Isolation and Staining

1. Grow yeast in 5 mL of liquid culture to mid-log phase (OD₆₀₀ of 0.5–1.0).
2. Centrifuge the cells at 2500 rpm for 5 min at 4 °C and decant the liquid.
3. Resuspend the cell pellet in 500 μ L water and transfer to an Eppendorf tube.
4. Spin down in a microfuge for 2 min at full speed, aspirate the liquid.
5. Resuspend cells in 500 μ L 70% ethanol. Fix overnight at 4 °C (*see Note 9*).
6. The next day, recover the cells by centrifugation for 30 s at full speed in a microfuge.
7. Aspirate the supernatant and rehydrate cells by resuspending the pellet in 50 mM Tris–HCl (pH 8.0) by vortexing.
8. Pellet the cells, aspirate the supernatant and resuspend the cells in 1 mL of a *freshly made* RNase A digestion solution by vortexing.
9. Make sure that the cells are well-dispersed and incubate at 37 °C for at least 2 h. Mix by inversion approximately every 30 min. (*see Note 10*).
10. Recover the cells by centrifugation for 30 s in a microfuge at full-speed. Remove the RNase A digestion solution and resuspend the pellet in 200 μ L of Pepsin digestion solution.

11. Incubate the cells for 60 min at 37 °C, mixing every 15 min (*see Note 11*).
12. Spin down the cells for 30 s in a microfuge at full-speed and remove the Pepsin digestion solution.
13. Neutralize the samples by adding 1 mL 50 mM Tris–HCl (pH 8.0). Pellet the cells in a microfuge at full speed for 30 s, aspirate the supernatant and resuspend the pellet in 500 μ L propidium iodide staining solution by vortexing.
14. Stain the cells in the propidium iodide staining solution overnight at 4 °C in the dark (*see Note 12*).

3.2.2 Sample Processing and Analysis

1. Just prior to flow cytometry sample analysis, vortex the stained cells and remove 50 μ L of each sample and add it to 2.5 mL 50 mM Tris–HCl (pH 8.0) in a FACS sample tube.
2. Sonicate to break apart clumps using a Branson Sonifier (or equivalent), 20% duty cycle, output control of 3. Perform 20 quick pulses on each sample and then store on ice and protect from light until ready to process.
3. Flow cytometry can be performed using a LSR II Flow Cytometer and FACSDiva software (or equivalent). 10,000 individual cells per sample are selected by gating on a PI area versus width dot plot to exclude cell aggregates and cell debris. Cells are excited using a 488 nm argon laser and emission is detected at 585 nm. A PE setting of 715 can be used for most haploid yeast strains.
4. Cell cycle distribution profiles (using .fcs files) can be analyzed using ModFit software to determine the percentage of cells in G₁, S, and G₂/M phases of the cell cycle through integration of the area under the curve. Briefly, after opening the file, parameter = PE-A (area). Define gate 1 as PE-A (X) and PE-W (Y). Set the size of the rectangle to encompass the majority of data points. Use the Mod icon to turn off “autodebris and autoaggregates” and to move the G₁ and G₂ gates. Use the Fit icon to calculate numbers for percentage of cells in each cell cycle stage. The reduced chi-square (RCS) value should ideally be between 0.9 and 3 using these settings.
5. Save each analyzed file as a .mfl file and print/save as a .pdf file.
6. Histograms that are representative of at least three independent experiments can be displayed (Fig. 2). Quantitative analysis of cell cycle distribution can be plotted by calculating the percentage of cells in G₁, S, and G₂/M phases based on DNA content for each of the indicated strains. Data can be displayed as the mean percentage of cells \pm standard deviation. A two-tailed Student’s *t* test can be performed using GraphPad Prism to test whether differences between strains are statistically significant.

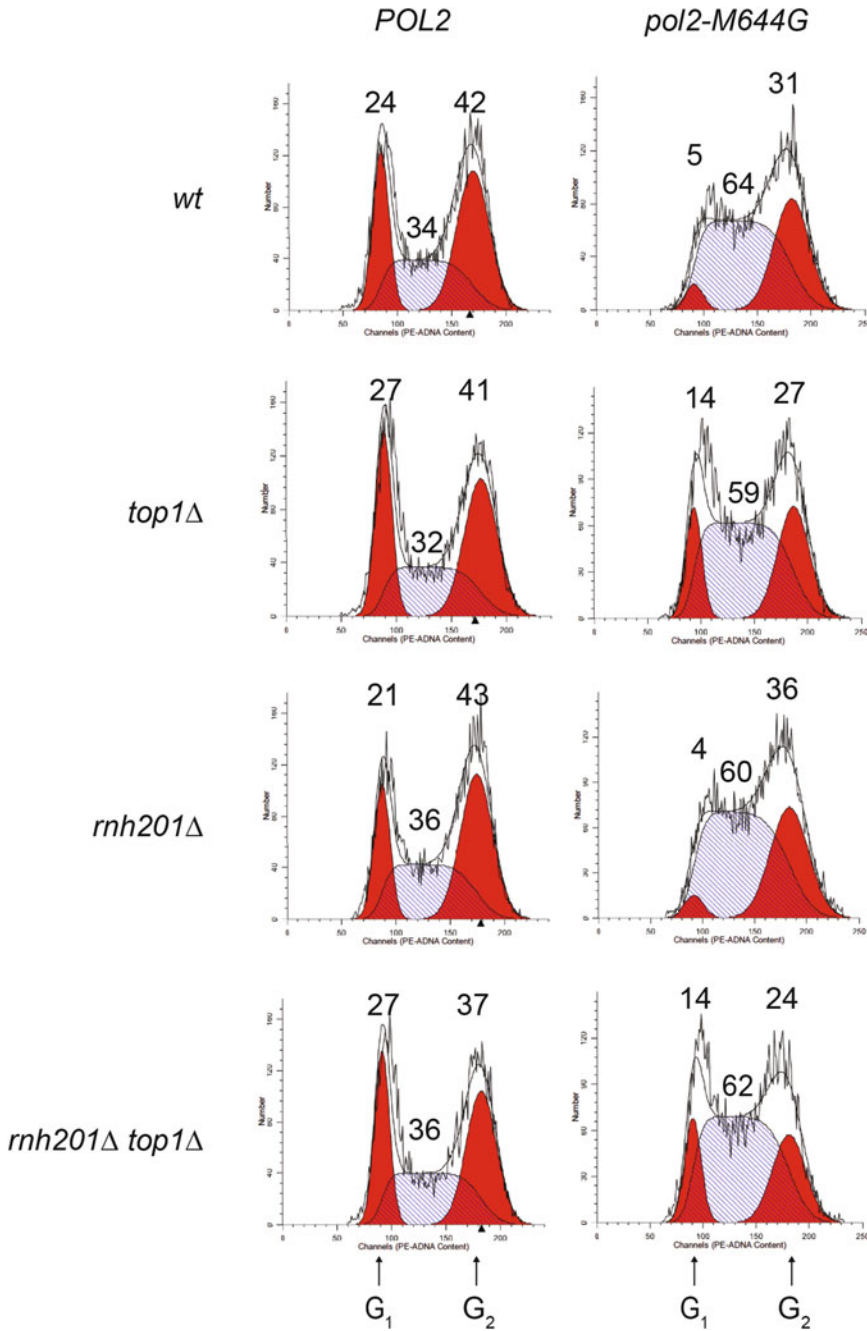


Fig. 2 Flow cytometry analysis of DNA content in each strain is displayed as a histogram, where the horizontal axis represents the fluorescence parameter and the vertical axis represents the number of cells. *Plotted black lines* represent the raw data and the smoothed data generated by ModFit software analysis. The *red shaded areas* represent cells in G₁ or G₂/M phases and the striped area represents cells in S phase. G₁ and G₂ peaks are indicated, with % of cells for each indicated above the appropriate peak. The middle number (in a lower position) is the % of cells in S phase for each strain

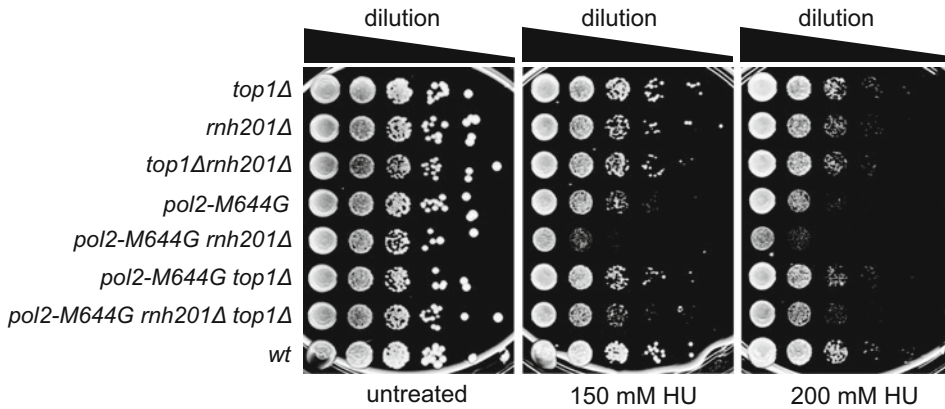


Fig. 3 Tenfold serial dilutions of exponentially growing cells from the indicated strains were grown on YPDA (untreated) or on YPDA plates containing 150 mM or 200 mM hydroxyurea (HU). Plates were incubated at 30 °C for 3 days and photographed. The *pol2-M644G rnh201Δ* mutant displays HU-sensitivity that is largely dependent on Top1 as it is reduced in the *pol2-M644G rnh201Δ top1Δ* strain

3.3 Spot Dilution Assay of Genotoxin Sensitivity

Replication stress resulting from Top1-cleavage at unrepaired ribonucleotides can be measured qualitatively by plating yeast cells onto medium containing the replication fork-stalling agent, HU. Sensitivity to HU can be reflective of replication stress (Fig. 3), including genome instability caused by Top1-cleavage at unrepaired ribonucleotides in a *pol2-M644G rnh201Δ* strain.

1. Grow yeast in 5 mL of YPD liquid medium to mid-log phase (OD_{600} 0.3–0.8). (see **Note 13**).
2. After measuring the OD_{600} of each strain, normalize the OD_{600} for each strain so that the left-most column (Column 1) has the equivalent of an OD_{600} of 0.6 in a volume of 200 μ L (see **Note 14**). For example, if your strain culture has an OD_{600} of 0.8, you would divide 0.6/0.8 and then multiply by 200 (as 200 μ L is the total volume in each well) resulting in a value of 150 μ L of culture added to 50 μ L of water.
3. Dilutions can be set up in a 96-well round bottom plate. The strains are organized vertically (by row). Dilutions are organized horizontally (by column). Each well will have a total volume of 200 μ L. Dilutions are made with sterile water, and 180 μ L of water can be added to each well in Columns 2–6.
4. After column 1 is set up for each of your strains, use a multi-channel pipette to move 20 μ L from column 1 into column 2, mix 20 times pipetting up and down, then 20 μ L into column 3, etc. (see **Note 15**). Do this until you have made dilutions for all 6 columns.
5. Sterilize the metal replicator by dipping the prongs into 100% ethanol, briefly touching this to a Bunsen burner flame, and

then letting the ethanol burn off. Alternatively, you can sterilize without ethanol by flaming the replicator prongs until the replicator is too hot to touch and setting it down, prongs up, on your bench to cool.

6. Once cooled, dip the prongs into your 96-well plate containing dilutions. Dip up and down and shake side to side being careful not to splash liquid across wells. Once liquid has been picked up and can be seen on each prong, lower the replicator onto your agar plate. (*see Note 16*).
7. After letting the replicator sit on the plate for approximately 10–20 s, pull it up slowly using one uniform motion.
8. Repeat **steps 6** and **7** for each test plate (*see Note 17*).
9. Once spots have dried, incubate plates at the desired temperature and scan after 2–7 days of growth (Fig. 3).
10. Sterilize the replicator.

3.4 Immunoblotting to Detect Spontaneous Checkpoint Activation

Top1-cleavage at ribonucleotides causes slow growth and accumulation of cells in the G₂/M phase of the cell cycle in an RNase H2-deficient *pol2-M644G* strain [4, 5]. This suggests activation of a cell cycle checkpoint, a phenotype that can be measured by monitoring the protein level of Rnr3, a subunit of the Ribonucleotide reductase enzyme responsible for biosynthesis of all four dNTPs. The genome integrity checkpoint is a conserved pathway that can be activated by endogenous replication stress caused by Top1-cleavage at ribonucleotides.

3.4.1 Whole Cell Extract Preparation

1. Grow 20 mL of cells in YPDA at 30 °C to mid-log phase. Include a wild-type (or other checkpoint-proficient) strain that has been grown to early/mid-log phase and treated with 200 mM HU for 3 h. This will serve as a positive control.
2. Measure the OD₆₀₀ of each culture and spin down the volume of cells equivalent to 10 mL of cells at OD₆₀₀ 0.5 for each for 5 min at 2500 rpm at 4 °C.
3. Pour off supernatant and resuspend cell pellet in 0.5 mL water by vortexing. Move the samples to screw-cap Eppendorf tubes.
4. Microfuge for 30 s at full speed.
5. Aspirate supernatant and flash-freeze the cell pellet by dropping the tube into liquid nitrogen. Store at –80 °C.
6. When ready to make cell extracts, thaw tubes briefly on ice and resuspend cells in 0.5 mL water by vortexing.
7. Add 70 µL fresh β-mercaptoethanol/NaOH solution, vortex.
8. Incubate on ice for 10 min.
9. Add 175 µL of 100% TCA and mix by inversion (DO NOT vortex).

10. Incubate on ice for 10 min.
11. Spin in a microfuge for 10 min at full speed.
12. Aspirate supernatant and wash the pellet twice with 500 μ L acetone.
13. Air dry pellet at room temperature on the bench for at least 10 min.
14. Resuspend pellet in 100 μ L 1 \times NuPage LDS sample buffer (containing β -ME).
15. Vortex extensively and incubate for 10 min at 70 $^{\circ}$ C (*see Note 18*).
16. Vigorously resuspend the insoluble pellet with your pipette tip and incubate for another 10 min at 70 $^{\circ}$ C.
17. Vortex samples, spin down in a microfuge at full speed for 2 min.

3.4.2 Western Blotting for Rnr3

1. Run 20 μ L of the aqueous phase per lane on a 10% Bis-Tris gel for 1.5 h at 150 V. Include a protein standard with size markers that encompass the size of Rnr3 (97 kDa). Include the sample treated with 200 mM HU for 3 h as the positive control.
2. Transfer protein to a nitrocellulose membrane using the Invitrogen XCell Sure Lock Novex minicell gel and transfer apparatus. Transfer at 25 V for 2 h at room temperature.
3. Disassemble transfer stack, perform 7 quick rinses with 1 \times TBST.
4. Block for 1 h at room temperature in 4% BSA/1 \times TBST with agitation.
5. Incubate in the primary antibody at a dilution of 1:1000 overnight at 4 $^{\circ}$ C with agitation (in 4% BSA/1 \times TBST).
6. Decant the antibody solution, wash blot 3 times for 10 min each in 1 \times TBST at room temperature with agitation.
7. Incubate in secondary antibody (mouse anti-rabbit HRP conjugate) at a dilution of 1:5000 at room temperature for 1 h with agitation (in 4% milk in 1 \times TBST).
8. Decant, wash blot 3 times for 10 min each in 1 \times TBST at room temperature with agitation.
9. Develop using WesternBright Sirius kit by mixing components 1 and 2 in a 1:1 ratio in a total volume of 5–10 mL. Add to the blot and allow 2 min for it to react.
10. Drain excess reagent by blotting the edge on a paper towel.
11. Cover damp blot with plastic wrap.
12. Image with a CCD camera or by exposure to X-ray film.

4 Notes

1. Adenine only needs to be included in the medium if strains being used are adenine auxotrophs.
2. Do not adjust the pH, 5-FOA efficiency is optimal at low pH.
3. The oligonucleotides that we use for PCR amplification and sequencing of the *URA3* reporter located adjacent to the ARS306 origin of replication are the following: URA3-F: 5'-CGCATATGTGGTGTGAAGAA; URA3-R: 5'-TGTGAGTTTAGTATACATGCA.
4. Ensure that round-bottomed 96-well plates are used. This is necessary in order to consistently pick up liquid on the prongs of the metal replicator.
5. If the strains are adenine auxotrophs, add an additional 100 mg adenine powder per 400 mL YPDA before dispensing into culture tubes for growth. This will ensure that the cultures do not turn pink during growth. A pink or red color is a toxic byproduct of the adenine biosynthesis pathway.
6. When working with mutant strains for the first time, it is useful to perform a pilot experiment with a small number of cultures (between 2 and 4 for each genotype) in order to test which dilutions will be appropriate in order to recover between 30 and 300 colonies on a plate. This should be done for the 5-FOA plates, and is often helpful to test for the COM plates also.
7. Sterile 3 mm beads can be added to each petri plate before the liquid culture is added. Plates can be stacked and shaken at the same time.
8. Not every 5-FOA-resistant mutant will have a mutation in *URA3*, as resistance may also result from epigenetic silencing, they may contain sequence changes in the promoter or 3' untranslated region of *URA3* or they may contain mutations in other genes that confer resistance to 5-FOA. Because these mutants contribute to the overall mutation rate, they are included in the calculation of rates for individual mutation classes.
9. The cells may be stored this way for several weeks at 4 °C. They should be fixed at least overnight.
10. This incubation can go 4–6 h.
11. Do not incubate longer than 60 min.
12. These samples are stable for several weeks when stored at 4 °C in the dark.
13. OD₆₀₀ measurement can be used as an approximate measurement of cell density for many yeast strains. In situations where

cell size and morphology may be very different among strains being compared, a more accurate cell count using a hemocytometer should be performed.

14. If not all of your strains have grown to an OD₆₀₀ of 0.6, just normalize the OD₆₀₀ to be used in column 1 to the OD₆₀₀ of the slowest growing strain. You may then want to use fivefold dilutions instead of tenfold dilutions in this case.
15. One option is to exchange pipet tips when moving from well-to-well in order to avoid transferring excess cells.
16. Make sure your plates are relatively dry, as you'll want to have your spots dried into the plates before incubation at 30 °C.
17. There is no need to sterilize the replicator when picking up a new set of spots as the replicator prongs are being lowered into the same well each time.
18. If the sample turns yellow due to acidity, add 2 μL of 2 M NaOH.

Acknowledgments

We thank Mercedes Arana and Salahuddin Syed for thoughtful comments on the manuscript, and all Kunkel lab members for helpful discussions. This work was supported by Project Z01 ES065070 to T.A.K. from the Division of Intramural Research of the National Institutes of Health (NIH), National Institute of Environmental Health Sciences (NIEHS).

References

1. Williams JS, Lujan SA, Kunkel TA (2016) Processing ribonucleotides incorporated during eukaryotic DNA replication. *Nat Rev Mol Cell Biol* 17(6):350–363. <https://doi.org/10.1038/nrm.2016.37>
2. Rydberg B, Game J (2002) Excision of misincorporated ribonucleotides in DNA by RNase H (type 2) and FEN-1 in cell-free extracts. *Proc Natl Acad Sci U S A* 99(26):16654–16659. <https://doi.org/10.1073/pnas.262591699>
3. Sparks JL, Chon H, Cerritelli SM, Kunkel TA, Johansson E, Crouch RJ, Burgers PM (2012) RNase H2-initiated ribonucleotide excision repair. *Mol Cell* 47(6):980–986. <https://doi.org/10.1016/j.molcel.2012.06.035>
4. Williams JS, Smith DJ, Marjavaara L, Lujan SA, Chabes A, Kunkel TA (2013) Topoisomerase I-mediated removal of ribonucleotides from nascent leading-strand DNA. *Mol Cell* 49(5):1010–1015. <https://doi.org/10.1016/j.molcel.2012.12.021>
5. Williams JS, Clausen AR, Lujan SA, Marjavaara L, Clark AB, Burgers PM, Chabes A, Kunkel TA (2015) Evidence that processing of ribonucleotides in DNA by topoisomerase I is leading-strand specific. *Nat Struct Mol Biol* 22(4):291–297. <https://doi.org/10.1038/nsmb.2989>
6. Potenski CJ, Niu H, Sung P, Klein HL (2014) Avoidance of ribonucleotide-induced mutations by RNase H2 and Srs2-Exo1 mechanisms. *Nature* 511(7508):251–254. <https://doi.org/10.1038/nature13292>
7. Nick McElhinny SA, Kumar D, Clark AB, Watt DL, Watts BE, Lundstrom EB, Johansson E, Chabes A, Kunkel TA (2010) Genome instability due to ribonucleotide incorporation into DNA. *Nat Chem Biol* 6(10):774–781. <https://doi.org/10.1038/nchembio.424>

8. Kim N, Huang SN, Williams JS, Li YC, Clark AB, Cho JE, Kunkel TA, Pommier Y, Jinks-Robertson S (2011) Mutagenic processing of ribonucleotides in DNA by yeast topoisomerase I. *Science* 332(6037):1561–1564. <https://doi.org/10.1126/science.1205016>
9. Sparks JL, Burgers PM (2015) Error-free and mutagenic processing of topoisomerase I-provoked damage at genomic ribonucleotides. *EMBO J* 34(9):1259–1269. [10.15252/embj.201490868](https://doi.org/10.15252/embj.201490868)
10. Huang SY, Ghosh S, Pommier Y (2015) Topoisomerase I alone is sufficient to produce short DNA deletions and can also reverse nicks at ribonucleotide sites. *J Biol Chem* 290(22):14068–14076. <https://doi.org/10.1074/jbc.M115.653345>
11. Lujan SA, Williams JS, Pursell ZF, Abdulovic-Cui AA, Clark AB, Nick McElhinny SA, Kunkel TA (2012) Mismatch repair balances leading and lagging strand DNA replication fidelity. *PLoS Genet* 8(10):e1003016. <https://doi.org/10.1371/journal.pgen.1003016>
12. Lujan SA, Williams JS, Clausen AR, Clark AB, Kunkel TA (2013) Ribonucleotides are signals for mismatch repair of leading-strand replication errors. *Mol Cell* 50(3):437–443. <https://doi.org/10.1016/j.molcel.2013.03.017>
13. Clausen AR, Lujan SA, Burkholder AB, Orebaugh CD, Williams JS, Clausen MF, Malc EP, Mieczkowski PA, Fargo DC, Smith DJ, Kunkel TA (2015) Tracking replication enzymology in vivo by genome-wide mapping of ribonucleotide incorporation. *Nat Struct Mol Biol* 22(3):185–191. <https://doi.org/10.1038/nsmb.2957>
14. Clausen AR, Williams JS, Kunkel TA (2015) Measuring ribonucleotide incorporation into DNA in vitro and in vivo. *Methods Mol Biol* 1300:123–139. https://doi.org/10.1007/978-1-4939-2596-4_9
15. Orebaugh CD, Lujan SA, Burkholder AB, Clausen AR, Kunkel TA (2017) Mapping ribonucleotides incorporated into DNA by hydrolytic end-sequencing. *Methods Mol Biol* 1672:329–345. https://doi.org/10.1007/978-1-4939-7306-4_23
16. Treco DA, Lundblad V (2001) Preparation of yeast media. *Curr Protoc Mol Biol* Chapter 13: Unit 13 11. <https://doi.org/10.1002/0471142727.mb1301s23>
17. Shcherbakova PV, Kunkel TA (1999) Mutator phenotypes conferred by MLH1 overexpression and by heterozygosity for mlh1 mutations. *Mol Cell Biol* 19(4):3177–3183
18. Clark AB, Lujan SA, Kissling GE, Kunkel TA (2011) Mismatch repair-independent tandem repeat sequence instability resulting from ribonucleotide incorporation by DNA polymerase epsilon. *DNA Repair (Amst)* 10(5):476–482. <https://doi.org/10.1016/j.dnarep.2011.02.001>

A Fluorescence-Based Assay for Identification of Bacterial Topoisomerase I Poisons

Thirunavukkarasu Annamalai, Bokun Cheng, Neelam Keswani,
and Yuk-Ching Tse-Dinh

Abstract

Bacterial Topoisomerase I is a potential target for the identification of novel topoisomerase poison inhibitors that could provide leads for a new class of antibacterial compounds. Here we describe in detail a fluorescence-based cleavage assay that is successfully used in HTS for the discovery of bacterial topoisomerase I poisons.

Key words Bacterial topoisomerase I, Topoisomerase I poisons, Fluorescence-based assay, High-throughput screening

1 Introduction

Topoisomerases are enzymes that play an important role in maintaining the structure and integrity of genome by relieving the topological stress on the DNA during cellular processes such as DNA replication, transcription, and repair [1, 2]. Topoisomerases may utilize different mechanisms to relieve the topological stress on DNA, but they all share one common intermediate step: transient cleavage of DNA through an active site tyrosine [3, 4]. Stabilization or trapping of this transient cleavage complex between DNA and the topoisomerase enzyme is lethal to cells and is of immense therapeutic value. Inhibitors that can cause cell death by trapping the covalent intermediate after DNA cleavage by topoisomerases are known as topoisomerase poison inhibitors [3, 5]. Many anti-cancer (including camptothecin derivatives targeting type IB human topoisomerase I and etoposide targeting type IIA human topoisomerase II) and antibacterial (fluoroquinolones targeting type IIA gyrase and topoisomerase IV) drugs are prominent examples of topoisomerase poisons [3, 6] (Chapter 3, this book).

Bacterial topoisomerase I, a type IA topoisomerase, is present in all bacteria [7, 8] and regulates DNA topology by cleaving and rejoining single stranded DNA. Similar to type IB and type IIA topoisomerases, bacterial topoisomerase I could be a potential target for a poison drug capable of trapping the transient cleavage complex between the single-stranded DNA and the topoisomerase enzyme [3, 9, 10]. Our lab has validated this concept in several studies wherein, bacterial topoisomerase I mutants deficient in DNA rejoining have been utilized to trigger the cell death pathway in *Escherichia coli* similar to that of a quinolone induced bactericidal pathway [5, 11–14]. Nonetheless, discovery of a topoisomerase poison with stringent specificity toward bacterial topoisomerase I remains elusive. Here, we describe a protocol for a fluorescence based HTS (high-throughput screening) assay we have developed as a part of our ongoing pursuit of bacterial topoisomerase I poisons.

1.1 Overview of the Assay

This assay employs a single-stranded oligonucleotide substrate (30–40 bases long) that forms a stem-loop structure with a fluorophore and a quencher at the 5' and 3' stem end respectively (Fig. 1). The single-stranded loop that connects both the stem ends is designed to include the preferred cleavage site(s) of the

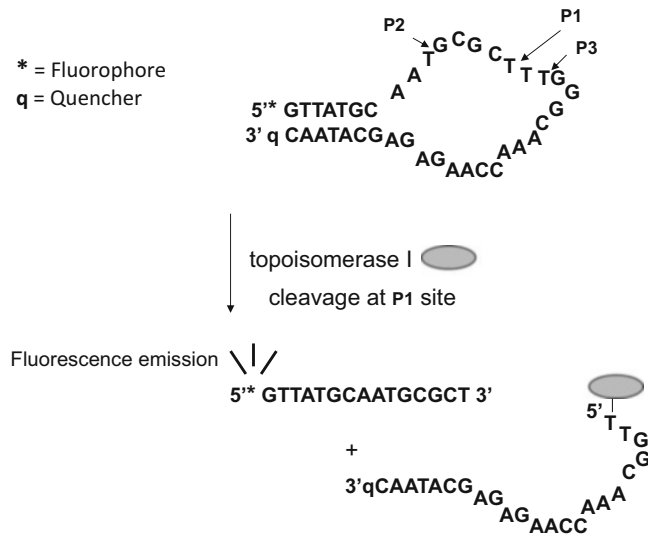


Fig. 1 Scheme of fluorescence assay to identify compounds that can increase the level of DNA cleavage product from bacterial topoisomerase I due to increase in fluorescence emission from fluorophore. The structure shown for a substrate used for *E. coli* and *Y. pestis* topoisomerase I is predicted by mfold, with constraints for the first and last bases be paired to quench the emission from the fluorophore, and the cleavage sites P1, P2, P3 be in single-stranded region of the structure (Reproduced from [22] by open access license)

bacterial topoisomerase I that is going to be targeted in this assay. In the absence of bacterial topoisomerase I, fluorescence signal is quenched due to base pairing in the short stem of the structure. The substrate alone in solution yields very low fluorescence. A cleavage in the loop region by bacterial topoisomerase I destabilizes the stem-loop conformation and a small increase in fluorescence is observed. In the presence of poison inhibitors that are capable of increasing the cleavage product, fluorescence signal further increases. Potential hits in the screening assay are scored by picking compounds that show an increase in fluorescence in comparison to the background of DMSO (negative control) that does not contain any compound.

1.2 Choice of Fluorophore

Fluorophore reporter at the 5' end of the oligo should have excitation/emission maxima in the longer wavelength in the red color range such as CAL Fluor Red 610 which can be paired with quencher BHQ-2. At longer wavelengths, the interferences of the drug like library compounds are minimal, since they exhibit autofluorescence or absorption usually only at shorter wavelengths [15, 16]. This helps in decreasing the number of false positives hits.

1.3 Oligonucleotide Substrate Design

In general, the oligonucleotide substrate is designed along the general guidelines of a molecular beacon (forming a hairpin structure) with a stem of around 5–7 bp and melting temperature around 50–60°C [17]. Loop regions range from 18–28 bases and should be designed to include one or more sequences that are preferred cleavage sites of the bacterial topoisomerases I for which the poison inhibitor is sought after [18, 19]. All bacterial topoisomerase I cleavage sites examined so far have a cytosine base 4 bases upstream of the cleavage site, but the different bacterial topoisomerase I can vary in cleavage products formed at individual cleavage sites [18]. Secondary hairpin structure of the oligonucleotide can be predicted by using software programs such as mfold before the actual synthesis [20].

1.4 Substrate Stability

Once the oligonucleotide substrate is synthesized, it is imperative to check experimentally if the fluorescence signal is minimal and stable at the closed (quenched) position; and also if there is an increase when the stem loop structure is perturbed, mimicking the increase in cleaved oligo by bacterial topoisomerase I poison. High temperature melts the secondary structures of the substrate DNA and causes an increase in fluorescence signal. Thermal melt profiles (Fig. 2) of three substrates with sequence differences in the stem region are shown here as an example. All of the substrates have the same loop region, which includes a preferred cutting site for *Mycobacterium tuberculosis* topoisomerase I [18]. Thermal melt profiles help in the selection of optimal substrates that form a stable secondary structure with minimal sacrifice in highest fluorescence signal increase.

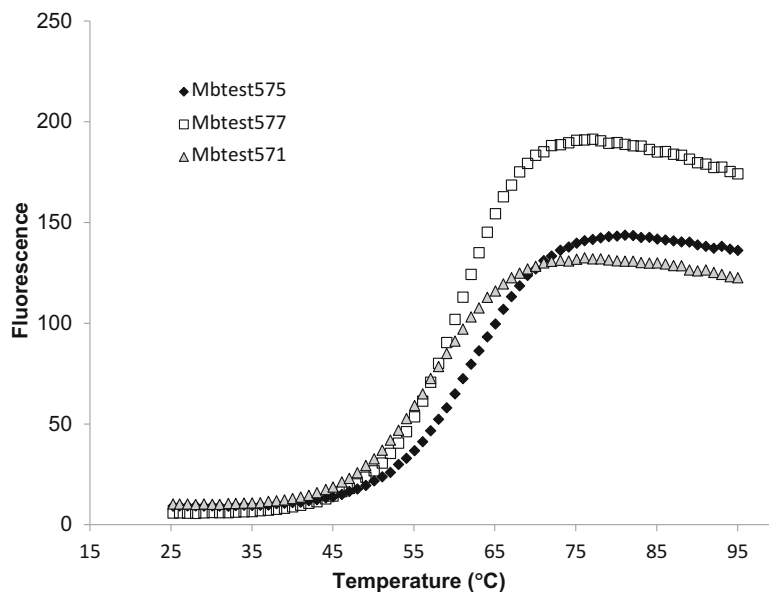


Fig. 2 Thermal melt profile of fluorescent oligonucleotide substrates. Three substrates designed for *M. tuberculosis* topoisomerase I, Mbtest571 (5'-CTTATGCAGT↓GTGATTTGGGATAATTAAGAGAGCATAAG-3'), Mbtest575 (5'-CCTATGCAGT↓GTGATTTGGGATAATTAAGAGAGCATAGG-3'), and Mbtest577 (5'-CTTTATGCAGT↓GTGATTTGGGATAATTAAGAGAGCATAAAG-3'), at a concentration of 100 nM in a buffer (10 mM Tris, pH 8.0) containing 0.5 mM MgCl₂ are subjected to thermal melt (25–95 °C) in a fluorescence spectrophotometer (Cary Eclipse, Varian)

1.5 Setting Up and Validation of HTS Assay

Robustness and sensitivity of a HTS screening assay is validated using a well-known statistic called as Z-factor [21]. Z-factor determination requires a good positive control that can result in a topoisomerase I specific signal increase. NSC28086, a positive control compound identified in a pilot screen of NCI diversity set I, is successfully utilized in several of our HTS regimens involving *Yersinia pestis* bacterial topoisomerase I to achieve a Z' factor of 0.7–0.8 [22, 23]. In the presence of *Y. pestis* topoisomerase I or *M. tuberculosis* topoisomerase I, NSC28086 shows a five or sixfold respective increase in fluorescence signal when compared to the DMSO negative control that does not contain any compound [9] (Fig. 3). Although there is a signal increase when incubated with the fluorescent oligo substrate alone, the fluorescence signal increase is greater by 25 or 35% in the presence of *Y. pestis* topoisomerase I [9] or *M. tuberculosis* topoisomerase I (Fig. 3) respectively.

1.6 Identification of Screening Hits and Counter Screens

Potential hits in the screening assay are scored by picking compounds that show at least two fold increase in fluorescence in comparison to the negative control (containing only the DMSO

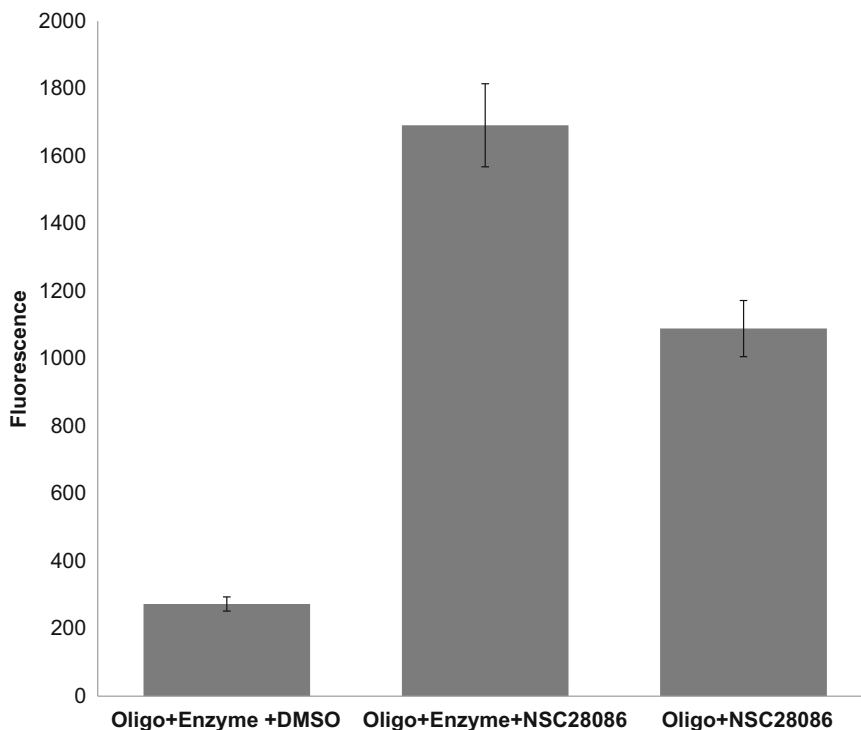


Fig. 3 Fluorescence cleavage increase by positive control NSC28086. Fluorescent oligonucleotide substrate Mbtest575 (Oligo) is incubated with NSC28086 (0.25 mM) in the presence and absence of *M. tuberculosis* topoisomerase I (Enzyme) at room temperature for 60 min. Assay containing DMSO was included as control. Fluorescence was read at Ex/Em 590/610

solvent). Potential hits are then evaluated in a counter-assay, wherein the hit compounds are incubated with oligonucleotide substrate in the absence of bacterial topoisomerase I. This counter-assay will eliminate the false positives that exhibit auto-fluorescence. Hits refined after this step are further evaluated in a dose dependent manner in primary assay (in the presence of enzyme) and in counter-assay (in the absence of enzyme) to identify compounds that show a consistent enzyme-dependent increase in fluorescence. Hit compounds are then confirmed as true poison inhibitors by gel-based cleavage assays to demonstrate an increase in the cleavage products.

Our HTS of different compound libraries for *Y. pestis* topoisomerase I poisons conducted at NERCE/NSRB resulted in identification of anziaic acid (a depside, from the lichen *Hypotrachyna* sp) and two organomercuric compounds that were shown to interfere with the cleavage religation mechanism of *Y. pestis* topoisomerase I or *E.coli* topoisomerase I [22, 23]. A dose response evaluation of the organomercuric compounds NSC201410 or NSC268879 with fluorescently labelled oligonucleotide substrate in the presence or absence of enzyme is shown in Fig. 4 [22]. While

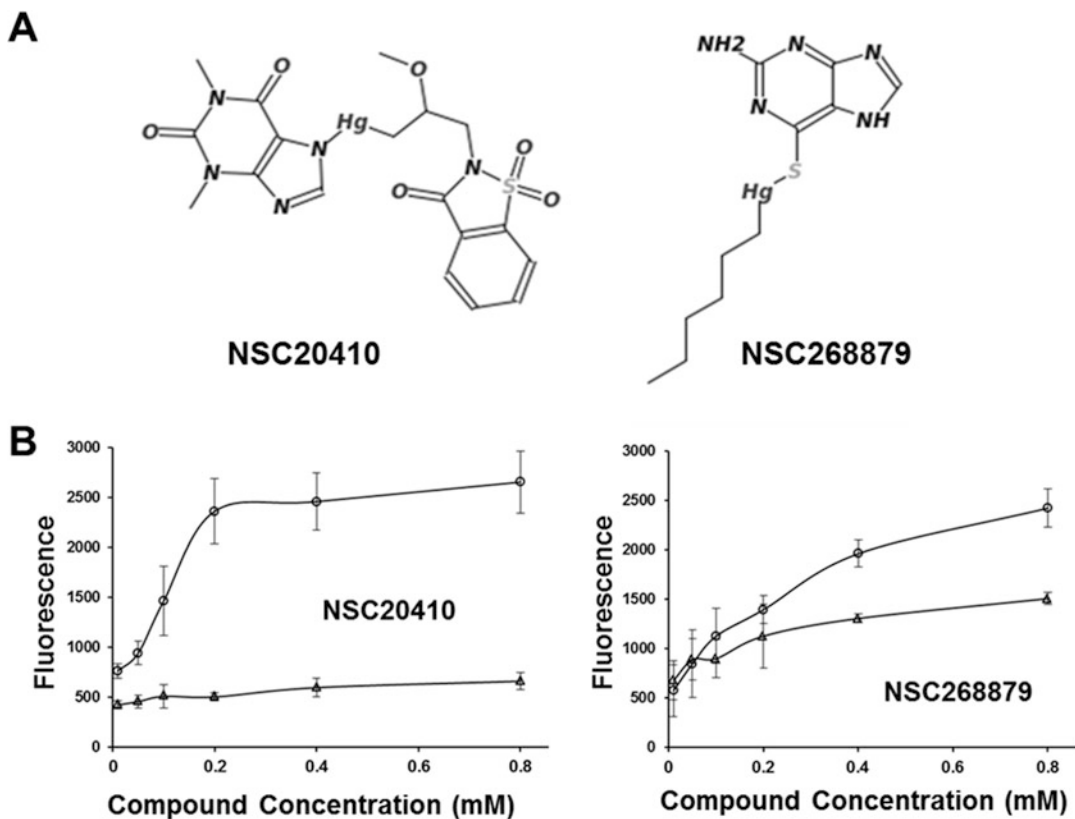


Fig. 4 Organomercury hits from fluorescence based assay. (a) Structures of organomercury hits from fluorescence based assay for increase in bacterial topoisomerase I mediated oligonucleotide cleavage. B. Dose response of increase fluorescence reading (in arbitrary units) upon addition of the two hit compounds (0.05–0.8 mM) in the absence (Δ) and presence (\circ) of *Y. pestis* topoisomerase I. Error bars correspond to standard deviations from at least three sets of data. (Reproduced from [22] by open access license)

both the compounds show an enzyme dependent increase of fluorescence in dose response assay, NSC20410 specifically increases the fluorescence only in the presence of the topoisomerase enzyme (Fig. 4b). In a gel based cleavage assay [22], NSC201410 and NSC268879 show an increase in the total cleavage products when compared with the DMSO control.

2 Materials

1. Substrate: Fluorescent Oligonucleotide substrate with CAL Fluor Red 610 fluorophore ((Ex/Em wavelengths of 590/610 nm) at the 5'-end and BHQ-2 quencher at the 3' end synthesized with dual (AX +RP) HPLC grade of purity by Bio-search technologies, CA, USA. Oligonucleotides are normally resuspended as 100 μ M (1000 \times) stocks in 10 mM Tris

(pH 8.0). Several aliquots are stored at -20°C in microcentrifuge tubes covered with aluminum foil.

2. Bacterial Topoisomerase I: Recombinant *Y. pestis* topoisomerase I, *E. coli* topoisomerase I or *M. tuberculosis* topoisomerase I [11, 13, 18] (*see Note 1*). Fresh working stocks (10–20 μM) of the enzyme are prepared in storage buffer (0.1 M KH_2PO_4 , 0.2 mM EDTA, 50% glycerol, 0.2 mM DTT, pH 7.4).
3. Negative control (DMSO), Positive control (NSC28086).
4. 384-well plates (Corning) (*see Note 2*).
5. Automatic liquid dispensers such as Matrix WellMate (Thermo Scientific).
6. Plate reader (Envision3, Perkin Elmer).

3 Methods

1. Dispense 10- μL volume of freshly prepared assay mix (10 mM Tris, 0.5 mM MgCl_2 , 100 nM fluorescent oligonucleotide substrate, and 100 nM bacterial topoisomerase I) using automatic liquid dispenser into each well of the 384-well plates (*see Note 3*). Total volume of the assay mix needed is determined by the number of compounds that are available for screening. Two columns of 18 wells each should be left blank for the addition of negative control or positive control assay mix.
2. Spin down the plates at $200 \times g$ for 1 min.
3. Compounds are added to each well (33 nl/10 μL assay mix) using automated capillary pin transfers (*see Note 4*).
4. Prepare negative control (assay mix containing 0.33% DMSO) or positive control compound (assay mix containing 0.25 mM NSC28086) separately and aliquot into the designated empty column of the assay plates.
5. Spin down the plates at $200 \times g$ for 1 min.
6. Seal the plates with TemPlate sealing foil (USA scientific) and incubate at 25°C for 30–60 min.
7. Read the plates in a fluorescent plate reader (Ex/Em, 590/610) after spinning them down at $200 \times g$ for 1 min.
8. Compounds that show an increase in the fluorescence (\geq two-fold) when compared to the negative (DMSO control) are scored as potential positives.
9. Counter-assay: These potential positives are subjected to counter-assays to eliminate false positives and nonspecific compounds. Potential positives are assayed with the same protocol as above at the screening concentration but in the absence of enzyme. Compounds that do not show the same increase in

fluorescence when compared to the initial screening are chosen for the dose-response assay.

10. Dose-response assay: Chosen positive compounds (in different concentrations) are assayed in the presence and absence of the bacterial topoisomerase I. Compounds that show an increase in fluorescence (in a dose dependent manner) in the presence of the enzyme more than in the absence of the enzyme are likely to be poison inhibitors of the enzyme.

4 Notes

1. Nuclease free preparation of bacterial topoisomerase I is necessary for eliminating nonspecific fluorescence signal increase in the assay due to contaminating nuclease. While topoisomerase I alone in the absence of compounds will show a small increase in the fluorescence signal that does not change with time (Fig. 5), presence of contaminating nucleases will increase the signal substantially over time even in the absence of any poison inhibitor.
2. Choice of plates plays an important role in the success of any HTS assay. As the assay volume is only 10 μL , a low volume plate is ideal. We have found that consistent robust signal can be obtained from non-treated black plates such as Corning #3821.
3. Assay mix is stable for up to 45–60 min prior to the screening assay.
4. Order and mode of compound addition does not affect results. We have had different HTS regimes with different methods of dispensing compound libraries in to the assay wells. In some,

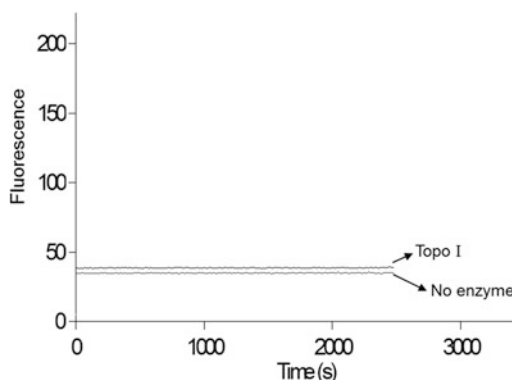


Fig. 5 Time course evaluation of cleavage assay. Mbtest575 is incubated in the presence or absence of *M. tuberculosis* topoisomerase I (Topo I) (as described in the methods) at 25 °C and fluorescence monitored over time

compounds are dispensed into the assay wells containing the assay mix, while in others, the assay plates are spotted with the compound libraries and then the assay mix is dispensed into those wells. Final screening concentration and the volume of compounds added in the assay depends on the actual library concentration. A screening concentration of 10 μM is reasonably common and we have found that the assay can tolerate a DMSO concentration of up to 2%

Acknowledgments

We thank the staff at NERCE/NSRB for access to screening libraries and HTS facilities, assistance in assay setup, data processing and analysis. This work was supported by funding from TB Alliance and National Institutes of Health grants R21NS067592, R01AI069313 to YT.

References

1. Wang JC (2002) Cellular roles of DNA topoisomerases: a molecular perspective. *Nat Rev Mol Cell Biol* 3(6):430–440. <https://doi.org/10.1038/nrm831>
2. Chen SH, Chan N, Hsieh T (2013) New mechanistic and functional insights into DNA topoisomerases. *Annu Rev Biochem* 82:139–170. <https://doi.org/10.1146/annurev-biochem-061809-100002>
3. Pommier Y (2013) Drugging topoisomerases: lessons and challenges. *ACS Chem Biol* 8(1):82–95. <https://doi.org/10.1021/cb300648v>
4. Vos SM, Tretter EM, Schmidt BH et al (2011) All tangled up: how cells direct, manage and exploit topoisomerase function. *Nat Rev Mol Cell Biol* 12(12):827–841. <https://doi.org/10.1038/nrm3228>
5. Liu LF (1989) DNA topoisomerase poisons as antitumor drugs. *Annu Rev Biochem* 58:351–375. <https://doi.org/10.1146/annurev.bi.58.070189.002031>
6. Aldred KJ, Kerns RJ, Osheroff N (2014) Mechanism of quinolone action and resistance. *Biochemistry* 53(10):1565–1574. <https://doi.org/10.1021/bi5000564>
7. Forterre P, Gabelle D (2009) Phylogenomics of DNA topoisomerases: their origin and putative roles in the emergence of modern organisms. *Nucleic Acids Res* 37(3):679–692. <https://doi.org/10.1093/nar/gkp032>
8. Tse-Dinh YC (1998) Bacterial and archeal type I topoisomerases. *Biochim Biophys Acta* 1400(1–3):19–27
9. Tse-Dinh Y (2015) Targeting bacterial topoisomerase I to meet the challenge of finding new antibiotics. *Future Med Chem* 7(4):459–471. <https://doi.org/10.4155/fmc.14.157>
10. Tse-Dinh Y (2009) Bacterial topoisomerase I as a target for discovery of antibacterial compounds. *Nucleic Acids Res* 37(3):731–737. <https://doi.org/10.1093/nar/gkn936>
11. Sorokin EP, Cheng B, Rathi S et al (2008) Inhibition of Mg^{2+} binding and DNA religation by bacterial topoisomerase I via introduction of an additional positive charge into the active site region. *Nucleic Acids Res* 36(14):4788–4796. <https://doi.org/10.1093/nar/gkn460>
12. Narula G, Annamalai T, Aedo S et al (2011) The strictly conserved Arg-321 residue in the active site of *Escherichia coli* topoisomerase I plays a critical role in DNA rejoining. *J Biol Chem* 286(21):18673–18680. <https://doi.org/10.1074/jbc.M111.229450>
13. Cheng B, Shukla S, Vasunilashorn S et al (2005) Bacterial cell killing mediated by topoisomerase I DNA cleavage activity. *J Biol Chem* 280(46):38489–38495. <https://doi.org/10.1074/jbc.M509722200>

14. Sutherland JH, Cheng B, Liu I et al (2008) SOS induction by stabilized topoisomerase IA cleavage complex occurs via the RecBCD pathway. *J Bacteriol* 190(9):3399–3403. <https://doi.org/10.1128/JB.01674-07>
15. Chen T (2009) A practical guide to assay development and high-throughput screening in drug discovery. CRC Press, Boca Raton
16. Acker MG, Auld DS (2014) Considerations for the design and reporting of enzyme assays in high-throughput screening applications. *Perspect Sci* 1(1–6):56–73. <https://doi.org/10.1016/j.pisc.2013.12.001>
17. Vet JM, Marras SE (2005) Design and optimization of molecular beacon real-time polymerase chain reaction assays. In: Herdewijn P (ed) *Oligonucleotide synthesis*. Humana Press, New York, pp 273–290
18. Annamalai T, Dani N, Cheng B et al (2009) Analysis of DNA relaxation and cleavage activities of recombinant *Mycobacterium tuberculosis* DNA topoisomerase I from a new expression and purification protocol. *BMC Biochem* 10:18. <https://doi.org/10.1186/1471-2091-10-18>
19. Sikder D, Nagaraja V (2000) Determination of the recognition sequence of *Mycobacterium smegmatis* topoisomerase I on mycobacterial genomic sequences. *Nucleic Acids Res* 28(8):1830–1837
20. Zuker M (2003) Mfold web server for nucleic acid folding and hybridization prediction. *Nucleic Acids Res* 31(13):3406–3415. <https://doi.org/10.1093/nar/gkg595>
21. Zhang JH, Chung TD, Oldenburg KR (1999) A simple statistical parameter for use in evaluation and validation of high throughput screening assays. *J Biomol Screen* 4(2):67–73
22. Cheng B, Annamalai T, Sandhaus S et al (2015) Inhibition of Zn(II) binding type IA topoisomerases by Organomercury compounds and hg(II). *PLoS One* 10(3):e0120022. <https://doi.org/10.1371/journal.pone.0120022>
23. Cheng B, Cao S, Vasquez V et al (2013) Identification of anziaic acid, a lichen depside from *Hypotrachyna* sp., as a new topoisomerase poison inhibitor. *PLoS One* 8(4):e60770. <https://doi.org/10.1371/journal.pone.0060770>

Chapter 19

Fluoroquinolone-Gyrase-DNA Cleaved Complexes

Gan Luan and Karl Drlica

Abstract

The quinolones are potent antibacterials that act by forming complexes with DNA and either gyrase or topoisomerase IV. These ternary complexes, called cleaved complexes because the DNA moiety is broken, block replication, transcription, and bacterial growth. Cleaved complexes readily form *in vitro* when gyrase, plasmid DNA, and quinolone are combined and incubated; complexes are detected by the linearization of plasmid DNA, generally assayed by gel electrophoresis. The stability of the complexes can be assessed by treatment with EDTA, high temperature, or dilution to dissociate the complexes and reseal the DNA moiety. Properties of the complexes are sensitive to quinolone structure and to topoisomerase amino acid substitutions associated with quinolone resistance. Consequently, studies of cleaved complexes can be used to identify improvements in quinolone structure and to understand the biochemical basis of target-based resistance. Cleaved complexes can also be detected in quinolone-treated bacterial cells by their ability to rapidly block DNA replication and to cause chromosome fragmentation; they can even be recovered from lysed cells following CsCl density-gradient centrifugation. Thus, *in vivo* and cell-fractionation tests are available for assessing the biological relevance of work with purified components.

Key words DNA topoisomerase, Quinolone, DNA gyrase, Cleaved complexes, Fluoroquinolone, Plasmid DNA isolation

1 Introduction

The quinolones, which account for a quarter of the US antibacterial prescriptions [1], act by trapping gyrase and topoisomerase IV on DNA [2–5]. The resulting drug-enzyme-DNA complexes, called cleaved complexes because the DNA is broken, rapidly block DNA replication [4, 6, 7] and transcription [8, 9]. The reversible complexes are the molecular explanation for bacterial growth inhibition and MIC (minimal inhibitory concentration) [10]. At elevated quinolone concentrations, the complexes lead to chromosome fragmentation, stimulation of ROS accumulation, and cell death [11–13]. Thus, cleaved complexes play a central role in fluoroquinolone action.

Cleaved-complex formation with purified components is measured in a three-step process involving (1) incubation of

quinolone with gyrase and circular, supercoiled plasmid DNA, (2) denaturation of the complexes and proteolytic removal of covalently attached gyrase, and (3) detection of linear DNA by gel electrophoresis. Complex stability is assessed by dissociation of the quinolone and resealing of the plasmid DNA. Cleaved-complex reversal is elicited by removal of divalent cations [2, 14, 15], by elevated temperature [16, 17], or by dilution [18, 19]. Some effects can be interpreted at the atomic level, since X-ray structures of cleaved complexes have been determined [19–23]. In those structures, two drug molecules are bound to each enzyme heterodimer, thereby defining a primary binding site. A secondary drug binding site is also observed using genetic and drug-binding assays; the location of this site is still undefined. The secondary site can be observed as cross-linking between a chloroacetyl derivative of ciprofloxacin (Cip-AcCl) and gyrase having a GyrA G81C substitution (*E. coli* numbering); preparation of Cip-AcCl is described.

The next level of investigation is to understand how cleaved complexes lead to quinolone-mediated cell death. Two types of downstream events occur: a surge in toxic reactive oxygen species, and with some very active quinolone derivatives, a proposed drug-induced destabilization of the complexes that leads to lethal chromosome fragmentation. Whether these two events derive from an “activated intermediate” cleaved complex is unknown.

2 Materials

2.1 Regents and Solutions

1. LB broth: Dissolve 10 g tryptone, 5 g yeast extract, and 10 g NaCl in 950 mL water, adjust pH to 7.0 with 1 N NaOH; add water to 1 L. Autoclave at 121 °C for 15 min; store at room temperature.
2. TAE buffer: Prepare as 50× stock solution. Dissolve 242 g Trizma base in water, adding 57.1 mL glacial acetic acid and 100 mL of 500 mM ethylenediaminetetraacetic acid (EDTA) (pH 8.0); bring the final volume to 1 L.
3. Gyrase storage buffer: 50 mM HEPES (pH 7.5), 500 mM KCl, 1 mM EDTA (pH 8.0), 30% (v/v) glycerol, and 2 mM 2-mercaptoethanol.
4. Gyrase dilution buffer: 50 mM Tris-HCl (pH 7.9), 30% (v/v) glycerol, 500 mM potassium glutamate.
5. 5× reaction buffer: 10 mM MgCl₂, 125 mM potassium glutamate, 75 mM Tris-HCl (pH 7.9).
6. ATP stock solution: 100 mM adjusted to pH 8.0 with NaOH.
7. Agarose: This reagent is available from a variety of sources including ACROS Organics.

8. Loading buffer: 6× loading buffer contains 30% (v/v) glycerol and 0.25% (w/v) bromophenol blue; store in aliquots at -80°C .
9. Ethidium bromide staining solution: stock solution contains 10 mg/mL ethidium bromide; dilute to 0.5 $\mu\text{g}/\text{mL}$ in water for DNA staining.
10. Gyrase subunits: gyrase subunits are available commercially (New England Biolabs and Inspiralis); they can also be prepared from cloned genes using an *E. coli* expression system. The method used by the Berger laboratory [24] produces separate subunits that are stored in gyrase storage buffer (Subheading 2.1, item 3).
11. Supercoiled plasmid DNA: A variety of plasmids having a size of approximately 4 kbp are suitable substrates for gyrase action; supercoiled pBR322 is commercially available (Inspiralis, UK). If many assays are likely to be performed, it may be cost-effective to prepare supercoiled plasmid DNA (Subheading 3.1).

2.2 Apparatus

1. Horizontal gel box for electrophoresis: Lucite gel boxes (20×50 cm) are available from Fisher Scientific. The apparatus contains two buffer reservoirs separated by a raised platform on which an agarose gel is formed. Walls are present on two sides of the platform; prior to pouring molten agarose onto the platform, walls must be formed at the two ends of the platform that communicate with the buffer reservoirs. These walls can be formed with paper tape that is removed after the gel solidifies. Each reservoir contains an electrode that is connected to a power source after the gels are formed and samples are loaded.
2. Sample-well comb: Teflon combs with teeth of various sizes are available from vendors of gel boxes. Combs are placed on the gel box at 90° to the platform prior to forming the gel to create wells for sample loading.
3. Electrophoresis power source: Fisher Biotech FB105 electrophoresis power supply is suitable.
4. UV transilluminator: model: EN-140 L from Spectroline (wavelength 365 nm) is suitable.
5. Densitometer/Camera: molecular Imager Gel DocTM XR+ with Image LabTM software (Bio-Rad, #1708195) is suitable.

3 Methods

3.1 Preparation of Supercoiled Plasmid DNA

1. An *E. coli* K-12 strain is transformed with plasmid pBR322 using a standard calcium chloride procedure [25]; the resulting transformants are selected on LB agar containing ampicillin at 100 $\mu\text{g}/\text{mL}$.

2. Plasmid DNA is extracted using a commercial kit according to the manufacturer's instructions. Examples are GeneJET Plasmid Maxiprep Kit from Thermo Scientific and Maxiprep kit from Qiagen. The resulting DNA samples usually contain some nicked and linear species in addition to the predominant supercoiled form (*see Note 1*).
3. For gel purification of supercoiled plasmid DNA, a 1% agarose gel is prepared that is 20 cm by 25 cm and about 0.5 cm thick. A bulk loading well is prepared that is about 15 cm long and 0.5 cm wide to accommodate a large volume of plasmid preparation (from Subheading 3.2). Near each end of the bulk loading well, but separate from it, prepare a narrow marker well (marker wells are typically 0.5 cm wide).
4. The two reservoirs of the gel box are filled with 1× TAE running buffer; plasmid DNA is loaded into the two marker wells and the bulk loading well. Running buffer covers the horizontal gel as a thin layer. Electrophoresis is performed at room temperature for about 2 h at 90 volts to move the supercoiled plasmid DNA to the middle of the gel.
5. To locate the supercoiled DNA, excise the two marker lanes with a razor blade or scalpel and transfer the DNA-containing agarose to a dish containing ethidium bromide (0.5 mg/L) staining solution (the shape of the excised regions should be unique for replacement in the gel in their original orientation). After 15 min, replace the ethidium bromide with water to destain; incubate at room temperature with gentle shaking for about 30 min.
6. Each marker lane is examined on a UV transilluminator to locate the supercoiled plasmid DNA band.
7. The position of the band is marked with 2 μ L 6× loading dye injected into the excised portions of the gel with a pipetman; the excised portions are then replaced in the gel such that the location of the supercoiled plasmid DNA is marked by the dye.
8. A collecting well is cut in the gel about 2 cm downstream from the supercoiled plasmid, determined by the position of plasmid DNA in the marker lanes.
9. The collecting well, which is parallel to the bulk loading well, is about 0.5 cm wide; it extends the full length of the bulk loading lane and the full depth of the gel.
10. The collecting well is filled with 1× TAE buffer (about 3 mL), and buffer on the upper surface of the gel is removed by blotting.
11. Electrophoresis is resumed for 3 min and then stopped.

12. All buffer in the collecting well is removed to a test tube on ice.
13. The collecting well is refilled with $1 \times$ TAE buffer, electrophoresis is restored for another 3 min, and the buffer in the collecting well is removed to a second test tube on ice.
14. **Steps 10–13** are repeated for about 35 fractions that are removed at 3-min intervals; during that time the dye placed in the marker lanes migrates beyond the collecting well by at least twice the distance from the collecting well to the position of the marker prior to creating the collecting well.
15. The plasmid-containing tubes are assayed for supercoiled plasmid by electrophoresis of a small aliquot (10–20 μ L) in a second agarose gel.
16. The contents of plasmid-containing tubes are pooled and concentrated using a Centrifugal Filter Unit (30 kDa, Merck Millipore, UFC903008).
17. Depending on the amount of DNA in the initial, bulk plasmid sample, the final preparation can contain about 1 mg plasmid DNA.

3.2 Preparation of Quinolones

1. Quinolones are obtained in powdered form, either from a commercial supplier (e.g., Sigma Chemical Co., St. Louis MO) or a pharmaceutical company.
2. Weigh quinolone sample (use minimal amount necessary for accurate weighing).
3. Dissolve in dimethyl sulfoxide (DMSO) to 20 mM; store in aliquots at -80°C (*see Note 2*).
4. Dilute in water prior to addition to reaction mixtures.

3.3 Preparation of Agarose Gel

1. Weigh the appropriate amount of powdered agarose, place in flask, add $1 \times$ TAE buffer to make a 1% w/v agarose suspension.
2. Place the flask containing agarose suspension in a microwave oven and briefly bring to a boil to generate a clear, uniform solution; do not overheat.
3. Allow the agarose solution to cool to roughly 45°C .
4. If necessary, apply a small amount of molten agarose to the taped ends of the gel-box platform to prevent leakage of the gel into the reservoirs during solidification (some gel boxes have a removable platform that allows gel formation without taping the ends).
5. With the comb in place, pour the molten agarose onto the gel box platform and allow the agarose to solidify; check for leakage around the tape.
6. Remove the tape from the ends of the platform, exposing the ends of the gel to the reservoirs.

7. Fill gel box reservoirs with $1\times$ TAE buffer such that a thin layer covers the gel.
8. Carefully remove the comb from the gel such that the wells fill with buffer; a thin layer of agarose should remain at the bottom of the wells.

3.4 Preparation of Gyrase

1. Immediately before preparing reaction mixtures, equimolar aliquots of GyrA and GyrB are thawed on ice, combined, and diluted in gyrase dilution buffer (*see Note 3*).
2. Dilution is performed gradually in twofold increments on ice with minimal aeration during mixing (mix by repeatedly drawing into a pipetman tip 10–20 times).
3. The final gyrase concentration will vary depending on the experiment, but good activity is achieved at 20 nM.

3.5 Formation of Cleaved Complexes

1. Prepare a protocol sheet indicating the reagents and reaction variables for each incubation (*see Note 4*).
2. Prepare a set of 0.5 mL Eppendorf tubes or PCR tubes that are numbered for identification and correspondence with each reaction mixture.
3. Add reagents to Eppendorf tubes on ice: 4 μ L $5\times$ reaction buffer, 0.4 μ L 100 mM ATP (2 mM final concentration), supercoiled pBR322 DNA (0.2 μ g, 4 nM), quinolone, water, and gyrase (as last ingredient); final volume is 20 μ L.
4. Mix with minimal aeration (drawing 20 times into a pipetman tip).
5. Transfer tubes to a water bath at the desired temperature (usually 37 °C); incubate for 15 min.
6. After incubation, transfer reaction tubes to ice and add sodium dodecyl sulfate (SDS) to 0.75% (w/v) final concentration.
7. Add proteinase K to 0.1 mg/mL, and incubate at 37 °C for 15 min to remove gyrase covalently bound to linear and nicked DNA.
8. Place tubes on ice.

3.6 Gel Electrophoresis

1. Warm samples briefly at 37 °C to dissolve SDS that may have precipitated during cooling on ice.
2. Add $6\times$ loading buffer (1/6 final volume) and mix by vortexing.
3. Load entire reaction volume from one tube into a well of the agarose gel; repeat for each reaction tube (*see Note 5*).
4. Apply voltage (100 V; 4 V/cm of gel) for 3 h at room temperature.

5. Manually remove gel from the gel box, place the gel in a glass dish containing ethidium bromide staining solution (0.5 mg/L) for 30 min with gentle agitation (*see Note 6*).
6. Destain by replacing ethidium bromide solution with distilled water that is replaced several times at 15-min intervals.

3.7 DNA Quantification by Densitometry

1. Place the destained gel on the UV transilluminator that is part of the densitometry apparatus (*see Note 7*).
2. Determine relative fluorescence intensity of the DNA bands (nicked, linear, and supercoiled).
3. Obtain data for multiple exposure times to assure that the fluorescent signal is not saturating (we routinely use five different exposure times). The fluorescence of total DNA is determined by adding the signal from the linear, nicked, and supercoiled bands.

3.8 Data Interpretation

1. For each sample lane, determine the fraction of DNA in the linear form.
2. Plot percent linear DNA on y axis, quinolone concentration or other variable on the x axis.
3. A point on the ascending portion of the curve at which 20% of the DNA is in the linear form can serve for comparison of compounds and treatments (*see Note 8*).
4. Generation of linear DNA by gyrase alone is taken as background; if this type of background is present, the drug-induced cleavage is considered reliable if it exceeds the background by a factor 3 [26].

3.9 Reversal by EDTA

1. After formation of cleaved complexes, as described in Subheading 3.5, chill the reaction mixtures on ice.
2. Add EDTA to various concentrations plus distilled water to balance the EDTA volume.
3. Incubate at 37 °C for 15 min.
4. Chill on ice and add SDS to 0.75% to stop the reaction.
5. Add proteinase K to 0.1 mg/mL, incubate at 37 °C for 15 min.
6. Perform gel electrophoresis as described in Subheading 3.6; quantify supercoiled and linear bands as in Subheading 3.7.
7. Plot percent linear DNA (y axis) against EDTA concentration (x axis); a U-shaped curve should be observed [15].

3.10 Reversal by High Temperature

1. After formation of cleaved complexes, as described in Subheading 3.5, chill reaction mixtures on ice.

2. Reincubate for 5 min at various temperatures (a thermocycler is suitable, since temperature can be quickly changed and multiple samples can be incubated concurrently) (*see Note 9*).
3. Chill on ice and add SDS to 0.75% to stop the reaction.
4. Add proteinase K to 0.1 mg/mL, incubate at 37 °C for 15 min.
5. Perform agarose gel electrophoresis as described in Subheading 3.6; quantify supercoiled and linear bands as in Subheading 3.7.
6. Plot percent linear DNA (*y* axis) against incubation temperature (*x* axis) to generate a reversal curve; determine midpoint (50% reversal) as a representative value.

3.11 Reversal by Dilution

1. Prepare cleaved complexes as described in Subheading 3.5 and chill on ice.
2. Dilute samples 20-fold in reaction buffer and incubate at 37 °C for various times (*see Note 10*).
3. Stop the reaction by adding SDS to 0.75%.
4. Add proteinase K to 0.1 mg/mL, and incubate at 37 °C for 15 min.
5. Transfer aliquot containing enough DNA for detection to an agarose gel.
6. Perform agarose gel electrophoresis as in Subheading 3.6 (increase sample well size to accommodate dilution) and analysis as in Subheading 3.7.

3.12 Preparation of Cip-AcCl

1. Dissolve 35 mg (0.1 mmol) ciprofloxacin hydrochloride in 1.5 mL of anhydrous dimethyl sulfoxide (DMSO) in the presence of 0.3 mmol of diisopropylethylamine.
2. Add 10 μ L chloroacetyl chloride followed by vigorous agitation.
3. Incubate for 5 min at ambient temperature.
4. Precipitate the product by adding 10 mL of 0.1 M citric acid and collect the precipitate by centrifugation at $2000 \times g$ for 10 min.
5. Wash the precipitate with water and vacuum-dry.
6. Dissolve the precipitate in 1 mL acetonitrile.
7. Perform preparative silica gel thin layer chromatography (TLC) in a chloroform/ethanol (8:1) developing system.
8. Identify product spot under UV light and collect it into a 15 mL tube.
9. Elute the product from the silica gel with 10 mL methanol.
10. Centrifuge at $2000 \times g$ for 10 min and collect the supernatant fluid.

11. Remove the methanol by evaporation in a rotary evaporator under reduced pressure; the remaining solid is the final product.
12. The product can be stored at -80°C ; it can be dissolved in dimethylformamide (DMF) at 10 mM to make a stock solution that can also be stored at -80°C .

3.13 Cross-Linking to Cleaved Complexes

1. Prepare reaction mixtures as described in Subheading 3.5 except that Cip-AcCl is the quinolone used and the GyrA subunit contains a cysteine substitution at position 81 (*E. coli* numbering; see Note 11).
2. Chill samples on ice after completion of the reaction; treat samples using one of the reversal protocols (Subheadings 3.9–3.11), most readily by adding EDTA to 10 mM.
3. Add SDS to 0.75% and proteinase K to 0.1 mg/mL, followed by incubation at 37°C for 15 min.
4. Chill samples by placing on ice.
5. Warm samples, add loading buffer, and place samples in wells of gel for electrophoresis and analysis as described in Subheadings 3.6 and 3.7.

3.14 Cleaved Complexes Assayed by Inhibition of DNA Synthesis

1. Prepare exponentially growing culture of bacteria in a flask with shaking; the strategy is to take samples at various times after adding quinolone and measure the rate of DNA synthesis using short pulses of radioactive thymidine and measurement of acid-precipitable radioactivity.
2. Prepare a series of test tubes on ice, each containing 1 μCi of ^3H -thymidine (Perkin Elmer) in a small volume (10 μL) (see Note 12).
3. Split culture into two flasks, one to serve as an untreated control and one to be treated with quinolone; label as flask 1 and flask 2, respectively, and continue shaking at 37°C .
4. Transfer 2–3 tubes containing ^3H -thymidine, as replicates, to a rack in a 37°C water bath.
5. Place 200 μL cell culture from flask 1 in each of the 2–3 tubes at 37°C .
6. Incubate for 2 min.
7. Stop growth in tubes by transferring to ice and immediately adding 1 mL cold 10% trichloroacetic acid.
8. Repeat steps 4–7 at 15-min intervals to generate a growth curve for untreated cells (time points of -30 , -15 , -5 , $+15$, and $+30$ min are suitable, with time zero occurring when quinolone is added to the second culture (flask 2), prepared at step 3.

9. At time zero (*see* **step 8**), add quinolone to growing culture of bacteria in flask 2.
10. Repeat **steps 4–7** using culture from flask 2 (quinolone treated) at specified intervals that will overlap with samples taken from untreated culture in flask 1 (3-min intervals are suitable, *see* **steps 4–10**).
11. Place glass-fiber filters on filter apparatus; prewet with 10% trichloroacetic acid.
12. Pour contents of each tube from **step 7** onto filter; wash filters with 10 mL ice-cold 1 N HCl to remove soluble radioactivity.
13. Wash with 10 mL ice-cold water to remove acid.
14. Wash with 5 mL 95% ethanol to remove water.
15. Dry and determine radioactivity by scintillation counting.

4 Notes

1. Plasmid preparations using commercial kits often contain several species (supercoiled, nicked, and sometimes linear forms). To obtain maximal sensitivity in the cleaved-complex assay, it is desirable to have all of the plasmid substrate in a supercoiled form. Preparative gel purification can be used to obtain pure supercoiled DNA. Other methods include preparative density-gradient centrifugation, either as velocity gradients using sucrose or as equilibrium gradients using CsCl. In the gel electrophoresis method we describe (Subheading 3.1), the bulk plasmid preparation is not exposed to ethidium bromide to avoid breakage—aliquots or parallel lanes containing small samples are used to track the plasmid DNA during purification.
2. We prefer to dissolve quinolones in dimethyl sulfoxide (DMSO), because using either alkaline or acid conditions to dissolve the compounds requires neutralization of small volumes prior to being added to reaction mixtures. In some cases, slight warming to 50 °C is required to dissolve the compounds. While quinolones are generally quite stable, that is not always the case; thus, we avoid storing dilute solutions at 4 °C. It may be desirable to store concentrated quinolone solutions in small aliquots to avoid repeated freezing and thawing. Include controls in experiments to assure stability. Prior to use, dilute quinolones in water, which removes effects of DMSO on reactions; however, when high concentrations of quinolone are used, controls for DMSO effects may be needed.
3. Purified subunits are stored in aliquots of about 5 μ L at -80 °C at a concentration of about 200 μ M. Repeated freezing and thawing may reduce activity, and for some experiments

reproducibility can be improved by using an aliquot only once. With *E. coli* gyrase, the GyrB subunit tends to dimerize, which needs to be taken into account when determining the molar concentration.

4. Two control reactions are important: one lacks gyrase to assess the integrity of the supercoiled DNA during the reaction, and the other lacks quinolone to assess the formation of linear DNA by gyrase alone. Additional marker lanes containing only plasmid DNA (supercoiled, linear, and nicked species) identify substrates and reaction products.
5. Care is taken to have lanes correspond to tube numbering—avoid symmetrical patterns to minimize errors in correspondence between samples and wells.
6. Ethidium bromide is a mutagen; gloves should be used. All ethidium bromide solutions are decontaminated by the extractor for ethidium bromide (Sigma Chemical Co., Z361569); the processed buffer can be discarded.
7. After electrophoresis, gels are photographed for laboratory records using the UV transilluminator; the intensity of the DNA bands is quantified using molecular Imager Gel Doc™ XR+ with Image Lab™ software (Bio-Rad, #1708195).
8. As quinolone concentration is increased, the percent linear DNA typically shows a sharp increase, up to about 50% linearization. At higher quinolone concentrations, a plateau and often a drop in percent linear DNA is observed. The plateau and drop derive from multiple cleavage events occurring in the plasmid DNA (at high quinolone concentration, a smear of DNA is seen in the gels due to DNA fragments that are smaller than the unit-length plasmid). Thus, the plateau or peak value should NOT be taken as maximal reaction and cannot be used as a 100% value for normalization.
9. Reversal of complexes is blocked by high temperature, presumably because gyrase is denatured. Thus, if thermal reversal is assayed by incubation at high temperature for various times [16], it is important to avoid the complication of gyrase denaturation.
10. Reversal by dilution of reaction mixtures following cleaved-complex formation tends to occur slowly (several hours). It also requires adjustments for dilution to have enough DNA for detection following gel electrophoresis. Sample wells can be enlarged, and concentrations of reactants can be increased (preliminary optimization experiments may be necessary). Procedures are described in [16, 19]. Reversal is also readily seen in living cells [17, 27]. In living cells, inhibition of replication is measured by adding quinolone to exponentially growing cultures, and at various times aliquots are removed for

pulse-labeling with ^3H -thymidine and determination of acid-precipitable radioactivity (Subheading 3.14). To effect reversal, cells of cultures treated with quinolone are collected on a sterile filter, washed with warm, drug-free medium, and introduced into warm drug-free medium by transferring the filter to which the cells are attached. Cells are removed from the filter by vigorous shaking. Aliquots are removed periodically for determination of DNA synthesis rate by pulse labeling. Data from a typical experiment are shown in ref. [17].

11. X-ray structures of cleaved-complex crystals show one binding mode for quinolones in which the quinolone C7 ring binds near GyrB-466 (*E. coli* gyrase numbering); the quinolone C3 carboxyl is located near the quinolone-resistance-determining region of GyrA helix-4. The cross-linking procedure described in Subheading 3.13 defines a secondary mode of binding in which the C7 ring binds near GyrA helix-4 (GyrA-81). Substitution of glycine at GyrA-81 with cysteine allows cross-linking between Cip-AcCl and gyrase that is not reversible by EDTA or high temperature. Cross-linking to GyrB-E466C gyrase serves to indicate the primary binding mode seen by X-ray crystallography.
12. A straightforward way to detect cleaved complexes in intact cells is by their ability to block DNA synthesis. Within a few minutes after quinolone addition, a nadir of synthesis rate is observed. The extent of inhibition of DNA synthesis seen after 5–10 min of quinolone treatment is related to MIC [10]. Skill is required to take accurate samples at closely spaced time points; we generally consider making these measurements to be a two-person task. After determination of radioactivity on the glass-fiber filters, remove filters from vials and recount. If no radioactivity transferred from the filters to the vials, only the filters need to be disposed as radioactive waste.

Acknowledgments

We thank the following for critical comments on the manuscript: Arkady Mustaev and Marila Gennaro.

References

1. Suda K, Hicks L, Roberts R, RJKunkler DL (2013) A national evaluation of antibiotic expenditures by healthcare setting in the United States, 2009. *J Antimicrob Chemother* 68:715–718
2. Gellert M, Mizuuchi K, O’Dea MH, Itoh T, Tomizawa JI (1977) Nalidixic acid resistance: a second genetic character involved in DNA gyrase activity. *Proc Natl Acad Sci U S A* 74:4772–4776
3. Sugino A, Peebles C, Kruezer K, Cozzarelli N (1977) Mechanism of action of nalidixic acid: purification of *Escherichia coli nalA* gene product and its relationship to DNA gyrase and a

- novel nicking-closing enzyme. *Proc Natl Acad Sci U S A* 74:4767–4771
4. Snyder M, Drlica K (1979) DNA gyrase on the bacterial chromosome: DNA cleavage induced by oxolinic acid. *J Mol Biol* 131:287–302
 5. Kato J, Nishimura Y, Imamura R, Niki H, Hiraga S, Suzuki H (1990) New topoisomerase essential for chromosome segregation in *E. coli*. *Cell* 63:393–404
 6. Hiasa H, Yousef D, Marians K (1996) DNA strand cleavage is required for replication fork arrest by a frozen topoisomerase-quinolone-DNA ternary complex. *J Biol Chem* 271:26424–26429
 7. Wentzell L, Maxwell A (2000) The complex of DNA gyrase and quinolone drugs on DNA forms a barrier to the T7 DNA polymerase replication complex. *J Mol Biol* 304:779–791
 8. Willmott CJR, Critchlow SE, Eperon IC, Maxwell A (1994) The complex of DNA gyrase and quinolone drugs with DNA forms a barrier to transcription by RNA polymerase. *J Mol Biol* 242:351–363
 9. Manes SH, Pruss GJ, Drlica K (1983) Inhibition of RNA synthesis by oxolinic acid is unrelated to average DNA supercoiling. *J Bacteriol* 155:420–423
 10. Chow R, Dougherty T, Fraimow H, Bellin E, Miller M (1988) Association between early inhibition of DNA synthesis and the MICs and MBCs of carboxyquinolone antimicrobial agents for wild-type and mutant [*gyrA nfxB (ompF) acrA*] *Escherichia coli* K-12. *Antimicrob Agents Chemother* 32(8):1113
 11. Drlica K, Malik M, Kerns RJ, Zhao X (2008) Quinolone-mediated bacterial death. *Antimicrob Agents Chemother* 52:385–392
 12. Zhao X, Drlica K (2014) Reactive oxygen species and the bacterial response to lethal stress. *Curr Opin Microbiol* 21:1–6
 13. Dwyer D, Collins J, Walker G (2015) Unraveling the physiological complexities of antibiotic lethality. *Annu Rev Pharmacol Toxicol* 55:9.1–9.20
 14. Pan XS, Dias M, Palumbo M, Fisher LM (2008) Clerocidin selectively modifies the gyrase-DNA gate to induce irreversible and reversible DNA damage. *Nucleic Acids Res* 36:5516–5529
 15. Drlica K, Mustaev A, Towle T, Luan G, Kerns R, Berger J (2014) Bypassing fluoroquinolone resistance with quinazolinodiones: studies of drug-gyrase-DNA complexes having implications for drug design. *ACS Chem Biol* 9:2895–2904
 16. Aldred K, McPherson S, Wang P, Kerns R, Graves D, Turnbough C et al (2012) Drug interactions with *Bacillus anthracis* topoisomerase IV: biochemical basis for quinolone action and resistance. *Biochemistry* 51:370–381
 17. Mustaev A, Malik M, Zhao X, Kurepina N, Luan G, Oppegard L et al (2014) Fluoroquinolone-gyrase-DNA complexes: two modes of drug binding. *J Biol Chem* 289:12300–12312
 18. Aldred K, McPherson S, Turnbough C, Kerns R, Osheroff N (2013) Topoisomerase IV-quinolone interactions are mediated through a water-metal ion bridge: mechanistic basis of quinolone resistance. *Nucleic Acids Res* 41:4628–4639
 19. Blower TR, Williamson BH, Kerns RJ, Berger JM (2016) Crystal structure and stability of gyrase-fluoroquinolone cleaved complexes from *Mycobacterium tuberculosis*. *Proc Natl Acad Sci U S A* 113:1706–1713
 20. Laponogov I, Pan X, Veselkov D, McAuley K, Fisher L, Sanderson M (2010) Structural basis of gate-DNA breakage and resealing by type II topoisomerases. *PLoS One* 5:e11338
 21. Laponogov I, Sohi M, Veselkov D, Pan X, Sawhney R, Thompson A et al (2009) Structural insight into the quinolone-DNA cleavage complex of type IIA topoisomerases. *Nat Struct Mol Biol* 16:667–669
 22. Bax B, Chan P, Eggleston D, Fosberry A, Gentry D, Gorrec F et al (2010) Type IIA topoisomerase inhibition by a new class of antibacterial agents. *Nature* 466:935–940
 23. Wohlkonig A, Chan P, Fosberry A, Homes P, Huang J, Kranz M et al (2010) Structural basis of quinolone inhibition of type IIA topoisomerases and target-mediated resistance. *Nat Struct Mol Biol* 17:1152–1153
 24. Schoeffler A, May A, Berger J (2010) A domain insertion in *Escherichia coli* GyrB adopts a novel fold that plays a critical role in gyrase function. *Nucleic Acids Res* 38:7830–7844
 25. Cohen S, Chang A, Hsu L (1972) Nonchromosomal antibiotic resistance in bacteria: genetic transformation of *Escherichia coli* by R-factor DNA. *Proc Natl Acad Sci U S A* 69:2110–2114
 26. Oppegard LM, Streck K, Rosen J, Shwanz HA, Drlica K, Kerns RJ et al (2010) Comparison of in vitro activities of fluoroquinolone-like 2,4- and 1,3-diones. *Antimicrob Agents Chemother* 54:3011–3014
 27. Goss W, Deitz W, Cook T (1965) Mechanism of action of nalidixic acid on *Escherichia coli*. II. Inhibition of deoxyribonucleic acid synthesis. *J Bacteriol* 89:1068–1074

Detection of Topoisomerase Covalent Complexes in Eukaryotic Cells

Jay Anand, Yilun Sun, Yang Zhao, Karin C. Nitiss, and John L. Nitiss

Abstract

DNA topoisomerases carry out topological transformations of DNA by introducing transient DNA breaks. The covalent intermediate of topoisomerase reactions include the topoisomerase protein covalently bound to DNA by a phosphotyrosine intermediate. Anti-cancer drugs that target topoisomerases typically trap the covalent intermediate, and generate cytotoxic enzyme dependent DNA damage. More recently, structural alterations in DNA such as DNA damage have also been shown to trap covalent intermediates of topoisomerase reactions. Understanding the action of drugs that target topoisomerases as well as determining the importance of trapped topoisomerases on genome stability requires assays that can accurately and sensitively measure levels of topoisomerase/DNA complexes. This chapter describes two approaches that have been developed to quantitate topoisomerase DNA complexes. These assays termed ICE (in vivo complex of enzymes) and RADAR (rapid approach to DNA adduct recovery) rely on isolation of genomic DNA under conditions that preserve proteins covalently bound to DNA. Covalently bound proteins are then quantitated using antibodies directed against specific topoisomerases. We describe assays in both mammalian cells and the yeast *Saccharomyces cerevisiae* that can measure topoisomerase/DNA covalent complexes, and give examples that can be used to enhance the quantitative reliability of these assays.

Key words ICE assay, RADAR assay, CsCl ultracentrifugation, Antibody detection

1 Introduction

Topoisomerase reactions depend on enzyme mediated DNA breakage through the generation of protein linked DNA [1]. Anticancer drugs that target DNA topoisomerases typically inhibit the ligation step of the enzyme catalytic cycle, and therefore cause enzyme mediated DNA damage. The enzyme mediated damage consists of protein covalently bound to DNA, with either single or double strand DNA breaks [2, 3]. The efficacy of anticancer drugs that target topoisomerases is related in part to the levels of these topoisomerase/DNA covalent complexes [4]. Therefore, accurate quantitation of complexes is important for studying the action of topoisomerase targeting anticancer drugs [5]. Additionally, recent evidence suggests that a variety of natural processes, including

natural products, DNA lesions, and even the normal process of transcription can lead to elevated levels of enzyme topoisomerase covalent complexes [6]. Therefore assays for these complexes will be useful for workers studying a variety of cellular processes.

Assays for topoisomerase/DNA complexes are relatively straightforward *in vitro* [7]. Early studies of topoisomerase targeting drugs in cells relied on DNA breakage assays such as alkaline elution or the Comet assay to quantitate topoisomerase induced DNA damage. These assays are obviously not specific for topoisomerase/DNA covalent complexes. Subsequently, a commonly used assay was the band depletion assay, which measured the loss of free topoisomerase, i.e., enzyme not covalently bound to DNA and therefore having normal mobility in SDS gels [8].

A significant advance was the development of the ICE assay by Muller and colleagues [7, 9]. This assay relies on purification of DNA under conditions that do not result in protein linked DNA. At the time the assay was developed, cesium chloride ultracentrifugation was a method of choice for DNA purification. The assay therefore relied on CsCl gradients, recovery of purified cellular DNA, and quantitation of topoisomerase covalently bound to the DNA by antibodies directed against topoisomerases. Since the ICE assay continues to be an important assay for both trapped topoisomerase I and topoisomerase II, this chapter includes protocols for this assay. ICE assays have mainly been applied to mammalian cells, and have not been applied to yeast, an important model system for studying topoisomerases [10]. This chapter includes appropriate modifications to the ICE assay for use in yeast.

More recently an alternate assay for quantitating topoisomerase DNA covalent complexes has been developed by Maizels and colleagues [11]. This assay termed the RADAR assay (rapid approach to DNA adduct recovery), uses purification of DNA by chaotropic agents such as guanidinium isothiocyanate. Since this assay can be performed without an ultracentrifuge, it has also become a mainstay for many laboratories. This chapter includes a detailed protocol for the RADAR assay. A more recent version of this assay has also been described [12]. Since our laboratory has not had extensive experience with this modified assay, we have not included the assay in this chapter. However, our protocols for the RADAR assay in this chapter should allow investigators the main framework for using the modified RADAR assay.

For each of the major assays described in this chapter, we have provided experiments that illustrate application of these techniques. In almost all cases we illustrate results with technical replicates. While these techniques are robust, and have been applied in many laboratories, we feel that careful experimental design, including multiple biological and technical replicates are essential for using these assays. A good rule of thumb is to include duplicate technical replicates for each experiment, and to perform a minimum of three biological replicates.

2 Materials

2.1 ICE Assay (In Vivo Complex of Enzyme Bioassay)

2.1.1 Cell Culture

1. Cells of interest: we used RH30 human rhabdomyosarcoma cell line.
2. Cell growth media: we used RH30 growth media (RPMI 1640) supplemented with 10% fetal bovine serum (FBS) and penicillin–streptomycin.

2.1.2 Drug Treatment

1. Etoposide (Sigma).
2. Camptothecin (CPT) (Sigma).

2.1.3 Cell Lysis and Ultracentrifugation

1. 1× TE buffer, pH 7.5: 10 mM Tris–HCl, 1 mM EDTA.
2. Lysis buffer: 1% 1× (w/v) sarkosyl in 1× TE buffer, protease inhibitor cocktail.
3. Cell scraper.
4. 15 mL centrifuge tubes.
5. 1 mL latex-free syringe with 25G5/8 needle (BD biosciences).
6. 150% (w/v) cesium chloride (CsCl) solution in H₂O.
7. 3 mL latex-free syringe with 16G1/2 needle (BD biosciences).
8. Floor standing ultracentrifuge or tabletop ultracentrifuge.
If using floor standing ultracentrifuge centrifuge:
9. OptiSeal centrifuge tubes, 4.9 mL (Beckman coulter #362185).
10. NVT65.2 ultracentrifuge rotor (Beckman coulter) or equivalent.
If using tabletop ultracentrifuge:
11. OptiSeal centrifuge tubes, 3.3 mL (Beckman coulter #361627).
12. TLN-100 ultracentrifuge rotor (Beckman coulter) or equivalent.

2.1.4 DNA Topoisomerase Covalent Complexes Recovery

1. Sharp blade or CentriTube splicer (Beckman coulter).
2. 70% ethanol.
3. 1× TE buffer pH 7.5.
4. Parafilm M.
5. Water bath or heating block, 65 °C.
6. UV spectrophotometer.

**2.1.5 DNA Transfer
to Nitrocellulose Membrane
and Immunodetection
of Covalently Bound
Topoisomerases**

1. 25 mM NaPO₄ (Sodium phosphate), pH 6.5.
2. Nitrocellulose membrane (Bio-Rad).
3. Bio-Dot SF filter paper (Bio-Rad #1620161).
4. Slot blot apparatus (Bio-Rad SF apparatus #1706542).
5. 1× Tris-buffered saline–Tween 20 (TBS-T): dilute 10× TBS to 1× TBS and add 0.1% (v/v) Tween 20.
6. 5% (w/v) nonfat dry milk (nestle) in 1× TBS-T.
7. Rabbit anti-Human Topo II Alpha antibody (Bethyl #A300-054A) (1:10,000 dilution).
8. Mouse anti-Human Topo II Beta antibody (BD transduction laboratories #611493) (1:10,000 dilution).
9. Rabbit anti-TOP1 antibody (Bethyl #A302-590A) (1:20,000 dilution).
10. Anti-rabbit IgG, horseradish peroxidase-linked whole antibody (GE Healthcare #NA934) (1:10,000 dilution).
11. Anti-mouse IgG, horseradish peroxidase-linked whole antibody (GE Healthcare #NXA931) (1:10,000 dilution).
12. Supersignal west femto maximum sensitivity substrate (Thermo Scientific #34095).

**2.2 RADAR Assay
(Rapid Approach
to DNA Adduct
Recovery)**

2.2.1 Cell Culture
(See Subheading 2.1.1)

2.2.2 Drug Treatment
(See Subheading 2.1.2)

2.2.3 Cell Lysis

1. 1× phosphate buffered saline (PBS).
2. M Lysis buffer: 5 M guanidinium isothiocyanate (*see Note 1*), 10 mM Tris–HCl pH 6.5, 20 mM EDTA, 4% Triton X-100, 1% Sarkosyl, 1% dithiothreitol (DTT) (*see Note 2*).

**2.2.4 DNA
Topoisomerase Covalent
Complexes Recovery**

1. 1.5 mL centrifuge tubes.
2. 100% ethanol.
3. Centrifuge.
4. 75% ethanol.
5. 8 mM NaOH (*see Note 3*).
6. UV spectrophotometer.

2.2.5 DNA Transfer to Nitrocellulose Membrane and Immunodetection of Covalently Bound Topoisomerases (See Subheading 2.1.5).

2.3 DNA Hybridization
Technique to Measure Human DNA Loaded on Nitrocellulose Membrane Using Biotinylated D17Z1 Probes

2.3.1 DNA Hybridization

1. Nitrocellulose membrane with DNA loaded using slot blot apparatus (*see Note 4*).
2. UV cross-linker (*see Note 5*).
3. Heat incubator.
4. Biotin-labeled D17Z1 oligonucleotide probes (5'-biotin-TAGAAGCATTCTCAGAACTACTTTGTGATGATTG-CATTC-3', custom made through Sigma-Aldrich).
5. North2South chemiluminescent hybridization and detection kit (Thermo Scientific): North2South hybridization buffer, North2South hybridization stringency wash buffer (2×), Blocking buffer, 4× wash buffer, Stabilized streptavidin-horseradish peroxidase conjugate.

2.3.2 Chemiluminescence-Based Detection

1. Chemiluminescent substrates (Luminol/enhancer solution and Stable peroxide solution; included in North2South chemiluminescent hybridization and detection kit).

2.4 Detection of Topoisomerase II-DNA Covalent Complexes (Top2ccs) in the yeast *Saccharomyces cerevisiae*

1. Yeast growth medium: synthetic complete medium (SC medium) without uracil is used for strain YMM10, a *S. cerevisiae* strain that contains gene deletions in several drug efflux pumps and is used to enhance etoposide sensitivity, carrying plasmid pDEDITOP2-3×HA, a single copy yeast plasmid that overexpresses HA-tagged Top2 from the yeast DED1 promoter and contains URA3 gene as the selectable marker. Per litre: 1.7 g yeast nitrogen base without ammonium sulfate, 5 g ammonium sulfate, 20 g glucose, 0.77 g complete supplement mixture minus uracil (BIO 101, Inc. 4511-212); adjust the pH to 6.0 with sodium hydroxide and autoclave.
2. Yeast lysis buffer (YLB): 6 M guanidinium thiocyanate (GTC) or guanidinium chloride, 1% Sarkosyl, 4% Triton X-100, 1 M Tris-HCl, 1 mM EDTA, pH 7.5; Add yeast protease inhibitor cocktail (Sigma-Aldrich P8215, 5 μL is recommended for 100 mg of yeast cells) and dithiothreitol (final concentration 0.1 M) prior to the lysis.
3. 150% (w/v) CsCl solution: 150 g of cesium chloride in 100 mL 1× TE buffer. The CsCl solution is prepared at $\rho_{(\text{CsCl})} = 1.783$ g/mL for precipitating nucleic acids, the percent by weight of

CsCl is calculated by the formula: $\% \text{ wt}(\text{CsCl})/\text{wt}(\text{total}) = 137.48-138.11/\rho$.

4. $10\times$ micrococcal nuclease reaction buffer: 50 mM CaCl_2 , 0.5 M Tris-HCl, pH 7.9.
5. Rabbit anti-HA antibody 1:1000 (Santa Cruz, sc-805).

3 Methods

3.1 ICE Assay (In Vivo Complexes Of Enzyme Bioassay)

1. Grow $0.5-2 \times 10^6$ cells per 100 mm culture plate per treatment condition (control, plus one plate each per treatment condition) for analysis (*see Note 6*).

3.1.1 Cell Culture

3.1.2 Drug Treatment

1. After 24 h, as per experimental design treat cells with drug or test reagent and incubate for chosen length of time (*see Note 7*).

3.1.3 Cell Lysis and Ultracentrifugation

1. Aspirate growth medium using suction
If using floor standing ultracentrifuge:
2. Lyse cells using 1.5 mL 1% Sarkosyl containing protease inhibitors.
3. Scrap cells using cell scraper and transfer cell lysate to 15 mL centrifuge tube.
4. Using 1 mL latex-free syringe, shear DNA by passing it through 25G8/5 needle. Repeat ten times.
5. After shearing DNA, add additional 1.5 mL lysis buffer to each 15 mL tubes to make final volume equal to 3 mL.
6. Take new 4.9 mL OptiSeal centrifuge tubes equal to number of samples and label them (*see Note 8*). Add 2 mL 150% (w/v) CsCl solution to each OptiSeal tubes using 1 mL micropipette.
7. Using 3 mL syringe and 16G1/2 needle, layer 3 mL of cell lysate on CsCl in OptiSeal tubes. Close the OptiSeal tube by placing tube plug (supplied with OptiSeal tubes) into the stem of the tube. Wipe off any fluid on the OptiSeal tube using Kimwipes.
8. Place OptiSeal tubes into the NVT65.2 ultracentrifuge rotor and seal them as per manufacturer's instruction and run ultracentrifuge. Condition for NVT65.2 rotor is: 20 h; 42,000 rpm; 25 °C (*see Note 9*).
If using tabletop ultracentrifuge:
9. Lyse cells using 1 mL 1% sarkosyl containing protease inhibitors.

10. Scrap cells using cell scraper and transfer cell lysate to 1.5 mL eppendorf tube.
11. Using 1 mL latex-free syringe, shear DNA by passing it through 25G8/5 needle. Repeat ten times.
12. After shearing DNA, aliquot cell lysate into two 1.5 mL eppendorf tubes. Add additional 0.5 mL lysis buffer to each 1.5 mL eppendorf tubes to make final volume equal to 1 mL per tube and net lysate volume 2 mL.
13. Take new 3.3 mL OptiSeal centrifuge tubes equal to number of samples and label them (*see Note 8*). Add 1.3 mL 150% (w/v) CsCl solution to each OptiSeal tubes using 1 mL micropipette.
14. Using 3 mL syringe and 16G1/2 needle, layer 2 mL of cell lysate on CsCl in OptiSeal tubes. Close the OptiSeal tube by placing tube plug (supplied with OptiSeal tubes) into the stem of the tube. Wipe off any fluid on the OptiSeal tube using Kimwipes.
15. Place OptiSeal tubes into the TLN-100 ultracentrifuge rotor and seal them as per manufacturer's instruction and run ultracentrifuge. Condition for TLN-100 rotor is: 14 h; 61,000 rpm; 25 °C (*see Note 9*).

3.1.4 DNA Topoisomerase Covalent Complexes Recovery

1. Once ultracentrifuge is done, following manufacturer's instructions carefully remove OptiSeal tubes from the ultracentrifuge rotor. Using 1 mL micropipette, remove approximately 1–2 mL of cell lysate CsCl solution from each OptiSeal tube (approx. 1 mL for 3.3 mL OptiSeal tubes; approx. 2 mL for 4.9 mL OptiSeal tubes).
2. Cut each OptiSeal tubes just above the liquid layer using sharp blade or CentriTube splicer (Beckman) (*see Note 10*).
3. Carefully discard liquid by pouring without dislodging DNA pellet (*see Note 11*).
4. Wash DNA pellet using 0.5 mL 70% ethanol. Carefully aspirate ethanol using suction or by pouring from the side opposite to the pellet without dislodging DNA pellet. Air-dry the DNA pellet for about 15 s.
5. Add 0.5 mL 1× TE buffer (pH 7.5) to each tube and dissolve DNA pellet.
6. Cover each tube with Parafilm M. To complete dissolve DNA put sealed tubes on a shaker at 4 °C, overnight.
7. Remove tubes from 4 °C and place them on a 65 °C water bath or heat block for 5 min. Allow the tubes to cool to room temperature.
8. Measure DNA concentration using UV spectrophotometer.

**3.1.5 DNA Transfer
to Nitrocellulose Membrane
and Immunodetection
of Covalently Bound
Topoisomerases**

1. Apply samples to nitrocellulose membrane using slot blot apparatus. We apply 2 μg DNA per slot of slot blot apparatus. Dilute DNA samples using NaPO_4 so that the total volume to be applied to each slot of slot blot apparatus is 200 μL . Equilibrate nitrocellulose membrane and slot-dot filter paper in NaPO_4 (pH 6.5) for 15 min. Construct slot blot apparatus assembly as per manufacturer's guidelines. Wash the membrane slots using 200 μL of NaPO_4 applying vacuum. Remove vacuum and allow the wash to pass through the membrane. Reapply vacuum, add samples (200 μL per slot) to membrane slots and remove vacuum. Reapply vacuum, wash membrane slots using 200 μL of NaPO_4 and remove vacuum until the wash has passed through the membrane. Open the slot blot apparatus and remove the membrane.
2. Wash the membrane using $1\times$ TBS-T (make a 1:10 dilution of $10\times$ TBS and add 0.1% Tween 20) for 5 min. Discard wash and block nitrocellulose membrane using 5% nonfat dry milk in $1\times$ TBS-T for 1 h at room temperature on a shaker at medium speed.
3. Discard the blocking solution and incubate membrane with desired primary antibody [Topoisomerase I (anti-Top1), Topoisomerase II alpha (anti-Topo II alpha) or Topoisomerase II beta (anti-Topo II beta)] at appropriate dilution in 5% nonfat dry milk prepared using $1\times$ TBS-T at 4 $^\circ\text{C}$ on a shaker, overnight.
4. After overnight incubation, rinse and then wash the membrane with $1\times$ TBS-T for 5 min on a shaker at room temperature, thrice.
5. Incubate with appropriate secondary antibody at suitable dilution in 5% nonfat dry milk prepared using $1\times$ TBS-T for 1 h at room temperature on a shaker. Rinse and then wash with $1\times$ TBS-T for 5 min on a shaker at room temperature, thrice.
6. Detect DNA topoisomerase covalent complexes using enhanced Chemiluminescence (ECL) kit following manufacturer's instructions. Examples of the ICE assay detecting Top2 covalent complexes and Top1 covalent complexes are shown in Figs. 1 and 2, respectively.

**3.2 RADAR Assay
(Rapid Approach
to DNA Adduct
Recovery)**

1. Grow $0.5\text{--}1 \times 10^6$ cells per 100 mm culture plate per treatment condition (control, plus one plate each per treatment condition) for analysis (*see* Note 12).

3.2.1 Cell Culture

3.2.2 Drug Treatment

See Subheading 3.1.2.

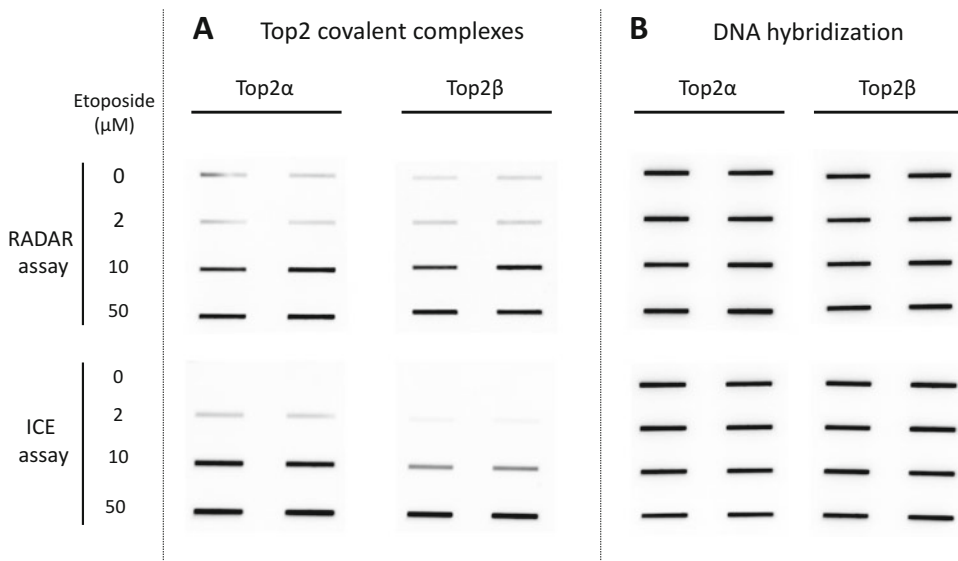


Fig. 1 ICE assay and RADAR assay for Top2 covalent complexes with DNA hybridization. RH30 cells were treated with different concentrations of etoposide for 1 h. Either ICE assay or RADAR assay was performed as described in the protocol to recover DNA with covalently bound Top2. Slot blots of recovered DNA probed with anti-Top2α or anti-Top2β antibodies is shown in *panel a*. *Panel b* shows DNA on membrane hybridized with biotinylated D17Z1 probe

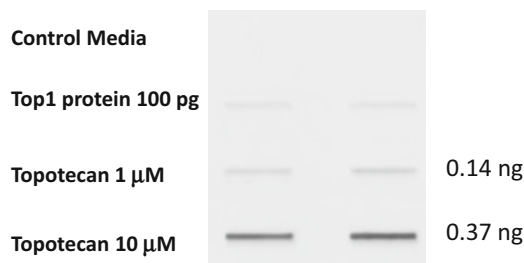


Fig. 2 ICE assay for Top1 covalent complexes. H446 cells were treated with various topotecan concentrations for 1 h. DNA was purified using the ICE assay using a tabletop ultracentrifuge. In the experiment shown, 100 pg of purified human topoisomerase I was spotted onto the membrane as a quantitation control, and the quantity of recovered Top1 is also indicated

3.2.3 Cell Lysis

1. Following drug treatment, aspirate the growth medium using suction, wash with PBS and immediately lyse cells by adding 1 mL M lysis buffer (*see Note 13*).

3.2.4 DNA

Topoisomerase Covalent Complexes Recovery

1. To recover DNA with covalently bound protein, transfer cell lysate to 1.5 mL eppendorf tube and add ½ volume (i.e., 0.5 mL for 1 mL cell lysate) of 100% ethanol to it. Incubate eppendorf tube at low temperature (−20 °C for 5 min) and

then centrifugation for 15 min at maximum speed (we centrifuged at 14,000 rpm) (*see Note 14*). Decant or aspirate the supernatant using suction or pipette, and wash DNA pellet by vortexing in 1 mL 75% ethanol followed by 10 min centrifugation, twice (*see Note 15*).

2. Quickly dissolve DNA pellet in 0.2–0.5 mL of freshly made 8 mM NaOH. Resuspend DNA pellet by repeated pipetting or incubate on a tube rotator at 4 °C overnight for thoroughly dissolving. Samples can be stored at –20 °C or below for later use.
3. Incubate DNA samples in water bath or heat block at 65 °C for 5 min. Allow the samples to cool and then quantify DNA concentration using appropriate method. We use UV spectrometer to quantify DNA. Typical DNA yield is around 100 ng/μL.

3.2.5 DNA Transfer to Nitrocellulose Membrane and Immunodetection of Covalently Bound Topoisomerases

See Subheading 3.1.5.

Examples of the RADAR assay detecting Top2 covalent complexes and Top1 covalent complexes are shown in Figs. 1 and 3, respectively.

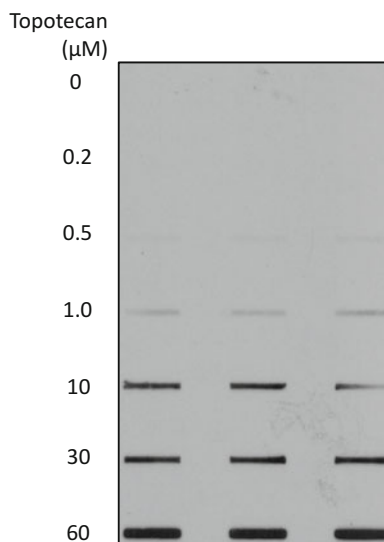


Fig. 3 RADAR assay for Top1 covalent complexes. H446 cells were treated with various topotecan concentrations for 1 h. The slot blots of DNA recovered from H446 cells were probed with an antibody directed against Top1. The figure shown includes three technical replicates

3.3 DNA Hybridization Technique to Measure DNA Loaded on Nitrocellulose Membrane Using Biotinylated D17Z1 Probes

3.3.1 DNA Hybridization (See Note 4)

DNA on the membrane was measured using North2South Chemiluminescent hybridization and detection kit and following manufacturer's instructions. Steps are briefly mentioned below.

1. Following detection of DNA-topoisomerase covalent complexes, rinse nitrocellulose membrane with $1\times$ TBS-T and allow it dry on a Whatman 3MM paper.
2. Once membrane is completely dry, place membrane in a UV light cross-linker box, and immobilize DNA by irradiating (UVP CL-1000 Ultraviolet cross-linker; $12,000\text{ mJ/cm}^2$; thrice) (*see Note 5*).
3. Prehybridization: Equilibrate North2South hybridization buffer at room temperature. Place membrane into hybridization tube and add sufficient hybridization buffer (use at least 0.1 mL hybridization buffer per cm^2 of membrane). Incubate the tube with membrane in a heat incubator rotator at $55\text{ }^\circ\text{C}$ for at least 30 min (*see Note 16*).
4. Hybridization: Add D17Z1 probes to hybridization buffer and continue incubation at $55\text{ }^\circ\text{C}$ (150 pmoles D17Z1 probes for 10 mL hybridization buffer). Incubate overnight to get stronger signal.
5. Dilute $2\times$ stringency buffer to $1\times$. Wash membrane with diluted $2\times$ stringency buffer at $55\text{ }^\circ\text{C}$, twice.
6. Transfer the membrane to a box, and block membrane with blocking buffer for $15\text{--}30\text{ min}$ at room temperature.
7. Transfer blocking buffer to a tube and add streptavidin-HRP conjugate. Retransfer blocking buffer containing streptavidin-HRP to membrane and incubate on shaker for $15\text{--}30\text{ min}$ at room temperature.
8. Dilute $4\times$ stringency buffer to $1\times$ using H_2O . Wash membrane with $1\times$ stringency buffer for 5 min at room temperature, thrice.
9. Incubate membrane in equilibrium buffer for 5 min at room temperature with gentle shaking.

3.3.2 Chemiluminescence-Based Detection

1. Detect biotin-streptavidin complex bound to DNA through D17Z1 probes using enhanced Chemiluminescence as per the manufacturer's instructions.

An example of the DNA hybridization on nitrocellulose membrane using D17Z1 probes is shown in Fig. 1.

**3.4 Detection
of Topoisomerase
II–DNA Covalent
Complexes (Top2ccs)
in the yeast
Saccharomyces
cerevisiae**

Day 1:

1. Inoculate yeast strain YMM10 pDEP1TOP2-3×HA into 20 mL SC medium lacking uracil and grow in a shaker incubator at 30 °C overnight.

Day 2:

2. The next morning, read the cells' optical density (OD) at $\lambda = 600$ nm on spectrophotometer, and dilute to 0.8 ODU/mL. 20 mL of culture per drug concentration will be needed. Allow the cells to grow ~2 h to reenter log phase.
3. Read OD again to make sure that cells are at log phase, and treat cells with etoposide or other Top2 poisons. Incubate at 30 °C for 30 min.
4. Centrifuge the cells at 3000 rpm for 5 min, 4 °C. Discard the supernatant and resuspend the pellet in 1 mL yeast lysis buffer (YLB).
5. Transfer the cells in 2 mL screw-cap microcentrifuge tubes and centrifuge at 14,000 rpm for 1 min, 4 °C. Discard the supernatant and resuspend in 700 μ L YLB.
6. Add approximately 0.7 mL acid-washed glass beads to the microcentrifuge tubes. Lyse the cells in a beadbeater-type homogenizer at full speed for 50 s, 4 °C. Let the machine cool for 5 min and run it again.
7. Incubate the lysates at 65 °C for 15 min.
8. Centrifuge at 14,000 rpm for 10 min.
9. Transfer maximum 400 μ L to each 1.5 mL eppendorf tube and add 700 μ L 1% sarkosyl solution (*see Note 18*).
10. Centrifuge again for 15 min at 14,000 rpm, room temperature.
11. Transfer 1 mL to each 15 mL falcon tube, add 2 mL 1% sarkosyl solution and mix.
12. Add 2 mL of 150% (w/v) cesium chloride solution to each new 5 mL OptiSeal tube (Beckman Coulter). Layer 3 mL of cell lysate prepared as described in **step 10** on top of the CsCl solution with 16G \times 1 1/2" needles and 3 mL syringes. After addition of yeast lysate to CsCl solution, $\rho_{(\text{CsCl})}$ is decreased to approximately 1.3 g/mL.
13. Ultracentrifuge at 42,000 rpm for 22 h, 25 °C. (NVT65.2 rotor, Beckman Coulter).

Day 3:

14. Remove the tubes from the ultracentrifuge rotor. At the tube bottom is the pellet containing DNA, RNA, and Top2–DNA covalent complexes. To retrieve the pellet, remove about 1.5 mL of the solution then cut off about 1.5 cm from the neck of the tube using a razor blade. Pour off the rest of the

solution while avoid dislodging the pellet. A translucent round pellet will become visible as soon as the solution is removed (*see Note 19*).

15. Wash the pellets with 500 μL of 70% ethanol. Gently remove the ethanol and set aside the tube for 5 min to allow any residual ethanol to evaporate.
16. Dissolve the pellet with 200 μL of nuclease-free H_2O . Make sure the volume added is sufficient for the pellet to be completely immersed. Vortex and incubate at 65 °C for 5 min.
17. Take the tubes from the heat block. Incubate at room temperature on a shaker for 1 h.
18. Transfer the solution to 1.5 mL eppendorf tubes. Add RNase A to the tubes to a final concentration of 30 $\mu\text{g}/\text{mL}$, and incubate for 30 min and 37 °C.
19. Add 20 μL of 3 M sodium acetate (1/10 volume) to the solution, then add 500 μL of 100% ethanol (~2 volumes). Mix well.
20. Incubate at -20 °C for 5 min.
21. Collect the precipitated DNA by centrifugation at room temperature for 5 min at 14,000 rpm. Discard the supernatant and dissolve the pellet containing DNA and Top2-DNA covalent complexes in 100 μL of nuclease-free H_2O .
22. Incubate at 65 °C for 5 min then incubate at room temperature on a shaker for 1 h.
23. Measure the DNA concentration of the samples using an UV spectrophotometer. The A260/A280 ratio should be approximately 1.9 by now. (The A260/A280 ratio should be around 2.2 before RNase A treatment).
24. Transfer equal amounts of DNA of the samples to new tubes. Make the volumes of the transferred samples equal by adding nuclease-free H_2O .
25. Add 1/9 volume 10 \times micrococcal nuclease reaction buffer to the tube and mix well. Add 0.5 μL of micrococcal nuclease (New England Biolabs) to the tube and mix well. Incubate at 37 °C for 30 min.
26. Add 1/3 volume 4 \times laemmli sample buffer with β -mercaptoethanol to the tube, and mix well.
27. Boil the samples in laemmli buffer at 100 °C for 5 min. Samples can be aliquoted and stored at -20 °C for future use.
28. Load equal amounts of DNA into the wells of a gradient SDS-PAGE gel, along with molecular weight marker.
29. Run the gel for 1.5 h at 100 V.
30. Transfer the DNA samples from the gel to PVDF membrane at 100 V for 1 h.

31. Block the membrane for 15 min at room temperature.
32. Incubate the membrane with anti-HA antibody (1:1000) in blocking buffer overnight at 4 °C.

Day 4:

33. Wash the membrane in three washes of 1× TBS-T, 10 min each.
 34. Incubate the membrane with the recommended dilutions of HRP-conjugated secondary antibodies in blocking buffer at room temperature for 1 h.
 35. Wash the membrane in three washes of 1× TBS-T, 10 min each.
 36. Prepare ECL solution for signal development by following the kit manufacturer’s introduction.
 37. Acquire image using darkroom development techniques or gel imaging systems for chemiluminescence detection.
- See Fig. 4 for an example of the assay detecting yeast Top2cc in YMM10 pDED1TOP2-3XHA treated with etoposide.

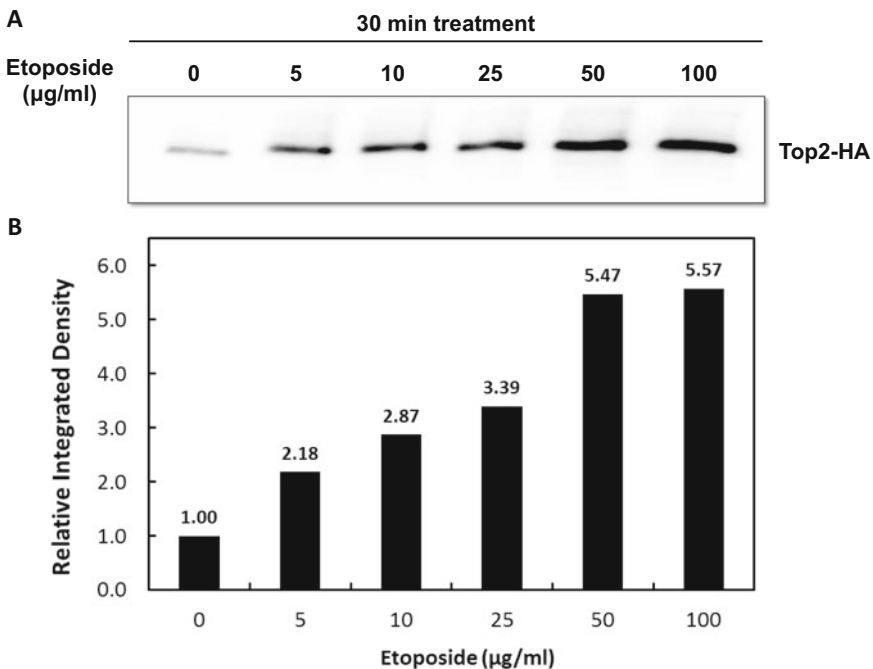


Fig. 4 Detection of Top2cc in *Saccharomyces cerevisiae*. Yeast strain YMM10 pDEP1yTOP2-3×HA were treated with etoposide of a series of doses for 30 min. Yeast Top2cc detection assay was performed as described in the protocol to collect yeast Top2 covalently bound to DNA. After SDS electrophoresis, immunoblotting of DNA-linked Top2 probed with anti-HA antibody is shown in *Panel A*. *Panel B* shows quantitation of Top2cc levels by densitometric analysis using ImageJ. Integrated density of Top2cc signal of each drug-treated group was normalized to that of control cells treated with solvent DMSO

4 Notes

1. Take appropriate precautions while handling GTC as it is highly toxic. Read the product MSDS.
2. Add DTT just before cell lysis to M lysis buffer.
3. Every time make fresh 8 mM NaOH from less than 6 months old 1 M NaOH stock.
4. For DNA hybridization detection using D17Z1 probes, DNA should be denatured before loading on to the nitrocellulose membrane. To denature DNA, boil DNA sample for 10 min and immediately put it on ice for 5 min.
5. If UV cross-linker is not available, UV transilluminator can be used. Place membranes in a UV transparent plastic wrap and keep DNA side down. Nitrocellulose membrane can be store in a dry place for a month at room temperature after sandwiching between Whatman filter papers.
6. Plate minimum 0.5×10^5 cells to obtain necessary DNA yield for further analysis. Plating more than 2×10^6 cells gives vicious cell lysate, which can obstruct DNA recovery. For optimal DNA yield and reproducibility of the experiments plate $0.5\text{--}1 \times 10^6$ cells per plate.
7. Length of drug treatment will depend on the goal and design of the experiment. In our hands, etoposide treatment ($10 \mu\text{M}$; 1 h) gives strong signal in different cell lines like RH30, Nalm6, HeLa, MDA-MB-231, HEK293, and HCT116.
8. Label OptiSeal tubes both at the top and the bottom. This will help keep track of samples after cutting the top of the OptiSeal tubes in **step 2** of Subheading 3.1.4. Sarkosyl is a detergent and it can remove the marker label on the OptiSeal tubes. If one label is removed, second label will be a useful backup.
9. Follow manufacturer's recommendations while using an ultracentrifuge. Ultracentrifuge conditions vary according to the rotor. Adjust conditions according to your ultracentrifuge rotor type.
10. While cutting the OptiSeal tube, place it in a stand and keep it steady to avoid dislodging of DNA pellet.
11. Pour liquid slowly avoiding dislodging of pellet. DNA pellet will be translucent and oval in shape.
12. If plating less than 0.5×10^5 cells, DNA yield will be low and frequently one will not have enough DNA to run duplicate samples on a slot blot in **step 10**. If plating more than 1×10^6 cells, cell lysate obtained in **step 3** will be too viscous. This can obstruct DNA recovery in **step 4**. One way to overcome this problem is to use 2 mL of M lysis buffer in **step 3** and transferring each 1 mL cell lysate to two separate eppendorf tubes.

After DNA recovery in **step 4**, combine DNA pellets from both the tubes for further steps. Another way is to shear the cell lysate to reduce its viscosity. Use 1 mL latex-free syringe with 25G/8 gauge needle to pass 1 mL of each cell lysate through syringe. Repeat ten times for each sample.

13. Cell lysate can be stored at -80°C for later processing. We were able to detect Top2 covalent complexes using sample stored for one and half months.
14. We were also able to isolate DNA by gently inverting (4–5 times) eppendorf tube containing cell lysate and 100% ethanol, and spooling DNA using pipette tip.
15. If GTC solidifies in eppendorf tube during low temperature incubation at -20°C , add 100% ethanol directly to cell lysate in the plate, gently shake the plate and after brief low temperature incubation, transfer supernatant to a 1.5 mL eppendorf tube and centrifugation for 15 min at maximum speed to obtain DNA pellet).
16. Decant or aspirate supernatant carefully without throwing out DNA pellet, which may or may not be visible.
17. Hybridization can be performed using hybridization bags but we have not tried that [13].
18. Higher volume ($> 500\ \mu\text{L}$) of the lysate will result in low density of CsCl solution, leading to protein contamination.
19. Yeast nucleic acid pellet is more smooth and slippery than mammalian nucleic acid pellet. The yeast pellet can be easily lost when pouring off the solution. Make sure the side of the tube where the solution flows out is perpendicular to the side at which the pellet stays due to centrifugal force. The solution can be poured into a petri dish plate. If the pellet is gone with the solution, add 95% ethanol to the plate to visualize the pellet and retrieve the pellet with a pipette.

References

1. Vos SM, Tretter EM, Schmidt BH, Berger JM (2011) All tangled up: how cells direct, manage and exploit topoisomerase function. *Nat Rev Mol Cell Biol* 12(12):827–841
2. Dewese JE, Osheroff N (2009) The DNA cleavage reaction of topoisomerase II: wolf in sheep's clothing. *Nucleic Acids Res* 37(3):738–748
3. Chen SH, Chan NL, Hsieh TS (2013) New mechanistic and functional insights into DNA topoisomerases. *Annual Rev Biochem* 82:139–170
4. Walker JV, Nitiss JL (2002) DNA topoisomerase II as a target for cancer chemotherapy. *Cancer Invest* 20(4):570–589
5. Pommier Y (2013) Drugging topoisomerases: lessons and challenges. *ACS Chem Biol* 8(1):82–95
6. Pommier Y, Sun Y, Huang SN, Nitiss JL (2016) Roles of eukaryotic topoisomerases in transcription, replication and genomic stability. *Nat Rev Mol Cell Biol* 17(11):703–721
7. Nitiss JL, Soans E, Rogojina A, Seth A, Mishina M (2012) Topoisomerase assays. *Curr Protoc Pharmacol Chapter 3:Unit 3 3*

8. Nitiss JL (2001) Topoisomerase assays. *Curr Protoc Pharmacol* Chapter 3:Unit3 3
9. Subramanian D, Rosenstein BS, Muller MT (1998) Ultraviolet-induced DNA damage stimulates topoisomerase I-DNA complex formation in vivo: possible relationship with DNA repair. *Cancer Res* 58(5):976–984
10. Nitiss JL, Rose A, Sykes KC, Harris J, Zhou J (1996) Using yeast to understand drugs that target topoisomerases. *Ann N Y Acad Sci* 803:32–43
11. Kiiianitsa K, Maizels N (2013) A rapid and sensitive assay for DNA-protein covalent complexes in living cells. *Nucleic Acids Res* 41 (9):e104
12. Kiiianitsa K, Maizels N (2014) Ultrasensitive isolation, identification and quantification of DNA-protein adducts by ELISA-based RADAR assay. *Nucleic Acids Res* 42(13):e108
- 13 Brown T (2001) Hybridization analysis of DNA blots. In: Ausubel FM, Brent R, Kingston RE, Moure DD, Seidman JG, Smith JA, Struhl K (eds) *The current protocols in molecular biology*. Wiley and Sons, New York, pp 2.10.1-2.10.16

Visualization and Quantification of Topoisomerase–DNA Covalent Complexes Using the Trapped in Agarose Immunostaining (TARDIS) Assay

Ian G. Cowell and Caroline A. Austin

Abstract

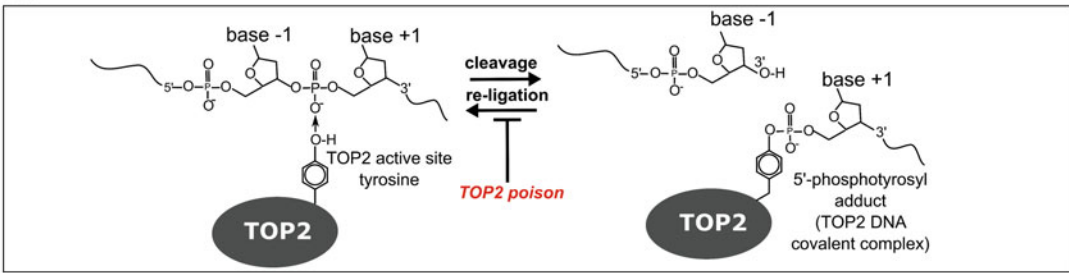
The TARDIS assay was originally developed as a means of detecting and quantifying melphalan and cisplatin DNA adducts at the single cell level, but it has since been adapted to quantify topoisomerase DNA complexes that result from the actions of topoisomerase poisons and this is currently the main use of the assay. The method employs sensitive immunofluorescent detection to quantify topoisomerase molecules covalently coupled to DNA in what are often referred to as cleavage complexes. Free topoisomerase molecules, and other cellular constituents are first removed using salt-detergent extraction of agarose-embedded, unfixed cells. Using these stringent extraction conditions, genomic DNA remains in place in the agarose as “nuclear ghosts,” and any covalent attached molecules can be detected and quantified by immunofluorescence with a low background.

Key words Topoisomerase, Covalent complex, TARDIS, Immunostaining

1 Introduction

Topoisomerase enzymes create transient DNA strand breaks enabling changes in DNA topology. In the case of type IB DNA topoisomerases such as mammalian TOP1, the enzyme introduces a single-strand break, allowing rotation of the DNA fibre. Type II topoisomerases such as mammalian TOP2 introduce a staggered double-strand break and enable the passage of a second DNA duplex through the break, thus changing supercoil linking number or allowing decatenation of two DNA segments [1]. After DNA strand cleavage, both TOP1 and TOP2 topoisomerases remain covalently linked to the cleaved DNA via their active-site tyrosine residues in a 3'- or 5'- DNA phosphotyrosyl linkage respectively. At the end of the reaction cycle, the strand breaks are resealed and the enzyme released (Fig. 1a). Various chemical compounds can interfere at different points in the TOP1 and TOP2 reaction cycles, and one class, the topoisomerase poisons, are widely used in anticancer

A



B

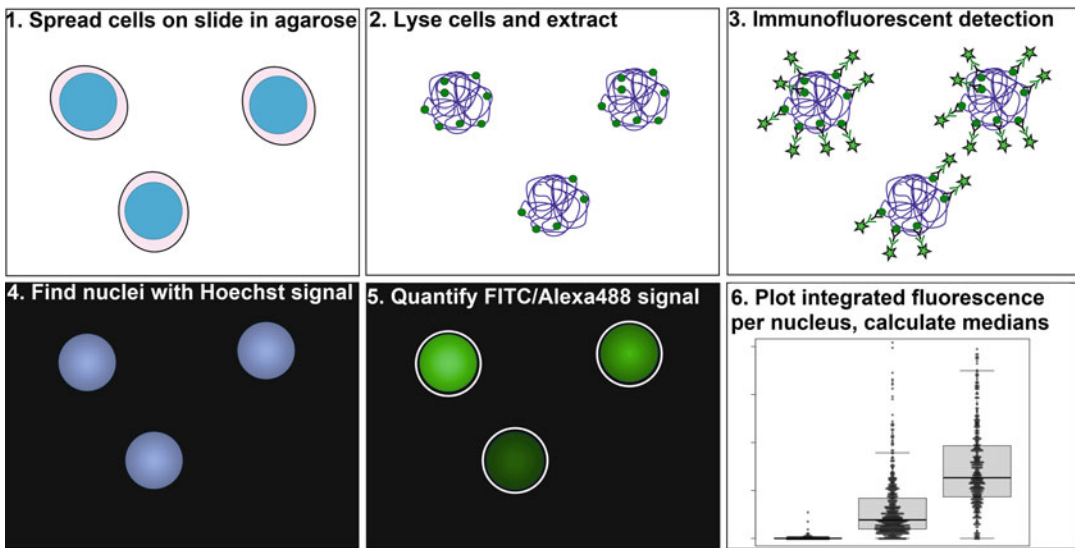


Fig. 1 TARDIS assay principle. **(a)** TOP2 is a dimeric enzyme and introduces a DNA double-strand break via nucleophilic attack by active site tyrosines on the DNA sugar phosphate backbone. TOP2 subunits remain covalently linked to the cleaved DNA strand via a 5'-phosphotyrosyl linkage (only one DNA strand is shown in the figure). The covalent TOP2–DNA complexes are transient and reversible, but are stabilized by TOP2 poisons and can be detected and quantified by the TARDIS assay. TOP1 acts via an analogous mechanism, attacking a single strand, and remaining attached to the cleaved DNA strand via a 3'-phosphotyrosyl linkage. **(b)** Processing of samples for TARDIS analysis can be divided into the following steps. 1 Cells are spread in a thin layer of agarose onto glass microscope slides. 2 The slides are submerged in lysis and extraction buffers. This leaves “nuclear ghosts” consisting of genomic DNA (*twisted lines*) which is too large to escape the agarose. Any protein molecules covalently linked to the DNA (indicated as *small circles*) also remain in the agarose. 3 Covalently linked molecules such as TOP2 are detected by immunofluorescence, in this example using a FITC or Alexa-488 linked secondary antibody. Slides are counterstained with Hoechst. 4 and 5 Images are obtained for both the Hoechst and FITC/Alexa-488 signals. After shade correction, the Hoechst signal is used to locate objects (nuclei) and the corresponding FITC/Alexa-488 signal is determined for each object separately. 6 The data can be conveniently displayed as a scatter plot where each dot represents the integrated fluorescence of a single nucleus, from which median values and other parameters can be calculated

therapy. Topoisomerase poisons inhibit the religation step (*see* Fig. 1a), resulting in the accumulation of single- or double-strand breaks with covalently coupled topoisomerase molecules. These topoisomerase–DNA covalent complexes, or as they are often called, “cleavage complexes,” can be detected and quantified using the TARDIS assay. In addition to clinically used anticancer drugs, some natural compounds are also topoisomerase poisons, including curcumin [2], dietary flavonoids [3, 4], and selenite [5]. The ability to detect and quantify specific protein–DNA complexes provides a useful tool in genome stability studies, drug development and in evaluating natural compounds. Initially, the TARDIS assay was developed as a method to quantify melphalan–DNA adducts and was subsequently adapted to detect topoisomerase–DNA covalent complexes [6–9], and to our knowledge it is still the only approach that allows sensitive and specific detection of these complexes at the single cell level. Since it relies on specific antibodies for detection, the TARDIS assay can discriminate between TOP1 complexes and TOP2 complexes and between the two human TOP2 orthologs, TOP2A and TOP2B. However, in principle the assay could be used to detect and quantify any covalently linked DNA adduct, including posttranslational modifications of topoisomerases providing suitable antibodies are available. The method relies on immunofluorescent detection using a sensitive CCD camera, but differs from standard immunofluorescence approaches in that unfixed cells are spread on slides in agarose and then extracted *in situ* in detergent and high salt buffers (Fig. 1b). These conditions remove histones (Fig. 2a, b) and other proteins from the cells, leaving only genomic DNA with any covalently attached molecules in the agarose as “nuclear ghosts,” and these can be detected without interference from other cellular components.

2 Materials

2.1 Microscopy Equipment

TARDIS is a quantitative immunofluorescence-based technique. It relies on a microscope setup with a sensitive monochrome camera and good quality 10× or 20× objective (*see* Notes 1 and 2).

2.2 Slide Preparation

1. Microscope slides with frosted end for labeling.
2. A tray about 20 × 30 cm in area and deep enough to hold crushed ice 2–3 cm deep.
3. A glass plate that will fit inside the tray on top of the ice.
4. Coplin jars or Wheaton staining dishes

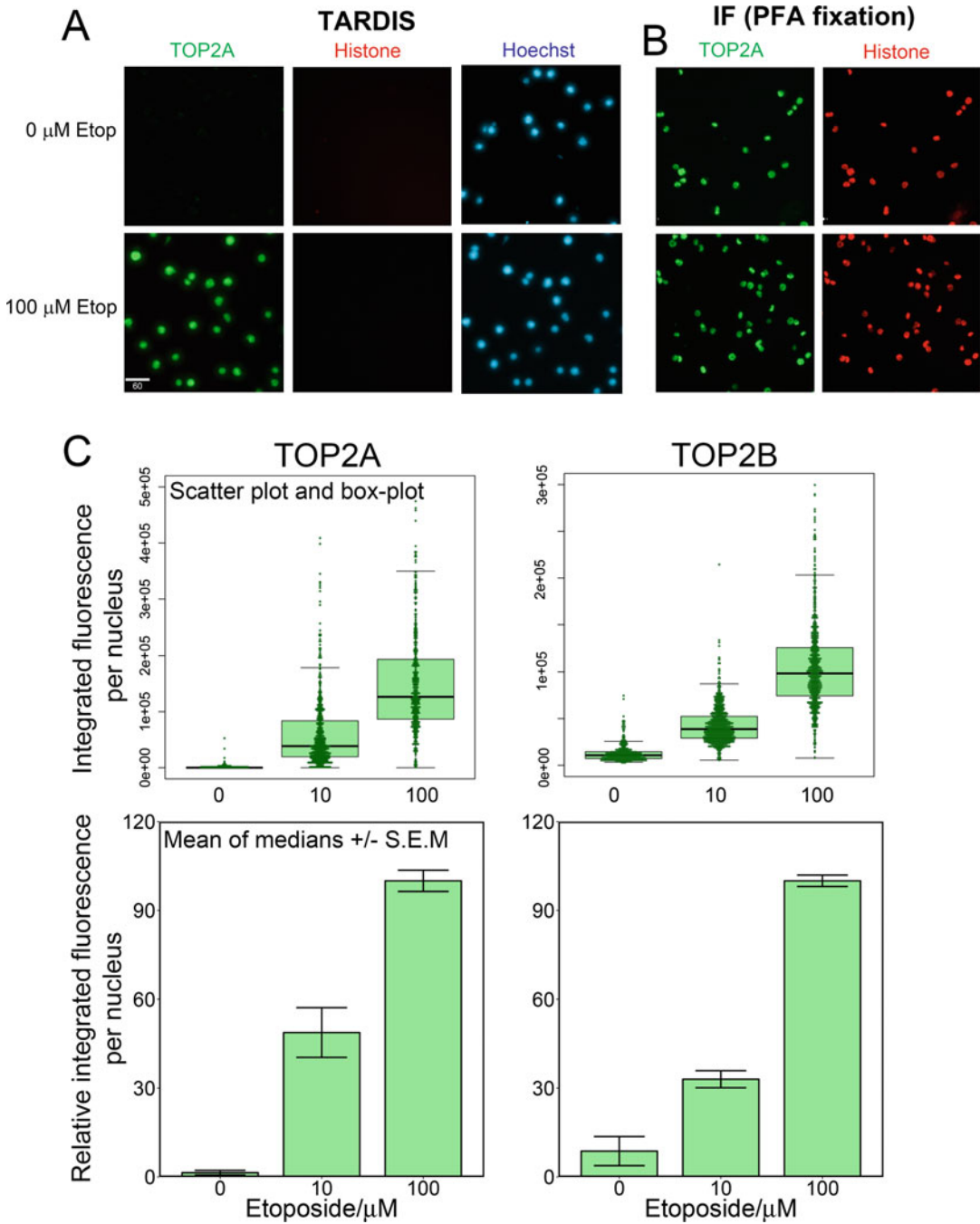


Fig. 2 Example TARDIS experiment. (a and b) Fluorescent micrographs of etoposide-treated cells processed for TARDIS (a) or standard immunofluorescence with paraformaldehyde fixation (b). In both cases cells were stained with rabbit anti-TOP2A and mouse anti-histone primary antibodies and anti-rabbit Alexa-488 (green)/anti-mouse Alexa-594 (red) secondary antibodies. The lysis and extraction conditions employed for TARDIS analysis removed histone protein and TOP2A in untreated cells, but in etoposide treated cells a proportion of the TOP2A (but not histone) was retained on the DNA (anti-histone was included here for demonstration

5. 0.5% agarose: Prepare 0.5% agarose (Sea-prep ultralow gelling temp, cat # 50302) using water in a glass universal bottle or similar. Store at 4 °C.
6. Phosphate buffered saline (PBS): 10 mM sodium phosphate, 2.68 mM potassium chloride, 140 mM sodium chloride, pH 7.2. Typically made up from Gibco PBS tablets (Cat-no 18912) dissolved in 500 mL deionized water.
7. 2% Agarose: Prepare 2% agarose (Sea-prep cat # 50302) in PBS in glass universal bottles or similar. Store at 4 °C. Prior to use, melt in a microwave oven at low power and keep at 37 °C until ready to make slides.
8. Lysis buffer: 1% SDS (w/v); 20 mM sodium phosphate, 10 mM EDTA, pH 6.5. Typically prepare 1 L.
9. Protease inhibitors: Benzamidine, 100 mM stock, use stock at 1% (v/v); PMSF, 100 mM use stock use at 1% (v/v); leupeptin, stock 2 mg/mL, use stock at 0.1% (v/v); pepstatin, stock 2 mg/mL, use stock at 0.1% (v/v). Alternatively, use a protease inhibitor cocktail such as Sigma P8340 (*see Note 3*).

2.3 Immuno-fluorescence

1. Wash buffers: PBS, PBS-T (PBS + 0.1% Tween 20).
2. Antibody dilution/blocking buffer: PBS-T + 1% BSA.
3. Primary antibodies: Antibodies that work well in standard immunofluorescence applications should be suitable for TARDIS (*see Note 4*).
4. Secondary antibodies: Fluorescently conjugated secondary antibodies suitable for use with chosen primary antibodies. We typically use AlexaFluor-488 coupled anti-rabbit IgG (Thermo A-11034) diluted 1:250 (*see Note 5*).
5. Hoechst 33258 dye solution: Prepare at 1 mM in water, dilute this stock to 1 mM in PBS for use.

3 Methods

3.1 Agarose Coating of Slides

It is necessary to precoat the slides with agarose so that the cell-containing agarose layer prepared in Subheading 3.3 adheres soundly to the slide.

1. Melt the 0.5% agarose using a microwave oven at low power.

Fig. 2 (Continued) purposes and is not required routinely for TARDIS analysis). (c) Example TARDIS data comparing untreated cells and cells exposed to 10 μ M or 100 μ M etoposide. Data from individual experiments can be displayed as scatter plots or combined scatter and box plots (*top*). Median values from replicate experiments can then be analysed to give means of medians (*bottom*)

2. Lay the required number of slides on the bench, and one at a time place one drop of 0.5% agarose onto the end of a slide.
3. Immediately smear the agarose across the slide using another (dry) slide by dragging the agarose along the length of the slide.
4. Repeat for the next slide.
5. Allow slides to air-dry and then store in an air-tight container. Prepare slides up to a few days in advance.
6. Slides must be evenly but thinly coated.

3.2 Cell Treatments and Collection

The protocols for treating cells will depend on the nature of the compound/s of interest and the cells used. As an example, for the analysis of TOP2 protein–DNA complexes induced by the TOP2 poison etoposide, we routinely treat cells for 1–2 h before collecting the cells in ice-cold PBS. It is useful to include a positive control treatment, both to check for the success of the experiment and to use as a standard for comparison between experiments. We routinely use 100 μ M etoposide treatment for this purpose which gives a strong, reproducible signal for TOP2A and TOP2B. The steps below describe the cell treatment and collection routine for mammalian suspension or adherent cells.

3.2.1 Suspension Cells

1. For suspension cells such as K562 cells, cells should be at a density of $2\text{--}5 \times 10^5$ cells/mL before starting the experiment, and should not be in yellow, exhausted medium. If the medium looks yellow or if the cells are above this density, dilute cells and start the experiment on the next day.
2. Drug exposure can be carried out either in 6-well plates or in 15 mL Falcon tubes. Since the cells will later be spun and washed with PBS, using tubes can be more convenient if the drug incubation time is short (≤ 2 h). Plate 2 mL of cells for each drug treatment.
3. Add drug, or solvent control (*see Note 6*) to each well or tube, mix thoroughly and return cells to the incubator.
4. After the appropriate time, pellet the cells in a benchtop centrifuge using 15 mL Falcon tubes. Wash cells in ice-cold PBS. Carefully remove as much of the PBS as possible and place the cell pellets on ice. Once all samples are collected, proceed immediately to the cell lysis stage (Subheading 3.3).

3.2.2 Adherent Cells

1. For adherent cells such as MEFS, seed cells in wells of a 6-well plate at a density of 3×10^4 per well and incubate for 48 h before adding drug.
2. Add drug or solvent control to each well, and ensure mixing.

3. At the end of the drug treatment, wash cell monolayer with PBS and trypsinize. Add 5 mL of ice-cold PBS to each well and collect trypsinized cells by centrifugation in a bench-top centrifuge. Wash cell pellet in 10 mL ice-cold PBS. After pelleting the cells, remove as much of the supernatant as possible and place the cells on ice. Once all samples are collected, proceed immediately to the cell lysis stage (Subheading 3.3).

3.3 Slide Preparation and Cell Lysis

Carry out **steps 1–4** below during drug exposure (Subheading 3.2). Cell lysis and antibody washes are performed using one or more Coplin staining jar, Wheaton dish or equivalent to hold slides. For clarity, we will refer to “staining dish” in the steps below.

1. Melt the 2% agarose using a microwave oven at low power, keep molten in a 37 °C water bath.
2. Arrange a series of pre-agar-treated slides (Subheading 3.1) on the bench, label with a pencil. If the aim is to analyse the samples with two antibodies on different slides in the same experiment (e.g., anti-TOP2A and anti-TOP2B *see* **Note 4**), or to produce duplicate slides for each treatment, arrange the slides in two columns, one for each antibody or duplicate.
3. Label a series of 1.5 mL Eppendorf tubes, one for each drug treatment.
4. Partly fill a deep tray with ice, and place a glass plate of approximately 15 × 20 cm in size on top of the ice. This is used to quickly set the agarose once spread on the slides.
5. Remove any remaining PBS from the cell pellets and for all samples resuspend the cells in 100 µl ice cold PBS per tube and return to ice.
6. Taking one cell suspension at a time, transfer 50 µl of the cell suspension into one of the labeled Eppendorf tubes and place the tube in a 37 °C water bath in a floating rack. Incubate for 30 s, then remove the tube from the water bath and add 50 µl molten 2% agarose. Gently suck the mixture up and down 2–3 times using a Gilson P200 or similar to thoroughly mix.
7. Using a Gilson P200 place a drop of the agarose–cell suspension at the nonfrosted end of a precoated prepared slide. Immediately smear the cell-suspension-in-agarose from one side of the slide to the other evenly with a dry slide using a single gentle movement. The aim is to get a thin layer of cells in agarose covering the entire non-frosted part of the slide (*see* **Note 7**). If doing two antibodies on pairs of slides, or preparing replicate slides on the same samples, place the cell suspension on one slide from each column (*see* **step 2** above).

8. Also prepare one slide as above, from an agarose sample diluted with PBS, but with no cells: this is used to subtract background fluorescence during microscopy.
9. As the slides are prepared, place each slide on top of the ice-cooled glass plate to set the agarose quickly.
10. Once all of the slides are prepared and the agarose has set, place the slides in a staining dish containing lysis buffer + protease inhibitors (*see Note 3*). Add protease inhibitors just before placing the slides in the lysis buffer.
11. Incubate the slides in lysis buffer for 30 min at room temperature.
12. Although we prefer to continue directly with the processing, slides can be stored frozen at this stage to continue with the processing at a later date (*see Note 8*).
13. If not freezing slides for later processing, discard the lysis buffer and replace with 1 M NaCl + protease inhibitors (*see Note 3*). Incubate for 30 min at room temperature.
14. Discard the NaCl solution and wash slides three times in PBS initially for 30 s, then twice for 5 min. The second two washes should contain protease inhibitors (*see Note 3*).

3.4 Antibody Staining

Immunofluorescent staining can be performed using a slide staining tray with a lid or directly on the bench on Parafilm strips. The advantage of the former is that the level can be adjusted easily if the bench is not perfectly horizontal, potentially reducing the volume of antibody required. For the steps below we will assume the second arrangement.

1. Discard the wash buffer and taking each slide one at a time, remove from the staining dish with fine pointed forceps and drain off as much buffer as possible, touching the corner of each slide on tissue paper to blot. Place slides on strips of Parafilm on the bench-top, agarose side up.
2. Dilute the primary antibody in antibody dilution/blocking buffer. Enough antibody should be used to just cover the slide; this is typically 200 μ l per slide. Place the lid of a staining tray or equivalent over slides and incubate for 1.5 h (*see Note 9*).
3. At the end of the primary antibody treatment place slides in a staining dish containing PBS-T. After 30 s discard the buffer and wash slides two more times for 5 min each and once for 10 min in PBS-T, the last wash containing protease inhibitors.
4. At the end of the last wash remove the slides from the dish using forceps, drain off excess liquid and place slides on fresh Parafilm as above.

5. From this step onward keep the slides in dark or in subdued light. Dilute the fluorescent secondary antibody in antibody dilution/blocking buffer (*see Note 5*). Pipette diluted secondary antibody onto slides. Place the lid of a staining tray or equivalent over slides and incubate for 1.5 h.
6. At the end of the incubation with the secondary antibody return the slides to a staining dish containing PBS-T. After 30 s discard the buffer and wash slides two more times for 5 min each.
7. At this stage slides can be stored in the dark overnight at 4 °C in PBS-T + protease inhibitors before examining the slides (*see Note 3*). Alternatively, carry out a last PBS wash for 20 min (without protease inhibitors) if the slides are to be examined on the same day.
8. Remove the slides from the staining dish with fine pointed forceps and drain off as much buffer as possible, touching the corner of each slide on tissue paper to blot. Place slides on Parafilm strips on the bench and pipette 0.5 mL of 1–2 mL of 1 μ M Hoechst 33258 in PBS onto each slide. Cover slides with a tray lid and incubate for 5 min.
9. Drain off surplus Hoechst solution and mount coverslips onto each slide using Vectashield mounting medium (without DAPI) or equivalent using 50 \times 20mm coverslips. Seal corners of coverslip with clear nail varnish.

3.5 Microscopy

1. Carry out microscopy as soon as possible, ideally straight away, but slides can be stored for 2–3 days at least in the dark at 4 °C without noticeable loss of quality.
2. Starting with the sample that is expected to give the highest immunofluorescent signal (e.g., we routinely use a 100 μ M etoposide positive control) set the microscope camera exposure, being careful to avoid saturation of the sensor (*see Notes 10 and 11*). For all subsequent images in the session keep the exposure settings the same.
3. For each slide record several fields of cells, avoiding the extreme edges of the slides and areas where the cells are clumped or overlapping or where they are very sparse (*see Note 12*). For each field record separate grey-scale images for both Hoechst and FITC channels.
4. Also record one or more images from the control (no cell) slide and from evenly fluorescing bright slides (*see Note 13*).
5. Ensure that all images corresponding to the same antibody employ the same exposure settings, and record all images for one experiment in one session.
6. Once images are collected, proceed to image processing (*see Notes 14–16*).

4 Notes

1. A conventional immunofluorescence microscope is suitable for these studies. Systems can be fully manual or motorized, but image acquisition can be quicker with a partially automated motorized system. Certain equipment details need to be considered in order to obtain useful detection sensitivity and reproducibility: (a) good quality $10\times$ and/or $20\times$ planar apochromatic objectives with high NA and low levels of autofluorescence associated with the glass and adhesives used to assemble the lenses; (b) a bright stable fluorescent light source. We have used a xenon arc lamp and metal halide X-cite system (EXFO) system. Recent LED illumination should also be suitable; (c) appropriate narrow band filter sets for FITC (or other fluorochrome) and Hoechst fluorescence; (d) sensitive monochrome cooled CCD camera (*see Note 2*). Specifications for the original system used for TARDIS analysis are described by Frank et al. [8] and we also have a similar system based on a full manual Leica DMLB microscope [6]. Our current primary system for TARDIS analysis is based on an Olympus IX81 inverted microscope with metal halide X-cite 120Q illumination, $10\times$ VPLA NA 0.3 objective and a Hamamatsu Orca-AC cooled CD camera.
2. CCD cameras are continually being developed. Our current set ups employ a Hamamatsu Orca-AG and Photometrics Cool-snap HQ2 cameras which have similar specifications. Fluorescent signals associated with TARDIS analysis are faint compared to typical standard immunofluorescence, requiring a sensitive cooled CCD camera. Other pertinent characteristics include low dark-current, large photosite full-well capacity and high quantum efficiency of the sensor. These relate to the accumulation of electrons in photosites in the absence of illumination, the number of electrons to fill the photosites and the efficiency of converting photons to electrons at the photosite respectively. In turn these factors determine the sensitivity, and dynamic range of the sensor. Suitable sensors contain about a million photosites (1 megapixel) and can be operated in 2×2 binning mode, whereby 2×2 squares of photosites act as if they were a single larger site and have at least 12-bit analogue to digital conversion. The technical specifications of the cameras mentioned above are given in Table 1.

Table 1
Cooled CCD Camera data from manufacturer's datasheets

	Hamamatsu Orca-AG	Photometrics Coolsnap HQ2
Photosite size (mm)	6.45 × 6.45	6.45 × 6.45
Number of photosites	1344 × 1024	1393 × 1040
Full-well capacity	18 K e ⁻	16 K or 30 K e ⁻ binned
Dark current	0.03 e ⁻ /pixel/s	0.001 e ⁻ /pixel/s (-30 °C)
A-D conversion	12/16 bit	14 bit

3. Protease inhibitors are essential for TARDIS analysis of topoisomerase complexes. Subheading 3 describes at which point they are required. Individual protease inhibitors can be used, as listed in Subheading 2.2. However, it is more convenient to use a premade protease inhibitor cocktail such as Sigma P8340. In this case, the cocktail is used at 0.25% v/v in the SDS lysis buffer, 0.1% in the 1 M NaCl wash and at 0.05% in wash buffers where protease inhibitors are indicated.
4. The success of the TARDIS assay depends on good primary antibodies. For TOP2, we have found rabbit polyclonal antibodies to give a more robust signal than mouse monoclonals. We routinely assay for TOP2A and TOP2B–DNA complexes in the same experiment using one set of slides each for each topoisomerase isoform. However, in principle it is possible to quantify two targets in the same slides, using primary antibodies raised in different species and suitable secondary antibodies.
5. We originally used FITC-conjugated goat anti-rabbit IgG secondary antibodies. However, with the development of brighter more photostable fluorochromes, we now routinely use Alexa Fluor 488-conjugated secondary antibodies.
6. When treating cells, ensure that all treatments contain the same concentration of solvent in which the drug of interest is dissolved, such as methanol or DMSO. This includes a solvent control, where the cells have received just the solvent.
7. When spreading agarose-cell suspension over slides the aim is to get a thin even layer over the whole nonfrosted part of the slide. The agarose should be spread in a single action using a second clean slide held at about 45 degrees to horizontal. Before carrying out the first TARDIS experiment, it could be useful to practice spreading agarose on slides in this way to obtain an even layer.

8. To store cells for later processing, place slides in twos back-to-back in 50 mL Falcon tubes containing 10% v/v glycerol in PBS. Store at $-20\text{ }^{\circ}\text{C}$. After removal from the freezer, wash slides once in PBS, before continuing to Subheading 3.3, step 13.
9. We routinely carry out our antibody incubations for 90 min at room temperature, although we obtain equivalent results with overnight incubations at $4\text{ }^{\circ}\text{C}$. Other antibodies may require different conditions.
10. Setting a correct exposure time is essential. Exposure times must be set to record a robust fluorescent image from the brightest samples but not saturate the recording device. For TOP2 TARDIS, we typically include a $100\text{ }\mu\text{M}$ etoposide treatment as a positive control, and use this to set the exposure for the rest of the experiment. However, if the samples to be analysed all give much lower fluorescent signals than $100\text{ }\mu\text{M}$ etoposide, $10\text{ }\mu\text{M}$ etoposide is preferable as the control. Most camera set ups have an auto-exposure facility. This can be used to determine the optimum exposure time for the positive control, but must then be disabled so that all subsequent images (for that antibody) are recorded with the same settings for the duration of the session. Exposure times are typically in the range of 100 ms to 1 s for topoisomerase TARDIS, depending on the sample, the camera and the microscope optics. Samples can also be susceptible to photo-bleaching during imaging, which can result in lower than expected fluorescence values. Modern fluorochromes are less prone to bleaching, but it can easily be checked for by taking a series of three consecutive images of the same field of nuclei. A fall of the median immunofluorescent signal per nucleus would indicate bleaching, and suggest using lower excitation intensity or a more photostable fluorochrome.
11. Other camera settings that need to be considered are: (a) binning, for the cameras listed in Table 1, and similar devices, binning should be set to 2×2 ; (b) gain should be set to its lowest value (usually 0); (c) shutter controls should be arranged for maximum image protection, which essentially means that the shutter is only open (and the sample illuminated) for purposes of framing and focussing and image recording.
12. Obtaining an optimum density of cells on the slides is important. If the cells are too sparse, more images will be required to record data from sufficient cells. Whereas, if the cells are too densely packed, it can be difficult or impossible to separate

individual nuclei during image analysis due to clumping and overlapping cells. The cell numbers given in the protocol (Subheading 3.2) aim to give optimal cell densities on the slides, but numbers can be adjusted if necessary. Uneven spreading of the cell-agarose suspension in step (Subheading 3.3) can also result in clumping of nuclei at one end of the slide.

13. In addition to the samples themselves, two other types of slides are required; a Dark-Reference slide and a Bright-Reference slide. The former is used correct for extraneous light and fluorescence coming from the microscope optics, the slide and agarose; the latter is used to correct for any unevenness in the sample illumination. Together they produce a “Shade-Correction” which is applied to all sample images (*see Note 14*). The Dark-Reference slide is prepared along with the sample slides, but contains no cells. The Bright-Reference slides are simply evenly fluorescing samples. In the original method describe by Frank et al. [8] these were solutions of 3 μM fluorescein and 200 μM 4-methylumbeliferone in 20 μm -deep observation chambers, but a piece of evenly fluorescent plastic of a suitable shape and size also suffices. Dark- and Bright-Reference slides are required for both fluorescence channels, typically Hoechst and FITC/AlexaFluor-488. Dark-Reference images must be recorded using the same exposure settings as were used for the samples. The Bright-Reference images are recorded at a suitable exposure that does not saturate the sensor, typically determined using the auto-exposure function.
14. Image analysis can be divided into three parts. We currently use Volocity (Perkin Elmer) software for image analysis, but the steps involved would be equivalent for other analysis software. Firstly, Hoechst and FITC/AlexaFluor-488 shade-corrections are generated from the Bright- and Dark-Reference slide images (*see Note 13*) and these corrections are applied to the sample images to correct for background and any illumination unevenness. Secondly, for each pair of images (Hoechst and FITC/Alexa-488), the outline and position of each nucleus is determined using the Hoechst fluorescence image (Fig. 1b). For each nucleus thus identified, parameters including number of pixels, average pixel intensity and integrated fluorescence values are determined for both Hoechst and FITC channels. The result for, each image, is a table of values including the

integrated fluorescence value for each nucleus in both the Hoechst and FITC/AlexaFluor-488 channel. In the third stage, these data are exported into a spreadsheet for further analysis and presentation (*see* **Note 15**).

15. As described above, we use Volocity software (PerkinElmer) for image management and analysis. The data is output as a series of integrated fluorescence per nucleus values for each image. It is convenient and informative to plot this data (FITC/AlexaFluor-488 integrated fluorescence) as a scatter plot or as a scatter plot with superimposed box plot as shown in Figs. 1b and 2c, upper panels. We have used Graphpad Prism software for this, and also R-studio (r-project.org, rstudio.com) using ggplot2 and beeswarm packages. The graphs in Fig. 2 were generated with the latter, and the R-script to produce the superimposed scatter- and box plots is given in Table 2. For this script the data should be contained in a CSV (comma-separated-value) file (TOP2A.CSV in the example), consisting of two columns; the first with the header “Etop” is the relevant treatment, in this case etoposide concentration. The second column with the header INTFLUOR consists of the integrated fluorescence values. All the data is arranged in these two (long) columns (*see* bottom of Table 2).
16. Data analysis described to this point refers to a single biological replicate experiment. A typical TARDIS study consists of a series of biological replicates. Example data is shown in Fig. 2c. The top panels depict a single experiment. The lower panels represent the mean of the median values for each treatment, derived from this and two further replicate experiments. In this case the means of the medians have also been normalized to the mean of the 100 μ M treatments, which aids comparison between different experiments.

Table 2
R-script code and data layout to generate scatter-plot and box-plots—see Note 15

R-script (R 3.1.1, requires ggplot2 and beeswarm libraries)

```
## A. Load relevant R libraries
library(beeswarm)
library(ggplot2)

## B. Read data from csv file - i.e. put the name of your .csv file containing the data between the quoted
marks
data1 <- read.csv("TOP2A.csv")
data1

##Plot - Plot title and axis labels can be changed by altering the text between quote marks
par(oma=c(8,3,3,3))
beeswarm(INTFLUOR ~ Etop, data1, cex=0,
xlab="Etoposide / uM ",
ylab="Integrated fluorescence per nucleus",
cex.lab=1.5,
cex.axis=1.5,
#Use ylim to set specific limits to Y axis
#ylim=c(0, 2e+05),
las=3)
#Different colours can be substituted for lightgreen below
A <- boxplot(INTFLUOR ~ Etop, data1,col = "lightgreen", outline=FALSE, main=" PLOT TITLE",
xaxt="n",
yaxt="n",
add=TRUE)
#Symbol shapes and sizes can be altered by changing the pch an cex values below
beeswarm(INTFLUOR ~ Etop, data1,
pch = 1, col= "darkgreen",cex=.5,
corral="wrap",
method="center",
cex.lab=1.5,
las=3,
corralWidth=.5,
add=TRUE)

#corralWidth=.25

## The following code displays and saves the summary data as "TOP2A_Rep1_sumtable.csv"
##You will need to manually change the csv filename to something suitable
sumtable <- A$stats
colnames(sumtable)<-A$names
rownames(sumtable)<-c('min','lower quartile','median','upper quartile','max')
sumtable
write.csv(sumtable, "TOP2A_Rep1_sumtable.csv", row.names = TRUE)
```

First 3 rows of data table (TOP2A.csv)

Etop	INTFLUOR
0	4731
0	1538

References

1. Vos SM, Tretter EM, Schmidt BH, Berger JM (2011) All tangled up: how cells direct, manage and exploit topoisomerase function. *Nat Rev Mol Cell Biol* 12:827–841
2. Lopez-Lazaro M, Willmore E, Jobson A et al (2007) Curcumin induces high levels of topoisomerase I- and II-DNA complexes in K562 leukemia cells. *J Nat Prod* 70:1884–1888
3. Lopez-Lazaro M, Calderon-Montano JM, Burgos-Moron E, Austin CA (2011) Green tea constituents (–)-epigallocatechin-3-gallate (EGCG) and gallic acid induce topoisomerase I- and topoisomerase II-DNA complexes in cells mediated by pyrogallol-induced hydrogen peroxide. *Mutagenesis* 26:489–498
4. Lopez-Lazaro M, Willmore E, Austin CA (2010) The dietary flavonoids myricetin and fisetin act as dual inhibitors of DNA topoisomerases I and II in cells. *Mutat Res* 696:41–47
5. Lopez-Lazaro M, Willmore E, Elliott SL, Austin CA (2008) Selenite induces topoisomerase I and II-DNA complexes in K562 leukemia cells. *Int J Cancer* 123:2217–2221
6. Cowell IG, Tilby MJ, Austin CA (2011) An overview of the visualisation and quantitation of low and high MW DNA adducts using the trapped in agarose DNA immunostaining (TARDIS) assay. *Mutagenesis* 26:253–260. <https://doi.org/10.1093/mutage/geq094>
7. Frank AJ, Tilby MJ (2003) Quantification of DNA adducts in individual cells by immunofluorescence: effects of variation in DNA conformation. *Exp Cell Res* 283:127–134. [https://doi.org/10.1016/S0014-4827\(02\)00026-5](https://doi.org/10.1016/S0014-4827(02)00026-5)
8. Frank AJ, Proctor SJ, Tilby MJ (1996) Detection and quantification of melphalan-DNA adducts at the single cell level in hematopoietic tumor cells. *Blood* 88:977–984
9. Willmore E, Frank AJ, Padget K et al (1998) Etoposide targets topoisomerase II α and II β in leukemic cells: isoform-specific cleavable complexes visualized and quantified in situ by a novel immunofluorescence technique. *Mol Pharmacol* 54:78–85

Study of Plasmid-Mediated Quinolone Resistance in Bacteria

George A. Jacoby

Abstract

Plasmid-mediated quinolone resistance (PMQR) involves genes for proteins that protect the quinolone targets, an enzyme that inactivates certain quinolones as well as aminoglycosides, and pumps that efflux quinolones. Quinolone susceptibility is reduced by these mechanisms but not to the level of clinical resistance unless chromosomal mutations are also present. PCR primers and conditions for PMQR gene detection are described as well as how to establish a plasmid location.

Key words Quinolone resistance, Conjugation, Gene location, Plasmid characterization

1 Introduction

Plasmid-mediated quinolone resistance (PMQR) involves (1) Qnr proteins that compete with quinolones for binding to their intracellular targets, the topoisomerase type II enzymes DNA gyrase and topoisomerase IV, (2) the aminoglycoside acetyltransferase variant AAC(6′)-Ib-cr that modifies those quinolones with an amino nitrogen on the piperazinyl ring, such as ciprofloxacin but not levofloxacin, and (3) QepAB or OqxAB pumps that efflux quinolones from the bacterial cell. The increasing incidence of quinolone resistance in clinical isolates is mainly due to mutations in subunits of DNA gyrase and topoisomerase IV abetted by activation of endogenous efflux pumps and restriction of porin channels for quinolone entry. PMQR reduces quinolone susceptibility although not to the level of clinical resistance (Table 1), but it supplements other resistance mechanisms and facilitates further mutations to higher-level resistance.

Plasmids carrying PMQR have been mainly found in *Enterobacteriaceae*, especially *Escherichia coli*, and species of *Klebsiella*, *Enterobacter*, and *Salmonella*, but only rarely in *Acinetobacter*, *Pseudomonas*, and other nonfermenting species, and not at all in

Table 1
Effect of different quinolone resistance mechanisms on quinolone susceptibility of *E. coli*

<i>E. coli</i> strain	MIC $\mu\text{g/ml}$		
	Ciprofloxacin	Levofloxacin	Nalidixic acid
J53	0.008	0.015	4
J53 <i>gyrA</i> (S83 L)	0.25	0.5	≥ 256
J53 pMG252 (<i>qnrA1</i>)	0.25	0.5	16
J53 pMG298 (<i>qnrB1</i>)	0.25	0.5	16
J53 pMG306 (<i>qnrS1</i>)	0.25	0.38	16
J53 pMG320 (<i>aac(6')-Ib-cr</i>)	0.06	0.015	4
J53 pAT851 (<i>qepA</i>)	0.064	0.032	4
CLSI susceptibility breakpoint	≤ 1.0	≤ 2.0	≤ 16

gram-positive species. In both gram-positive and gram-negative, especially aquatic, bacteria *qnr* genes related to those found on plasmids are located on the bacterial chromosome. Alleles of *qnrB* are found on the chromosome of members of the *Citrobacter freundii* complex [1, 2]. *oqxAB* is also commonly chromosomal in *K. pneumoniae* and *Enterobacter* spp. Hence, depending on the investigation it may be necessary to show whether a PMQR gene is mediated by a plasmid or the chromosome in particular bacterial isolates.

PMQR has been found in both quinolone susceptible and quinolone resistant clinical isolates. A phenotype of low level reduced fluoroquinolone susceptibility combined with only low level nalidixic acid resistance (see Table 1) suggests the presence of PMQR [3, 4]. In clinically quinolone resistant isolates molecular methods are needed for PMQR detection. Because it is often linked on plasmids with resistance to other agents, especially β -lactams, a higher frequency of PMQR will be found in clinical samples selected for resistance to ceftazidime or other antibiotics. Other enzymes can confer kanamycin resistance besides AAC(6')-Ib-cr, but this quinolone resistance mechanism can be ruled out in a kanamycin susceptible isolate. On the other hand *qepAB* has often been found on plasmids also encoding ribosomal methylase *rmtB*, so resistance to aminoglycosides may be a clue to the presence of this efflux pump. The frequency of PMQR detection in unselected clinical samples is usually <5% but frequencies as high as 39% in *E. cloacae* isolates at a hospital in China have been reported [5]. *aac(6')-Ib-cr* is the most common PMQR; *qnrB* and *qnrS* are the next most common. *qnrD* is particularly likely to be found in *Proteus* spp. and other *Proteaceae*. *qnrC* has been found only once. *qnrVC* is

Table 2
PCR primers

Gene	Primer sequence	Annealing temperature (C ⁰)	Product size (bp)	References
<i>qnrA</i>	ATTTCTCACGCCAGGATTG TGCCAGGCACAGATCTTGAC	60	573	[11]
<i>qnrB</i>	CTCTGGCRYTMGTYYGGCG TTYGCBGYCCGCCAGTCGAA	64	504	[1]
<i>qnrC</i>	CACCTACCCATTTATTTTCA GGGTTGTACATTTATTGAATCG	56	307	[12]
<i>qnrD</i>	CGAGATCAATTTACGGGGAATA AACAAGCTGAAGCGCCTG	60	581	[13]
<i>qnrS</i>	ACTGCAAGTTCATTGAACAG GATCTAAACCGTCGAGTTCG	60	416	[11]
<i>aac(6)-Ib-cr</i>	TTGCGATGCTCTATGAGTGGCTA CTCGAATGCCTGGCGTGTTT	55	482	[14]
<i>qepA</i>	AACTGCTTGAGCCCGTAGAT GTCTACGCCATGGACCTCAC	60	596	[12]
<i>oqxA</i>	CTCGGCGCGATGATGCT CCACTCTTCACGGGAGACGA	57	392	[15]
<i>psp</i> [1]	AAATTTAAYCAGAAAAAAGC			[1]
<i>sdr</i> [2]	GCTSARGAGAACAGCTATAC		972 ^a	[1]
<i>orf</i> [3]	AAGAGTGGAATAATTTCCACA		914 ^a	[1]
<i>orf</i> [4]	ATGGCTGAAGTTGAGATTAT		1068 ^a	[1]

^aProduct size when paired with *psp* [1]

the newest variety to be recognized on plasmids [6]. PMQR has also been found in samples from a variety of animals. The topic of PMQR has been frequently reviewed [7–10].

Six families of *qnr* genes are known: *qnrA*, *qnrB*, *qnrC*, *qnrD*, *qnrS*, and *qnrVC*. The families differ from each other by 30% or more with variation within each family of generally 10% or less. A listing of plasmid-mediated *qnr* genes is maintained at <http://www.lahey.org/qnrStudies/>. There are currently 6 alleles of *qnrVC*, 8 alleles of *qnrA*, 9 alleles of *qnrS*, 2 alleles of *qnrD*, only a single *qnrC*, and more than 80 alleles of *qnrB*. PCR reactions with primers such as those in Table 2 allow the presence of a member of each PMQR family to be detected. The *aac(6)-Ib-cr* gene differs from *aac(6)-Ib* by only a few nucleotides, and the primers listed in Table 2 will amplify both genes, but they can be distinguished by digesting the amplification product with a restriction endonuclease that cleaves the wild-type gene but not the –cr variant [14]. A PCR method that detects the –cr variant directly has been described

[16], as well as a gap-ligase chain reaction technique [17], methods involving high-resolution DNA melting analysis [18, 19], a pyrosequencing method [20, 21], a disc-based method [22], and a strategy utilizing MALDI-TOF [23]. A multiplex PCR assay for *qnrA*, *qnrB*, *qnrC*, *qnrD*, *qnrS*, *aac(6)-Ib-cr*, *qepA*, and *oqxAB* [24] has been reported as well as a multiplex real time PCR assay for all PMQR genes except *oqxAB* and *qnrVC* [25].

2 Materials

2.1 Growth Media

1. LB (Luria Bertani) broth: 10 g tryptone, 5 g yeast extract, 10 g NaCl in 1 L distilled water (pH 7.0 with 5 N NaOH as necessary). Commercially available.
2. Medium A: 7 g K₂HPO₄, 3 g KH₂PO₄, 0.5 g Na₃Citrate-2H₂O, 0.1 g MgSO₄-7H₂O, 1 g (NH₄)₂SO₄ in 1 L, pH 7.0 at 25 °C.
3. Minimal Agar: Medium A, 2% agar, 0.5% glucose plus growth factors as required, such as 30 µg/ml L-methionine and 50 µg/ml L-proline.
4. MH (Mueller Hinton) Agar: 2 g beef extract, 17.5 g casein hydrolysate, 1.5 g starch, 17 g agar in 1 L distilled water, pH 7.3 at 25 °C. Commercially available.

2.2 PCR

1. Oligonucleotide primers (Listed in Table 2) (*see Note 1*).
2. PCR SuperMix High Fidelity (Invitrogen; www.thermofisher.com):
A 22 U/ml DNA mixture of Taq DNA polymerase and DNA polymerase from *Pyrococcus* species GB-D in 66 mM Tris-SO₄ (pH 9.1 at 25 °C), 19.8 mM (NH₄)₂SO₄, 2.2 mM MgSO₄, 220 µM dGTP, 220 µM dATP, 220 µM dTTP, 220 µM dCTP, and stabilizers. PCR SuperMix High Fidelity is supplied at a 1.1× concentration to allow approximately 10% of the final reaction volume to be used for the addition of primer and template solutions. Store at −20 °C.

2.3 Restriction Endonuclease

BtsCI (New England Biolabs, neb.com).

2.4 Control Strains and Plasmids

1. *Escherichia coli* J53 Azide^R (K12 *met pro* R⁻), ATCC[®] BAA-2731[™], conjugation recipient and common host strain [26].
2. J53 Az^RpMG252, ATCC[®] BAA-2728[™], *qnrA1* standard for PCR [27].
3. J53 Az^RpMG298, ATCC[®] BAA-2729[™], *qnrB1* and *aac(6)-Ib-cr* standard for PCR [28].

4. J53 Az^R pMG306, ATCC[®] BAA-2730[™], *qnrS1* standard for PCR [29].
5. pBC SK (+) Phagemid (agilent.com). Carries a chloramphenicol resistance gene and a polylinker with 21 unique restriction sites.

3 Methods

3.1 Detection of PMQR Genes

1. Grow a single test colony overnight at 37 °C in 2 ml LB broth plus selective antibiotic if concerned about plasmid stability.
2. Centrifuge 1 ml of culture for 2–3 min.
3. Discard supernatant. Resuspend pellet in 500 µl distilled water in a microcentrifuge (Eppendorf) tube.
4. Boil solution for 10 min in a heat block or water bath.
5. Centrifuge the boil prep for 1–2 min.
6. Remove supernatant to fresh Eppendorf tube for analysis. This is the template DNA.
7. Set up reaction tubes on ice.
8. Add to each tube a) 45 µl PCR SuperMix High Fidelity b) Primer solution (recommended final concentration of each 200 nM) c) 3.5 µl of template solution. Total volume of primer and template solutions added can be 0.5–5 µl.
9. Mix contents of tubes and cover with mineral or silicone oil (depending on the model of thermal cycler used, the oil may be unnecessary).
10. Cap tubes and load thermal cycler at 94 °C.
11. Cycling parameters: One cycle of 94 °C for 2 min (preamplification denaturation); 31 cycles of 94 °C for 45 s (denaturing); X °C for 45 s (annealing); 72 °C for 1 min (extension); finally 72 °C for 3 min, 4 °C Hold. Where X is the annealing temperature given in Table 2 (*see Note 2*).
12. Include positive and negative controls in each run.
13. Identify amplification products by their size after electrophoresis on a 1.8% agarose gel at 130 V for 30 min, staining with ethidium bromide, and band visualization by UV light.
14. Positive results for *qnr* genes can be confirmed by direct sequencing of PCR products.
15. PCR products positive for *aac(θ)-Ib* are further analyzed by digestion with BtsCI to identify *aac(θ)-Ib-cr*, which lacks the BtsCI restriction site present in the wild-type gene (17). The wild-type *aac(θ)-Ib* PCR product yields 210-bp and 272-bp fragments after restriction.

3.2 Sequencing *qnr* Alleles

1. Many *qnrB* alleles are bounded by *pspF* and *sdr* or *orf2* genes, which can be used to amplify the entire intervening *qnrB* allele for sequencing [1]. Table 2 shows primers that can be paired with one for *pspF* for this purpose.
2. For other *qnr* genes cloning into a vector such as pBC SK and sequencing the insert using T7 and T3 primers is convenient.
3. A web site listing the defining amino acid alterations in different Qnr alleles can be found at <http://www.lahey.org/qnrStudies/>.

3.3 Susceptibility Testing

1. MICs are determined by agar dilution on Mueller-Hinton agar at 37 °C with an inoculum of $\sim 10^4$ colony forming units according to CLSI guidelines [30] using *E. coli* J53 and ATCC 25922 as susceptible standards for quality control. Alternatively, Etest strips can be used.
2. Qualitative antimicrobial susceptibility is determined by zone diameters around antibiotic disks placed on a lawn of test bacteria on Mueller-Hinton agar plates incubated overnight at 37 °C following CLSI guidelines.

3.4 Establishing Gene Location

1. The easiest proof of a plasmid location is to demonstrate resistance transfer by conjugation with a susceptible recipient such as *E. coli* J53 Az^R.
2. Donor and recipient bacteria are grown overnight at 37 °C in LB broth.
3. 0.5 ml of each are added together to 4 ml fresh LB broth and incubation continued for at least 3–4 h or overnight. Controls include 0.5 ml of each added separately to 4.5 ml LB broth.
4. Spread 0.1 ml of controls and 0.1 ml of undiluted, 1/10 and 1/100 dilutions in medium A of the mating mixture on MH agar plates containing 200 µg/ml sodium azide (to prevent growth of the donor) and selective antibiotic (to prevent growth of the recipient). Incubate at 37 °C overnight or for up to 48 h.
5. If the donor is ampicillin resistant, add 100 µg/ml ampicillin to the selective plates in hope that PMQR will be cotransferred. Depending on the resistance of the donor other antibiotics can also be used, e.g., 50 µg/ml chloramphenicol, 10 µg/ml gentamicin, or 20 µg/ml tetracycline. 0.2 µg/ml ciprofloxacin can be used directly for selection but expect a background of ciprofloxacin resistant mutants in the recipient. The resistance phenotype (Table 1) is helpful in distinguishing transconjugants from mutants while a positive PCR result is the final confirmation that transfer has been successful.

6. Quantitative transfer frequencies can be obtained by having recipient in fivefold excess and counting the number of input donor colonies by dilution.
7. A few donors give rise to a confusing background of azide resistant mutants, which can be easily distinguished from transconjugants by the methionine and proline requirements of J53 for growth on minimal media.
8. If conjugation fails (*see Note 3*) and one or more plasmids can be visualized by agarose gel electrophoresis in the donor (*see Note 4*), transformation may be successful. Use a kit appropriate for the plasmid size to isolate plasmid DNA and electroporate it into J53 with selection on MH agar containing 0.2 µg/ml ciprofloxacin or other antibiotics with appropriate controls for background mutations.
9. A large (>100 kb) plasmid may not be transformable, but can be shown to contain a particular PMQR by hybridization with a labeled gene probe [15] (*see Note 5*).
10. Purify transconjugants or transformants once on selective media and characterize their resistances by disk or MIC (*see Note 6*).

4 Notes

1. The sequence variability of *qnrB* is such that additional primers may be required to detect all *qnrB* alleles.
2. The annealing temperature can be adjusted for yield and specificity, and may be different if another polymerase is used for PCR.
3. Occasional plasmids transfer more efficiently at 30 °C or by filter mating. For the latter the donor and recipient pair as well as controls with each alone is impinged on sterile filters, which are placed on the surface of a plain MH plate. After incubation overnight at 37 °C, growth is resuspended in medium A, and appropriate dilutions are plated on selective media.
4. Visualization of large PMQR plasmids may require specialized techniques [31].
5. A chromosomal location can be inferred by digestion of genomic DNA with I-Ceu I, an endonuclease specific for ribosomal RNA genes [32], and demonstrating hybridization to a specific fragment with a PMQR gene probe [33].
6. Additional possible plasmid characterization includes sizing by agarose gel electrophoresis in comparison with standards [34] and determination of incompatibility specificity (Inc group) by PCR [35].

References

- Jacoby GA, Griffin CM, Hooper DC (2011) *Citrobacter* spp. as a source of *qnrB* alleles. *Antimicrob Agents Chemother* 55 (11):4979–4984. <https://doi.org/10.1128/AAC.05187-11>. AAC.05187-11 [pii]
- Ribeiro TG, Novais A, Branquinho R, Machado E, Peixe L (2015) Phylogeny and comparative genomics unveil independent diversification trajectories of *qnrB* and genetic platforms within particular *Citrobacter* species. *Antimicrob Agents Chemother* 59 (10):5951–5958. <https://doi.org/10.1128/AAC.00027-15>
- Gunell M, Webber MA, Kotilainen P, Lilly AJ, Caddick JM, Jalava J, Huovinen P, Siitonen A, Hakanen AJ, Piddock LJ (2009) Mechanisms of resistance in nontyphoidal *Salmonella enterica* strains exhibiting a nonclassical quinolone resistance phenotype. *Antimicrob Agents Chemother* 53(9):3832–3836. <https://doi.org/10.1128/AAC.00121-09>. AAC.00121-09 [pii]
- Rodriguez-Martinez JM, Lopez-Cerero L, Diaz-de-Alba P, Chamizo-Lopez FJ, Polo-Padillo J, Pascual A (2016) Assessment of a phenotypic algorithm to detect plasmid-mediated quinolone resistance in Enterobacteriaceae. *J Antimicrob Chemother* 71 (3):845–847. <https://doi.org/10.1093/jac/dkv392>
- Zhao X, Xu X, Zhu D, Ye X, Wang M (2010) Decreased quinolone susceptibility in high percentage of *Enterobacter cloacae* clinical isolates caused only by Qnr determinants. *Diagn Microbiol Infect Dis* 67:110–113. <https://doi.org/10.1016/j.diagmicrobio.2009.12.018>. S0732-8893(09)00509-4 [pii]
- Fonseca EL, Vicente AC (2013) Epidemiology of *qnrVC* alleles and emergence out of the *Vibrionaceae* family. *J Med Microbiol* 62 (Pt 10):1628–1630. <https://doi.org/10.1099/jmm.0.062661-0>
- Strahilevitz J, Jacoby GA, Hooper DC, Robicsek A (2009) Plasmid-mediated quinolone resistance: a multifaceted threat. *Clin Microbiol Rev* 22(4):664–689. <https://doi.org/10.1128/CMR.00016-09>. 22/4/664 [pii]
- Poirel L, Cattoir V, Nordmann P (2012) Plasmid-mediated quinolone resistance; interactions between human, animal, and environmental ecologies. *Front Microbiol* 3:24. <https://doi.org/10.3389/fmicb.2012.00024>
- Ruiz J, Pons MJ, Gomes C (2012) Transferable mechanisms of quinolone resistance. *Int J Antimicrob Agents* 40(3):196–203. <https://doi.org/10.1016/j.ijantimicag.2012.02.011>
- Jacoby GA, Strahilevitz J, Hooper DC (2014) Plasmid-mediated quinolone resistance. *Microbiol Spectr* 2(5). <https://doi.org/10.1128/microbiolspec.PLAS-0006-2013>. PLAS-0006-2013
- Jacoby GA, Gacharna N, Black TA, Miller GH, Hooper DC (2009) Temporal appearance of plasmid-mediated quinolone resistance genes. *Antimicrob Agents Chemother* 53 (4):1665–1666. <https://doi.org/10.1128/AAC.01447-08>. AAC.01447-08 [pii]
- Kim HB, Park CH, Kim CJ, Kim EC, Jacoby GA, Hooper DC (2009) Prevalence of plasmid-mediated quinolone resistance determinants over a 9-year period. *Antimicrob Agents Chemother* 53(2):639–645. <https://doi.org/10.1128/AAC.01051-08>. AAC.01051-08 [pii]
- Cavaco LM, Hasman H, Xia S, Aarestrup FM (2009) *qnrD*, a novel gene conferring transferable quinolone resistance in *Salmonella enterica* serovar Kentucky and Bovismorbificans strains of human origin. *Antimicrob Agents Chemother* 53(2):603–608. <https://doi.org/10.1128/AAC.00997-08>. AAC.00997-08 [pii]
- Park CH, Robicsek A, Jacoby GA, Sahm D, Hooper DC (2006) Prevalence in the United States of *aac(6)-Ib-cr* encoding a ciprofloxacin-modifying enzyme. *Antimicrob Agents Chemother* 50:3953–3955
- Kim HB, Wang M, Park CH, Kim EC, Jacoby GA, Hooper DC (2009) *oqxAB* encoding a multidrug efflux pump in human clinical isolates of *Enterobacteriaceae*. *Antimicrob Agents Chemother* 53(8):3582–3584. <https://doi.org/10.1128/AAC.01574-08>. AAC.01574-08 [pii]
- Wareham DW, Umoren I, Khanna P, Gordon NC (2010) Allele-specific polymerase chain reaction (PCR) for rapid detection of the *aac(6)-Ib-cr* quinolone resistance gene. *Int J Antimicrob Agents* 36(5):476–477. <https://doi.org/10.1016/j.ijantimicag.2010.07.012>
- Warburg G, Korem M, Robicsek A, Engelstein D, Moses AE, Block C, Strahilevitz J (2009) Changes in *aac(6)-Ib-cr* prevalence and fluoroquinolone resistance in nosocomial isolates of *Escherichia coli* collected from 1991 through 2005. *Antimicrob Agents Chemother* 53(3):1268–1270. <https://doi.org/10.1128/AAC.01300-08>. AAC.01300-08 [pii]
- Hidalgo-Grass C, Strahilevitz J (2010) High-resolution melt curve analysis for identification of single nucleotide mutations in the quinolone resistance gene *aac(6)-Ib-cr*. *Antimicrob*

- Agents Chemother 54(8):3509–3511. <https://doi.org/10.1128/AAC.00485-10>. AAC.00485-10 [pii]
19. Bell JM, Turnidge JD, Andersson P (2010) *aac*(δ')-*Ib-cr* genotyping by simultaneous high-resolution melting analyses of an unlabeled probe and full-length amplicon. Antimicrob Agents Chemother 54(3):1378–1380. <https://doi.org/10.1128/AAC.01476-09>. AAC.01476-09 [pii]
 20. Guillard T, Duval V, Moret H, Brasme L, Vernet-Garnier V, de Champs C (2010) Rapid detection of *aac*(δ')-*Ib-cr* quinolone resistance gene by pyrosequencing. J Clin Microbiol 48(1):286–289. <https://doi.org/10.1128/JCM.01498-09>. JCM.01498-09 [pii]
 21. Guillard T, Fontaine N, Limelette A, Lebreil AL, Madoux J, de Champs C (2013) A simplified and cost-effective method combining real-time PCR and pyrosequencing for detection of *aac*(δ')-*Ib-cr* gene. J Microbiol Methods 95(2):268–271. <https://doi.org/10.1016/j.mimet.2013.09.015>
 22. Wachino J, Yamane K, Arakawa Y (2011) Practical disk-based method for detection of *Escherichia coli* clinical isolates producing the fluoroquinolone-modifying enzyme AAC(δ')-*Ib-cr*. J Clin Microbiol 49(6):2378–2379. <https://doi.org/10.1128/JCM.00278-11>
 23. Pardo CA, Tan RN, Hennequin C, Beyrouthy R, Bonnet R, Robin F (2016) Rapid detection of AAC(δ')-*Ib-cr* production using a MALDI-TOF MS strategy. Eur J Clin Microbiol Infect Dis. <https://doi.org/10.1007/s10096-016-2762-1>
 24. Ciesielczuk H, Hornsey M, Choi V, Woodford N, Wareham DW (2013) Development and evaluation of a multiplex PCR for eight plasmid-mediated quinolone-resistance determinants. J Med Microbiol 62(Pt 12):1823–1827. <https://doi.org/10.1099/jmm.0.064428-0>
 25. Guillard T, Moret H, Brasme L, Carlier A, Vernet-Garnier V, Cambau E, de Champs C (2011) Rapid detection of *qnr* and *qepA* plasmid-mediated quinolone resistance genes using real-time PCR. Diagn Microbiol Infect Dis 70(2):253–259. <https://doi.org/10.1016/j.diagmicrobio.2011.01.004>. S0732-8893(11)00010-1 [pii]
 26. Jacoby GA, Han P (1996) Detection of extended-spectrum β -lactamases in clinical isolates of *Klebsiella pneumoniae* and *Escherichia coli*. J Clin Microbiol 34(4):908–911
 27. Martínez-Martínez L, Pascual A, Jacoby GA (1998) Quinolone resistance from a transferable plasmid. Lancet 351(9105):797–799
 28. Jacoby GA, Walsh KE, Mills DM, Walker VJ, Oh H, Robicsek A, Hooper DC (2006) *qnrB*, another plasmid-mediated gene for quinolone resistance. Antimicrob Agents Chemother 50(4):1178–1182. <https://doi.org/10.1128/AAC.50.4.1178-1182.2006>. 50/4/1178 [pii]
 29. Gay K, Robicsek A, Strahilevitz J, Park CH, Jacoby G, Barrett TJ, Medalla F, Chiller TM, Hooper DC (2006) Plasmid-mediated quinolone resistance in non-Typhi serotypes of *Salmonella enterica*. Clin Infect Dis 43(3):297–304
 30. Clinical and Laboratory Standards Institute (2016) Performance standards for antimicrobial susceptibility testing; 26th informational supplement. CLSI document M100-S26. Clinical and Laboratory Standards Institute, Wayne, PA
 31. Barton BM, Harding GP, Zuccarelli AJ (1995) A general method for detecting and sizing large plasmids. Anal Biochem 226(2):235–240
 32. Liu SL, Hessel A, Sanderson KE (1993) Genomic mapping with *I-Ceu I*, an intron-encoded endonuclease specific for genes for ribosomal RNA, in *Salmonella* spp., *Escherichia coli*, and other bacteria. Proc Natl Acad Sci U S A 90(14):6874–6878
 33. Kehrenberg C, Friederichs S, de Jong A, Schwarz S (2008) Novel variant of the *qnrB* gene, *qnrB12*, in *Citrobacter werkmanii*. Antimicrob Agents Chemother 52(3):1206–1207
 34. Takahashi S, Nagano Y (1984) Rapid procedure for isolation of plasmid DNA and application to epidemiological analysis. J Clin Microbiol 20(4):608–613
 35. Carattoli A, Bertini A, Villa L, Falbo V, Hopkins KL, Threlfall EJ (2005) Identification of plasmids by PCR-based replicon typing. J Microbiol Methods 63(3):219–228. <https://doi.org/10.1016/j.mimet.2005.03.018>. S0167-7012(05)00113-2 [pii]

INDEX

A

- Agarose gel electrophoresisv, 64, 66, 67, 69, 70, 78, 80–82, 84, 85, 100, 105, 187, 275, 276, 323
- Aminocoumarin49, 50
- Anaphase 191, 201, 217, 219–222, 224, 226–228, 231, 232, 234, 236, 238
- Antibacterial drugs48–51, 55, 57
- Antibody detection 283
- Assayv, vi, 8, 14, 23, 26, 29, 35, 64, 68, 89, 96, 105, 116, 121, 122, 125, 158, 161–170, 174–180, 186, 187, 200, 215, 218, 219, 228, 231, 232, 234, 244, 246, 252, 253, 259, 260, 262–264, 266, 270, 271, 273, 277, 278, 284, 288–292, 296, 301, 302, 304, 311, 315

B

- Bacteria v, vi, 4, 11, 12, 14, 15, 48–52, 56, 57, 63–65, 67, 71, 72, 131, 162, 168, 260, 277, 278, 317–319
- Bacterial topoisomerase I 141, 259, 260, 262–264, 266
- Bright-field microscopy 145, 146
- Budding yeast 22, 23, 29, 35, 109, 119, 217

C

- Catenation9, 75–86, 139, 191
- Cell-based 8
- ChIP-seq (chromatin immunoprecipitation) 89, 91–93, 105, 107, 111–113, 186, 187
- Chromatid resolution 192, 194, 196–199
- Chromatin 97, 98, 110–113, 117–119, 123, 125, 127, 153, 183–187, 195, 199, 201, 202, 213, 229
- Chromatin immunoprecipitation (ChIP)vi, 32, 111, 114, 117, 119, 125, 127, 183–187
- Chromosome condensation 192, 200, 202, 217, 218, 224, 229, 231, 232, 234
- Chromosome individualization 192, 197–199
- Circular RNA 161–164, 166, 168, 170
- Cleaved complexes vi, 269

- Condensation 154, 194–198, 200, 217, 224–232
- Conjugation 218, 219, 320, 322, 323
- Covalent complexes vi, 283–298, 301–315
- CsCl ultracentrifugation 289

D

- 2D agarose gel electrophoresis76, 154–157
- Deoxyribonucleic acid (DNA)
- gyrase 2, 4, 47–53, 55–57, 87, 317
- replication23, 29, 31, 34, 49, 51–53, 56, 63, 75, 77, 110, 111, 113, 131, 132, 173, 191, 218, 220, 259, 269
- supercoilingv, 63–72, 95, 96, 98, 105
- topoisomerasev, 1, 2, 6, 7, 14, 47–58, 63, 71, 72, 153, 161, 183, 217–239, 283, 285, 286, 289–291, 293, 301
- topologyv, 2, 75–77, 139, 153, 183, 260, 301
- 2D gels77, 85
- Double Holliday junctions (dHj)12, 153, 154
- Drug discovery 173

E

- 5-Ethynyl-2'-deoxyuridine (EdU)v, 132–137

F

- Flow cell 91, 140, 141, 145–149, 151
- Fluorescence-based assay vi, 259–267
- Fluoroquinolonevi, 48, 259, 269–280, 318
- Functionalized DNA 143

G

- Gene location 322, 323
- Genome instability 12, 38, 110, 241, 242, 252

H

- Hemicatenanev, 11, 14, 153–158
- High-throughput genomics 95

328 | DNA TOPOISOMERASES: METHODS AND PROTOCOLS

Index

High-throughput screening (HTS) 56, 260,
262, 263, 266

I

ICRF-193 192, 193, 195,
197–199, 202, 204, 211

Immunostaining 111, 301,
302, 304, 311, 315

In-vivo complexes of enzyme bioassay
(ICE assay) 284–286, 288–291

K

Knot 5, 9, 161–163,
166, 168–171

M

Magnetic tweezers (MT) v, 139, 141, 146, 150
Mutagenesis 31, 38, 131,
242, 243, 246–248

Mutation vi, 8, 9, 27, 29,
38, 50, 53–56, 113, 191–193, 195–199, 206,
241–243, 246–249, 255, 317, 323

N

Non-covalent antibody attachment 140, 147
NorflIP 88, 89, 91–93
Norfloxacin 51, 88, 89, 92, 93

O

OriC 51, 131–137

P

Plasmid characterization 323
Plasmid DNA isolation 72
Psoralen v, 95–107

Q

Quinolone vi, 5, 48–56, 260,
269, 270, 272, 274, 275, 277–280, 317–323
Quinolone resistance vi, 53, 54, 317–319

R

Rapid assay for DNA adduct recovery
(RADAR assay) 284, 286,
287, 290–292

Replication v, 5, 13, 14, 21,
23, 26, 29, 35, 37, 49–52, 56, 75–77, 87, 109,
131, 136, 153, 154, 161, 241, 252, 255, 279

Replication stress 241, 242, 252, 253

Ribonucleotide excision repair (RER) 29, 241

Ribonucleotides vi, 29–36, 38,
165, 241, 242, 246, 248, 249, 251–253

R-loops v, 12,
14, 24–29, 35–38

RNA:DNA hybrids 29, 109–127

RNA:DNA immunoprecipitation
(DRIP) 111–116, 119, 120, 122

RNase H2 29, 31,
34, 35, 38, 110, 241, 242, 246, 248, 253

S

S9.6 antibody 111, 113,
118, 119, 123, 124, 126

Saccharomyces cerevisiae 22, 77,
80, 109, 111–113, 217, 219–228, 230, 232, 287,
288, 294

Single-molecule v, 14, 139–151

Spindle elongation 219, 221, 227, 236

Supercoiling v, 11, 12,
21, 47, 50, 63–65, 67, 71, 72, 95–97, 102, 104,
132, 139, 141–143, 148

Supercoiling density 64, 65, 67, 68, 70, 71

T

TopA 6–9, 27, 132, 136

TopB 132, 136

Top1 174, 241–256

Top2 75, 83, 110,
174, 183, 184, 217, 218, 221, 223–227, 231,
290–292, 294–296, 301–303, 306, 311, 312

Top3 β 162, 163, 168

Topoisomerase I 2, 21–38, 47, 57, 58,
70, 71, 132, 259–262, 264, 265, 284, 291

Topoisomerase I poisons 259, 260,
262–264, 266

Topoisomerase II 2, 48, 183–188,
191–215, 217, 219–228, 230, 232, 259, 284,
290, 294–296

Topoisomerase II checkpoint 217,
219–228, 230, 232

Topoisomerase III 48, 154, 161

Topoisomerase IV 48, 87–93,
259, 269, 317

Topoisomerase poison 50, 51,
56, 183, 259, 260, 301, 303

Topoisomerases 283, 284,
286, 287, 290, 292

Transcription v, 1, 11–14,
21, 24, 26–29, 31, 32, 37, 38, 95–97, 102, 104,
109–112, 131, 132, 136, 153, 161, 163, 165,
173, 259, 269, 284

Trapped in agarose immunostaining
(TARDIS) 301, 302, 304, 311, 315

Type IA v, 1–14, 110, 132, 170

Tyrosyl-DNA phosphodiesterase 1 (TDP1) vi, 23, 28,
173–180